ELSEVIER

CURRENT TRENDS AND FUTURE DEVELOPMENTS ON (BIO-) MEMBRANES

PHOTOCATALYTIC MEMBRANES AND PHOTOCATALYTIC MEMBRANE REACTORS

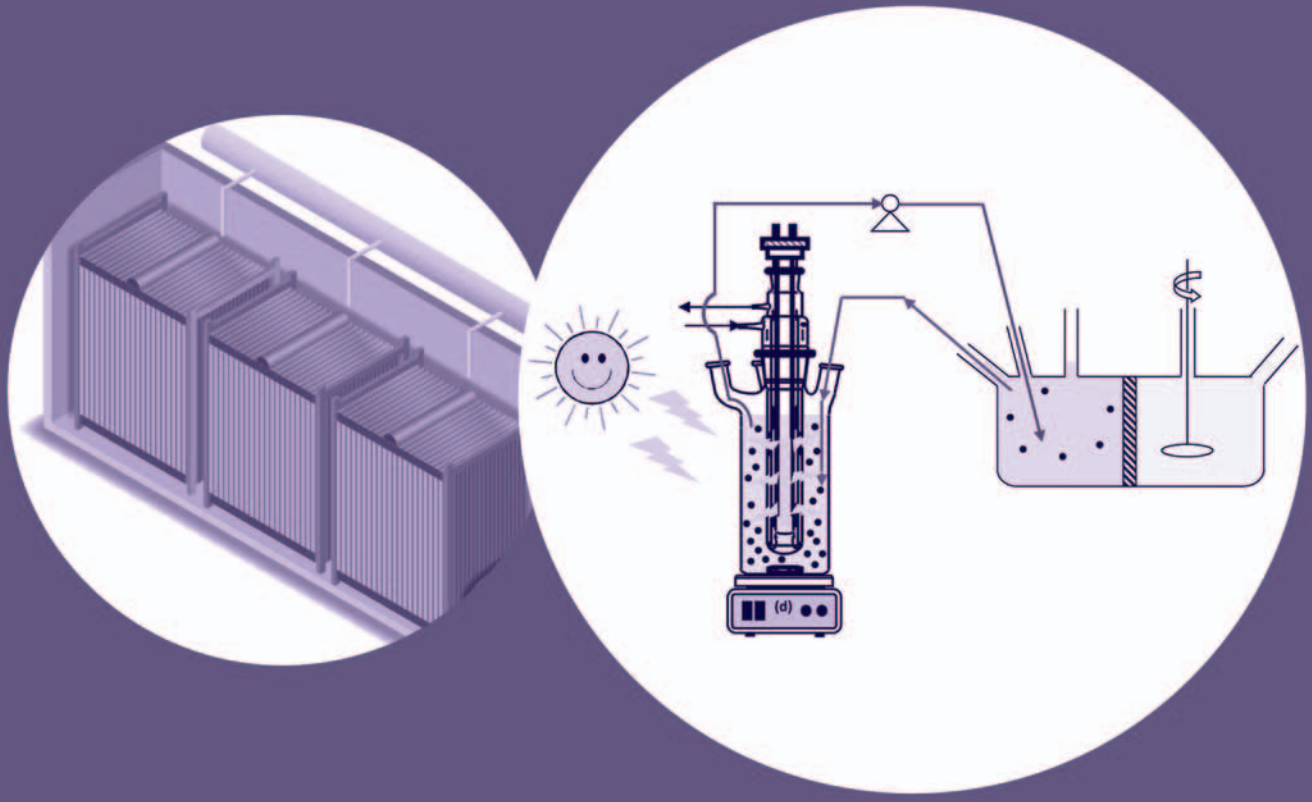

EDITORS
ANGELO BASILE, SYLWIA MOZIA, RAFFAELE MOLINARI

Current Trends and Future Developments on (Bio-) Membranes

This page intentionally left blank

Current Trends and Future Developments on (Bio-) Membranes

Photocatalytic Membranes and Photocatalytic Membrane Reactors

Edited by

Angelo Basile

Sylwia Mozia

Raffaele Molinari

Elsevier
Radarweg 29, PO Box 211, 1000 AE Amsterdam, Netherlands
The Boulevard, Langford Lane, Kidlington, Oxford OX5 1GB, United Kingdom
50 Hampshire Street, 5th Floor, Cambridge, MA 02139, United States

Notices
Knowledge and best practice in this field are constantly changing. As new research and experience broaden our understanding, changes in research methods, professional practices, or medical treatment may become necessary.

Practitioners and researchers must always rely on their own experience and knowledge in evaluating and using any information, methods, compounds, or experiments described herein. In using such information or methods they should be mindful of their own safety and the safety of others, including parties for whom they have a professional responsibility.

To the fullest extent of the law, neither the Publisher nor the authors, contributors, or editors, assume any liability for any injury and/or damage to persons or property as a matter of products liability, negligence or otherwise, or from any use or operation of any methods, products, instructions, or ideas contained in the material herein.

Library of Congress Cataloging-in-Publication Data
A catalog record for this book is available from the Library of Congress

British Library Cataloguing-in-Publication Data
A catalogue record for this book is available from the British Library

ISBN: 978-0-12-813549-5

Publisher: Susan Dennis
Acquisition Editor: Kostas KI Marinakis
Editorial Project Manager: Emily Thomson
Production Project Manager: Bharatwaj Varatharajan
Cover Designer: Mark Rogers

Typeset by TNQ Technologies

Contents

List of Contributors

Norfazliana Abdullah Universiti Teknologi Malaysia, Skudai, Johor, Malaysia
Pietro Argurio University of Calabria, Rende (CS), Italy
Marianna Bellardita University of Palermo, Palermo, Italy
Giovanni Camera-Roda University of Bologna, Bologna, Italy
Xiaofang Chen Monash University, Clayton, VIC, Australia; CSIRO Manufacturing, Clayton, VIC, Australia
Kwang-Ho Choo Kyungpook National University, Daegu, Republic of Korea
Mohd Hafiz Dzarfan Othman Advanced Membrane Technology Research Center (AMTEC), Universiti Teknologi Malaysia, Johor Bahru, Malaysia; Faculty of Chemical & Energy Engineering (FCEE), Universiti Teknologi Malaysia, Johor Bahru, Malaysia
Yaoxin Hu Monash University, Clayton, VIC, Australia; CSIRO Manufacturing, Clayton, VIC, Australia
Siti K. Hubadillah Advanced Membrane Technology Research Center (AMTEC), Universiti Teknologi Malaysia, Johor Bahru, Malaysia; Faculty of Chemical & Energy Engineering (FCEE), Universiti Teknologi Malaysia, Johor Bahru, Malaysia
Ahmad F. Ismail Advanced Membrane Technology Research Center (AMTEC), Universiti Teknologi Malaysia, Johor Bahru, Malaysia; Faculty of Chemical & Energy Engineering (FCEE), Universiti Teknologi Malaysia, Johor Bahru, Malaysia
Juhana Jaafar Universiti Teknologi Malaysia, Skudai, Johor, Malaysia
Anastasios J. Karabelas Centre for Research and Technology – Hellas (CERTH), Thessaloniki, Greece
Vittorio Loddo University of Palermo, Palermo, Italy
Leila Mahmoodi Shiraz University, Shiraz, Iran
Takeshi Matsuura Faculty of Chemical & Energy Engineering (FCEE), Universiti Teknologi Malaysia, Johor Bahru, Malaysia; University of Toronto, Toronto, ON, Canada
Raffaele Molinari University of Calabria, Rende (CS), Italy
Ali Moslehyani Advanced Membrane Technology Research Center (AMTEC), Universiti Teknologi Malaysia, Johor Bahru, Malaysia; University of Ottawa, Ottawa, ON, Canada; University of Toronto, Toronto, ON, Canada
Sylwia Mozia West Pomeranian University of Technology, Szczecin, Poland
Minh Tan Nguyen Hanoi University of Science and Technology, Hanoi, Vietnam

Leonardo Palmisano University of Palermo, Palermo, Italy
Francesco Parrino University of Palermo, Palermo, Italy
Konstantinos V. Plakas Centre for Research and Technology – Hellas (CERTH), Thessaloniki, Greece
Mohammad R. Rahimpour Shiraz University, Shiraz, Iran
Mukhlis A. Rahman Universiti Teknologi Malaysia, Skudai, Johor, Malaysia
Wolfgang M. Samhaber Johannes Kepler University Linz, Linz, Austria
Vasileios C. Sarasidis Centre for Research and Technology – Hellas (CERTH), Thessaloniki, Greece
Huanting Wang Monash University, Clayton, VIC, Australia; CSIRO Manufacturing, Clayton, VIC, Australia
Zongli Xie Monash University, Clayton, VIC, Australia; CSIRO Manufacturing, Clayton, VIC, Australia

Preface

Advanced oxidation processes, such as those using light and a semiconductor (the photocatalyst), named heterogeneous photocatalysis, to generate oxidizing/reducing species, have been extensively studied since 1972 when Fujishima and Honda discovered the photocatalytic splitting of water on TiO_2 electrodes. Then a large amount of studies related to environment recovery by the total degradation to innocuous substances of organic and inorganic pollutants, removal of toxic metals, and synthesis of organic compounds, has been carried out.

The main difference of photocatalysis compared with conventional catalysis is the photonic activation mode of the catalyst, which replaces the thermal activation. So, in perspective, the Sun as energy source can be used to carry out a variety of reactions.

Photocatalysis is based on green chemistry principles. Its important characteristics include the following:

1. mild operating conditions (ambient temperature and pressure, very few auxiliary additives, and short reaction times);
2. possibility to abate refractory, very toxic, and nonbiodegradable molecules;
3. avoids the use of environmentally and unhealthy dangerous heavy metal catalysts by using safer photocatalysts (mainly TiO_2);
4. avoids the use of strong oxidants/reducing agents;
5. permits the real destruction of the contaminants with the formation of innocuous by-products;
6. can be applied to a wide range of substrates in aqueous, solid, and gaseous phase;
7. applicable to solutions at low concentrations;
8. offers a good alternative to the energy-intensive conventional treatment methods;
9. permits to use renewable solar energy;
10. can be combined with other physical and chemical technologies (e.g., membrane separations).

Coupling of photocatalysis and membranes is a powerful approach that is achieved in photocatalytic membrane reactors (PMRs). A PMR can be defined as a device existing in various configurations, which combines a photocatalyst and a membrane to produce chemical transformations. PMRs improve the potentialities of classical photoreactors (PRs)

and those of membrane processes (separation at molecular level), giving a synergy for both technologies and thus minimizing environmental and economical impacts.

Recently, a particular interest has been directed toward PMRs with photocatalytic membranes (PMs) or suspended photocatalyst. First reports on the possibilities of combining photocatalysis and membrane separation were published in the 1990s of the 20th century. A significant growth of interest in this area has been observed, however, especially in the last 4 years. Implementation of PMRs into large-scale applications could be beneficial in terms of environmental protection (wastewater treatment), standard of living (production of water free from harmful contaminants), and chemical industry (synthesis of useful compounds).

Detailed investigations are still needed to improve the hybrid photocatalysis—membrane processes performance.

The main aim of this book is to give, with contributions from some of the best scientists in the field, a comprehensive remark on the present state of the art in the area of PMs and PMRs as well as an update on recent publications in this field. The reader will get an overview of basis of photocatalysis and membrane separation; basic aspects of PMs and PMRs; and applications, modeling, and economical aspects of PMs and PMRs. The book addresses the main issues associated with PMR design and tries to answer the question: how far from the laboratory scale is the application of PMRs in industry?

Going a bit into the details, there are 11 chapters, each one related to a specific aspect of PMs and PMRs. The volume opens with a chapter (Loddo, Bellardita, Camera-Roda, Parrino, and Palmisano) that presents the fundamentals of the processes of heterogeneous photocatalysis. Various models and equations are used to describe the influence of some parameters (pH, T, etc.) on the rate of photocatalysis. Chapter 2 (Abdullah, Rahman, Othman, Jaafar, and Ismail) provides the actual status on the development of membrane (materials, geometry, morphology, etc.) and membrane processes (microfiltration, ultrafiltration, nanofiltration, reverse osmosis, forward osmosis, gas separation, and membrane distillation). A discussion on the major issues in membrane applications is also presented. In Chapter 3 (Chen, Hu, Xie, and Wang), the recent progresses of PMs in water purification, disinfection, energy conversion are presented. Various methods (dip coating, spin coating, etc.) for the fabrication of PMs are also discussed in detail. Chapter 4 (Mozia, Molinari, and Argurio) overviews PMRs utilizing pressure-driven membrane techniques (microfiltration, ultrafiltration, and nanofiltration). Some aspects of possible strategies of mitigation of membrane fouling in PMRs, including backwashing, air sparging, intermittent permeation, control of hydraulic conditions, etc., are also introduced and discussed in detail. The various factors affecting the permeate quality are also considered. Examples of various configurations of PMRs (pressurized and submerged systems with photocatalyst in a slurry or PMs) are also introduced, compared, and discussed in detail. Chapter 5 (Camera-Roda, Loddo, Palmisano, and Parrino) shows how PMRs utilizing non—pressure-driven membrane processes can exploit various mechanisms to obtain a substantial improvement of the overall process. An important aspect of this chapter is that it illustrates the reasons that currently limit the application of these MRs. An interesting look into the very promising future perspectives is also given. Chapter 6 (Rahimpour and Mahmoodi) illustrates the most recent

progress in the application of PMRs using PMs. The chapter concludes with a discussion on the further investigations that are still necessary for enhancing the performance of these membrane systems versus the various benefits with respect to the conventional photoreactors. Chapter 7 (Moslehyani, Hubadillah, Othman, Ismail, and Matsuura) discusses the use of PMRs for organic pollutant (oil, dye, phenols, pesticides, etc.) degradation in both water and wastewater treatments. The authors' analysis confirms that PMRs must be considered a promising technology for the treatment of organic pollutants in water; however, the composition of permeate in terms of oxidation by-products should be taken into account during PMR optimization. Chapter 8 (Molinari and Argurio) presents and discusses in detail some recent results present in the specialized literature on both photocatalytic partial oxidations (benzene to phenol and ferulic acid to vanillin) and photocatalytic reductions (acetophenone to phenylethanol, CO_2 to fuels, and nitrite to ammonia). The authors give the reasons to affirm that the main benefits (i.e., enhanced system productivity and selectivity) of the hybrid processes are due both to the complete confining of the photocatalyst in the reacting environment and to the selective separation of the product simultaneously to the reaction. Chapter 9 (Karabelas, Plakas, and Sarasidis) underlines why, despite extensive research on several aspects of PMRs, no significant large-scale applications have been reported in the area of water treatment. The authors also stress the concept that a development work is still needed for promoting PMRs ready for commercialization. According to the authors, some advantages of the novel PMRs over conventional techniques may be the decisive proof in favor of large-scale PMR applications. Chapter 10 (Choo) is particularly focused on the modeling of PMRs. The author stresses the concept that the simulation of PMRs, combined with the reaction kinetics, is essential for optimal process designs and operations. To better understand different types of reactor operation schemes and flow regimes, this chapter at first focuses on the process configuration. And afterward, the kinetic model equations used to evaluate the reaction rate in photocatalytic membrane systems under various operating conditions are also considered and discussed. As a conclusion, the model prediction needs to be further improved by varying some variables such as light sources, radiation methods, process designs, and operation modes. The last chapter (Samhaber and Nguyen) introduces the economical aspects of PMRs. To find synergies in practical applications, system examples and cost aspects of various membrane techniques (reverse osmosis, nanofiltration, ultrafiltration, and microfiltration) coupled with photocatalytic reactor systems are described and critically discussed.

To conclude, the editors would like to express special thanks to each one of the authors for their strong contributions to this volume. Other very special thanks are surely addressed to all the staff of Elsevier who helped us in all the various steps for realizing this work in the best way.

Sylwia Mozia
Raffaele Molinari
Angelo Basile

This page intentionally left blank

CHAPTER 1

Heterogeneous Photocatalysis: A Promising Advanced Oxidation Process

Vittorio Loddo[1], Marianna Bellardita[1], Giovanni Camera-Roda[2], Francesco Parrino[1], Leonardo Palmisano[1]

[1]University of Palermo, Palermo, Italy; [2]University of Bologna, Bologna, Italy

1.1 Introduction

Since the pioneering research of Fujishima and Honda in 1972 on the photocatalytic cleavage of water into H_2 and O_2 (Fujishima and Honda, 1972), basic and applied research have been devoted to heterogeneous photocatalysis (PC), especially for the oxidation of organic pollutants in water or in air (Schiavello, 1995; Fujishima et al., 1999; Augugliaro et al., 1997, 1999a,1999b, 2004; Maira Vidal et al., 1997). Heterogeneous PC is defined in the following way (Braslavsky et al., 2011): "*Change in the rate of a chemical reaction or its initiation under the action of ultraviolet, visible, or infrared radiation in the presence of a substance, the photocatalyst, that absorbs light and is involved in the chemical transformation of the reaction partners.*" The possibility of solar light exploitation makes PC in aqueous media a promising tool for green chemistry applications.

The occurrence of an oxidation reaction is linked to a transfer of one or more electrons from a reductant (electron donor) to an oxidant (electron acceptor).

These electron transfers result in a chemical transformation of both the oxidant and the reductant species. Sometimes chemical species with an odd number of valence electrons (radicals) are produced, and these species are highly unstable and reactive.

The radicals generated could further react with other species present in the reaction environment (both organic and inorganic) until thermodynamically stable oxidation products are formed.

The ability of an oxidant to react with other species is related to its oxidation potential. The most effective oxidants are fluorine, hydroxyl radicals ($^{\bullet}OH$), ozone, and chlorine with oxidation potentials of 2.85, 2.70, 2.07, and 1.49 eV, respectively (Dorfman and Adams, 1973). The final products of a complete oxidation (i.e., mineralization) of organic compounds are carbon dioxide (CO_2), mineral acids, and water (H_2O).

Current Trends and Future Developments on (Bio-) Membranes. https://doi.org/10.1016/B978-0-12-813549-5.00001-3

The phenomena occurring during an advanced oxidation process (AOP) are (1) formation of primary oxidizing species (e.g., hydroxyl radicals) and (2) reaction of these species with organic/inorganic contaminants in water (Glaze et al., 1987). Examples of advanced oxidation processes (AOPs) are processes that include O_3, H_2O_2, and/or UV light, cavitation, electron beam irradiation, and Fenton's reaction. Nevertheless, AOPs will be used also to refer to a more general group of processes that involve semiconductor PC.

The rationales of these AOPs are based on the in situ generation of the highly reactive transitory species aforementioned for mineralization of refractory organic compounds, water pathogens, and disinfection by-products (Esplugas et al., 2002; Pera-Titus et al., 2004).

Heterogeneous PC uses semiconductor oxides irradiated with UV, near-UV, or visible light at ambient temperature and pressure and in the presence of oxygen. The fundamental mechanism of PC consists in the generation of electron−hole pairs, which, once separated, determine the occurrence of redox reactions of species adsorbed on the active surface. This method has been successfully used for wastewater treatment, and it is suitable to perform the complete degradation of organic and inorganic pollutants, the reduction of metal ions, the inactivation of many aerobic bacteria, etc. (Chen and Ray, 2001; Sunada et al., 2003).

Titanium dioxide is extensively used as photocatalyst because of its high chemical stability, low cost, optical electronic properties (Linsebigler et al., 1995), and nontoxicity. However, TiO_2, due to its relatively high bandgap (3.2 eV), uses only a small fraction of the solar spectrum.

The photocatalytic activity of TiO_2 for the removal of aquatic pollutants depends on different parameters. Mainly, it is strongly related to the interaction between the active surface and the chemical species, efficiency of the charge transfer recombination, and type of reactive oxygen species generated primarily by electron−hole pairs. As these behaviors are strongly dependent on the surface properties of TiO_2, to improve the performance of the photocatalytic process, different strategies have been used.

A variety of surface modification methods have been developed to enhance the photocatalytic activity and improve the efficiency of TiO_2 in a photocatalytic process; they include carbon material coating (Moon et al., 2014; Gao et al., 2013; Jiang et al., 2011; Andriantsiferana et al., 2015), metal deposition (Anderson, 2012), anion adsorption (Kim et al., 2012; Sheng et al., 2013), and hybridization with other semiconductors (Dhatshanamurthi et al., 2015; Wang et al., 2009). These modifications can induce a displacement of TiO_2 absorbance toward the visible region of the spectrum.

The previous modifications affect the quantum yield of the photocatalytic process and/or the absorption rate of the photons. Moreover, these modifications could increase the lifetime of the photogenerated electron−hole pairs.

An alternative option to increase the performance of a photocatalytic system is to add very oxidant species such as ozone, hydrogen peroxide (Pera-Titus et al., 2004) also in the presence of Fe(II) ions (Chen and Ray, 2001), peroxydisulfate and periodate ions (Sunada et al., 2003).

However, PC is also capable of selective oxidations or reductions to produce high value chemicals from a number of substrates (Palmisano et al., 2007; Yurdakal et al., 2008, 2009, 2013; Augugliaro et al., 2012; Bellardita et al., 2012, 2013, 2014a, 2014b). On the other hand, poor selectivity and costs related to the separation of the powdered photocatalyst are the major drawbacks that hinder industrial applications.

Coupling PC with membrane separation processes has been proposed as a promising solution for these problems (Loddo et al., 2009; Camera-Roda et al., 2011, 2013). Moreover, the two technologies can be straightforwardly integrated because of the similar conditions at which they may operate (relatively low temperature, low concentration of the chemicals, low energy demand). Interdisciplinary competences are required and some engineering issues should be deeply approached to prove the convenience to apply photocatalytic membrane reactors (PMRs) to the synthesis of valuable products.

This chapter reports the fundamentals of heterogeneous PC. In particular, different kinetic models and the influence of some parameters (such as pH, temperature, light intensity) on the rate of PC are described, and the effects of some photocatalyst modifications are discussed. Methods for photoreactor modeling are analyzed and the coupling of PC with other AOPs using H_2O_2, O_3, and peroxydisulfate are discussed.

1.2 Fundamentals and Mechanisms of TiO_2 Photocatalysis

1.2.1 Conductors, Insulators, and Semiconductors

The molecular orbital theory is useful to explain the structure and the geometry of the molecules.

The starting point of this theory is to consider that not only the valence electrons but all the electrons of the molecule contribute to the bond between the atoms. Electrons do not exist in the molecule that belongs to individual atoms, but they are all redistributed on energetic levels, named molecular orbitals. The molecular orbitals are centered around the nuclei of a molecule.

Molecular orbitals of a solid consisting of n equal atoms are obtained by means of a linear combination of atomic orbitals. The number of molecular orbitals formed is equal to that of the atomic ones. By increasing the number of atoms, the difference between the energetic levels decreases and a continuous band of energy is formed for high values of n.

To determine if a crystalline solid is a conductive or an insulating material, the energy band model for electrons can be applied. Indeed, the properties of a solid can be determined by the difference of energy between the different bands and the distribution of the electrons within.

The width of the various bands and the separation among them depend on the internuclear equilibrium distance between adjacent atoms. If the energetic levels of isolated atoms are not so different, the progressive enlargement of the bands may lead to their overlapping by decreasing the internuclear distance. The most external energetic band full of electrons is called *valence band* (VB).

In conducting materials, the VB is totally or partially filled and overlaps with empty higher energy band. In this case, electrons can freely move allowing conduction as in the case of metals.

On the contrary, the VB of insulating materials is completely filled, but it is separated by a high energy gap from the subsequent empty band. In this situation, no electrons can move even if high electric fields are applied.

Finally, if the forbidden energy gap is not so high, some electrons could pass in the energetic empty band by means of some kinds of excitation (e.g., thermal or light) and the material behaves as a weak conductor, i.e., as a semiconductor. The empty band, which allows the movement of the electrons, is called *conduction band* (CB).

The energy difference between the lowest conduction band edge and the highest VB edge is called *bandgap* (E_G). A material is generally considered a semiconductor when $E_G \leq 3$ eV, whereas it is considered a wide bandgap semiconductor when its bandgap value is in the $3 \div 4$ eV range.

Fig. 1.1 shows the position of the energy bands of different types of materials.

1.2.2 Properties of Semiconductor Materials

The probability that an energetic level of a solid is occupied by electrons can be determined by the Fermi–Dirac distribution function f(E) (Dekker, 1957). It applies to fermions (particles with half-integer spin, including electrons, photons, neutrons, which must obey the Pauli exclusion principle) and states that a given allowed level of energy E is a function of temperature and the Fermi level (E_F).

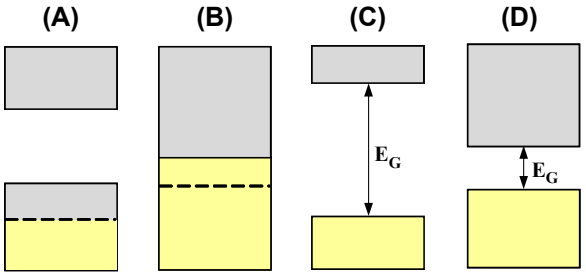

Figure 1.1
Schematic representation of the energetic bands for: (A) conductors with partially filled valence band; (B) conductors with overlapped bands; (C) insulators; (D) semiconductors.

The value of E_F is equivalent to the electrochemical potential of the electron, i.e., it can be considered as the work necessary to transport an electron from infinite distance to the semiconductor.

The Fermi level is the term used to describe the top of the electron energy levels at absolute zero temperature. An imaginary horizontal line of energy, called Fermi energy, represents the level above which the probability of electron states being filled is under 50%, and below which the probability of electron states being filled is over 50%. We call holes the empty states in the VB. Both VB holes and conduction band electrons contribute to the conductivity.

Some types of impurities and imperfections may drastically affect the electric properties of a semiconductor. In fact, the conductivity of a semiconductor can be significantly increased by adding foreign atoms in the lattice (doping) that make available electrons in the conduction band and holes in the VB. The addition of atoms having one valence electron more, with respect to the chemical valence of the atoms of the semiconductor, will lead to an excess of positive charge (Fig. 1.2A) because of the transfer of an electron from the foreign atom to the conduction band (donor doping). If the foreign atom has one valence electron less, it can accept one electron from the VB (acceptor doping) (Fig. 1.2B).

In the first case, an energetic level close to the conduction band is introduced; consequently, electrons can pass more easily in it. In this case, the solid is called “n”-type semiconductor, and the Fermi level will be close to the conduction band (Fig. 1.3B). In the second case, an energetic level close to the VB is formed, in which electrons can be promoted with the formation of holes. The semiconductor is of “p”-type, and its Fermi level will result close to the VB (Fig. 1.3C).

When a semiconductor is placed in contact with an electrolytic solution, a potential difference is established at the interface. Also in this case, it is possible to extend the concept of energetic levels of electrons in solids (Gerischer, 1970).

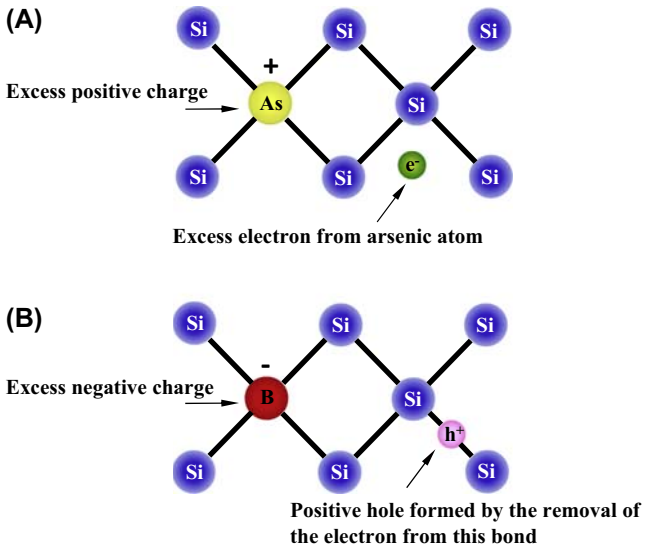

Figure 1.2
Silicon as intrinsic semiconductor (A) with arsenic impurity an electron is available for conduction; (B) with boron impurity a positive hole is available.

The energetic states of the reduced species correspond to the occupied electronic levels, whereas the energetic states of the oxidized species correspond to the not occupied ones. The Fermi level of the redox couple, $E_{F,redox}$, is equal to the electrochemical potential of electrons in the redox system, and it is equivalent to the reduction potential, V. Two different scales are used to compare the energetic levels of a semiconductor with those of a redox couple in an electrolyte. The first is expressed in eV, the other one in V (Fig. 1.4A). The difference between the two scales is due to the fact that the reference in electrochemistry is the potential of the normal hydrogen electrode (NHE), whereas in solid state physics, zero is the level of the electron in vacuum. The correlation between the two scales can be calculated from the value of potential of NHE which is equal to −4.5 eV when it is referred to that of the electron in vacuum (Lohmann, 1967).

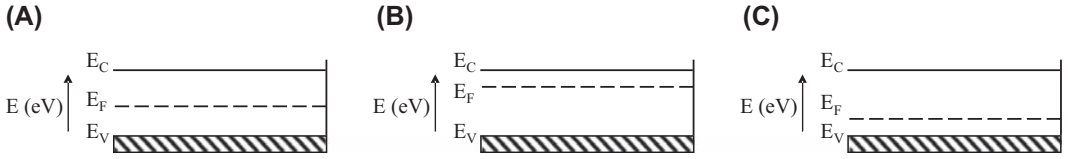

Figure 1.3
Energetic levels of a semiconductor: (A) intrinsic semiconductor; (B) "n"-type semiconductor; (C) "p"-type semiconductor. E_C: energy of CB and E_V: energy of VB.

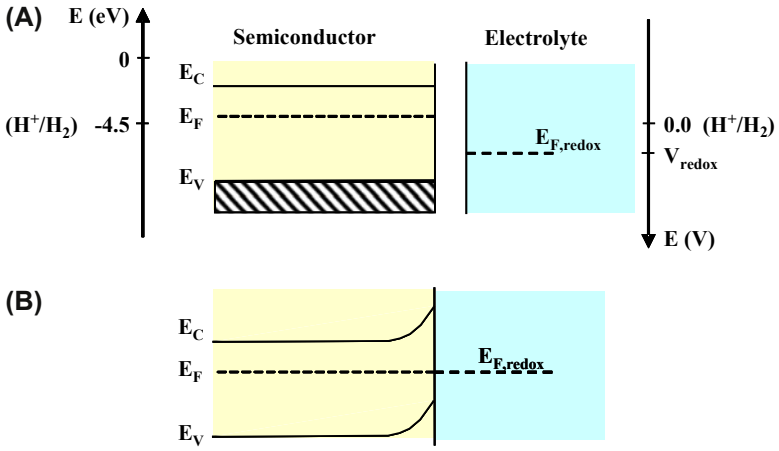

Figure 1.4
Formation of a junction between an "n"-type semiconductor and a solution (A) before the contact and (B) at equilibrium.

After the contact of the semiconductor and the solution containing the redox couple, the equilibrium is reached when the Fermi levels of both phases become equal because of an electron exchange between the solid and the electrolyte. This electronic exchange leads to the generation of a charge inside the semiconductor that is distributed in a spatial charge region near to the surface. The values of hole and electron concentrations on the surface and inside the semiconductor differ considerably. In Fig. 1.4A, the energetic levels of an "n"-type semiconductor and a redox electrolyte before the contact are drawn. In this particular case, being the energy of the Fermi level higher than that of the electrolyte, the equilibrium is reached by electron transfer from the semiconductor to the solution. The electric field produced by this transfer is represented by the upward band bending (Fig. 1.4B). Holes in excess generated in the spatial charge region move toward the semiconductor surface because of the presence of the field, whereas electrons in excess migrate from the surface to the bulk of the solid. Fig. 1.5 shows the behavior during a contact between a redox electrolyte and a "p"-type semiconductor. In this case, transfer of electrons occurs from the electrolyte to the semiconductor and the band bending is downward.

If a semiconductor is irradiated by a suitable radiation of energy equal or higher than that of the bandgap, electrons can be excited from the VB to the conduction band with the formation of electron–hole pairs because of the absorption of photons by the semiconductor. This bound state electron–hole pair is called exciton. Fig. 1.6 shows the scheme of generation of excitons.

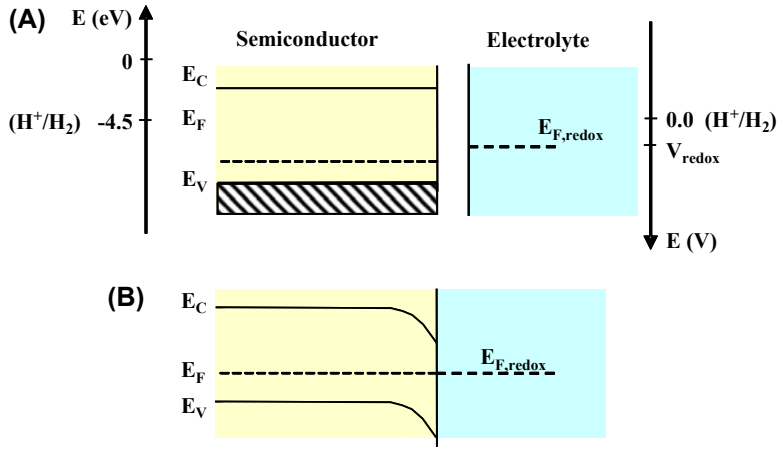

Figure 1.5
Formation of a junction between a "p"-type semiconductor and a solution (A) before the contact and (B) at equilibrium.

The separation of the photogenerated pairs is allowed by the electric field in the spatial charge region. Electrons migrate toward the bulk, whereas holes move to the surface in the case of "n"-type semiconductors (Fig. 1.6A). In the case of "p"-semiconductors, on the contrary, holes move inward of the semiconductor and electrons toward the surface (Fig. 1.6B).

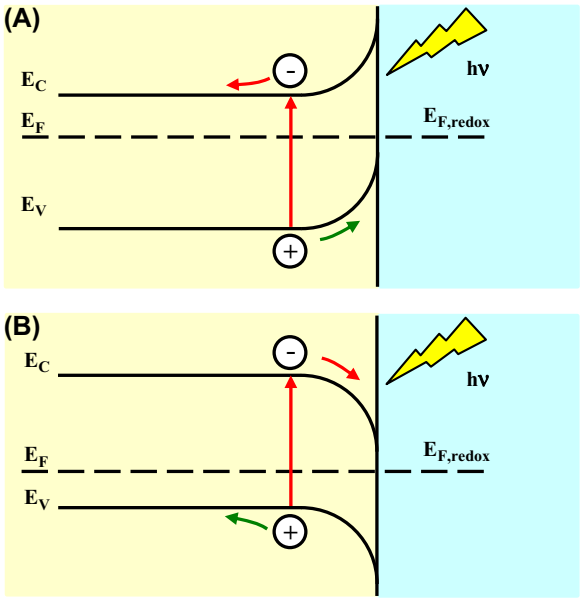

Figure 1.6
Generation of electron–hole pair due to irradiation of (A) "n"-type semiconductor and (B) "p"-type semiconductor.

Holes and electrons, during their migration, can (1) recombine, dissipating their energy as heat or as electromagnetic radiation (photons emission) or (2) can react with electron-donor or electron-acceptor species present at the semiconductor–electrolyte interface.

The potential of the photogenerated electrons corresponds to the energy of the conduction band edge, E_C, whereas the potential of the holes corresponds to the energy of the VB edge, E_V. If the value of E_C is more negative than the potential of a species present in solution, electrons reaching the interface are able to reduce the oxidized form of the redox couple. Conversely, if the potential of E_V is more positive than that of the redox couple, photoproduced holes can oxidize its reduced form (Fig. 1.7). The knowledge of the relative edge positions of the bands and of the energetic levels of the redox couples is essential to establish if oxidation and/or reduction of the species in solution occur.

Fig. 1.8 shows the values of bandgap and the positions of valence and conduction band edges for different semiconductors.

1.2.3 Photocatalytic Processes

The photocatalytic properties of a semiconductor depend on the mobility and mean lifetime of the photogenerated electrons and holes, position of the energetic levels, light absorption coefficient, and nature of the interface. Moreover, the photoactivity depends on different physicochemical properties of the semiconductor, which is mainly influenced by

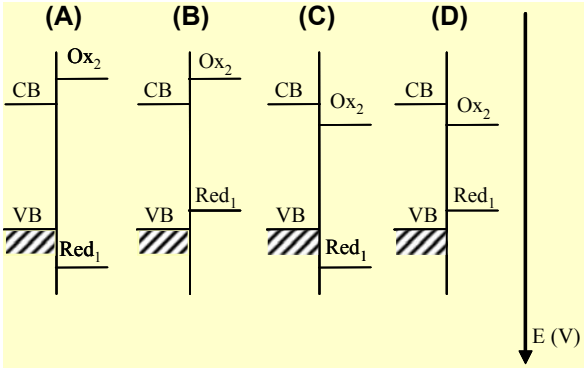

Figure 1.7
Relative positions of the valence and conduction bands with respect to the energies of two redox couples. Only for (d), both reduction and oxidation reactions are thermodynamically allowed. Ox_2 and Red_1 represent the oxidized and the reduced species, respectively, of two different redox couples.

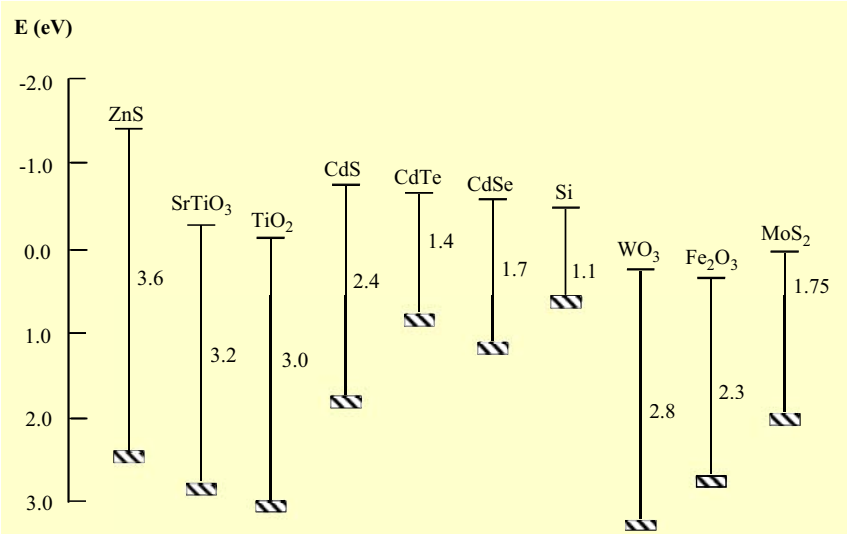

Figure 1.8
Positions of the band edges for some semiconductors in contact with aqueous electrolyte at pH = 0.

the methods of preparation of the solids, as the crystalline structure, the surface area, and the distribution of the particle size.

In a photocatalytic system, each single particle of semiconductor can be seen as a photoelectrochemical cell constituted by a semiconductor electrode in contact with an electrode of an inert metal (Bard, 1979). In a photoelectrochemical cell, an oxidation or reduction reaction may occur on the semiconductor electrode, whereas in a semiconductor particle immersed in an electrolyte solution, both reactions occur simultaneously by hole transfer from the VB and by electron transfer from the conduction band (see Fig. 1.9).

When the semiconductor is used as powder in suspension, each particle acts as a small photocell, and in 100 mg of powder, consisting for example of 0.1 mm diameter particles, more than 10^{11} independent particles are present, thus making the system very effective.

When aqueous suspensions of semiconductor powders are irradiated with light of suitable energy at the solid–liquid interface, very reactive radical species, generated in the presence of O_2 and H_2O, can induce a great variety of photochemical oxidation reactions that are able to degrade many organic and inorganic molecules. The following scheme shows the events that can occur at the semiconductor–water interface when TiO_2 is used as the photocatalyst:

$$TiO_2 + h\nu \rightarrow TiO_2\left(e^-_{(CB)} + h^+_{(VB)}\right) \tag{1.1}$$

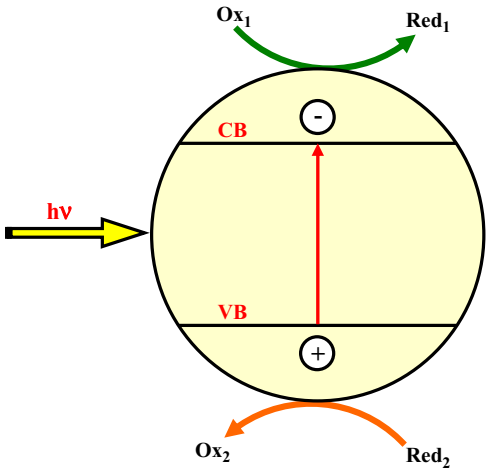

Figure 1.9
Scheme of the photocatalytic process occurring on an illuminated particle in contact with a redox system. The oxidizing agent Ox_1 is generally oxygen, and the reducing one is an organic substrate.

$$OH^- + h^+_{(VB)} \rightarrow {}^{\cdot}OH \tag{1.2}$$

$$O_2 + e^-_{(CB)} \rightarrow {}^{\cdot}O_2^- \tag{1.3}$$

$${}^{\cdot}O_2^- + H^+ \rightarrow HO_2^{\cdot} \tag{1.4}$$

$$2HO_2^{\cdot} \rightarrow O_2 + H_2O_2 \tag{1.5}$$

$$H_2O_2 + {}^{\cdot}O_2^- \rightarrow OH^- + {}^{\cdot}OH + O_2 \tag{1.6}$$

The photocatalytic method allows, also, reduction reactions, in the absence of O_2, which are able to eliminate many inorganic ionic pollutants present in water, reducing them in their elemental form on the surface of the photocatalyst particle:

$$M^{n+}_{(aq)} + ne^-_{(CB)} \rightarrow M_{(surf)} \tag{1.7}$$

or reducing them in less noxious species. For example, the reduction of Cr(VI) to Cr(III) allows the elimination of chromium by means of its subsequent precipitation as hydroxide.

The photoactivity of a semiconductor can be increased by depositing small amounts of noble metals on the particle surface. Indeed, the photooxidation rate of organic compounds is generally limited by the rate of transfer of electrons to oxygen adsorbed on the

semiconductor surface. The more the electrons are available for oxygen reduction, the higher the reaction rate is.

The positive effect of the presence of a noble metal (e.g., Pt) can be explained by comparing a photoelectrochemical cell and a process occurring by irradiating an "n"-type semiconductor particle partially covered with "isles" of Pt (see Fig. 1.10).

The photocatalytic activity of a semiconductor powder is based on the contemporaneous occurrence of oxidation and reduction processes on different zones of the same particle. In the presence of noble metals (such as Pt, Ag, Pd, and Au) physically separated reaction sites, similar to a cell consisting of an "n"-type semiconductor and a platinum counterelectrode for the photogenerated pairs, exist in which oxidation occurs on the semiconductor, whereas reduction on the metallic electrode.

Indeed, the photogenerated electrons are transferred to the metallic isles, whereas the holes remain on the semiconductor, with the consequent decrease of the electron–hole recombination rate and the acceleration of the process kinetics (Panagiotopoulou et al., 2013).

The same beneficial effect can be obtained by partially covering the particle surface with oxides such as RuO_2 or NiO (Domen et al., 1982).

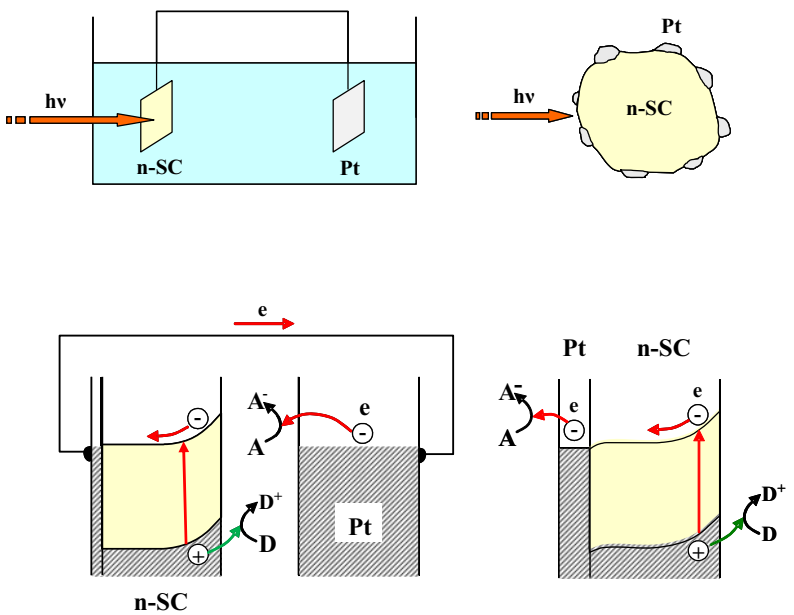

Figure 1.10
Photocatalytic processes in a photoelectrochemical cell and on an irradiated "n"-type semiconductor particle covered with "isles" of platinum.

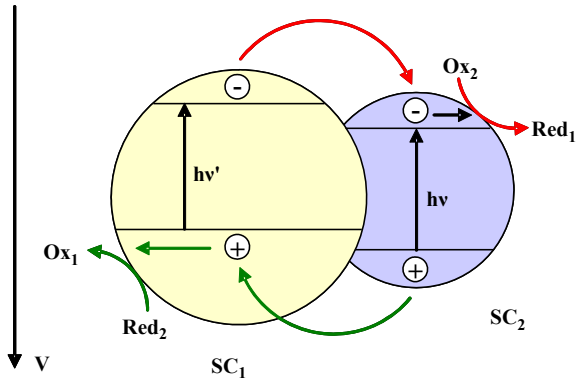

Figure 1.11
Scheme of the charge transfer processes that occur on two different coupled semiconductors.

Another method to realize an efficient electron–hole pair separation is to use mixtures of two different semiconductor powders with suitable energies of VB and CB. Fig. 1.11 shows the scheme of the coupling. Typical mixtures are CdS (SC_1) with TiO_2 (SC_2) (Serpone et al., 1995) or WO_3 (SC_1) with WS_2 (SC_2) (Di Paola et al., 1999).

It can be noticed that the heterojunction between semiconductors with different energies of the valence and conduction bands, such as those shown in Fig. 1.11, allows the transfer of electrons and holes from a semiconductor to the other, improving their separation, thus decreasing the probability of their recombination.

1.3 Visible Light Activity of Modified TiO_2

Titanium dioxide is close to be an ideal photocatalyst, being nontoxic, abundant, chemically stable, and cheap. However, its practical application is limited because it does not absorb visible light so that only the UV part of the solar spectrum (c. 4%) is useful to activate photocatalytic reactions. A shift of the absorption edge of TiO_2 to longer wavelengths is highly desirable as it would increase the solar light conversion efficiency.

Visible light photosensitization may be induced by four different approaches: (1) bulk doping, (2) use of metal–semiconductor composites, (3) coupling of different semiconductors, and (4) surface modification.

Bulk doping consists in the insertion of suitable species into the lattice of the semiconductor. Nitrogen can be easily introduced in the TiO_2 structure, as its atomic size is comparable with that of oxygen. The first report on nitrogen doping dates back to

1986 when Sato (Sato, 1986) discovered the visible light responsiveness of nitrogen-doped TiO_2. Since then, many papers reported TiO_2 modifications starting from plenty of nitrogen-containing compounds (Asahi et al., 2014). In most cases, interstitial or substitutional nitrogen insertion has been obtained (Bellardita et al., 2009), whereas more rarely, as in the case of melamine-modified TiO_2, surface loaded materials have been synthesized (Mitoraj and Kisch, 2008). Bandgap narrowing has been achieved for carbon- (Irie et al., 2003; Sakthivel and Kisch, 2003; Nagaveni et al., 2004), phosphorus- (Han et al., 2001), boron- (Xu et al., 2009), and sulfur-doped TiO_2 (Umebayashi et al., 2002; Ohno et al., 2003). On the other hand, fluorine doping does not result in bandgap narrowing but improves the surface acidity and promotes formation of Ti^{3+} ions, thus increasing photocatalytic activity (Czoska et al., 2008).

Cr, Co, V, and Fe inserted into the TiO_2 lattice mainly by ion implantation extend the spectral response of TiO_2 toward the visible region, also improving photocatalytic activity (Borgarello et al., 1982; Zhu et al., 2006). However, transition metals may also act as recombination centers, and metal islands on the surface of the semiconductor may block the reaction sites (Kang, 2005).

Noble metal deposition generally results in surface modification by creating metal−semiconductor nanocomposites. The presence of Ag, Au, Pt, and Pd islands on the surface of TiO_2 enhances the photocatalytic efficiency under light because the metals act as electron sinks reducing the charge recombination (You et al., 2005; Abd-Elaal et al., 2015; Bellardita et al., 2017). The plasmon resonance of the metal nanoparticles on the surface of TiO_2 is generally responsible for the visible light responsiveness of the materials.

Coupled semiconductors (Qian et al., 2001; Hamrouni et al., 2015) often result in photocatalytic efficiency higher than that obtained in the presence of the single materials. This is generally attributed to heterojunctions between the semiconductors, which improve spatial charge separation. Visible light activity is observed when one of the components is able to absorb in this region or when the electronic interactions between the semiconductors are strong enough to alter the electronic structure of the composite (Tada et al., 2011).

The most commonly used technique of TiO_2 photosensitization is surface modification. Visible light activity may be induced through formation of covalent or ionic bonds between a semiconductor surface and chromophoric molecules (sensitization mechanism) or upon interaction of the semiconductor with molecules that are able to generate chromophoric surface species (charge transfer complex mechanism CTC) (Kisch, 2015). Sensitization of TiO_2 has been achieved by adsorption on its surface of various organic dyes (Guarisco et al., 2014; Ingrosso et al., 2005) and metal complexes,

D (Dai et al., 2009). The mechanism underlying the photoactivity of these materials, known also as photoinduced electron transfer, is summarized in Eqs. (8) and (9).

$$TiO_2 \cdots D + h\nu \rightarrow TiO_2 \cdots D^* \tag{1.8}$$

$$TiO_2 \cdots D^* \rightarrow TiO_2\left(e^-\right) \cdots {}^{\cdot}D^+ \tag{1.9}$$

The species D adsorbed onto the TiO_2 surface absorbs the radiation of suitable energy, and its excited state (D*) injects an electron into the conduction band of the semiconductor.

The CTC mechanism could allow visible light activation of a system in which neither the photocatalyst nor the adsorbate (S) absorbs visible light by itself. The adsorbate could be colorless but becomes colored when adsorbed on TiO_2 (Parrino et al., 2012).

This mechanism is also known as optical electron transfer and could be summarized as in Eqs. (10) and (11).

$$TiO_2 + S \rightleftarrows [TiO_2 - S] \tag{1.10}$$

$$[TiO_2 - S] + h\nu \rightarrow TiO_2\left(e^-\right) - {}^{\cdot}S^+ \tag{1.11}$$

It can be noticed that in both the sensitization and the CTC mechanisms, TiO_2 does not absorb visible light by itself, but the dye and the CT complex, respectively, are the light-absorbing species. In these cases, the process may be defined "indirect semiconductor PC". Notably, in both the mentioned indirect PC mechanisms, only electrons are localized on the semiconductor, while the oxidized substrate plays the role of the hole.

A very simple and inexpensive low-frequency ultrasound method has been used to induce oxygen vacancies formation in TiO_2 powders. The generation of oxygen vacancies by sonication could introduce new procedures for the economical and easy synthesis of photocatalysts active under solar/visible light irradiation (Osorio-Vargas et al., 2012; Bellardita et al., 2017). Indeed, the bulk oxygen deficiency could result in a narrowing bandgap and in visible light absorption.

1.4 Photocatalytic Syntheses Versus Photodegradations

Heterogeneous PC has been mainly applied for environmental purposes. Indeed, the highly oxidizing capability of the hydroxyl radicals thereby generated allows the photodegradation and mineralization of almost all organic compounds. The term mineralization generally refers to the complete degradation of the organic pollutant to water, CO_2, nitrate, phosphate, halide ions, etc. However, the toxicity of the intermediates deriving from the first oxidation steps of mineralization and the by-products may be higher than that of the starting contaminant. Therefore, when

investigating photodegradation of emerging contaminants, it is necessary to deeply study the degradation path and to determine the percentage of the initial substrate converted into small and stable molecules with the highest oxidation state by means of total organic carbon (TOC) analyses.

If one of the reaction products is selectively obtained in appreciable yield, one can speak of photocatalytic synthesis. Oxidative reactions are generally easier to be performed. On the other hand, photocatalytic reductions must be carried out under strict experimental conditions (oxygen absence, presence of a proton source) and are usually less efficient. This is mainly due to two reasons: (1) the conduction band electron has a significantly lower reducing ability with respect to the oxidizing power of the VB hole, (2) few organic substrates efficiently compete with oxygen in trapping photogenerated electrons (Li and Wang, 1993).

Although reactions in water as the solvent are highly desirable, generally photocatalytic syntheses are carried out in harmful organic solvents such as acetonitrile, mainly due to the low solubility of reactants and products in water and to the generally lower selectivity values achieved in aqueous medium. Some reactions have been performed with remarkable selectivity values in water or other green solvents such as dimethyl carbonate (Bellardita et al., 2014a). For instance, the oxidation of alcohols (Palmisano et al., 2007; Yurdakal et al., 2008, 2009; Addamo et al., 2008; Sivaranjani and Gopinath, 2011; Bellardita et al., 2014b; Yurdakal et al., 2013), amines (Li et al., 2013), bioactive molecules such as trans-ferulic acid (Augugliaro et al., 2012), isoeugenol, glycerol (Maurino et al., 2008; Augugliaro et al., 2010a; Minero et al., 2012; Chong et al., 2014), and glucose (Bellardita et al., 2016); selective cyclization of aromatic acids (Ohtani et al., 2003); synthesis of bromine (Parrino et al., 2016) and vitamin B_3 (Alfe et al., 2014; Spasiano et al., 2015; Yurdakal et al., 2017) have been reported.

1.5 Operational Parameters

1.5.1 pH

The pH values of the aqueous reacting media are a key parameter that strongly influences the photocatalytic activity. First, the protonation or deprotonation of the substrates may significantly change their physicochemical behavior in photocatalytic systems. Furthermore, the photocatalyst surface dramatically changes with the pH of the dispersion. In particular, the TiO_2 surface, schematically depicted in Fig. 1.12, presents titanium and oxygen atoms that are not coordinatively saturated giving rise to the so-called surface defects. Water molecules can fill up these sites through dissociative adsorption so that the surface presents a high concentration of OH groups (about 5 OH groups per nm^2) (Beranek, 2011). It is worth to note that although hydroxyl groups are generally

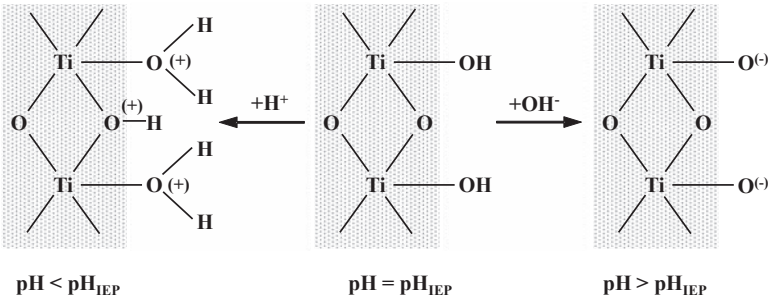

Figure 1.12
Simplified scheme of the protonation and deprotonation of the TiO_2 surface. *Adapted from Beranek, 2011.*

considered as active sites, a higher hydroxylation degree does not necessarily imply higher photocatalytic activity (Di Paola et al., 2014).

The hydroxyl groups may have acid (pKa = 2.9) or basic character (pKa = 12.7), if they are bidentate or monodentate, respectively (Herrmann and Boehm, 1969).

For these reasons the TiO_2 surface can be protonated or deprotonated depending on the pH value of the aqueous suspension (Fig. 1.12).

The pH value at which the net surface charge is zero is called pH_{IEP} (isoelectric point). If $pH > pH_{IEP}$ the surface is negatively charged, whereas if $pH < pH_{IEP}$ positive charges are present on the surface. Such a pH dependence of the surface not only strongly influences the adsorption of charged or polarizable compounds, but it determines the energetic position of the valence and conduction band, and in other words the thermodynamic feasibility of the interfacial electron transfer.

1.5.2 Oxygen Concentration

The presence of oxygen is generally required for the photocatalytic degradation of organic compounds and for photocatalytic oxidative syntheses (Al-Ekabi et al., 1991). Owing to its electrophilic character, oxygen generally plays the role of electron trap, thus reducing electron–hole recombination routes (Ollis et al., 1991). Furthermore, reduction of oxygen gives rise to formation of reactive oxygen species that initiate radical chain oxidative reactions (Eqs. 3–6). However, high oxygen concentrations have been reported to be detrimental and responsible for the decrease of the reaction rate because of the competition with the reacting substrates for the adsorption sites (Braun and Oliveros, 1997). The role of dissolved molecular oxygen has been investigated for the photocatalytic oxidation of 3,4-dichlorophenol (Axelsson and Dunne, 2001). The presence of oxygen

gives rise to hydroxylation of the substrate, whereas partial dechlorination of dichlorophenol mainly occurs in the absence of oxygen.

1.5.3 Temperature Dependence

Temperatures between 293 and 353 K are reported to weakly influence the oxidation rates of photocatalytic reactions (Fox and Dulay, 1993). The apparent activation energy increases at lower temperatures (between 233 and 273 K) while it becomes negative at temperatures higher than 353 K (Herrmann, 1999). In any case, the activation energies reported for photocatalytic reactions are lower (few $kJ \cdot mol^{-1}$) than those measured for thermal reactions. In particular, Matthews (1987) and Okamoto et al. (1985) reported activation energies equal to c. 10 kJ mol^{-1} for the photocatalytic degradation of salicylic acid and phenol.

It has been proposed that hydroxyl radical reactions predominantly contribute to the activation energy of photocatalytic reactions (Elliot and Simsons, 1984). On the other hand, Herrmann (1999) suggested that the desorption of oxidation products may be the rate limiting step influencing the activation energy of photocatalytic reactions (Herrmann et al., 1987).

Kiwi (1985) observed that increasing the temperature improved the interfacial electron transfer due to small changes in the quasi-Fermi level of the semiconductor (ΔV = ca. 0.04 V). Based on these results, it was often reported that minor changes in temperature do not influence the photocatalytic activity. However, recently, it was proposed, on the basis of experimental evidences, that the activation energy, considered as an indirect measure of the temperature dependence of a photocatalytic reaction, is related to the dynamics of water adsorbed on the photocatalyst surface, being the morphological features of the powder and the interactions with the adsorbed molecule-determining factors (Parrino et al., 2017).

1.6 Photocatalytic Reactor Modeling

The main peculiarity that differentiates a photoreactor from a chemical reactor is the presence of photons, which can be considered as an immaterial reagent having the function of generating electron–hole pairs in heterogeneous systems. Then it is important to consider the radiant field in the reaction environment when modeling a photoreactor. The model should take into account the following aspects of the process: (1) the reactive system; (2) the type of reactor and its geometry; (3) the radiation source; (4) the type of photocatalyst. The knowledge of the features previously listed allows to correctly describe the phenomenological processes involved and to obtain the corresponding mathematical relationships. The modeling procedure requires the

application of mass and momentum balances and of the kinetic law. Moreover, it is clear that the activation of the reaction by the absorption of photons makes necessary the knowledge of the rate of photon absorption, which locally cannot be experimentally measured and may significantly change from point to point within a real photocatalytic reactor.

The law of radiant energy transport reflects that it is almost impossible to control the distribution of the photons throughout the reactor. Indeed, the "convection" term, which is present in a mass balance equation, is absent in the radiative transport equation (RTE). Therefore, the photons participating to the reaction as immaterial reagents (consumed by the reaction) cannot be mechanically "mixed" unlike the real reactants. For these reasons, the geometry and the properties of the irradiation system, together with the geometry of the reactor and the optical properties of the reacting system are of fundamental importance to obtain an efficient distribution of the radiation inside the reactor.

The two most important dimensionless parameters for the modeling of a photocatalytic reactor are the albedo, ω, which is a weight of the importance of scattering with respect to light extinction, and the optical thickness, τ, which is a measure of the degree of opacity of the photoreactor (Bandini et al., 1977; Spadoni et al., 1980).

$$\omega = \frac{\sigma^*}{\sigma^* + \kappa^*} \tag{1.12}$$

$$\tau = (\sigma^* + \kappa^*) C_{Cat} \cdot \delta \tag{1.13}$$

where C_{Cat} is the concentration of the photocatalyst, δ is the thickness of the reaction space, and σ^* and κ^* are the specific scattering and absorption coefficients, respectively, averaged over the useful spectrum of the incident radiation. Different laws can be applied for describing the scattering phenomena involved, depending on the particles size. Indeed, in the presence of very small particles ($d_p < .03-.06$ μm for near-UV radiation), elastic scattering, named Rayleigh scattering, takes place. Mie theory for particles of any size, and geometrical optics (specular and diffuse reflectance models) for particles having a relatively large size ($d_p > .5$ μm for near-UV radiation) (Siegel and Howell, 1992) are others examples. In the pertinent literature, it is possible to find experimental methods that are able to determine these optical parameters in particular experimental conditions (Loddo et al., 2006). Both absorption and scattering coefficients of aqueous suspensions of commercial TiO_2 powders irradiated by monochromatic light were determined by measuring the transmitted photon flow as a function of the photocatalyst mass and by applying an asymptotic form of the Kubelka–Munk solution of the radiative transfer equation (RTE). Satuf et al. (2005) report the physical and optical characterization of TiO_2 suspended in water. Experiments were carried out in a specially designed spectrophotometer with conventional cells and with an integrating sphere accessory operating in transmission mode.

The influence of the optical thickness (i.e., photocatalyst load) on the reaction rate depends on the type of solid, on particle size, and on the optical parameters previously described. Generally, by increasing the amount of photocatalyst, the dependence between the observed reaction rate and the concentration of the photocatalyst is linear, then a plateau is reached at a certain photocatalyst concentration and for higher amounts the reaction rate remains practically constant.

The effect of absorption and scattering occurring in the reaction medium (Cassano and Alfano, 2000) is studied by solving the RTE. Then, the obtained radiant field allows to carry out a kinetic analysis to obtain the intrinsic kinetics of photocatalytic reactions (Martin et al., 1999; Arancibia-Bulnes et al., 2002; Alfano et al., 1994). Recently, it has been also shown how with a so-called "photodifferential" reactor it is possible to obtain the intrinsic values of the kinetic parameters and the absorbed radiant power without experimentally measuring this latter and without solving the RTE (G. Camera Roda et al., 2017).

The local values of the volumetric rate of radiant energy absorption (VREA) are also obtained by the solution of the RTE (Cassano et al., 1995):

$$e'''_{\lambda} = \kappa_{\lambda} \int_{4\pi} I_{\lambda,\Omega} d\Omega \tag{1.14}$$

where κ_{λ} is the spectral absorption coefficient, $I_{\lambda,\Omega}$ is the intensity along the Ω direction, $d\Omega$ is the differential solid angle associated with the direction Ω. The volumetric rate of photon absorption (VRPA) for a monochromatic radiation is directly related to the VREA through the Planck's equation.

In most cases a wide spatial and angular variation of the intensity is expected to occur in a slurry photocatalytic reactor because of absorption (which is necessary to activate the reaction), scattering, and geometrical redistribution of the radiant energy.

The intrinsic rate of a photocatalytic reaction depends on the quantum yield and on the absorbed radiation.

Generally speaking, it is possible to write (G. Camera Roda et al., 2017):

$$\widehat{r} = \eta \cdot \widehat{\varphi} \tag{1.15}$$

where $\widehat{r}$ is the reaction rate per unit mass of photocatalyst, $\widehat{\varphi}$ is the specific rate of photon absorption (SRPA) (moles of absorbed photons per unit time and per unit mass of photocatalyst), and η the quantum yield. The SRPA can be written as:

$$\widehat{\varphi}_{\lambda} = \frac{\varphi_{\lambda}}{C_{Cat}} = \dot{e}'''_{\lambda} \frac{\lambda}{h \cdot c \cdot N_{Av}} \cdot \frac{1}{C_{Cat}} \tag{1.16}$$

where h is the Plank constant, c is the speed of light, and N_{Av} is the Avogadro's number.

In general, the primary quantum yield can be defined as the ratio between the number of molecules following the expected path in the primary process (in our case the activation that leads exclusively to chemical reaction) and the number of absorbed quanta of radiation at wavelength λ:

$$\eta_{\lambda} = \frac{\text{number of molecules}_{\text{prim}}}{\text{number of photons at } \lambda \text{ absorb.}} \tag{1.17}$$

In practical applications, a different definition of quantum yield is used, the "overall quantum yield." This is a highly "process-dependent" value, and it is not an intrinsic kinetic property.

It is defined as the ratio between the number of molecules of a given reactant or product finally disappeared or formed and the number of absorbed quanta of photons at wavelength λ:

$$\eta_{\text{overall},\lambda} = \frac{\text{number of molecules reacted}}{\text{number of photons at } \lambda \text{ absorb.}} \tag{1.18}$$

Its evaluation comprises the primary event and all the other secondary reactions that follow thereafter (Cassano et al., 1995).

Consequently, in any kinetic experiment, due to the inhomogeneity of the radiation inside the reactor volume, it is necessary to distinguish between the local values of the parameters (SRPA, reaction rate, quantum yield) and their average values, which possibly an external observer could be able to measure. In particular, the quantum yield determined for irradiation having a discrete range of wavelengths is called "quantum efficiency." The local values cannot be experimentally measured, but they represent the values that, in theory, should be known for the evaluation of the "intrinsic kinetics," that is the rate which takes into account only the events occurring at a molecular level. Therefore, the intrinsic kinetics represents a "law," which is invariant with respect to all the phenomena (e.g., mass and radiant energy transport) taking place on a macroscopic scale in a real reactor. For geometrical simple systems, it is possible to determine experimentally the values of quantum yield (Loddo et al., 2006) and quantum efficiency (Augugliaro et al., 1995).

The above considerations mainly concern slurry systems in which the photocatalyst is dispersed in solution. The use of powders, in particular when their particle size is small (20−100 nm, i.e., high surface to volume ratios), generates a series of problems, such as the possible dispersion in the environment of these solids during the manipulation of the photocatalyst and their problematic separation from the effluent streams (Kagaya et al., 1999; Sopajaree et al., 1999). When the photocatalyst is supported on a solid surface as a film, most of the practical drawbacks can be

avoided, but other problems arise and additional efforts are required in the design of the reactor. Indeed, mass transfer phenomena outside and/or inside the film can limit the obtainable reaction rate (Turchi and Ollis, 1988; Subramanian et al., 2003; Chen and Dionysiou, 2007).

Camera-Roda et al. (Edwards et al., 1996; Camera-Roda and Santarelli, 2007a) studied and supported "thick" photocatalytic film, determining that the extent of the limitations due to internal diffusion of the reactant and transport of the photons can be evaluated by the effectiveness factor of the photocatalytic film, η_F, defined as:

$$\eta_F = \frac{\text{observed reaction rate}}{\text{reaction rate at } C_S = C_{S0} \text{ and } I = I_0},$$

where C_S is the substrate concentration, C_{S0} is the initial substrate concentration; I is the local radiation intensity, and I_0 is the intensity of the radiant energy that enters the film.

They identified the intervening parameters that affect the effectiveness, indicating simple methods to assess the value of the parameters and consequently identify the possible limiting processes, which should be improved. Finally, the determination of the optimal thickness that maximizes the obtainable reaction rate was done.

It was shown (Chen et al., 2001; Herz, 2004; Camera-Roda and Santarelli, 2007a,b) that the observed rate of degradation increases monotonically toward an asymptote if photons and reactants enter the reactor from the same side (SS case), whereas it reaches a maximum at an optimal thickness if the film is illuminated from the opposite side (OS case) the reactants enter the film. Interestingly, at the optimal thickness of the OS case the observed reaction rate is already close to the asymptotic value.

Vezzoli et al. (2013) added mass external transport to internal diffusion to study the effects of their combination on the observed reaction rate for an LH-type kinetics.

1.6.1 Kinetics of Photocatalytic Processes

In 1835, Berzelius coined the term catalysis to describe the influence of certain substances on the nature of diverse reactions, the substances themselves apparently being unchanged by the reaction. One of the fundamental principle of catalysis is that of catalytic cycle, based on the definition proposed by Boudart: "*A catalyst is a substance that transforms reactants into products, through an uninterrupted and repeated cycle of elementary steps in which the catalyst is changed through a sequence of reactive intermediates, until the last step in the cycle regenerates the catalyst in its original form.*"

Heterogeneous PC could be studied by using the same methods used for heterogeneous catalysis and similar problems must be faced.

Indeed, a catalytic reaction is accelerated by the presence of small amounts of a particular substance called catalyst, and a photocatalyst is a "*substance able to produce, by absorption of ultraviolet, visible, or infrared radiation, chemical transformations of the reaction partners, repeatedly coming with them into intermediate chemical interactions and regenerating its chemical composition after each cycle of such interactions*" (Augugliaro et al., 2010b).

When a photocatalyst is exposed to a suitable irradiation, its surface undergoes a series of changes needed for the occurrence of a photoprocess (Bickley, 1985a, 1985b). The interaction of a photon with the solid semiconductor could give rise to an increase of the vibrational state of the lattice, i.e., it generates an excited state of the solid. The adsorption–desorption equilibrium established in the dark is perturbated by irradiation with light of energy greater than that of the bandgap, determining a net photoadsorption or photodesorption of species. A new equilibrium is achieved when the species and the solid acquire the same electrochemical potential (Bickley, 1985a, 1985b).

The absorption of photons by a solid semiconductor is related to the nature of the crystal sites, which can be regular or imperfections can be present as intrinsic and extrinsic lattice defects, resulting in four different types of electronic excitations. Absorption in a perfect lattice can produce only intrinsic photoexcitations with (1) promotion of electrons from the valence band to the conduction band with formation of free electron–hole pairs (electrons and holes separated); (2) formation of free bulk excitons (combination of an electron and a positive hole which are free to move through a nonmetallic crystal as a unit). The presence of defects in the lattice could cause extrinsic absorption of light, in particular (3) photon absorption by defects generating electronically excited defects and bound and/or self-trapped excitons; (4) photon absorption generating ionization of defects (transitions between localized and delocalized electronic states). The scheme of Fig. 1.13 shows the processes above described (Emeline et al., 2001; Ryabchuk, 2004).

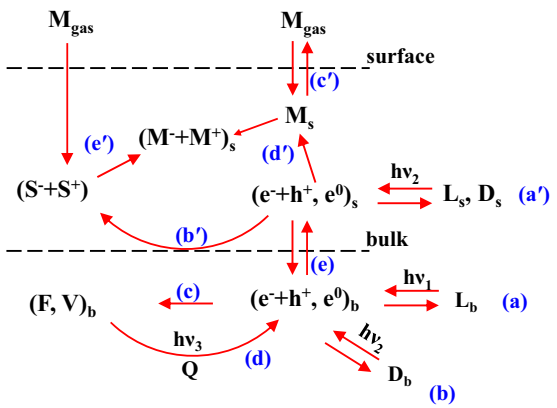

Figure 1.13
Scheme of photoinduced processes occurring in a heterogeneous system containing a wide bandgap semiconductor.

The fundamental absorption of light with energy of the photons higher or equal to that of the bandgap ($h\nu_1 \geq E_G$) allows the intrinsic photoexcitation of the lattice, L_b, (a) with the formation of free electrons (e^-) and holes (h^+) or excitons (e^0) that can recombine (band to band recombination of free charge carriers).

Preexisting bulk defects (D_b) can lead to an extrinsic photoexcitation (b) by light with energy $h\nu_2 < h\nu_1$ with the formation of free electrons and holes. The reverse process is the recombination and exciton decay through defects.

The presence of bulk defects could allow another bulk process that is the trapping of free charge carriers and excitons (c) to form color centers or deep traps (F-type: vacancies occupied by electrons, and V-type; vacancies occupied by holes). Photobleaching ($h\nu_3$) or thermoannealing of color centers (d) leads to generation of free electrons and holes.

As far as the surface processes are concerned, light absorption ($h\nu_2$) by regular, L_s, and irregular, D_s, surface states (a') leads to the formation of free charge carriers and excitons. Their surface recombination is likely accompanied by luminescence, whereas their trapping by surface defects, S, (b') yields surface active centers (S^- and S^+) for adsorption and PC.

Adsorption of molecules in the gas or liquid phase (c') generates adsorption–desorption equilibria on the solid surface. The interaction of adsorbed molecules, M_s, (d') with the surface charge carriers and excitons can promote surface chemical processes by the LH-like mechanism, whereas the interaction of molecules with surface active centers (e') can initiate surface chemical processes by Eley–Rideal mechanism. Finally, the exchange of free charge carriers and excitons between the bulk and the surface can occur by diffusion or drift (e).

In the LH mechanism, both molecules A_g and B_g adsorb on an active site S_s of the photocatalyst, according to Eqs. (19) and (20), respectively (Langmuir, 1918), and undergo a bimolecular reaction (Eq. 21):

$$A_g + S_s \rightleftharpoons AS_{ads.} \tag{1.19}$$

$$B_g + S_s \rightleftharpoons BS_{ads.} \tag{1.20}$$

$$AS_{ads.} + BS_{ads.} \rightarrow \text{Product} \tag{1.21}$$

On the contrary, in the Eley–Rideal mechanism, proposed in 1938 by Rideal and Eley (1950), only one molecule adsorbs while the other one reacts with it directly from the gas phase, without adsorbing:

$$A_g + S_s \rightleftharpoons AS_{ads.} \tag{1.22}$$

$$AS_{ads.} + B_g \rightarrow \text{Product} \tag{1.23}$$

Fig. 1.14 shows the two mechanisms.

The observed kinetics of most of the photocatalytic reactions in liquid–phase is in very good agreement with the LH model used to describe heterogeneous surface reactions (Ollis, 1985; Turchi and Ollis, 1989; Ollis et al., 1989; Matthews, 1987; Hoffmann et al., 1995). Thus, assuming LH kinetics for a general photocatalytic degradation of a species A, an expression for the initial reaction rate, r_A, is:

$$r_A = k_{LH} \cdot \theta_A \cdot \theta_{Ox} \tag{1.24}$$

where k_{LH} is the second-order surface rate constant for the degradation reaction, which depends mainly on the radiation flux, I, and θ_A and θ_{Ox} are the fractional sites coverages by A and O_2 on the surface of the semiconductor particles.

The θ_A and θ_{Ox} terms are related to A and O_2 concentrations in solution by the Langmuir model:

$$\theta_A = \frac{K_A C_A}{1 + K_A C_A} \tag{1.25}$$

$$\theta_{Ox} = \frac{K_{Ox} C_{Ox}}{1 + K_{Ox} C_{Ox}} \tag{1.26}$$

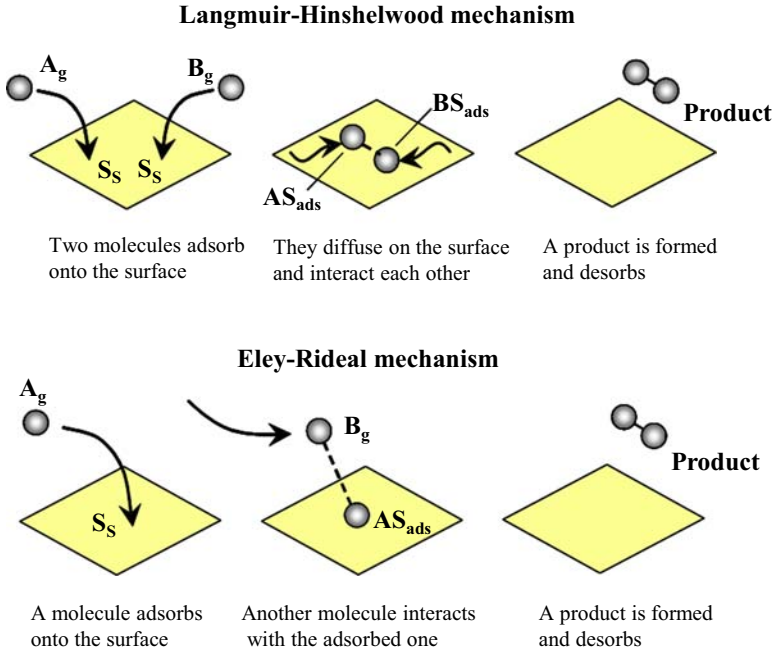

Figure 1.14
Graphic models of Langmuir–Hinshelwood and Eley–Rideal mechanisms.

in which K_A and K_{Ox} are the equilibrium adsorption constants, and C_A and C_{Ox} the concentrations of A and oxygen, respectively.

The LH model states that the adsorption of the species on the photocatalytic surface is a rapid equilibrium process and that the slow rate-controlling surface step involves the presence of both reactants in monolayer at the solid–liquid interface. Eq. (24) can be written as:

$$r_A = k_{LH} \cdot \frac{K_A C_A}{1 + K_A C_A} \cdot \frac{K_{Ox} C_{Ox}}{1 + K_{Ox} C_{Ox}} \tag{1.27}$$

Generally, in well-mixed photocatalytic systems, oxygen or air is continuously bubbled, and dissolved oxygen concentration can be considered constant. Eq. (27), consequently, can be rewritten as:

$$r_A = k'_{LH} \cdot \frac{K_A C_A}{1 + K_A C_A} \tag{1.28}$$

with

$$k'_{LH} = k_{LH} \cdot \frac{K_{Ox} C_{Ox}}{1 + K_{Ox} C_{Ox}} \tag{1.29}$$

Studies in the past years have highlighted that adsorption isotherm and reaction rate may each follow the same analytic form, i.e., a saturation function of the Langmuir adsorption isotherm form and of the LH kinetic rate form, whereas the dark adsorption equilibrium constant K_A is not found to be the same as the apparent adsorption constant. The LH-type kinetic expression for semiconductor PC can be written as:

$$r_A = k'_{LH} \cdot \frac{K'_A C_A}{1 + K'_A C_A} \tag{1.30}$$

where $k'_{LH} = k \cdot I^{\alpha}$ is a proportionality constant (being I the incident irradiance), which varies depending on the test system. The power term, α, is related to I and its values are 1 and 0.5 at low and high values of I, respectively. K′A is the Langmuir apparent adsorption constant that can be experimentally calculated together with k'_{LH} by plotting the reciprocal of the initial reaction rate as a function of the reciprocal of C_A that generally yields a straight line.

Turchi and Ollis (1990) showed that the meaning of the Langmuir adsorption coefficient, K'_A, may vary from one mechanism to another.

Several papers, which studied the influence of the reactant concentration C_A and the light intensity I in the same photocatalyzed reaction, show that both k'_{LH} and the apparent binding constant, K'_A, are influenced by the light intensity (Emeline et al., 2000; Xu and

Langford, 2000; Davydov and Smirniotis, 2000). In particular, the derived adsorption constant decreases with increasing the light intensity, while the rate constant increases (Xu and Langford, 2000). As the adsorption equilibrium dark constant, K_A, is the ratio between the adsorption rate constant and the desorption rate constant (in the dark), it must be independent of the light intensity.

The dependence of the adsorption constant on light irradiance can be easily obtained by taking into account the following steps (Emeline et al., 2005).

$$S + h\nu \rightarrow S^* \tag{1.31}$$

$$S^* \rightarrow S \tag{1.32}$$

$$S^* + M \rightarrow \text{Product} \tag{1.33}$$

The photoinduced deactivation of the excited state of surface site, S*, is represented by the following equation:

$$S^* + h\nu \rightarrow S \tag{1.34}$$

Others steps to be considered are the trapping of free charge carriers by the surface defects (see Fig. 1.13b′):

$$S + e^-\left(h^+\right) \rightarrow S^-\left(S^+\right) \tag{1.35}$$

$$S^-\left(S^+\right) + h^+\left(e^-\right) \rightarrow S \tag{1.36}$$

Ollis (2005) recommends the steady-state approach for the coverage of reactant molecules, as in heterogeneous PC, the fast adsorption/desorption equilibria may not be established during the photoreaction. By considering the mechanism described by reactions 31−34, the reaction may either be Eley−Rideal type (Eq. 37) if M are molecules in the liquid or gas phase, or LH type if M is an adsorbed molecule.

$$r_A = \frac{k_1 k_2 I^{\alpha} C_A}{1 + k_2 C_A} \tag{1.37}$$

In Eq. (37), k_1, k_2, and α are fitting constants.

Different equations have been developed by modifying the LH model as the disrupted adsorption models (Eq. 38, k_1, k_2, k_3, and α fitting constants)

$$r_A = \frac{k_1 I^{\alpha} C_A}{1 + k_2 I^{\alpha} + k_3 C_A} \tag{1.38}$$

or others based on the direct and/or indirect transfer mechanism with various parameters (Mills and O'Rourke, 2015).

Among the kinetic models developed by Minero et al. (Minero, 1995, 1999; Minero et al., 2013), an interesting approach was adopted (Minero et al., 2013), which developed an equation which explicitly takes into account the effect of most of the widely accepted intervening variables (rate of photon absorption, concentration of substrate, oxygen, and photocatalyst) with only one kinetic parameter (see Eq. 39).

$$r_A = k\left(\sqrt{1 + 2\frac{\varphi/C_{cat}}{kC_{Ox}\,C_A}} - 1\right)\cdot C_{Ox}\,C_{cat}\,C_A \tag{1.39}$$

where k is a kinetic constant; φ is the (local) VRPA; and C_{Ox}, C_{cat}, C_A are the oxygen, photocatalyst, and substrate concentrations, respectively.

The reaction can be rewritten in a form in which the dependence on the photocatalyst concentration disappears if the specific absorption coefficient is constant (Camera-Roda et al., 2017).

$$\hat{r}_A = \eta\cdot\hat{\varphi} = k\cdot C_{Ox}C_A\left(\sqrt{1 + \hat{\varphi}\cdot\frac{2}{k\cdot C_{Ox}C_A}} - 1\right) \tag{1.40}$$

where $\hat{r}_A$ is the reaction rate per unit of photocatalyst mass, $\hat{\varphi}$ is the SRPA (i.e., the moles of absorbed photons per unit time per unit mass of photocatalyst), η is the quantum yield.

The number of kinetic parameters is an important characteristic of the rate law. A lower number is appreciable because it avoids overfitting, but concurrently the law should be able to reproduce satisfactorily all the essential features of the reaction.

In PC, the activation of the reaction occurs by photon absorption, thus it is necessary to have knowledge of the value of the rate of photon absorption, which locally cannot be measured and may vary very much from point to point inside a real photocatalytic reactor.

Indeed, the photons participate to the reaction as reagents (albeit immaterial reagents) consumed by the reaction (Camera-Roda et al., 2005). The mole (Einstein) is the unit to measure the number of photons, and the first step of a photocatalytic event is often expressed by Eq. (1).

The aforementioned considerations indicate that the assessment of the rate law of slurry photocatalytic reactions is a hard task, as the average rate of reaction, which is experimentally determined, could be very different from the "true" (intrinsic) rate of reaction, which cannot be measured directly.

The paper by Camera Roda et al. (2005) shows how a proper mathematical model allows the utilization of the differential and/or the integral methods of kinetic analysis. Moreover, this study gives a survey of the difficulties encountered in the assessment of

the rate law of a photocatalytic slurry reaction and to identify some guidelines to solve these problems.

1.6.2 Coupling Photocatalysis With Other Advanced Oxidation Processes

One of the main limiting processes in TiO_2 PC carried out in liquid phase is the recombination of electrons (e^-) and holes (h^+) (Dionysiou et al., 2004). These photogenerated pairs may reach the surface and generate primary oxidant species (i.e., superoxide radical anion and hydroxyl radical, respectively), but most of them recombine in the bulk or at the surface of the photocatalyst. Recombination is detrimental for the photocatalytic process and the photon energy is lost as heat. For this reason, the quantum yields (i.e., number of primary chemical reactions per photon absorbed) of photocatalytic processes are low (Hoffmann et al., 1995). Over the past 10 years, research has focused on reducing the effect of charges recombination or enhancing PC performances by applying different techniques including electrochemical methods (Yu et al., 1997), surface modification of TiO_2 (Makarova et al., 2000), and adding an external electron acceptor such as hydrogen peroxide, peroxydisulfate ions, or ozone.

1.6.3 TiO_2/H_2O_2 Photocatalysis

The enhancement of the photocatalytic activity by using hydrogen peroxide is due to the fact that it is a better electron acceptor than oxygen (potential for oxygen reduction $= -0.13$ V; potential for H_2O_2 reduction $= 0.72$ V) (Dionysiou et al., 2004). It has been reported that trapping of photogenerated electrons in the conduction band by oxygen reduction represents the rate-controlling step in the mechanism (Gerischer and Heller, 1991). Accordingly, conditions that promote the removal of conduction band electrons, such as enhanced oxygen concentrations (Dionysiou et al., 2002) and addition of other efficient electron acceptors as H_2O_2, could have a positive effect on the photocatalytic process.

Moreover, the addition of hydrogen peroxide can enhance the rate of generation of hydroxyl radicals. This can be the consequence of different mechanisms. One is the generation of hydroxyl radicals by direct photolysis of hydrogen peroxide to form hydroxyl radicals. Indeed, radiation of wavelength lower than 300 nm has sufficient energy to generate the photocleavage of the H_2O_2 molecule. Another pathway is the reaction of hydrogen peroxide with superoxide radical and, moreover, hydrogen peroxide could react with photogenerated intermediates. Hydrogen peroxide can also be beneficial in situations where there is limited availability of oxygen.

The following reactions, along with those expressed by Eqs. (1)–(6), may occur in the presence of hydrogen peroxide and irradiated TiO_2 (Dionysiou et al., 2004 and references therein):

$$H_2O_2 + h\nu \rightarrow 2\ {}^{\cdot}OH \tag{1.41}$$

$$H_2O_{(ads)} + h^+ \rightarrow {}^{\cdot}OH + H^+ \tag{1.42}$$

$${}^{\cdot}O_2^- + HO_2^{\cdot} \rightarrow HO_2^- + O_2 \tag{1.43}$$

$$HO_2^- + H^+ \rightarrow H_2O_2 \tag{1.44}$$

$$H_2O_{2(ads)} + e^- \rightarrow {}^{\cdot}OH + OH^- \tag{1.45}$$

$$H_2O_{2(ads)} + 2h^+ \rightarrow O_2 + 2H^+ \tag{1.46}$$

$$H_2O_{2(ads)} + 2H^+ + 2e^- \rightarrow 2H_2O \tag{1.47}$$

$$H_2O_{2(ads)} + h^+ \rightarrow HO_2^{\cdot} + H^+ \tag{1.48}$$

$$O_{2(ads)} + 2e^- + 2H^+ \rightarrow H_2O_{2(ads)} \tag{1.49}$$

$${}^{\cdot}O_2^- + H^+ \rightleftharpoons HO_2^{\cdot} \tag{1.50}$$

$${}^{\cdot}O_2^- + h_{tr}^+ \rightarrow O_2 \tag{1.51}$$

$$H_2O_2 + {}^{\cdot}OH \rightarrow H_2O + HO_2^{\cdot} \tag{1.52}$$

$$HO_2^{\cdot} + {}^{\cdot}OH \rightarrow H_2O_2 + \tfrac{1}{2}\ O_2 \tag{1.53}$$

$$^{\cdot}OH + {}^{\cdot}OH \rightarrow H_2O_2 \tag{1.54}$$

$$HO_2^{\cdot} + H_2O_2 \rightarrow {}^{\cdot}OH + H_2O + O_2 \tag{1.55}$$

Notably, e^- and h^+ refer to conduction band electron and VB hole, respectively, generated during the photoexcitation process (Eq. 1). On the other hand, $h_{tr}{}^+$ (Eq. 51) refers to a trapped hole with redox potential equal to 1.5 V (Hirakawa and Nosaka, 2002).

In the presence of hydrogen peroxide, additional $^{\cdot}OH$ radicals could be produced through the reaction between H_2O_2 and $^{\cdot}O_2^-$ or e^- (Eqs. 6 and 45, respectively).

However, an excess of H_2O_2 would trap $^{\cdot}OH$ radicals to form the weaker oxidant $HO_2^{\cdot}$ radicals (Eq. 52).

An increase of dissolved oxygen could be obtained also through decomposition of hydrogen peroxide.

$$2H_2O_2 \rightarrow 2H_2O + O_2 \tag{1.56}$$

1.6.4 $TiO_2/S_2O_8^{2-}$ Photocatalysis

Another way to overcome the recombination of electron–hole pairs is to add other (irreversible) electron acceptors to the reaction mixture. Peroxydisulfate ion is a very effective electron trap as its one-electron reduction potential is 1.1 V ($S_2O_8^{2-}/SO_4^{\bullet -}$).

This oxidant is normally available as a salt associated with ammonium, sodium, or potassium. It has been reported that potassium peroxydisulfate is effective for degrading organics in hazardous wastewater in acidic or basic media through direct chemical oxidation (McCallum et al., 2000). Because $S_2O_8^{2-}$ reacts slowly with many organics, it is generally activated via photochemical, thermal, radiolytic, or redox decomposition to generate the stronger oxidant sulfate radical ($SO_4^{\bullet -}$) (Zhao et al., 2010). In the presence of irradiated TiO_2, these radicals, with redox potential of 2.6 V, together with generated $^{\bullet}OH$ radicals are responsible for the degradation of organic pollutants in solution. The formation of these strong oxidizing radicals occurs according to the following reactions:

$$S_2O_8^{2-} + e^- \rightarrow SO_4^{2-} + SO_4^{-}\cdot \tag{1.57}$$

$$SO_4^{\cdot -} + H_2O \rightarrow SO_4^{2-} + {}^{\cdot}OH + H^+ \tag{1.58}$$

$$SO_4^{\cdot-} + OH^- \rightarrow {}^{\cdot}OH + SO_4^{2-} \tag{1.59}$$

If the system is irradiated with light having a wavelength lower than 310 nm, the peroxydisulfate ion can be excited generating oxidizing radicals by the following reactions (Saien et al., 2011):

$$S_2O_8^{2-} + h\nu \rightarrow 2SO_4^{\cdot-} \tag{1.60}$$

In some cases found in literature (Hegedűs et al., 2015), the addition of persulfate apparently hinders the photocatalytic process. This phenomenon may be attributed to the occupation of the TiO_2 surface active sites by persulfate or sulfate ions.

1.6.5 TiO_2/O_3 Photocatalysis

Oxidation processes based on ozonation have received much attention. The use of ozone in combination with heterogeneous PC has been studied in liquid phase (Addamo et al., 2005 and references therein). In all cases a significant improvement of oxidation process performance has been reported. A likely explanation of the onset of this effect is that ozone is able to generate $^{\bullet}OH$ radicals on the TiO_2 surface by means of the formation of $O_3^{\bullet-}$ ozonide radicals. The production of $HO^{\bullet}$ radicals on the irradiated surface of the photocatalyst would be more effective in the presence of ozone than oxygen.

Indeed, it is well known (Oyama, 2000) that ozone reacts in water solution with organic or inorganic compounds by following two pathways, the direct selective reaction with specific functional groups (double bonds, nucleophilic positions) and the reaction through free radicals generated from ozone decomposition. Hoigne and Bader (1983) investigated the ozonation of oxalic acid at pHs ranging from 2 to 8 and concluded that the direct reaction of ozone with oxalate anion can be considered negligible. On this basis, it may be assumed that the oxidation of organic species in homogeneous systems is due to the attack by free radicals generated by O_3 decomposition. It is known that O_3 molecules react with hydroxyl ions at alkaline pHs eventually producing the strong oxidant hydroxyl radicals:

$$O_3 + OH^- \rightarrow {}^{\cdot}O_2^- + HO_2^{\cdot} \tag{1.61}$$

$$O_3 + HO_2^{\cdot} \rightarrow 2O_2 + {}^{\cdot}OH \tag{1.62}$$

or alternatively:

$$2HO_2^{\cdot} \rightarrow O_2 + H_2O_2 \tag{1.63}$$

$$H_2O_2 + {}^{\cdot}O_2^- \rightarrow OH^- + {}^{\cdot}OH + O_2 \tag{1.64}$$

In the presence of TiO_2 and irradiation, ozone acts as a very strong electrophilic species forming $O_3^{\bullet-}$ ozonide radicals that lead to hydroxyl radicals:

$$O_{3(ads)} + e^- \rightarrow {}^{\cdot}O_3^- \tag{1.65}$$

$${}^{\cdot}O_3^- + H_2O \rightarrow {}^{\cdot}OH + OH^- + O_2 \tag{1.66}$$

Notably, the above reported mechanism gives rise to formation of a hydroxyl radical per each trapped electron, whereas three electrons are needed for generation of a hydroxyl radical when O_2 acts as the electron trap (Parrino et al., 2015).

Coupling different AOPs could lead to a certain level of synergy between the methods. Determination of the optimum condition to obtain the maximum synergy, i.e., a "process intensification" (Stankiewicz and Moulijn, 2000), is possible by evaluating the "intensification factor," E_i, of the integrated process (Camera-Roda and Santarelli, 2007b). E_i is defined as the ratio between the oxidation rate of the integrated process and the sum of the rates of the photocatalytic process and the homogenous ones in the presence of other oxidants:

$$E_i = \frac{\text{oxidation rate in integrated process}}{\text{oxidation rate in PC} \quad + \quad \text{oxidation rate in AOP}} \tag{1.67}$$

The higher the value of E_i, the more important the synergetic effect is. Of course, E_i depends on the experimental conditions. Indeed, when a synergy holds between two processes that contribute to accomplish the same task (in this case the oxidation of organic compounds), it is expected that the extent of the synergy depends primarily on the ratio, δ, between the rates of the two processes carried out individually under the same experimental conditions.

1.7 Conclusions and Future Trends

This chapter describes the fundamentals of heterogeneous PC focusing on the influence both of the physicochemical and photoelectronic behavior of the photocatalysts and of

the operative parameters such as pH, temperature, irradiation power, oxygen, and substrate concentrations. Furthermore, the LH-type kinetic equation, often used to describe the kinetics of heterogeneous photocatalytic reactions, has been discussed along with its modifications. In particular, it has been recognized that kinetic models of heterogeneous photocatalytic reactions are simply a manifestation of saturation type kinetics. Methods for photoreactor modeling have been described, and studies for their simplifications cited. Finally, the coupling of PC with other AOPs using H_2O_2, O_3, and peroxydisulfate has been discussed. Coupling different technologies results in a real intensification of the global efficiency only for specific ratios of the rates of the single processes. The presented results point out that a precise evaluation of the efficiency of a process is a challenging but necessary task to be approached to allow real applications of the AOPs.

The world's energy consumption is continuously rising because of the global rise in population and standards of living. Therefore energy generation capacity will continue to increase in the future. Solar energy, as a renewable and abundant supply, can become a possible sustainable solution to the increasing energy demand of the world.

To effectively capture and utilize solar energy, the following issues need to be addressed. The first issue is the low density of solar radiation per unit of earth surface (c. 0.4−1 kW m^{-2}). Therefore, providing energy via an established technology such as photovoltaic−thermal systems would require large nonshaded areas occupied with expensive systems. The second issue concerns the intermittent and fluctuant nature of solar radiation. Then, the solar energy must be converted in a form of energy that can be stored so that a continuous (24 h) energy demand can be satisfied. Hydrogen, as an energy carrier, could be a potential promising candidate to address these issues.

Over the past decades, substantial progress has been accomplished on semiconductor-based photocatalytic H_2 generation by means of water splitting. Indeed, overall water splitting is an important reaction that offers an ideal method for supplying hydrogen as a clean and renewable energy carrier.

Although TiO_2-based materials are the most studied ones for photocatalytic applications, they are only responsive to ultraviolet light that represents not more than 4% of the solar spectrum. The bandgap value of TiO_2 (3.2 eV), indeed, greatly restricts the practical application of this oxide. Therefore, it is still an urgent challenge to explore novel photocatalytic materials with visible light response, which can directly harvest energy with a satisfactory yield from solar light and produce H_2, offering a desirable way to solve energy and environmental issues.

Additional interesting studies could be the transformation of organic waste species in fine chemicals through selective oxidation or reduction reactions. The development of

techniques able to prepare photocatalysts with suitable characteristics to increase the selectivity toward product(s) of interest is welcome. One way to increase the efficiency of the photocatalytic systems is to couple photoreactor with a membrane separation device. However, research in the field of PMRs for synthetic purposes may be still defined at a nascent level, being PMRs mainly used for environmental remediation. Notably, interdisciplinary competences and scientific collaborations are required, and some engineering issues should be deeply approached to prove the applicative viability of PMRs for the synthesis of valuable products.

List of Acronyms and Symbols

A Electron acceptor
A_g, B_g Molecules in the gas phase
AOP Advanced oxidation process
C_A Concentrations of A in the solution
CB Conduction band
c Speed of light
C_{Ox} Oxygen concentration in the solution
C_S Substrate concentration
C_{S0} Initial substrate concentration
D Electrons donor
D_b Bulk defects
D_s Irregular surface states
$e^-_{(CB)}$ Electron in the conduction band
E Energy
e^0 Exciton
E_C Energy of CB
$E_{F,redox}$ Fermi level of the redox couple
E_F Fermi level energy
E_G Energy bandgap
E_V Energy of VB
F Vacancies occupied by electrons
$\hat{\varphi}$ Specific rate of photon absorption, i.e., the moles of absorbed photons per unit time per unit mass of photocatalyst
h Planck constant
$h^+_{(VB)}$ Hole in the valence band
hν Energy of the photon
I Radiation flux
I_0 Incident radiation flux
k Surface rate constant
k_1, k_2, α Fitting constants
K_A Adsorption equilibrium constant
k_{LH} Surface rate constant obtained by the Langmuir–Hinshelwood model
K_{Ox} O_2 equilibrium adsorption constant
L_b Lattice
LH Langmuir–Hinshelwood model
L_s Regular surface states
M Molecule

M^- Reduced adsorbed molecule
M^+ Oxidized adsorbed molecule
M_s Adsorbed molecule
NHE Normal hydrogen electrode
η Quantum yield
η_F Effectiveness factor
n-SC n-type semiconductor
Ox Oxidized species
PC Photocatalysis
PMR Photocatalytic membrane reactor
r Initial reaction rate
r_A Initial reaction rate related to A species
$\hat{r}_A$ Reaction rate per unit of photocatalyst mass
Red Reduced species
S* Excited state of surface site
S^- Negative surface active centers
S Surface site
S^+ Positive surface active centers
SC Semiconductor
UV Ultraviolet
V Vacancies occupied by holes
VB Valence band
δ Ratio between the rates of the two processes carried out individually under the same operating conditions
θ_A Fractional sites coverages by the species A on the surface of the semiconductor particles
θ_{Ox} Fractional sites coverages by O_2 on the surface of the semiconductor particles
ν Frequency
φ Local volumetric rate of photon absorption

References

Abd-Elaal, A., Parrino, F., Ciriminna, R., Loddo, V., Palmisano, L., Pagliaro, M., 2015. Alcohol selective oxidation in water under mild conditions via a novel approach to hybrid composite photocatalysts. ChemistryOpen 4, 779–785.

Addamo, M., Augugliaro, V., Bellardita, M., Di Paola, A., Loddo, V., Palmisano, G., Palmisano, L., Yurdakal, S., 2008. Environmentally friendly photocatalytic oxidation of aromatic alcohol to aldehyde in aqueous suspension of brookite TiO_2. Catal. Lett. 126, 58–62.

Addamo, M., Augugliaro, V., García-López, E., Loddo, V., Marcì, G., Palmisano, L., 2005. Oxidation of oxalate ion in aqueous suspensions of TiO_2 by photocatalysis and ozonation. Catal. Today 107–108, 612–618.

Al-Ekabi, H., Safarzadeh-Amiri, A., Sifton, W., Story, J., 1991. Advanced technology for water purification by heterogeneous photocatalysis. Int. J. Environ. Pollut. 1, 125–136.

Alfano, O.M., Cabrera, M.I., Cassano, A.E., 1994. Modeling of light scattering in photochemical reactors. Chem. Eng. Sci. 49, 5327–5346.

Alfe, M., Spasiano, D., Gargiulo, V., Vitiello, G., Di Capua, R., Marotta, R., 2014. TiO_2/graphene-like photocatalysts for selective oxidation of 3-pyridine-methanol to vitamin B_3 under UV/solar simulated radiation in aqueous solution at room conditions: the effect of morphology on catalyst performances. Appl. Catal. A 487, 91–99.

Anderson, J.A., 2012. Simultaneous photocatalytic degradation of nitrate and oxalic acid over gold promoted titania. Catal. Today 181, 171–176.

Andriantsiferana, C., Mohamed, E.F., Delmas, H., 2015. Sequential adsorption-photocatalytic oxidation process for wastewater treatment using a composite material TiO_2/activated carbon. Environ. Eng. Res. 20, 181−189.

Arancibia-Bulnes, C.A., Bandala, E.R., Estrada, C.A., 2002. Radiation absorption and rate constants for carbaryl photocatalytic degradation in a solar collector. Catal. Today 76, 149−159.

Asahi, R., Morikawa, T., Irie, H., Ohwaki, T., 2014. Nitrogen-doped titanium dioxide as visible-light-sensitive photocatalyst: designs, developments, and prospects. Chem. Rev. 114, 9824−9852.

Augugliaro, V., Camera Roda, G., Loddo, V., Palmisano, G., Palmisano, L., Parrino, F., Puma, M.A., 2012. Synthesis of vanillin in water by TiO_2 photocatalysis. Appl. Catal. B Environ. 111−112, 555−561.

Augugliaro, V., Bianco Prevot, A., Cáceres Vázquez, J., García-López, E., Loddo, V., Malato-Rodríguez, S., Marcì, G., Palmisano, L., Pramauro, E., 2004. Photocatalytic oxidation of acetonitrile in aqueous suspension of titanium dioxide irradiated by sunlight. Adv. Environ. Res. 8, 329−335.

Augugliaro, V., Bianco Prevot, A., Cáceres Vázquez, J., García-López, E., Loddo, V., López-Muñoz, M.J., Malato-Rodríguez, S., Marcì, G., Palmisano, L., Schiavello, M., Soria-Ruiz, J., 1999a. Photocatalytic oxidation of cyanide in aqueous TiO_2 suspensions irradiated by sunlight in mild and strong oxidant conditions. Catal. Today 54, 245−253.

Augugliaro, V., Coluccia, S., Loddo, V., Marchese, L., Martra, G., Palmisano, L., Schiavello, M., 1999b. Photocatalytic oxidation of gaseous toluene on anatase TiO_2 catalyst: mechanistic aspects and FTIR investigation. Appl. Catal. B 20, 15−27.

Augugliaro, V., El Nazer, H.H., Loddo, V., Mele, A., Palmisano, G., Palmisano, L., Yurdakal, S., 2010a. Photocatalytic oxidation of glycerol in TiO_2 water suspensions. Catal. Today 151, 21−28.

Augugliaro, V., Loddo, V., Marcì, G., Palmisano, L., López-Muñoz, M.J., 1997. Photocatalytic oxidation of cyanides in aqueous titanium dioxide suspensions. J. Catal. 166, 272−283.

Augugliaro, V., Loddo, V., Pagliaro, M., Palmisano, G., Palmisano, L. (Eds.), 2010b. Clean by Light Irradiation: Practical Applications of Supported TiO_2. RSC Publishing, Cambridge.

Augugliaro, V., Loddo, V., Palmisano, L., Schiavello, M., 1995. Performance of heterogeneous photocatalytic systems: influence of operational variables on photoactivity of aqueous suspensions of TiO_2. J. Catal. 153, 32−40.

Axelsson, A.K., Dunne, L.J., 2001. Mechanism of photocatalytic oxidation of 3, 4-dichlorophenol on TiO_2 semiconductor surfaces. J. Photochem. Photobiol. A 144, 205−213.

Bandini, E., Stramigioli, C., Santarelli, F., 1977. A rigorous approach to photochemicals reactors,. Chem. Eng. Sci. 32, 89−96.

Bard, A.J., 1979. Photoelectrochemistry and heterogeneous photo-catalysis at semiconductors. J. Photochem. 10, 59−75.

Bellardita, M., Addamo, M., Di Paola, A., Palmisano, L., Venezia, A.M., 2009. Preparation of N-doped TiO_2: characterization and photocatalytic performance under UV and visible light. Phys. Chem. Chem. Phys. 11, 4084−4093.

Bellardita, M., Augugliaro, V., Loddo, V., Megna, B., Palmisano, G., Palmisano, L., Puma, M.A., 2012. Selective oxidation of phenol and benzoic acid in water via home-prepared TiO_2 photocatalysts: distribution of hydroxylation products. Appl. Catal. A 441−442, 79−89.

Bellardita, M., Di Paola, A., García-López, E., Loddo, V., Marcì, G., Palmisano, L., 2013. Photocatalytic CO_2 reduction in gas-solid regime in the presence of bare, SiO_2 supported or Cu-loaded TiO_2 samples. Cur. Org. Chem. 17, 2440−2448.

Bellardita, M., El Nazer, H.A., Loddo, V., Parrino, F., Venezia, A.M., Palmisano, L., 2017. Photoactivity under visible light of metal loaded TiO_2 catalysts prepared by low frequency ultrasound treatment. Catal. Today 284, 92−99.

Bellardita, M., Loddo, V., Mele, A., Panzeri, W., Parrino, F., Pibiri, I., Palmisano, L., 2014a. Photocatalysis in dimethyl carbonate green solvent: degradation and partial oxidation of phenanthrene on supported TiO_2. RSC Adv. 4, 40859−40864.

Bellardita, M., Loddo, V., Palmisano, G., Pibiri, I., Palmisano, L., Augugliaro, V., 2014b. Photocatalytic green synthesis of piperonal in aqueous TiO_2 suspension. Appl. Catal. B 144, 607–613.

Bellardita, M., García-López, E., Marcì, G., Palmisano, L., 2016. Photocatalytic formation of H_2 and value-added chemicals in aqueous glucose (Pt)-TiO_2 suspension. Int. J. Hydrogen Energ. 41, 5934–5947.

Beranek, 2011. (Photo)electrochemical methods for the determination of the band edge positions of TiO_2-based nanomaterials. Advanc. Phys. Chem. Article ID 786759.

Bickley, R.I., 1985a. Photoelectrochemistry. In: Schiavello, M. (Ed.), Photocatalysis and Photoreactors, Fundamentals and Developments. Reidel, Dordrecht, pp. 379–388.

Bickley, R.I., 1985b. In: Schiavello, M. (Ed.), Photoelectrochemistry, Photocatalysis and Photoreactors, Fundamentals and Developments. Reidel, Dordrecht, pp. 491–502.

Borgarello, E., Kiwi, J., Gratzel, M., Pelizzetti, E., Visca, M., 1982. Visible light induced water cleavage in colloidal solutions of chromium-doped titanium dioxide particles. J. Am. Chem. Soc. 104, 2996–3002.

Braslavsky, S.E., Braun, A.M., Cassano, A.E., Emeline, A.V., Litter, M.I., Palmisano, L., Parmon, V.N., Serpone, N., 2011. Glossary of terms used in photocatalysis and radiation catalysis (IUPAC Recommendations 2011). Pure Appl. Chem. 83, 931–1014.

Braun, A.M., Oliveros, E., 1997. How to evaluate photochemical methods for water treatment. Water Sci. Technol. 35, 17–23.

Camera Roda, G., Augugliaro, V., Cardillo, A., Loddo, V., Palmisano, G., Palmisano, L., 2013. A pervaporation photocatalytic reactor for the green synthesis of vanillin,. Chem. Eng. J. 224, 136–143.

Camera Roda, G., Santarelli, F., Augugliaro, V., Loddo, V., Palmisano, G., Palmisano, L., Yurdakal, S., 2011. Photocatalytic process intensification by coupling with pervaporation. Catal. Today 161, 209–213.

Camera-Roda, G., Loddo, V., Palmisano, L., Parrino, F., 2017. Guidelines for the assessment of the rate law of slurry photocatalytic reactions. Catal. Today 281, 221–230.

Camera-Roda, G., Santarelli, F., 2007a. Optimization of the thickness of a photocatalytic film on the basis of the effectiveness factor. Catal. Today 129, 161–168.

Camera-Roda, G., Santarelli, F., 2007b. Intensification of water detoxification by integrating photocatalysis and pervaporation. J. Sol. Energy Eng. 129, 68–73.

Camera-Roda, G., Santarelli, F., Martin, C.A., 2005. Design of photocatalytic reactors made easy by considering the photons as immaterial reactants. Sol. Energy 79, 343–352.

Cassano, A.E., Alfano, O.M., 2000. Reaction engineering of suspended solid heterogeneous photocatalytic reactors. Catal. Today 58, 167–197.

Cassano, A.E., Martin, C.A., Brandi, R.J., Alfano, O.M., 1995. Photoreactor analysis and design: fundamentals and applications. Ind. Eng. Chem. Res. 34, 2155–2201.

Chen, D., Li, F., Ray, A.K., 2001. External and internal mass transfer effect on photocatalytic degradation. Catal. Today 66, 475–485.

Chen, D., Ray, A.K., 2001. Removal of toxic metal ions from wastewater by semiconductor photocatalysis. Chem. Eng. Sci. 56, 1561–1570.

Chen, Y., Dionysiou, D.D., 2007. A comparative study on physicochemical properties and photocatalytic behavior of macroporous TiO_2-P25 composite films and macroporous TiO_2 films coated on stainless steel substrate. Appl. Catal. A Gen. 317, 129–137.

Chong, R., Li, J., Zhou, X., Ma, Y., Yang, J., Huang, L., Han, H., Zhang, F., Li, C., 2014. Selective photocatalytic conversion of glycerol to hydroxyacetaldehyde in aqueous solution on facet tuned TiO_2-based catalysts. Chem. Commun. 50, 165–167.

Czoska, A.M., Livraghi, S., Chiesa, M., Giamello, E., Agnoli, S., Granozzi, G., Finazzi, E., Di Valentin, C., Pacchioni, G., 2008. The nature of defects in fluorine-doped TiO_2. J. Phys. Chem. C 112, 8951–8956.

Dai, Z., Burgeth, G., Parrino, F., Kisch, H., 2009. Visible light photocatalysis by a Titania–Rhodium(III) complex. J. Organomet. Chem. 694, 1049–1054.

Davydov, L., Smirniotis, P., 2000. Quantification of the primary processes in aqueous heterogeneous photocatalysis using single-stage oxidation reactions. J. Catal. 191, 105–115.

Dekker, A.J., 1957. Solid State Physics. Prentice-Hall, Englewood Cliffs, N.J.

Dhatshanamurthi, P., Subash, B., Shanthi, M., 2015. Investigation on UV-A light photocatalytic degradation of an azo dye in the presence of CdO/TiO_2 coupled semiconductor. Mater. Sci. Semicond. Process. 35, 22−29.

Di Paola, A., Bellardita, M., Palmisano, L., Barbieriková, Z., Brezová, V., 2014. Influence of crystallinity and OH surface density on the photocatalytic activity of TiO_2 powders. J. Photochem. Photobiol. A 273, 59−67.

Di Paola, A., Palmisano, L., Venezia, A.M., Augugliaro, V., 1999. Coupled semiconductor systems for photocatalysis. Preparation and characterization of polycrystalline mixed WO_3/WS_2 powders. J. Phys. Chem. B 103, 8236−8244.

Dionysiou, D.D., Burbano, A.A., Suidan, M.T., Baudin, I., Laîné, J.-M., 2002. Effect of oxygen in a Thin-Film ootating disk photocatalytic reactor. Environ. Sci. Technol. 36, 3834−3843.

Dionysiou, D.D., Suidan, M.T., Baudin, I., Laîné, J.-M., 2004. Effect of hydrogen peroxide on the destruction of organic contaminants-synergism and inhibition in a continuous-mode photocatalytic reactor. Appl. Catal. B 50, 259−269.

Domen, K., Naito, S., Domen, K., Onishi, T., Tamara, K., Soma, M., 1982. Study of the photocatalytic decomposition of water vapor over a $NiO\text{-}SrTiO_3$ catalyst. J. Phys. Chem. 86, 3657−3661.

Dorfman, L.M., Adams, G.E., 1973. Reactivity of the Hydroxyl Radical, National Bureau of Standards. Report No. NSRDS-NBS-46.

Edwards, M.E., Villa, C.M., Hill Jr., C.G., Chapman, T.W., 1996. Effectiveness factors for photocatalytic reactions occurring in planar membranes. Ind. Eng. Chem. Res. 35, 712−720.

Elliot, A.J., Simsons, A.S., 1984. Rate constants for reactions of hydroxyl radicals as a function of temperature. Radiat. Phys. Chem. 24, 229−231.

Emeline, A.V., Ryabchuk, V.K., Serpone, N., 2005. Dogmas and misconceptions in heterogeneous photocatalysis. Some enlightened reflections. J. Phys. Chem. B 109, 18515−18521.

Emeline, A., Ryabachuk, V., Serpone, N., 2000. Factors affecting the efficiency of a photocatalyzed process in aqueous metal-oxide dispersions: prospect of distinguishing between two kinetic models. J. Photochem. Photobiol. A A133, 89−97.

Emeline, A., Salinaro, A., Ryabchuk, V.K., Serpone, N., 2001. Photo-induced processes in heterogeneous nanosystems. From photoexcitation to interfacial chemical transformations. Int. J. Photoen. 3, 1−16.

Esplugas, S., Giménez, J., Conteras, S., Pascual, E., Rodríguez, M., 2002. Comparison of different advanced oxidation processes for phenol degradation. Water Res. 36, 1034−1042.

Fox, M.A., Dulay, M.T., 1993. Heterogeneous photocatalysis. Chem. Rev. 93, 341−357.

Fujishima, A., Hashimoto, K., Watanabe, T., 1999. TiO_2 Photocatalysis: Fundamentals and Applications. Bkc, Tokyo.

Fujishima, A., Honda, K., 1972. Electrochemical photolysis of water at a semiconductor electrode. Nature 238, 37−38.

Gao, P., Liu, Z., Tai, M., Sun, D.D., Ng, W., 2013. Multifunctional graphene oxide-TiO_2 microsphere hierarchical membrane for clean water production. Appl. Catal. B 138−139, 17−25.

Gerischer, H., 1970. Semiconductor electrochemistry. In: Eyring, H., Henderson, D., Host, W. (Eds.), Physical Chemistry, an Advanced Treatise, vol. IX. Academic Press, New York.

Gerischer, H., Heller, A., 1991. The role of oxygen in photooxidation of organic molecules on semiconductor particles. J. Phys. Chem. B 95, 5261−5267.

Glaze, W.H., Kang, J.W., Chapin, D.H., 1987. The chemistry of water treatment processes involving ozone, hydrogen peroxide, and ultraviolet radiation. Ozone Sci. Eng. 9, 335−352.

Guarisco, C., Palmisano, G., Calogero, G., Ciriminna, R., Di Marco, G., Loddo, V., Pagliaro, M., Parrino, F., 2014. Visible-light driven oxidation of gaseous aliphatic alcohols to the corresponding carbonyls via TiO_2 sensitized by a perylene derivative. Environ. Sci. Pollut. Res. 21, 11135−11141.

Hamrouni, A., Moussa, N., Di Paola, A., Palmisano, L., Houas, A., Parrino, F., 2015. Photocatalytic activity of binary and ternary $SnO_2\text{-}ZnO\text{-}ZnWO_4$ nanocomposites. J. Photochem. Photobiol. A 309, 47−54.

Han, S., Sun, J., Guo, S., Jiang, L., He, D., 2001. Phosphorus doped titania materials: synthesis, characterization and visible-light photocatalytic activity. Advanc. Mater. Res. 183–185, 2059–2062.

Hegedűs, P., Szabó-Bárdos, E., Horváth, O., Horváth, K., Hajós, P., 2015. TiO_2-mediated photocatalytic mineralization of a non-ionic detergent: comparison and combination with other advanced oxidation procedures. Materials 8, 231–250.

Herrmann, J.M., 1999. Heterogeneous photocatalysis: fundamentals and applications to the removal of various types of aqueous pollutants. Catal. Today 53, 115–129.

Herrmann, J.M., Boehm, H.P., 1969. Saure Hydroxylgruppen auf der Oberflaeche. Zeitschrift fuer Anorganische und Allgemeine Chemie 368, 73–86.

Herrmann, J.M., Gravelle-Rumeau-Mailleau, M., Gravelle, P.C., 1987. A microcalorimetric study of metal-support interaction in the Pt TiO_2 system. J. Catal. 104, 136–146.

Herz, R.K., 2004. Intrinsic kinetics of first-order reactions in photocatalytic membranes and layers. Chem. Eng. J. 99, 237–245.

Hirakawa, T., Nosaka, Y., 2002. Properties of $O_2^{\bullet-}$ and $OH^{\bullet}$ formed in TiO_2 aqueous suspensions by photocatalytic reaction and the influence of H_2O_2 and some ions. Langmuir 18, 3247–3254.

Hoffmann, M.R., Martin, S.T., Choi, W., Bahnemann, D.W., 1995. Environmental applications of semiconductor photocatalysis. Chem. Rev. 95 (1), 69–96.

Hoigne, J., Bader, H., 1983. Rate constants of reactions of ozone with organic and inorganic compounds in water-II. Dissociating organic compounds. Water Res. 17, 185–194.

Ingrosso, C., Petrella, A., Curri, M.L., Striccoli, M., Cosma, P., Cozzoli, P.D., Agostiano, A., 2005. Optical and electrochemical properties of Zn(II)phthalocyanine/ZnO nanocrystals heterojunctions. Appl. Surf. Sci. 246, 367–371.

Irie, H., Watanabe, Y., Hashimoto, K., 2003. Carbon-doped anatase TiO_2 powders as a visible-light sensitive photocatalyst. Chem. Lett. 32, 772–773.

Jiang, G., Lin, Z., Chen, C., Zhu, L., Chang, Q., Wang, N., Wei, W., Tang, H., 2011. TiO_2 nanoparticles assembled on graphene oxide nanosheets with high photocatalytic activity for removal of pollutants. Carbon 49, 2693–2701.

Kagaya, S., Shimizu, K., Arai, R., 1999. Separation of titanium dioxide photocatalyst in its aqueous suspensions by coagulation with basic aluminium chloride. Water Res. 33, 1753–1755.

Kang, M., 2005. The superhydrophilicity of Al–TiO_2 nanometer sized material synthesized using a solvothermal method. Mater. Lett. 59, 3122–3127.

Kim, S., Kim, M., Hwang, S.-H., Lim, S.K., 2012. Enhancement of photocatalytic activity of titania–titanate nanotubes by surface modification. Appl. Catal. B 123–124, 391–397.

Kisch, H., 2015. Semiconductor Photocatalysis: Principles and Applications. Wiley-VCH Verlag GmbH, Weinheim.

Kiwi, J., 1985. Direct observation of the variation of energy levels in powdered titanium dioxide as a function of temperature. Beneficial effects for energy conversion through semiconductor devices. J. Phys. Chem. 89, 2437–2439.

Langmuir, I., 1918. The adsorption of gases on plane surfaces of glass, mica and platinum. J. Am. Chem. Soc. 40, 1361–1403.

Li, N., Lang, X., Ma, W., Ji, H., Chen, C., Zhao, J., 2013. Selective aerobic oxidation of amines to imines by TiO_2 photocatalysis in water. Chem. Commun. 49, 5034–5036.

Li, Y., Wang, L., 1993. Semiconductor–mediated photocatalysis for organic synthesis. In: Kamat, P.V., Meisel, D. (Eds.), Semiconductor Nanoclusters: Physical, Chemical, and Catalytic Aspects, vol. 103. Elsevier, Amsterdam.

Linsebigler, A.L., Lu, G., Yates, J.T., 1995. Photocatalysis on TiO_2 surfaces: principles, mechanisms, and selected results. Chem. Rev. 95, 735–758.

Loddo, V., Addamo, M., Augugliaro, V., Garrone, E., Palmisano, L., Schiavello, M., 2006. Optical properties and quantum yield determination in photocatalytic suspensions. AIChE J. 52, 2565–2574.

Loddo, V., Augugliaro, V., Palmisano, L., 2009. Photocatalytic membrane reactors: case studies and perspectives. Asia Pac. J. Chem. Eng. 4, 380−384.

Lohmann, F., 1967. Fermi-Niveau und Flachbandpotential von Molekülkristallen aromatischer Kohlenwasserstoffe. Z. Naturforsch. A22, 843−844.

Maira Vidal, A.J., Soria, J., Augugliaro, V., Loddo, V., 1997. Oxidation of ethanol in gas phase via heterogeneous photocatalysis. Chem. Biochem. Eng. Quart. 11, 89−95.

Makarova, O.V., Rajh, T., Thurnauer, M.C., 2000. Surface modification of TiO_2 nanoparticles for photochemical reduction of nitrobenzene. Environ. Sci. Technol. 34, 4797−4806.

Martin, C.A., Camera-Roda, G., Santarelli, F., 1999. Effective design of photocatalytic reactors: influence of radiative transfer on their performance. Catal. Today 48, 307−313.

Matthews, R.W., 1987. Photooxidation of organic impurities in water using thin films of titanium dioxide. J. Phys. Chem. 91, 3328−3333.

Maurino, V., Bedini, A., Minella, M., Rubertelli, F., Pelizzetti, E., Minero, C., 2008. Glycerol transformation through photocatalysis: a possible route to value-added chemicals. J. Adv. Oxid. Technol. 11, 184−192.

McCallum, J.E.B., Madison, S.A., Alkan, S., Depinto, R.L., Wahl, R.U.R., 2000. Analytical studies on the oxidative degradation of the reactive textile dye Uniblue A. Environ. Sci. Technol. 34, 5157−5164.

Mills, A., O'Rourke, C., 2015. A revised disrupted Langmuir-adsorption model of photocatalysis. J. Phys. Chem. C 119, 19941−19946.

Minero, C., 1995. A rigorous kinetic approach to model primary oxidative steps of photocatalytic degradation. Sol. Energ. Mat. Sol. C 38, 421−430.

Minero, C., Bedini, A., Maurino, V., 2012. Glycerol as a probe molecule to uncover oxidation mechanism in photocatalysis. Appl. Catal. B 128, 135−143.

Minero, C., Maurino, V., Vione, D., 2013. Photocatalytic mechanisms and reaction pathways drawn from kinetic and probe molecules. In: Pichat, P. (Ed.), Photocatalysis and Water Purification: From Fundamentals to Recent Applications, first ed. Wiley-VCH Verlag GmbH & Co. KGaA (Chapter 3).

Minero, C., 1999. Kinetic analysis of photoinduced reactions at the water semiconductor interface. Catal. Today 54, 205−216.

Mitoraj, D., Kisch, H., 2008. The nature of nitrogen-modified titanium dioxide photocatalysts active in visible light. Angew. Chem. Int. Edit. 47, 9975−9978.

Moon, G-h., Kim, D-h., Kim, H-i., Bokare, A.D., Choi, W., 2014. Platinum-like behavior of reduced graphene oxide as a cocatalyst on TiO_2 for the efficient photocatalytic oxidation of arsenite. Environ. Sci. Technol. Lett. 1, 185−190.

Nagaveni, K., Hedge, M.S., Ravishankar, N., Subbanna, G.N., Madras, G., 2004. Synthesis and structure of nanocrystalline TiO_2 with lower band gap showing high photocatalytic activity. Langmuir 20, 2900−2907.

Ohno, T., Mitsui, T., Matsumura, M., 2003. Photocatalytic Activity of S-doped TiO_2 Photocatalyst under Visible Light, vol. 32, pp. 364−365.

Ohtani, B., Pal, B., Ikeda, S., 2003. Photocatalytic organic syntheses: selective cyclization of amino acids in aqueous suspensions. Catal. Surv. Asia 7, 165−176.

Okamoto, K., Yamamoto, Y., Tanaka, H., Itaya, A., 1985. Kinetics of heterogeneous photocatalytic decomposition of phenol over anatase TiO_2 powder. Bull. Chem. Soc. Jpn. 58, 2023−2028.

Ollis, D.F., 2005. Kinetics of liquid phase photocatalyzed reactions: an illuminating approach. J. Phys. Chem. B 109, 2439−2444.

Ollis, D.F., 1985. Contaminant degradation in water. Environ. Sci. Technol. 19, 480−484.

Ollis, D.F., Pelizzetti, E., Serpone, N., 1989. Heterogeneous photocatalysis in the environment: application to water purification. In: Serpone, N., Pelizzetti, E. (Eds.), Photocatalysis: Fundamentals and Applications. John Wiley & Sons, New York, pp. 603−637.

Ollis, D.F., Pelizzetti, E., Serpone, N., 1991. Photocatalyzed destruction of water contaminants. Environ. Sci. Technol. 25, 1522−1529.

Osorio-Vargas, P.A., Pulgarin, C., Sienkiewicz, A., Pizzio, L.R., Blanco, M.N., Torres-Palma, R.A., Pétrier, C., Rengifo-Herrera, J.A., 2012. Ultrason. Sonochem 19, 383.

Oyama, S.T., 2000. Chemical and catalyticp of ozone. Catal. Rev. Sci. Eng. 42, 279–322.
Palmisano, G., Yurdakal, S., Augugliaro, V., Loddo, V., Palmisano, L., 2007. Photocatalytic selective oxidation of 4-methoxybenzyl alcohol to aldehyde in aqueous suspension of home-prepared TiO_2 catalyst. Adv. Synth. Catal. 349, 964–970.
Panagiotopoulou, P., Karamerou, E.E., Kondarides, D.I., 2013. Kinetics and mechanism of glycerol photo-oxidation and photo-reforming reactions in aqueous TiO_2 and Pt/TiO_2. Catal. Today 209, 91–98.
Parrino, F., Augugliaro, V., Camera-Roda, G., Loddo, V., López-Muñoz, M.J., Márquez-Álvarez, C., Palmisano, G., Palmisano, L., Puma, M.A., 2012. Visible-light-induced oxidation of trans-ferulic acid by TiO_2 photocatalysis. J. Catal. 295, 254–260.
Parrino, F., Camera Roda, G., Loddo, V., Palmisano, L., 2016. Elemental bromine production by TiO_2 photocatalysis and/or ozonation. Angew. Chem. Int. Edit. 55, 10391–10395.
Parrino, F., Camera-Roda, G., Loddo, V., Augugliaro, V., Palmisano, L., 2015. Photocatalytic ozonation: maximization of the reaction rate and control of undesired by-products. Appl. Catal. B 178, 37–43.
Parrino, F., Conte, P., De Pasquale, C., Laudicina, V.A., Loddo, V., Palmisano, L., 2017. Influence of adsorbed water on the activation energy of model photocatalytic reactions. J. Phys. Chem. C 121, 2258–2267.
Pera-Titus, M., García-Molina, V., Baños, M.A., Giménez, J., Esplugas, S., 2004. Degradation of chlorophenols by means of advanced oxidation processes: a general review. Appl. Catal. B 47, 219–256.
Qian, X., Qin, D., Bai, Y., Li, T., Tang, X., Wang, E., Dong, S., 2001. Photosensitization of TiO_2 nanoparticulate thin film electrodes by CdS nanoparticles. J. Solid State Electrochem. 5, 562–567.
Rideal, E.K., Eley, D.D., 1950. Adsorption and catalysis on metals. Discuss. Faraday Soc. 8, 96–104.
Ryabchuk, V., 2004. Photophysical processes related to photoadsorption and photocatalysis on wide band gap solids: a review. Int. J. Photoen. 6, 95–113.
Saien, J., Ojaghloo, Z., Soleymani, A.R., Rasoulifard, M.H., 2011. Homogeneous and heterogeneous AOPs for rapid degradation of Triton X-100 in aqueous media via UV light, nano titania hydrogen peroxide and potassium persulfate. Chem. Eng. J. 167, 172–182.
Sakthivel, S., Kisch, H., 2003. Daylight photocatalysis by carbon-modified titanium dioxide. Angew. Chem. Int. Ed. 42, 4908–4911.
Sato, S., 1986. Photocatalytic activity of NO_x-doped TiO_2 in the visible light region. Chem. Phys. Lett. 123, 126–128.
Satuf, M.L., Brandi, R.J., Cassano, A.E., Alfano, O.M., 2005. Experimental method to evaluate the optical properties of aqueous titanium dioxide suspensions. Ind. Eng. Chem. Res. 44, 6643–6649.
Schiavello, M. (Ed.), 1995. Heterogeneous Photocatalysis. John Wiley &Sons, New York.
Serpone, N., Maruthamuthu, P., Pichat, P., Pellizzetti, E., Hidaka, H., 1995. Exploiting the interparticle electron transfer process in the photocatalysed oxidation of phenol, 2-chlorophenol and pentachlorophenol: chemical evidence for electron and hole transfer between coupled semiconductors. J. Photochem. Photobiol. A 85, 247–255.
Sheng, H., Li, Q., Ma, W., Ji, H., Chen, C., Zhao, J., 2013. Photocatalytic degradation of organic pollutants on surface anionized TiO_2: common effect of anions for high hole-availability by water. Appl. Catal. B 138–139, 212–218.
Siegel, R., Howell, J.R., 1992. Thermal Radiation Heat Transfer. Hemisphere Publishing Corporation, USA.
Sivaranjani, K., Gopinath, C., 2011. Porosity driven photocatalytic activity of wormhole mesoporous $TiO_{2-x}N_x$ in direct sunlight. J. Mater. Chem. 21, 2639–2647.
Sopajaree, K., Quasim, S.A., Basak, S., Rajeshwar, K., 1999. An integrated flow reactor-membrane filtration system for heterogeneous photocatalysis. Part II: experiments on the ultrafiltration unit and combined operation. J. Appl. Electrochem. 29, 1111–1118.
Spadoni, G., Stramigioli, C., Santarelli, F., 1980. Rigorous and simplified approach to the modelling of continuous photoreactors. Chem. Eng. Sci. 35, 925–931.
Spasiano, D., Marotta, R., Di Somma, I., Mancini, G., 2015. Production of pyridinecarboxy aldehydes, nicotinic and isonicotinic and picolinic acids by TiO_2-sacrificial photocatalysis at ambient conditions and in aqueous solution through artificial solar radiation. Appl. Catal. B 163, 248–257.

Stankiewicz, A., Moulijn, J.A., 2000. Process intensification: transforming chemical engineering. Chem. Eng. Prog. 96, 22−34.

Subramanian, V., Kamat, P.V., Wolf, E.E., 2003. Mass-transfer and kinetic studies during the photocatalytic degradation of an azo dye on optically transparent electrode thin film. Ind. Eng. Chem. Res. 42, 2131−2138.

Sunada, K., Watanabe, T., Hashimoto, K., 2003. Studies on photokilling of bacteria on TiO_2 thin film. J. Photochem. Photobiol. A Chem. 156, 227−233.

Tada, H., Jin, Q., Nishijima, H., Yamamoto, H., Fujishima, M., Okuoka, S., Hattori, T., Sumida, Y., Kobayashi, H., 2011. Titanium(IV) dioxide surface-modified with iron oxide as a visible light photocatalyst. Angew. Chem. Int. Ed. 50, 3501−3505.

Turchi, C.S., Ollis, D.F., 1990. Photocatalytic degradation of organic water contaminants: mechanisms involving hydroxyl radical attack. J. Catal. 122, 178−192.

Turchi, C.S., Ollis, D.F., 1988. Comment. Photocatalytic reactor design: an example of mass-transfer limitations with an immobilized catalyst. J. Phys. Chem. 92, 6852−6853.

Turchi, C.S., Ollis, D.F., 1989. Mixed reactant photocatalysis: intermediates and mutual rate inhibition. J. Catal. 119, 483−496.

Umebayashi, T., Yamaki, T., Itoh, H., Asai, K., 2002. Band gap narrowing of titanium dioxide by sulfur doping. Appl. Phys. Lett. 81, 454−456.

Vezzoli, M., Farrell, T., Baker, A., Psaltis, S., Martens, W.N., Bell, J.M., 2013. Optimal catalyst thickness in titanium dioxide fixed film reactors: mathematical modelling and experimental validation. Chem. Eng. J. 234, 57−65.

Wang, C., Shao, C., Zhang, X., Liu, Y., 2009. SnO_2 nanostructures-TiO_2 nanofibers heterostructures: controlled fabrication and high photocatalytic properties. Inorg. Chem. 48, 7261−7268.

Xu, J., Ao, Y., Chen, M., Fu, D., 2009. Low-temperature preparation of Boron-doped titania by hydrothermal method and its photocatalytic activity. J. Alloy Compd. 484, 73−79.

Xu, Y., Langford, C., 2000. Variation of Langmuir adsorption constant determined for TiO_2-photocatalyzed degradation of acetophenone under different light intensity. J. Photochem. Photobiol. A 133, 67−71.

You, X., Chen, F., Zhang, J., Anpo, M., 2005. A novel deposition precipitation method for preparation of Ag-loaded titanium dioxide. Catal. Lett. 102, 247−250.

Yu, J.C., Lin, J., Kwok, R.W.M., 1997. Enhanced photocatalytic activity of $Ti_{1-x}V_xO_2$ solid solution on the degradation of acetone. J. Photochem. Photobiol. A 111, 199−203.

Yurdakal, S., Palmisano, G., Loddo, V., Alagöz, O., Augugliaro, V., Palmisano, L., 2009. Selective photocatalytic oxidation of 4-substituted aromatic alcohols in water with rutile TiO_2 prepared at room temperature. Green Chem. 11, 510−516.

Yurdakal, S., Palmisano, G., Loddo, V., Augugliaro, V., Palmisano, L., 2008. Nanostructured Rutile TiO_2 for selective photocatalytic oxidation of aromatic alcohols to aldehydes in water. J. Am. Chem. Soc. 130, 1568−1569.

Yurdakal, S., Tek, B.S., Alagöz, O., Augugliaro, V., Loddo, V., Palmisano, G., Palmisano, L., 2013. Photocatalytic selective oxidation of 5-(hydroxymethyl)-2-furaldehyde to 2,5-furandicarbaldehyde in water by using anatase, rutile and brookite TiO_2 nanoparticles. ACS Sustain. Chem. Eng. 1, 456−461.

Yurdakal, S., Yanar, Ş.Ö., Çetinkaya, S., Alagöz, O., Yalçın, P., Özcan, L., 2017. Green photocatalytic synthesis of vitamin B_3 by Pt loaded TiO_2 photocatalysts. Appl. Catal. B 202, 500−508.

Zhao, J., Zhang, Y., Quan, X., Chen, S., 2010. Enhanced oxidation of 4-chlorophenol using sulfate radicals generated from zero-valent iron and peroxydisulfate at ambient temperature. Sep. Purif. Technol. 71, 302−307.

Zhu, J., Chen, F., Zhang, J., Chen, H., Anpo, M., 2006. Fe^{3+}-TiO_2 photocatalysts prepared by combining sol−gel method with hydrothermal treatment and their characterization. J. Photochem. Photobiol. A 180, 196−204.

This page intentionally left blank

CHAPTER 2

Membranes and Membrane Processes: Fundamentals

Norfazliana Abdullah, Mukhlis A. Rahman, Mohd Hafiz Dzarfan Othman, Juhana Jaafar, Ahmad F. Ismail

Universiti Teknologi Malaysia, Skudai, Johor, Malaysia

2.1 Introduction

Membrane technology plays a vital role in the broad range of industrial applications. The concept of membrane-based separation has been introduced since the 18th century and regarded to have advantages over most conventional separation processes, e.g., distillation, adsorption, and absorption due to energy saving and less space consumption attributed to its characteristics (Hsieh, 1991). The membrane is described based on its role as a permselective barrier between two phases where the separation of desired species occurs in the presence of driving forces, i.e., pressure gradient, vapor partial pressure gradient, concentration gradient, or electrical potential gradient (Mulder, 1996). Fig. 2.1 presents the illustration of a membrane acting as a permselective barrier (Lu et al., 2007).

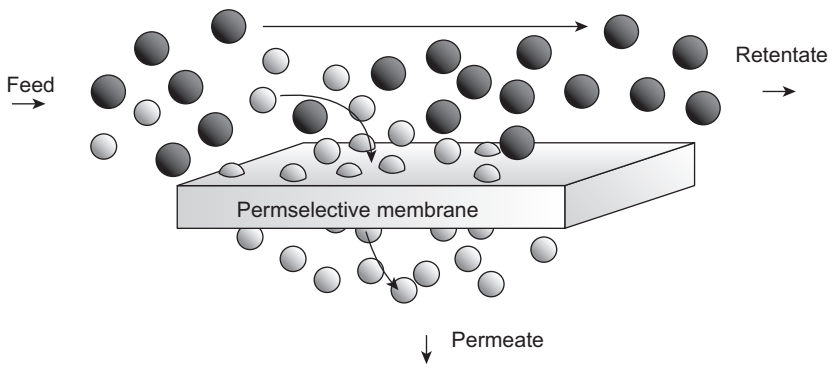

Figure 2.1
A diagram representation of membrane system. *From Lu et al., 2007. With permission from Elsevier.*

Current Trends and Future Developments on (Bio-) Membranes. https://doi.org/10.1016/B978-0-12-813549-5.00002-5

Membrane performance is typically measured using flux and selectivity (Mulder, 1996). Flux of a membrane can be expressed as the volume, mass, or number of moles of a substance that flow through the membrane per unit membrane area and time. The unit of volumetric flux is $m^3\ m^2\ s^{-1}$, although usually $L\ m^2\ h^{-1}$ is used. The permeation rate is influenced by various driving forces such as electrical flow, pressure, concentration, or partial pressure. Selectivity of a membrane to a fluid mixture is related to retention or separation factor. However, the separation factor is normally used for gas mixtures and organic liquid mixtures.

Membrane processes can be performed through two types of filtrations, namely, the dead-end filtration and the cross-flow filtration. These filtration types are based on the direction of the feed stream relative to the orientation of the membrane surface, as shown in Fig. 2.2 (Lee and Darling, 2016). The dead-end filtration is normally applied for small-scale separation, particularly in laboratory batch separation modules. In this filtration approach, the feed and permeate are both perpendicular to the surface of the membrane (Hsieh, 1991). This filtration type is prone to fouling; therefore backwashing is suggested to improve membrane permeability. On the other hand, the cross-flow filtration refers to the system in which feed flows parallel to the membrane surface while permeate penetrates through the membrane. The shear force exerted by the flowing feed stream on the membrane surface helps to remove the deposits that cause a decrease of permeate flux.

Membrane processes have been applied in various applications related to the separation of gas mixtures, wastewater treatment, water recycling, enhanced oil recovery, separations of organic liquids, oil to gas conversion, and others. The separation processes using membranes have been classified into various categories. Each category has specific driving

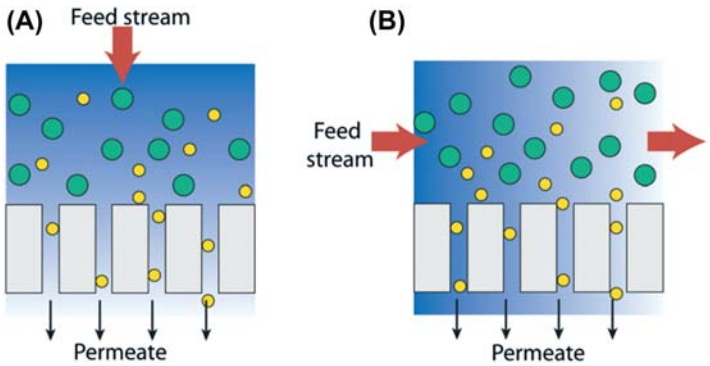

Figure 2.2

Schematic diagram of membrane process according to (A) dead-end filtration mode and (B) cross-flow mode. *From Lee and Darling, 2016. With permission from The Royal Society of Chemistry.*

Table 2.1: Membrane separation processes according to different operating parameters and applications.

Process	Pore Size	Driving Force	Transport Mechanism
Microfiltration	0.05–10 μm	Pressure, 1–2 bar	Sieving
Ultrafiltration	0.001–0.05 μm	Pressure, 2–5 bar	Sieving
Nanofiltration	<2.0 nm	Pressure, 5–15 bar	Preferential sorption–capillary flow
Reverse osmosis	<1.0 nm	Pressure, 15–100 bar	Preferential sorption–capillary flow
Gas separation	Nonporous	Pressure, 15–100 bar	Solution-diffusion
Pervaporation	Nonporous	Partial pressure difference	Solution-diffusion
Dialysis	10–30 Å	Concentration difference	Sieving—diffusivity difference
Electrodialysis	MW < 200	Electrical potential	Ion migration
Electrodeionization	MW < 200	Electrical potential	Ion migration
Membrane contactor	Porous hydrophobic	Vacuum	Sieving

From Singh, R., 2005. Water and membrane treatment. Hybrid Membr. Syst. Water Purif. 1, 57–130. With permission from Elsevier.

force. Depending on the driving force and solute to be separated, these categories have unique mode of separation such as size exclusion, solution-diffusion mechanism, Knudsen diffusion, molecular diffusion, etc. Table 2.1 lists the various separation processes with respective applied driving force and mode of separation.

2.2 History of Membrane Technology

The development of membrane technology started in the 18th century with the phenomenon of water permeation through a pig bladder that was used to store alcohol. This phenomenon was observed by a physicist, Jean Antoine Nollet. He was probably the first to recognize the relation between a semipermeable membrane and the osmotic pressure. Later on, Thomas Graham conducted more detailed investigations on the diffusion of gases through different media (Mulder, 1996). Consequently, a rapid advancement of membrane technology was observed in the following decades through the works of Adolf Fick and Jacobus Henricus van 't Hoff, who explained the diffusion of solutes in liquid media. The early stage of membrane technology had focused mainly on providing a theoretical explanation for membrane processes. Moreover, Leonor Michaelis, Erich Manegold, and James William proposed a reverse osmosis (RO) prototype in the period between 1926 and 1931. During the same period, Torsten Teorell, Kurt H. Meyer, and J.F. Sievers designed and introduced electrodialysis membrane and modern electrodes, whereas the first clinical hemodialysis using the membrane technology was successfully developed by Willem Johan Kolff in 1945. In the 1950s, a number of membrane technologies were developed for treatment of drinking water in Europe, particularly electrodialysis, microfiltration (MF), and ion-exchange membranes. This led to the first

commercial plant for the production of potable water from seawater using electrodialysis and ion-exchange membrane, which operated in 1954 (Wang et al., 2011).

In the meantime, perhaps the most significant achievement in the history of membrane technology is the preparation of defect-free, high-flux, anisotropic RO membrane by using asymmetric cellulose acetate (CA) membrane by Loeb and Sourirajan in 1962 (Baker, 2012; Li, 2007; Wang et al., 2011). Its fabrication method is known as the phase inversion, which initiated the production of an artificial membrane. The fabrication technique introduced by Loeb and Sourirajan also dominated the membrane development for gas separation applications. Then, in the late 1960s and early 1970s, Permea had successfully installed a polysulfone (PSF) hollow fiber membrane for the separation and recovery of hydrogen from the purge gas streams of ammonia plants. This effort had encouraged other companies, such as Cynara, Separex, and GMS, to use CA for the removal of carbon dioxide from natural gas (Baker, 2002). At the same time, Generon introduced a membrane system to separate nitrogen from air. Mostly, these membranes comprise polymers, and the selectivity was improved by using a very thin skin layer. Fig. 2.3 shows the milestone of membrane technology, particularly for gas separation (Baker, 2002).

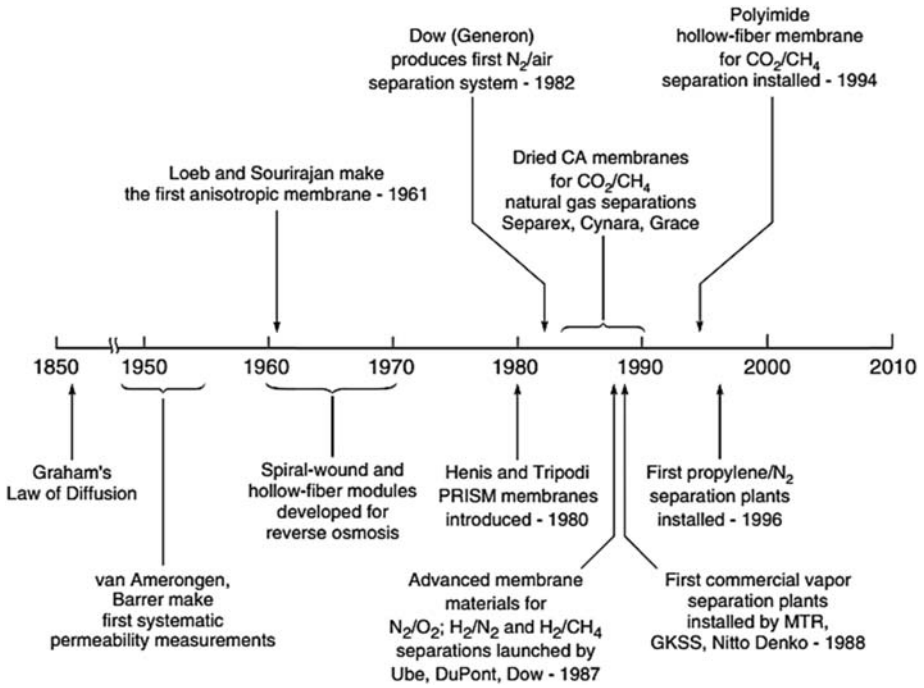

Figure 2.3

Milestone development of membrane gas separation. *From Baker, 2002. With permission from American Chemical Society.*

2.3 Classification of Membranes

Membranes can be generally classified into different categories, i.e., membrane materials, membrane geometry, and membrane morphology. The details are discussed in the following sections.

2.3.1 Membrane Materials

Most of the available membranes used polymeric material because of various reasons, i.e., low price, availability, ease of preparation, etc. Various types of polymers have been explored to maximize both flux and separation factor. CA, one of the organic polymers, is commonly used in membrane preparation. CA is a polysaccharide with a regular repeating structure that forms a strong intermolecular hydrogen bond between the hydroxyl groups and contributes to the increase of the level of crystallinity. This characteristic prevents CA from dissolving in water. However, CA can dissolve in various organic solvents, i.e., N-methylmorpholine-N-oxide (NMMO), N,N-dimethylacetamide (DMAC), and N-methylpyrrolidone (NMP) (Liu and Hsieh, 2002). CA exhibits a strong hydrophilic characteristic (Chen et al., 2004) but has a poor resistance at the pH ranging from 4 to 6.5 (Wang et al., 2009). Apart from CA, PSF is also favored for membrane preparation. PSF is an amorphous high-performance polymer, which demonstrates a high degree of chemical and thermal stability (Wang et al., 2011). PSF is commonly used in UF, MF, and gas separation membranes and as a support layer for RO and NF. Unlike CA, PSF can tolerate a wide range of pH and is stable under acidic and alkaline solutions (Han and Nam, 2002). A number of works have also used polyvinylidene fluoride (PVDF) for membrane preparation (Rajabzadeh et al., 2008; Song et al., 2012; Yuliwati and Ismail, 2011). PVDF is a hydrophobic and semicrystalline polymer, which is suitable for membrane fabrication because of its good chemical resistance and thermal stability. This material is soluble in various organic solvents, which makes it advantageous for membrane preparation. Polyamide (PA) is another type of polymer used for membrane preparation. This synthetic polymer contains an amide group (−NHCO−) as the main polymer chain (Buonomenna, 2013; Wang et al., 2011). PA is commonly used as a thin dense layer in composite membranes for RO and NF applications. In this regard, Table 2.2 lists the polymers commonly used as membrane materials.

Recently, the use of ceramic membrane in fluid separation has gained much interest, as it offers various advantages, such as high resistance under acidic and alkali medium, high thermal stability, high chemical stability, and excellent mechanical strength compared with polymeric membrane. The commonly used materials for the ceramic membrane are aluminum oxide or alumina (Al_2O_3); titanium dioxide/titania (TiO_2); zirconium dioxide/zirconia (ZrO_2); silicon dioxide/silica (SiO_2); mixed ionic-electronic conduction (MIEC) materials such as lanthanum, strontium, cobalt ferrite; and the combination of ceramic

Table 2.2: Advantages and disadvantages of different types of polymers.

Polymer[a]	Advantages	Disadvantages	Process[b]
CA	Inexpensive More fouling resistant than PA	A poor resistance at the pH ranging from 4 to 6.5	**RO**, NF, UF
PA	More all-around stability than CA More permselectivity than CA	Very limited chlorine tolerance (<0.1 mg L^{-1})	**RO**, NF
PAN	High resistance to hydrolysis High resistance to oxidation	Hydrophobic Requires copolymers to make less brittle	UF, RO substrate
PSF, PES	Very good all-around stability Mechanically strong	Hydrophobic	UF, RO substrate
PVDF, PTFE	Extremely high chemical stability High thermal stability	Highly hydrophobic Limited mechanical stability Limited intrinsic permeability Expensive	UF, **MF**
PEI	High chemical stability Very high thermal stability Mechanically strong	Hydrophobic Less solvent resistant than PVDF Poorer alkaline stability than PSF or PAN	**UF**, RO substrate
PP	Inexpensive	Hydrophobic	UF, **MF**

[a]*CA*, cellulose acetate (predominantly di- or tri-acetate); *PA*, polyamide (aromatic); *PAN*, polyacrylonitrile; *PEI*, polyetherimide; *PES*, polyethersulfone; *PP*, polypropylene; *PSF*, polysulfone; *PVDF*, poly(vinylidene fluoride); *PTFE*, polytetrafluoroethylene.
[b]Most usual application in bold type.
From Judd, S., Jefferson, B., 2003. Membrane Technology. Membranes for Industrial Wastewater Recovery and Re-use: 3.1 the Power Industry, first ed. Elsevier Ltd, UK. With permission from Elsevier.

materials (Li, 2007). Each of these materials has its own commercial values. Alumina is commonly used in mechanical devices, manufacturing products (thermal insulator, ceramic jar, pottery, etc.), and membrane support, whereas titania has a great potential in photocatalytic applications such as air purification, water purification, and heavy metal removal (Fujishima et al., 2000; Puskelova et al., 2014). Zirconia is a commonly studied ceramic material used in medical devices (Manicone et al., 2007) and fuel cell membrane study (Meng et al., 2013; Wei and Li, 2008). Meanwhile, silica is used primarily as a precursor for glass, silicon productions, and microporous membrane (Gao et al., 2014), and MIEC materials have unique characteristics to be used as membranes at higher temperature applications, particularly in air separation industry (Jiang et al., 2011). Ceramic material is brittle in nature but still can be shaped into membrane module, and its mechanical strength can be improved by sintering at an elevated temperature.

2.3.2 Membrane Geometry

There are four types of membrane geometries used in membrane applications, namely, flat sheet, tubular, capillary, and hollow fibers (El-ghaffar and Tieama, 2017).

These configurations will have different membrane modules for separation process for various applications. The flat sheet membranes can be shaped into either plate-and-frame or spiral-wound configurations. The plate-and-frame design refers to a number of flat sheet membranes sandwiched between rigid porous supports and the flow channel (Lonsdale, 1982; Baker, 2012). This configuration is typically used in the development of electrodialysis cells. The spiral-wound has similar configuration to the plate-and-frame system, but the membranes are arranged between flexible porous supports wrapped around a central porous tube, as shown in Fig. 2.4 (Wang et al., 2011). This type of membrane configuration has various components including the membrane, the feed and permeate channels, the spacer, the permeate tube, and the membrane housing (Schwinge et al., 2004). The membrane filtration area, per unit volume of the module, is approximately one and half times to that of plate-and-frame design (Wang et al., 2011). The drawback of both

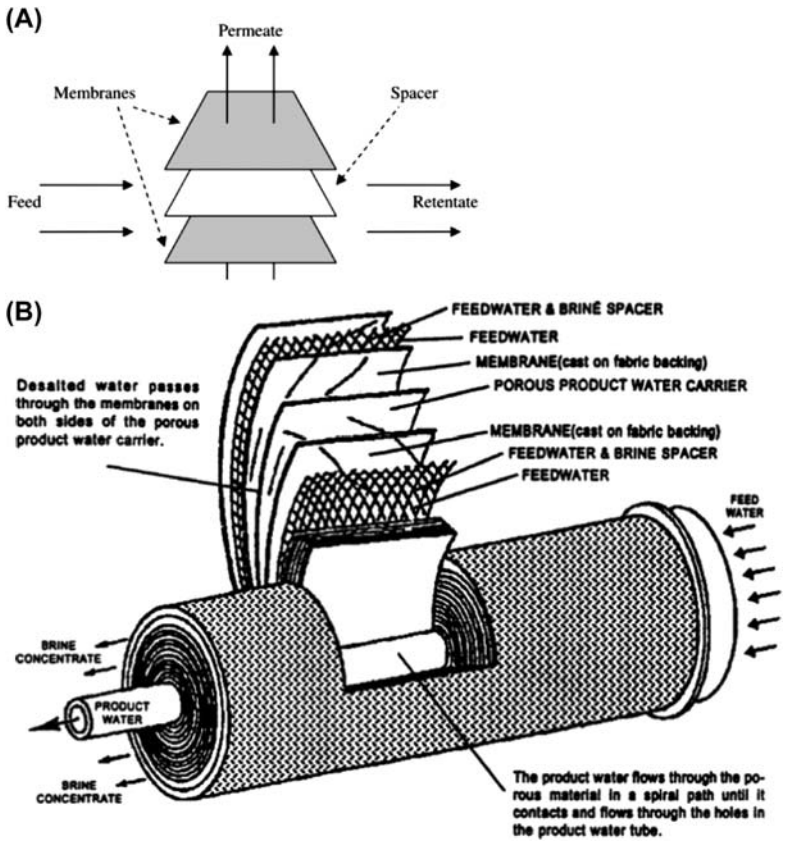

Figure 2.4
Schematic diagram of (A) plate-and-frame module and (B) spiral-wound module. *From Wang et al., 2011. With permission from Springer.*

configurations is mechanical cleaning, which is very difficult, hence it is not suitable for the application that has particulates in the feed streams.

The membranes with circular cross section can be formed into either tubular, capillary, or hollow fiber form (Giorno and Drioli, 2000). The classification of these membranes is based on their diameter. The tubular configuration resembles that in a shell and tube heat exchanger. This arrangement enables the tube to be cleaned, plugged off, or replaced. It can give benefit in terms of membrane maintenance and replacement, but it requires tedious work when hundreds of membranes are assembled together. Hollow fiber configuration is known to have the smallest outer diameter, as shown in Fig. 2.5, which offers maximum packing density (Wang et al., 2011) compared with other membrane configurations. The hollow fiber membrane has a diameter ranging from 50 to 3000 μm. A hollow fiber module may consist of thousands of hairlike hollow membrane fibers assembled into a bundle and contained in a vessel (Hsieh, 1991; Lonsdale, 1982). This configuration has been used extensively in fluid separation. For the hollow fiber membrane that has an outer diameter larger than 200−500 μm, the feed fluid is typically applied to the lumen of the fiber and permeate is collected from the outer surface (Baker, 2012). This technique is used for low-pressure gas separations and applications such as hemodialysis or UF. Smaller hollow fiber membranes with outer diameters ranging from 50 to 200 μm

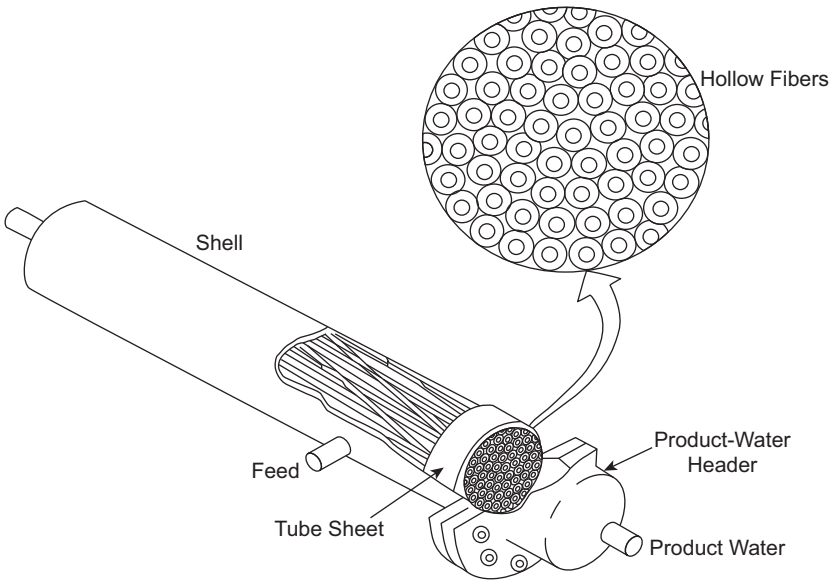

Figure 2.5
Schematic diagram of a hollow fiber module with high packing density. *From Wang et al., 2011. With permission from Elsevier.*

have also been produced, which are known as hollow fine fibers. These membranes have the ability to withstand a very high hydrostatic pressure applied on their outer surface. They are designed specifically for RO or high-pressure gas separation applications, where the applied pressure is 6.9 MPa or more (Baker, 2012). The feed fluid is applied on the outer surface of the fibers, and product flow is collected from the fiber lumen.

2.3.3 Membrane Morphology

Membrane morphology can be divided into two types, isotropic or symmetric membrane and anisotropic or asymmetric membrane, as shown in Fig. 2.6 (Lee and Darling, 2016). Isotropic microporous membrane has a rigid, interconnected pore and void structure with pores distributed randomly (pore diameter is in the order of 0.01−10 μm) (Baker, 2012). The separation process is influenced by the pore size distribution of the microporous membrane and the hydrodynamic conditions. The microporous membranes can be prepared using the phase inversion, track etching, stretching or leaching, and

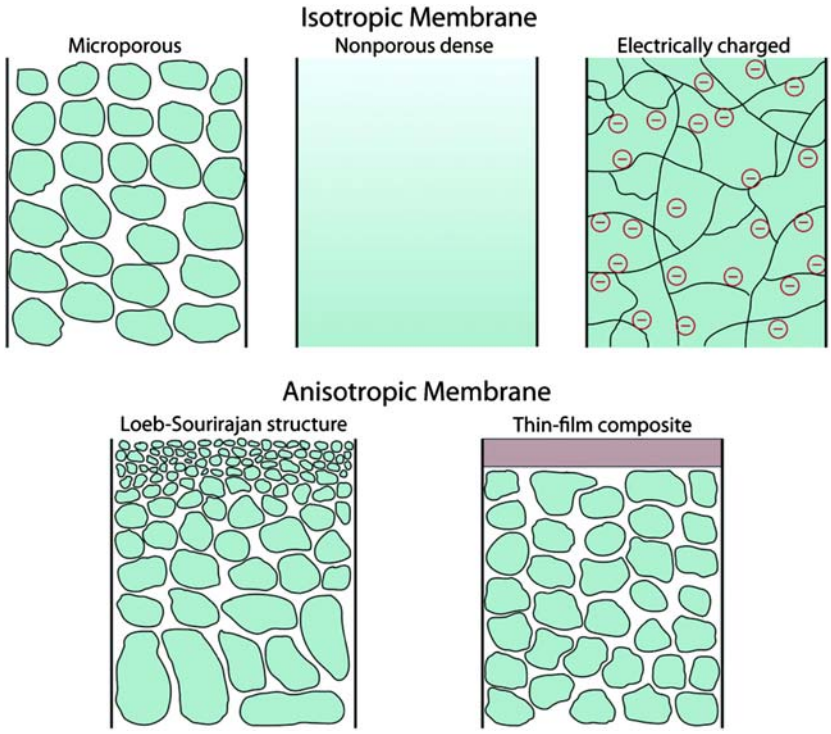

Figure 2.6
Isotropic and anisotropic membranes. *From Lee and Darling, 2016. With permission from The Royal Society of Chemistry.*

electrospinning (Lalia et al., 2013). The phase inversion method is the most important method for the isotropic microporous membrane formation. Electrically charged membranes are referred to either anion-exchange membranes or cation-exchange membranes that possess dense/microporous structures carrying fixed positive or negatively charged ions distributed uniformly (Baker, 2012; Wang et al., 2011). The charge and the concentration of the ions in membrane are the key aspects to control the separation process using this membrane.

Anisotropic membranes comprise the layered structures, changing the porosity and pore size over the whole membrane cross section (Baker, 2012). Anisotropic membranes typically have a very thin surface layer supported on a thick microporous layer. The thin layer is used as the selective layer to perform separation. Owing to the thickness of the selective layer, the membrane fluxes are usually very high. Integrally asymmetric membranes, composite membranes, and supported liquid membranes can be categorized under the anisotropic membranes. Loeb and Sourirajan developed integrally asymmetric membranes using the phase inversion method applying a single polymer (Loeb and Sourirajan, 1963). The porosity and pore size changed throughout the cross section of the membrane. A selective thin layer on the top surface was created on the gradually looser layer. The thin skin layer and porous substrate are coupled with each other as they are formed simultaneously in the phase inversion process.

2.4 Fabrication of Polymeric Membranes

A typical method of preparation of a polymeric membrane with an asymmetrical structure is the phase inversion technique. In this process, the solidification of polymer matrix from liquid (or soluble) state occurs in a controlled manner (Lalia et al., 2013). There are a number of the phase inversion routes occurring in the fabrication of polymeric membranes, including immersion precipitation (Ahmad et al., 2005; Kong and Li, 2001; Wang et al., 2009; Peng et al., 2007), thermally induced phase separation (TIPS) (Gu et al., 2006; Matsuyama et al., 2000, 2003; Rajabzadeh et al., 2008; Tanaka and Lloyd, 2004), evaporation-induced phase separation (Samuel et al., 2011; Yamamura et al., 2002), and vapor-induced phase separation (Li et al., 2010; Menut et al., 2008; Su et al., 2009; Tsai et al., 2010). During the immersion precipitation, the solvent and nonsolvent must be miscible. This is one of the phase inversion processes where the demixing and precipitation occur after homogeneous polymer solution in the solvent is in contact with nonsolvent as shown in Fig. 2.7 (Lalia et al., 2013). After immersing the polymer solution in a nonsolvent bath, the solvent will diffuse into the coagulation bath (at flux $= J_2$), whereas the nonsolvent will diffuse into the cast membrane film (at flux $= J_1$) (Lalia et al., 2013). This process will continue until the polymer solution becomes thermodynamically unstable, allowing the demixing to form a solid polymeric membrane with asymmetrical structure.

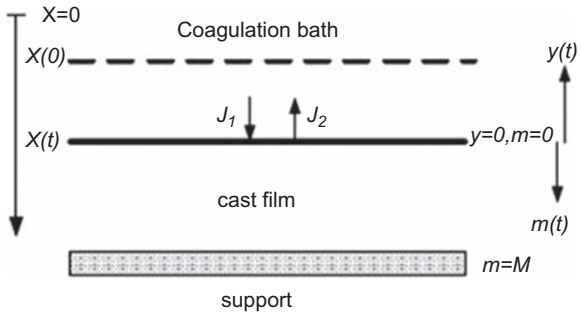

Figure 2.7

Schematic representation of a film/bath interface: J_1 is the nonsolvent flux, and J_2 is the solvent flux. X is the position of the interface between the film and the coagulation bath, x is the spatial position coordinate normal to the membrane surface, $y = -x - X(t)$ is the position coordinate that moves with the interface. m is the position coordinate in the polymer-fixed frame of reference, and M is a support. *From Lalia et al., 2013. With permission from Elsevier.*

TIPS occurs when a homogeneous polymeric solution prepared at an elevated temperature is cooled to allow the induction of the polymer precipitation phase (Gu et al., 2006; Matsuyama et al., 2000, 2003; Rajabzadeh et al., 2008; Tanaka and Lloyd, 2004). After the polymer-rich phase is solidified by the glass transition or crystallization, the porous membrane structure can be created by removing the solvent via extraction, evaporation, or freeze drying (Cao et al., 2004; Lalia et al., 2013). The evaporation-induced phase inversion is also known as the solution casting method. The polymer solution is casted on a flat substrate using the doctor blade technique, and when the volatile solvent evaporates from the casted solution, a thin polymer film is formed on the support. The vapor-induced phase inversion occurs when the polymer solutions are exposed to the atmosphere leading to the precipitation of polymer phase.

The phase inversion process can be explained using the ternary phase diagram of polymeric system, which involves polymer, solvent, and nonsolvent, as shown in Fig. 2.8 (Jamil et al., 2015). The entire phase inversion process of a polymeric solution is represented by the path from A to D. The original polymeric solution is at point A, where no precipitation agent (nonsolvent) is present in the solution. After immersion of the polymeric solution into a nonsolvent coagulation bath, the solvent diffuses out of the polymer solution, while the nonsolvent diffuses into the solution. The polymer concentration at the interface increases, and the polymer starts to precipitate (as represented by point B). The continuous replacement of solvent with nonsolvent would result in the solidification of the polymer-rich phase (point C). Further solvent/nonsolvent exchange would cause shrinkage of the polymer-rich phase, before finally reaching point

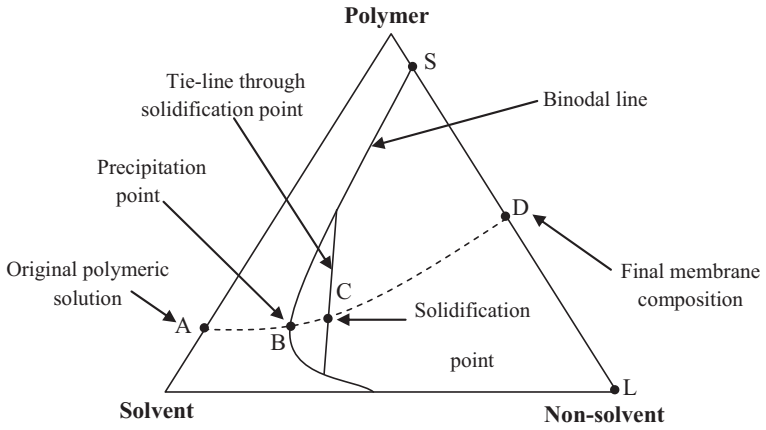

Figure 2.8
Schematic ternary phase diagram for polymer/solvent/nonsolvent systems. *From Jamil et al., 2015. With permission from Elsevier.*

D, where two phases (solid and liquid) are in equilibrium. A solid (polymer-rich) phase, which forms the membrane structure, is represented by point S, and a liquid (polymer-poor) phase, which constitutes the membrane pores filled with nonsolvent, is represented by point L (Jamil et al., 2015).

During the phase inversion process, macrovoids can be formed in the membrane structure. The macrovoids refer to very large elongated pores that can extend over the membrane thickness. They have various shapes, such as tearlike, pinlike, fingerlike, affected by the manner of nonsolvent diffusion. Macrovoids are usually referred as defects, which are undesirable as they can reduce the mechanical strength of a membrane. The formation of macrovoids in the phase inversion process has been studied extensively in past literature (Barth et al., 2000; Peinemann et al., 2007; Pinnau and Freeman, 1999). Various mechanisms have been proposed to describe the formation of macrovoids, such as the shrinkage of polymer matrix, surface tension gradient−induced convection, osmotic pressure, instantaneous phase demixing, and concentration gradient−induced instability (Smolders et al., 1992; Strathmann et al., 1975). There were a number of works that studied the macrovoid formation with the viscous fingering phenomenon in the polymer and gelation systems (Kawaguchi et al., 1997; Wang and Lai, 2013). In this phenomenon, a nascent porous membrane structure is formed under the nascent skin layer. Owing to the steep concentration gradient, the nonsolvent is diffusing into the polymer-poor phase, which is formed in the nascent porous membrane structure. This unstable condition causes the formation of some macrovoids, as illustrated in Fig. 2.9 (Wang et al., 2011).

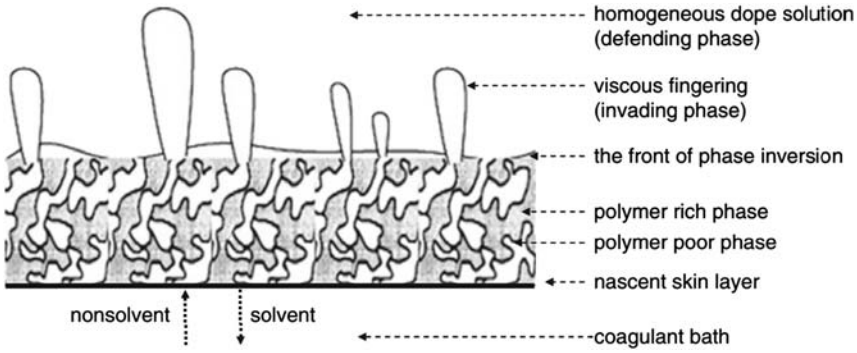

Figure 2.9
Formation of macrovoids in phase inversion process. *From Wang et al., 2011. With permission from Springer.*

Typically, hollow fiber membranes are prepared using the phase inversion method using the spinning possess asymmetric structure. Fig. 2.10 shows a typical set up to prepare polymeric membrane with hollow fiber configuration (Xu et al., 2014). Various parameters can influence the formation of hollow fiber membrane, including the evaporation time of the solution exiting the spinneret, the compositions of the bore fluid and the coagulation bath (Hasbullah et al., 2011; Peng et al., 2012). The position of the dense anisotropic skin can be adjusted by varying the bath and bore solutions; if water is used as the bore fluid and the coagulation bath contains some solvent, precipitation will occur first and most

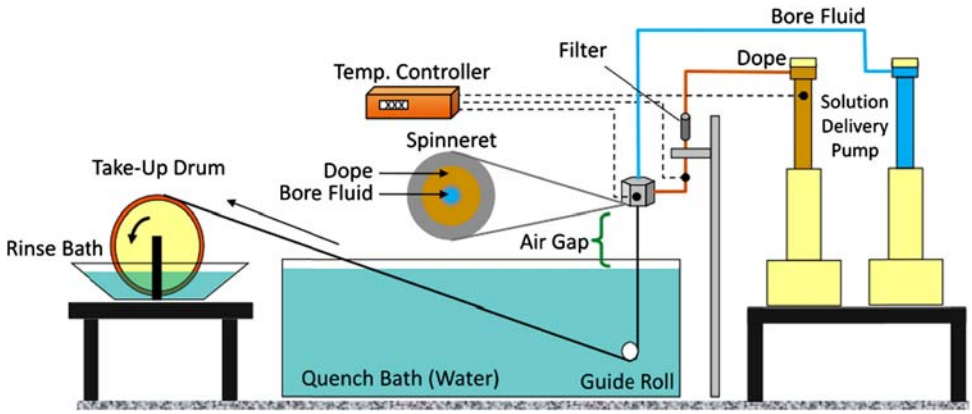

Figure 2.10
Schematic diagram of spinning system for fabrication of polymeric membrane by phase inversion. *From Xu et al., 2014. With permission from Elsevier.*

rapidly on the inside surface of the fiber (Mulder, 1996). On the other hand, if the bore solution contains some solvent and the coagulation bath comprises water, a skin will be formed on the outer surface of the fiber. A common case is precipitation on both surfaces of the fibers leading to formation of a dense layer on both inside and outside surfaces (Li et al., 1994; Ulbricht, 2006).

2.5 Membrane Operations

2.5.1 Examples of Pressure-Driven Membrane Operations

There are four categories of pressure-driven membrane processes, namely MF, ultrafiltration (UF), nanofiltration (NF), and RO. Basically, these techniques require transmembrane pressure (TMP) (ΔP) to facilitate the separation process.

2.5.1.1 Microfiltration

MF refers to the filtration processes that use membranes to separate the suspended particles or macromolecules with diameters ranging from 0.1 to 10 μm (Hwang and Lin, 2002; Chen et al., 2004; Ulbricht, 2006) under pressures ranging from 100 to 400 kPa. The separation is typically based on the sieving mechanism. For MF, both isotropic and anisotropic membranes can be used, but the separation layer should be preferably around 10−50 μm and c. 1 μm, respectively (Mulder, 1996). Polymeric materials are mostly used to prepare this type of membrane. Focus has been made on morphology of the membrane so as to improve the performance of MF process. The study also emphasized on the preparation techniques and polymeric functionality of MF membrane (Hwang and Lin, 2002; Ulbricht, 2006; Van Der Bruggen et al., 2003).

2.5.1.2 Ultrafiltration

UF membrane is similar to MF membrane, but this membrane enables to reject smaller molecules. UF membranes are practically used to separate macromolecules, colloids, and solutes with molecular weight larger than 10,000 Da. The TMP ranging from 100 to 1000 kPa is used as driving force. The selectivity of UF membrane is based on the difference in solute size, membrane properties, and the hydrodynamic conditions (Wang et al., 2011). This membrane is easily prepared using the phase inversion process, which leads the membrane to possess asymmetric porous structure (Khayet et al., 2002; Susanto and Ulbricht, 2009; Ulbricht, 2006; Xu and Qusay, 2004).

2.5.1.3 Nanofiltration

NF membrane typically has high rejections to most dissolved organic solutes with molecular weight above 100−200 Da and good salt rejection at the salt concentrations below 1000−2000 ppm (Baker, 2012; Buonomenna, 2013). The membranes are more

permeable than brackish and seawater RO membrane. This type of membrane can operate under pressures as low as 0.34−1 MPa. Owing to this, the membrane is preferable to be used in water softening or as an initial pretreatment unit for the production of ultrapure water.

2.5.1.4 Reverse Osmosis

RO is a pressure-driven membrane separation process to remove most of the dissolved contaminants from water. This process uses the reverse of the natural osmosis process. The pressure applied in the RO process is influenced by the concentration of solute at the feed. Water can be produced when the magnitude of pressure applied is higher than the osmotic pressure of the concentrated solution (Kang and Cao, 2012; Lee et al., 2011; Malaeb and Ayoub, 2011). An approximate osmotic pressure of fresh or brackish water is approximately 6895 Pa (1 psi) for every 100 mg L^{-1} difference in TDS concentration on opposite sides of the membrane. Therefore, the higher the solute concentration, the higher the pressure required to produce RO water. Nevertheless, RO can eliminate various contaminants and salt from water by using a semipermeable membrane that permits only water to pass through its structure. Furthermore, RO is effective in rejecting various organic solutes with large molecular weights, such as fulvic acids, lignins, humic acids, and detergents.

In general, RO units used in potable water treatment plants consist of raw water pumps, pretreatment systems (usually consisting of chemical coagulation, filtration [fine filtration, UF or MF], scaling control [e.g., softening], and acidification for regulating the pH), membrane units, disinfection stage, storage and distribution elements. These units are able to process virtually the desired quantity or quality of water by configuring them sequentially to reprocess waste brine from the earlier stages of the process. The pressure applied in RO units ranges from 1.5 to 2.5 MPa for brackish water and from 5.5 to 8.5 MPa for seawater (Buonomenna, 2013), and the most commercially successful RO configurations is spiral-wound. Brackish water RO plants can typically recover 50%−80% of the feed water, with 90%−98% of salt rejection (Wang et al., 2008). For seawater, recovery rates vary from 20% to 40% with 90%−98% of salt rejection (Wang et al., 2011). The details of RO system can be found in other works such as Malaeb and Ayoub (2011), Lee et al. (2011), Kang and Cao (2012).

2.5.2 Examples of Concentration-Driven Membrane Operations

This section discusses forward osmosis (FO), which uses concentration difference as its driving force. Separated by a thin layer of membrane, draw solution with high concentration and feed solution with low concentration can create a steep concentration gradient to allow separation to occur. The detail of the process is discussed as follows.

2.5.2.1 Forward Osmosis

FO is an osmosis process that involves the use of draw solution with higher concentration compared with feed solution. Fig. 2.11 shows the mechanism of water transport via the membrane due to high osmotic pressure gradient (Chung et al., 2012). During separation process, a draw solution with high osmotic pressure is used to induce a net flow of water through a semipermeable membrane into the draw solution under an osmotic pressure gradient, thus, effectively separating the feed water from its solutes (Cath et al., 2006; Peng et al., 2012). The water that permeates through the membrane can be recovered if a second separation unit is installed to extract the freshwater from the less concentrated draw solution. Unlike the RO system, FO process does not require a significant energy input. Energy consumption will be needed only for the water purification at second separation unit and for the regeneration of the draw solution. FO has been studied for applications such as water and wastewater treatments, sea/brackish water desalination, food processing, drug delivery, and electric power production (Chung et al., 2012; Zhao et al., 2012). Focus has been made in the development of robust and efficient membranes and the development of draw solutions that can induce high osmotic pressure with low energy requirements for regeneration or reconcentration (Achilli et al., 2010; Ling et al., 2010; McCutcheon et al., 2006). The differences between RO and FO are listed in Table 2.3 (Chung et al., 2012).

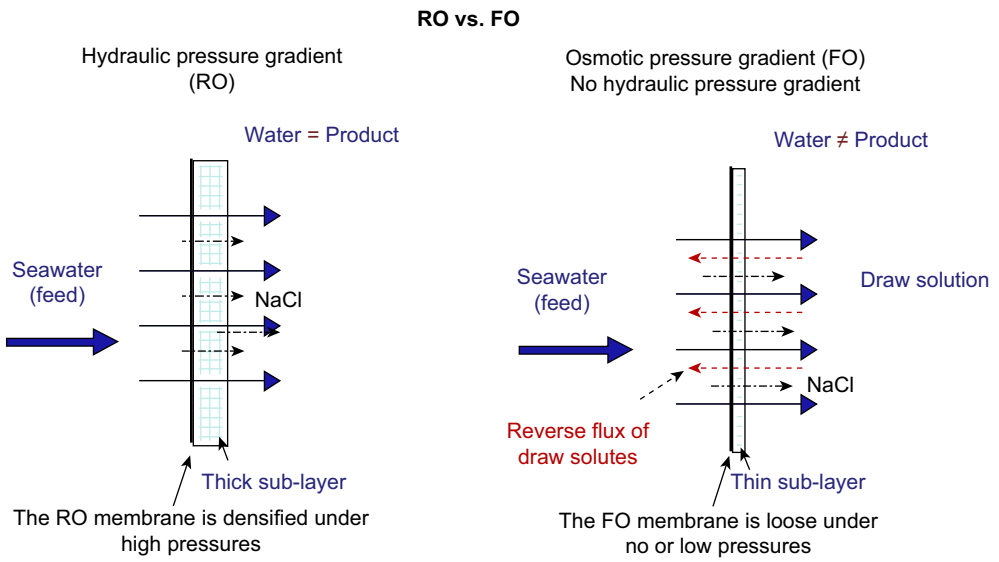

Figure 2.11
Difference between reverse osmosis and forward osmosis. *From Chung et al., 2012. With permission from Elsevier.*

Table 2.3: Main difference between reverse osmosis (RO) and forward osmosis (FO) systems.

Process	Advantages	Disadvantages	Challenges
FO	• Less energy intensive for water transport across the semipermeable membrane • More reversible fouling	• Permeate water product • Requires a second separation step	• Ineffective membranes • Lack of cost-effective draw solutes • Limited studies on fouling
RO	Permeate water = high-quality product	• High energy consumption • Some irreversible fouling	• How to improve energy recovery efficiency • How to mitigate membrane fouling

From Chung, T.S., Li, X., Ong, R.C., Ge, Q., Wang, H., Han, G., 2012. Emerging forward osmosis (FO) technologies and challenges ahead for clean water and clean energy applications. Curr. Opin. Chem. Eng. 1 (3), 246–257. With permission from Elsevier.

2.5.3 Examples of Partial Pressure–Driven Membrane Operations

This section explains the examples of membrane processes that separate using a partial pressure difference. Gas separation and membrane distillation (MD) are membrane applications that used partial pressure to perform separation processes. The principles of both operations are as follows.

2.5.3.1 Gas Separation

Gas separation mostly uses nonporous/isotropic membranes (Pandey and Chauhan, 2001; Seo et al., 2006). In the process of preparing the membrane for gas separation, defects can occur, which reduce the membrane performance. Therefore, the top surface of the membrane is coated with a very thin layer to seal the defects. The coating layer has the function to remove defect but does not contribute to the intrinsic separation properties of the membranes. There is another membrane for gas separation, which uses a composite coating as a selective layer. The material is used to facilitate the intrinsic separation properties of the membranes but the original microporous membrane is only a support for the material (Budd et al., 2005). This type of membrane is mainly applied for the separation of O_2/N_2 and volatile organic compounds (VOCs/N_2). Compared with conventional technology used in gas separation, membrane technology offers minimal operating cost. Gas separation using membranes does not require gas-to-liquid (GTL) phase change in the gas mixture, thus, significantly decreasing the energy costs. Gas separation membranes have been successfully applied in hydrogen separation, CO_2 capture, organic vapor removal, and natural gas separation.

For gas separation, the gas permeation mechanism can be explained using the Knudsen diffusion, surface diffusion, multilayer diffusion, capillary condensation, or molecular sieving (i.e., configurational diffusion). These mechanisms are strongly dependent on the pore size, the pore size distribution of the membrane, operating temperature and pressure,

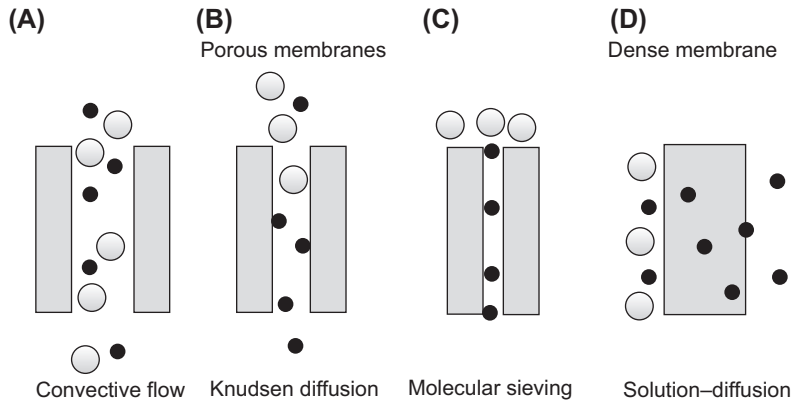

Figure 2.12
Different mechanisms of gas separation through porous membrane and dense membrane. (A) Convective flow. (B) Knudsen diffusion. (C) Molecular sieving (D) Solution-diffusion. *From Khatib and Oyama, 2011. With permission from Elsevier.*

and the nature of the membrane and the permeating molecules (Pandey and Chauhan, 2001; Baker, 2002). Knudsen diffusion is a likely mechanism to control the transport rate if the pore diameter is smaller than the mean free path of the molecule involved. In this case, the gases permeate in proportion to their molecular velocity, and hence in inverse proportion to the square root of their molecular weight. If the gasses are strongly adsorbed in the membrane pores, surface diffusion will enhance the permeation rate relative to the Knudsen diffusion. Molecular sieving mechanism may take place if the membrane pores are roughly similar to the diameter of the gas molecule. This mechanism is characterized by strong temperature dependence. Through this mechanism, larger gas molecules will experience a sharp decline in permeability. The different mechanisms for gas separation are shown in Fig. 2.12 (Khatib and Oyama, 2011).

2.5.3.2 Membrane Distillation

MD relies primarily upon thermal evaporation at the feed/membrane interface. The microporous hydrophobic membrane is used to pass vapor, which later condensed on permeate side. The rejection of nonvolatile compounds is theoretically 100%; however, if feed contains volatile substances, they will pass through the membrane together with water vapor. MD operates on the principle of vapor−liquid equilibrium as a basis for separation. The driving force of the process is supplied by the vapor pressure difference caused by temperature gradient imposed between the liquid and vapor interfaces (Alkhudhiri et al., 2012; Alklaibi and Lior, 2005; Curcio and Drioli, 2005; El-Bourawi et al., 2006).

MD separates contaminants from aqueous solutions and yields highly purified permeate. MD process can be used as a substitute for conventional desalination process in producing

pure water. Compared with other processes, MD has various advantages. MD that possesses low operating feed temperature enables the use of waste heat as a preferable energy source. This system also requires lower vapor space compared with traditional distillation. Furthermore, MD requires no external pressure applied as a driving force and possesses almost a complete rejection of dissolved and nonvolatile species. The performance of the membrane is not limited by high osmotic pressure or concentration polarization (Gryta, 2008; Srisurichan et al., 2005; Warsinger et al., 2015). Although MD technology has advantages over other membrane technologies, the main obstacles that slow the implementation of MD are lack of membranes design, membrane wettability, cost of feed heating, and rather low permeate flux (Gryta, 2008; Srisurichan et al., 2005; Warsinger et al., 2015).

2.6 Fouling Issues

Fouling is a major concern especially in the pressure-driven membrane separation processes. Membrane fouling is a result of the concentration polarization and pore blocking that reduces membrane performance. The effects of membrane fouling are permeate flux reduction, shortening of the membrane life span, and incurring of high cost due to the high TMP (Marchese et al., 2003; Sablani et al., 2001). A concentration gradient is created between the concentrations of nonpermeating species with adjacent fluid at the outer surface of the membrane, and this occurrence is known as concentration polarization (reversible) (Lowe and Hossain, 2008; Yuan and Zydney, 2000). Pore blocking occurs when the particulates or solutes with small size distributions are introduced to membrane's body, and this can cause severe fouling (De Barros et al., 2003; Hwang and Lin, 2002).

Fouling can be categorized into organic fouling, inorganic fouling (scaling), biological fouling, and colloidal fouling. Colloidal fouling is common in membrane processes, which can be regarded as the most serious fouling problem. Organic fouling occurs when natural organic matter (NOM) appears during the filtration process. Inorganic fouling can occur due to the precipitation of deposits on membrane resulting in bulk and membrane crystallization. Biological fouling occurs when biofilm forms on the membrane surface. This undesired phenomenon can be alleviated using solution-compatible membranes, i.e., highly hydrophilic membranes and low fouling membranes, as well as optimization of the pretreatment process.

Conventional cleaning can remove the fouling deposits but with low efficiency. To maintain the membrane performance, numerous conventional cleaning treatments have been used, specifically, biological, chemical, and physical treatments. Physical treatment has the ability to remove loose particles attached to the surface of the membranes, whereas chemical cleaning is used to remove the adhered particles, and biological cleaning involves the use of bioactive species such as enzymes. The conventional backwashing process is illustrated in Fig. 2.13 (Singh, 2005). The summary of the physical and chemical cleaning treatment mechanisms is presented in Table 2.4 (Le and Nunes, 2016).

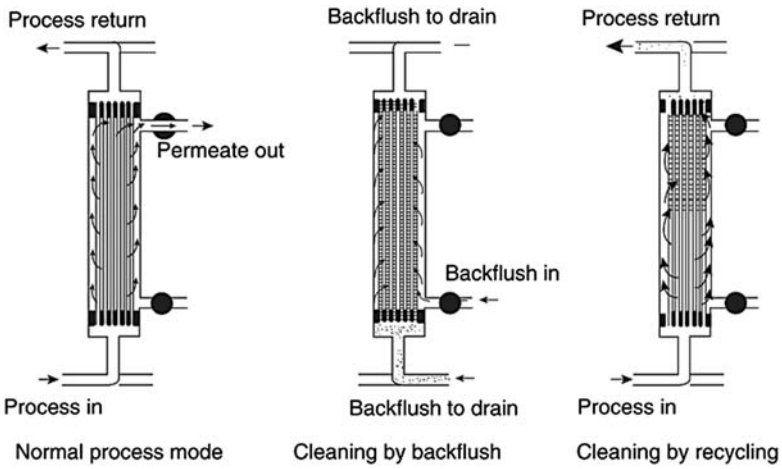

Figure 2.13
Backwashing in co-current flow. *From Singh, 2005. With permission from Elsevier.*

Table 2.4: Summary of different cleaning treatments.

Solution	Methods	Effects	Affecting Factors	Challenges
Pretreatment	Coagulation, precipitation, media filtration, sonication, boiling, membrane filtration, pH changes, and chlorination	Alter the physicochemical and/or biological properties of the feed water, and reduce the foulant concentration	Agent, temperature, dosing point, solution and foulant properties, and the characteristics of the membrane	Ineffective pretreatment can lead to high rates of membrane fouling
Operation optimization	Gas bubbling	Increase shear rate at the surface to intermittently remove fouling layers	Size of bubbles, gas flow rate	Mainly effective in addressing external membrane fouling
	Temperature and flow reversal	Inhibit the homogeneous precipitation of salts and disrupt the nucleation of salt crystals	Temperature, flow rate	No in-depth explanation on the nucleation kinetics and scale formation
Chemical treatment	Rinse with acid or base	Rinsing with acid is particularly effective in removing inorganic scaling, whereas rinsing with base is relatively effective in reducing organic fouling	Type, amount of agents	May cause membrane structural damage

From Le, N.L., Nunes, S.P., 2016. Materials and membrane technologies for water and energy sustainability. Sustain. Mater. Technol. 7, 1–28. With permission from Elsevier.

2.7 Conclusions and Future Trends

This chapter provides a comprehensive discussion on membranes and the membrane processes to provide an insightful understanding on the membrane fundamental principles. The membrane technology has expanded and emerged as the viable separation systems based on its simple concept and operation, modular nature, ease to scale-up, cost and space-saving properties, and most importantly, low energy consumption. Research and development of this technology is growing for a wide range of industrial applications, i.e., wastewater treatment, gas separation, oil recovery, chemical conversions, etc.

List of Symbols

$\alpha_{A/B}$ Selectivity factor
J Nonsolvent flux
ΔP Transmembrane pressure

List of Abbreviations

CA Cellulose acetate
DMAC N,N-dimethylacetamide
DMF Dimethylformamide
DMSO Dimethylsulfoxide
FO Forward osmosis
GTL Gas-to-liquid
MF Microfiltration
MIEC Mixed ionic−electronic conduction
MD Membrane distillation
MW Molecular weight
NF Nanofiltration
NMMO N-methylmorpholine-N-oxide
NMP N-methylpyrrolidone
NOM Natural organic matter
ppm Part per million
PSF Polysulfone
PES Polyethersulfone
PEI Polyetherimide
PA Polyamide
PAN Polyacrylonitrile
PP Polypropylene
PTFE Polytetrafluoroethylene
PVA Poly(vinyl alcohol)
PVDF Polyvinylidene fluoride
RO Reverse osmosis
TIPS Thermally induced phase separation
TEP Triethyl phosphate
TMP Transmembrane pressure
UF Ultrafiltration
USA United States of America
VOC Volatile organic compound

Acknowledgments

The authors gratefully acknowledge financial support from various parties, namely, Higher Institution Centre of Excellence (HICoE) Research Grant (R. J090301.7846.4J176) and Universiti Teknologi Malaysia (UTM) through the Research University grants (Q.J130000.2446.03G37, Q.J130000.2546.12H22). Appreciation also goes to UTM Research Management Centre for both financial and technical support.

References

Achilli, A., Cath, T.Y., Childress, A.E., 2010. Selection of inorganic-based draw solutions for forward osmosis applications. J. Membr. Sci. 364 (1−2), 233−241.

Ahmad, A.L., Sarif, M., Ismail, S., 2005. Development of an integrally skinned ultrafiltration membrane for wastewater treatment: effect of different formulations of PSf/NMP/PVP on flux and rejection. Desalination 179, 257−263.

Alkhudhiri, A., Darwish, N., Hilal, N., 2012. Membrane distillation: a comprehensive review. Desalination 287, 2−18.

Alklaibi, A.M., Lior, N., 2005. Membrane-distillation desalination: status and potential. Desalination 171 (2), 111−131.

Baker, R.W., 2002. Future directions of membrane gas separation technology. Ind. Eng. Chem. Res. 41 (6), 1393−1411.

Baker, R.W., 2012. Membrane Technology and Applications, third ed. John Wiley and Sons, Chichester, UK.

Barth, C., Gonçalves, M.C., Pires, A.T.N., Roeder, J., Wolf, B.A., 2000. Asymmetric polysulfone and polyethersulfone membranes: effects of thermodynamic conditions during formation on their performance. J. Membr. Sci. 169 (2), 287−299.

Budd, P.M., Msayib, K.J., Tattershall, C.E., Ghanem, B.S., Reynolds, K.J., McKeown, N.B., Fritsch, D., 2005. Gas separation membranes from polymers of intrinsic microporosity. J. Membr. Sci. 251 (1−2), 263−269.

Buonomenna, M.G., 2013. Membrane processes for a sustainable industrial growth. RSC Adv. 3 (17), 5694.

Cao, C., Chung, T.S., Chen, S.B., Dong, Z., 2004. The study of elongation and shear rates in spinning process and its effect on gas separation performance of Poly(ethersulfone) (PES) hollow fiber membranes. Chem. Eng. Sci. 59, 1053−1062.

Cath, T.Y., Childress, A.E., Elimelech, M., 2006. Forward osmosis: principles, applications, and recent developments. J. Membr. Sci. 281 (1−2), 70−87.

Chen, Z., Deng, M., Chen, Y., He, G., Wu, M., Wang, J., 2004. Preparation and performance of cellulose acetate/polyethyleneimine blend microfiltration membranes and their applications. J. Membr. Sci. 235 (1−2), 73−86.

Chung, T.S., Li, X., Ong, R.C., Ge, Q., Wang, H., Han, G., 2012. Emerging forward osmosis (FO) technologies and challenges ahead for clean water and clean energy applications. Curr. Opin. Chem. Eng. 1 (3), 246−257.

Curcio, E., Drioli, E., 2005. Membrane distillation and related operations—a review. Separ. Purif. Rev. 34 (1), 35−86.

De Barros, S.T.D., Andrade, C.M.G., Mendes, E.S., Peres, L., 2003. Study of fouling mechanism in pineapple juice clarification by ultrafiltration. J. Membr. Sci. 215 (1−2), 213−224.

El-Bourawi, M.S., Ding, Z., Ma, R., Khayet, M., 2006. A framework for better understanding membrane distillation separation process. J. Membr. Sci. 285 (1−2), 4−29.

El-ghaffar, M.A.A., Tieama, H.A., 2017. A review of membranes classifications, configurations, surface modifications, characteristics and its applications in water purification. Chem. Biomol. Eng. 2 (2), 57−82.

Fujishima, A., Rao, T.N., Tryk, D.A., 2000. Titanium dioxide photocatalysis. J. Photochem. Photobiol. C Photochem. Rev. 1, 1−21.

Gao, X., Diniz da Costa, J.C., Bhatia, S.K., 2014. Adsorption and transport of gases in a supported microporous silica membrane. J. Membr. Sci. 460, 46−61.

Giorno, L., Drioli, E., 2000. Biocatalytic membrane reactors: applications and perspectives. Trends Biotechnol. 18 (8), 339−349.

Gryta, M., 2008. Fouling in direct contact membrane distillation process. J. Membr. Sci. 325 (1), 383−394.

Gu, M., Zhang, J., Wang, X., Tao, H., Ge, L., 2006. Formation of poly(vinylidene fluoride) (PVDF) membranes via thermally induced phase separation. Desalination 192 (1−3), 160−167.

Han, M.J., Nam, S.T., 2002. Thermodynamic and rheological variation in polysulfone solution by PVP and its effect in the preparation of phase inversion membrane. J. Membr. Sci. 202 (1−2), 55−61.

Hasbullah, H., Kumbharkar, S., Ismail, A.F., Li, K., 2011. Preparation of polyaniline asymmetric hollow fiber membranes and investigation towards gas separation performance. J. Membr. Sci. 366, 116−124.

Hsieh, H.P., 1991. Inorganic membrane reactor. Catal. Revi. Sci. Eng 33 (1), 1−70.

Hwang, K.J., Lin, T.T., 2002. Effect of morphology of polymeric membrane on the performance of cross-flow microfiltration. J. Membr. Sci. 199 (1−2), 41−52.

Jamil, S.M., Othman, M.H.D., Rahman, M.A., Jaafar, J., Ismail, A.F., Li, K., 2015. Recent fabrication techniques for micro-tubular solid oxide fuel cell support : a review. J. Eur. Ceram. Soc. 35, 1−22.

Jiang, Q., Faraji, S., Slade, D.A., Stagg-williams, S.M., 2011. A Review of Mixed Ionic and Electronic Conducting Ceramic Membranes as Oxygen Sources for High-Temperature Reactors, first ed. Elsevier BV.

Judd, S., Jefferson, B., 2003. Membrane Technology. Membranes for Industrial Wastewater Recovery and Re-use: 3.1 the Power Industry, first ed. Elsevier Ltd, UK.

Kang, G., Cao, Y., 2012. Development of antifouling reverse osmosis membranes for water treatment: a review. Water Res. 46 (3), 584−600.

Kawaguchi, M., Makino, K., Kato, T., 1997. Viscous fingering patterns in polymer solutions. Physica D 109 (3−4), 325−332.

Khatib, S.J., Oyama, S.T., 2011. Review of silica membranes for hydrogen separation prepared by chemical vapor deposition. Membr. Sci. Technol. 14, 25−60.

Khayet, M., Feng, C.Y., Khulbe, K.C., Matsuura, T., 2002. Preparation and characterization of polyvinylidene fluoride hollow fiber membranes for ultrafiltration. Polymer 43, 3879−3890.

Kong, J., Li, K., 2001. Preparation of PVDF hollow-fiber membranes via immersion precipitation. J. Appl. Polym. Sci. 81 (7), 1643−1653.

Lalia, B.S., Kochkodan, V., Hashaikeh, R., Hilal, N., 2013. A review on membrane fabrication: structure, properties and performance relationship. Desalination 326, 77−95.

Le, N.L., Nunes, S.P., 2016. Materials and membrane technologies for water and energy sustainability. Sustain. Mater. Technol. 7, 1−28.

Lee, A., Darling, S.B., 2016. Membrane materials for water purification: design, development, and application. Environ. Sci. Water Res. Technol. 2 (1), 17−42.

Lee, K.P., Arnot, T.C., Mattia, D., 2011. A review of reverse osmosis membrane materials for desalination-Development to date and future potential. J. Membr. Sci. 370 (1−2), 1−22.

Li, K., 2007. Ceramic Membranes for Separation and Rection. In: UK (Ed.), second ed. John Wiley and Sons.

Li, S., Koops, G.H., Mulder, M.H.V., Boomgaard, T.V.D., Smolders, C.A., 1994. Wet spinning of integrally skinned hollow fiber membranes by a modified dual-bath coagulation method using a triple orifice spinneret. J. Membr. Sci. 94, 329−340.

Li, C.L., Wang, D.M., Deratani, A., Quémener, D., Bouyer, D., Lai, J.Y., 2010. Insight into the preparation of poly(vinylidene fluoride) membranes by vapor-induced phase separation. J. Membr. Sci. 361 (1−2), 154−166.

Ling, M.M., Wang, K.Y., Chung, T.S., 2010. Highly water-soluble magnetic nanoparticles as novel draw solutes in forward osmosis for water reuse. Ind. Eng. Chem. Res. 49 (12), 5869−5876.

Liu, H., Hsieh, Y.L., 2002. Ultrafine fibrous cellulose membranes from electrospinning of cellulose acetate. J. Polym. Sci. B Polym. Phys. 40 (18), 2119–2129. https://doi.org/10.1002/polb.10261.

Loeb, S., Sourirajan, S., 1963. Seawater demineralization by means of osmotic membrane. Advances in Chemistry Series 38, 117–132.

Lonsdale, H.K., 1982. The growth of membrane technology. J. Membr. Sci. 10 (2–3), 81–181.

Lowe, J., Hossain, M.M., 2008. Application of ultrafiltration membranes for removal of humic acid from drinking water. Desalination 218 (1–3), 343–354.

Lu, G.Q., Diniz da Costa, J.C., Duke, M., Giessler, S., Socolow, R., Williams, R.H., Kreutz, T., 2007. Inorganic membranes for hydrogen production and purification: a critical review and perspective. J. Colloid Interface Sci. 314 (2), 589–603.

Malaeb, L., Ayoub, G.M., 2011. Reverse osmosis technology for water treatment: state of the art review. Desalination 267 (1), 1–8.

Manicone, P.F., Rossi Iommetti, P., Raffaelli, L., 2007. An overview of zirconia ceramics: basic properties and clinical applications. J. Dent. 35 (11), 819–826.

Marchese, J., Ponce, M., Ochoa, N.A., Prádanos, P., Palacio, L., Hernández, A., 2003. Fouling behaviour of polyethersulfone UF membranes made with different PVP. J. Membr. Sci. 211, 1–11.

Matsuyama, H., Yuasa, M., Kitamura, Y., Teramoto, M., Lloyd, D.R., 2000. Structure control of anisotropic and asymmetric polypropylene membrane prepared by thermally induced phase separation. J. Membr. Sci. 179, 91–100.

Matsuyama, H., Okafuji, H., Maki, T., Teramoto, M., Kubota, N., 2003. Preparation of polyethylene hollow fiber membrane via thermally induced phase separation. J. Membr. Sci. 223 (1–2), 119–126.

McCutcheon, J.R., McGinnis, R.L., Elimelech, M., 2006. Desalination by ammonia-carbon dioxide forward osmosis: influence of draw and feed solution concentrations on process performance. J. Membr. Sci. 278 (1–2), 114–123.

Meng, X., Gong, X., Yang, N., Tan, X., Yin, Y., Ma, Z.F., 2013. Fabrication of Y2O3-stabilized-ZrO_2(YSZ)/$La_{0.8}Sr_{0.2}MnO_{3-\alpha}$-YSZ dual-layer hollow fibers for the cathode-supported micro-tubular solid oxide fuel cells by a co-spinning/co-sintering technique. J. Power Sources 237, 277–284.

Menut, P., Su, Y.S., Chinpa, W., Pochat-Bohatier, C., Deratani, A., Wang, D.M., Huguet, P., Kuo, C.Y., Lai, J.Y., Dupuy, C., 2008. A top surface liquid layer during membrane formation using vapor-induced phase separation (VIPS)-Evidence and mechanism of formation. J. Membr. Sci. 310 (1–2), 278–288.

Mulder, M., 1996. Basic Principles of Membrane Technlogy. Kluwer Academic Publishers, Boston, London.

Pandey, P., Chauhan, R.S., 2001. Membranes for gas separation. Prog. Polym. Sci. 26 (6), 853–893.

Peinemann, K.-V., Abetz, V., Simon, P.F.W., 2007. Asymmetric superstructure formed in a block copolymer via phase separation. Nat. Mater. 6 (12), 992–996.

Peng, Y., Han, H., Fan, H.W., 2007. Characterization and performance of PVA/PSf composite hollow fiber UF membrane prepared with interfacial polymerization. Engineering 47, 21–25.

Peng, N., Widjojo, N., Sukitpaneenit, P., Teoh, M.M., Lipscomb, G.G., Chung, T.S., Lai, J.Y., 2012. Evolution of polymeric hollow fibers as sustainable technologies: past, present, and future. Prog. Polym. Sci. 37 (10), 1401–1424.

Pinnau, I., Freeman, B.D., 1999. Formation and Modification of Polymeric Membranes: Overview. Membrane Formation and Modification. In: ACS Symposium Series, vol. 744. American Chemical Society, Washington, DC, pp. 1–22.

Puskelova, J., Baia, L., Vulpoi, A., Baia, M., Antoniadou, M., Dracopoulos, V., Stathatos, E., Gabor, K., Pap, Z., Danciu, V., Lianos, P., 2014. Photocatalytic hydrogen production using TiO_2–Pt aerogels. Chem. Eng. J. 242, 96–101.

Rajabzadeh, S., Maruyama, T., Sotani, T., Matsuyama, H., 2008. Preparation of PVDF hollow fiber membrane from a ternary polymer/solvent/nonsolvent system via thermally induced phase separation (TIPS) method. Separ. Purif. Technol. 63 (2), 415–423.

Sablani, S., Goosen, M., Al-Belushi, R., Wilf, M., 2001. Concentration polarization in ultrafiltration and reverse osmosis: a critical review. Desalination 141 (3), 269–289.

Samuel, A.Z., Umapathy, S., Ramakrishnan, S., 2011. Functionalized and postfunctionalizable porous polymeric films through evaporation-induced phase separation using mixed solvents. ACS Appl. Mater. Interf. 3 (9), 3293−3299.

Schwinge, J., Neal, P.R., Wiley, D.E., Fletcher, D.F., Fane, A.G., 2004. Spiral wound modules and spacers: review and analysis. J. Membr. Sci. 242 (1−2), 129−153.

Seo, Y., Kim, S., Hong, S.U., 2006. Highly selective polymeric membranes for gas separation. Polym. Commun. 47, 4501−4504.

Singh, R., 2005. Water and membrane treatment. Hybrid Membr. Syst. Water Purif. 1, 57−130.

Smolders, C.A., Reuvers, A.J., Boom, R.M., Wienk, I.M., 1992. Microstructures in phase-inversion membranes. Part 1. Formation of macrovoids. J. Membr. Sci. 73 (2−3), 259−275.

Song, H., Shao, J., He, Y., Liu, B., Zhong, X., 2012. Natural organic matter removal and flux decline with PEG-TiO_2-doped PVDF membranes by integration of ultrafiltration with photocatalysis. J. Membr. Sci. 405−406, 48−56.

Srisurichan, S., Jiraratananon, R., Fane, A.G., 2005. Humic acid fouling in the membrane distillation process. Desalination 174 (1), 63−72.

Strathmann, H., Kock, K., Amar, P., Baker, R.W., 1975. The formation mechanism of asymmetric membranes. Desalination 16 (2), 179−203.

Su, Y.S., Kuo, C.Y., Wang, D.M., Lai, J.Y., Deratani, A., Pochat, C., Bouyer, D., 2009. Interplay of mass transfer, phase separation, and membrane morphology in vapor-induced phase separation. J. Membr. Sci. 338 (1−2), 17−28.

Susanto, H., Ulbricht, M., 2009. Characteristics, performance and stability of polyethersulfone ultrafiltration membranes prepared by phase separation method using different macromolecular additives. J. Membr. Sci. 327 (1−2), 125−135.

Tanaka, T., Lloyd, D.R., 2004. Formation of poly(L-lactic acid) microfiltration membranes via thermally induced phase separation. J. Membr. Sci. 238 (1−2), 65−73.

Tsai, J.T., Su, Y.S., Wang, D.M., Kuo, J.L., Lai, J.Y., Deratani, A., 2010. Retainment of pore connectivity in membranes prepared with vapor-induced phase separation. J. Membr. Sci. 362 (1−2), 360−373.

Ulbricht, M., 2006. Advanced functional polymer membranes. Polymer 47 (7), 2217−2262.

Van Der Bruggen, B., Vandecasteele, C., Van Gestel, T., Doyen, W., Leysen, R., 2003. A review of pressure-driven membrane processes in wastewater treatment and drinking water production. Environ. Prog. 22 (1), 46−56.

Wang, D.M., Lai, J.Y., 2013. Recent advances in preparation and morphology control of polymeric membranes formed by nonsolvent induced phase separation. Curr. Opin. Chem. Eng. 2 (2), 229−237.

Wang, X., Zhang, L., Sun, D., An, Q., Chen, H., 2009. Formation mechanism and crystallization of poly(vinylidene fluoride) membrane via immersion precipitation method. Desalination 236 (1−3), 170−178.

Wang, L.K., Chen, J.P., Hung, Y.T., Shammas, N.K. (Eds.), 2011. Membrane and Desalination Technologies. Humana Press, London.

Warsinger, D.M., Swaminathan, J., Guillen-Burrieza, E., Arafat, H.A., Lienhard, V.J.H., 2015. Scaling and fouling in membrane distillation for desalination applications: a review. Desalination 356, 294−313.

Wei, C.C., Li, K., 2008. Yttria-Stabilized Zirconia (YSZ) -based hollow fiber solid oxide fuel cells. Ind. Eng. Chem. Res. 47 (5), 1506−1512.

Xu, Z.L., Qusay, F.A., 2004. Polyethersulfone (PES) hollow fiber ultrafiltration membranes prepared by PES/non-solvent/NMP solution. J. Membr. Sci. 233 (1−2), 101−111.

Xu, L., Zhang, C., Rungta, M., Qiu, W., Liu, J., Koros, W.J., 2014. Formation of defect-free 6FDA-DAM asymmetric hollow fiber membranes for gas separations. J. Membr. Sci. 459, 223−232. https://doi.org/10.1016/j.memsci.2014.02.023.

Yamamura, M., Nishio, T., Kajiwara, T., Adachi, K., 2002. Evaporation-induced pattern formation in polymer films via secondary phase separation. Chem. Eng. Sci. 57 (15), 2901−2905.

Yuan, W., Zydney, A.L., 2000. Humic acid fouling during ultrafiltration. Environ. Sci. Technol. 34 (23), 5043−5050.

Yuliwati, E., Ismail, A.F., 2011. Effect of additives concentration on the surface properties and performance of PVDF ultrafiltration membranes for refinery produced wastewater treatment. Desalination 273 (1), 226−234.

Zhao, S., Zou, L., Tang, C.Y., Mulcahy, D., 2012. Recent developments in forward osmosis: opportunities and challenges. J. Membr. Sci. 396, 1−21.

CHAPTER 3

Materials and Design of Photocatalytic Membranes

Xiaofang Chen[1,2], Yaoxin Hu[1,2], Zongli Xie[1,2], Huanting Wang[1,2]
[1]Monash University, Clayton, VIC, Australia; [2]CSIRO Manufacturing, Clayton, VIC, Australia

3.1 Introduction

Global warming, air and water pollution, rising energy shortages are expected to get worse if not properly solved in the coming decades. It is an urgent task to develop sustainable strategies for two of the global issues: environmental remediation and clean energy. Photocatalytic membrane technology is a promising technology for environment restoration (Elahifard et al., 2007; Horng et al., 2009; Liu et al., 2016a,b,c) and power generation in a green and renewable way (Irie et al., 2003; Derichter et al., 2013; Yang et al., 2013; Liu et al., 2016a,b,c; Padmanaban et al., 2016). The conventional approaches of decontamination usually involve a huge amount of chemical and energy consumption. Photocatalysis could be used for the removal of organic or inorganic pollutants from the environment by a photooxidizing process driven by light, which takes place at ambient temperature and without requiring other energy inputs (Thiruvenkatachari et al., 2005; Mitoraj and Kisch, 2008; Tacchini et al., 2011; Chen et al., 2016). Solar hydrogen can be obtained from the photocatalytic water splitting reaction. It is potentially the most abundant and sustainable energy because water as the fuel precursor and solar light as the driving force are both plentiful on Earth (Prodhomme et al., 2010; Yang et al., 2013; Sasaki et al., 2013). Besides, photocatalytic reduction of CO_2 into fuels by solar energy is attractive to simultaneously capture the major greenhouse gas and address the shortage of energy.

Membrane technology exhibits various distinct characteristics such as low chemical and energy consumption, automatic control, and steady operation, which lead it to be a desirable candidate in industrial applications (Kim et al., 2006; Han et al., 2010; Liu et al., 2010). Membranes can be used in continuous processes with low maintenance costs and facile scaling-up by a simple connection between different membrane modules (Roso et al., 2011; Jhaveri and Murthy, 2016). Besides, membrane technology can solve the separation of photocatalysts in practical applications. Fundamentally, a membrane is

Current Trends and Future Developments on (Bio-) Membranes. https://doi.org/10.1016/B978-0-12-813549-5.00003-7

essentially considered as a physical wall, which isolates different phases and restrains the transfer of different species with special characteristics in an individually selective procedure (Huo et al., 2013; Yee et al., 2015). Combining membrane and photocatalytic technology has been proposed recently, namely photocatalytic membrane (Bosc et al., 2003, 2004, 2005; Choi et al., 2006). New developments in design and manufacturing of photocatalytic membranes have made a great contribution to the photocatalytic application. Hybridizing photocatalysis with membrane offers photocatalytic reaction and products separation in a single step and well control of the products and by-products retention (Thiruvenkatachari et al., 2005; Lee et al., 2006; Zamfirescu et al., 2011). Photocatalytic membranes used in reaction systems save considerable energy and time, making significant contributions to enhancing photocatalytic processes. Photocatalytic membranes have great potential for water purification, wastewater treatment, and self-cleaning applications because of their antifouling, antimicrobial, and superhydrophilic properties, as well as concurrent photocatalytic oxidation and separation (Ziegmann et al., 2010; Papageorgiou et al., 2012; Ahmad et al., 2016).

However, we are still facing the challenges in exploring the feasibility of hybridizing membrane with photocatalytic technology for practical application. The current key issues for the application of photocatalytic hybrid membrane are how to develop systems that deal with sensible flows while ensuring all of the photocatalyst particles are active and how to make sure the membrane resistance to fouling. Fouling is a process of adsorption or deposition of particles, colloids, salt, macromolecules on the surface or inside pores of membranes, causing a decrease of permeation flux, selectivity, and separability of the membrane and even shortening the membrane life. It has been demonstrated that the intrinsic hydrophobicity of membrane materials is one of the main reasons for fouling because organic foulants can be easily adsorbed on the hydrophobic membrane. The simple cleaning or backwashing cannot remove these organic foulants. To solve this problem, many efforts have been devoted to improve the surface properties of the membrane in the fabrication process. Besides, Zhang et al. (2006b) found that some polymeric membrane substrates could not endure the UV light irradiation, which caused damages to the membrane in applications. Various technical problems were encountered, such as membrane structure deterioration, loss of deposited photocatalyst layer in application processes, and low photocatalytic activity. Coupling photocatalysis with pressure-driven membrane processes induced a decrease of the permeate flux owing to membrane fouling (Huo et al., 2013). All of these problems need to be addressed before photocatalytic membranes become a viable technology for industrial processes.

The aim of the chapter is to summarize the general features of the materials for photocatalytic membranes and the fabrication of photocatalytic membranes.

3.2 Design of Photocatalytic Membrane

The photocatalytic membrane is attractive because the photocatalytic reaction can take place on the surface of the membrane without the aggregation of nanosized particles, difficulty in recycling use, and the loss of photocatalyst particles. In the photocatalytic membrane, the membrane functions as a barrier to separate different phases and control the mass transport between them, facilitating the separation of products and hence enhancing the photocatalytic efficiency. The photodegradation of organic pollutants may improve the permeate quality of membrane. Therefore, the introduction of photocatalyst into conventional membrane reduces also the membrane fouling in wastewater treatment process (Mozia et al., 2007; Li et al., 2017). However, immobilization of photocatalysts usually causes a loss of photocatalytic activity compared with the suspended system. The photocatalyst nanoparticles are likely to block the substrate pores in the membrane fabrication process. Moreover, the support should be strongly resistant to UV irradiation and oxidation by active radicals in photocatalytic reaction. Therefore, the selection of proper membrane and photocatalyst and the preparation method deserves more attention.

The substrates, designed materials, and preparation methods of photocatalytic membranes are discussed in the following sections.

3.2.1 Substrate of Photocatalytic Membrane

The materials for the production of photocatalytic membranes mainly depend on their thermal and chemical stability and on the corresponding application field. Most of the semiconductor photocatalysts are inorganic materials such as TiO_2, ZnO_2, Bi_2O_3, etc. (Madaeni and Ghaemi, 2007; Wang et al., 2011; Gan et al., 2013). Suitable polymers or ceramic substrates are required for fabrication of photocatalytic membranes. It is known that the most commonly studied membranes can be produced from different materials including polymer, metal, ceramic, or even zeolite (Bet-moushoul et al., 2016). Many polymers (Table 3.1) such as polyamide (PA), polysulfone (PS), polyethersulfone (PES),

Table 3.1: Summary of polymers used for membranes fabrication.

Name	Abbreviation	Formula
Cellulose acetate	CA	$(C_6H_7O_2(OH)_3)_n$
Polysulfone	PS	$(C_{27}H_{26}O_6S)$
Polyamide	PA	$(CONH_2)_n$
Polyvinylidene fluoride	PVDF	$(CH_2CF_2)_n$
Polyacrylonitrile	PAN	$(C_3H_3N)_n$
Polyethersulfone	PES	$C_6H_4{-}SO_2{-}C_6H_4{-}O)_n$
Polyvinylpyrrolidone	PVP	$(C_6H_9NO)_n$
Polyvinyl alcohol	PVA	$(C_2H_6O_2)_n$

polyvinylidene fluoride (PVDF), and polyvinylpyrrolidone (PVP) can be used to fabricate porous membrane substrate for photocatalysts (Bet-moushoul et al., 2016; Jhaveri and Murthy, 2016). Polymeric membranes have good thermal stability, high energy efficiency, and low price, which are attractive for industrial applications (Kim et al., 2003; Daels et al., 2014). However, some polymeric membranes could not resist against the UV irradiation and oxidation of active radicals in the photocatalytic process.

The ceramic membranes made of zirconia, alumina, or titania can work as the support for fabrication of photocatalytic membrane (Zhang et al., 2006b; Tian et al., 2012). Compared with polymeric membranes, ceramic membranes show higher durability in practical operation because of their excellent chemical and thermal stability and mechanical strength (Lu et al., 2004). However, the ceramic membranes are much more expensive than the common polymer membranes because of the high costs of raw materials and membrane fabrication.

Carbon-based materials have shown great potential to be fabricated into membranes. Carbon paper, carbon nanotube (CNT), and carbon fiber cloth (Table 3.2) were applied in photocatalytic membranes and membranes in fuel cells (Zhao et al., 2013; Li et al., 2014; Zhang et al., 2015). These carbon-based materials can be used in various fields, based on their different properties such as hydrophobicity, conductivity, resistance against corrosion, and mechanical stability (Li et al., 2017; Liu et al., 2014). Moreover, in contrast to the polymeric membranes, carbon-based membranes are resistant to UV light.

The photocatalysts are fabricated into membranes using different preparation methods even without any substrates. Some pure photocatalytic membranes, namely free-standing

Table 3.2: Summary of photocatalytic membranes with different substrates and their applications.

Type of Membrane	Application	References
TiO_2/Al_2O_3 composite membrane	Methylene blue (MB) degradation	Choi et al. (2006)
$FeTiO_2$/PS hybrid photocatalytic membrane	Removal of NO	Li et al. (2016)
$CoFe_2O_4$/rGO/PVDF/carbon paper membrane	Removal of tetracycline hydrochloride antibiotics	Li et al. (2017)
TiO_2 hollow fiber membrane	Acid orange 7 (AO7) degradation	Zhang et al. (2014)
TiO_2/carbon/Al_2O_3 membrane	Removal of natural organic matter	Wang et al. (2015)
CNT/ZnO/TiO_2 membrane	Removal of AO7	Bai et al. (2015b)
g-C_3N_4/rGO/CA membrane	Removal of rhodamine B (RhB)	Zhao et al. (2016)
Silica/titania nanorods/ nanotubes membrane	Removal of sodium dodecylbenzene sulfonate	Zhang et al. (2006c)
TiO_2/carbon paper membrane	Removal of MB	He et al. (2016)

CA, cellulose acetate; *CNT*, carbon nanotube; *PS*, polysulfone; *PVDF*, polyvinylidene fluoride; *rGO*, reduced graphene oxide.

photocatalytic membranes, have been explored (Zhang et al., 2006a; He et al., 2016). For instance, the one-dimensional and free-standing photocatalytic membranes were prepared (Liu et al., 2013); however, scaling up of such a one-dimensional photocatalytic membrane is still a big challenge.

3.2.2 Fabrication of Photocatalytic Membranes

To prepare a photocatalytic membrane, the most significant step is to attach photocatalysts or their precursors onto different supports. Various fabrication methods have been investigated, such as dip coating, spin coating, electrospinning, physical deposition (vacuum filtration) and immersion precipitation.

3.2.2.1 Dip Coating

Dip coating is a facile method and thus widely used to immobilize photocatalyst on either polymeric membranes or inorganic membranes. The polymeric membranes are preferred to be modified with as-prepared photocatalysts because the photocatalysts are often synthesized under harsh conditions such as high temperature and corrosive solution, under which polymeric membranes may be damaged. Fundamentally, dip coating is a capillary filtration process on a microscale. During the dipping, the porous surface of the support is wetted by the dispersion solution. The capillary suction induced by the porous structure drives the dispersed particles to concentrate at the substrate, forming a coating. In the preparation process, photocatalyst particles can be dispersed in a variety of solvents such as water, ethanol, and 2-propanol (Ziegmann et al., 2010). The solvent with low boiling point is more suitable for obtaining more uniform photocatalyst layer by dip coating, as its fast vaporization eases the immobilization of particles when the substrate is drying out of the suspension. Therefore, the dipping time is one of the main factors to determine the membrane structure. The number of dip-coating layers is another critical parameter in the producing process of a photocatalytic membrane from both scientific and engineering prospectives. Choi et al. (2006) confirmed that increasing the membrane thickness could bring better results in terms of adsorption capacity and photocatalytic performance of the photocatalytic membrane to some extent, yet it caused the increase of synthesis time and cost. However, these photocatalytic membranes with multiple dip-coated layers of photocatalysts should have highly porous and interconnected structure for the free migration of reactants in a photocatalytic process; otherwise, the inner-layer photocatalyst could be a shield from the light illumination. Besides, increasing the membrane thickness via multicoatings could enhance organic retention to a large extent but could also increase the filtration resistance and possibility for crack formation in wastewater treatment systems. The permeability of TiO_2/Al_2O_3 membrane decreased from 11.0 L m^{-2} h^{-1} bar^{-1} for the alumina support to 3.55 L m^{-2} h^{-1} bar^{-1} for five coating layers of TiO_2.

In practical application, the high shear stress induced by the filtration velocity or long-term operations is likely to result in the detachment of photocatalyst particles, and hence the photocatalytic membrane would likely lose its properties. To solve this problem, Kim et al. (2003) prepared an aromatic PA support with the COOH functional group. This polymer substrate was dipped in the transparent TiO_2 colloidal solution to deposit TiO_2 particles on the membrane surface. The coordination and the H-bonding interaction between TiO_2 and functional groups drove the TiO_2 particles self-assembled on a polymer substrate with sufficient binding strength for the actual application (Fig. 3.1). Optimizing combination of preparation conditions, such as polymer solution concentration, cross-linking agent concentration, dipping time, can yield better composite membrane.

In the case of inorganic membranes such as ceramic membranes, the precursors of photocatalysts can be uniformly dip-coated on their surface and the photocatalysts would be tightly attached on the surface or inside of the porous supports by further heat annealing. The heating process greatly improves the adhesion between the photocatalysts and their supports. Therefore, the photocatalytic membranes synthesized by this process show good reusability. For instance, the Al_2O_3 membrane was dipped in TiO_2 sol solution, followed by heating treatment to form anatase TiO_2 layer on the membrane (Zhang et al., 2006b). Controlling the immersing time and dipping time could lead to a well-defined TiO_2 layer with high photocatalytic activity and permeation flux. During the dip coating process, the photocatalyst nanoparticles can be adsorbed onto the membrane surface and the walls of membrane pores, which easily cause the decrease of the water flux. Matching the nanoparticle size of photocatalysts with a pore size of the membrane is important to prevent these nanoparticles from blocking the pores.

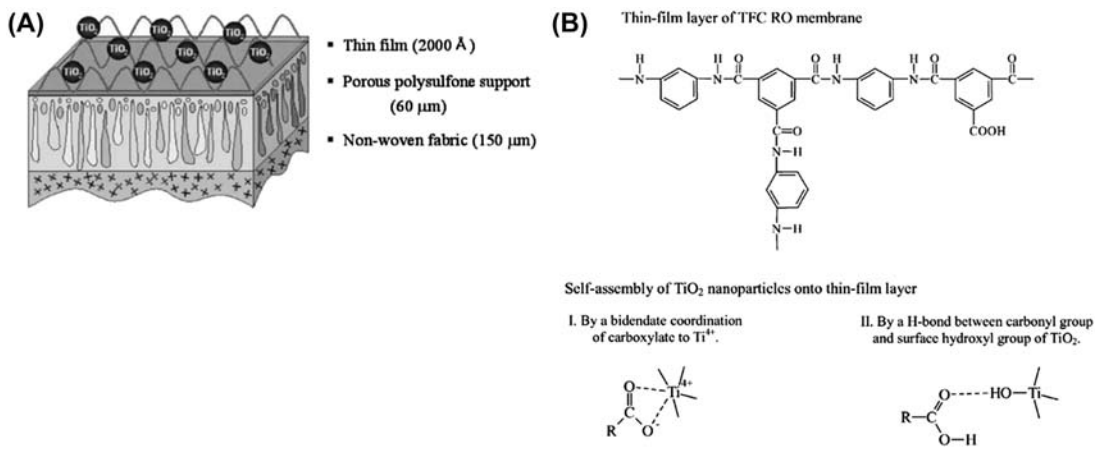

Figure 3.1

(A) Schematic drawing of the hybrid membrane; (B) Mechanism of self-assembly of TiO_2 nanoparticles. *Reprinted with permission from Kim et al., 2003, copyright 2003, Elsevier.*

3.2.2.2 Spin Coating

Spin coating is a laboratory technique for rapidly producing membranes. In general, this technique is used to prepare thin membranes by spinning out the precursor solution over the edge of the support. The process is to add the coating solution onto the surface of support, and the centrifugal force drives the solution to spread in a thin film where the solvent rapidly evaporates to produce a uniform coating layer on the substrate, as shown in Fig. 3.2 (Le Roux and Paul, 1992). The thickness of the membrane can be determined by three experimental parameters, namely solvent evaporation rate, velocity of the spinning substrate (spin rate), and the viscosity of the coating solution. Therefore the parameters such as precursor volume, rotational speed, rotational time, solution or solid concentration are important for controlling membrane formation. In this method, some organic additives are often added to adjust the solid loading, viscosity, and volatility of the coating solution. This method is particularly suited to produce an ultrathin film on various substrates. Emslie et al. (1958) proposed a model of the spin coating process to predict the film thickness as a function of certain physical parameters as follows:

$$h = \frac{h_0}{\left(1 + \frac{4\omega^2 h_0^2 t}{3\eta}\right)^{1/2}}$$

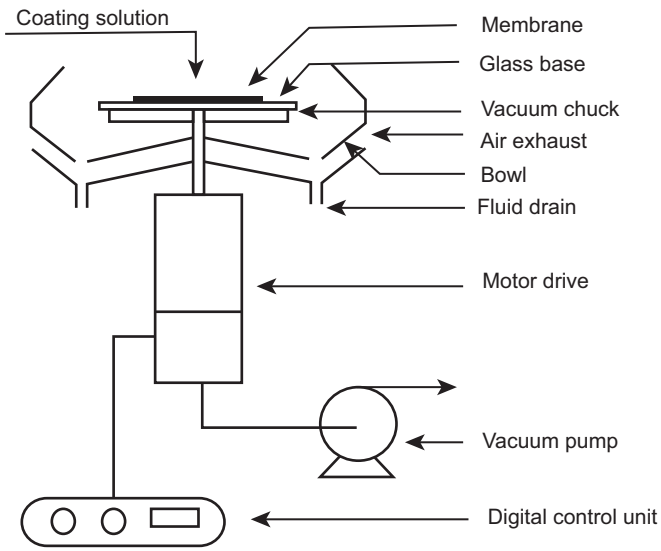

Figure 3.2
Schematic illustration of the spin-coating apparatus used for making composite membranes.
Reprinted with permission from Le Roux and Paul, 1992, copyright 1992, Elsevier.

where h_0 is the initial film thickness, ω the spin rate, and η the viscosity. This equation was rarely used because the various operating conditions merely satisfy the assumption. However, this function can be taken as a model for correlating the dip-coating parameters. Based on this function, Huang and Chou (2003) further proposed that the viscosity of solution significantly depends upon the shear rate due to viscosity related to the shear stress. Theoretically, the membrane thickness is mainly determined by the shear forces from viscosity and spinning of solution. The less viscous precursor solution for spin coating would produce a thinner, yet more uniform membrane.

Burmann et al. (2014) demonstrated that the rotational time had no effect on the membrane thickness, whereas the solvent evaporation effect plays a significant role in using the spin coating for membrane casting. However, the fast solvent evaporation could generate defective and unstable membranes.

Hashizume and Kunitake (2003) reported self-supporting ultrathin films of TiO_2 by a spin coating process. The ultrathin layer of polyvinyl alcohol (PVA) was first formed by spin coating on a soluble polymer, followed by coating with titanium tetrabutoxide. By dissolving the soluble polymer, the self-supporting ultrathin PVA/titania composite film was finally produced (Fig. 3.3). The spin coating is commonly used in laboratories to

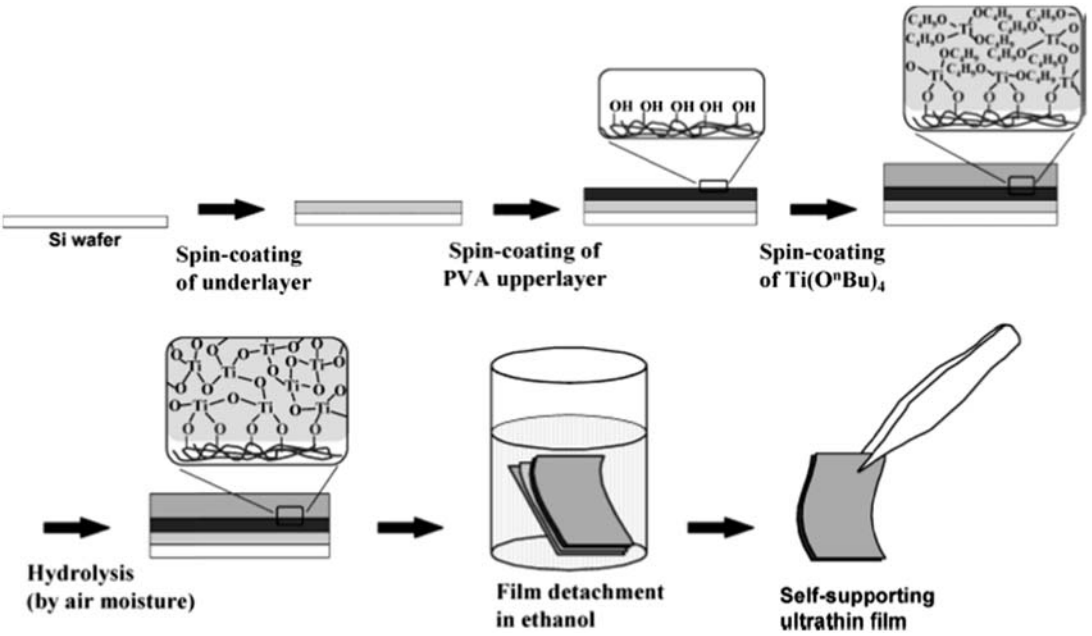

Figure 3.3

Preparative procedure of a self-supporting ultrathin film by spin coating. *Reprinted with permission from Hashizume and Kunitake, 2003, copyright 2003, American Chemical Society.*

prepare small-sized membranes, but it is not suitable for large-scale manufacturing of photocatalytic membranes for practical applications.

3.2.2.3 Electrospraying and Electrospinning

The conventional electrohydrodynamic processes, including electrospraying and electrospinning, are facile, cost-effective, and flexible methods for fiber production. These methods are thereby carried out to produce fibrous membranes. The electrosprayed or electrospun membranes are currently employed for applications in air filtrations and water filtrations especially the microfiltration and ultrafiltration because of their high porosity and low permeation resistance. The polymer solution can be sprayed and spun in the presence of high potential electric field to produce fiber and particles (Figs. 3.4 and 3.5). In particular, these methods are used to fabricate highly porous membranes by electrospinning or electrospraying organic polymer nanofibers.

These processes are driven by electrical forces. Varying electrospinning and electrospraying parameters and polymer solution properties can result in different morphologies (Wang and Hsiao, 2016). The electrospinning technique offers an ideal route to construct nanofiber filtration membrane with controllable pore size and pore size distribution. The high surface areas of electrospun membranes have attracted significant

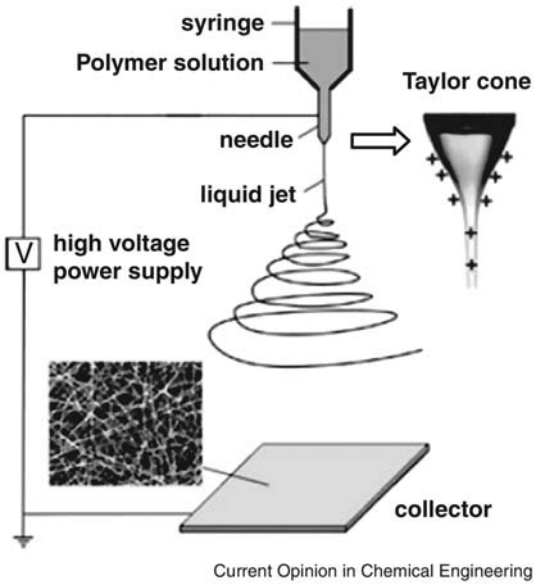

Figure 3.4
Schematic illustration of the electrospinning process. *Reprinted with permission from Wang and Hsiao, 2016, copyright 2016, Elsevier.*

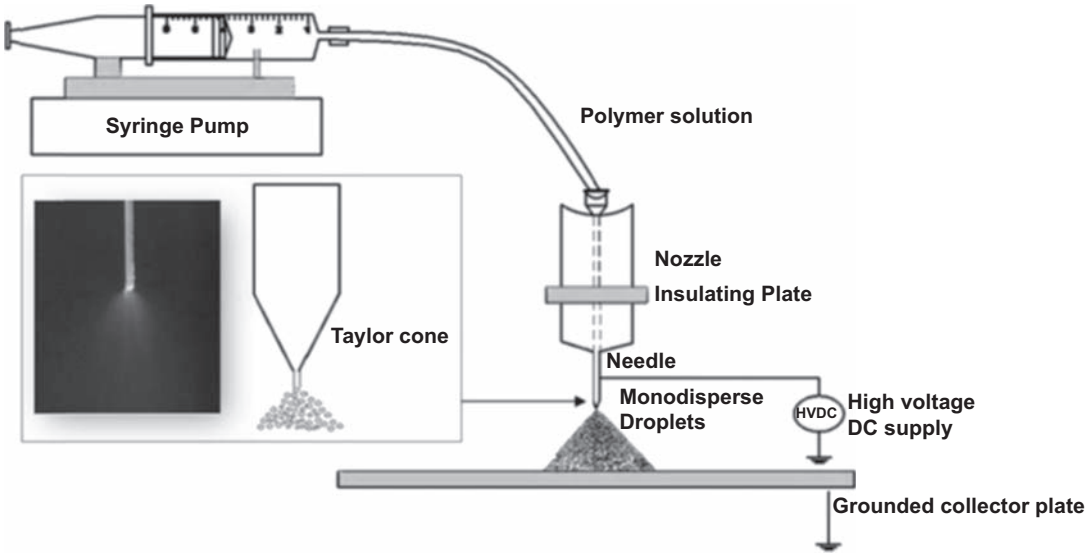

Figure 3.5
A typical electrospraying setup. The inset shows the digital image and representation of electrospraying process. *Reprinted with permission from Bhushani and Anandharamakrishnan, 2014, copyright 2014, Elsevier.*

interest for their practical applications, such as protective clothes, high-performance filter media, and even electronic devices. A variety of materials such as the polymer-solvent systems and polymerless sol−gel systems can be electrospun. Electrospinning can produce highly porous nanofiber network structures with interconnected flow-through pores. Typically, the precursor of photocatalysts or as-prepared photocatalyst particles is mixed with the polymer solution to produce polymeric membranes coupled with photocatalysts. The $H_4SiW_{12}O_{40}$/chitosan (CS)/polycaprolactam (PA6) sandwich nanofibrous membrane was produced by electrospinning of solutions dissolved within PA6 and $H_4SiW_{12}O_{40}$ (Cui et al., 2016). The membrane was a nonwoven-like structure that was piled up randomly deposited nanofibers. In the case of electrospinning method, the fiber diameter influences the porous structure of the membrane. The flow-through pore size decreased with a decrease in the fiber diameter. Besides, the fiber diameter, surface morphology, and internal structure of nanofibers can control the functionalities of nanofibers and performances of nanofibrous membranes. However, using electrospinning approach to prepare photocatalytic membranes generally requires the incorporation of nanoparticles of photocatalysts into nanofibers, which is typically realized by mixing the nanoparticles with polymer solutions before electrospinning. In this fabrication process, the nanoparticles could be covered by polymer material, and they thereby may not be fully exposed on the surface for photocatalytic applications.

3.2.2.4 Vacuum Filtration

Another method for preparing photocatalytic membrane is vacuum filtration, by which photocatalyst particles are physically deposited on a membrane surface. Different amounts of photocatalyst particles can be deposited on the support, controlled by the concentration of photocatalyst particles and filtration pressure. For example, CNT/ZnO/TiO_2 composite was uniformly assembled on the cellulose acetate membrane (Bai et al., 2015b). The hierarchically structured nanocomposite layer was compressed onto the substrate membrane. This method allows for achieving relatively large thickness and density of the membrane. However, the photocatalyst particles may flow into the substrate pores and thus easily block them. Moreover, the pure water flux could be decreased because of the dense photocatalyst layer. This preparation method also requires the photocatalyst particles to be well dispersed; otherwise, the resulting photocatalytic membrane may not be uniform due to the aggregation of particles. Importantly, this method is particularly suited to assembling two-dimensional (2D) materials onto the support membranes. A number of 2D materials, including graphene, graphitic carbon nitride, MoS_2 nanosheets, have been fabricated into the membrane by this method (Gang et al., 2016; Zhao et al., 2016; Wang et al., 2017). For the vacuum filtration method, the downstream pressure and concentration of filtrated solution are the typical factors influencing the properties of the photocatalytic membrane. The downstream pressure dramatically influences the solvent flux, and thus the uniformity of membrane, whereas the concentration of 2D materials determines the thickness as well as uniformity of membranes.

3.2.2.5 Immersion Precipitation

Phase inversion via immersion precipitation is a widely used membrane preparation approach. A polymer plus solvent (polymer solution) is casted on a proper support and then submerged in a coagulation bath containing nonsolvent. Owing to the solvent and nonsolvent exchange, precipitation takes place. The polymer must be soluble in solvent mixture. The combination of phase separation and mass transfer affects the membrane structure. During the immersion phase inversion process, the kinetic and thermodynamic properties of the casting solution are the two key aspects that influence the morphology and properties of the resulted membranes (for more details, see Chapter 2). To prepare photocatalytic membranes, the photocatalyst particles or the precursor of photocatalysts are blended with the casting solution, where the blending ratio, polymer concentration, and the selection of the solvent and nonsolvent significantly influence the properties of the final membranes. Jiang et al. (2016) prepared poly(L-lactide) (PLLA)/TiO_2 composite membranes by immersion precipitation method. The introduction of TiO_2 improved the membrane hydrophilicity and mitigated the membrane fouling in the wastewater treatment. In addition, the pore size and porosity of the PLLA surface varied with the increase of TiO_2 loading. However, one of the key issues to be solved in case of application of

immersion precipitation method is aggregation of nanoparticles, especially at high concentration, that results in a low dispensability in the casting solution and affects membrane properties and performance.

3.2.3 Types of Photocatalysts Coupled With Membranes

3.2.3.1 TiO_2-Based Photocatalytic Membrane

Considerable progress has been made in the development of photocatalytic membrane materials. TiO_2 is one of the most commonly studied photocatalytic materials and has been integrated with membranes to achieve photocatalytic degradation of organic pollutants and antifouling properties in the membrane systems. In particular, the antifouling properties can be achieved by improved membrane hydrophilicity and photocatalytic degradation of organic foulants deposited on the membrane. Apart from the proper selection of the membrane support, it is important to improve the photocatalytic efficiency of TiO_2.

3.2.3.1.1 Morphology Effects of TiO_2 on Photocatalytic Membrane

Morphology of TiO_2 particles significantly affects properties of membranes such as the roughness, pore structure, and the antifouling performance. It is reported that application of the TiO_2 nanoparticles with smoother structure resulted in less pore blocking, compared with commercial Degussa P-25 (Ciston et al., 2006; Goei and Lim, 2014b). TiO_2 nanoparticles with controllable sizes can be easily synthesized and incorporated into porous substrates (Choi et al., 2006; Bet-moushoul et al., 2016). Many studies have been carried out to investigate the morphology of nanostructured TiO_2 and its role in the interface-related membrane processes. Moreover, the hierarchical structure of TiO_2 is an important feature of the photocatalyst because of the high surface area and efficient medium diffusion in reaction systems.

Tan et al. (2016) used TiO_2 nanowire as the main substrate for the fabrication of TiO_2/Fe_2O_3 composite membrane (Fig. 3.6) because of its superhydrophilic property and photocatalytic performance. The TiO_2/Fe_2O_3 composite membrane was synthesized by the solvothermal method. This composite membrane displayed excellent oil rejection rate, outstanding anti−oil fouling, and self-cleaning properties. Li et al. (2015) demonstrated a superoleophobic porous membrane based on hierarchical TiO_2 nanotubes. This membrane was fabricated by electrochemical anodization of porous Ti membrane. This functional porous membrane showed superhydrophilicity and underwater-superoleophobicity, achieving distinctive oil−water separation properties. Fischer et al. (2014) reported that the self-supported TiO_2 nanotubes were very brittle and fragile; on the contrary, the TiO_2 nanotubes were well attached onto a porous PES substrate, and the membrane showed good stability and flexibility. They found that the pores were blocked by the TiO_2 nanotube array, and the TiO_2 nanotube film thickness was limited to 400 nm to avoid the

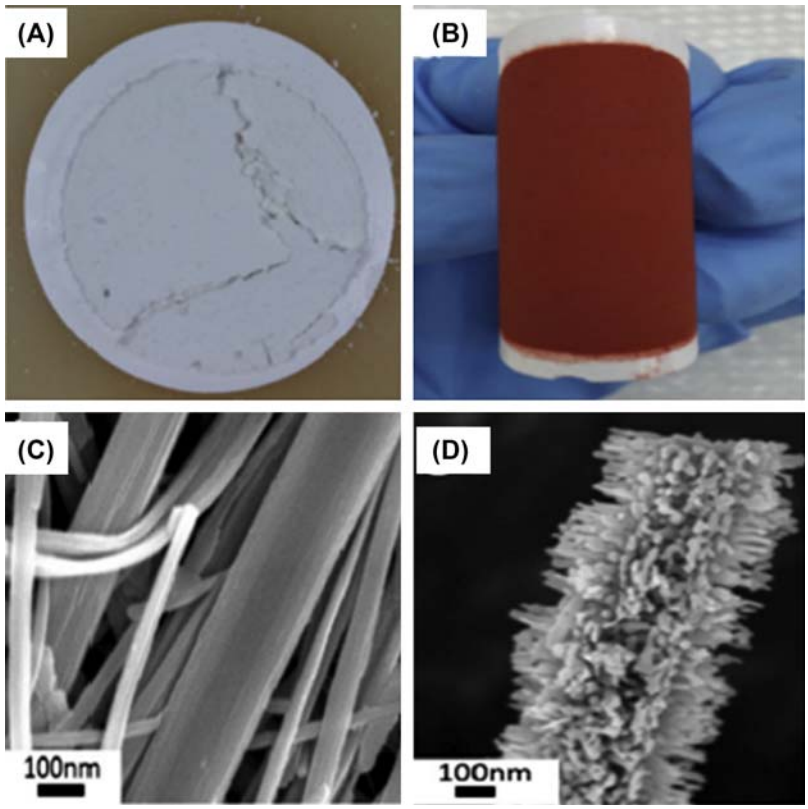

Figure 3.6
(A) Photograph illustrating the effect of TiO_2 nanowire membrane after bending; (B) Field emission scanning electron microscope (FESEM) image of pure TiO_2 nanowires; (C) FESEM image of the pure TiO_2 nanowire membrane; (D) photograph illustrating the mechanical flexibility of TiO_2/Fe_2O_3 composite membrane. *Reprinted with permission from Tan et al., 2016, copyright 2015, John Wiley and Sons.*

destruction of the membrane. Mesoporous TiO_2 spheres were immobilized on porous alumina discs by dip coating (Leong et al., 2016). The mesoporous TiO_2 reduced the effective pore size of the membrane and improved removal efficiency of humic acid under UV light irradiation. With the aid of filtration, the degradation efficiency of humic acid was improved from 58.6% to 92%.

Apart from the influence on photocatalytic activity, the nanostructured photocatalysts also affect the water flux, fouling, and stability of membranes (Table 3.3). For example, hot pressing methods were used by the application of pressure and heat to improve the connectivity between the TiO_2 fiber and PVDF membrane intersection (Nor et al., 2016).

Table 3.3: Photocatalytic membranes with nanostructured photocatalysts.

Photocatalytic Membrane	Structure	Performance	References
TiO_2/PVDF membrane	TiO_2 nanofiber	Removal of bisphenol A, efficiency 85% within 300 min, UV irradiation	Nor et al. (2016)
Silica/TiO_2 membrane	Titania nanorods/ nanotubes	Removal of sodium dodecylbenzene sulfonate, efficiency 89% within 100 min, UV light irradiation, 89% retention of 20,000 g mol^{-1} at pressure 0.5 bar	Zhang et al. (2006a)
$SrTiO_3/TiO_2$	Nanofiber	Removal of acid orange 7 (AO7), efficiency around 100% within 24 h, UV irradiation	Bai et al. (2015a)
TiO_2/carbon/Al_2O_3 membrane	Nanoparticle	Removal of humic acid (HA), TOC removal 62%, UV light irradiation, pure water flux 314 L m^{-2} h^{-1} bar^{-1}, rejection efficiency of standard polystyrene microspheres (528.4 nm) 97.3%	Wang et al. (2015)
TiO_2/PES membrane	Nanoneedle and nanotubular	Removal of MB, efficiency: six times higher compared with TiO_2 nanoparticle membrane, UV light irradiation	Fischer et al. (2014)

MB, methylene blue; *PES*, polyethersulfone; *PVDF*, polyvinylidene fluoride; *TOC*, total organic carbon.

No leaching was observed from the membrane throughout the photocatalytic reaction due to strong adhesion of photocatalyst and PVDF membrane. The hot-pressed TiO_2/PVDF membrane at a lower temperature (100°C) was hydrophilic, exhibited higher pure water flux, and showed strong UV and visible absorption. With increasing the hot-pressing temperature, the pure water flux and the mean pore size of the TiO_2/PVDF membrane showed a decrease; the bisphenol A rejection was increased because the mean pore size of the membrane was reduced. The removal efficiency of bisphenol A increased from 63% to 85% after the TiO_2/PVDF membrane was treated with UV illumination.

3.2.3.1.2 TiO_2 Modification

In the past few decades, TiO_2 has been considered as a green environmental protection material and widely applied in various fields. Its excellent properties such as nontoxicity, low cost, high chemical stability, and high photocatalytic activity have attracted much attention. However, the wide bandgap (~3.2 eV) limits its absorption of visible light, thereby restraining its practical application (Mozia et al., 2009; Ahn et al., 2014). Various approaches were studied for the development of TiO_2 with visible light–responsive feature. Impurity doping, dye sensitization, and semiconductor coupling have been

performed to modify TiO_2, resulting in enhanced visible light activity. In the photocatalytic membrane system, the aforementioned modification methods were also investigated to improve the activity of TiO_2 photocatalyst and the synergetic effect with the membrane. Chen et al. (2017) introduced nitrogen to TiO_2 to efficiently reduce its energy bandgap between conduction and valence bands and graphene, greatly enhancing visible light activity of ultrafiltration membrane. The N-doped TiO_2/graphene oxide (GO) membrane can improve the hydrophilicity of photocatalytic membrane due to TiO_2 and oxygen-containing functional groups in GO.

Apart from the nonmetal doping, the composite TiO_2 material has also shown the improvement of properties, such as crystal phase, surface area, defects in the lattice, crystal facets, uncoordinated surface sites, and degree of crystallinity, which determine the photocatalytic activity of the semiconductor (Dahl et al., 2014). Some metal sulfide, metal, metal oxide, and even carbon-based materials were coupled with TiO_2 to improve the photocatalytic performance. The metal sulfide such as CdS, ZnS, and SnS have also been used to modify TiO_2 (Luengas et al., 2015; Banerjee et al., 2008; Schneider et al., 2014). The CdS-sensitized TiO_2 structure showed a high photocatalytic efficiency for the degradation of pollutants (Fig. 3.7) (Pant et al., 2017). Immobilization of CdS/TiO_2 composite on carbon nanofibers avoided the leaching of cadmium ions and enhanced the reaction rate of degradation of dyes owing to the carbon fiber substrate (Pant et al., 2017).

Silver and gold nanoparticles were the most common metal-modification options because of their antibacterial and plasma effects (Grunwaldt et al., 1999; Elahifard et al., 2007). TiO_2-coated PVDF membrane showed effective improvement in hydrophilicity and antifouling properties compared with the neat membrane (Nor et al., 2016). The presence of silver nanoparticles on TiO_2/PVDF membrane further improved the biofouling and organic fouling resistance (Goei and Lim, 2014b).

Although metal sulfide and noble metal could enhance the visible light response of TiO_2 photocatalyst, they showed a weak chemical stability in the photocatalytic reaction. For metal oxide modification, ZnO (Bai et al., 2015b), Fe_2O_3 (Tan et al., 2016), ZrO_2 (Grunwaldt et al., 1999), and WO_3 (Zou et al., 2008) are promising candidates to modify TiO_2 semiconductor. The heterojunctioned architectures, $SrTiO_3$/TiO_2, were facilely produced via hydrothermal treatment of electrospun nanofibers (Bai et al., 2015a). The heterojunctioned $SrTiO_3$/TiO_2 nanofiber architectures and their structured porous functional layer resulted in high photodegradation efficiency and high permeate flux.

Hybridizing membrane filtration with photocatalytic technology offers multifunctions including both filtration and photodegradation of organic pollutants. However, the photocatalytic activity is often restrained by the quick recombination of photo-generated electron/hole pairs. Carbon-based materials exhibit good conductivity and high chemical stability. The hierarchically structured TiO_2/carbon/Al_2O_3 composite was constructed via

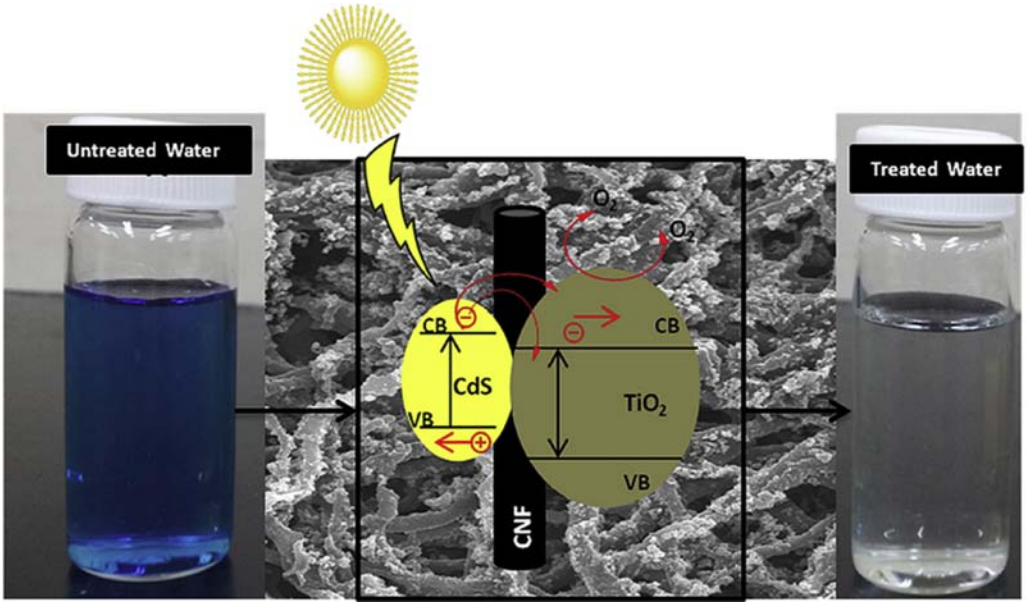

Figure 3.7
Illustration of adsorptive and photocatalytic properties of carbonized eggshell membrane decorated with CdS/TiO_2 nanoparticles during the removal of methylene blue under visible light irradiation. *CB*, conduction band; *VB*, valence band. *Reprinted with permission from Pant et al., 2017, copyright 2017, Elsevier.*

sequential deposition of graphitic carbon and TiO_2 nanoparticle layer on Al_2O_3 membrane (Wang et al., 2015). The TiO_2/carbon/Al_2O_3 (Fig. 3.8) membrane applied for photoelectrocatalytic filtration showed 1.2 or 1.7 times higher efficiency of organic pollutant removal and 1.3 or 3 times higher permeate flux than that observed for the membrane during filtration with UV irradiation or filtration alone. The rejection and permeability performance of the membrane was affected by the thickness of the TiO_2 layer and carbon layer. Li et al. (2017) demonstrated that the presence of reduced graphene oxide (rGO) greatly improved the photocatalytic activity of $CoFe_2O_4$-rGO/PVDF membrane.

The TiO_2 photocatalytic membrane often has good hydrophilicity and antifouling properties because of the presence of coated TiO_2. However, the degree of hydrophilicity of the membrane is not proportional to the degree of antifouling as reported (Leong et al., 2014). The introduction of TiO_2 influences the hydrophilicity and structure of the membrane support, thereby affecting the water flux of the membrane. The pure water flux of the photocatalytic membrane often decreases with increase in the concentration of TiO_2 in the coating process, owing to the blockage of the membrane pores by the photocatalyst

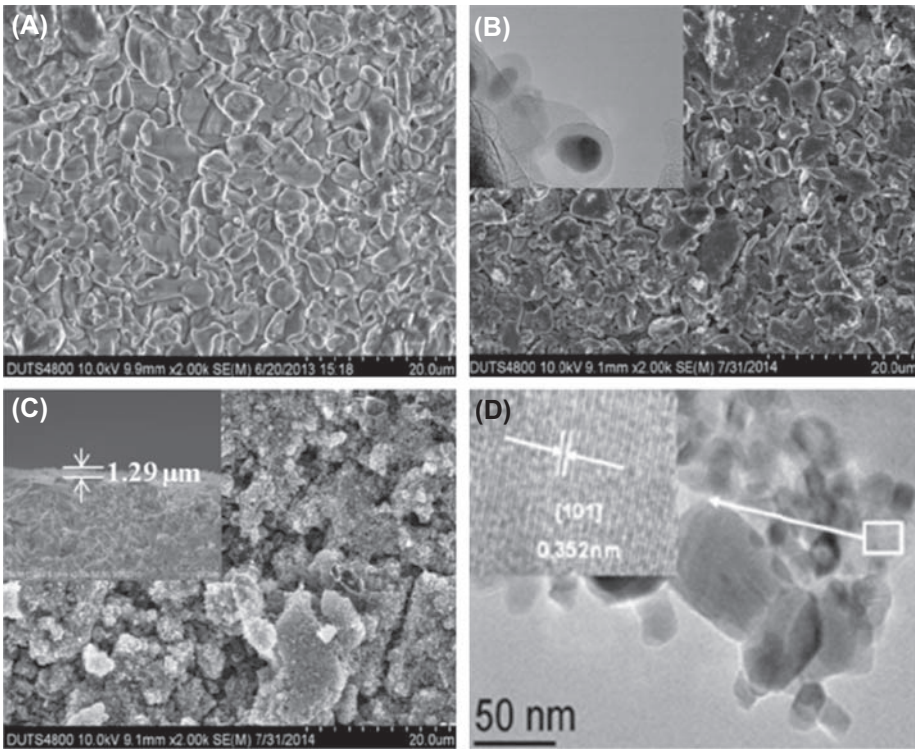

Figure 3.8

SEM images of (A) Al_2O_3 membrane support, (B) carbon/Al_2O_3 membrane, and (C) TiO_2/carbon/Al_2O_3 membrane. TEM image of (D) TiO_2/carbon/Al_2O_3 membrane. *SEM*, scanning electron microscope; *TEM*, transmission electron microscopy. *Reprinted with permission from Wang et al., 2015, Copyright 2015, Elsevier.*

nanoparticles. Besides, the dense structure of coated TiO_2 layer could dramatically decrease the pure water flux. However, Ahn et al. (2014) demonstrated that TiO_2-coated aromatic PA thin film composite membrane exhibited better flux and stability than the neat membrane after 3 days under the UV illumination in a reverse osmosis (RO) system. Liu et al. (2008) reported that the pure water flux was increased by the introduction of 6 wt% TiO_2 to PES membrane. The increased water flux was due to the large pores formed on the membrane surface by TiO_2 nanoparticle aggregation. A thick layer of TiO_2 on ceramic membranes could reduce the water flux of the photocatalytic membrane. Meng et al. (2008) compared the permeate flux of photocatalytic membrane with and without UV light irradiation and found that the permeate flux under UV light illumination showed better results. It was explained that the improved permeate flux was due to the destruction of the bacterial residues, which left on the membrane surface by the active radicals formed in the photocatalytic process.

Adhesion of TiO_2 with membrane support is determined by the coating method and the type of membranes. The attachment of TiO_2 on the support is usually not strong enough, as some of the TiO_2 nanoparticles could detach from the membrane after a long-time operation. It was found that TiO_2 on the polymer membrane detached after 30 min under RO-pressurized operation, yet not further loss was observed (Leong et al., 2014). In the case of TiO_2 blended into polymer membranes, the casting solution could induce the change of the structure of the membrane and the blending of TiO_2 could result in the more porous membrane and stronger adhesion of TiO_2 with support, unlike the surface coating method. To strengthen the photocatalytic membrane and avoid the decrease of water flux, Bai et al. (2015b) proposed a hierarchical structure of TiO_2/CNT/ZnO deposited on cellulose acetate support (Table 3.4). The CNT/ZnO/TiO_2 functional layer was in favor of the flux improvement. This structured membrane showed the highest filtration flux, compared with the nanocomposite integrated cellulose acetate membranes. This functional layer was beneficial for the fouling control by adsorbing or rejecting the

Table 3.4: TiO_2-based photocatalytic membranes and their performance.

Photocatalytic Membrane	Light Source	Performance	References
Ag/TiO_2 membrane	UV light	Removal of RhB, efficiency: 1007 mg m^{-2} h^{-1}; pure water flux 123 L m^{-2} h^{-1}	Goei and Lim (2014a)
CdS—TiO_2/carbonized eggshell membrane	Visible light	Removal of MB, 53% decomposed by TiO_2/membrane, 96% decomposed by CdS—TiO_2 membrane within 60 min	Pant et al. (2017)
TiO_2/aromatic polyamide membrane	UV light	Bactericidal effect: 63% of cells removed within 4 h	Kim et al. (2003)
$SrTiO_3$/TiO_2 membrane	UV light	Removal of AO7, efficiency: around 100% within 24 h	Bai et al. (2015a)
TiO_2 hollow fiber membrane	UV light	Removal of AO7, efficiency: 70% decomposed within 1 h	Sholl and Johnson (2006)
C, N, and Ce-doped TiO_2 membrane	Visible light	Removal of MO, 100% decomposed within 160 min, permeability: 300 L m^{-2} h^{-1} bar^{-1}	Zhang et al. (2009)
TiO_2/silica nanotube membrane	UV light	Removal of direct black, efficiency: 85% within 100 min; permeability: 55—65 L m^{-2} h^{-1} bar^{-1}	Cao et al. (2012)
CNT/ZnO/TiO_2 membrane	UV light	Removal of AO7: 100% decomposed within 25 min The highest filtration flux among the nanocomposite integrated cellulose acetate membranes	Bai et al. (2015b)
N-doped TiO_2/graphene oxide membrane	UV/visible light	Removal of MB, efficiency: about 85% within 5 h	Chen et al. (2017)

AO7, acid orange 7; *CNT*, carbon nanotube; *MB*, methylene blue; *MO*, methyl orange; *RhB*, rhodamine B.

organic pollutants on the structured surface instead of forming a dense fouling layer. By contrast, in the filtration process of cellulose acetate membrane, severe membrane fouling layer would be formed on the surface or trapped in the pores of the membrane. Moreover, the TiO_2 nanowires served as the supporting matrix, whereas the amorphous CNT/ZnO nanorods showed a bridging property to conjugate the entire CNT/ZnO/TiO_2 nanocomposite structure, thus enhancing the mechanical strength of the structured membrane.

3.2.3.2 Non−TiO_2 Photocatalytic Membrane

Although enormous studies of the immobilization of TiO_2 nanoparticles on the surface of supports have been performed, the TiO_2 membrane, as a functional layer, suffers from limited performance because of the wide bandgap of the semiconductor and fast recombination of photo-generated electron/hole pairs (Zhang et al., 2014; Goei and Lim, 2014a). Moreover, TiO_2 is only photoexcited by UV light; expensive ceramic membranes with good tolerance to serve as the support result in high cost of membrane products (Ciston et al., 2006; Goei and Lim, 2014b). Therefore, some non−TiO_2 photocatalysts with high visible light activity were used to prepare a photocatalytic layer on the porous supports (Zhang et al., 2006b; Zou et al., 2008; Kou et al., 2012; Li et al., 2017; Cui et al., 2016). The 2D material, graphitic carbon nitride nanosheet, is a promising metal-free photocatalyst and option for fabrication of photocatalytic membrane. Zhao et al. (2016) proposed immobilization of g-C_3N_4 nanosheets/rGO composite on commercial cellulose acetate membrane by vacuum filtration and high-pressure process (Table 3.5). The 2D structure of g-C_3N_4 nanosheets and rGO nanosheets was helpful to enhance the flexibility of membrane. The g-C_3N_4/rGO membrane showed high pure water flux of 957 L m^{-2} h^{-1}, 33.8% higher than that of cellulose acetate membrane modified with TiO_2 P25, attributed to the large lateral size of g-C_3N_4/rGO sheets, which prevented them from depositing into the pores. This membrane also showed high removal efficiency of organic pollutants and antifouling performance. $H_4SiW_{12}O_{40}$ (SiW_{12})/CS/PA6 sandwich nanofibrous membrane was synthesized by electrospinning (Cui et al., 2016). The permeate flux initially declined with the running time increased and was stable at 140 L m^{-2} h^{-1} after 1 h, which was 3.7 times higher than that in dark. The enhanced permeate flux was due to the destruction of bacteria formed on the membrane surface as a result of the action of reactive oxygen species generated by photocatalysis. The SiW_{12} with Keggin structure has properties comparable to the well-known photocatalysts such as TiO_2, CdS, ZnO, etc. However, the high solubility of SiW_{12} in aqueous solution makes it impossible to be separated for recycling. Combining CS and SiW_{12} with suitable support could make them more recoverable. This membrane exhibited an excellent performance with a high adsorption capacity toward Cr(VI) (78.5 mg g^{-1}), high removal efficiency of methyl orange (MO) (96.7%), and good stability because of its high porosity, good hydrophilicity, and superior water tolerance.

Table 3.5: Non−TiO_2 photocatalytic membranes and their performance.

Photocatalytic Membrane	Light Source	Performance	References
g-C_3N_4 nanosheet/reduced graphene oxide (rGO)	Visible light	Permeate flux higher than that of filtration alone, inactivation of *Escherichia coli* at three orders of magnitude higher than that of filtration alone	Zhao et al. (2016)
$FeTiO_2$/polysulfone membrane		NO removal efficiency up to 85.7% in 270 days, the maximum elimination capacity up to 159.8 g NO m^{-3} h^{-1}, biochemical degradation rate 6.12 mg m^{-2} h^{-1}, catalytic reaction rate 1.67 mg m^{-2} h^{-1}	Wei et al. (2016)
Graphene quantum dots-Cu_2O/bipolar membrane (GQDs-Cu_2O/BPM)	Sunlight	Hydrogen evolution: efficiency of GQDs-Cu_2O/BPM 88.8% and 14.5% more efficient than BPM at the current density of 90 mA cm^{-2} and under sunlight irradiation	Liu et al. (2016a,b,c)
$CoFe_2O_4$-rGO/PVDF/carbon fiber cloth	Visible light	Pure water flux 927.28 L m^{-2}, six times higher that pure PVDF membrane; removal of tetracycline hydrochloride: efficiency 85% within 90 min	Li et al. (2017)
$H_4SiW_{12}O_{40}$/chitosan/PA6 nanofiber membrane	Visible light	High adsorption capacity toward Cr(VI) (78.5 mg g^{-1}); high removal efficiency of MO (96.7%)	Cui et al. (2016)

MO, methyl orange; *PA6*, polycaprolactam; *PVDF*, polyvinylidene fluoride.

3.3 Conclusions and Future Trends

TiO_2 photocatalytic membranes show much enhanced filtration performance compared with the traditional membranes. TiO_2 can be coated on the porous supports or fabricated into free-standing membranes. Both polymer and ceramic membranes have been widely studied as supports of photocatalysts, but the stability of polymer membrane under the UV illumination is a concern and requires further investigation. Owing to the limitation of the wide bandgap, TiO_2 can be doped with nonmetal elements or modified with other metals and semiconductors to improve its photocatalytic performance and the filtration efficiency of photocatalytic membranes. The non−TiO_2 photocatalysts are also developed and hybridized with porous membrane supports such as g-C_3N_4/GO deposited on polymer membranes and $H_4SiW_{12}O_{40}$ (SiW_{12})/CS/PA6 membrane. These non−TiO_2 photocatalysts show better performance than TiO_2 in terms of pure water, disinfection, and energy conversion. The photocatalytic membranes also have unique properties including

superhydrophilicity, antifouling performance, photocatalytic oxidation and reduction, separation, and antimicrobial ability. The photocatalytic membranes can be fabricated via various methods: dip coating, spin coating, electrospraying and electrospinning, immersion precipitation, vacuum filtration. The fabrication method is the key to photocatalytic membrane properties and performances.

Even though photocatalytic membranes have shown great potential in water treatment, antifouling, disinfection, and energy conversion, many technical problems still need to be addressed before this technique can be practically applied in the industry. More efforts are required to improve the photocatalytic efficiency of photocatalytic membranes, such as immobilized photocatalysts. Photocatalytic membranes are facing the challenge of the lower contact area among photocatalyst, target pollutant, and light than in the conventional slurry photocatalysis systems. Most of the photocatalytic membranes in small-scale applications still work under UV light, even though a large number of visible light−absorption photocatalysts have been reported. Therefore, solar light−induced photocatalytic membranes are yet to be investigated in the future. The synthesis of novel photocatalysts will be always beneficial for developing photocatalytic membrane with high photocatalytic activity, high permeate flux, and desirable antifouling properties.

List of Abbreviations

AO7 Acid orange 7
BPM Bipolar membrane
CA Cellulose acetate
CB Conduction band
CNT Carbon nanotube
CS Chitosan
GQDs Graphene quantum dots
HA Humic acid
MB Methylene blue
MO Methyl orange
PA Polyamide
PA6 Polycaprolactam
PAN Polyacrylonitrile
PES Polyethersulfone
PLLA Poly(L-lactide)
PS Polysulfone
PVA Polyvinyl alcohol
PVDF Polyvinylidene fluoride
PVP Polyvinylpyrrolidone
rGO Reduced graphene oxide
RhB Rhodamine B
RO Reverse osmosis
TOC Total organic carbon
VB Valence band

References

Ahmad, R., Kim, J.K., Kim, J.H., Kim, J., 2016. Well-organized, mesoporous nanocrystalline TiO_2 on alumina membranes with hierarchical architecture: antifouling and photocatalytic activities. Catal. Today 282.

Ahn, S.H., Kim, D.J., Chi, W.S., Kim, J.H., 2014. Hierarchical double-shell nanostructures of TiO_2 nanosheets on SnO_2 hollow spheres for high-efficiency, solid-state, dye-sensitized solar cells. Adv. Funct. Mater. 24, 5037−5044.

Bai, H., Zan, X., Juay, J., Sun, D.D., 2015a. Hierarchical heteroarchitectures functionalized membrane for high efficient water purification. J. Membr. Sci. 475, 245−251.

Bai, H., Zan, X., Zhang, L., Sun, D.D., 2015b. Multi-functional CNT/ZnO/TiO_2 nanocomposite membrane for concurrent filtration and photocatalytic degradation. Sep. Purif. Technol. 156, 922−930.

Banerjee, S., Mohapatra, S.K., Das, P.P., Misra, M., 2008. Synthesis of coupled semiconductor by filling 1D TiO_2 nanotubes with CdS. Chem. Mater. 20, 6784−6791.

Bet-moushoul, E., Mansourpanah, Y., Farhadi, K., Tabatabaei, M., 2016. TiO_2 nanocomposite based polymeric membranes: a review on performance improvement for various applications in chemical engineering processes. Chem. Eng. J. 283, 29−46.

Bhushani, J.A., Anandharamakrishnan, C., 2014. Electrospinning and electrospraying techniques: potential food based applications. Trends Food Sci. Technol. 38, 21−33.

Bosc, F., Ayral, A., Albouy, P.A., Datas, L., Guizard, C., 2004. Mesostructure of anatase thin films prepared by mesophase templating. Chem. Mater. 16, 2208−2214.

Bosc, F., Ayral, A., Albouy, P.A., Guizard, C., 2003. A simple route for low-temperature synthesis of mesoporous and nanocrystalline anatase thin films. Chem. Mater. 15, 2463−2468.

Bosc, F., Ayral, A., Guizard, C., 2005. Mesoporous anatase coatings for coupling membrane separation and photocatalyzed reactions. J. Membr. Sci. 265, 13−19.

Burmann, P., Zornoza, B., Tellez, C., Coronas, J., 2014. Mixed matrix membranes comprising MOFs and porous silicate fillers prepared via spin coating for gas separation. Chem. Eng. Sci. 107, 66−75.

Cao, X.P., Li, D., Jing, W.H., Xing, W.H., Fan, Y.Q., 2012. Synthesis of visible-light responsive C, N and Ce co-doped TiO_2 mesoporous membranes via weak alkaline sol-gel process. J. Mater. Chem. 22, 15309−15315.

Chen, W., Ye, T., Xu, H., Chen, T., Geng, N., Gao, X., 2017. An ultrafiltration membrane with enhanced photocatalytic performance from grafted N−TiO_2/graphene oxide. RSC Adv. 7, 9880−9887.

Chen, X.F., Wei, J., Hou, R.J., Liang, Y., Xie, Z.L., Zhu, Y.G., Zhang, X.W., Wang, H.T., 2016. Growth of g-C_3N_4 on mesoporous TiO_2 spheres with high photocatalytic activity under visible light irradiation. Appl. Catal. B Environ. 188, 342−350.

Choi, H., Stathatos, E., Dionysiou, D.D., 2006. Sol-gel preparation of mesoporous photocatalytic TiO_2 films and TiO_2/Al_2O_3 composite membranes for environmental applications. Appl. Catal. B Environ. 63, 60−67.

Ciston, S., Chen, L., Li, G., Hausner, M., Lueptow, R.M., Gray, K.A., 2006. Effects of TiO_2 nanostructure and various ceramic supports in photocatalytic membranes for water treatment. In: 2006 AIChE Annual Meeting San Francisco, CA.

Cui, X.X., Li, T.T., Yao, S.W., An, L.B., Li, Y.Q., Zhou, Z., Guo, M.C., Zhang, Z.M., 2016. Electrospun $H_4SiW_{12}O_{40}$/chitosan/polycaprolactam sandwich nanofibrous membrane with excellent dual-function: adsorption and photocatalysis. RSC Adv. 6, 96237−96244.

Daels, N., Radoicic, M., Radetic, M., Van Hulle, S.W.H., De Clerck, K., 2014. Functionalisation of electrospun polymer nanofibre membranes with TiO_2 nanoparticles in view of dissolved organic matter photodegradation. Sep. Purif. Technol. 133, 282−290.

Dahl, M., Liu, Y.D., Yin, Y.D., 2014. Composite titanium dioxide nanomaterials. Chem. Rev. 114, 9853−9889.

Derichter, R.K., Ming, T., Caillol, S., 2013. Fighting global warming by photocatalytic reduction of CO_2 using giant photocatalytic reactors. Renew. Sustain. Energy Rev. 19, 82−106.

Elahifard, M.R., Rahimnejad, S., Haghighi, S., Gholami, M.R., 2007. Apatite-coated Ag/AgBr/TiO_2 visible-light photocatalyst for destruction of bacteria. J. Am. Chem. Soc. 129, 9552−9553.

Emslie, A.G., Bonner, F.T., Peck, L.G., 1958. Flow of a viscous fluid on a rotating disk. J. Appl. Phys. 29 (5), 858.

Fischer, K., Gläser, R., Schulze, A., 2014. Nanoneedle and nanotubular titanium dioxide − PES mixed matrix membrane for photocatalysis. Appl. Catal. B Environ. 160−161, 456−464.

Gan, H., Zhang, G., Huang, H., 2013. Enhanced visible-light-driven photocatalytic inactivation of *Escherichia coli* by $Bi_2O_2CO_3/Bi_3NbO_7$ composites. J. Hazard. Mater. 250−251, 131−137.

Gang, M., He, G., Li, Z., Cao, K., Li, Z., Yin, Y., Wu, H., Jiang, Z., 2016. Graphitic carbon nitride nanosheets/sulfonated poly(ether ether ketone) nanocomposite membrane for direct methanol fuel cell application. J. Membr. Sci. 507, 1−11.

Goei, R., Lim, T.T., 2014a. Ag-decorated TiO_2 photocatalytic membrane with hierarchical architecture: photocatalytic and anti-bacterial activities. Water Res. 59, 207−218.

Goei, R., Lim, T.T., 2014b. Asymmetric TiO_2 hybrid photocatalytic ceramic membrane with porosity gradient: effect of structure directing agent on the resulting membranes architecture and performances. Ceram. Int. 40, 6747−6757.

Grunwaldt, J.D., Maciejewski, M., Becker, O.S., Fabrizioli, P., Baiker, A., 1999. Comparative study of Au/TiO_2 and Au/ZrO_2 catalysts for low-temperature CO oxidation. J. Catal. 186, 458−469.

Han, J., Qiu, W., Gao, W., 2010. Adsorption of estrone in microfiltration membrane filters. Chem. Eng. J. 165, 819−826.

Hashizume, M., Kunitake, T., 2003. Preparation of self-supporting ultrathin films of titania by spin coating. Langmuir 19, 10172−10178.

He, X.F., Chen, R., Zhu, X., Liao, Q., An, L., Cheng, X., Li, L., 2016. Optofluidics-based membrane microreactor for wastewater treatment by photocatalytic ozonation. Ind. Eng. Chem. Res. 55, 8627−8635.

Horng, R.Y., Huang, C., Chang, M.C., Shao, H., Shiau, B.L., Hu, Y.J., 2009. Application of TiO_2 photocatalytic oxidation and non-woven membrane filtration hybrid system for degradation of 4-chlorophenol. Desalination 245, 169−182.

Huang, Y.Y., Chou, K.S., 2003. Studies on the spin coating process of silica films. Ceram. Int. 29, 485−493.

Huo, Y., Xie, Z., Wang, X., Li, H., Hoang, M., Caruso, R.A., 2013. Methyl orange removal by combined visible-light photocatalysis and membrane distillation. Dyes Pigment 98, 106−112.

Irie, H., Watanabe, Y., Hashimoto, K., 2003. Carbon-doped anatase TiO_2 powders as a visible-light sensitive photocatalyst. Chem. Lett. 32, 772−773.

Jhaveri, J.H., Murthy, Z.V.P., 2016. A comprehensive review on anti-fouling nanocomposite membranes for pressure driven membrane separation processes. Desalination 379, 137−154.

Jiang, B., Wang, B.Y., Zhang, L.H., Sun, Y.L., Xiao, X.M., Hao, L., Yang, N., 2016. Enhancing antifouling performance of poly (L-lactide) membranes by TiO_2 nanoparticles. J. Appl. Polym. Sci. 133 (24), 8.

Kim, J.O., Jung, J.T., Choi, W.Y., 2006. Application of photocatalytic metal membrane system for water purification. Key Eng. Mater. 1317−1320.

Kim, S.H., Kwak, S.Y., Sohn, B.H., Park, T.H., 2003. Design of TiO_2 nanoparticle self-assembled aromatic polyamide thin-film-composite (TFC) membrane as an approach to solve biofouling problem. J. Membr. Sci. 211, 157−165.

Kou, H., Jia, L., Wang, C., 2012. Electrochemical deposition of flower-like ZnO nanoparticles on a silver-modified carbon nanotube/polyimide membrane to improve its photoelectric activity and photocatalytic performance. Carbon 50, 3522−3529.

Lee, J.W., Kwon, T.O., Thiruvenkatachari, R., Moon, I.S., 2006. Adsorption and photocatalytic degradation of bisphenol A using TiO_2 and its separation by submerged hollow fiber ultrafiltration membrane. J. Environ. Sci. 18, 193−200.

Leong, S.W., Low, Z.-X., Liu, Q., Hapgood, K., Zhang, X., Wang, H., 2016. Preparation of supported photocatalytic membrane from mesoporous titania spheres for humic acid removal from wastewater. Asia Pac. J. Chem. Eng. 11, 611−619.

Leong, S.W., Razmjou, A., Wang, K., Hapgood, K., Zhang, X.W., Wang, H.T., 2014. TiO_2 based photocatalytic membranes: a review. J. Membr. Sci. 472, 167−184.

Le Roux, J.D., Paul, D.R., 1992. Preparation of composite membranes by a spin coating process. J. Membr. Sci. 74, 233−252.

Li, B.R., Chen, Z.Y., Wang, J.B., Zhang, Z.L., Fan, Q.J., Wei, Z.S., 2016. Nitric oxide removal with a Fe-TiO_2/PSF hybrid catalytic membrane bioreactor. Huanjing Kexue 37, 847−853.

Li, L., Liu, Z., Zhang, Q., Meng, C., Zhang, T., Zhai, J., 2015. Underwater superoleophobic porous membrane based on hierarchical TiO_2 nanotubes: multifunctional integration of oil−water separation, flow-through photocatalysis and self-cleaning. J. Mater. Chem. A 3, 1279−1286.

Li, L., Wang, G., Chen, R., Zhu, X., Wang, H., Liao, Q., Yu, Y., 2014. Optofluidics based micro-photocatalytic fuel cell for efficient wastewater treatment and electricity generation. Lab Chip 14, 3368−3375.

Li, Y.H., Sun, J.Q., Liu, L.F., Yang, F.L., 2017. A composite cathode membrane with $CoFe_2O_{4-r}$GO/PVDF on carbon fiber cloth: synthesis and performance in a photocatalysis-assisted MFC-MBR system. Environ. Sci. Nano 4, 335−345.

Liu, H., Dao, A.Q., Fu, C., 2016a. Activities of combined TiO_2 semiconductor nanocatalysts under solar light on the reduction of CO_2. J. Nanosci. Nanotechnol. 16, 3437−3446.

Liu, L.F., Zhang, P.H., Yang, F.L., 2010. Adsorptive removal of 2,4-DCP from water by fresh or regenerated chitosan/ACF/TiO_2 membrane. Sep. Purif. Technol. 70, 354−361.

Liu, S., Wang, X.T., Zhao, W.X., Wang, K., Sang, H.X., He, Z., 2013. Synthesis, characterization and enhanced photocatalytic performance of Ag_2S-coupled ZnO/ZnS core/shell nanorods. J. Alloys Compd. 568, 84−91.

Liu, X., Cong, R., Cao, L., Liu, S., Cui, H., 2014. The structure, morphology and photocatalytic activity of graphene-TiO_2 multilayer films and charge transfer at the interface. New J. Chem. 38, 2362−2367.

Liu, X., Jian, X., Yang, H.M., Song, X.L., Liang, Z.H., 2016b. A photocatalytic graphene quantum dots-Cu_2O/bipolar membrane as a separator for water splitting. New J. Chem. 40, 3075−3079.

Liu, X.F., Xing, Z.P., Zhang, H., Wang, W.M., Zhang, Y., Li, Z.Z., Wu, X.Y., Yu, X.J., Zhou, W., 2016c. Fabrication of 3D mesoporous black TiO_2/MoS_2/TiO_2 nanosheets for visible-light-driven photocatalysis. ChemSusChem 9, 1118−1124.

Liu, Z., Zhang, X., Nishimoto, S., Jin, M., Tryk, D.A., Murakami, T., Fujishima, A., 2008. Highly ordered TiO_2 nanotube arrays with controllable length for photoelectrocatalytic degradation of phenol. J. Phys. Chem. C 112, 253−259.

Lu, X.P., Dai, W.X., Wang, X.X., Fu, X.Z., Shao, Y., Liu, P., Li, D.Z., 2004. Electrophoretic deposition of TiO_2 colloid particles on aluminum alloy surface and the photocatalytic property of the resulted TiO_2 membrane. Chin. J. Inorg. Chem. 20, 734−738.

Luengas, A., Barona, A., Hort, C., Gallastegui, G., Platel, V., Elias, A., 2015. A review of indoor air treatment technologies. Rev. Environ. Sci. Biotechnol. 14, 499−522.

Madaeni, S.S., Ghaemi, N., 2007. Characterization of self-cleaning RO membranes coated with TiO_2 particles under UV irradiation. J. Membr. Sci. 303, 221−233.

Meng, X.F., Qian, Z.Z., Wang, H.T., Gao, X.W., Zhang, S.M., Yang, M.S., 2008. Sol-gel immobilization of SiO_2/TiO_2 on hydrophobic clay and its removal of methyl orange from water. J. Sol Gel Sci. Technol. 46, 195−200.

Mitoraj, D., Kisch, H., 2008. The nature of nitrogen-modified titanium dioxide photocatalysts active in visible light. Angew. Chem. Int. Ed. 47, 9975−9978.

Mozia, S., Morawski, A.W., Toyoda, M., Inagaki, M., 2009. Application of anatase-phase TiO_2 for decomposition of azo dye in a photocatalytic membrane reactor. Desalination 241, 97−105.

Mozia, S., Toyoda, M., Inagaki, M., Tryba, B., Morawski, A.W., 2007. Application of carbon-coated TiO_2 for decomposition of methylene blue in a photocatalytic membrane reactor. J. Hazard. Mater. 140, 369−375.

Nor, N.A.M., Jaafar, J., Ismail, A.F., Mohamed, M.A., Rahman, M.A., Othman, M.H.D., Lau, W.J., Yusof, N., 2016. Preparation and performance of PVDF-based nanocomposite membrane consisting of TiO_2 nanofibers for organic pollutant decomposition in wastewater under UV irradiation. Desalination 391, 89−97.

Padmanaban, V.C., Giri Nandagopal, M.S., Madhangi Priyadharshini, G., Maheswari, N., Janani Sree, G., Selvaraju, N., 2016. Advanced approach for degradation of recalcitrant by nanophotocatalysis using nanocomposites and their future perspectives. Int. J. Environ. Sci. Technol. 13, 1591−1606.

Pant, B., Park, M., Kim, H.-Y., Park, S.-J., 2017. CdS-TiO_2 NPs decorated carbonized eggshell membrane for effective removal of organic pollutants: a novel strategy to use a waste material for environmental remediation. J. Alloys Compd. 699, 73−78.

Papageorgiou, S.K., Romanos, G.E., Katsaros, F.K., 2012. Alginate based materials in environmental applications: from metal sorption to advanced catalytic and membrane processes. In: Alginates: Production, Types and Applications. Nova Science Publishers, Inc., pp. 61−95

Prodhomme, P., Warren, S., Cortes, R., Jurca, H.F., Maroun, F., Allongue, P., 2010. Epitaxial growth of gold on H-Si (111): the determining role of hydrogen evolution. ChemPhysChem 11, 2992−3001.

Roso, M., Lorenzetti, A., Besco, S., Monti, M., Berti, G., Modesti, M., 2011. Application of empirical modelling in multi-layers membrane manufacturing. Comput. Chem. Eng. 35, 2248−2256.

Sasaki, Y., Kato, H., Kudo, A., 2013. $[Co\ (bpy)_3)]^{3+/2+}$ and $[Co\ (phen)_3]^{3+/2+}$ electron mediators for overall water splitting under sunlight irradiation using Z-scheme photocatalyst system. J. Am. Chem. Soc. 135, 5441−5449.

Schneider, J., Matsuoka, M., Takeuchi, M., Zhang, J., Horiuchi, Y., Anpo, M., Bahnemann, D.W., 2014. Understanding TiO_2 photocatalysis: mechanisms and materials. Chem. Rev. 114, 9919−9986.

Sholl, D.S., Johnson, J.K., 2006. Making high-flux membranes with carbon nanotubes. Science 312, 1003−1004.

Tacchini, I., Terrado, E., Ansón, A., Martínez, M.T., 2011. Anatase nanotubes synthesized by a template method and their application as a green photocatalyst. J. Mater. Sci. 46, 2097−2104.

Tan, B.Y., Juay, J., Liu, Z., Sun, D., 2016. Flexible hierarchical TiO_2/Fe_2O_3 composite membrane with high separation efficiency for surfactant-stabilized oil-water emulsions. Chem. Asian J. 11, 561−567.

Thiruvenkatachari, R., Kwon, T.O., Moon, I.S., 2005. Application of slurry type photocatalytic oxidation-submerged hollow fiber microfiltration hybrid system for the degradation of bisphenol A (BPA). Sep. Sci. Technol. 40, 2871−2888.

Tian, Y., Zhao, Y., Gong, C., Chai, Y., 2012. Mechanism and the influences of different substrates on photocatalytic property of TiO_2 membrane. In: ISCEMP 2012, pp. 1200−1204.

Wang, D.K., Elma, M., Motuzas, J., Hou, W.C., Xie, F.W., Zhang, X.W., 2017. Rational design and synthesis of molecular-sieving, photocatalytic, hollow fiber membranes for advanced water treatment applications. J. Membr. Sci. 524, 163−173.

Wang, G.L., Chen, S., Yu, H.T., Quan, X., 2015. Integration of membrane filtration and photoelectrocatalysis using a TiO_2/carbon/Al_2O_3 membrane for enhanced water treatment. J. Hazard. Mater. 299, 27−34.

Wang, X., Wang, W., Liu, P., Wang, P., Zhang, L., 2011. Photocatalytic degradation of *E. coli* membrane cell in the presence of ZnO nanowires. J. Wuhan Univ. Technol. Mater. Sci. 26, 222−225.

Wang, X.F., Hsiao, B.S., 2016. Electrospun nanofiber membranes. Curr. Opin. Chem. Eng. 12, 62−81.

Wei, Z.S., Li, B.R., Wang, J.B., Huang, Z.S., He, Y.M., Chen, Z.Y., 2016. Coupling membrane catalysis and biodegradation for nitric oxide removal in a novel hybrid catalytic membrane biofilm reactor. Chem. Eng. J. 296, 154−161.

Yang, S., Gong, Y., Zhang, J., Zhan, L., Ma, L., Fang, Z., Vajtai, R., Wang, X., Ajayan, P.M., 2013. Exfoliated graphitic carbon nitride nanosheets as efficient catalysts for hydrogen evolution under visible light. Adv. Mater. 25, 2452−2456.

Yee, K.F., Yeang, Q.W., Ong, Y.T., Vadivelu, V.M., Tan, S.H., 2015. Water remediation using nanoparticle and nanocomposite membranes. In: Nanomaterials for Environmental Protection. Wiley Blackwell, pp. 269−291.

Zamfirescu, C., Dincer, I., Naterer, G.F., 2011. Analysis of a photochemical water splitting reactor with supramolecular catalysts and a proton exchange membrane. Int. J. Hydrog. Energy 36, 11273−11281.

Zhang, H., Quan, X., Chen, S., Zhao, H., 2006a. Fabrication and characterization of silica/titania nanotubes composite membrane with photocatalytic capability. Environ. Sci. Technol. 40, 6104−6109.

Zhang, H., Quan, X., Chen, S., Zhao, H., Zhao, Y., 2006b. Fabrication of photocatalytic membrane and evaluation its efficiency in removal of organic pollutants from water. Sep. Purif. Technol. 50, 147−155.

Zhang, H., Quan, X., Chen, S., Zhao, H., Zhao, Y., 2006c. The removal of sodium dodecylbenzene sulfonate surfactant from water using silica/titania nanorods/nanotubes composite membrane with photocatalytic capability. Appl. Surf. Sci. 252, 8598−8604.

Zhang, J., Zhang, M., Lin, L., Wang, X., 2015. Sol processing of conjugated carbon nitride powders for thin-film fabrication. Angew. Chem. Int. Ed. 54, 6297−6301.

Zhang, X., Wang, D.K., Lopez, D.R.S., Diniz da Costa, J.C., 2014. Fabrication of nanostructured TiO_2 hollow fiber photocatalytic membrane and application for wastewater treatment. Chem. Eng. J. 236, 314−322.

Zhang, X.W., Pan, J.H., Du, A.J., Fu, W.J., Sun, D.D., Leckie, J.O., 2009. Combination of one-dimensional TiO_2 nanowire photocatalytic oxidation with microfiltration for water treatment. Water Res. 43, 1179−1186.

Zhao, H., Chen, S., Quan, X., Yu, H., Zhao, H., 2016. Integration of microfiltration and visible-light-driven photocatalysis on g-C_3N_4 nanosheet/reduced graphene oxide membrane for enhanced water treatment. Appl. Catal. B Environ. 194, 134−140.

Zhao, H., Li, H., Yu, H., Chang, H., Quan, X., Chen, S., 2013. CNTs-TiO_2/Al_2O_3 composite membrane with a photocatalytic function: fabrication and energetic performance in water treatment. Sep. Purif. Technol. 116, 360−365.

Ziegmann, M., Saravia, F., Torres, P.A., Frimmel, F.H., 2010. The hybrid process TiO_2/PAC: performance of membrane filtration. Water Sci. Technol. 62, 1205−1212.

Zou, L., Ding, H., Dong, L., Ouyang, M., 2008. Synthesis of $WO_3 \cdot H_2O$ nanowire arrays film and its photocatalytic activity. Fuhe Cailiao Xuebao 25, 123−128.

Further Reading

Liao, J.J., Lin, S.W., Pan, N.Q., Li, S.P., Cao, X.K., Cao, Y., 2012. Fabrication and photocatalytic properties of free-standing TiO_2 nanotube membranes with through-hole morphology. Mater. Charact. 66, 24−29.

CHAPTER 4

PMRs Utilizing Pressure-Driven Membrane Techniques

Sylwia Mozia[1], Pietro Argurio[2], Raffaele Molinari[2]
[1]West Pomeranian University of Technology, Szczecin, Poland; [2]University of Calabria, Rende (CS), Italy

4.1 Introduction: General Overview of Photocatalytic Membrane Reactors Utilizing Pressure-Driven Membrane Techniques

Photocatalytic membrane reactors (PMRs) represent an interesting alternative technology useful both in the field of water and air purification and as a synthetic pathway.

A PMR can be defined as a device existing in various configurations, which combines heterogeneous photocatalysis and membrane separations to produce chemical transformations (Molinari et al., 2017).

In a PMR, the membrane has the dual role of maintaining the photocatalyst (e.g., in suspension or immobilized) and the substrate and (sometimes) by-products in the reaction environment and controlling their residence time (RT). In the case of using PMRs for organic pollutants removal, the RT must be adequate to guarantee complete degradation of recalcitrant substances. When the PMR is used as a synthetic pathway, the main objective of the membrane can be the selective separation of the product, thus minimizing its successive transformation (e.g., oxidation) that leads to undesirable by-products.

Several characteristics make PMRs a useful green technology that improves the potentialities of classical photoreactors and membrane processes (separation at molecular level), giving a synergy for both technologies in which each technique complements the advantages and overcomes the challenges of the other (Anpo, 2000; Herrmann et al., 2007; Molinari et al., 2008; Ollis, 2000; Palmisano et al., 2007), e.g.,: (1) use of green and safe photocatalyst, as TiO_2; (2) use of mild oxidants, such as molecular oxygen; (3) possibility to work under mild reaction conditions (closer to room temperature and pressure); (4) possibility to abate refractory, very toxic, and nonbiodegradable molecules with no production of harmful chemicals; (5) possibility to use renewable solar energy, and (6) possibility to operate in continuous mode in systems in which the recovery of the photocatalyst (immobilized or in suspension), the reactions, and the separation of the

Current Trends and Future Developments on (Bio-) Membranes. https://doi.org/10.1016/B978-0-12-813549-5.00004-9

products simultaneously occur. Higher energy efficiency, modularity, and easy scale-up are some other potential advantages of PMRs.

The choice of an appropriate membrane and the knowledge of the parameters influencing the photocatalytic process represent important steps in the design of a PMR.

Various types of membrane photoreactors were built with the purpose of achieving an easy separation of the photocatalyst from the reaction environment and an efficient removal of pollutants from aqueous media.

The most-studied configurations of PMRs are pressurized systems (Mascolo et al., 2007; Molinari et al., 2002a; Tang and Chen, 2004) in which pressure-driven membrane techniques, such as nanofiltration (NF), ultrafiltration (UF), and microfiltration (MF), are combined with a photocatalytic process. These pressurized PMRs (PPMRs) can be built in two configurations: (1) PPMRs that employ powdered TiO_2 suspended in the reaction mixture and (2) PPMRs that utilize TiO_2 immobilized on a substrate material (e.g., glass, quartz, mesoporous materials, stainless steel, or polymers) acting as a membrane. In both cases, the photocatalyst is confined in the pressurized side of the permeation cell. Based on the greater available active surface area compared with immobilized system, the first configuration has been largely used in literature, finding it more efficient than that using immobilized photocatalysts (Dijkstra et al., 2001; Mascolo et al., 2007; Molinari et al., 2004).

In the pertinent literature (Molinari et al., 2004), it was demonstrated that ultraviolet (UV) irradiation mode (UV source immersed in the photoreactor, mounted above the photoreactor/above the membrane module, etc.) and the type of light source (i.e., the emission spectrum of the lamp) strongly affect the rate of pollutant photodegradation.

Different aspects have been studied to improve the performance of PPMRs such as use of different membrane module geometry (e.g., hollow fiber [HF] instead of flat sheet membranes), use of specific operating procedure as membrane backflushing, and increase of flux to decrease photocatalyst deposition and membrane fouling to improve the photocatalytic activity and productivity. Despite all these technological developments and accuracies, the suitability of PPMRs for industrial applications seems to be limited, thus the research is addressed toward the use of other configurations of membrane photoreactors (Le-Clech et al., 2006; Lee et al., 2001; Molinari et al., 2006).

Several studies in literature (Chin et al., 2007a, 2007b; Fernandez et al., 2014; Fu et al., 2006; Huang et al., 2007; Kertesz et al., 2014; Sarasidis et al., 2014) were performed using submerged membrane modules coupled to photocatalysis. In the submerged membrane photocatalytic reactors (SMPRs), also known as submerged PMRs (SPMRs), the photocatalyst is suspended in the reaction environment, the membrane (usually HF type) is immersed in the batch photoreactor and it works in depressurized mode, that is,

the permeate is sucked by means of a pump. On these bases, this kind of system was indicated by some authors as depressurized PMR. A useful strategy, to obtain stable continuous operation (i.e., constant transmembrane pressure (TMP) and constant permeate flux during long-term operations), is represented by the coupling of gas sparging (e.g., air bubbling) at the bottom of the membrane unit (Chan et al., 2007; Ghosh, 2006) with adequate membrane backflushing protocol.

Despite the potentialities of PMR systems with suspended photocatalyst, mainly in the configuration of SPMRs, fouling and light scattering by photocatalyst particles addressed the research toward the use of photocatalytic membranes (PMs) obtained by immobilizing the photocatalyst into the membrane matrix (Anderson et al., 1988; Athanasekou et al., 2015; Moosemiller et al., 1989; Zhang et al., 2006). In such a system, the membrane has the simultaneous task of acting as a selective barrier for the species to be degraded and as support for the photocatalyst. However, also in these PMs, some drawbacks exist, e.g., (1) necessity to irradiate the membrane surface, resulting in possible membrane photodegradation and technical difficulties; (2) moderate loss of photoactivity because of the photocatalyst coverage and lower availability to irradiation; (3) restricted processing capacities owing to mass transfer limitations; and (4) unsatisfactory system lifetime owing to the possible photocatalyst deactivation and washout. On these bases, it is fundamental to prepare systems with appropriate porosity and effective dispersion of the photocatalyst particles. The performances of photocatalytic reactors using PMs are reported in Chapter 6.

Other interesting configurations of PMRs were obtained by coupling the photocatalytic process with membrane operations such as (1) direct contact membrane distillation (DCMD) (Mozia et al., 2007), having the main advantages of avoiding flux decline caused by a photocatalyst and producing a permeate, which is practically pure water, although the high-energy consumption constitutes a disadvantage in terms of process costs; (2) pervaporation (PV) (Camera-Roda and Santarelli, 2007), thus reducing the heating cost of the solution needed in the case of DCMD; (3) dialysis (Azrague et al., 2007), thus reducing operating costs and avoiding the fouling of membrane because the separation occurs due to a diffusion of the pollutant through the membrane, no TMP is needed. The applications of these kinds of PMRs are described in Chapter 5.

4.2 Membrane Fouling in Photocatalytic Membrane Reactors

PMRs have been proposed by many authors (Ahmad et al., 2017; Rajca, 2016; Shon et al., 2008) to solve the limitations of membrane technology in water and wastewater treatment, caused by membrane fouling from the solute content in feed. The increasing concentration of the retentate during membrane filtration constantly accelerates membrane fouling and decreases membrane life. An integrated photocatalysis–membrane hybrid system can lead

to a near-zero fouling by the organic pollutants because the photocatalytic reactions degrade and modify the organic foulant in wastewater. Besides, if UV is irradiated directly on the membrane surface, the photocatalytic reaction can convert the foulant accumulated on the membrane surface, thereby reducing membrane fouling.

The results reported in literature (Du et al., 2017; Ganiyu et al., 2015; Ou et al., 2015; Zangeneh et al., 2015) clearly demonstrate that pressurized and depressurized PMRs were successfully applied in the photodegradation of numerous organic pollutants, including dyes, pharmaceutically active compounds (PhACs), and substances generally indicated as organic matter (OM) contained in aqueous media, both in the case of suspended and immobilized TiO_2. Despite these encouraging results, the major problems encountered in developing efficient slurry PPMRs (photoreactors in which the photocatalyst is suspended in the reaction media and the membrane is pressure driven type) are related to membrane fouling regardless of the type of organic pollutant. Membrane fouling, caused by both organic pollutants and photocatalyst accumulation on the membrane surface, generates a decrease of membrane permeability. On this aspect, both Molinari et al. (2004, 2008) and Hairom et al. (2015), during their experiments on dyes or PhACs photodegradation, demonstrated that slurry PPMRs could be interesting by an application point of view for the decontamination of highly concentrated effluents once the problems related to membrane fouling, which caused a 60%−65% flux decline, have been opportunely minimized. A similar hybrid system, in which a photocatalytic step was followed by a filtration through a flat sheet MF membrane, was tested by Shon et al. (2008) in the removal of OM from wastewater. The results evidenced that the use of MF not only permitted the selective permeation of OM but also acted as a barrier in maintaining the TiO_2 photocatalyst into the reacting environment. Although the proposed hybrid system removed 97% of the OM, the permeate flux was still observed lower than the pure water flux (PWF), confirming that a flux decline took place in the presence of TiO_2 slurry (i.e., in suspension). Besides, considering that membrane fouling can be due to both OM and photocatalyst accumulation on the membrane surface, the authors demonstrated that the lower the OM contents in wastewater the more significant is the TiO_2 slurry effect on the membrane flux. It was also confirmed that the use of an integrated photocatalysis−membrane hybrid system with respect to a simple membrane filtration permits to reduce flux decline caused by contaminant accumulation on the membrane.

It is also important to have good knowledge of feedwater properties because they affect PMR performance, both in terms of photocatalytic activity and membrane permeability. Fernandez et al. (2014), by testing an SPMR, operated at constant permeate flow rate for the photocatalytic degradation of 33 organic contaminants from aqueous media, observed no fouling problems when pure water was the aqueous matrix (TMP remained constant), whereas a significant membrane fouling, attributed to the retained macromolecules, was

observed in the presence of OM background, evidencing the necessity to increase TMP from 0.3 to 0.8 bar to maintain a constant permeation flux.

Sarasidis et al. (2014) evaluating the performance of a laboratory pilot SMPR, operated continuously in degradation of diclofenac (DCF), demonstrated that use of air bubbling and adequate membrane backflushing represents an interesting approach to limit membrane fouling. Ultrapure water (UW), tap water (TW), and groundwater (GW) were tested as aqueous matrices, thus evaluating the influence of water matrix on the performance of the photocatalytic system both in terms of degradation and membrane fouling. The feedwater characteristics showed an important role in terms of removal efficiency, which decreased by using TW and GW, whereas no difference was observed in terms of membrane fouling. In particular, operating with an automatic periodic membrane backwashing (duration 1 min) every 9 min of filtration, fouling was controlled, thus permitting stable continuous operation (TMP practically constant during the 72 h of operation at constant permeate flux). So, the developed automatic backwashing protocol effectively contrasts membrane fouling independently from the aqueous matrix. These results demonstrated that fouling of the submerged membrane can be controlled (not avoided) by optimizing the operating parameters and, in particular, membrane backflushing parameters, i.e., frequency, duration, and intensity. Besides, membrane backflushing also allows maintaining the required photocatalyst concentration in the reaction mixture (Kertesz et al., 2014).

The efficiency of SPMR with fine bubble aeration and membrane backflushing in removing different organic pollutants from aqueous systems and limiting the problems related to membrane fouling was also confirmed by other authors (Fu et al., 2006; Zheng et al., 2015). The demonstrated possibility to operate at constant permeate flow and TMP represents a technical requirement in running some membrane plants in continuous mode to treat a constant feed flow rate.

Fu et al. (2006) reported that photocatalyst dimension is another important parameter to be considered for controlling membrane fouling. In particular, their work demonstrated that the use of nanostructured TiO_2 instead of commercial TiO_2 P25 powder gave an increase of permeate flux, and therefore a reduction of membrane fouling. This trend was ascribed to the higher average particle size of nanostructured TiO_2 (50 μm vs 30 nm), which permitted photocatalyst suspension avoiding membrane fouling and allowed its easy separation.

Another strategy to mitigate membrane fouling in SPMR was investigated by Chin et al. (2007a): an intermittent permeation method, consisting in alternate permeation/suction stopping during the operation. When suction was stopped and no permeate was collected, the shear stress was created on the membrane surface by the aeration facilitating the

detachment of photocatalyst particles and, therefore, avoiding their accumulation on the membrane, which is the principal cause of membrane fouling.

The effectiveness of this approach was also demonstrated by other researchers (Choi, 2006; Huang et al., 2007; Zheng et al., 2015). The results obtained by Huang et al. (2007) in a study on the operational conditions of SPMR evidenced that the sedimentation of the suspended photocatalyst can be controlled by applying fine bubble aeration and an intermittent membrane filtration. Choi (2006) reported that during degradation of 4-chlorophenol (4-CP) in a pilot-scale SPMR, no fouling of the membrane was observed when an intermittent operation was used. A similar approach was applied by Zheng et al. (2015), who studied virus removal from aqueous media. They used the experimental setup, schematized in Fig. 4.1, operated under constant flux mode. The influences of filtration flux and permeation mode (continuous or intermittent) were tested. The optimal operating condition was determined to be the intermittent suction mode with a filtration flux of 40 L m^{-2} h^{-1}. Above this value, irreversible fouling was observed.

The presence of a sustainable permeate flux (i.e., a flux value below which reversible membrane fouling is detected (but it can be easily removed by membrane backflushing), whereas above this value irreversible fouling is observed) was also evidenced in their work by Kertesz et al. (2014). They found a sustainable permeate flux of 40 L m^{-2} h^{-1} by operating an SPMR in dead-end mode for the photocatalytic degradation of Acid Red 1 (AR1) in aqueous suspension of TiO_2.

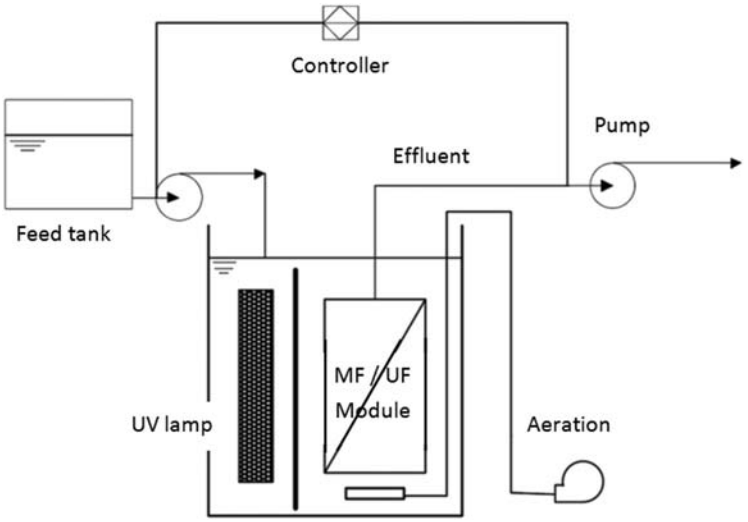

Figure 4.1
Schematization of the submerged photocatalytic membrane reactor employed by Zheng et al. (2015). *MF*, microfiltration; *UF*, ultrafiltration; *UV*, ultraviolet.

The operating pH plays a significant role in controlling the photocatalytic efficiency and fouling behavior in the PPMR system, as it may affect (1) the surface charge of the photocatalyst and then its interaction with the substrate and/or the membrane and (2) the size of photocatalyst particles. On this aspect, Hairom et al. (2015) tested ZnO nanoparticles self-synthesized via precipitation method for industrial dye wastewater treatment in a pressurized slurry PMR. They observed a severe fouling at pH 2, 7, and 8 because of the weak electrostatic repulsion among the membrane surface, ZnO particles, and the dye in the wastewater, being all the pHs near to their isoelectric point.

Membrane permeability was strongly affected by hydraulic conditions, thus their optimization permits to limit membrane fouling. On the basis of this, Choo et al. (2008) tested a slurry PMR using a hollow fiber MF module for the degradation of toxic organic compounds such as trichloroethylene (TCE) in water. They evidenced that an improvement of 60% in flux was achieved when the tangential velocity increased from 0.19 to 1.45 m s^{-1}, owing to the lower deposition of TiO_2 particles on the membrane surface. The addition of a typical background species, such as humic acids, to the wastewater did not give a significant effect on TCE degradation while it played a significant role in the decline of permeability by 60%.

Summarizing, from our point of view, SPMRs operated under optimized conditions with fine bubble aeration and membrane backflushing can have, at present, greater perspective of industrial applications than the PPMRs because they are able to remove different organic pollutants from waters limiting the problems related to membrane fouling.

4.3 Stability of Membranes in Photocatalytic Membrane Reactors

Membranes applied in PMRs are exposed to harsh process conditions prevailing in these systems resulting from the action of UV irradiation, the oxidizing environment created by the reactive oxygen species (ROS) (mainly $^{\bullet}OH$ radicals), and the abrasive effect of photocatalyst particles. Taking this into account, the choice of a membrane material is a key issue when designing the hybrid photocatalysis–membrane systems. Both polymeric and inorganic membranes have been applied in PMRs described in literature. Ceramic membranes exhibit properties that make them especially attractive for this application, which is associated with their high chemical and thermal stability. However, due to lower price as well as ease of manufacturing and structure design, the polymeric membranes are of higher interest than the inorganic ones.

In PMR configurations in which the radiation source is located above/in a membrane module, the polymeric membranes are directly exposed to the action of UV irradiation, which creates a danger of their destruction. The stability of the membranes under such

conditions depends on the type of polymer applied as a membrane material. Analysis of 11 commercial polymeric membranes (Table 4.1) revealed (Molinari et al., 2000) that samples made of polyacrylonitrile (PAN), fluoride + polypropylene (PP), and polysulfone (PSU) + PP exhibited higher resistance to UV-A irradiation ($\lambda_{max} = 365$ nm) than those made of PSU, polyethersulfone (PES), polyamide (PA), or even polyvinylidene fluoride (PVDF). Similar conclusions were drawn on a basis of investigations on 7 MF and 3 UF polymeric membranes (Table 4.1) realized by other researchers (Chin et al., 2006). Based on the differences between the PWF measured for new and UV-A–irradiated samples, they reported that the stability of the membranes decreased in the following order: PES > PSU > PP = CA > PVDF-MP > PC > PVDF Pall = PTFE = PAN = PVDFphobic.

Table 4.1: Commercial polymeric membranes applied in UV stability tests (Chin et al., 2006; Molinari et al., 2000).

Polymer	Membrane Symbol	Manufacturer	Molecular Weight Cut-off or Pore Size	Stability	Source
PSU	MPPS 0000 u002	Separem	15 kDa	++	Molinari et al. (2000)
PSU	MPPS 0000 u006	Separem	40 kDa	++	
PES	PES	TechSep	40 kDa	+	
PA	MPCU 0000 u25	Separem	2.5 kDa	+++	
PA	MPCU 0000 u20	Separem	2.0 kDa	+++	
PEEK	P-12-10	Homemade	–	++	
PVDF	PVDF	Techsep	0.1 μm	++	
PAN	PAN	Techsep	40 kDa	+++	
PSU + PP	GR 51 PP	Techsep	50 kDa	+++	
CA + PP	CA 600 PP	Dow	20 kDa	+	
Fluoride + PP	FS 50 PP	Dow	50 kDa	+++	
PSU	PS	Osmonics	600 kDa	+	Chin et al. (2006)
PES	PES	Millipore	50 kDa	+	
PVDF	PVDFphobic	Millipore	0.22 μm	+++	
PVDF	PVDF-MP	Millipore	0.22 μm	++	
PVDF	PVDF-Pall	Pall Filtration	0.1 μm	+++	
PAN	PAN	Cleanseas	~40 kDa	+++	
CA	CA	MFS	0.2 μm	++	
PP	PP	Osmonics	0.1 μm	++	
PC	PC	Millipore	0.1 μm	++	
PTFE	PTFE	Cole Parmer	0.2 μm	+++	

CA, cellulose acetate; *PA*, polyamide; *PAN*, polyacrylonitrile; *PC*, polycarbonate; *PEEK*, polyetheretherketone; *PES*, polyethersulfone; *PP*, polypropylene; *PSU*, polysulfone; *PTFE*, polytetrafluoroethylene; *PVDF*, polyvinylidene fluoride; *UV*, ultraviolet.

Chemical changes in a polymeric membrane structure induced by UV irradiation are a complex phenomenon that includes chain scission and/or cross-linking followed by reactions with oxygen resulting in formation of functional groups such as carbonyl (C═O), carboxyl (COOH), peroxide (O−O), etc. (Rupiasih et al., 2013). Fig. 4.2 presents as an example of the mechanism of degradation of PSU—a polymer with relatively low stability under UV illumination. The high susceptibility of PSU to destruction by UV irradiation results in low stability of membranes made of this polymer. Rupiasih et al. (2013) reported that even after less than 15 min of exposure of a PSU membrane to the action of a 15-W germicidal lamp ($\lambda_{max} = 254$ nm, $I = 0.28$ W m^{-2}) the pore size and pore number increased, whereas a 45-min exposure resulted in cracks and other damages. The membrane destruction led to about 225%−370% increase of PWF.

The membrane damage under UV irradiation was also reported in case of PMs, e.g., TiO_2-modified PSU membranes exhibiting self-cleaning properties (Feng et al., 2015). The polymer chains in such membranes can be broken not only by UV radiation but also by ROS, e.g., $^{\bullet}OH$ radicals formed during photocatalytic process. Feng et al. (2015) proposed application of an intermediate polydopamine (PDA) layer, serving as a free radical scavenger, protecting the PSU membrane against UV irradiation. The authors reported that a membrane without the protective layer was completely destroyed after 9 days of UV irradiation, whereas under the same conditions the membrane with the PDA layer exhibited a stable performance (in terms of permeate flux and rejection) and its matrix remained complete.

PVDF membranes have been found to be more resistant to damage by UV irradiation than the PSU or PES ones (Chin et al., 2006; Molinari et al., 2000). Zhao et al. (2016) in their recent paper reported that also TiO_2-modified PVDF PMs exhibited excellent chemical stability under photocatalytic conditions during 2 h of UV irradiation. However, the research by Lee et al. (2016) revealed that long-term exposition of TiO_2-PVDF PMs to UV-A irradiation resulted in severe damage of their structure. Numerous surface cracks

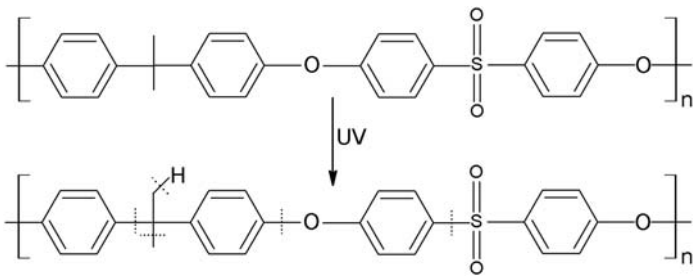

Figure 4.2
Scheme of possible bond dissociation or scission of polysulfone under ultraviolet (UV) irradiation (Jyothi et al., 2014).

Table 4.2: Influence of UV-A irradiation on permeate flux, mechanical strength, and thermal stability of TiO_2-PVDF photocatalytic membrane (Lee et al., 2016).

UV Exposure Time (h)	Permeate Flux ($L\ m^{-2}\ h^{-1}$)	Tensile Strength (MPa)	Elongation at Break (%)	Decomposition Temperature (°C)
0	10.9	1.93	326	406
40	11.5	1.90	160	421
60	16.0	1.82	128	406
120	21.8	1.73	120	390

PVDF, polyvinylidene fluoride; *UV*, ultraviolet.

were observed after 40 h of illumination, whereas after 120 h of UV exposure the separation layer of the membrane was severely destructed, which was accompanied by reduction of its thickness from 153 to <120 μm. Extension of the irradiation time above 120 h resulted in a complete damage of the membrane, which turned to powder form. The proceeding membrane destruction with UV exposure time was accompanied by a continuous increase of permeate flux and a deterioration of mechanical properties and thermal stability (Table 4.2).

The results presented by Lee et al. (2016) clearly show how important are long-term investigations in evaluation of membrane stability. The short-term experiments, which are very commonly present in the literature, often lead to misleading conclusions about high lifespan of polymer-based PMs.

Another issue related to stability of membranes in PMRs is membrane damage due to abrasive action of photocatalyst particles (Darowna et al., 2017; Mozia et al., 2015a, 2015b; Szymański et al., 2016). The mechanical destruction of membrane separation layer in the slurry PMRs refers to both polymeric (organic) and ceramic (inorganic) membranes. Based on changes of rejection of model compounds (dextrans) by four commercial PES UF membranes (Table 4.3) after their operation in a PPMR, it was concluded

Table 4.3: Properties of commercial PES membranes applied in stability tests in PPMR (Mozia et al., 2015a).

Membrane	UFPT	UFPW	UE10	UE50
Manufacturer	GE Osmonics, USA	GE Osmonics, USA	Trisep Corp.	Trisep Corp.
MWCO (kDa)[a]	5	10	10	100
PWF at TMP = 1 bar ($L\ m^{-2}\ h^{-1}$)	49	130	150	760
Contact angle (degrees)	67.1	55.8	73.9	68.5

MWCO, molecular weight cut-off; *PES*, polyethersulfone; *PPMR*, pressurized photocatalytic membrane reactor; *PWF*, pure water flux; *TMP*, transmembrane pressure.
[a]According to manufacturer.

(Mozia et al., 2015a; Darowna et al., 2017) that the severity of membrane damage due to abrasion depends on membrane type, photocatalyst type, process parameters (i.e., feed flow rate and TMP), and feed composition. The polymeric membrane destruction was observed for a very short time of their operation in a PPMR, which amounted in some cases to 35 h only.

In general, membranes with very fine pores and a delicate, thin separation layer were found to be less resistant to abrasion than the ones exhibiting thicker skin with larger pores. The destruction of a membrane surface was more severe when photocatalyst agglomerates were small and sharp edged than in case of large, round-shaped particles. Large particles caused formation of deep cracks but did not destroy the whole surface, whereas small particles polished the membrane surface leading to a severe damage of skin layer. The effect of TMP on stability of membranes was found to be much more significant than the influence of feed crossflow velocity (CFV). In general, operation under low TMP (1 bar) restricted the deterioration of the separation properties of the membranes and, additionally, prevented from membrane fouling. Moreover, the abrasive action of TiO_2 particles was more damaging when the particles were suspended in UW than in case of feed containing OM (humic acids) and inorganic salts (sulfates, phosphates, and bicarbonates). That was due to different shape and size of TiO_2 aggregates formed in the presence of various compounds in the treated water (Mozia et al., 2015a). It was also reported (Mozia et al., 2015a) that abrasion of the PES membrane surface by TiO_2 particles contributed to the loss of their separation properties to a greater extent than the action of oxidative species, such as H_2O_2, even when applied at very high concentration (10 g L^{-1}).

It must be stated clearly that not only polymeric but also ceramic UF membranes were found to undergo damage by abrasive action of photocatalyst particles (Mozia et al., 2015b). The investigations on three commercial ceramic TiO_2 membranes with various separation characteristics (Filtanium series, TAMI Industries, France) revealed that the membrane with the finest pores (molecular weight cut-off [MWCO] = 5 kDa) underwent significant destruction and lost completely its separation properties toward polyethylene glycol (PEG) applied as a model compound just after 100 h of operation. Based on an observed increase in the membrane roughness after its exploitation in the PMR compared with the brand new membrane (Fig. 4.3), it was concluded that the gentle skin layer was simply scraped by the flowing TiO_2 particles. On the opposite, in case of an MF membrane (pore size of 0.2 μm) an increase of rejection efficiency in time was observed, which was attributed to the deposition of TiO_2 particles in the membrane pores. The separation characteristics of a UF membrane with MWCO of 100 kDa were found to be stable during 100 h of operation (Mozia et al., 2015b). However, extension of its exploitation time up to 400 h resulted in an observable loss of the separation properties. The rejection of 70-kDa dextran decreased from 95% at the beginning of

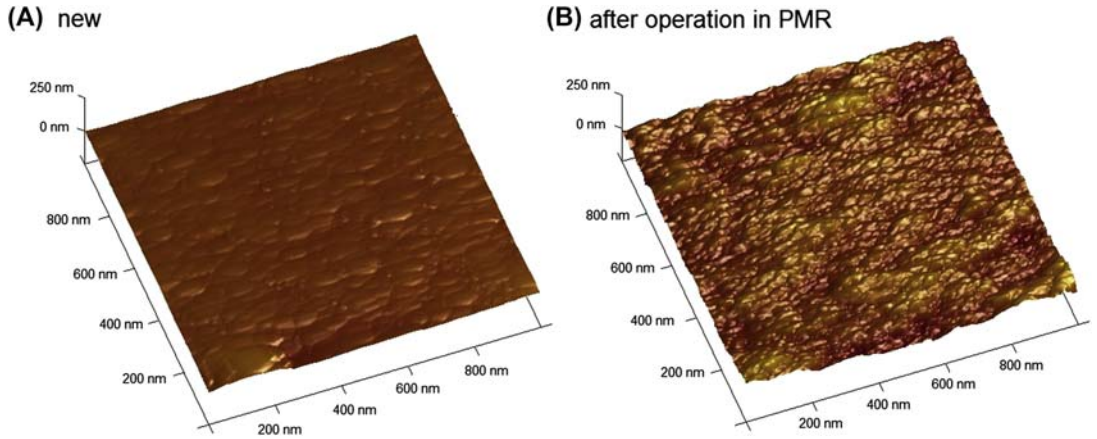

Figure 4.3

Atomic force microscopy (AFM) images of the brand new Filtanium 5 membrane (A) and the membrane after operation in photocatalytic membrane reactor (PMR) (B) (Mozia et al., 2015b).

the process to 46% after 400 h of the experiments realized in the presence of TiO_2 (Szymański et al., 2016). These results confirm how important, before the development of a PMR setup, are long-term investigations on the resistance of a membrane not only to the action of UV irradiation and ROS but also to the abrasive damage by the photocatalyst particles.

When stability of PMs applied in PMRs is considered, two additional factors should also be taken into account: (1) the strength of attachment/binding of photocatalyst particles, which prevents from their washing out from the membrane matrix or surface and (2) maintaining/recovery of membrane photoactivity. The highest risk of washing out of photocatalyst particles exists in the case of PMs prepared by the dip coating technique or simple physical deposition via filtration. During long-term operations or high shear stress introduced by the filtration velocity, the particles might be detached (Mozia et al., 2013). As a result, the membrane might be losing its properties after some time. The stability of membrane photoactivity results from the stability of the photocatalyst activity and is strongly associated with the strength of photocatalyst binding. Both parameters are influenced by process conditions and feed composition and, therefore, should be evaluated under conditions similar to the real ones.

The presented overview clearly shows that a successful scale-up of PMRs requires development of novel membranes resistant to the severe conditions prevailing in these systems. The membranes should exhibit excellent lifespan, especially in terms of resistance to oxidation by hydroxyl radicals and other oxidative species as well as abrasion by photocatalyst particles. To prove this resistance the long-term lifespan or aging tests are necessary. However, it must be considered that a careful design of the membrane

photoreactor can reduce these drawbacks (e.g., separating the reaction zone from the membrane separation zone).

4.4 Operating Variables Influencing Permeate Quality in Photocatalytic Membrane Reactors

The quality of permeate in pressure-driven PMRs depends on both photocatalytic and membrane separation components. The efficiency of photodegradation arises strictly from the factors associated with the photocatalysis itself, such as light wavelength and intensity, photocatalyst type and loading, solution composition, reactor configuration, etc. The parameters related to the membrane process, which affect permeate quality mainly include the following (Table 4.4):

- hydraulic retention time (HRT, RT) associated with the permeate flux;
- operational mode (e.g., batch vs continuous flow, dead end vs crossflow, intermittent vs continuous operation, with/without backwash, etc.);
- hydraulic process parameters (CFV, TMP);
- separation characteristics of a membrane, and
- module packing density (MPD).

HRT is strictly associated with permeate flux, which in turn is connected with TMP and membrane characteristics. Long RT is desirable when an improvement of photodegradation efficiency is considered. An increase in TMP results in shortening of HRT, which leads to a decrease of permeate quality. Controlling of RT is especially important in case of MF or UF that are characterized by high permeate fluxes and limited rejection of low molecular organic compounds, being the products of photodegradation. Nonetheless, optimization of the process in terms of RT is required for a given system, and feed composition taking into account that low pollutant concentrations as well as low-molecular-weight compounds may require shorter HRT and vice versa (Sarasidis et al., 2014). Fig. 4.4 presents, as an example, the influence of RT on treatment efficiency during removal of 1,4-dioxane as a model contaminant in an SPMR equipped with PVDF MF membrane.

PMRs can be operated either in batch or in continuous modes. In some cases the semibatch systems can also be applied. In general, the treatment efficiency in continuous flow PMRs is lower than in the batch ones (Molinari et al., 2001, 2002b; Mozia et al., 2013). This is associated mainly with shorter HRT in case of the former systems. The batch mode is recommended when the volumes of the treated feed are relatively small. On the opposite, in case of large feed quantities, the continuous flow PMRs are more promising, even though the treatment efficiency compared with the batch systems is lower (Molinari et al., 2002a).

Table 4.4: Operating variables influencing permeate quality in pressure-driven PMRs (Jiang and Choo, 2016; Moustakas et al., 2014; Mozia et al., 2013; Ong et al., 2014; Wang and Lim, 2012).

Operating Variable	Description
Effectiveness of photocatalytic degradation of pollutants	Associated with the parameters influencing the photocatalytic process: reactor design, light wavelength and intensity, photocatalyst type and loading (i.e., concentration in a slurry or mass deposited in/on a membrane), pH, oxygen content, solution composition (e.g., concentration of pollutants, presence of inorganic ions, etc.). In general, improvement of photodegradation (mineralization) efficiency results in improvement of permeate quality.
Hydraulic retention time (HRT) (residence time, RT)	Elongation of HRT contributes to enhancement of photodegradation efficiency and improvement of permeate quality. In general, lower the permeate flux better the permeate quality.
Operational Mode	
• Batch versus continuous flow	Batch mode was found to be more efficient than the continuous flow one. Considering the potential industrial application, the continuous system is, however, more favorable.
• Intermittent versus continuous	The effect of intermittent permeation on the degradation efficiency and product quality was found to be negligible. However, intermittent operation can help in prevention from deposition of photocatalyst on a membrane leading to an improved degradation efficiency.
• With or without back-washing/backpulsing	Backwashing/backpulsing contributes to removal of deposited photocatalyst from a membrane surface, thus increasing its concentration in the bulk and enhancing photocatalysis.
• With or without aeration (SPMR)	Air bubbles formed during aeration can interfere with photocatalysis due to light scattering, which might lead to decrease of degradation efficiency.
Hydraulic Process Parameters	
• CFV	Increase of CFV can mitigate or prevent from deposition of photocatalyst on a membrane, which results in improved degradation efficiency.
• TMP	• Increase of degradation efficiency at lower TMP due to increase of HRT. • Decrease of degradation efficiency at higher TMP due to enhanced deposition of photocatalyst particles on/in a membrane and shortening of HRT.
Type of the membrane process and separation characteristics of the membrane	For the pressure-driven processes the quality of permeate increases with decreasing the pore size of the membranes (MF < UF < NF).
Module packing density (PMRs with photocatalytic membranes)	An increase of module packing density results in an increase of active surface of photocatalytic membranes and thus an increase of photodegradation efficiency. However, at too high packing density the membrane fibers tend to attach each other and the active surface is reduced.

CFV, crossflow velocity; *MF*, microfiltration; *NF*, nanofiltration; *PMR*, photocatalytic membrane reactor; *SPMR*, submerged photocatalytic membrane reactor; *TMP*, transmembrane pressure; *UF*, ultrafiltration.

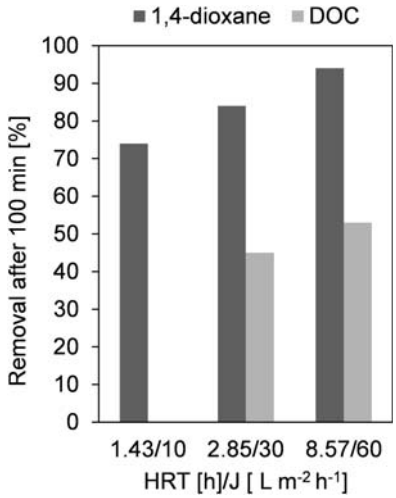

Figure 4.4
Influence of hydraulic retention time (HRT) on removal of 1,4-dioxane and dissolved organic carbon (DOC) in submerged photocatalytic membrane reactor utilizing microfiltration. Parameters: TiO_2 P25 concentration, 5.0 g L^{-1}; initial 1,4-dioxane concentration, 0.85 mg L^{-1}; initial DOC concentration, 4.4 mg L^{-1}; membrane, polyvinylidene fluoride (0.4 μm). J—permeate flux. *Based on Lee et al., 2015.*

The treatment in PMRs utilizing submerged membranes can be realized either in the continuous or in the intermittent suction mode. Application of intermittent permeation could lead to improvement of permeate flux and reduction of membrane fouling (Mozia et al., 2013). Nonetheless, no substantial effect of intermittent operation on the quality of permeate compared with the continuous mode was observed. Furthermore, no significant influence of the intermittent frequency (IF) on the efficiency of organics removal in the SPMRs was found (Chin et al., 2007b; Ryu et al., 2005).

The intermittent operation can, however, help in prevention from deposition of photocatalyst particles on a membrane surface. Another scenarios are backwashing (backpulsing, backflushing), aeration (air bubbling), or membrane module vibration (Wang et al., 2013). The deposition of photocatalyst on a membrane surface (and other parts of installation) leads to a decrease in its concentration in the treated solution, which might result in a deterioration of photodegradation efficiency. With backwashing the photocatalyst particles can be efficiently dislodged from the membrane surface back to the photoreactor, resulting in an almost constant photocatalyst concentration in the slurry (Wang and Lim, 2012).

Backpulsing was found to be more beneficial than continuous aeration when treatment efficiency in SPMRs was evaluated (Jiang and Choo, 2016). In case of aeration the air

bubbles interfere with photocatalysis due to light scattering, whereas in bubble-free backpulsing or when aeration zone is separated from reaction zone (Fu et al., 2006) such phenomenon does not occur.

Another group of factors affecting permeate quality are hydraulic process parameters: CFV and TMP. In a slurry PMR, an increase of CFV can improve the photodegradation efficiency, which is due to mitigation or even prevention from deposition of photocatalyst particles on a membrane surface or within its pores. A decrease in TMP can influence the efficiency of photodegradation positively because at lower driving force the permeate flux is also lower, which translates to increased HRT (Wang and Lim, 2012). On the opposite, an increase in TMP leads to a decrease in permeate quality. Moustakas et al. (2014) based their investigations on methyl orange and methylene blue (MB) removal in a PMR equipped with PMs. They reported that a higher flow rate through the membrane pores resulted in a significant decrease of the photocatalytic efficiency due to shorter contact time of the contaminant with the photocatalytic surface. In slurry PMRs an unfavorable effect of TMP increase on photodegradation efficiency is associated with enhanced deposition of photocatalyst particles on/in a membrane.

Quality of PMR permeate depends also on the membrane properties and membrane process applied (Mozia et al., 2013). Membranes utilized in MF and UF assure efficient separation of photocatalyst particles, but they are not able to reject low-molecular-weight compounds, both initial pollutants as well as products/by-products of their photodegradation. Therefore, these substances can freely permeate through the membranes, thus lowering product quality. Taking the above into consideration, it is clear that efficient photodegradation of contaminants in feed solution is a key issue when MF/UF membranes are utilized.

The quality of permeate in PMRs utilizing NF is higher than in the systems in which MF or UF are used. However, even in case of NF, the low-molecular-weight products of photodegradation or the initial compounds can permeate through the membranes (Molinari et al., 2004). It should be remembered, however, that the separation mechanism in MF/UF is different from that in NF. In the former case the sieve effect takes place, whereas during NF the solution-diffusion mechanism and the Donnan effect must be taken into account. The repulsive or attractive interactions between the substrate molecules and the membrane surface resulting from the Donnan effect can increase or decrease the rejection, respectively, thus affecting the permeate quality (Mozia et al., 2013).

The influence of MPD on the permeate quality in PMRs was recently reported by Ong et al. (2014). During the investigations on oil removal in SPMR equipped with HF TiO_2-PVDF PMs, the authors observed that an increase of MPD from 17.6% to 35.3% (i.e., by factor of 2) contributed to an improvement of total organic carbon (TOC) degradation. However, further increase in packing density up to 52.9% (i.e., by factor of 3) led to a

decrease of TOC removal compared with that at MPD of 35.3%. The results were explained in terms of reduction of the membrane active surface available for UV radiation and photocatalysis due to attachment of membrane fibers to each other.

The above overview clearly shows that at the stage of PMR design, numerous factors should be taken into consideration to assure optimized permeate quality.

4.5 Examples of Photocatalytic Membrane Reactor Configurations and Designs

Concerning the development of PMRs in which pressure-driven membrane processes (MF, UF, NF) were coupled with photocatalysis, the first works reported in the literature (Molinari et al., 2000, 2001; Sopajaree et al., 1999) were performed with the aim to choose a suitable membrane material, stable in the reactive environment, and to identify the variables influencing the performance of the membrane photoreactor.

Molinari et al. (2002a) studied the performance of two different PPMR configurations in the degradation of 4-nitrophenol using TiO_2 as photocatalyst. In particular, the configurations studied were (1) lamp positioned up the permeating cell containing the membrane, where the irradiation of the photocatalyst takes place (see Fig. 4.5); (2) lamp immersed in the photocatalytic reactor, so that the irradiation of the photocatalyst in suspension was performed in the recirculation tank (see Fig. 4.5). Moreover, in the first configuration, the efficiency of the process was investigated with the photocatalyst suspended, coated, or included in the membrane.

Obtained results evidenced that the second configuration, in which the lamp was immersed in the photocatalytic reactor, was the more interesting one in terms of irradiation efficiency and membrane permeability. Besides, the separation of the irradiation zone from the permeation zone also allows selecting the membrane type depending on the photocatalytic process under study, without the constraint of choosing a UV-resistant membrane.

In a successive work (Molinari et al., 2004), by studying the photodegradation of the dyes Congo red (CR) and Patent Blue (PB), the same group confirmed that the rate of pollutant photodegradation was strongly affected by the UV irradiation mode. In particular, by comparing the results obtained in two types of photoreactors, with external lamp and with immersed lamp, it was observed that the rate of photodegradation in the latter configuration was three times higher than that in the configuration with external lamp, although the power of the last was four times greater. On the basis of this consideration, successive experiments in the PPMR were carried out by using the immersed lamp. Some tests in continuous regime were carried out by continuously injecting the feed solution contained in the feed tank ((n) in Fig. 4.5) and continuously withdrawing the permeate into the waste tank ((o) in Fig. 4.5). The results reported in Fig. 4.6 in terms of CR

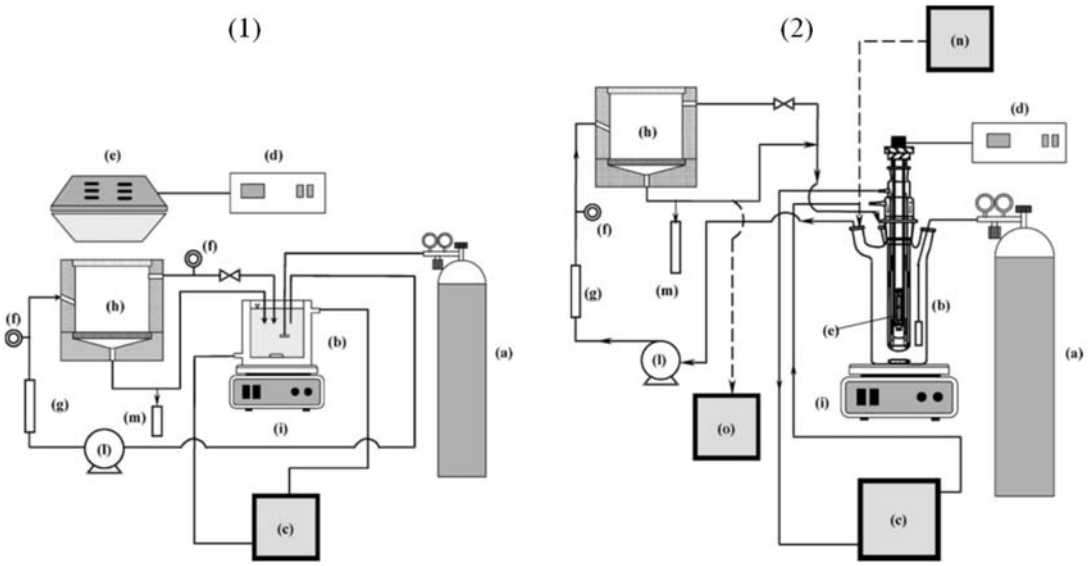

Figure 4.5

Scheme of the two different photocatalytic membrane reactor configurations: (1) with the lamp positioned on the permeation cell; (2) with the lamp immersed in the photocatalytic reactor. (a) Oxygen cylinder; (b) cylindrical reactor with cooling jacket; (c) thermostatic bath; (d) power supply; (e) medium-pressure Hg lamp; (f) manometer; (g) rotameter; (h) permeation cell; (i) magnetic stirrer; (l) pump; (m) graduate cylinder for permeate sampling; (n) feed tank (continuous regime); (o) waste tank (continuous regime) (Molinari et al., 2004).

concentration in the permeate and in the retentate, versus the time, show that the NF membrane effectively acted as a barrier for both the photocatalyst and the substrate. The obtained permeate contained a very low concentration of CR (c. 0.1%) with respect to 500 mg L^{-1} of the feed. Thus it was demonstrated that it is possible to successfully treat highly concentrated solutions of dyes by a continuous process, which is an important feature of a PPMR. Despite these encouraging results, permeate flux throughout the run decreased from the initial value of 74.2 L m^{-2} h^{-1} to the value of 29.8 L m^{-2} h^{-1} (60% flux decrease) because of membrane fouling caused by photocatalyst deposition on the membrane.

Some years later (Molinari et al., 2008) the same PPMR system was tested in the photodegradation of Gemfibrozil (GEM) using suspended TiO_2 P25 as a photocatalyst. Good operational performance was observed by working in continuous regime at a constant TMP of 6 bar, reaching a steady state in approximately 120 min, with complete GEM removal, 60% mineralization and constant permeate flux of 38.6 L h^{-1} m^{-2}, which remained stable until the end of the run. Some intermediate products permeated across the membrane, as evidenced by a TOC rejection of about 62% at steady state, indicating the need to select a better membrane with higher rejection to the photodegradation products.

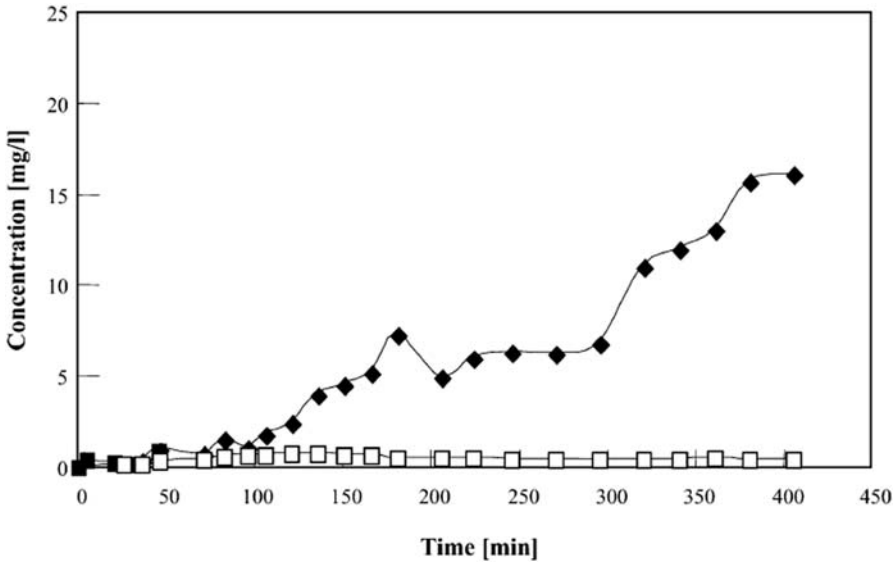

Figure 4.6

Congo red concentration in the retentate and in the permeate versus time: (◆) retentate; (□) permeate. (V = 500 mL; T = 303K; $C(O_2)$ = 22 ppm; TiO_2 = 1 g L^{-1}; C_{feed} = 500 mg L^{-1}; lamp = 125-W medium pressure Hg immersed lamp; initial pH = 6.42; P = 3.5 bar.) *Elaborated from Molinari et al., 2004.*

Photocatalyst deposition on the membrane surface and fouling caused a flux decline during the photocatalytic process. A washing of membranes with an enzymatic detergent restored the flux at acceptable values.

All previous works confirm that the use of PMRs obtained by coupling slurry photoreactor with pressurized flat sheet membrane systems could be interesting on an application point of view for the decontamination of highly concentrated effluents once membrane fouling, mainly due to photocatalyst deposition on the membrane, causing a flux decline will be opportunely controlled.

The use of a hollow fiber membrane (HFM) represents an interesting approach to overcome this problem. On the basis of this, Sopajaree et al. (1999) proposed a hybrid system obtained by integrating a slurry-based heterogeneous photoreactor with a pressurized hollow fiber UF (HFM-UF) unit (Fig. 4.7). TiO_2 Degussa P25 was the photocatalyst and MB the pollutant.

The results evidenced that the used HFM-UF unit permitted to maintain the photocatalyst into the reacting environment. A 98% dye removal was obtained, but 26% of TOC was detected in the permeate, evidencing that some degradation intermediates crossed the membrane. A progressive flux decrease, owing to photocatalyst deposition on the

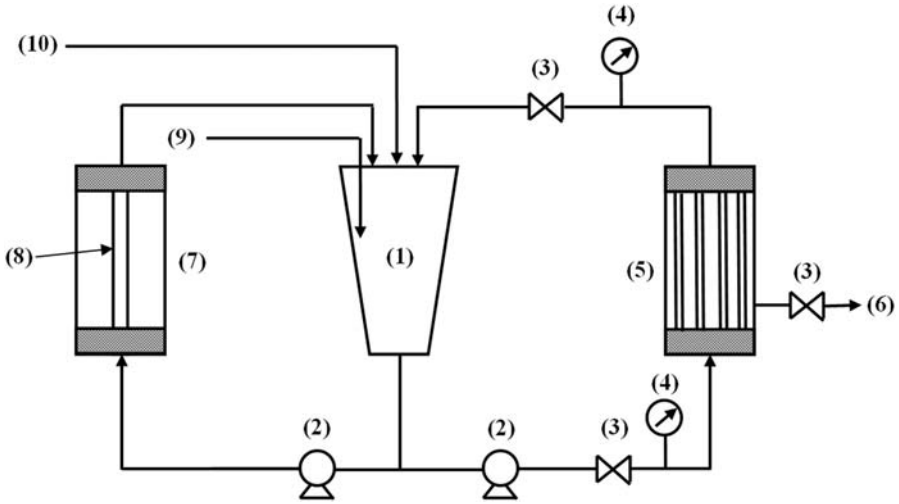

Figure 4.7
Schematic diagram of the hollow fiber membrane (HFM) UF unit: (1) reservoir; (2) peristaltic pump; (3) lamination valve; (4) pressure gauges; (5) HFM module; (6) permeate outlet; (7) photocatalytic reactor; (8) irradiation source; (9) air supply; (10) wastewater. *Elaborated from Sopajaree et al., 1999.*

membrane, was observed during the operation. Membrane backflushing was used to obtain a quite stable permeate flux. Despite these encouraging results in term of fouling reduction, a systematic decrease of photocatalytic performance in the subsequent cycles was observed (86% MB removal after the 10th cycle of operation). Dynamic light scattering measurements of the solution contained into the photocatalytic reactor during the UF process (photocatalyst accumulation) and during the membrane backflushing (photocatalyst redispersion) evidenced a progressive and irreversible photocatalyst agglomeration, causing the observed decrease of the photocatalytic activity.

The performance of HFM systems mainly in terms of membrane permeability can be enhanced by operating in depressurized mode, i.e., the permeate is sucked inside HFM that is immersed in the reacting solution/suspension. In these systems, indicated as SPMRs, gas sparging represents a promising strategy to control the hydrodynamic conditions near membrane surface, thus reducing photocatalyst deposition and then membrane fouling.

Kertesz et al. (2014) performed the photocatalytic degradation of an azo dye, AR1 in an aqueous dispersion of TiO_2, in SPMR where the photoreactor was integrated with a submerged HFM module (see Fig. 4.8).

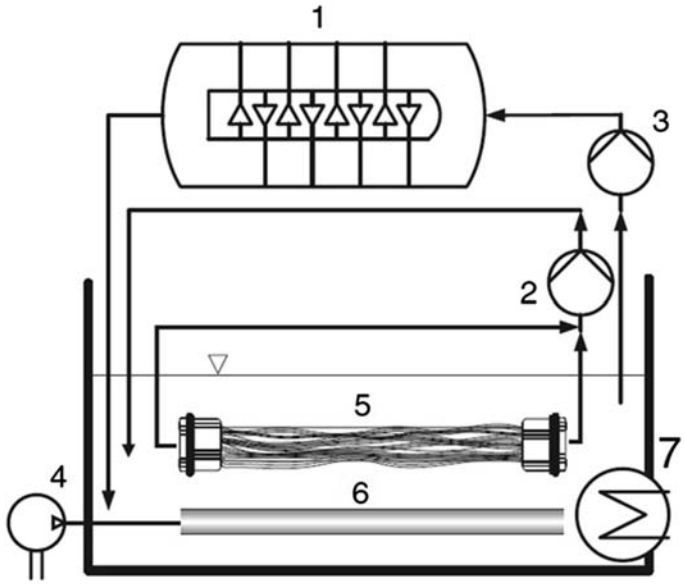

Figure 4.8
Schematic diagram of the photocatalytic membrane reactor experimental setup: (1) ultraviolet reactor, (2) permeate pump, (3) circulation pump, (4) air compressor, (5) membrane module, (6) air diffuser, (7) temperature control system (Kertesz et al., 2014).

The feasibility of this system in treating industrial wastewaters containing dyes was validated by the results because the aqueous solution containing AR1 was successfully decolorized. Besides, the photocatalyst was completely maintained into the reacting environment. Air bubbling is permitted to control the rapid flux decline, thus achieving a dual purpose: TiO_2 particle removal from the surface of the fibers and oxygen saturation promoted photodegradation reactions (Chin et al., 2007a; Fu et al., 2006; Huang et al., 2007). As previously reported, a sustainable permeate flux of 40 L m^{-2} h^{-1} was found.

A similar approach was proposed by Fu et al. (2006) for fulvic acid (FA) photodegradation from aqueous media. By using SPMRs with air bubbling schematized in Fig. 4.9, the authors evidenced that photocatalyst concentration, airflow, and pH showed important effects on the performance of the overall process: the optimal conditions for FA degradation were 0.5 g L^{-1} photocatalyst concentration, 0.06 m^3 h^{-1} airflow, and acidic conditions.

Molinari et al. (2008) also proposed the use of a depressurized PMR obtained by changing the permeation cell of Fig. 4.5 with the depressurized permeation system schematized in Fig. 4.10. It was constituted by assembling commercial capillary PES membranes (exposed membrane surface area of 4.19×10^{-3} m^2) in a homemade module. The oxidant was fed by means of oxygen bubbling in the permeation module, having the dual purpose previously described (Hairom et al., 2015).

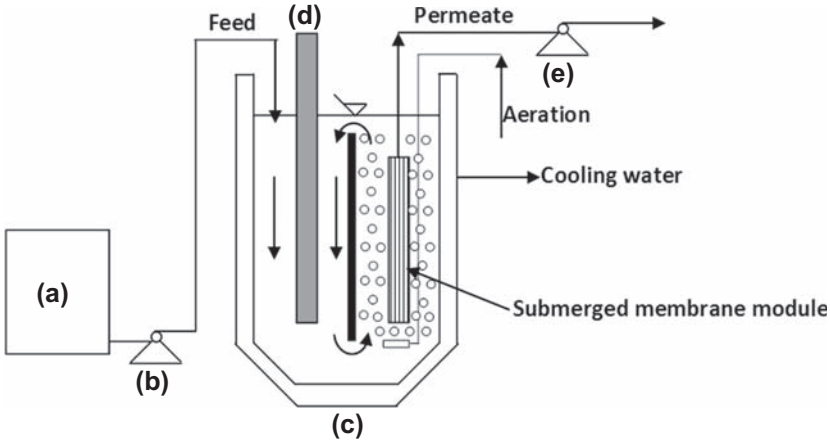

Figure 4.9

Schematic diagram of the submerged membrane photocatalytic reactor system: (a) feed tank; (b) feed pump; (c) thermostated jacket photoreactor; (d) ultraviolet lamp; (e) suction pump. *Elaborated from Fu et al., 2006.*

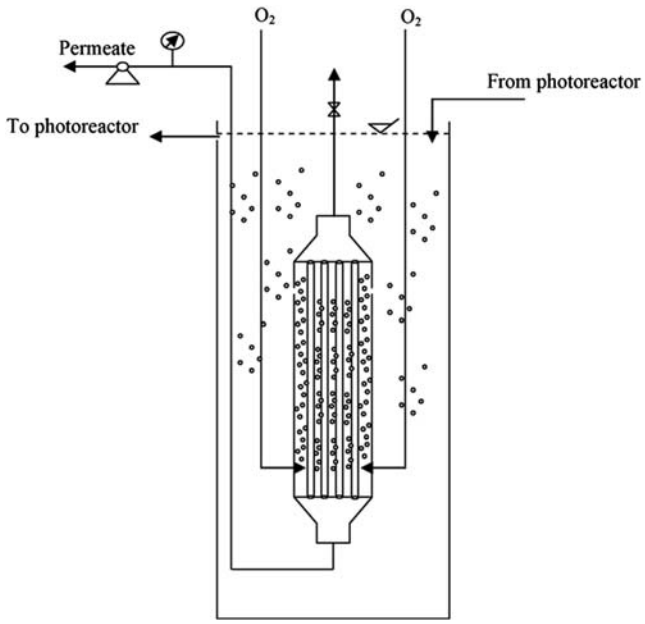

Figure 4.10

Scheme of the depressurized permeation cell with submerged membranes (Molinari et al., 2008).

Obtained results evidenced that only the photocatalyst was retained by the membrane in the reaction environment, while GEM and its photodegradation by-products moved in the permeate. Despite this drawback, the proposed SPMR permitted to obtain a steady-state flux (65.1 L h^{-1} m^{-2} at a vacuum of 0.133 bar) higher than those obtained operating with the PPMR, showing it interesting for application purposes, provided a suitable permselective membrane versus the substrate is used.

As previously reported, the performances of SPMRs can be improved by coupling an adequate membrane backflushing with air bubbling by optimizing frequency, duration, and intensity. The experimental setup used by Sarasidis et al. (2014) in their continuous tests of degradation of DCF, built to run a membrane backflushing procedure, is schematized in Fig. 4.11.

In this system the automated periodic membrane backwashing was carried out by using two three-way valves controlled by means of a timer to mitigate membrane fouling.

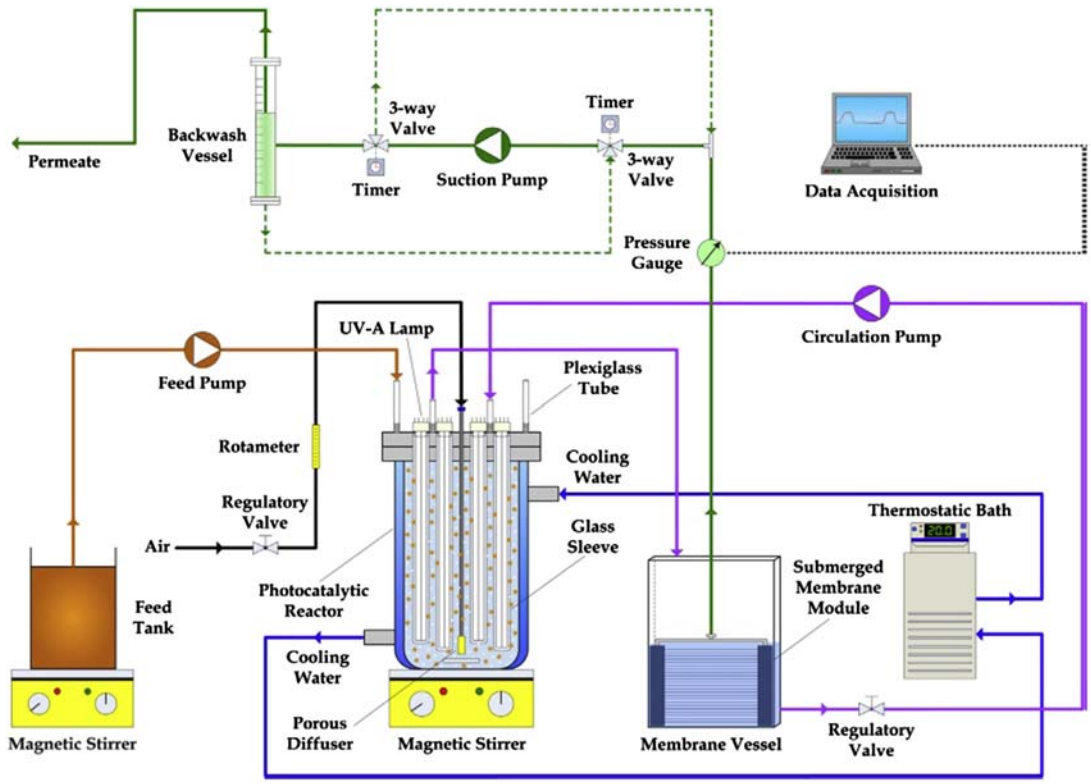

Figure 4.11
Schematic diagram of the laboratory pilot submerged photocatalytic membrane reactor, with immersed UV-A lamps, tested by Sarasidis et al. (2014). *UV*, ultraviolet.

Quite all the previous configurations of SPMRs with suspended photocatalyst, both in pressurized and depressurized modes, were built by separating the photocatalytic zone (i.e., the photoreactor where the solution containing the pollutant and the photocatalyst is irradiated by the light source) and the membrane separation zone, where a permeation module plays the dual role of maintaining both the photocatalyst and the unreacted substrate into the reacting environment, permitting to obtain a purified permeate. In these systems, the distribution of the PMR volumes between these two zones is another important design parameter that needs to be optimized (Hairom et al., 2015; Molinari et al., 2004).

Only Fu et al. (2006) did not physically separate the photocatalytic zone from the membrane separation zone, and the membrane module was immersed directly into the photoreactor. Despite this characteristic, the direct irradiation of membrane module by the UV lamp was avoided by using an appropriate black baffle. So, also in this case the membrane can be chosen without the necessity of selecting photoresistant materials.

Another attempt to avoid membrane damage under UV radiation conditions is application of ceramic, instead of polymeric, membranes. Recently, Szymański et al. (2016) presented a PMR equipped with tubular ceramic UF membranes (Fig. 4.12) for removal of humic acids from water.

The main elements of the system were two flow-through photoreactors equipped with UV-C lamps, where the photocatalytic process took place, and a tubular membrane module

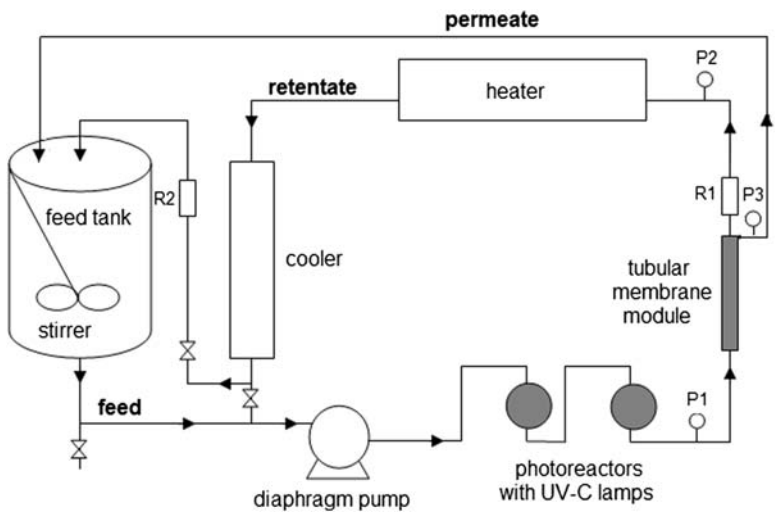

Figure 4.12
Schematic diagram of laboratory scale photocatalytic membrane reactor with a ceramic tubular membrane: R1, R2—rotameters, P1, P2, P3—manometers (Szymański et al., 2016). *UV*, ultraviolet.

with a ceramic membrane for separation of photocatalyst and contaminants. The membrane was working in the "inside-out" mode, i.e., the feed flowed in the lumen side and the permeate was collected from the shell side of the membrane. An air-operated double diaphragm pump was used to deliver the feed. The feed tank was equipped with a motorized mechanical stirrer to assure efficient mixing of feed containing suspended photocatalyst. The system configuration allowed to realize membrane backflush using permeate as a flushing medium. Both backflush frequency and backpulse duration were possible to be set at a desired value. To control the process temperature the cooler was used. Additionally, the PMR was equipped with a heater to heat the acid or base solutions applied during membrane cleaning.

As can be found from the above overview of PMR configurations, in majority of the systems described in literature the mercury lamps, both low- and high-pressure types, are utilized as radiation sources. This results from the fact that the most common photocatalyst, i.e., TiO_2 requires UV irradiation to proceed the photocatalytic reactions. However, a very interesting approach, especially when the energy efficiency is considered, is utilization of visible light-emitting diode (vis-LED) light sources. Wang et al. proposed application of visible light active C−N−S tri-doped TiO_2 activated with vis-LED light for removal of pharmaceuticals such as penicillin G and carbamazepine in two configurations of PMRs: PPMR (Wang and Lim, 2012) and SPMR (Wang et al., 2013). In case of PPMR the photoreactor and the MF membrane module were separated (Fig. 4.13), whereas in case of SPMR the MF membrane was mounted inside the photoreactor (Fig. 4.14).

As was pointed out by the authors (Wang and Lim, 2012), the vis-LED has increasingly attracted attention of researchers as visible light source in photocatalytic processes because of its advantages such as long lifetime, energy efficiency, high spectral purity, flexible

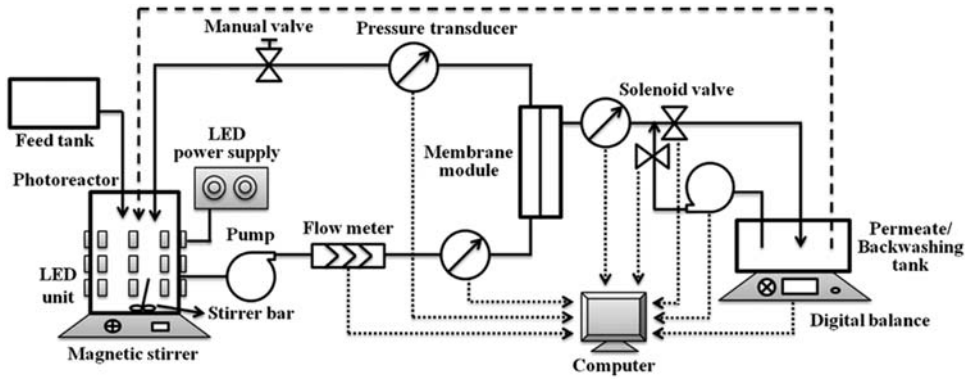

Figure 4.13

Schematic diagram of PPMR with a flat sheet PVDF MF membrane and vis-LED light source (Wang and Lim, 2012). *MF*, microfiltration; *PPMR*, pressurized photocatalytic membrane reactor; *PVDF*, polyvinylidene fluoride; *vis-LED*, visible light-emitting diode.

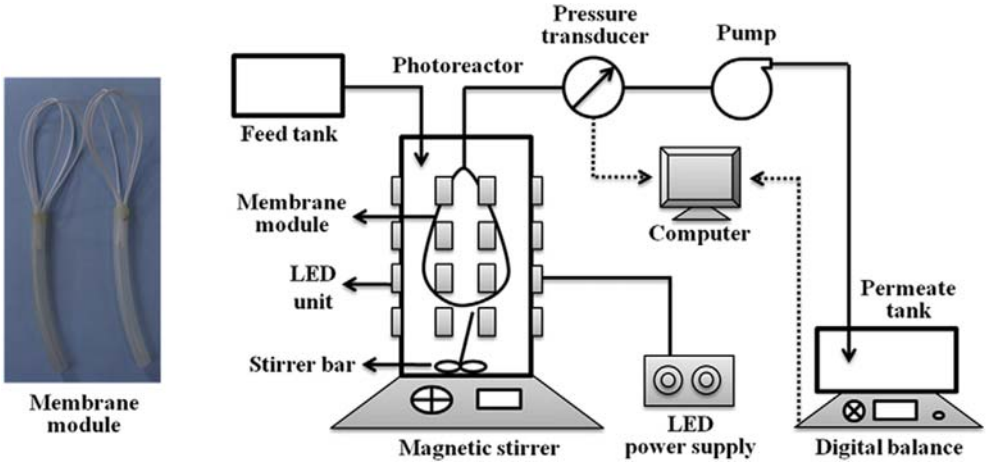

Figure 4.14

Schematic diagram of SPMR with a hollow fiber PVDF MF membrane and vis-LED light source (Wang et al., 2013). *MF*, microfiltration; *PVDF*, polyvinylidene fluoride; *SPMR*, submerged photocatalytic membrane reactor; *vis-LED*, visible light-emitting diode.

configuration, and small footprint (Wang and Lim, 2012). Nonetheless, despite these merits, the application of vis-LED sources in PMRs is still very limited, mainly because of difficulties in development of high quantities of vis-active photocatalysts that can be applied in these systems.

4.6 Summary and Conclusions

PMRs utilizing pressure-driven membrane techniques can be built in various configurations with a positive or negative pressure on the active permselective layer of the membrane obtaining PPMRs and SPMRs, respectively. Further, the PMRs configurations can be divided into systems with suspended (photocatalyst in a slurry) or immobilized photocatalyst (PMs); the systems with light source immersed in the photoreactor or mounted above the photoreactor/above the membrane module, or the systems in which the photoreaction and membrane separation are realized in one unit or in separated zones.

Regardless of the PMR configuration, a significant attention should be paid to membrane selection in terms of its resistance to harsh conditions prevailing in these systems. Polymeric membranes in immobilized systems are in danger of destruction by UV radiation and ROS, but in the suspended systems this risk can be minimized in some type of configurations (separation of reaction from membrane zones). Moreover, both polymeric and ceramic membranes can be damaged by abrasive action of photocatalyst particles in the slurry-type PMRs. Therefore, long-term investigations on stability of membranes before their selection are recommended.

A key issue in every type of PMR is permeate quality, which is affected by numerous factors, e.g., parameters related to efficiency of photodegradation, HRT and hydraulic process parameters, operational mode, separation characteristics of a membrane, and MPD. All these factors should be taken into consideration to optimize permeate quality.

Among the various PMR configurations, the SPMR seems to be especially promising for industrial applications, which is mainly due to the possibility of significant mitigation of membrane fouling and relatively low energy consumption. Nonetheless, from the economical point of view, it is also desired to consider, during the development of the SPMR systems, the utilization of visible light active photocatalysts and visible light sources, such as vis-LED ones.

List of Abbreviations

4-CP 4 Chlorophenol
AR1 Acid Red 1
CA 600 PP Symbol of a commercial membrane (see Table 4.1)
CA Cellulose acetate
CFV Crossflow velocity
CR Congo red
DCF Diclofenac
DCMD Direct contact membrane distillation
DOC Dissolved organic carbon
FA Fulvic acid
FS 50 PP Symbol of a commercial membrane (see Table 4.1)
GEM Gemfibrozil
GR 51 PP Symbol of a commercial membrane (see Table 4.1)
GW Groundwater
HF Hollow fiber
HFM Hollow fiber membrane
HRT Hydraulic retention time
IF Intermittent frequency
LED Light-emitting diode
MB Methylene blue
MF Microfiltration
MPCU 0000 u020 Symbol of a commercial membrane (see Table 4.1)
MPCU 0000 u025 Symbol of a commercial membrane (see Table 4.1)
MPD Module packing density
MPPS 0000 u002 Symbol of a commercial membrane (see Table 4.1)
MPPS 0000 u006 Symbol of a commercial membrane (see Table 4.1)
MWCO Molecular weight cut-off
NF Nanofiltration
OM Organic matter
P-12-10 Symbol of a commercial membrane (see Table 4.1)
PA Polyamide
PAN Polyacrylonitrile
PB Patent Blue

PC Polycarbonate
PDA Polydopamine
PEEK Polyetheretherketone
PEG Polyethylene glycol
PES Polyethersulfone
PhACs Pharmaceutically active compounds
PM Photocatalytic membrane
PMR Photocatalytic membrane reactor
PP Polypropylene
PPMR Pressurized photocatalytic membrane reactor
PSU Polysulfone
PTFE Polytetrafluoroethylene
PV Pervaporation
PVDF Polyvinylidene fluoride
PVDF-MP Symbol of a commercial membrane (see Table 4.1)
PVDF-Pall Symbol of a commercial membrane (see Table 4.1)
PVDFphobic Symbol of a commercial membrane (see Table 4.1)
PWF Pure water flux
ROS Reactive oxygen species
RT Residence time
SMPR Submerged membrane photocatalytic reactor
SPMR Submerged photocatalytic membrane reactor
TCE Trichloroethylene
TMP Transmembrane pressure
TOC Total organic carbon
TW Tap water
UE10 Symbol of a commercial membrane (see Table 4.3)
UE50 Symbol of a commercial membrane (see Table 4.3)
UF Ultrafiltration
UFPT Symbol of a commercial membrane (see Table 4.3)
UFPW Symbol of a commercial membrane (see Table 4.3)
UV Ultraviolet
UW Ultrapure water
vis-LED Visible light-emitting diode

References

Ahmad, R., Kim, J.K., Kim, J.H., Kim, J., 2017. Well-organized, mesoporous nanocrystalline TiO_2 on alumina membranes with hierarchical architecture: antifouling and photocatalytic activities. Catal. Today 282, 2−12.

Anderson, M.A., Gieselmann, M.J., Xu, Q.J., 1988. Titania and alumina ceramic membranes. J. Membr. Sci. 39, 243−258.

Anpo, M., 2000. Utilization of TiO_2 photocatalysts in green chemistry. Pure Appl. Chem. 72, 1265−1270.

Athanasekou, C.P., Moustakas, N.G., Morales-Torres, S., Pastrana-Martínez, L.M., Figueiredo, J.L., Faria, J.L., Silva, A.M.T., Dona-Rodriguez, J.M., Romanos, G.E., Falaras, P., 2015. Ceramic photocatalytic membranes for water filtration under UV and visible light. Appl. Catal. B Environ. 178, 12−19.

Azrague, K., Aimar, P., Benoit-Marquié, F., Maurette, M.T., 2007. A new combination of a membrane and a photocatalytic reactor for the depollution of turbid water. Appl. Catal. B Environ. 72, 197−204.

Camera-Roda, G., Santarelli, F., 2007. Intensification of water detoxification by integrating photocatalysis and pervaporation. J. Sol. Energy Eng. 129, 68−73.

Chan, C.C.V., Bérubé, P.R., Hall, E.R., 2007. Shear profiles inside gas sparged submerged hollow fiber membrane modules. J. Membr. Sci. 297, 104–120.

Chin, S.S., Chiang, K., Fane, A.G., 2006. The stability of polymeric membranes in a TiO_2 photocatalysis process. J. Membr. Sci. 275, 202–211.

Chin, S.S., Lim, T.M., Chiang, K., Fane, A.G., 2007a. Factors affecting the performance of a low-pressure submerged membrane photocatalytic reactor. Chem. Eng. J. 130, 53–63.

Chin, S.S., Lim, T.M., Chiang, K., Fane, A.G., 2007b. Hybrid low-pressure submerged membrane photoreactor for the removal of bisphenol A. Desalination 202, 253–261.

Choi, W., 2006. Pure and modified TiO_2 photocatalysts and their environmental applications. Catal. Surv. Asia 10, 16–28.

Choo, K.-H., Chang, D.-I., Park, K.-W., Kim, M.-H., 2008. Use of an integrated photocatalysis/hollow fiber microfiltration system for the removal of trichloroethylene in water. J. Hazard. Mater. 152, 183–190.

Darowna, D., Wróbel, R., Morawski, A.W., Mozia, S., 2017. The influence of feed composition on fouling and stability of a polyethersulfone ultrafiltration membrane in a photocatalytic membrane reactor. Chem. Eng. J. 310, 360–367.

Dijkstra, M.F.J., Buwalda, H., De Jong, A.F., Michorius, A., Wilkelman, J.G.M., Beenackers, A.A.C.M., 2001. Experimental comparison of three reactor designs for photocatalytic water purification. Chem. Eng. Sci. 56, 547–555.

Du, X., Qu, F.-S., Liang, H., Li, K., Bai, L.-M., Li, G.-B., 2017. Control of submerged hollow fiber membrane fouling caused by fine particles in photocatalytic membrane reactors using bubbly flow: shear stress and particle forces analysis. Sep. Purif. Technol. 172, 130–139.

Feng, K., Hou, L., Tang, B., Wu, P., 2015. A self-protected self-cleaning ultrafiltration membrane by using polydopamine as a free-radical scavenger. J. Membr. Sci. 490, 120–128.

Fernandez, R.L., McDonald, J.A., Khan, S.J., Le-Clech, P., 2014. Removal of pharmaceuticals and endocrine disrupting chemicals by a submerged membrane photocatalysis reactor (MPR). Sep. Purif. Technol. 127, 131–139.

Fu, J., Ji, M., Wang, Z., Jin, L., An, D., 2006. A new submerged membrane photocatalysis reactor (SMPR) for fulvic acid removal using a nano-structured photocatalyst. J. Hazard. Mater. 131, 238–242.

Ganiyu, S.O., Van Hullebusch, E.D., Cretin, M., Esposito, G., Oturan, M.A., 2015. Coupling of membrane filtration and advanced oxidation processes for removal of pharmaceutical residues: a critical review. Sep. Purif. Technol. 156, 891–914.

Ghosh, R., 2006. Enhancement of membrane permeability by gas-sparging in submerged hollow fibre ultrafiltration of macromolecular solutions: role of module design. J. Membr. Sci. 274, 73–82.

Hairom, N.H.H., Mohammad, A.W., Ng, L.Y., Kadhumb, A.A.H., 2015. Utilization of self-synthesized ZnO nanoparticles in MPR for industrial dye wastewater treatment using NF and UF membrane. Desalin. Water Treat. 54, 944–955.

Herrmann, J.-M., Duchamp, C., Karkmaz, M., Thu Hoai, B., Lachheb, H., Puzenat, E., Guillard, C., 2007. Environmental green chemistry as defined by photocatalysis. J. Hazard. Mater. 146, 624–629.

Huang, X., Meng, Y., Liang, P., Qian, Y., 2007. Operational conditions of a membrane filtration reactor coupled with photocatalytic oxidation. Sep. Purif. Technol. 55, 165–172.

Jiang, L., Choo, K.H., 2016. Photocatalytic mineralization of secondary effluent organic matter with mitigating fouling propensity in a submerged membrane photoreactor. Chem. Eng. J. 288, 798–805.

Jyothi, M.S., Nayak, V., Padaki, M., Balakrishna, R.G., Ismail, A.F., 2014. The effect of UV irradiation on PSf/TiO_2 mixed matrix membrane for chromium rejection. Desalination 354, 189–199.

Kertesz, S., Cakl, J., Jirankova, H., 2014. Submerged hollow fiber microfiltration as a part of hybrid photocatalytic process for dye wastewater treatment. Desalination 343, 106–112.

Le-Clech, P., Lee, E.-K., Chen, V., 2006. Hybrid photocatalysis/membrane treatment for surface waters containing low concentrations of natural organic matters. Water Res. 40, 323–330.

Lee, S.-A., Choo, K.-H., Lee, C.-H., Lee, H.-I., Hyeon, T., Choi, W., Kwon, H.-H., 2001. Use of ultrafiltration membranes for the separation of TiO_2 photocatalysts in drinking water treatment. Ind. Eng. Chem. Res. 40, 1712–1719.

Lee, K.-C., Beak, H.-J., Choo, K.-H., 2015. Membrane photoreactor treatment of 1,4-dioxane-containing textile wastewater effluent: performance, modeling, and fouling control. Water Res. 86, 58−65.

Lee, M.J., Ong, C.S., Lau, W.J., Ng, B.C., Ismail, A.F., Lai, S.O., 2016. Degradation of PVDF-based composite membrane and its impacts on membrane intrinsic and separation properties. J. Polym. Eng. 36, 261−268.

Mascolo, G., Comparelli, R., Curri, M.L., Lovecchio, G., Lopez, A., Agostiano, A., 2007. Photocatalytic degradation of methyl red by TiO_2: comparison of the efficiency of immobilized nanoparticles versus conventional suspended catalyst. J. Hazard. Mater. 142, 130−137.

Molinari, R., Mungari, M., Drioli, E., Di Paola, A., Loddo, V., Palmisano, L., Schiavello, M., 2000. Study on a photocatalytic membrane reactor for water purification. Catal. Today 55, 71−78.

Molinari, R., Grande, C., Drioli, E., Palmisano, L., Schiavello, M., 2001. Photocatalytic membrane reactors for degradation of organic pollutants in water. Catal. Today 67, 273−279.

Molinari, R., Palmisano, L., Drioli, E., Schiavello, M., 2002a. Studies on various reactor configurations for coupling photocatalysis and membrane processes in water purification. J. Membr. Sci. 206, 399−415.

Molinari, R., Borgese, M., Drioli, E., Palmisano, L., Schiavello, M., 2002b. Hybrid processes coupling photocatalysis and membranes for degradation of organic pollutants in water. Catal. Today 75, 77−85.

Molinari, R., Pirillo, F., Falco, M., Loddo, V., Palmisano, L., 2004. Photocatalytic degradation of dyes by using a membrane reactor. Chem. Eng. Process 43, 1103−1114.

Molinari, R., Pirillo, F., Loddo, V., Palmisano, L., 2006. Heterogeneous photocatalytic degradation of pharmaceuticals in water by using polycrystalline TiO_2 and a nanofiltration membrane reactor. Catal. Today 118, 205−213.

Molinari, R., Caruso, A., Argurio, P., Poerio, T., 2008. Degradation of the drugs gemfibrozil and tamoxifen in pressurized and de-pressurized membrane photoreactors using suspended polycrystalline TiO_2 as catalyst. J. Membr. Sci. 319, 54−63.

Molinari, R., Lavorato, C., Argurio, P., 2017. Recent progress of photocatalytic membrane reactors in water treatment and in synthesis of organic compounds. A review. Catal. Today 281, 144−164.

Moosemiller, M.D., Hill Jr., C.G., Anderson, M.A., 1989. Physicochemical properties of supported γ-Al_2O_3 and TiO_2 ceramic membranes. Sep. Sci. Technol. 24, 641−657.

Moustakas, N.G., Katsaros, F.K., Kontos, A.G., Romanos, G.Em., Dionysiou, D.D., Falaras, P., 2014. Visible light active TiO_2 photocatalytic filtration membranes with improved permeability and low energy consumption. Catal. Today 224, 56−69.

Mozia, S., Tomaszewska, M., Morawski, A.W., 2007. Photocatalytic membrane reactor (PMR) coupling photocatalysis and membrane distillation—effectiveness of removal of three azo dyes from water. Catal. Today 129, 3−8.

Mozia, S., Morawski, A.W., Molinari, R., Palmisano, L., Loddo, V., 2013. Photocatalytic membrane reactors: fundamentals, membrane materials and operational issues. In: Basile, A. (Ed.), Handbook of Membrane Reactors, Reactor Types and Industrial Applications, vol. 2. Woodhead Publishing Limited, Cambridge, UK, pp. 236−295 (Chapter 6).

Mozia, S., Darowna, D., Wróbel, R., Morawski, A.W., 2015a. A study on the stability of polyethersulfone ultrafiltration membranes in a photocatalytic membrane reactor. J. Membr. Sci. 495, 176−186.

Mozia, S., Szymański, K., Michalkiewicz, B., Tryba, B., Toyoda, M., Morawski, A.W., 2015b. Effect of process parameters on fouling and stability of MF/UF TiO_2 membranes in a photocatalytic membrane reactor. Sep. Purif. Technol. 142, 137−148.

Ollis, D.F., 2000. Photocatalytic purification and remediation of contaminated air and water. C. R. Acad. Sci. Ser. IIC Chem. 3, 405−411.

Ong, C.S., Lau, W.J., Goh, P.S., Ng, B.C., Ismail, A.F., 2014. Investigation of submerged membrane photocatalytic reactor (sMPR) operating parameters during oily wastewater treatment process. Desalination 353, 48−56.

Ou, W., Zhang, G., Yuan, X., Su, P., 2015. Experimental study on coupling photocatalytic oxidation process and membrane separation for the reuse of dye wastewater. J. Water Process Eng. 6, 120−128.

Palmisano, G., Augugliaro, V., Pagliaro, M., Palmisano, L., 2007. Photocatalysis: a promising route for 21st century organic chemistry. Chem. Commun. 33, 3425−3437.

Rajca, M., 2016. The effectiveness of removal of nom from natural water using photocatalytic membrane reactors in PMR-UF and PMR-MF modes. Chem. Eng. J. 305, 169−175.

Rupiasih, N.N., Suyanto, H., Sumadiyasa, M., Wendri, N., 2013. Study of effects of low doses UV radiation on microporous polysulfone membranes in sterilization process. Open J. Org. Polym. Mater. 3, 12−18.

Ryu, J., Choi, W., Choo, K.-H., 2005. A pilot-scale photocatalyst-membrane hybrid reactor: performance and characterization. Water Sci. Technol. 51, 491−497.

Sarasidis, V.C., Plakas, K.V., Patsios, S.I., Karabelas, A.J., 2014. Investigation of diclofenac degradation in a continuous photo-catalytic membrane reactor. Influence of operating parameters. Chem. Eng. J. 239, 299−311.

Shon, H.K., Phuntsho, S., Vigneswaran, S., 2008. Effect of photocatalysis on the membrane hybrid system for wastewater treatment. Desalination 225, 235−248.

Sopajaree, K., Qasim, S.A., Basak, S., Rajeshwar, K., 1999. An integrated flow reactor-membrane filtration system for heterogeneous photocatalysis. Part I: experiments and modeling of a batch-recirculated photoreactor. J. Appl. Electrochem. 29, 533−539.

Szymański, K., Morawski, A.W., Mozia, S., 2016. Humic acids removal in a photocatalytic membrane reactor with a ceramic UF membrane. Chem. Eng. J. 305, 19−27.

Tang, C., Chen, V., 2004. The photocatalytic degradation of reactive black 5 using TiO_2/UV in an annular photoreactor. Water Res. 38, 2775−2781.

Wang, P., Lim, T.-T., 2012. Membrane vis-LED photoreactor for simultaneous penicillin G degradation and TiO_2 separation. Water Res. 46, 1825−1837.

Wang, P., Fane, A.G., Lim, T.-T., 2013. Evaluation of a submerged membrane vis-LED photoreactor (sMPR) for carbamazepine degradation and TiO_2 separation. Chem. Eng. J. 215−216, 240−251.

Zangeneh, H., Zinatizadeh, A.A.L., Habibi, M., Akia, M., Hasnain Isa, M., 2015. Photocatalytic oxidation of organic dyes and pollutants in wastewater using different modified titanium dioxides: a comparative review. J. Ind. Eng. Chem. 26, 1−36.

Zhang, H., Quan, X., Chen, S., Zhao, H., Zhao, Y., 2006. Fabrication of photocatalytic membrane and evaluation its efficiency in removal of organic pollutants from water. Sep. Purif. Technol. 50, 147−155.

Zhao, J., Liao, Ch., Liu, J., Shen, X., Tong, H.J., 2016. Development of mesoporous titanium dioxide hybrid poly(vinylidene fluoride) ultrafiltration membranes with photocatalytic properties. Appl. Polym. Sci. 133 (43427), 11.

Zheng, X., Wang, Q., Chen, L., Wang, J., Cheng, R., 2015. Photocatalytic membrane reactor (PMR) for virus removal in water: performance and mechanisms. Chem. Eng. J. 277, 124−129.

This page intentionally left blank

CHAPTER 5

PMRs Utilizing Non–Pressure-Driven Membrane Techniques

Giovanni Camera-Roda[1], Vittorio Loddo[2], Leonardo Palmisano[2], Francesco Parrino[2]

[1]University of Bologna, Bologna, Italy; [2]University of Palermo, Palermo, Italy

5.1 Introduction

Photocatalytic processes have been and are being extensively studied for several potential utilizations because they present several features, which lead to more sustainable chemical transformations or complete abatement of recalcitrant pollutants, including the so-called "emerging pollutants" (Pelaez et al., 2012; Belgiorno et al., 2007). However, until now the number of real industrial applications remains rather low. The main reasons for this shortage are the relatively slow reaction rates and unsatisfactory yields, which have been obtained so far in photocatalysis. One of the most promising ways to achieve a substantial improvement of the system performance and make the process appealing and convenient is the coupling of photocatalysis with other processes in a "multifunctional reactor." "Multifunctional reactor," "hybrid process," "integrated process" are terms that indicate an operation where the different "functions" interact. It is expected that the interaction presents advantages and/or activates synergistic mechanisms, which ultimately have significant effect on the performance. "Process intensification," which is a substantial improvement of the process, can be the final potential result. "To produce much more and better while consuming much less" (Charpentier, 2012; Stankiewicz, 2003) is the "mission" of process intensification and represents a key objective not only for the economic convenience of the production process and for the safety but, in a more general vision, also for sustainability. The coupling (i.e., the integration) of the various "functions" is becoming the focus of the design and analysis of these systems, which, starting from a different point of view, need novel approaches and equipment with respect to those of the traditional chemical engineering, which is centered on the unit operation concept (Stankiewicz and Moulijn, 2000; Babi et al., 2016). Anyhow, at some extent, also "process integration" can be seen as a unit operation, which obeys certain general rules and laws regardless the specific involved processes. In many cases, the "function," which is combined to a reaction operation, is a separation process, possibly a membrane separation

Current Trends and Future Developments on (Bio-) Membranes. https://doi.org/10.1016/B978-0-12-813549-5.00005-0

process. Indeed, membrane separation processes are very suitable to be coupled with a photocatalytic unit operation in a "photocatalytic membrane reactor" (PMR). In fact, photocatalysis and membrane processes in liquid systems share almost the same mild operating conditions, which represent their strengths over other processes, and the coupling becomes easy and straightforward with a few aspects needing attention. A membrane reactor can use several different actions to obtain process intensification. Table 5.1 reports the most important of them. It is worth noting that some of the actions in Table 5.1 (namely, 1, 2, 3, 4, 6, 7, and 10) are caused by membrane separation and are beneficial for reaction, whereas others (8, 11, 12, and 13) are caused by reaction and are beneficial for membrane separation. Moreover, from Table 5.1, it is clear that the advantages of utilizing a membrane process in combination with photocatalysis can be far beyond the simple retention of the photocatalytic powders inside the reactor. On the other hand, the utilization of photocatalytic films deposited onto proper supports represents an alternative way to avoid the problematic postprocess separation of the photocatalyst powders from the fluid stream. This is a viable solution every time the retentate is the final product of the PMR.

PMRs can be classified according to different criteria, such as the type of the involved membrane process, the task to be accomplished, the form of the photocatalytic material (in suspension or immobilized), the arrangement of the units of reaction and separation, the driving force for the permeation across the membrane, the involved phases, etc. Almost all existing membrane processes have been tested for the coupling with photocatalysis with

Table 5.1: Actions that might contribute to process intensification with a membrane reactor.

1. Concentrate reactants in the reacting solution
2. Remove products that can hinder the desired reaction
3. Remove one or some products of a reversible reaction
4. Recover valuable intermediates that otherwise undergo further undesired reactions if maintained in the reactor
5. Arrange reaction and separation together, thus saving volume
6. Maintain the (photo)catalyst in the reactor
7. Continuously feed a reagent, which is consumed by the reaction
8. Utilize the heat of reaction for the separation
9. Attain a complementary use of an energy source
10. Create a more intimate contact between reagents and the (photo)catalyst (typical for catalytic membranes)
11. Produce compounds that can be more easily removed by the membrane separation with respect to the starting permeating species
12. Create a barrier for the permeation of a compound, thanks to the destruction of that compound by the reaction onto or into the membrane
13. Degrade the permeants, thus lowering their chemical potential downstream the membrane and increasing the driving force for the separation
14. Destroy through the reaction the agents that cause membrane fouling

Most of the reported actions are effective only if reaction and separation operate concurrently.

the objective of overcoming some of the difficulties encountered with the sole photocatalysis. Reverse osmosis, nanofiltration, ultrafiltration, and microfiltration have the common characteristic to be pressure-driven processes. They are considered in Chapter 4. In other membrane processes, the permeation is obtained without the use of a pressure difference because the driving force (given in general by the gradient of the chemical potential) for the flux of each permeant across the membrane is obtained in other ways, such as maintaining a temperature or a concentration gradient. The separation of the permeating species is the result of the differences between the individual driving forces and of the selective barrier effect of the membrane. Among the non—pressure-driven processes, pervaporation, dialysis, membrane distillation, and membrane contactors have been applied in PMRs and are considered in the present chapter.

Until now, the number of studies on the membrane reactors, which use the non—pressure-driven membrane processes, is not large, but they show encouraging potentialities for applications both in water treatment and in chemical synthesis of fine chemicals. They appear to be particularly apt to generate more sustainable processes. Furthermore, a review of them offers the opportunity to analyze their interesting and fascinating features, which under some aspects may offer advantages over pressure-driven processes and constitute a basis for future developments. For instance, unlike in pressure-driven processes, membrane fouling seems to be a minor problem (Zhang et al., 2016), and the opportunity to use nonpressurized equipment makes simpler the integration with photocatalysis and the layout of the plant. In Table 5.2, the list of studies, which deals with non—pressure-driven membrane processes, is organized on the basis of the type of membrane process and two main tasks (water treatment and chemical synthesis). Actually, the classification into these two tasks is not always simple. In fact, sometimes the objective could be twofold to obtain an environmental remediation while producing valuable products (fine chemicals or fuels) by the (photocatalytic) degradation of the original pollutant. “To kill two birds with one stone” looks appealing, so the valorization of waste streams through the conversion of pollutants into valuable products transforms a problem into an opportunity and represents a new frontier of sustainability.

A simple survey of the possible applications or types of PMRs utilizing non—pressure-driven membrane techniques is not the main objective of this chapter. On the contrary, particular attention is paid to the fundamentals, which the different types of PMRs have in common. The starting point is the analysis of specific types of PMR. This analysis usually allows to illustrate characteristic phenomena and to discuss the mechanisms, which embrace a wider set of membrane reactors and are important for the improvement of the process. In the overview of the different applications, minor details are omitted. On the other hand, a complete description can be found in the relevant articles and in the comprehensive reviews (Mozia, 2010; Molinari et al., 2017; Iglesias et al., 2016; Leong et al., 2014) that have been published on PMRs.

Table 5.2: Works on photocatalytic membrane reactors with non–pressure-driven membrane processes.

Objective →	Water Treatment and Purification	Synthesis of Fine Chemicals
Type of Membrane Process ↓		
Pervaporation	Camera-Roda and Santarelli (2007)[2,3,9,11]	Camera-Roda et al. (2011a)[1,2,4,6,9] Augugliaro et al. (2012)[1,2,4,6,9] Camera-Roda et al. (2013a)[1,2,4,6,9] Camera-Roda et al. (2014)[1,2,4,6,9]
Dialysis	Azrague et al. (2005)[6,7,13] Azrague et al. (2007)[6,7,13] Lekelefac et al. (2014)[4]	Camera-Roda et al. (2017c)[2,4,6,7]
Membrane contactors	Kumakiri et al. (2011)[6,7]	Molinari et al. (2009)[4,6,7] Molinari et al. (2015)[4,6,7]
Direct-contact membrane distillation	Mozia et al. (2005)[1,6,9], Mozia et al. (2007)[1,6], Mozia and Morawski (2012)[1,6], Mozia et al. (2013)[1,6], and Darowna et al. (2014)[1,6] Hou et al. (2017)[1]	–

The classification is based on the type of membrane process and the proposed application (water treatment or synthesis of fine chemicals). The numbers in the superscripts refer to the numbered actions listed in Table 5.1.

The characteristics of photocatalysis are described in Chapter 1, so in the present chapter they will be invoked only when necessary. Different types of PMRs are examined in the following sections, where a preliminary brief description of the relevant membrane process is also given. Finally, potential and prospective solutions are discussed in the conclusions.

5.2 Photocatalysis Integrated With Pervaporation

5.2.1 Principles of Pervaporation

Chemical compounds can dissolve and diffuse into some solid materials. Therefore, if these materials are used as the selective layer of a membrane, chemicals permeate through the membrane when a driving force is applied. This is the effective transport mechanism in pervaporation, where the membrane separates a vapor permeate from a liquid feed. Normally the membrane is nonporous (often referred to as dense or homogeneous) and the solution–diffusion model applies (Böddeker, 1990; Wijmans and Baker, 1995; Schaetzel et al., 2001). The term "pervaporation" derives from the two fundamental occurring steps: permeation through the membrane and evaporation at the membrane–permeate interface of the chemicals. The driving force for the permeation of a certain "permeant" is obtained by maintaining a difference of its partial pressure and, consequently, of its chemical potential between the two sides of the membrane. Referring to the upstream (U) and the

downstream (D) phases, the partial pressure of permeant A_i in the liquid phase upstream the membrane, $P_{i,U}$, is $P_{i,U} = P_i^*(T)\ \gamma_i\ x_i$, where $P_i^*(T)$ is the vapor pressure of A_i at the operating temperature T, γ_i is its activity coefficient in the liquid phase, and x_i is its molar fraction. The partial pressure in the vapor phase downstream the membrane, $P_{i,D}$, is given by the Dalton's law: $P_{i,D} = P_P\ y_i$, where P_P is the pressure downstream the membrane (i.e., in the permeate) and y_i is its molar fraction. So, the driving force for the permeation of A_i is $P_{i,U} - P_{i,D} = P_i^*(T)\ \gamma_i\ x_i - P_P\ y_i$ and it is favored by high temperatures (P_i^* increases), low permeate pressures, P_P, or low molar fractions, y_i, in the permeate. Conversely, the upstream pressure has little influence on the rate of permeation because it affects only marginally the chemical potential in a liquid phase. Therefore, it is impractical to operate at pressures higher than atmospheric pressure, and pervaporation is classified among the membrane processes that are not driven by pressure differences. The molar fraction in the permeate y_i could be maintained low by dilution with a carrier gas, but it is uncommon to operate this way because the dilution makes necessary a further separation step for the recovery of the permeants. Usually, it is more convenient to operate at low permeate pressure with condensation of the vapors and vacuum pumping of the incondensable gas.

Flux and selectivity describe the capabilities of this separation process. The flux (or more rigorously the flow density or flux density) is the mass (or volumetric or molar) overall flow rate per unit surface area and per unit time. Selectivity can be measured as a separation factor, $\alpha_{i,j}$, of component A_i with respect to component A_j, which is defined as $\alpha_{ij} = \frac{c_{i,D}/c_{j,D}}{c_{i,U}/c_{j,U}}$, where c_i and c_j are the concentrations of A_i and A_j, respectively. The separation factor is the equivalent of the relative volatility used in vapor–liquid equilibrium, so a direct comparison of the separation capabilities of pervaporation and one-stage distillation is made by considering the separation factor and the relative volatility, respectively. Often the separation capability of pervaporation equals the one obtained with hundreds of equilibrium stages in distillation (Baudot and Marin, 1997). The equivalent number of equilibrium distillation stages becomes infinite when pervaporation is able to break a vapor–liquid azeotrope (Wijmans and Baker, 1995). In pervaporation, when separating A_i from A_j, differences in the individual solubility and diffusivity represent an additional contribution for separation, which is not present in one-stage distillation. Often these differences are so important that the vapor permeate is enriched in the component with lower volatility, thus successfully counteracting the driving force.

In substitution of the separation factor, the selectivity may be referred to the enrichment factor, β_i, of the species A_i, with $\beta_i = \frac{c_{i,D}}{c_{i,U}}$. It is evident that $\alpha_{ij} = \frac{\beta_i}{\beta_j}$ and that $\alpha_{ij} \to \beta_i$ when $x_i \to 0$. Note that the enrichment factor of a "rejected" species is below 1, and it can be directly related to the "rejection," R_i, of that species because $R_i = 1 - \beta_i$.

In pervaporation, it is always opportune to choose a membrane, which is selective toward the minor component of the solution. This choice is a consequence of three well-established phenomena, which take place in pervaporation: the separation factor α_{ij} decreases when x_i increases, heat must be supplied to evaporate the permeate, and the flux through a dense membrane is typically low because the transport in the membrane takes place through slow molecular diffusion in a solid matrix. So, for a given extent of separation and a given production, the permeate flow rate (and consequently the membrane area) and the energy consumption are lower when the membrane is selective toward the minor component. Pervaporation membranes are classified into two main classes: hydrophilic and hydrophobic membranes. The first ones remove preferentially water, and their main application is in the purification of alcohol by removing the residual water from an ethyl alcohol−water solution with a composition close to the azeotrope (breaking of the azeotrope). Hydrophobic membranes (often named also as "organophilic" membranes) are mainly utilized to recover valuable or target compounds, such as aromas, from diluted aqueous solutions or to remove undesired chemicals, such as pollutants, from a water stream where they are present at low, but still unacceptable levels. With hydrophilic membranes, both sorption and diffusivity are in favor of the preferential permeation of water. On the contrary, in organophilic membranes the diffusivity of water, whose molecules are very small and mobile, is always greater than the one of the organics, but the sorption of the organic compounds can be so high that a preferential permeation of the organics is finally obtained. Two main applications of organophilic pervaporation exist: the recovery of aroma compounds from process streams (Karlsson and Trägårdh, 1993; Pereira et al., 2006; Trifunović et al., 2006) and the removal of volatile organic compounds (VOCs) from aqueous effluents (Wijmans et al., 1994; Lipnizki and Field, 2002; Urkiaga et al., 2002; Peng et al., 2003; Konieczny et al., 2008).

Various techniques are used to produce pervaporation membranes, which can be polymeric or inorganic, elastomeric or glassy, homogeneous or filled with functional powders. Often a very thin selective layer, supported onto a macro or microporous layer, is adopted. The main function of the support is to increase the mechanical resistance of the membrane, but sometimes the support affects also the selectivity.

The coupling of photocatalysis and pervaporation is simple and straightforward because both these processes take place at compatible operating conditions:

- Mild temperatures
- Atmospheric pressure
- Low concentrations of organics in water solution (for organophilic pervaporation membranes).

Furthermore, pervaporation photocatalytic reactors encompass all the features to be classified as green and sustainable processes.

At this regards it is observed that

- photocatalysis and pervaporation are typically carried out at mild operating conditions,
- no chemical additive is usually needed,
- it is possible a complimentary utilization of sunlight, whose ultraviolet (UV) fraction is used by photocatalysis to activate the reaction and whose thermal part by pervaporation to supply the latent heat of evaporation of the permeate.

"Pervaporation photocatalytic reactors" have been applied both for photocatalytic synthesis of fine chemicals and water detoxification. Pervaporation photocatalytic reactors have been used also as examples to illustrate some general and important aspects of membrane reactors, such as the effects of the main parameters and the methods to integrate reaction and separation. It is worthwhile to present these general elements before surveying the existing applications of photocatalytic pervaporation reactors because they represent the basis to get a better understanding of how these systems work.

5.2.2 Membrane Reactor as a Unit Operation

In textbooks, reviews, and articles, membrane reactors are considered a well-defined category of systems, thus recognizing more or less explicitly the existence of common principles and laws. The common features open the door to a "unit operation" approach for studying membrane reactors. The benefits of using a unit operation approach are well known. As a matter of facts, the knowledge of these laws and the possibility of applying them to any membrane reactor make the design and the analysis of new or existing systems more effective and systematic. These general laws should not be disregarded in the studies concerning membrane reactors.

Pervaporation photocatalytic reactors represent illustrative examples of membrane reactors. They have been used in some works to illustrate the common features that make membrane reactor a unit operation and to ascertain the general laws and principles. For this reason, this subject has been included in the section related to PMRs with pervaporation.

Principally, what membrane reactors have in common is the main relevant parameters of the process (and their effects on the performance of a membrane reactor) and the possible methods and rules of coupling reaction with separation. Most of these laws can be extended also to any integrated process (Schmidt-Traub and Górak, 2006).

First, it is worth observing that membrane reactors may operate in a continuous or semicontinuous way. Two output streams can be in general present. They are the permeate and the retentate. Usually one represents the product stream and the other a purge stream, but sometimes this latter stream is absent, in particular in semicontinuous systems. A feed stream is present only in continuous mode.

Starting from the mathematical models, which describe the behavior of a membrane reactor, and applying the Buckingham π theorem, it is possible to identify the main intervening parameters. They include the following:

- The Damköhler number, $\mathrm{Da} = \frac{t_{0r}}{t_r} = \frac{\mathrm{R}(c_{R,0})}{c_{R,0}} \frac{V_r}{\dot{V}_0}$, i.e., the ratio of a residence time, $t_{0r} = \frac{V_r}{\dot{V}_0}$, to the characteristic reaction time, $t_r = \frac{c_{R,0}}{\mathrm{R}(c_{R,0})}$, where $c_{R,0}$ is a reference value of the reactant concentration (usually the feed or the initial concentration), $\mathrm{R}(c_{R,0})$ is the reaction rate evaluated at the reference conditions (i.e., at $c_{R,0}$ and at the reference values of the other possible factors affecting the reaction rate), V_r is the reactor volume, and $\dot{V}_0$ is the feed volumetric flow rate.
- The Péclet number for membrane processes (Battersby et al., 2006; Moon and Park, 2000; Gómez-García et al., 2012).

  $Pe = \frac{\dot{V}_0}{\dot{V}_P} = \frac{t_{sep}}{t_{0r}}$ with $1 < Pe \leq \infty$, i.e., the ratio of the characteristic separation time, $t_{sep} = \frac{V_r}{A_m \ \dot{m}''/\rho}$, to the residence time, t_{0r}, where $\dot{V}_P = \frac{A_m \ \dot{m}''}{\rho}$ is the volumetric flow rate of the condensed permeate, A_m is the membrane area, $\dot{m}''$ is the mass flux of the permeate, and ρ is the density of the condensed permeate. The reciprocal of Pe, $1/Pe = \dot{V}_P/\dot{V}_0 = \frac{A_m \ \dot{m}''/\rho}{\dot{V}_0}$ with $0 \leq 1/Pe < 1$, is proportional to the permeate flow rate, that is to the membrane area, and very often it is more practical to refer to it rather than to Pe.

- The parameters assessing the selectivity of the membrane, i.e., $(N_c - 1)$ separation factors or enrichment factors where N_c is the number of components.

The presence of Da and Pe among the parameters, which govern the behavior of membrane reactors, is not surprising because they are typical parameters that govern the behavior of reactors and separators, respectively, regardless they take place in a membrane reactor or not.

However, in substitution of the Péclet number (or of the Damköhler number), it is possible to use the ratio of the characteristic reaction time to the characteristic separation time, $\delta = \frac{t_r}{t_{sep}} = \frac{1/Pe}{Da}$ (with $0 \leq \delta < \frac{1}{Da}$). This parameter is peculiar of integrated reaction–separation systems (Camera-Roda et al., 2013b; Mohan and Govind, 1988; Assabumrungrat et al., 2003; Lim et al., 2002).

Following from the previous definitions, $\delta = \frac{c_{R,0} \ A_m \ \dot{m}''/\rho}{\mathrm{R}(c_{R,0}) \ V_r}$. In this dimensionless group, the ratio of the membrane area to the reactor volume, $\frac{A_m}{V_r}$, appears in combination with other variables. This means that $\frac{A_m}{V_r}$, in spite of its widespread utilization, is not a sound and general parameter if it is used alone.

All of these parameters, with minor modifications of their expressions, but maintaining the same physical meaning, can be used in continuous or in semicontinuous systems. In fact, the definitions of *Da*, *Pe*, and δ, as ratios of peculiar characteristic times, can be easily extended to semicontinuous systems, thus obtaining analogous expressions.

The effect of the variation of these parameters has been discussed by Camera-Roda et al. (2014), who considered a PMR where pervaporation selectively recovers the valuable intermediate product, *I*, of consecutive photocatalytic reactions. A high enrichment factor of the product, β_I, is desirable because the recovery of the intermediate prevents its further degradation by photocatalytic oxidation, thus increasing the reaction selectivity toward the desired product. Alternatively, at a fixed production of I, a saving of the membrane area is the result of the increase of β_I. Conversely, low values of the enrichment factor of the reactant, β_R, are required. In fact, if the reactant is effectively rejected (rejection = 1-β_R with $\beta_R < 1$), the conversion increases for a fixed reactor volume or vice versa the reactor volume decreases for a given conversion. To obtain this beneficial effect, it is sufficient that the membrane rejects at some extent the reactant(s) ($\beta_R < 1$). Of course, the higher the rejection (i.e., the lower is β_R), the more important the advantages. Even if this outcome can be extended to any membrane reactor, the beneficial effects of the rejection of the reactants are sometimes overlooked.

For the production of the intermediate product I, an optimal value of Da, which depends on 1/*Pe*, maximizes the yield. The higher the 1/*Pe*, the higher the yield because the recovery of I from the reacting solution while it is produced increases and its further degradation by the consecutive reaction is thus prevented. An analysis of the performance of the PMR based on δ instead of 1/*Pe* is often more appropriate. The effects of δ, the ratio between the rate of permeation and the rate of reaction, deserve some reflections. Values of δ around unity guarantee that neither reaction nor separation prevails. This solution seems a good choice to avoid that one of the two processes limits the other. That should be correct if processes were operating in sequence, but most of the benefits are obtained only with a real "integration" of the processes. Essentially, the best value of δ depends on which is the process, between reaction and separation, that is beneficial for the other one. If membrane separation is beneficial for reaction, i.e., if some among actions 1, 2, 3, 4, 7, and 10 in Table 5.1 are operative, then the higher the rate of permeation ($\delta \rightarrow \infty$) the more important the benefits. This is the case, for instance, for the systems investigated by Camera-Roda et al. (2011a), Augugliaro et al. (2012), Camera-Roda et al. (2013a, 2014), Molinari et al. (2009, 2015) where one or more among actions 1, 2, and 4 apply. Action 6 (the retention of the catalyst in the reactor) has not to be accounted for because the retention of the photocatalyst is complete regardless of the rate of permeation. On the contrary, if the opposite is true, i.e., if some among actions 8, 11, 12, 13, and 14 are functional, then the extent of reaction should be as high as possible ($\delta \rightarrow 0$). In some systems, there establishes a mutual beneficial interaction, that is a true

synergy, between reaction and separation. In this case, both reaction is beneficial for separation and separation is beneficial for reaction and, therefore, an optimal finite value of δ, which is not necessarily around unity, maximizes the synergy. Camera-Roda and Santarelli (2007) found an optimal value $\delta = 0.1$ for water detoxification with a pervaporation photocatalytic reactor where actions 2, 3, and 11 are concurrently operative. Of course, also economic aspects, related to the costs, have a weight on the final choice of the most convenient value of δ.

There are two principal approaches to integrate reaction with a separation process: reaction and separation may take place in the same apparatus or in separate apparatuses. Some possible schemes are shown in Figs. 5.1 and 5.2.

In a single apparatus, the coupling of reaction and separation is more direct and simpler. In fact, in this case, both reaction and separation operate on the same bulk solution, with only mass or heat transfer that might limit the effectiveness of the coupling. If reaction and separation take place in separate apparatuses, the complexity of the layout increases with the appearance of some additional parameters. These additional parameters affect the performance of the system through the control of the "degree of integration" of reaction with separation.

It is worth pointing out that in photocatalysis, the simultaneous presence of photocatalyst, reactants, and photons is required. The shortage of just one of these "factors" makes the rate of reaction vanish. The lifetime of the oxidizing agents (principally hydroxyl radicals), which are produced directly or indirectly by the absorption of photons, is indeed very short (Zhang and Nosaka, 2014). Therefore, the reaction is always confined within the lighted zones of the reactor, even when the photocatalyst is distributed throughout the system as in slurry photocatalytic reactors with recirculation.

The utilization of separate apparatuses may present the following advantages, which are the result of the higher degree of freedom.

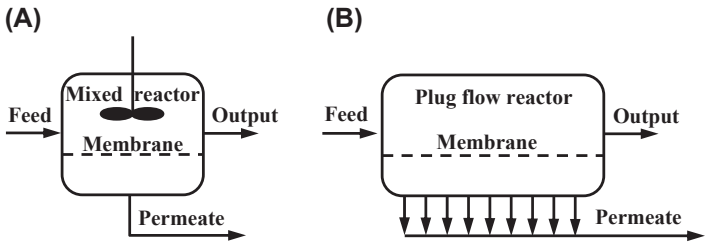

Figure 5.1
Possible schemes with reaction and membrane separation in the same apparatus: (A) mixed reactor, (B) plug flow reactor.

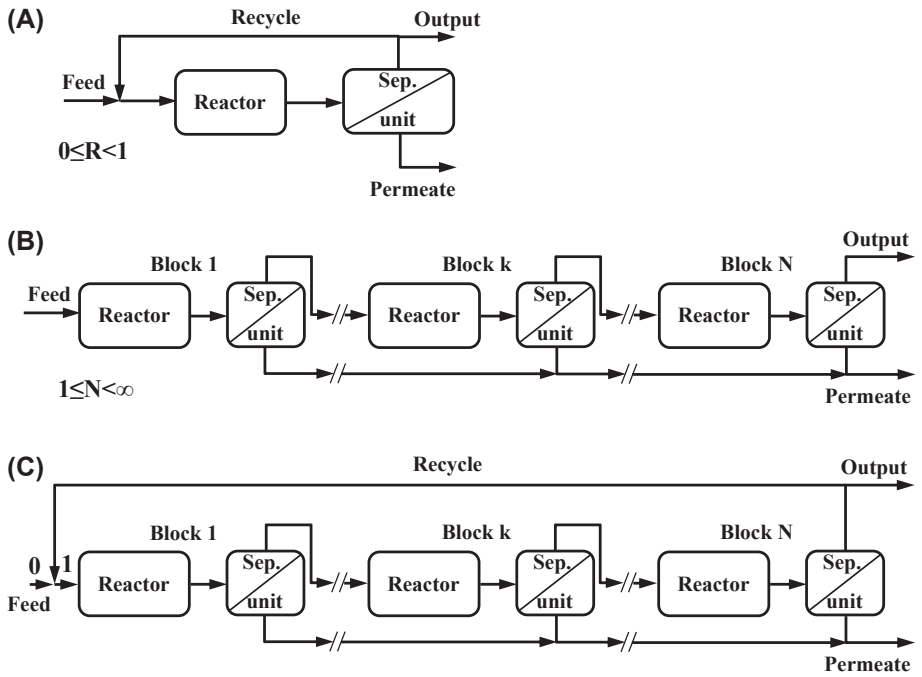

Figure 5.2

Possible schemes with reaction and membrane separation in separate apparatuses (A) with recycle, (B) with multiple blocks, (C) a more general scheme with recycle and multiple blocks. *Adapted from Camera-Roda et al., 2017a.*

- The parameter δ (which is related to the ratio of the membrane area to the reactor volume) can be varied at will with almost no limitation, whereas technical and space limitations exist if separation and reaction take place inside a single apparatus or, even worse, in a catalytic membrane.
- It is possible to design the apparatuses separately to better satisfy the individual mass and heat transfer requirements of reaction and separation. For instance, to limit fouling and concentration polarization, it is possible to optimize hydrodynamics in the membrane module without the constraints that must be respected in a single apparatus where also reaction takes place. Also radiant energy exploitation inside the photocatalytic reactor can be better satisfied if the membrane is not present.
- There is no need to shield the membrane from the radiation that activates the photocatalytic reaction (the UV radiation may damage polymeric membranes and reduce their life).
- Maintenance is simpler and can be carried out independently in each separate apparatus.
- Substitution of the photocatalyst and of the membrane can be carried out disjointedly.

- The modularity of both photocatalytic reactors and membrane separators can be conveniently exploited.

A general scheme, which allows the integration of reaction and separation while using separate apparatuses, is presented in Fig. 5.2C. Reaction and separation take place in N blocks in series, each one being composed by a reaction apparatus directly connected to a separation apparatus. For each block, except the first one, the retentate from the previous block constitutes the feed, and a retentate and a permeate are produced. The feed to the first block (stream #1) is the result of the mixing of the feed to the system (stream #0) with the recycle of the retentate from the last block. The recycle ratio, R, is defined as the ratio of the volumetric flow rate of the recycle, $\dot{V}_{recycle}$, to the volumetric flow rate of stream #1, $\dot{V}_1$, $\Rightarrow R = \frac{\dot{V}_{recycle}}{\dot{V}_1}$ with $0 \leq R < 1$. Permeates from the blocks (mixed together or not) and the retentate from the last block constitute the exiting streams of the system. Alternative layouts might include also a recycle internal to each block. Of course, it is possible to use only the recycle (scheme in Fig. 5.2A where $N = 1$) or only the fractionation into multiple blocks (scheme in Fig. 5.2B where $R = 0$). It is worth noting that the utilization of multiple blocks is simple in PMRs, thanks to the modular nature of both membrane separation and photocatalytic reaction.

The modularity of photocatalytic reactors is the result of the intrinsic modularity of any illumination system, including also solar radiation. Once the type of illumination system has been selected, the photocatalytic reactor must be designed specifically for it, with the objective of best reconciling some opposing demands. In photocatalytic systems, a satisfactory exploitation of the radiant energy entering the reactor is always in contrast with an effective utilization by the reaction of the reactor volume (Camera-Roda et al., 2005, 2009). Essentially, both of these targets depend on the photocatalyst concentration and on the geometry of the reactor illumination system. So, photocatalyst concentration and geometry of the system must be chosen taking into account the relevant advantages and disadvantages. In this respect, the ratio of the thickness of the reactor (a parameter related to the geometry of the system) to the mean free path of the photons (which, in view of the photon absorption by the photocatalyst, depends on the photocatalyst concentration) is the central parameter to be settled (Martin et al., 1999). This ratio is the so-called "optical thickness," τ, of the reactor and in practice represents the measurement of the geometrical thickness made by adopting the mean free path of the photons as unit of measure. The optical thickness is a fundamental parameter for any system where the absorption of radiation activates some phenomenon. The mean free path of the photons is essentially the reciprocal of the light extinction coefficient, β, an optical property of the medium (the reacting solution), which interacts with the radiation. Therefore $\tau = \beta \times l$, where l is the "geometrical" thickness of the reactor.

Furthermore, a high radiation intensity enhances the productivity but decreases the efficiency with which reaction utilizes the absorbed radiant energy (the quantum yield). Therefore, also the pros and cons of the change of the illumination level must be weighed up carefully. Once a satisfactory compromise has been found for these conflicting needs, which is usually based on the balancing of the capital costs (mostly related to the reactor) and the energy costs (mostly related to the illumination), there is no reason to alter the layout of the obtained reactor module, including the illumination system, when the production is "scaled up" or "scaled down." Scaling up or down is accomplished just by the addition or the removal of a sufficient number of equal reaction modules. The layout of the reaction module must be reconsidered and the system redesigned only when a new illumination system is adopted.

As a matter of fact, most of the mechanisms listed in Table 5.1 are operative only if reaction and separation are effectively coupled, that is when reaction and separation operate on a solution with almost the same composition. Therefore, reaction and separation should not operate sequentially even when a sequential arrangement of reactor and separator, as the ones in Fig. 5.2, is adopted. To this aim, it can be demonstrated that the recycle ratio R and the number of blocks N must be taken sufficiently high.

The importance of R and N on the degree of integration becomes evident when the Damköhler number of each reactor and the Péclet number of each separator are expressed in terms of the values of Da and Pe for the whole system.

Referring to the scheme in Fig. 5.2C, let $Da = \frac{\mathrm{R}(c_{R,0})}{c_{R,0}} \frac{V_{r,tot}}{\dot{V}_0}$ and $1/Pe = \frac{\dot{m}''/\rho A_{m,tot}}{\dot{V}_0}$, and for the k*th* block $Da_k = \frac{\mathrm{R}(c_{R,0})}{c_{R,0}} \frac{V_{r,k}}{\dot{V}_k}$ and $1/Pe_k = \frac{\dot{m}''/\rho A_{m,k}}{\dot{V}_k}$ where for the k*th* block, $V_{r,k}$, $A_{m,k}$, $\dot{V}_k$ represent the reactor volume, the membrane area, and the volumetric feed flow rate, respectively. The total reactor volume $V_{r,tot}$ and the total membrane area, $A_{m,tot}$, are fractionated into the different blocks $\left(V_{r,tot} = \sum_{k=1}^{N} V_{r,k} \text{ and } A_{m,tot} = \sum_{k=1}^{N} A_{m,k} \right)$.

In the hypothesis of constant density and if the reactor volume and the membrane area are the same in any block, it is $\dot{V}_1 = \frac{\dot{V}_0}{1-R}$, $V_{r,k} = \frac{V_{r,tot}}{N}$, $A_{m,k} = \frac{A_{m,tot}}{N}$, and $\dot{V}_k = \dot{V}_1 - \dot{m}''/\rho \frac{A_{m,tot}}{N}(k-1)$. After substitution and algebraic manipulation, one obtains $Da_k = \frac{Da \; Pe \; (1-R)}{N \; Pe-(1-R) \; (k-1)}$ and $1/Pe_k = \frac{1-R}{N \; Pe-(1-R) \; (k-1)}$ with $1 \leq \mathrm{k} \leq \mathrm{N}$. If the total volume and the total membrane area are fixed (i.e., Da and $1/Pe$ are fixed), it is clear that Da_k and $1/Pe_k$ tend to 0 when $R \to 1$ or when $N \to \infty$. Vanishing values of Da_k and $1/Pe_k$ imply that the variation of the composition in the passage through the reactor and the separator, respectively, is negligible and the apparatuses operate in a "differential" way. In practice, when $R \to 1$, the flow rate tends to infinity and consequently the residence time in the

apparatuses vanishes. When $N \rightarrow \infty$ the reactor volume and the membrane area in each block become so small that again the residence time in the apparatuses vanishes. Increasing R or N represents a simple way to approach the status of differential apparatuses (with Da_k and $1/Pe_k$ as low as desired), while maintaining at appropriate finite values the parameters (Da and $1/Pe$) that more directly affect the reaction and the separation performance of the overall system. In Fig. 5.3, it is apparent how the variance of the composition inside the apparatuses approaches 0 and the concentration in the reactor and in the separator become the same when $R \rightarrow 1$. A similar trend is obtained for $N \rightarrow \infty$. It is worth noting that, unlike most of traditional separation processes, non−pressure-driven membrane processes have costs, which are almost independent of the feed flow rate, because the costs arise mainly from the permeate flow rate (i.e., from the membrane area). Therefore, the relatively high feed flow rates, which are obtained if R is close to 1, are not disadvantageous. The same applies to photocatalytic reactors, whose costs depend mostly on the volume (and eventually on the radiant energy) but not on the flow rate.

After all, a complete integration is obtained both for $R \rightarrow 1$ and for $N \rightarrow \infty$ but with some differences. When $R \rightarrow 1$ and $N = 1$, the system approaches the behavior of a completely "integrated mixed reactor" (as the one represented in Fig. 5.1A) working with the same reactor volume and the same membrane area, whatever the type of reactor is. Conversely, when $N \rightarrow \infty$ and $R = 0$, the system performs as a completely "integrated

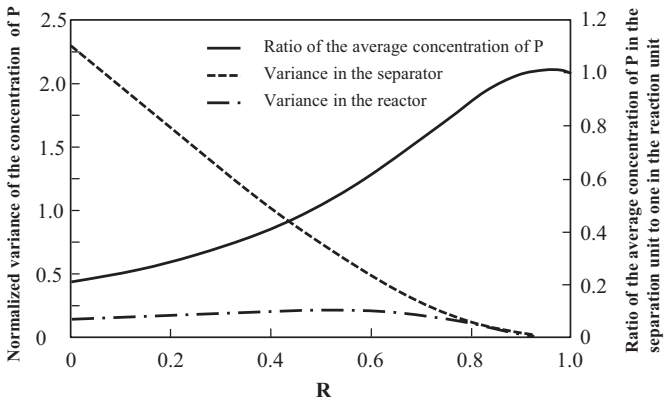

Figure 5.3

The effect of R on the distribution of the concentration of P for the system in Fig. 5.2A. The curves refer to the ratio of the average concentration of P in the separator to the one in the reactor and to the variance of the concentration of P inside the reactor and inside the separator versus the recycle ratio R. Kinetics and membrane separation properties are those for the pervaporation photocatalytic membrane studied by Camera-Roda et al. (2017a). The values are obtained for $Da = 0.296$ and $1/Pe = 0.4$.

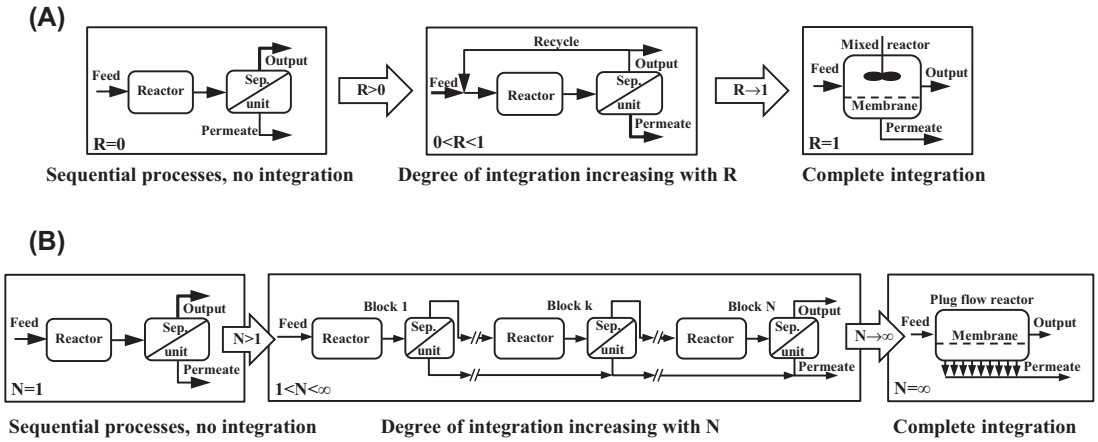

Figure 5.4

Graphical representation of the effect of (A) the recycle ratio, *R*, and (B) the number of blocks, *N*, on the behavior of the integrated process. *Adapted from Camera-Roda et al., 2017a.*

PFR" (as the one in Fig. 5.1B) with the same overall reactor volume and the same membrane area, whatever the type of reactor is. Fig. 5.4 depicts schematically this behavior.

The higher the degree of integration of reaction with separation the more important are the advantages for the production of the intermediate product, *P*, of reactions in series because the production and the recovery of *P* become more simultaneous, thus reducing the risks of the degradation of *P*. Therefore, the yield in *P* increases with *R* and/or with *N*. In Fig. 5.5, this effect is evident. The same figure shows also the beneficial effect of increasing $1/Pe$, i.e., of augmenting the membrane area.

When the adopted scheme combines the recycle and the fractionation into multiple blocks, the degree of freedom increases and the same extent of integration is reached with lower values of *R* and *N*. Generally, a higher degree of freedom is desirable because, even if it makes more complex the system, it offers more opportunities for a proper design and optimization and greater possibilities for the improvement of the process.

5.2.3 Applications of Pervaporation Photocatalytic Reactors

The abatement of recalcitrant pollutants (Ahmed et al., 2011; Chong et al., 2010; Thakur et al., 2010; Ray, 2009; Gaya and Abdullah, 2008; Occulti et al., 2008; Blanco-Galvez et al., 2007) and, in recent years, the synthesis of fine chemicals (Augugliaro et al., 2010, 2012;

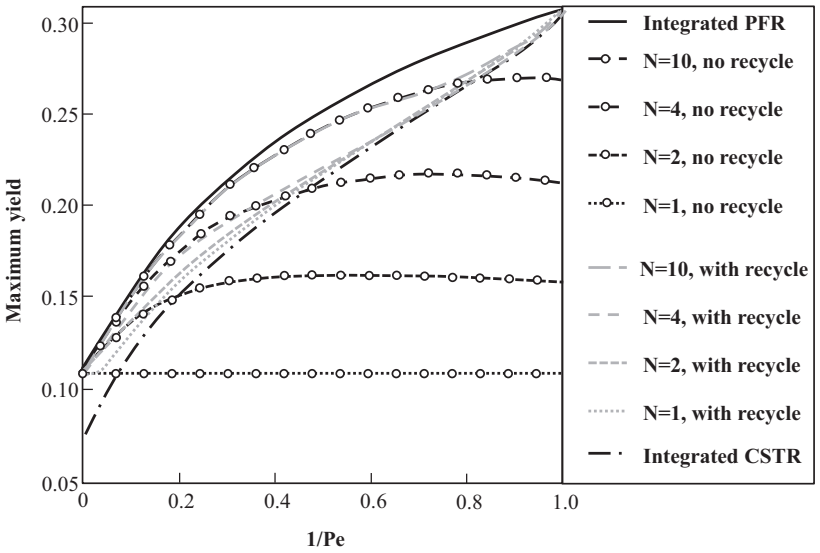

Figure 5.5
The maximum yield versus 1/*Pe* for different layouts of the integrated process. *Adapted from Camera-Roda et al., 2017a.*

Augugliaro et al., 2010; Hermann and Lacroix, 2010; Maurino et al., 2008; Shiraishi and Hirai, 2008; Palmisano et al., 2007) are two of the most promising applications of photocatalysis. In both of these areas, pervaporation has been coupled with photocatalysis to improve the overall process. The potential applications of pervaporation photocatalytic reactors appear interesting and the research on this process is expected to continue the growth.

Camera-Roda and Santarelli (2007) studied the advantages that can be obtained by the integration of photocatalytic oxidation with organophilic pervaporation in the abatement of 4-chlorophenol (4-CP) in aqueous solution. Chlorophenols are a class of chlorinated organic compounds, which enter in the environment and in particular into water, while they are being made or used, and are environmentally persistent. They are widely utilized as pesticides and are ubiquitously found in surface water and groundwater and are of public concern for their toxicity even at low concentrations. Biological degradation and other traditional methods are not sufficiently effective for their abatement, and adsorption does not transform them into harmless compounds. Photocatalysis is proposed as an interesting "advanced oxidation process" (Pera-Titus et al., 2004; Thiruvenkatachari et al., 2008) for their abatement, but complete mineralization is characterized by relatively low rates, which limit the interest on this technology. Also pervaporation has been considered for the removal of chlorinated compounds at very low concentrations from contaminated

waters (Dotremont et al., 1993; Pereira et al., 1998; Pattabhi Ramaiah et al., 2013; Mishima et al., 1999) because of some interesting features such as the flexibility in design and the low energy cost. However, even for pervaporation, the rate of removal is rather low and practical applications are rare. Camera-Roda and Santarelli (2007) showed that the rate of abatement of the organic pollutants is substantially improved when photocatalysis and pervaporation are integrated in a membrane reactor. Process intensification is the result of the synergy that establishes between the two processes. In fact, photocatalysis is favored by the continuous removal from the reactor of intermediate compounds (principally hydroquinone and benzoquinone), which slow down the reaction because they are competitive with 4-CP for adsorption and for the utilization of the photogenerated oxidizing agents (Camera-Roda and Santarelli, 2007; Camera-Roda et al., 2011a; Satuf et al., 2008; Theurich et al., 1996). Concurrently, benzoquinone is more permeable than the original substrate (4-CP), so the removal by pervaporation of organic pollutants becomes more efficient. Furthermore, the continuous removal of benzoquinone slows down the rate of the reverse reaction in the fast equilibrium reaction of transformation of hydroquinone into benzoquinone, and consequently also hydroquinone disappears as long as benzoquinone permeates. The mutual advantages for reaction and membrane separation cause an increase of the rate of detoxification. The rate of disappearance of the organic pollutants in the integrated process is even higher than the sum of the rates of the two uncoupled processes. An "intensification factor," E_i, is introduced to measure the "extent" of process intensification thus obtained. E_i is defined as

$$E_i = \frac{\text{Rate of disappearance of pollutants in the integrated system}}{\text{Sum of the characteristic rates of disappearance of pollutants in each uncoupled process}}$$

The characteristic rates at the denominator are those evaluated at the given concentration of 4-CP, which is operative in the integrated process. It is clear that these rates are at some extent higher than those that would be achieved if reaction and separation were arranged in sequence because in this latter case the concentration of 4-CP would be lower (and hence the driving force would be lower) at least in the second process of the series. Therefore, even if E_i represents a meaningful index of process intensification, it embodies a somehow conservative evaluation of this index.

This performance criterion, which considers the intensification factor to measure the extent of process intensification, can be applied every time the integrated process accomplishes the same task that the uncoupled processes might perform as well. It has been used also in photocatalytic ozonation (Parrino et al., 2015) and in a process where photocatalysis, ozonation, and adsorption processes are combined (Cataldo et al., 2016).

Thanks to the synergy between reaction and separation, E_i is greater than unity, as the experimentally measured values confirm. It is expected that δ should influence E_i because

it is the relative weight of separation to reaction (or vice versa) that affects the synergy. Specifically, the experiments carried out by varying the photocatalytic reactor and the type of membrane demonstrate that when a certain synergy mechanism is active, that is for a given pollutant (4-CP) and for a certain photocatalyst (Degussa P25), E_i depends solely on δ. It is obvious that when $\delta \to 0$ (without separation) or when $\delta \to \infty$ (without reaction), the numerator and the denominator in the definition of E_i become equal and $E_i \to 1$. Therefore, with the reasonable assumption that E_i varies continuously with δ, the Rolle's theorem proves that there exists a maximum of E_i at an optimal value of δ. For the system investigated by Camera-Roda and Santarelli (2007), the maximum value of the intensification factor is about 1.9 and it is obtained at $\delta \approx 0.1$, i.e., when the characteristic rate of pervaporation is only one-tenth of the characteristic rate of reaction. An important guideline can be drawn: whenever a synergy establishes as a result of the coupling of processes that are able to perform the same task (in the present case, water detoxification) the characteristic rates of the processes should be opportunely weighted to give the best process intensification.

Other interesting points include the following:

- The flow rate and the pollutant content of the permeate are much more favorable than the ones that would be obtained with pervaporation alone. With the integrated process, the disposal or the treatment of the permeate is neither problematic nor costly.
- It has been observed that UV-A radiation may damage the polymeric materials of the membranes. This negative phenomenon is easily prevented by keeping separate the membrane module from the photocatalytic reactor. The recycle of the retentate with a proper flow rate guarantees the effective coupling of reaction and separation.
- Membrane fouling is not a problem. Even at long times of operation of the membrane reactor (more than 500 h) no variation of the performances was detected.

It is worth noting that Camera-Roda and Santarelli (2007) inserted a mixed tank in the loop, which recirculates the retentate from the membrane module to the photocatalytic reactor. The presence of the tank allows to increase the total volume of the treated solution and consequently to slow down the disappearance of 4-CP from the system. So, the decrease of the rate of disappearance of 4-CP, which takes place when the concentration of the intermediate compounds builds up and their inhibition effect becomes significant, is more apparent. Without a sufficiently high value of the volume of the tank, V_{tank}, this phenomenon (the decrease of the rate of disappearance of 4-CP) would occur so rapidly that it might not be noticed. This highlights the importance of the ratio, V_{total}/V_r, of the total volume to the reactor volume, where $V_{total} \approx V_{tank} + V_r$. V_{total}/V_r is a parameter whose effects are important whenever a tank is inserted in the recirculation line to the reactor. Actually, a well-mixed tank is very often used in photocatalytic systems with recirculation of the reacting solution, regardless the reactor is coupled or not with a

membrane apparatus (Cassano and Alfano, 2000; Klausner et al., 1994; Davis and Hao, 1991; Wolfrum and Turchi, 1992). There are several reasons for its utilization:

1. To slow down the rate of disappearance of the reactants to experimentally observe more carefully some relatively fast phenomena.
2. To increase the productivity of a discontinuous (or semicontinuous if a permeate is continuously withdrawn) system.
3. To enhance the mixing of the solution.
4. To maintain by mixing the photocatalytic powders in suspension.
5. To allow for the possible continuous supply of consumed reagents (e g. oxygen) in an apparatus where mixing is easy and effective.
6. To approach the behavior of a discontinuous perfectly mixed system.

Regarding this last point, in a reactor with recirculation the evaluation of the average reaction rate, $\langle R \rangle$, can be carried out with the mass balance of the substrate. The mass balance in the case of a perfectly mixed overall system is $\langle R \rangle = -\frac{V_{total}}{V_r}\frac{dc_S}{dt} \approx R(c_S)$ where t is the time, V_{total} is the total volume of the reacting solution, and c_S is the concentration of the substrate. This simple model is sufficiently accurate whenever $Da \times V_r/V_{total} << 1$ with $\mathrm{Da} = \frac{R(c_{S,0})}{c_{S,0}}\frac{V_r}{\dot{V}}$ (Camera-Roda et al., 2017b), where $\dot{V}$ is the volumetric flow rate. This condition is satisfied when the tank has a relatively large volume and Da is low, as it usually happens with photocatalytic reactors.

Points 1 and 2 in the previous list are only apparently contradicting each other. If, for a given reactor volume, the volume of the tank increases, the reaction time for obtaining a given conversion of the substrate increases. During this time the reaction, which takes place only in the reactor, continues to transform the substrate with a rate that, at any time, corresponds to the substrate concentration at that time. Therefore, for a fixed χ conversion, the amount of substrate converted per unit of reaction time is almost independent of the V_{total}/V_r ratio. This statement can be easily demonstrated as follows. The productivity (i.e., the amount of substrate reacted per unit of reactor volume and per unit of process time) is evaluated as

$\text{Productivity} = \frac{n_{S,0}\ \chi}{V_r\ \left(t_r|_\chi + t_{sd}\right)} = \frac{V_{total}\ c_{S,0}\ \chi}{V_r\ \left(t_r|_\chi + t_{sd}\right)}$, where $n_{S,0} = V_{total}\ c_{S,0}$ is the initial number of moles of the substrate in the system; $t_r|_\chi$ is the reaction time to reach the desired conversion, χ; and t_{sd} is the shut down time for discharging the products, cleaning the reactor, and charging the reactants. $t_r|_\chi$ is obtained from the previous mass balance as $t_r|_\chi \approx \frac{V_{total}}{V_r}\int_{c_{S,0(1-\chi)}}^{c_{S,0}} \frac{dc_S}{R(c_S)}$. This equation demonstrates point 1 of the list because it shows that a longer reaction time is needed to get a given conversion when $\frac{V_{total}}{V_r}$ increases.

After substitution:

$$\text{Productivity} = \frac{c_{S,0}\ \chi}{\int_{c_{S,0(1-\chi)}}^{c_{S,0}} \frac{dc_S}{\mathrm{R}(c_S)} + \frac{t_{sd}}{V_{total}/V_r}}$$

. Looking at this equation, it is clear that, if only the reaction time is taken into account (that is only when $t_{sd} \to 0$), the productivity is independent of V_{total}/V_r. However, in a batch production carried out by continuously repeating the cycles of production, the productivity must take into account the total time of a production cycle ($t_{total} = t_r|_{\chi} + t_{sd}$), which, in addition to the reaction time, includes the shut down time. The "weight" of the shut down time on the total time decreases when V_{total}/V_r is raised. Consequently, the productivity augments with V_{total}/V_r even if the reaction time for achieving a given conversion becomes longer.

It is also evident that it makes no sense to compare the photocatalytic activities of different systems on the basis of the reaction time, which is necessary to get a given conversion, or on the basis of the conversion obtained after a certain reaction time. Actually, both of them depend on other parameters, such as V_{total}/V_r, and therefore, the reaction time or the conversion cannot be used for comparing different systems.

Green chemistry plays an important role in sustainability, which, nowadays, is a key objective of the industry from economic, social, and environmental points of view. Moreover, industry cannot ignore that the preferences of the consumers toward eco-friendly products rapidly increased in the last years (Straughan and Roberts, 1999; Laroche et al., 2001; Pickett-Baker and Ozaki, 2008). By considering that in photocatalysis no chemical additive is needed, the photocatalyst (generally, titanium dioxide) is a nontoxic substance, the operating conditions are mild, the energy demand is low, and it can be satisfied by the solar radiation, then it is clear that these important characteristics satisfy the green chemistry principles. This is the main reason why photocatalysis has been studied for the synthesis of fine chemicals. Yet, it is important to improve the yield of photocatalytic syntheses because the low performance of photocatalysis alone represents a bottleneck for practical applications. Process integration seems to be the most viable solution to obtain higher performance.

In photocatalysis, the economy of the process requires the substrate (that is the reactant) to be present at relatively low concentration. Therefore, the proposed membrane process must be able to extract products at low concentration. In this regard, pervaporation appears particularly suited for the coupling, in particular if the membrane module is kept apart from the photocatalytic reactor to avoid UV-A attack to the membrane. Relatively high temperatures, which anyway would not exceed 60–70°C, are necessary to ensure a sufficient permeate flux and are not so detrimental for a photocatalytic reaction as for a biological reaction. Photocatalysis is not thermally activated; hence the temperature does not affect significantly the rate of reaction because only at rather high temperatures,

adsorption properties and oxygen solubility are severely affected. Consequently, the requirements of pervaporation have a greater weight in the choice of the operating temperature.

The photocatalysts in the form of suspended (nano)powders have shown not to be harmful to polymeric PV membranes, and the possible fouling by these powders does not alter their performance (Camera Roda et al., 2011a). On the other hand, because of the higher rate of reaction (De Lasa et al., 2005), which is obtained in real reactors, photocatalyst powders are preferable to immobilized photocatalyst, but the powders usually necessitate a problematic postprocessing recovery. The retention of the photocatalyst in the reacting solution and the recovery of the products, to avoid their inhibition effect on the reaction and their further degradation in the reactor, are among the expected benefits of the integration. Moreover, in pervaporation photocatalytic reactors a complementary exploitation of the solar radiation is possible. In fact, photocatalysis may utilize the UV-A component of the solar spectrum, whereas most of the remaining thermal part is used to heat the fluid and to evaporate the permeate.

On this basis, pervaporation PMRs have been applied to the photocatalytic synthesis of a large class of important fine chemicals (aromatic aldehydes) (Camera-Roda et al., 2011b). The process, named AROMA (advanced recovery and oxidation method for aldehydes), encompasses many positive and interesting features, such as high yields, very simple operation, mild conditions, and possibility of using natural precursors and sunlight. These aldehydes are widely used to enrich the flavor of different types of products, and the utilization of eco-friendly aromas could give an extra value to the final product. The investigation involved some important aromas, such as vanillin, benzaldehyde, and anisaldehyde, whose market is really significant. In principle, many other aromatic aldehydes could be photocatalytically synthetized by partial oxidation of the corresponding primary alcohol in aqueous solution. Therefore, in the photocatalytic synthesis, these products are intermediate compounds in a scheme of reactions in series.

It is worth observing that it is not yet completely clear if, according to the current rules, the aromas, which are photocatalytically produced from natural substrates, can be labeled "natural." The regulations for natural flavor ingredients are at the same time complex and unclear so they are still open to interpretation (Paterson, 2010; Bomgardner, 2016). Furthermore, photocatalysis is an innovative process, which mimics nature and presents uncommon features for "catalytic" reactions (Childs and Ollis, 1980; Serpone et al., 2000; Parmon, 1997; Serpone, 2007). In this framework, the interpretation of the rules should not ignore positive characteristic of the photocatalytic process such as safety, sustainability, and eco-friendliness. Therefore, the product of photocatalysis should not be disadvantaged in comparison with other "natural" products obtained with processes that are much less effective under these points of view.

The effective integration of reaction and pervaporation, i.e., the simultaneity of these two operations is fundamental to obtain the expected improvements. It is anyway possible, as discussed previously, to utilize separate units with the advantage that the design of each apparatus can be optimized, thus obtaining the maximum performances. The pervaporation process uses polymeric, organophilic, dense membranes. In the integrated process, the role of the membrane is to recover selectively from the reactor the aldehyde as long as it is produced, by avoiding its further degradation by oxidation. The reagents are retained in the reactor with negligible loss in the permeate product with the positive effect of increasing the conversion. The rate of production is positively influenced by the removal of the products because the competition of the products with the original substrate for the utilization of the photocatalytic active sites and of the photogenerated oxidizing agents decreases. A simple way to quantify the detrimental effect of the presence of the intermediate on the rate of transformation of the substrate is to make experiments in presence of known concentrations of the intermediate compounds. By keeping constant the initial concentration of the substrate and varying the initial concentration of a given intermediate from 0 to likely values, the initial rate of substrate transformation shows how important is the decay of the rate. The concentration of the aldehyde in the permeate is much higher than the one in the reacting solution, making more easy or unnecessary a further purification. For instance, in the case of vanillin, part of the permeated product deposits directly as almost pure crystals at temperatures slightly below the ambient temperature (Camera-Roda et al., 2014). The running of the plant is very simple and safe because only the temperature and the permeate pressure must be controlled at mild values (temperature around 50−70°C and a sufficient vacuum degree in the permeate).

In summary the advantages deriving from the process integration include the following:

- A substantial improvement of the yield and of the selectivity.
- A satisfactory purification of the product, which in some cases does not need any further separation.
- The product stream is absolutely free from the photocatalytic powders.

Other strengths of the process include the following:

- Low energy demand for the separation step.
- Modularity (both the capacity of the photocatalytic and of the membrane separation apparatuses can be varied by adding or removing modules).
- Possibility of shifting from continuous to semicontinuous (batch) processing.
- Safe environment, thanks to the mild operating conditions and to the utilization of aqueous solutions.
- Simple control so that qualified technicians are not required and the actions of operators are minimized.

Of course, the choice of the membranes is based on the flux and the selectivity, which are obtained with the specific reacting solution. In the case of benzaldehyde and anisaldehyde, polyoctylmethylsiloxane membranes perform satisfactorily, while, with vanillin, polyether block amide (PEBA) membranes show more favorable flux and selectivity. Vanillin is a "high boiler" (Böddeker et al., 1993; Böddeker, 2008), which means that its boiling point is higher than the one of water. Actually, the boiling temperature of vanillin ($T_b \approx 285°C$) is really much higher than 100°C. With the very low vanillin vapor pressure that is obtained at moderate temperatures (50–70°C), the permeation takes place mainly by virtue of the high activity coefficient of vanillin in aqueous solution (>100 at infinite dilution). The enrichment of vanillin in the permeate is due to barrier interference (Böddeker, 2008; Camera-Roda et al., 2017c) of the membrane toward the passage of water, which is in orders of magnitude less soluble than vanillin into the polymeric matrix (even though water diffusivity is higher than vanillin diffusivity).

The retention of most of the other organic compounds (the substrate, i.e., ferulic acid, and the other products) that are present is exceptionally high. Camera-Roda et al. (2014) showed that the high retention is due to the very poor volatility of these compounds rather than to phenomena related to the dissociation of the molecules in aqueous solution, as hypothesized by Brazinha et al. (2011).

Pervaporation of vanillin in aqueous solution presents some unusual behaviors: vanillin permeates through the membrane with a negligible gradient of its partial pressure and the separation factor of vanillin with respect to water increases with the thickness, d, of the membrane. This latter behavior is a consequence of the fact that the variation of the vanillin flux with d is much more limited than the one, which the solution–diffusion model predicts for the transport through the membrane, whereas the water flux complies the solution–diffusion model because it decays proportionally to the thickness d (see Fig. 5.6).

The results of a mathematical model, which adopts the solution–diffusion model for the transport through the membrane plus viscous transport and Knudsen diffusion to describe the transport through the porous support of the membrane, are in optimal agreement with the experimental data (see the curves obtained with the model for vanillin and water in Fig. 5.6). In practice, the small variations of the pressure at the membrane–permeate interface, which are observed when the membrane thickness changes, have a high effect on the vanillin flux, but a negligible effect on the water flux. The model predicts also that the gradient of partial pressure of vanillin across the membrane is very low, according to the experimental evidence (Böddeker and Bengston, 1990; Böddeker et al., 1997). In practice, only a very small fraction of the theoretically maximum driving force of vanillin (i.e., the one that would be available if the vanillin partial pressure downstream the membrane were kept at 0) is active for permeation. This fraction is around 1% and slightly increases with d.

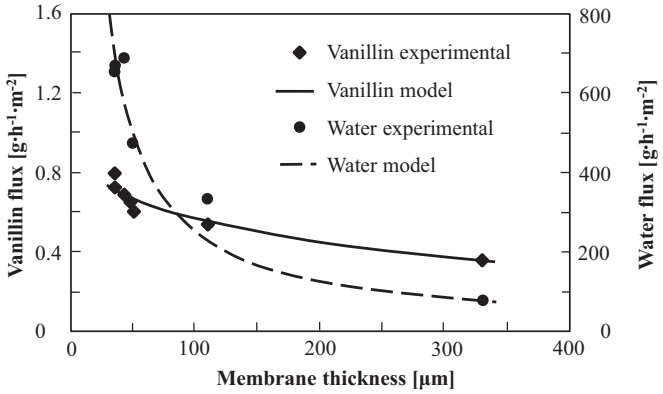

Figure 5.6

The fluxes of vanillin and water versus the membrane thickness. PEBA membranes, vanillin feed concentration = 420 ppm, temperature = 60°C, permeate pressure = 0.7 mbar.

In summary, it has been observed that (1) the theoretically maximum driving force for water permeation is more than 100 times higher than that of vanillin, (2) the driving force for vanillin permeation is very poorly exploited, (3) the diffusivity of water ($D_{water} = 3.5 \times 10^{-9}$ m^2/s) in the membrane is much higher than the diffusivity of vanillin ($D_{vanillin} = 9 \times 10^{-11}$ m^2/s). Looking at these numbers, it is surprising that vanillin permeates preferentially with respect to water.

5.3 Photocatalysis Integrated With Dialysis

5.3.1 Principles of Dialysis

The transport mechanism in dialysis is similar to the one in pervaporation, in particular if the membranes are not porous: the permeants dissolve into the membrane and diffuse through it. The substantial difference is that the permeate does not evaporate because both the phases, upstream and downstream the membrane, are liquid. Owing to the absence of the vapor phase, the volatility has no importance and the driving force is given by the difference of the activities of the permeating species between the two liquid phases. It is normal that in diluted aqueous solutions the values of the activity coefficients of a given permeant in the two liquid phases are very similar. In this case, the driving force for the permeation of a component can be expressed simply by its concentration difference. It is therefore clear that high boilers, such as vanillin, do not suffer the limitations (low volatility and difficulties in exploiting the potential driving force) that are encountered in pervaporation.

5.3.2 Applications of Dialysis Photocatalytic Reactors

On these bases, Camera-Roda et al. (2017c) studied the convenience of coupling dialysis in substitution of pervaporation with photocatalysis in a membrane reactor

where ferulic acid is partially oxidized to produce vanillin. The membrane separates the reacting solution at the side of the photocatalytic reactor (side 1) from the aqueous solution at the other side (side 2). The layout at the side of the photocatalytic reactor was almost the same adopted with pervaporation: a pump recycles the retentate from the membrane module to the annular photocatalytic reactor after the passage through a perfectly mixed tank. The same PEBA membranes, utilized in pervaporation, were used also in dialysis. The membrane module was redesigned to accommodate the plane membrane with a countercurrent tangential flow at the two sides of the membrane. The fluid at side 2 is continuously recycled to the membrane module after the passage through a mixed tank. Preliminary tests of dialysis alone were carried out, bypassing the photocatalytic reactor using diluted aqueous solutions of vanillin or ferulic acid. These preliminary experiments confirmed that dialysis overcomes most of the limitations, which are present in pervaporation. Under the same upstream concentration, the vanillin flux is more than 10 times higher than in pervaporation even at ambient temperature. However, no rejection of the substrate, ferulic acid, is obtained. In general, the permeability of all the aromatic organics, the substrate and any product, is high. A solution–diffusion model, which takes into account also mass transport in the two liquid phases, is able to accurately predict the experimental data (see Fig. 5.7). The only adjustable parameter of the model was the vanillin diffusivity in the polymer matrix, whose value was obtained by best fitting the experimental data of several runs carried out at different initial vanillin concentration and varying the flow rate upstream the membrane. The value of vanillin diffusivity in the membrane resulted to be almost independent of vanillin concentration (at least in the range of the investigated concentrations) and equal to 9 x 10^{-11} m^2/s. The high values of

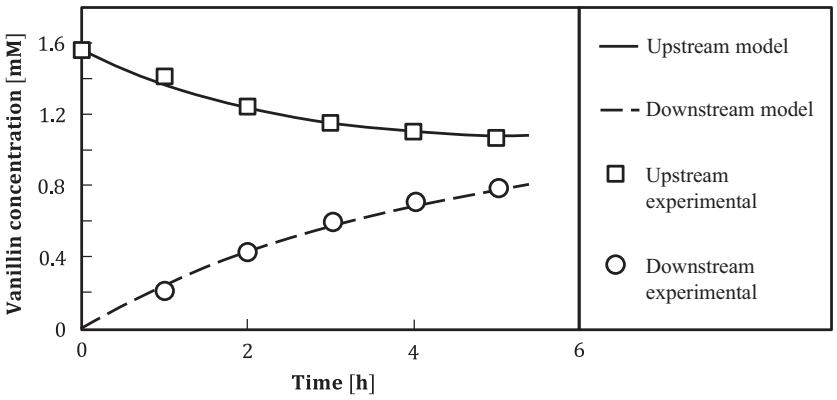

Figure 5.7

Vanillin concentration versus time in the tanks upstream and downstream the membrane. Temperature = 60°C, upstream volume = 1 L, downstream volume = 1 L, membrane area = 9.6 × 10^{-3} m^2, membrane thickness = 50 μm.

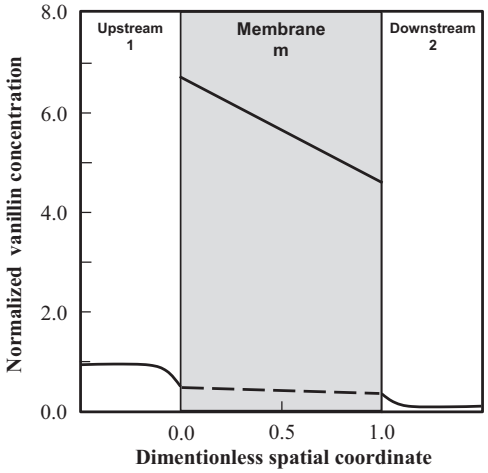

Figure 5.8

Spatial profile of normalized vanillin concentration (C_S/C_{S0}) after 1 h in the same dialysis experiment of Fig. 5.7 (*continuous line*). The *dashed line* represents the vanillin concentration in a hypothetical aqueous solution in local equilibrium.

vanillin diffusivity and solubility justify the high permeability of the membranes. Owing to the relatively high flux of vanillin, concentration polarization is no longer negligible, as it was in pervaporation (see Fig. 5.8). Therefore, it is advisable to operate at sufficiently high tangential velocity to limit this phenomenon.

Interestingly, the high permeability of the substrate does not allow the separation of the product from the substrate, but it can be exploited to continuously replace the substrate, which is consumed in the photocatalytic reactor. To this aim, solutions with the same concentration of the substrate were present initially both at side 1 and 2. In this way, vanillin is recovered from the reacting solution while it is produced, whereas ferulic acid permeates in the opposite direction, thus replacing almost completely the reactant consumed by the reaction.

In the dialysis membrane reactor, the membrane process enables the continuous recovery of the produced vanillin, the continuous feed of the substrate, and the retention of the photocatalytic powders with negligible fouling. Conversely, the postprocess purification of vanillin appears to be more demanding than pervaporation due to the absence in dialysis of an effective barrier against the permeation of the other aromatic compounds.

Azrague et al. (2005; 2007) studied the combination of dialysis and photocatalytic reaction for the depollution of turbid water. The investigated system is purely discontinuous because no output stream is present. The membrane is positioned between the "feed," which is initially composed by turbid water with the pollutant

(2,4-dihydroxybenzoic acid), and the reacting solution at the permeate side. A recycle connects in a loop the reactor to the membrane module. The membranes are permeable to the pollutant but are able to perfectly reject both the photocatalytic powders suspended in the reacting solution and the bentonite powders that are responsible of the turbidity. In this way, the permeated pollutant is degraded in the photocatalytic reactor. The advantages of the coupling are more numerous than the ones claimed by the authors. They include the following:

- Only the photocatalyst absorbs the photons in the reactor because the bentonite powders, which can absorb and waste radiant energy, are confined on the other side of the membrane.
- The pollutant is continuously fed to the reactor, thanks to permeation.
- The driving force for the permeation is enhanced in the coupled process because the concentration of the pollutant in the permeate is lowered by the photocatalytic degradation.
- The photocatalyst powders remain in the reactor.
- After the water is sufficiently purified, the treatment cycle can probably be repeated without substituting the photocatalyst.

Some of the advantages are for the reaction and one is for the separation. Therefore, it is not surprising that, as discussed in Section 5.2.2, the authors suggest to satisfy a given condition for the membrane area "to balance the photodegradation and mass transfer rates," thus "improving the effectiveness of the process." Actually, this condition represents merely the optimal value of δ, which corresponds to $\delta = 1$.

It is not completely clear which is the main "product" stream. It is more likely that the purified water upstream the membrane represents the product stream, even if it is evident that at the end of the treatment it necessitates a filtration step to obtain a clear water with a low content of bentonite powders.

A study on the utilization of dialysis to recover the intermediate products formed from the photocatalytic degradation of lignin sulfonate obtained has been made also by Lekelefac et al. (2014). The objective is twofold: lignin abatement to reduce the environmental impact of wastewaters from pulp and paper mills and the possible production of valuable chemicals as intermediate products of the photocatalytic degradation. In the investigated system, the photocatalytic reactor is connected to a dialysis filter, which should permeate preferentially aromatic compounds from the aqueous medium in the reactor. The organic compounds in the permeate are then extracted by an adsorption cartridge. Actually, the study appears to be more a preliminary attempt than a thorough investigation. So, the conclusion that "it did not matter if extraction was done after the reaction or during the reaction" is probably a contingent result, which is a consequence of the inadequately low membrane area.

5.4 Photocatalysis Integrated With Membrane Contactors

5.4.1 Principles of Membrane Contactors

"Membrane contactors" are used to carry out a separation, which is the membrane analog of the more traditional unit operation of extraction. As in extraction, the separation is given by the distribution of a component between two immiscible phases, where the solubility of that component is different. With membrane contactors a high value of the partition coefficient is beneficial both for the flux by increasing the driving force for mass transfer and the selectivity. The function of the membrane is to govern the interface between the two phases, while allowing the passage of the component between the two phases, which is driven by the necessity of approaching the thermodynamic equilibrium. In the traditional extractors the two phases are in direct contact through interfaces. The same happens in membrane contactors, but without the necessity of dispersing the phases by mixing, because the role of the membrane is to set the interface for mass exchange between the phases. Usually one phase (the wetting phase) penetrates (the pores of) the membrane and comes in contact with the other phase. The interface area per volume, which is obtainable using hollow fibers and capillary modules, can be (much) higher than the one in traditional dispersed phase contactors. This is the strength of a membrane contactor. The presence of the membrane adds a phase to the extraction process. Besides mass transfer in the feed phase and in the permeate phase, mass transfer through the membrane is in series in membrane contactors. This is a weakness of membrane contactors because the resistance to mass transfer through the membrane represents an additional contribution to the overall resistance. Gas−liquid, liquid−liquid, and liquid−gas membrane contactors are the possible cases, where the first term indicates the phase of the feed and the second one indicates the phase of the permeate. The process is not pressure driven, but, generally, the pressure must be regulated to maintain the pores filled by the wetting phase, thus avoiding both the leakage in one direction of the wetting phase into the other phase and the displacement of the wetting phase in the opposite direction.

5.4.2 Applications of Photocatalytic Reactors Integrated With Membrane Contactors

Photocatalytic synthesis of phenol by partial oxidation of benzene has been studied by Molinari et al. (2009) with and without the integration of a membrane contactor equipped with a polypropylene membrane. The reacting solution was an aqueous phase with a benzene concentration close to the limit of solubility and the photocatalyst powders suspended therein. The organic extractant was the same substrate, i.e., benzene. The benzene filled the pores of the polypropylene membrane by capillary forces. Therefore, it was necessary to operate with a pressure in the aqueous phase

slightly higher than the one in the organic phase to prevent the direct passage of the organic phase into the reacting solution. Anyhow, the pressure was kept below the critical "breakthrough" pressure that would displace the organic phase from the membrane pores.

The study was comprehensive, as the effects of many operating conditions and factors were investigated: the photocatalyst concentration, the pH, the presence of metal salts, the type of photocatalyst, the acidic compound used to lower pH, etc. In the proper operating conditions the rate of transformation of benzene into phenol was indeed satisfactory, but phenol is prone to be rapidly degraded by further oxidation in the reacting mixture. It was observed that phenol is photocatalytically produced from benzene, but photocatalysis further oxidizes it into undesired compounds at a relatively high rate.

The authors demonstrated that the presence of the membrane contactor equipped with a plane polypropylene membrane presents several advantages: the continuous recovery of phenol from the reacting solution by means of the membrane contactor; the complete retention of the photocatalytic powders; the continuous restocking of the consumed substrate (benzene), which passes from the organic phase to the reacting solution when its concentration falls below the solubility limit. Probably, benzene does not represent the best extractant, in view of the relatively low value of the partition coefficient (=2.1) of phenol. However, it avoids the introduction in the system of another organic solvent, which then has to be separated, and it is able to play the dual role of extractant and substrate. Therefore, its choice looks to be really profitable. Fouling seems to be a minor problem in particular if the photocatalyst concentration is not too high. It can be concluded that the benefits of the coupling are encouraging and make membrane contactors a technology worth of further investigation for future practical applications of photocatalytic synthesis.

Again in the field of the chemical synthesis of fine chemicals, another interesting application of hybrid photocatalysis–membrane contactor processes has been presented by Molinari et al. (2015). The photocatalytic hydrogenation of acetophenone to phenylethanol is the investigated reaction. Phenylethanol is an added-value chemical that is widely used in flavors and perfumery because of its pleasant floral odor of rose. Interestingly, this synthesis is a reduction. Therefore, all the precautions were taken in the photocatalytic reactor to favor acetophenone reduction instead of its oxidation. After having established the best operating conditions, the researchers investigated the capabilities of the concurrent action of a membrane contactor on the reacting solution. The reacting solution was an aqueous phase of acetophenone, and the layout of the laboratory apparatus was similar to the one adopted by Molinari et al. (2009). In particular, the membrane contactor was arranged in the same way with a plane polypropylene membrane of the same type. A different reactor was adopted in this

synthesis with two alternative types of illumination: a UV lamp or a light-emitting diode (LED) illumination, with an emission spectrum in the visible. The authors tested different feeding modes and extractants, but finally the preference went to the utilization of the substrate (acetophenone) as extractant because in this way the best solubilization in the reacting phase and a more effective extraction of phenylethanol were obtained, with the additional benefit of avoiding the presence of another compound. By comparison of the results obtained with and without the membrane contactor, the integrated process appears more performing. In fact, the recovery of the product avoids "its subsequent reduction" and "shift the hydrogenation reaction forward to the product." Even if the shift of the hydrogenation reaction has not been definitely proven, there is no doubt that the membrane contactor is beneficial. It is likely that the same mechanisms of improvement of the productivity are active also when the same synthesis is carried out under visible light. The activity of the photocatalyst in the visible light was obtained by doping with palladium. With this photocatalyst and under visible light illumination, the amount of produced and extracted phenylethanol was much higher than with undoped photocatalyst under UV light. It is obvious that, despite the study considered the effect of many parameters and factors, it is far to be concluded. For instance, the effect of the fundamental parameter δ has not been investigated in these works on membrane reactors, which utilize membrane contactors. Anyway, these interesting results are promising and create the basis for further developments.

Kumakiri et al. used a gas–liquid membrane contactor to supply continuously oxygen to a photocatalytic film during the degradation of organic acids. A layer of titanium dioxide was deposited with or without platinum onto the surface of two different porous α-alumina supports. In the laboratory apparatus, oxygen filled the pores, thanks to the overpressure that was maintained at the side of the gas phase. In this way, the oxygen comes in direct contact with the photocatalytic layer and may dissolve into the aqueous solution of the substrate without forming bubbles. Formic acid, oxalic acid, and humic acid were used as substrate. The effects of the presence of platinum, the absence of the light, and the shortage of oxygen on the rate of disappearance of the substrate were investigated. The results show that the highest rates are obtained when the membrane contactor feeds the oxygen to the photocatalytic layer under UV illumination, in particular if Pt is present in the layer. Therefore, the author argues that the membrane contactor represents a suitable way to supply the oxygen required for the reaction directly to the photocatalytic layer. In this way, the contact of oxygen with the photocatalyst is more direct than the one obtainable through the conventional techniques of oxygenation, such as bubbling the oxygen in the bulk of the solution. Other interesting findings are as follow: the lifetime of Pt is enhanced by the combination with the photocatalyst, the chemicals give no membrane fouling, and the initial catalytic activity is maintained after several months of testing and several months of storage in air.

Finally, it is worth mentioning the work by Sciubba et al. (2009), who evaluated the potential of using membrane contactors for the membrane-based solvent extraction of vanillin from a fermentation broth. Even if this study is finalized to the utilization in an integrated bioconversion—separation process, the results show that the same membrane contactor technology could be applied to a PMR for the recovery of vanillin with the advantages, which have been discussed in Section 5.2.3.

5.5 Photocatalysis Integrated With Membrane Distillation

5.5.1 Principles of Membrane Distillation

In membrane distillation, the role of the membrane is to block the passage of the liquid feed while allowing the passage of the produced vapors. In particular, in direct-contact membrane distillation (DCMD), the membrane keeps apart two aqueous phases, which are in direct contact with the membrane, whereas a gas phase with water vapor is present inside the pores. Until now, DCMD is the operation that has been considered for the combination with photocatalysis. The liquid feed is maintained at a higher temperature than the liquid permeate and, in this way, vapor is produced at the feed side, diffuses through the pores, and condensates in the permeate. The driving force is the difference of the vapor pressure, which is generated by the temperature difference. The membranes must be hydrophobic, with sufficiently high porosity and a narrow distribution of the pore size to avoid the passage of the fluids into the pores. The thinner the membrane the lower the resistance to vapor passage through the pores, but thin membranes offer also a poor thermal insulation between the two liquid phases. The pore size is usually in the range 0.1—1 μm. Hydrophobicity has the tendency to decrease with time especially in presence of organic solvents.

The main potential advantages of membrane distillation are

- possibility to operate at relatively low temperatures compared with conventional distillation or evaporation processes, thus allowing the treatment of heat-sensitive products and the utilization of solar and waste heat;
- low pressure compared with pressure-driven membrane processes because no external pressure is required to assure permeation as the driving force is mainly given by a temperature difference, which guarantees a partial pressure difference;
- possibility of operating also at high salt concentrations;
- lower membrane fouling than reverse osmosis or nanofiltration.

Gradients of the temperature inside the liquid phases (temperature polarization) and heat conduction between the two liquid phases have detrimental effect on the performance, so precautions shall be taken to limit these phenomena. Potential practical applications are water desalination and purification and the concentration of fruit juice.

5.5.2 Applications of Photocatalytic Reactors Integrated With Membrane Distillation

Systems where membrane distillation and photocatalysis operate concurrently have been analyzed to treat waters containing different types of pollutants. In these PMRs, photocatalysis operates upstream the membrane to degrade the pollutants, possibly up to mineralization, while water vapor passes through the pores of the hydrophobic membrane and condensate in the cold permeate. The main product is usually the distillated permeate, which consists of purified water, thanks to the low volatility of the pollutants and of the possible intermediate compounds, which are photocatalytically produced. The photocatalyst is used as suspended powders (Mozia et al., 2005, 2007, 2013; Mozia and Morawski, 2012; Darowna et al., 2014) or as an immobilized film on a support (Hou et al., 2017).

Several variations of the photocatalytic part of the system were investigated: UV-A, UV-C, or visible light; fluorescent lamp, discharge lamp, or LEDs; commercial or specially prepared photocatalyst; in the form of suspended powders (by the research group of Mozia); or as an immobilized film onto a glass support (Hou et al., 2017). The treated aqueous solutions are contaminated by some azo-dyes, ibuprofen, diclofenac, naproxen, or picrolonic acid. Pure water is the aqueous matrix where these pollutants are usually dissolved, but in some studies the pollutants are present also in tap water or primary or secondary effluents. Most of the works adopted polypropylene capillary membranes, whereas a flat sheet polytetrafluoroethylene membrane was used by Hou et al. (2017). Also the mode of operation has been varied: in most cases, discontinuous systems but also continuous systems (Mozia and Morawski, 2012) have been investigated. The study on the continuous system is particularly interesting in view of real practical applications.

Even if the types of pollutants and other features are different, the proposed systems present the following common features:

- The coupling is obtained by continuously recirculating the reacting solution in a loop that connects the membrane module and the photocatalytic reactor.
- Pollutants and the intermediate compounds that are produced by photocatalysis have a low volatility and do not permeate. The volatility of the original substrates is so low that the membrane is almost impermeable to them. Some intermediate compounds, which are photocatalytically produced, are detected in the permeate, but at such a low concentration, they do not represent an issue. Only effluents containing high concentrations of ammonia nitrogen produced a distillate of lower quality due to the passage of ammonia through the membrane.
- The rejection of photocatalytic powders by the membrane is total.
- Fouling by the photocatalytic powders is low and is not an issue.

In view of future practical applications, it must be considered that, unlike the other non—pressure-driven membrane processes, membrane distillation is an energy intensive process because latent heat is used for the evaporation of the permeate. The amount of permeate must satisfy the required production, whichever is the desired product between the permeate and the concentrate. To meet this goal a relatively high quantity of distillate must be produced. Also in pervaporation, the permeate evaporates, but the objective of the process is obtained with a (very) low flow rate of the permeate, that is with a low energy requirement. The debate on the economic convenience of membrane distillation is still open. In general, it is established that if waste heat is available, then membrane distillation can be suitable, but also other scenarios can be profitable (Al-Obaidani et al., 2008; Kesieme et al., 2013). Therefore, it can be stated that in various cases, membrane distillation is energetically convenient.

To establish the convenience of the integrated process, it is worth reviewing the reasons for the coupling.

In theory, the functions of membrane distillation (production of a pure permeate) and of photocatalysis (pollutant degradation) could be accomplished as well-operating membrane distillation and photocatalysis in this order in sequence. Therefore, the convenience of carrying out the two processes simultaneously is not a foregone conclusion. Furthermore, if the photocatalytic degradation takes place in series after membrane distillation, the quality of the distillate is certainly ensured because, unlike some intermediate compounds, the original substrates have such a low volatility that they are totally absent in the distillate.

Anyhow, some aspects are in favor of the hybrid systems. Among the invoked motivations for the coupling, the following ones are reported: (1) “minimize the size of the installation” (Mozia et al., 2007); (2) “in the case of the hybrid systems,” the pollutant “was removed also from the feed solution, which could be regarded as a solution of the problem of contaminated concentrate, occurring when DCMD is conducted alone” (Mozia et al., 2013).

Actually, point (1) needs further investigations because it has not been ultimately proven in the published studies and it is difficult to theoretically quantify the importance of the minimization of the size of the installation. Point (2) is correct, but the same would apply also to the sequential arrangement of membrane distillation before photocatalysis.

However, there are other reasons for the coupling, which appear to be stronger and justify the interest toward the photocatalysis-DCMD integrated systems. For instance, Mozia and Morawski (2012) showed that a TiO_2 layer deposits on the membrane surface with the coupled photocatalysis-DCMD process, thus preventing from deposition of $CaCO_3$ inside the membrane pores and “protecting the membrane from damage and elongating its

lifetime." So, coupling DCMD with photocatalysis has a positive influence on the mitigation of scaling, which often represents a serious problem, leading to membrane wetting or membrane mechanical destruction.

Moreover, the heat emitted by the light source can be exploited for heating the feed (Mozia et al., 2005), with the additional advantage of reducing or avoiding the utilization of cooling systems for the lamp.

Finally, an interesting rationale for the integration of photocatalysis with DCMD processes has been presented by Hou et al. (2017) who established that "membrane distillation process also promotes photocatalysis because it could retard the decrease of picrolonic acid concentration during its degradation by transporting water to the other side." In support of that statement, they showed that the rate of photocatalytic degradation of the pollutant, which is obtained in the integrated process, is higher than the one obtained without membrane distillation. The reason for this behavior is the continuous removal of water, which concentrates the reactants in the reacting solution with the consequential increase of the rate of reaction. In theory, also in a sequential arrangement, the reactant can be concentrated in a membrane distillation unit, so that the sequential reactor can operate with an initial (or inlet) higher reactant concentration. But, the integrated process is more favorable. In fact, it is easy to demonstrate that in a semicontinuous system, for a fixed quantity of distillate and a fixed pollutant abatement, the overall time (given by the sum of the time for membrane distillation plus the time for photocatalysis) for the sequential arrangement is longer than the time for the integrated process. In a continuous system, the same conclusion is drawn for the residence times. Interestingly, Hou et al. (2017) did not use the membrane to retain the photocatalyst because this latter is immobilized inside the photocatalytic reactor as a film deposited onto illuminated glass sheets.

5.6 Conclusions and Future Trends

PMRs that adopt non–pressure-driven membrane processes are characterized by some interesting qualities:

- The ability to retain the photocatalyst, even in the form of suspended nanopowders, without significant fouling phenomena.
- The possibility in many cases to selectively remove or recover the organic product(s) of the photocatalytic reaction from an aqueous solution (conversely, pressure-driven processes are able to permeate preferentially water). This capability enlarges significantly the opportunities of achieving interesting advantages from the reaction–separation integration.
- Simpler and cheaper modules because high pressures are not required.
- The easy and safe control of the process.

Other interesting features, which are in common with other types of PMRs, are the low energy demand, the reduced use of chemicals, the mild operating conditions, and the modularity.

Furthermore, they represent one of the most promising methods to surmount the limitations of the sole photocatalysis with the objective of filling the gap between research and industrial utilization.

A survey of the proposed applications using different membrane processes has shown the pros and the cons and the opportunities offered by the different studied solutions.

Many actions may contribute to meet the goal of process intensification, that is, a substantial improvement of the yields. Most of these actions are operative only if the coupling, i.e., the simultaneity, of reaction and membrane separation is effective. The parameters that affect the performance of the system and the methods to integrate reaction and membrane separation have been presented and discussed. The Damköhler number and the ratio of the characteristic rate of separation to the one of reaction are two main fundamental parameters that should always be considered in PMRs. Moreover, it is possible to adopt different configurations that are characterized by various degrees of freedom. As a general rule, the larger the degree of freedom, the higher the possibilities of optimizing the system and consequently of increasing the yield. From this point of view, separate apparatuses are preferable, provided that they are effectively coupled.

Substantially, PMRs have been proposed and studied for two types of applications: water treatment and chemical synthesis.

In the case of water treatment, PMRs appear among the best candidates for the final abatement of "emerging" micropollutants, such as drugs, pesticides, hormones, and pharmaceuticals, that sometimes are of public health concern even at concentrations levels of a few ng/L. With PMRs, it becomes possible to retain the photocatalyst and to improve the rate of abatement or removal of the pollutants.

In regard to chemical synthesis, as long as oil is "cheap," photocatalysis and PMRs cannot be economically convenient with respect to petrochemistry for the productions of basic chemicals. Nonetheless, the need of the industry of relocating toward green chemistry both to satisfy the preference of the consumers toward eco-friendly products and to reduce the environmental impact may turn photocatalysis into a serious competitor for the production of value-added fine chemicals. Also in this case, the coupling of non—pressure-driven membrane processes with photocatalysis appears as one of the best ways to achieve the levels of performance required for practical applications.

PMRs can be proposed also for the valorization of industrial waste and by-product streams through the transformation of unwanted compounds into chemicals or fuels. These

applications are just at the beginning but with interesting perspectives. At present, waste streams from the agro-food industry, such as olive oil mill wastewater and waste residue of wheat or rice bran, appear as the most likely candidates for this type of treatment.

However, certain problems, some of which are not of technical nature, remain to be solved.

The whole system must be reexamined by considering the specific needs of an integrated reaction–separation process. In particular, the main points that must be considered are the layout of the apparatuses, the effectiveness of the coupling, the optimization of the intervening parameters, and the design of the reactor modules and of the membrane modules. In that respect, there is large room for developments. Sometimes, the membrane modules are essentially inspired to reverse osmosis applications, with little or no attention to the necessities of the adopted non–pressure-driven membrane process fed by a reacting solution with suspended (nano)powders. Also the correct design of the photocatalytic reactor is complex mainly because the optimal utilization of the radiant energy is in contrast with the adequate exploitation of the reactor volume. In practice, the "best" photocatalytic reactor is determined by the more profitable compromise between the capital and the operating costs. Moreover, it has been shown that the modularity of both photocatalysis and membrane processes can be profitably utilized in PMRs, but currently it is largely underexploited.

The development of suitable membranes, studied for the specific utilization in PMRs, is far from being completed, and significant improvements can be expected in this field once more resources will be deserved. In practice, for non–pressure-driven processes, several types of membranes have been investigated on a laboratory scale because the interest toward these membrane processes is growing, but their development for a large-scale manufacturing and real practical application is in its infancy. Furthermore, the few commercially available membranes are still relatively expensive and this is a severe limit for the spread of PMRs based on these processes. Actually, nor the materials nor the manufacturing technology are more expensive than those for reverse osmosis membranes whose price is relatively low. Essentially, the absence of a real market for this type of membranes did not allow until now to lower their production cost. On the other hand, industries are quite reluctant to invest in new processes in cost-cutting times. The main progress is expected from the reduction of the thickness of the selective layer, the development of proper supports with higher porosity, and the selection of more selective materials toward the organic compounds because in general organophilic membranes are expected to be more beneficial in PMRs.

The interest for the photocatalytic production of fine chemicals is also limited by the current rules that regulate the food industry. It is emblematic in the case of many important aromas, such as vanillin, that, according to a strict interpretation of the EU and

USA regulations, cannot be labeled natural if photocatalytically produced. On the contrary, for the production of "natural" flavors, the regulations allow other processes, such as roasting, heating, distillation, and solvent extraction, which can be much less green and in some cases without a severe control may produce traces of toxic substances. On the other hand, the rules governing food industry are somehow atypical with respect to that for other industries. In fact, in the food industry, the regulations are not focused on the final properties of the product, as it would be logical and normal but fix the "recipe" for obtaining a given product. While this approach preserves the traditional methods of food processing, it limits the opportunities of the innovation, which could improve the quality of the product and the process including also safety, sustainability and eco-friendliness.

After all, the integration of photocatalysis with non−pressure-driven membrane processes can be really profitable because there are numerous mechanisms that can improve the yield. Therefore, the possibilities of process intensification are higher than with pressure-driven processes and the coupling is generally simpler. However, non−pressure-driven processes are not at the level of maturity of other membrane processes, such as reverse osmosis or ultrafiltration. Even if presently this represents a shortage, nonetheless it gives more future possibilities of improvement.

List of Symbols

A_i Component i
A_m Membrane area
$A_{m,k}$ Membrane area of the kth block
$A_{m,tot}$ Total membrane area in the system
c_i Molar concentration of component A_i
$c_{R,0}$ Reference value of the reactant concentration
c_S Concentration of the substrate
$c_{S,0}$ Initial concentration of the substrate
d Thickness of the membrane
$D_{vanillin}$ Vanillin diffusivity inside the membrane
D_{water} Water diffusivity inside the membrane
Da Damköhler number
E_i Intensification factor
I Intermediate product
l Geometrical thickness of the reactor
$\dot{m}''$ Mass flux of the permeate
N Number of reaction−separation blocks in series
N_c Number of components
$n_{S,0}$ Initial number of moles of the substrate
P Pressure
Pe Péclet number
P_i Partial pressure of component A_i
P_i^* Vapor pressure of component A_i
R Reaction rate
R Recycle ratio

R_i Rejection of component A_i
T Operating temperature
t Time
t_{0r} Residence time
t_r Characteristic time for reaction
$t_r|_\chi$ Reaction time to obtain a given conversion
t_{sd} Time of shut down
t_{sep} Characteristic time for the separation process
$\dot{V}_0$ Feed volumetric flow rate
$\dot{V}_1$ Volumetric flow rate of stream #1 in Fig. 5.2C
$\dot{V}_k$ Volumetric feed flow rate to the k*th* block
$\dot{V}_P$ Volumetric flow rate of the condensed permeate
V_r Reactor volume
$V_{r,k}$ Reactor volume of the k*th* block
$\dot{V}_{recycle}$ Volumetric flow rate of the recycle
V_{tank} Volume of the tank
$V_{r,tot}$ Total volume of the reactors
V_{total} Total volume of the system
x Molar fraction in the liquid phase
y Molar fraction in the gaseous phase

Greek Letters

$\alpha_{i,j}$ Separation factor of component A_i with respect to component A_j
β Extinction coefficient of the light
β_i Enrichment factor of component A_i
χ Conversion
δ Ratio of the characteristic reaction time to the characteristic separation time
γ Activity coefficient
ρ Density of the condensed permeate
τ Optical thickness

Subscripts

0 Refers to the feed stream or to a reference value
1 Refers to stream #1 in Fig. 5.2C
I Refers to an intermediate product
i Refers to component A_i
j Refers to component A_j
k Refers to the k*th* block
m Refers to the membrane
p Refers to permeate phase
r Refers to the reactor or to reaction
R Refers to a reactant
S Refers to the substrate
sep Refers to separation
tank Refers to the tank
U Refers to the phase "upstream the membrane" (at the feed side)
D Refers to the phase "downstream the membrane" (at the permeate side)

List of Acronyms

4-CP 4-Chlorophenol
DMCD Direct-contact membrane distillation
LED Light-emitting diode
PEBA Polyther block amide
PFR Plug flow reactor
PMR Photocatalytic membrane reactor
UV Ultraviolet
VOC Volatile organic compound

References

Ahmed, S., Rasulm, M.G., Brown, R., Hashib, M.A., 2011. Influence of parameters on the heterogeneous photocatalytic degradation of pesticides and phenolic contaminants in wastewater: a short review. J. Environ. Manag. 92, 311−330.

Al-Obaidani, S., Curcio, E., Macedonio, F., Di Profio, G., Al-Hinai, H., Drioli, E., 2008. Potential of membrane distillation in seawater desalination: thermal efficiency, sensitivity study and cost estimation. J. Membr. Sci. 323, 85−98.

Assabumrungrat, S., Phongpatthanapanich, J., Praserthdam, P., Tagawa, T., Goto, S., 2003. Theoretical study on the synthesis of methyl acetate from methanol and acetic acid in pervaporation membrane reactors: effect of continuous-flow modes. Chem. Eng. J. 95, 57−65.

Augugliaro, V., El Nazerb, H.A., Loddo, V., Mele, A., Palmisano, G., Palmisano, L., Yurdakal, S., 2010. Partial photocatalytic oxidation of glycerol in TiO_2 water suspensions. Catal. Today 151, 21−28.

Augugliaro, V., Camera-Roda, G., Loddo, V., Palmisano, G., Palmisano, L., Parrino, F., Puma, M.A., 2012. Synthesis ofvanillin water by TiO_2 photocatalysis. Appl. Catal. B Environ. 111-112, 555−561.

Azrague, K., Puech-Costes, E., Aimar, P., Maurette, M.T., Benoit-Marquié, F., 2005. Membrane photoreactor (MPR) for the mineralisation of organic pollutants from turbid effluents. J. Memb. Sci. 258, 71−77.

Azrague, K., Aimar, P., Benoit-Marquié, F., Maurette, M.T., 2007. A new combination of a membrane and a photocatalytic reactor for the depollution of turbid water. Appl. Catal. B Environ. 72, 197−204.

Babi, D.K., Cruz, M.S., Ganiet, R., 2016. Chapter 2, Fundamentals of process intensification: a process systems engineering view. In: Segovia-Hernández, J.G., Bonilla-Petriciolet, A. (Eds.), Process Intensification in Chemical Engineering. Springer International Publishing, Switzerland.

Battersby, S., Teixeira, P.W., Beltramini, J., Duke, M.C., Rudolph, V., Diniz Da Costa, J.C., 2006. An analysis of the Péclet and Damköhler numbers for dehydrogenation reactions using molecular sieve silica (MSS) membrane reactors. Catal. Today 116, 12−17.

Baudot, A., Marin, M., June 1997. Pervaporation of aroma compounds: comparison of membrane performances with vapour-liquid equilibria and engineering aspects of process improvement. Trans. IChemE 75 (Part C), 117−142.

Belgiorno, V., Rizzo, L., Fatta, D., Della Rocca, C., Lofrano, G., Nikolaou, A., Naddeo, V., Merica, S., 2007. Review on endocrine disrupting-emerging compounds in urban wastewater: Occurrence and removal by photocatalysis and ultrasonic irradiation for wastewater reuse. Desalination 215, 166−176.

Blanco-Galvez, J., Fernández-Ibáñez, P., Malato-Rodríguez, S., 2007. Solar photocatalytic detoxification and disinfection of water: recent overview. J. Sol. Energy Eng. 129, 4−15.

Böddeker, K.W., 1990. Terminology in pervaporation. J. Membr. Sci. 51, 259−272.

Böddeker, K.W., 2008. Liquid Separations With Membranes: An Introduction to Barrier Interference. Springer-Verlag, Berlin Heidelberg.

Böddeker, K.W., Bengston, G., 1990. Pervaporation of low volatility aromatics from water. J. Membr. Sci. 53, 143−158.

Böddeker, K.W., Bengtson, G., Pingel, H., Dozel, S., 1993. Pervaporation of high boilers using heated membranes. Desalination 90, 249–257.

Böddeker, K.W., Gatfield, I.L., Jähnig, J., Schorm, C., 1997. Pervaporation at the vapor pressure limit: Vanillin. J. Membr. Sci. 137, 155–158.

Bomgardner, M.M., 2016. The problem with vanilla. Chem. Eng. News 94, 38–42.

Brazinha, C., Barbosa, D.S., Crespo, J.G., 2011. Sustainable recovery of pure natural vanillin from fermentation media in a single pervaporation step. Green Chem. 13, 2197–2203.

Camera-Roda, G., Santarelli, F., 2007. Intensification of water detoxification by integrating photocatalysis and pervaporation. J. Sol. Energy Eng. 129, 68–73.

Camera-Roda, G., Santarelli, F., Martin, C.A., 2005. Design of photocatalytic reactors made easy by considering the photons as immaterial reactants. Sol. Energy 79, 343–352.

Camera-Roda, G., Santarelli, F., Panico, M., 2009. Study and optimization of an annular photocatalytic slurry reactor. Photochem. Photobiol. Sci. 8, 712–718.

Camera-Roda, G., Santarelli, F., Augugliaro, V., Loddo, V., Palmisano, G., Palmisano, L., Yurdakal, S., 2011a. Photocatalytic process intensification by coupling with pervaporation. Catal. Today 161, 209–213.

Camera-Roda, G., Augugliaro, V., Loddo, V., Palmisano, G., Palmisano, L.., 2011b. Production of aldehydes by oxidation in aqueous medium with recovery of the product by means of pervaporation. US Patent WO2011154925 A1.

Camera-Roda, G., Augugliaro, V., Cardillo, A., Loddo, V., Palmisano, G., Palmisano, L., 2013a. A pervaporation photocatalytic reactor for the green synthesis of vanillin. Chem. Eng. J. 224, 136–143.

Camera-Roda, G., Augugliaro, V., Loddo, V., Palmisano, L., 2013b. Pervaporation membrane reactors. In: Basile, A. (Ed.), Handbook of Membrane Reactors, Reactor Types and Industrial Applications, vol. 2. Woodhead Publishing Series in Energy, Cambridge, UK, pp. 107–151.

Camera-Roda, G., Cardillo, A., Loddo, V., Palmisano, L., Parrino, F., 2014. Improvement of membrane performance to enhance the yield of vanillin in a pervaporation reactor. Membranes 4, 96–112.

Camera-Roda, G., Loddo, V., Palmisano, L., Parrino, F., Santarelli, F., 2017a. Process intensification in a photocatalytic membrane reactor: analysis of the techniques to integrate reaction and separation. Chem. Eng. J. 310, 352–359.

Camera-Roda, G., Loddo, V., Palmisano, L., Parrino, F., 2017b. Guidelines for the assessment of the rate law of slurry photocatalytic reactions. Catal. Today 281, 221–230.

Camera-Roda, G., Loddo, V., Palmisano, L. and Parrino, F.., 2017c. A comparison of pervaporation and dialysis for the production of vanillin in a membrane reactor. To be submitted to J. Membr. Sci.

Cassano, A.E., Alfano, O.M., 2000. Reaction engineering of suspended solid heterogeneous photocatalytic reactors. Catal. Today 58, 167–197.

Cataldo, S., Iannì, A., Loddo, V., Mirenda, E., Palmisano, L., Parrino, F., Piazzese, D., 2016. Combination of advanced oxidation processes and active carbons adsorption for the treatment of simulated saline wastewater. Sep. Purif. Technol. 171, 101–111.

Charpentier, J.C., 2012. Did you say "Reactor Design & Process Intensification", or how to produce much more and better while consuming much less? Chem. Eng. Technol. 35, 1118–1119.

Childs, L.P., Ollis, D.F., 1980. Is photocatalysis catalytic? J. Catal. 66, 383–390.

Chong, M.N., Jin, B., Chow, C.W.K., Saint, C., 2010. Recent developments in photocatalytic water treatment technology: a review. Water Res. 44, 2997–3027.

Darowna, D., Grondzewska, S., Morawski, A.W., Mozia, S., 2014. Removal of non-steroidal anti-inflammatory drugs from primary and secondary effluents in a photocatalytic membrane reactor. J. Chem. Technol. Biotechnol. 89, 1265–1273.

Davis, A.P., Hao, O.J., 1991. Reactor dynamics in the evaluation of photocatalytic oxidation kinetics. J. Catal. 131, 285–288.

De Lasa, H., Serrano, B., Salaices, M., 2005. Photocatalytic Reaction Engineering. Springer Science+Business Media, New York. Chapter 2.

Dotremont, C., Goethaert, S., Vandecasteele, C., 1993. Pervaporation behaviour of chlorinated hydrocarbons through organophilic membranes. Desalination 91, 177−186.
Gaya, U.I., Abdullah, A.H., 2008. Heterogeneous photocatalytic degradation of organic contaminants over titanium dioxide: a review of fundamentals, progress and problems. J. Photochem. Photobiol. C 9, 1−12.
Gómez-García, M.Á., Dobrosz-Gómez, I., Fontalvo, J., Rynkowski, J.M., 2012. Membrane reactor design guidelines for ammonia decomposition. Catal. Today 191, 165−168.
Hermann, J.-M., Lacroix, M., 2010. Environmental photocatalysis for green chemistry. Kinet. Catal. 51, 793−800.
Hou, R., Gao, Y., Zhu, H., Yang, G., Liu, W., Huo, Y., Xie, Z., Li, H., 2017. Coupling system of Ag/BiOBr photocatalysis and direct contact membrane distillation for complete purification of N-containing dye wastewater. Chem. Eng. J. 317, 386−393.
Iglesias, O., Rivero, M.J., Urtiaga, A.M., Ortiz, I., 2016. Membrane-based photocatalytic systems for process intensification. Chem. Eng. J. 305, 136−148.
Karlsson, H.O., Trägårdh, G., 1993. Pervaporation of dilute organic-waters mixtures. A literature review on modelling studies and applications to aroma compound recovery. J. Membr. Sci. 76, 121−146.
Kesieme, U.K., Milne, N., Aral, H., Cheng, C.H., Duke, M., 2013. Economic analysis of desalination technologies in the context of carbon pricing, and opportunities for membrane distillation. Desalination 323, 66−74.
Klausner, J.F., Martin, A.R., Goswami, D.Y., Schanze, K.S., 1994. On the accurate determination of reaction rate constants in batch-type solar photocatalytic oxidation facilities. J. Sol. Energy Eng. 116, 19−24.
Konieczny, K., Bodzek, M., Panek, D., 2008. Removal of volatile compounds from the wastewaters by use of pervaporation. Desalination 223, 344−348.
Kumakiri, I., Diplas, S., Simon, C., Nowak, P., 2011. Photocatalytic membrane contactors for water treatment. Ind. Eng. Chem. Res. 50, 6000−6008.
Laroche, M., Bergeron, J., Barbaro-Forleo, G., 2001. Targeting consumers who are willing to pay more for environmentally friendly products. J. Consum. Mark. 18, 503−520.
Lekelefac, C.A., Hild, J., Czermak, P., Herrenbauer, M., 2014. Photocatalytic active coatings for lignin degradation in a continuous packed bed reactor. Int. J. Photoen. 10. Article ID 502326.
Leong, S., Razmjou, A., Wang, K., Hapgood, K., Zhang, X., Wang, H., 2014. TiO_2 based photocatalytic membranes: a review. J. Membr. Sci. 472, 167−184.
Lim, S.Y., Park, B., Hunga, F., Sahimi, M., Tsotsis, T.T., 2002. Design issues of pervaporation membrane reactors for esterification. Chem. Eng. Sci. 57, 4933−4946.
Lipnizki, F., Field, R.W., 2002. Hydrophobic pervaporation for environmental applications: process optimization and integration. Environ. Prog. 21, 265−272.
Martin, C.A., Camera-Roda, G., Santarelli, F., 1999. Effective design of photocatalytic reactors: influence of radiative transfer on their performance. Catal. Today 48, 307−313.
Maurino, V., Bedini, A., Minella, M., Rubertelli, F., Pelizzetti, E., Minero, C., 2008. Glycerol transformation through photocatalysis: a possible route to value-added chemicals. J. Adv. Oxid. Technol. 11, 184−192.
Mishima, S., Kaneoka, H., Nakagawa, T., 1999. Characterization and pervaporation of chlorinated hydrocarbon−water mixtures with fluoroalkyl methacrylate-grafted PDMS membrane. J. Appl. Polym. Sci. 71, 273−287.
Mohan, K., Govind, R., 1988. Effect of temperature on equilibrium shift in reactors with a permselective wall. Ind. Eng. Chem. Res. 27, 2064−2070.
Molinari, R., Caruso, A., Poerio, T., 2009. Direct benzene conversion to phenol in a hybrid photocatalytic membrane reactor. Catal. Today 144, 81−86.
Molinari, R., Lavorato, C., Argurio, P., 2015. Photocatalytic reduction of acetophenone in membrane reactors under UV and visible light using TiO_2 and Pd/TiO_2 catalysts. Chem. Eng. J. 274, 307−316.
Molinari, R., Lavorato, C., Argurio, P., 2017. Recent progress of photocatalytic membrane reactors in water treatment and in synthesis of organic compounds. A review. Catal. Today 281, 144−164.

Moon, W.S., Park, S.B., 2000. Design guide of a membrane for a membrane reactor in terms of permeability and selectivity. J. Membr. Sci. 170, 43–51.
Mozia, S., 2010. Photocatalytic membrane reactors (PMRs) in water and wastewater treatment. A review. Sep. Pur. Technol. 73, 71–91.
Mozia, S., Morawski, A.W., 2012. The performance of a hybrid photocatalysis–MD system for the treatment of tap water contaminated with ibuprofen. Catal. Today 193, 213–220.
Mozia, S., Tomaszewska, M., Morawski, A.W., 2005. A new photocatalytic membrane reactor (PMR) for removal of azo-dye Acid Red 18 from water. Appl. Catal. B Environ. 59, 131–137.
Mozia, S., Tomaszewska, M., Morawski, A.W., 2007. Photocatalytic membrane reactor (PMR) coupling photocatalysis and membrane distillation—effectiveness of removal of three azo dyes from water. Catal. Today 129, 3–8.
Mozia, S., Darowna, D., Przepiórski, J., Morawski, A.W., 2013. Evaluation of performance of hybrid photolysis-DCMD and photocatalysis-DCMD systems utilizing UV-C radiation for removal of diclofenac sodium salt from water. Pol. J. Chem. Tech. 15, 51–60.
Occulti, F., Camera-Roda, G., Berselli, S., Fava, F., 2008. Sustainable decontamination of an actual-site aged PCB-polluted soil through a biosurfactant-based washing followed by a photocatalytic treatment. Biotechnol. Bioeng. 99, 1525–1534.
Palmisano, G., Augugliaro, V., Pagliaro, M., Palmisano, L., 2007. Photocatalysis: a promising route for 21st century organic chemistry. Chem. Commun. 2007 (33), 3425–3437.
Parmon, V.N., 1997. Photocatalysis as a phenomenon: aspects of terminology. Catal. Today 39, 137–144.
Parrino, F., Camera-Roda, G., Loddo, V., Augugliaro, V., Palmisano, L., 2015. Photocatalytic ozonation: Maximization of the reaction rate and control of undesired by-products. Appl. Catal. B Environ. 178, 37–43.
Paterson, D., 2010. Vanilla: natural or not? Chem. Educ. N. Z. 118, 2–6.
Pattabhi Ramaiah, K., Satyasri, D., Sridhar, S., Krishnaiah, A., 2013. Removal of hazardous chlorinated VOCs from aqueous solutions using novel ZSM-5 loaded PDMS/PVDF composite membrane consisting of three hydrophobic layers. J. Hazard. Mat. 261, 362–371.
Pelaez, M., Nolan, N., Pillai, S., Seery, M., Falaras, P., 2012. A review on the visible light active titanium dioxide photocatalysts for environmental applications. Appl. Catal. B Environ. 125, 331–349.
Peng, M., Vane, L.M., Liu, S.X., 2003. Recent advances in VOCs removal from water by pervaporation. J. Hazard. Mater. B98, 69–90.
Pera-Titus, M., García-Molina, V., Baños, M.A., Giménez, J., Esplugas, S., 2004. Degradation of chlorophenols by means of advanced oxidation processes: a general review. Appl. Catal. B: Environ. 47, 219–256.
Pereira, C.C., Habert, A.C., Nobrega, R., Borges, C.P., 1998. New insights in the removal of diluted volatile organic compounds from dilute aqueous solution by pervaporation process. J. Memb. Sci. 138, 227–235.
Pereira, C.C., Ribeiro, C.P., Nobrega, R., Borges, C.P., 2006. Pervaporative recovery of volatile aroma compounds from fruit juices: review. J. Membr. Sci. 274, 1–23.
Pickett-Baker, J., Ozaki, R., 2008. Pro-environmental products: marketing influence on consumer purchase decision. J. Consum. Mark. 25, 281–293.
Ray, A.K., 2009. Photocatalytic reactor configurations for water purification: experimentation and modeling. Adv. Chem. Eng. 36, 145–184.
Satuf, M.L., Brandi, R.J., Cassano, A.E., Alfano, O.M., 2008. Photocatalytic degradation of 4-chlorophenol: a kinetic study. Appl. Catal. B Environ. 82, 37–49.
Schaetzel, P., Vauclair, C., Luo, G., Nguyen, Q.T., 2001. The solution–diffusion model. Order of magnitude calculation of coupling between the fluxes in pervaporation. J. Memb. Sci. 191, 103–108.
Schmidt-Traub, H., Górak, A. (Eds.), 2006. Integrated Reaction and Separation Operations. Springer-Verlag, Berlin/Heidelberg.
Sciubba, L., Di Gioia, D., Fava, F., Gostoli, C., 2009. Membrane-based solvent extraction of vanillin in hollow fiber contactors. Desalination 241, 357–364.

Serpone, N., Salinaro, A., Emeline, A., Ryabchuk, V., 2000. Turnovers and photocatalysis: a mathematical description. J. Photochem. Photobiol. A: Chem. 130, 83−94.
Serpone, N., 2007. Some remarks on so-called heterogeneous photocatalysis and on the mechanical application of the Langmuir-Hinshelwood kinetic model. J. Adv. Oxid. Technol. 10, 111−115.
Shiraishi, Y., Hirai, T., 2008. Selective organic transformations on titanium oxide-based photocatalysts. J. Photochem. Photobiol. C 9, 157−170.
Stankiewicz, A., Moulijn, J.A., 2000. Process intensification: transforming chemical engineering. Chem. Eng. Progr. 96, 22−34.
Stankiewicz, A., 2003. Reactive separations for process intensification: an industrial perspective. Chem. Eng. Proc. 42, 137−144.
Straughan, R.D., Roberts, J.A., 1999. Environmental segmentation alternatives: a look at green consumer behavior in the new millennium. J. Consum. Market. 16, 558−575.
Thakur, R.S., Chaudhary, R., Singh, C., 2010. Fundamentals and applications of the photocatalytic treatment for the removal of industrial organic pollutants and effects of operational parameters: a review. J. Renew. Sustain. Energy 2, 37, 042701.
Theurich, J., Linder, M., Bahnemann, D.W., 1996. Photocatalytic degradation of 4-chlorophenol in aerated aqueous titanium dioxide suspensions: a kinetic and mechanistic study. Langmuir 12, 6368−6376.
Thiruvenkatachari, R., Vigneswaran, S., Moon, I.S., 2008. A review on UV/TiO_2 photocatalytic oxidation process. Korean J. Chem. Eng. 25, 64−72.
Trifunović, O., Lipnizki, F., Trägårdh, G., 2006. The influence of process parameters on aroma recovery by hydrophobic pervaporation. Desalination 189, 1−12.
Urkiaga, A., Bolaño, N., De Las Fuentes, L., 2002. Removal of micropollutant in aqueous streams by organophilic pervaporation. Desalination 149, 55−60.
Wijmans, J.G., Baker, R.W., Athayde, A.L., 1994. Pervaporation: Removal of organics from water and organic/organic separations. In: Crespo, J.G., Böddeker, K.W. (Eds.), Membrane Processes in Separation and Purification. Spinger-Science+Business Media Dordrecht, pp. 283−316.
Wijmans, J.G., Baker, R.W., 1995. The solution-diffusion model: a review. J. Memb. Sci. 107, 1−21.
Wolfrumm, E.J., Turchi, C.S., 1992. Comments on "Reactor dynamics in the evaluation of photocatalytic oxidation kinetics". J. Catal. 136, 626−628.
Zhang, J., Nosaka, Y., 2014. Mechanism of the OH radical generation in photocatalysis with TiO_2 of different crystalline types. J. Phys. Chem. C 118, 10824−11083.
Zhang, W., Ding, L., Luo, J., Jaffrin, M.Y., Tang, B., 2016. Membrane fouling in photocatalytic membrane reactors (PMRs) for water and wastewater treatment: a critical review. Chem. Eng. J. 302, 446−458.

This page intentionally left blank

CHAPTER 6

Performance of Reactors With PMs

Mohammad R. Rahimpour, Leila Mahmoodi
Shiraz University, Shiraz, Iran

6.1 Introduction

Over the last few decades, focusing on photodegradation has been significantly taken especially about organic substances available in the water or wastewater in the presence of photocatalysts. The described photocatalytic membrane reactors (PMRs) published in the literature would be classified into two operative configurations: (1) reactors in which a photocatalyst is suspended in the reaction mixture and (2) reactors in which a photocatalyst is immobilized on a support (Fig. 6.1) (Molinari et al., 2013a). Although the active surface of the suspended photocatalyst is much greater than that of the immobilized

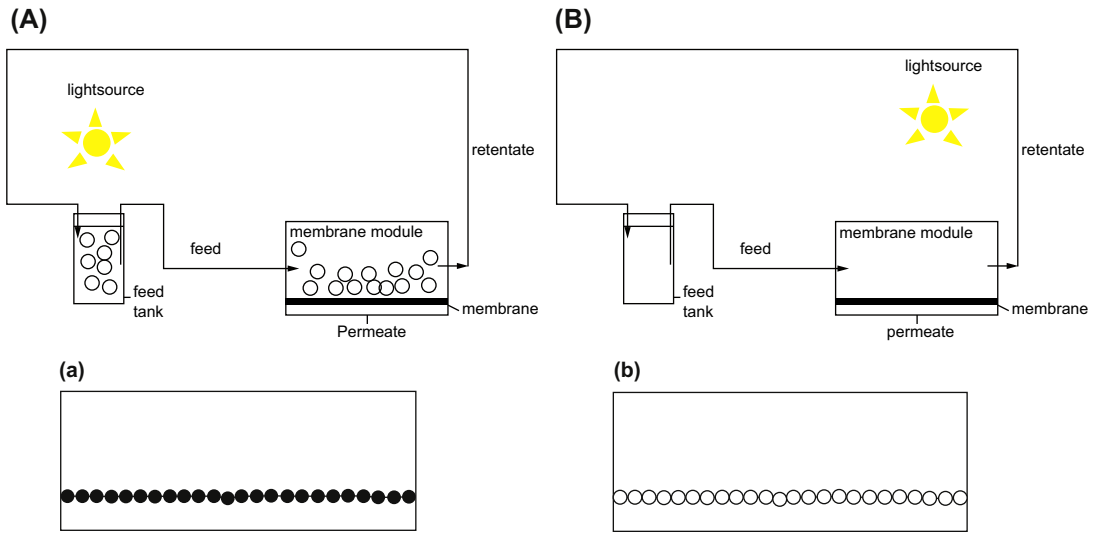

Figure 6.1
Photocatalytic membrane reactor utilizing photocatalyst (A) in suspension and (B) immobilized (a) on a membrane and (b) inside a membrane. *Reproduced from Mozia, 2010.*

Current Trends and Future Developments on (Bio-) Membranes. https://doi.org/10.1016/B978-0-12-813549-5.00006-2

one, the photocatalyst particles have to be separated to regenerate after the reaction. A very promising solution to solve photocatalyst separation problems, just like both by-products and products of photodegradation from the solution in the reactor, is the usage of PMRs (Mozia, 2010), being hybrid systems coupling membrane and photocatalysis. The membrane plays both the role of a selective hindrance for degraded molecules and support for the photocatalysts (Molinari et al., 2002a,b).

Because of photocatalytic reactions involved in the processes, which are really unselective, great investigations have been widely reported in water/wastewater treatment, as the most practical usage of PMRs, in which different organic and/or inorganic components such as phenols and chlorophenols (Barni et al., 1995), 4-nitrophenol (Molinari et al., 2001), dyes (Wang et al., 2006), and many other substances from water, in liquid and gas phases, are totally decomposed to innocuous components. However, some studies have been recently made to recognize the photocatalysis synthesis applications such as selective redox (reduction and oxidation) reactions, comprising the oxidation of ethanol and methanol (Tsuru et al., 2003); phenol (Colon et al., 2006); alkanes such as n-heptane, ethane, and methane (Bellobono et al., 2006), and trichloroethylene (Puma Li et al., 2009). These studies illustrated that, compared with conventional methods, high selective photooxidation/reduction reactions can be acquired by selecting or improving some photocatalytic parameters, such as the excitation wavelength or the semiconductor surface (Gazi and Ananthakrishnan, 2011; Flores et al., 2007). Furthermore, carbon dioxide removal is another interesting application of PMRs in which it would be converted to methanol, formaldehyde, and formic acid in the presence of semiconductors such as TiO_2, ZnO, CdS, GaP, WO_3 (Adachi et al., 1994; Varghese et al., 2009). Moreover, PMRs have been used to generate hydrogen, but in their early stages, compared with water treatment processes (Iglesias et al., 2016).

In spite of all PMR development, fouling is an important issue that should be considered before industrialization and commercialization of these systems. Fouling, being a result of a complex interaction between membrane and feed compositions (Lin et al., 2014), will reduce permeate flux, leading to an increase in energy consumption and cleaning frequency that reduces membrane lifetime and consequently leads to higher operational and replacement costs (Pidou et al., 2009). Although many efforts are made to understand membrane fouling clearly, there are limited up-to-date comprehensive investigations (Ganiyu et al., 2015; Leong et al., 2014; Mozia, 2010; Zhang et al., 2016) that demonstrate an overview of fouling mechanisms, fouling and photocatalysis relationships and reactions, and the strategies to control fouling in PMRs. Thus, fouling mechanisms, characteristics, and control strategies in PMRs are essential to study.

This chapter intends to help comprehend the performance of PMRs with photocatalytic membranes (PMs).

6.2 Configurations and Designs of Reactors With Photocatalytic Membranes

PMs are classified into two main configurations (Fig. 6.2). The first one, which is the most popular configuration, is a membrane with a photoactive layer, which simultaneously acts as a separation layer, and the active layer is supported by a porous nonphotoactive support. The second one consists of a nonphotoactive separation layer on the membrane with porous active support. In some cases, immersed UV lamps as light sources can be positioned inside the module or above it. Depending on the membrane type, UV light could be positioned either on the permeate side or the feed side. It is noteworthy that physical and chemical properties of the compound, the efficiency of photodegradation, and separation characteristics of the membrane are three substantial parameters directly affecting the composition of permeate stream.

In the first configuration, UV light radiation, located on the feed side, decomposes organic compounds in the feed stream on the membrane surface or within the pores of the membrane. On the other hand, permeate side contains final products, by-products, nondegraded substances, and water in the aqueous phase reactions.

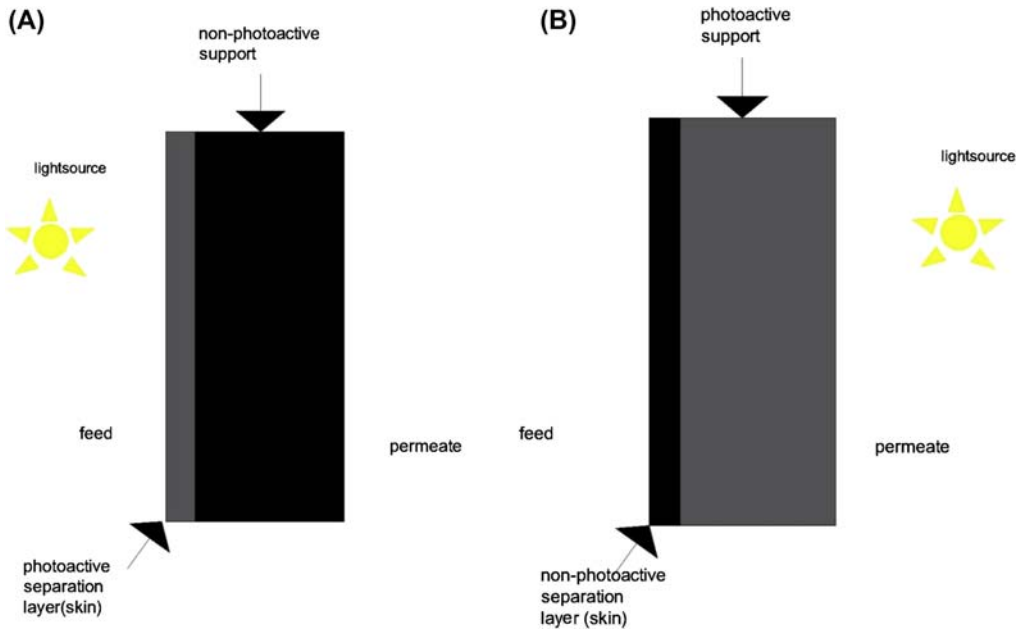

Figure 6.2
Asymmetrical photocatalytic membranes. (A) The photoactive separation layer is placed on a nonphotoactive porous support; (B) the nonphotoactive separation layer is placed on a photoactive porous support (Molinari et al., 2013a).

Because of decomposing of organic compounds, which leads to the formation of the gel layer and filtration cake, membrane fouling reduces and the permeate flux increases in water/wastewater treatment processes, which would be indeed noted as the main advantage of the first configuration.

The second configuration, which is less popular than the first one, utilizes a PM with photoactive support. In this case, the light source is located on the permeate side and the photocatalytic reaction takes place on the same side, whereas the membrane is just a separator. The main drawback of this configuration is that the permeate stream is the only purified stream. Moreover, rejected pollutants by the membrane are gathered into the concentrate stream (Molinari et al., 2013a).

The paramount difference between a PMR with PM and membrane installation is the membrane module's construction. The module design must be in a manner that ensures the light irradiates completely enough to the membrane surface to make the photocatalytic reaction. Advantages and disadvantages of PMRs with PMs are summarized in Table 6.1.

Tsuru et al. applied a PMR with a tubular PM coated by TiO_2 around which four or eight UV lamps were installed, for a gaseous phase oxidation of ethanol and methanol (Fig. 6.3). In comparison with photocatalysis without membrane, it is observed that at

Table 6.1: Advantages and disadvantages of photocatalytic membranes with photocatalytic membranes.

Advantages	Disadvantages
• No need to separate and recycle the photocatalyst • Photocatalyst exchange and membrane replacement can be performed simultaneously • Possibility of fouling mitigation due to enhanced hydrophilicity of the photocatalyst-modified membrane • Possibility of fouling mitigation due to decomposition of organic contaminants forming the gel layer or filtration cake • Contaminants could be decomposed either in feed or permeate • Higher decomposition rate in case of the gas phase reactions compared with conventional photoreactors with photocatalyst immobilized on a nonporous support	• In the case of aqueous phase reactions, the effectiveness of degradation is usually lower than in the case of photocatalyst in suspension • A posttreatment may need to be added for improving permeate quality • Risk of damage to polymer membranes by ultraviolet light or hydroxyl radicals • Necessity of membrane exchange when the photocatalytic membrane loses its activity during the filtration process • Fouling occurs if foulant concentration exceeds the degradation effectiveness

From Mozia, S., 2010. Photocatalytic membrane reactors (PMRs) in water and wastewater treatment, a review. Sep. Purif. Technol. 73, 71–91; Zhang, W., Ding, L., Luo, J., Jaffrin, M.Y., Tang, B., 2016. Membrane fouling in photocatalytic membrane reactors (PMRs) for water and wastewater treatment: a critical review. Chem. Eng. J. 302, 446–458.

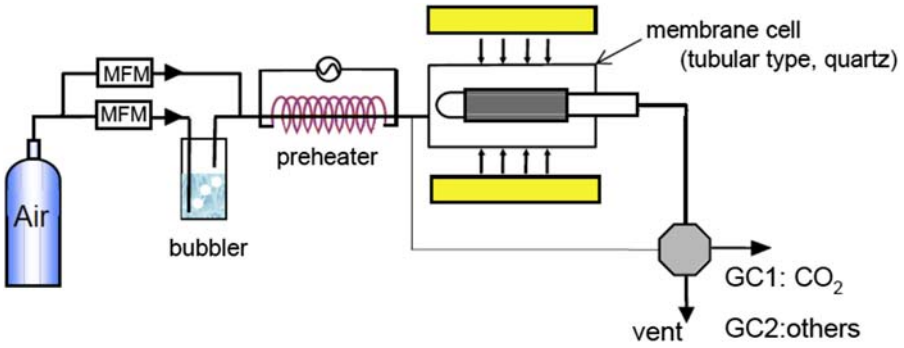

Figure 6.3
Schematic diagram of a photocatalytic membrane reactor (Tsuru et al., 2006). *MFM*, mass flow meter.

100−120°C, methanol decomposition rate, which is a function of residence time, is higher (Tsuru et al., 2003, 2006). As another experimental case, Zhang et al. (2006) used a crossflow-mode PMR with photocatalytic silica/titanium nanorods/nanotubes composite membranes, above which a UV lamp is placed, to decompose sodium dodecylbenzene sulfonate (SDBS) (Fig. 6.4). It is reported that, in spite of 89% decomposition rate of

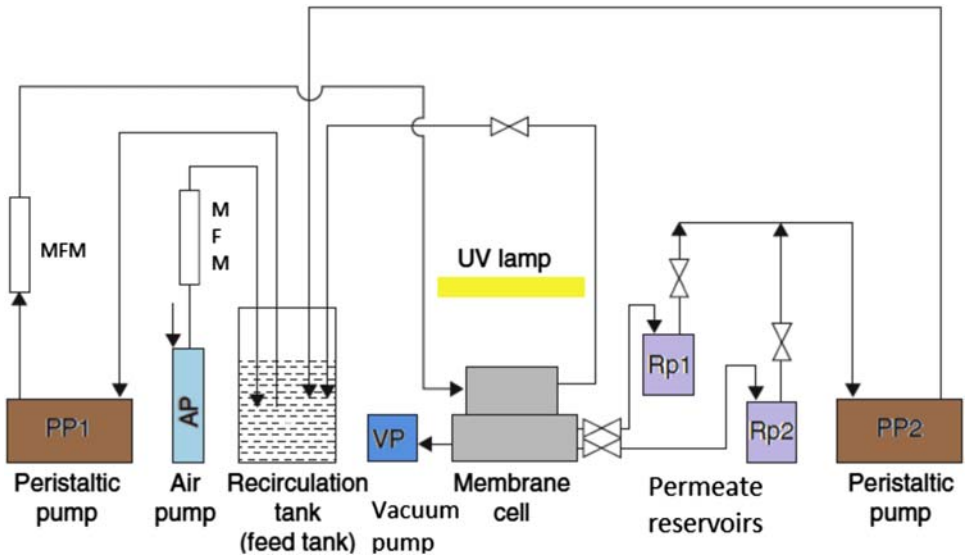

Figure 6.4
Schematic diagram of a photocatalytic membrane reactor with a photocatalytic membrane for liquid phase reaction operating in a crossflow mode. *MFM*, mass flow meter. *Adapted from Zhang et al., 2006*.

liquid phase SDBS, the permeate flux enhancement and membrane fouling decrement are obtained.

The mentioned experimental cases are in fact minor examples of chemical synthesis, and water treatment is an example of PMRs' application. Besides, more applications of reactors with PMs will be discussed in detail in the following sections.

6.3 Fouling in Reactors With Photocatalytic Membranes

A combination of photocatalysis and pressure-driven membrane processes, described in Chapter 4, such as microfiltration (MF), ultrafiltration (UF), and nanofiltration (NF), is the most common PMR configuration reported in the literature. In fact, the membrane fouling, especially in case of MF and UF membranes, is observed when the suspended photocatalyst is applied (Mozia, 2010).

Fouling is an undesired phenomenon that strongly decreases treatment efficiency because of decreasing permeate flux and productivity and increasing operation time, energy consumption, and cleaning frequency, which leads to short membrane life cycle and increased replacement costs (Pidou et al., 2009; Fernández et al., 2014; Choo et al., 2008; Wang et al., 2006; Patsios et al., 2013). Therefore, studying fouling formation, mechanisms, controlling and prevention methods in PMRs is indispensable.

Photocatalysis is actually called "advanced oxidation process" (AOP), in that reactive species such as hydroxyl radicals ($OH^{\cdot}$) are generated and could oxidize a wide spectrum of the organic substances quickly and nonselectively (Mozia, 2010). In essence, there are several complex photocatalysis reactions between photocatalysts and organic pollutants whose interactions with the membrane surface play a substantial role in fouling formation in PMs, which is assessed by the feed composition (Lin et al., 2014). Various compositions of different foulants show different fouling formation styles. For example, organic foulant filtration would form a thin layer, whereas pore blocking would be observed in the presence of UF and MF, which decreases the flux considerably (Gao et al., 2011). Moreover, inorganic foulants that are released in solution during degradation process, such as NH_4^+, SO_4^{2-}, Na^+, NO_3^-, etc., could be joined to photocatalyst particles and increase fouling layer (Damodar et al., 2010). The concept of two-membrane fouling mechanisms, i.e., cake layer and pore blocking, is schematically presented in Fig. 6.5.

Langmuir–Hinshelwood model is greatly fitted for the degradation rate of an organic foulant at different initial concentrations (Mozia, 2010):

$$-\frac{dC}{dt} = \frac{k_1 KC}{1 + KC} \tag{6.1}$$

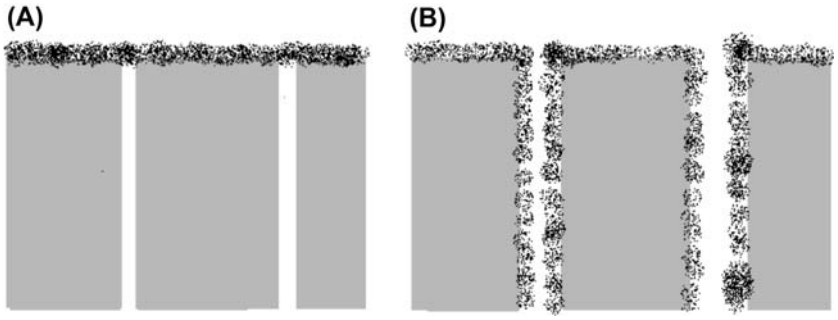

Figure 6.5
Schematic of two kinds of membrane fouling mechanisms. (A) Cake layer and (B) pore blocking (Bowen et al., 1995).

where C is the concentration of the foulant after time t of the photocatalytic degradation process, K is the adsorption equilibrium constant, and k_1 is a true rate constant, taking into account several parameters such as efficient photon flow, the mass of photocatalyst, O_2 layer, etc. (Mozia, 2010). Within a certain range, the probability of reaction between oxidizing species ($O_2^{\bullet-}$ and $OH^{\bullet}$ radicals) and organic foulants, as the initial concentration of organic foulants increase, leads to the growth of foulant decomposition rate. However, the degradation rate is decreased by an increase in redundant concentration and does not control fouling (Konstantinou and Albanis, 2004) according to three main reasons. The first one is that at high concentrations, $OH^{\bullet}$ radical generation on the photocatalyst surface is decreased because active sites are covered by organic foulants. Second, at high concentration, the organic foulant substances absorb more amount of UV than the photocatalyst particles, mainly TiO_2 particles, which reduces $O_2^{\bullet-}$ and $OH^{\bullet}$ radical formations. The last and most important reason is that at high concentration, the weak light irradiation increases (Huang et al., 2008), which results in foulant degradation rate reduction. Moreover, high-concentration organic foulants express a strong tendency to adsorb into membrane pores or attach to the membrane surface (Pidou et al., 2009; Fernández et al., 2014). Accordingly, to avoid the high-fouling formation, the concentration of organic foulants should be balanced.

6.3.1 Foulant Type

For efficient control of membrane fouling in PMRs, foulants should be classified according to their type. According to existing knowledge, fouling categorization is explained in the following sections (Zhang et al., 2016).

6.3.1.1 Organic Fouling

It is obvious from the "organic" term that the organic fouling is generated by the decomposition of the organic substances such as colloids, polysaccharides, proteins, humic

and fulvic acids, etc. It means that the organic foulants are adsorbed onto photocatalysts and make a compact gel or cake layer on the membrane surface. In addition to fouling layer formation, membrane pores could be blocked by the organic foulants existing in the systems, attaching onto membrane surfaces called pore blocking (Fig. 6.5) (Lee et al., 2001).

The characteristics and concentration of organic foulants affect directly the membrane fouling. For example, organic substances with higher hydrophobicity adhere to membrane surface more easily than those with lower hydrophobicity and cause more serious membrane fouling (Fernández et al., 2014). Moreover, in wastewater treatment processes integrated with PMRs, the primary effluent, including organic pollutants with a higher concentration than secondary effluent, has more weighty membrane fouling, leading to lower operating efficiency (Mozia et al., 2014).

6.3.1.2 Inorganic Fouling

In PMRs with suspended photocatalysts, inorganic fouling is generally related to photocatalyst particles that would form a fairly large porous cake layer on membrane surface (Zhang et al., 2016). In fact, because of the porous structure of these kinds of cake layers, which makes very low resistance for permeate flux, low membrane fouling and slight flux decline will be obtained (Lee et al., 2001). In case of PMRs with PMs, the fouling caused by photocatalyst cake, however, does not occur. In such a case the inorganic fouling (scaling) is associated with the precipitation of inorganic salts such as $CaSO_4$, $CaCO_3$, $Ca_3(PO_4)_2$, $Mg(OH)_2$, CaF_2, $BaSO_4$, $SrSO_4$, etc. Moreover, some inorganic ions and some groups of organic foulants could interact with each other, enter the gel or cake layer, and cross-link the structure, which leads to higher fouling. For example, in the presence of $CaCl_2$ and $NaHCO_3$, trichloroethylene caused severe membrane fouling (Choo et al., 2008).

6.3.1.3 Biofouling

In PMRs, no occurrence and presence of biofouling are reported compared with the traditional membrane system. The absence of biofouling may be because of strong capacity of $OH^{\bullet}$ to oxidize and kill the microorganisms, especially in water/wastewater treatment processes (Zhang et al., 2016). However, a trace of biofouling due to microorganisms' accumulation and their growth on the membrane surface would be observed.

6.3.2 Fouling Control Strategies

To control membrane fouling in PMRs, appropriate control strategies and impressive cleaning methods, which are divided into seven groups, are applied to inhibit the fouling

formation: (1) self-cleaning or photocatalytic oxidation process, (2) feed pretreatment, (3) membrane modification, (4) aeration, (5) applied electric field, (6) operating parameters optimization, and (7) membrane cleaning (Zhang et al., 2016). Some of these strategies are defined in the following sections.

6.3.2.1 Self-cleaning Process (Photocatalytic Oxidation)

Oxidizing agents such as $OH^{\bullet}$ and $O_2^{\bullet-}$ radicals, which are commonly produced in PMRs, can reduce fouling through photocatalytic oxidation of organic pollutants. Besides, some operational conditions such as light intensity, pH, and ion concentration should be optimized to improve photocatalytic oxidation process and decline fouling. It is reported that increasing irradiation time would make the fouling to be decreased as a result of improving organic foulant degradation (Pidou et al., 2009). Moreover, molecular characteristic changes of organic foulants [such as the removal of high hydrophobic molecules that is highly responsible for fouling (Huang et al., 2008)] could reduce fouling in photocatalytic reactions.

6.3.2.2 Feed Pretreatment

It is obvious that chemical, physical, and biological properties of the feed could directly affect membrane fouling. Mainly, modifying these kinds of feed properties through pH adjustment and coagulant addition would optimize the interactions between membrane and foulants and reduce the fouling. In PMRs, photocatalyst characteristics such as surface charge and hydrophilicity would be improved by pH adjustment (Damodar et al., 2012). Furthermore, coagulant addition during the feed pretreatment step has a capability to adsorb colloidal and suspended particles and mix them to form larger ones to enhance solid−liquid separation, and consequently decreasing fouling (Erdei et al., 2008).

6.3.2.3 Aeration

In PMRs with PMs, concentration polarization and fouling could be swept away by unstable flows and bubbles that are produced by aeration. Mass transfer enhancement and light attenuation by bubble clouds due to increasing aeration rate are two competing factors that limit the aeration process and must be adjusted and optimized to yield the greatest photocatalytic efficiency (Chin et al., 2007). Although aeration significantly mitigates membrane fouling and avoid serious flux reduction in PMRs, the complicated influence of bubbles and high-energy consumptions are its development bottlenecks and drawbacks (Zhang et al., 2016). Therefore more investigation is necessary for industrial aeration processes in PMRs in the future.

6.3.2.4 Membrane Cleaning

Physical and chemical cleaning are two types of membrane cleaning process according to fouling removal mechanisms in PMRs (Zhang et al., 2016). Physical cleaning, which

commonly removes reversible fouling such as cake layer and deposited solids, is not as effective as chemical cleaning and does not require any chemical reagents. In contrast to the physical cleaning, chemical cleaning is specified as an irreversible fouling removal process that uses chemical agents, including acid solution, bio-acid solution (bio-acids contain organic short-chain fatty acids (SCFA) such as lactic acid, propionic acid, and formic acid which improve water hygiene and manage the bacteria load in the water especially in food industries), and an alkaline solution, which are efficient for both inorganic and organic fouling removal (Zhang et al., 2016). Although chemical cleaning mostly helps permeability recovery, it is an expensive method, and sometimes the membrane may be damaged by incorrect chemical cleaning.

It is necessary to mention that in most cases of chemical cleaning, one kind of chemical agent cannot be useful and applicable to obviate the membrane fouling needs. For that reason, a combination of different agents in chemical cleaning methods is supposed to recover permeability and remove any kinds of foulants available on the membrane surface.

6.4 Overview of Applications of Reactors With Photocatalytic Membranes

PMRs have been applied to both water/wastewater treatment and chemical production. In the first case, the membrane is used to generate oxidant radicals to spoil organic pollutants. However, in chemical production, the PM contributes to separate two or more components.

6.4.1 Water Treatment

Today there are many remarkable recognized technologies for water recovery and purification. Among all of them, PMRs are mainly utilized for oxidizing organic matter contained in water. The aim of photocatalysis in this application is to mineralize organic substances to nontoxic compounds such as H_2O, CO_2 and also inorganic salts such as sulfates, nitrates, chlorides, etc. Today, PMRs are tested in a good number of applications dealing with water/wastewater treatment with the main advantages owing to the antifouling membrane properties and good permeate fluxes (Brunetti et al., 2018). Until now, many investigations report the development of PMs with mainly titanium dioxide deposition on or entrapment in membranes (Molinari et al., 2000, 2002a,b; Choi et al., 2006, 2007), especially for water and wastewater treatment, and also some pilot plant experiments were carried out for degradation of other organics (Bellobono et al., 1995; Barni et al., 1995; Choi et al., 2009; Dzinun et al., 2015).

Water/wastewater treatment application in PMRs would be defined completely in detail in Chapter 7.

6.4.2 H_2 Production

Today, hydrogen is considered as an environmentally friendly energy source because it produces no air pollutants or greenhouse gases when it burns as fuel in air, and also it possesses high energy capacity.

Hydrogen production from water considerably fascinates researchers working on transformation of solar energy into chemical energy (fuel) (Pathak et al., 2005; Kothari et al., 2010). Using a suitable membrane with equally suitable configuration are two key steps in this challenging research topic to produce hydrogen fuel from water. The PMRs for H_2 production are not still industrialized and commercialized, which means that their current configuration is at laboratory scale.

In laboratory hydrogen production scales, a dual photocatalysis system for water redox reactions (O_2 formation and H_2 generation) and also a membrane that is modified to enable the ion transport are used. Although there are various alternative proposed configurations for this process, many endeavors should be made to construct a robust system that can operate with high overall conversion efficiency. The photocatalyst configuration can be TiO_2/membrane/Pt or TiO_2/metal foil/Pt. The metal acts as a cathode for H^+ reduction and H_2 evolution (Gurunathan, 2004) (Fig. 6.6).

The decomposition of alcohols such as methanol and ethanol with the aim of H_2 production was investigated by Tsuru et al. (2003, 2006) (Fig. 6.3). A wide description on the recent progress in PMRs for H_2 production, their configurations, potentialities, and limitations can be found in the review published by Molinari et al. (2014).

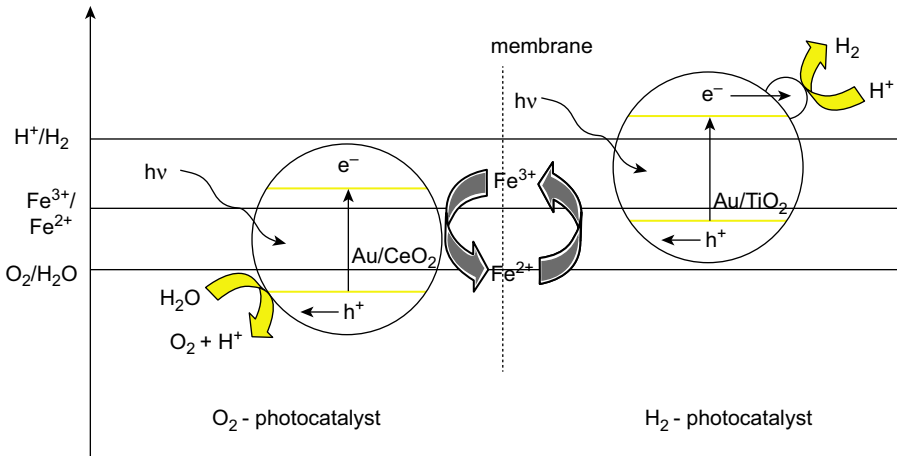

Figure 6.6
Idea of the photocatalytic membrane reactors for hydrogen and oxygen generation (Molinari et al., 2014).

6.4.3 CO_2 Conversion

Increasing the Earth's temperature is one of the major issues that encounter the environment. CO_2 is one of the main greenhouse gases in the atmosphere, which significantly contributes to the climate changes. Currently, carbon dioxide recovery from flue gas, biogas, and natural gas is attracting a great deal of attention (Brunetti et al., 2010, 2014). The best solution to both global warming and problems of lack of energy seems to be CO_2 conversion into valuable hydrocarbons. Carbon dioxide reduction by water to produce fuels through photocatalysis is one of the most promising novel investigations, as it is an attractive route from an environmental and economical point of view (Demeestere et al., 2007; Molinari et al., 2013a,b; Palmisano et al., 2007; Tsuru et al., 2006). In particular, the main interest is addressed to the production of methanol because of its ease of transportation, storage, and usage as gasoline additives, as well as the transformation of other useful chemicals using classic technologies (Wu, 2009). CO_2 can be converted by UV irradiation at common conditions of temperature and pressure (Wu, 2009; Koci et al., 2009) (Fig. 6.7).

Recently, Sellaro et al. (2015) reported the usage of a laboratory-scale continuous PMR based on TiO_2 photocatalyst for CO_2 conversion operated in steady-state condition, which produced 0.75 μmol/(gr catalyst.min) of methanol without any small amount of CH_4 nor CO formation. Moreover, it was observed that methanol production was highly achieved by the best distribution of photocatalysts on the PM in the PMR, which is a strong point in these systems. Some strategies are now being investigated and applied to modify the photocatalyst distribution at both low and high content (Brunetti et al., 2018).

Nonetheless, idea of industrialization of CO_2 conversion as an application of PMRs needs much work to do.

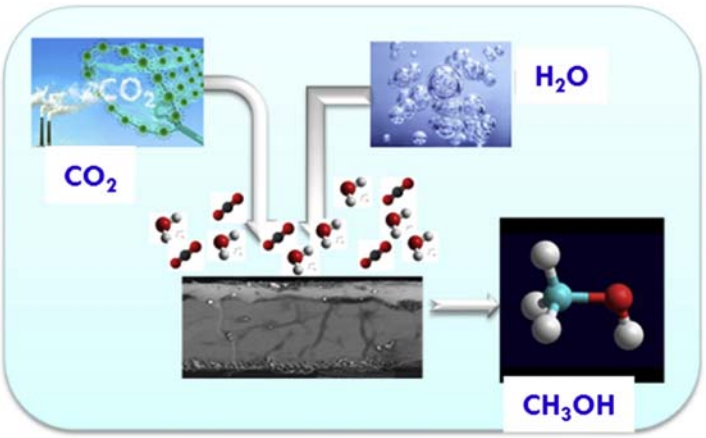

Figure 6.7
Scheme of CO_2 conversion by a photocatalytic membrane (Brunetti et al., 2018).

6.5 Conclusion and Future Trends

PMRs exhibit great advantages over the conventional photoreactors and can be considered useful "green" technology in case of both organic synthesis and water and wastewater treatment. However, further studies are still required to take their capability of industrialization.

Owing to membrane selective properties, PMRs permit achieving continuous operation in systems that allow regeneration of the photocatalysts and enhance the residence time. Moreover, various configurations of PMRs can be selected to affect the PM performance and possible solutions for some main problems such as control of photocatalyst activity, selectivity, fouling, and membrane rejection.

In this chapter, membrane fouling mechanisms, the parameters affecting fouling, and the strategies to control fouling in PMRs were presented. In fact, the fouling is caused by a complex interaction between PM and organic or inorganic components of feed. Therefore, the most important fouling consequences are transmembrane pressure increase, flux reduction, effective filtration area decrement, and accordingly shorter membrane lifespan. In addition, several fouling control methods, including aeration, membrane cleaning, feed pretreatment, and self-cleaning process, have been presented to mitigate PM fouling.

Moreover, as the number of reports concerning natural water and real wastewater is still inefficient and most conclusions have been obtained using model solution, it is worth to investigate real systems. More investigations on other possible PMR applications such as organic synthesis are also indispensable. Nevertheless, the major difficulty in the PMR application would be the light source such as the sun which could be considered as a clean and cheap source of light.

List of Abbreviations

AOP Advanced oxidation process
C Concentration
GC Gas chromatograph
K Adsorption equilibrium constant
k_1 True rate constant
MF Microfiltration
MFM Mass flow meter
NF Nanofiltration
PM Photocatalytic membrane
PMR Photocatalytic membrane reactor
SCFA Short-chain fatty acid
SDBS Sodium dodecylbenzene sulfonate
t Time
TMP Transmembrane pressure
UF Ultrafiltration
UV Ultraviolet

References

Adachi, K., Ohta, K., Mizuno, T., 1994. Photocatalytic reduction of carbon dioxide to hydrocarbon using copper-loaded titanium dioxide. Sol. Energy 53 (2), 187–190.

Barni, B., Cavicchioli, A., Riva, E., Zanoni, L., Bignoli, F., Bellobono, I.R., Gianturco, F., De Giorgi, A., Muntau, H., Montanarella, L., Facchetti, S., Castellano, L., 1995. Pilot-plant-scale photodegradation of phenol in aqueous solution by photocatalytic membranes immobilizing titanium dioxide (PHOTOPERM® process). Chemosphere 30, 1861–1874.

Bellobono, I.R., Barni, B., Gianturco, F., 1995. Pre-industrial experience in advanced oxidation and integral photodegradation of organics in potable waters and waste waters by PHOTOPERM™ membranes immobilizing titanium dioxide and promoting photocatalysts. J. Membr. Sci. 102, 139–147.

Bellobono, I.R., Stanescu, R., Costache, C., Canevali, C., Morazzoni, F., Scotti, R., Bianchi, R., Simona Mangone, E., Martini, G., Maria Tozzi, P., 2006. Laboratory-scale photomineralization of n-alkanes in gaseous phase by photocatalytic membranes immobilizing titanium dioxide. Int. J. Photoenergy 1, 1–8.

Bowen, W.R., Calvo, J.I., Hernández, A., 1995. Steps of membrane blocking in flux decline during protein microfiltration. J. Membr. Sci. 101, 153–165.

Brunetti, A., Scura, F., Barbieri, G., Drioli, E., 2010. Membrane technologies for CO_2 separation. J. Membr. Sci. 359, 115–125.

Brunetti, A., Drioli, E., Lee, Y.M., Barbieri, G., 2014. Engineering evaluation of CO_2 separation by membrane gas separation systems. J. Membr. Sci. 454, 305–315.

Brunetti, A., Zito, P.F., Giorno, L., Drioli, E., Barbieri, G., 2018. Membrane reactors for low temperature applications: an overview. Chem. Eng. Process 124, 282–307.

Chin, S.S., Lim, T.M., Chiang, K., Fane, A.G., 2007. Factors affecting the performance of a low-pressure submerged membrane photocatalytic reactor. Chem. Eng. J. 130, 53–63.

Choi, H., Sofranko, A.C., Dionysiou, D.D., 2006. Nanocrystalline TiO_2 photocatalytic membranes with a hierarchical mesoporous multilayer structure: synthesis, characterization and multifunction. Adv. Funct. Mater. 16, 1067–1074.

Choi, H., Stathatos, E., Dionysiou, D., 2007. Photocatalytic TiO_2 films and membranes for the development of efficient wastewater treatment and reuse systems. Desalination 202, 199–206.

Choi, S.H., Scura, F., Barbieri, G., Mazzei, R., Giorno, L., Drioli, E., Kim, J.H., 2009. Bio-degradation of phenol in wastewater by enzyme-loaded membrane reactor: numerical approach. Korean Membr. J. 19, 72–82.

Choo, K.H., Chang, D.I., Park, W.I., Kim, M.H., 2008. Use of an integrated photocatalysis/hollow fiber microfiltration system for the removal of trichloroethylene in water. J. Hazard. Mater. 152, 183–190.

Colon, G., Sanchez-Espana, J.M., Hidalgo, M.C., Navio, J.A., 2006. Effect of TiO_2 acidic pre-treatment on the photocatalytic properties for phenol degradation. J. Photochem. Photobiol. A Chem. 179 (1–2), 20–27.

Damodar, R.A., You, S.J., Ou, S.H., 2010. Coupling of membrane separation with photocatalytic slurry reactor for advanced dye wastewater treatment. Sep. Purif. Technol. 76, 64–71.

Damodar, R.A., You, S.J., Chiou, G.W., 2012. Investigation on the conditions mitigating membrane fouling caused by TiO_2 deposition in a membrane photocatalytic reactor (MPR) used for dye wastewater treatment. J. Hazard. Mater. 203, 348–356.

Demeestere, K., Dewulf, J., Van Langenhove, H., 2007. Heterogeneous photocatalysis as an advanced oxidation process for the abatement of chlorinated, monocyclic aromatic and sulfurous volatile organic compounds in the air: state of the art. Crit. Rev. Environ. Sci. Technol. 37, 489–538.

Dzinun, H., Othman, M.H.D., Ismail, A.F., Puteh, M.H., Rahman, M.A., Jaafar, J., 2015. Photocatalytic degradation of nonylphenol by immobilized TiO_2 in dual layer hollow-fibre membranes. Chem. Eng. J. 269, 255–261.

Erdei, E., Arecrachakul, A., Vigneswaran, S., 2008. A combined photocatalytic slurry reactor-immersed membrane module system for advanced wastewater treatment. Sep. Purif. Technol. 62, 382–388.

Fernández, R.L., McDonald, J.A., Khan, S.J., Le-Clech, P., 2014. Removal of pharmaceuticals and endocrine disrupting chemicals by a submerged membrane photocatalysis reactor (mpr). Sep. Purif. Technol. 127, 131–139.

Flores, S.O., Rios-Bernij, O., Valenzuela, M.A., Cordova, I., Gomez, R., Gutierrez, R., 2007. Photocatalytic reduction of nitrobenzene over titanium dioxide: by-product identification and possible pathways. Top. Catal. 44, 507−511.

Ganiyu, S.O., Hullebusch, E.D., van Cretin, M., Esposito, G., Oturan, M.A., 2015. Coupling of membrane filtration and advanced oxidation processes for removal of pharmaceutical residues: a critical review. Sep. Purif. Technol. 156, 891−914.

Gao, W., Liang, H., Ma, J., Han, M., Chen, Z., Han, Z., Li, G., 2011. Membrane fouling control in ultrafiltration technology for drinking water production: a review. Desalination 272, 1−8.

Gazi, S., Ananthakrishnan, R., 2011. Metal-free-photocatalytic reduction of 4-nitrophenol by resin-supported dye under the visible irradiation. Appl. Catal. B Environ. 105, 317−325.

Gurunathan, K., 2004. Photocatalytic hydrogen production using transition metal ions-doped γ-Bi_2O_3 semiconductor particles. Int. J. Hydrogen Energy 29, 933−940.

Huang, X., Leal, M., Li, Q., 2008. Degradation of natural organic matter by TiO_2 photocatalytic oxidation and its effect on fouling of low-pressure membranes. Water Res. 42, 1142−1150.

Iglesias, O., Rivero, M.J., Urtiaga, A.M., Ortiz, I., 2016. Membrane-based photocatalytic systems for process intensification. Chem. Eng. J. 305, 36−148.

Koci, K., Obalová, L., Matějová, L., Plachá, D., Lacný, Z., Jirkovský, J., Ŝolcová, O., 2009. Effect of TiO_2 particle size on the photocatalytic reduction of CO_2. Appl. Catal. B Environ. 89, 494−502.

Konstantinou, I.K., Albanis, T.A., 2004. TiO_2-assisted photocatalytic degradation of azo dyes in aqueous solution: kinetic and mechanistic investigations: a review. Appl. Catal. B Environ. 49, 1−14.

Kothari, R., Tyagi, V.V., Pathak, A., 2010. Waste-to-energy: a way from renewable energy sources to sustainable development. Renew. Sustain. Energy Rev. 14, 3164−3170.

Lee, S.A., Choo, K.H., Lee, C.H., Lee, H.I., Hyeon, T., Choi, W., Kwon, H.H., 2001. Use of ultrafiltration membranes for the separation of TiO_2 photocatalysts in drinking water treatment. Ind. Eng. Chem. Res. 40, 1712−1719.

Leong, S., Razmjou, A., Wang, K., Hapgood, K., Zhang, X., Wang, H., 2014. TiO_2 based photocatalytic membranes: a review. J. Membr. Sci. 472, 167−184.

Lin, H., Zhang, M., Wang, F., Meng, F., Liao, B., Hong, H., Chen, J., Gao, W., 2014. A critical review of extracellular polymeric substances (EPSs) in membrane bioreactors: characteristics, roles in membrane fouling and control strategies. J. Membr. Sci. 460, 110−125.

Molinari, R., Mungari, M., Drioli, E., Di Paola, A., Loddo, V., Palmisano, L., Schiavello, M., 2000. Study on a photocatalytic MR for water purification. Catal. Today 55, 71−78.

Molinari, R., Grande, C., Drioli, E., Palmisano, L., Schiavello, M., 2001. Photocatalytic membrane reactors for degradation of organic pollutants in water. Catal. Today 67, 273−279.

Molinari, R., Borgese, M., Drioli, E., Palmisano, L., Schiavello, M., 2002a. Hybrid processes coupling photocatalysis and membranes for degradation of organic pollutants in water. Catal. Today 75, 77−85.

Molinari, R., Palmisano, L., Drioli, E., Schiavello, M., 2002b. Studies on various reactor configurations for coupling photocatalysis and membrane processes in water purification. J. Membr. Sci. 206, 399−415.

Molinari, R., Palmisano, L., Loddo, V., Mozia, S., Morawski, A.W., 2013a. Photocatalytic membrane reactors: configurations, performance and applications in water treatment and chemical production. In: Basile, A. (Ed.), Handbook of Membrane Reactors, vol. 2. Woodhead Publishing Limited, pp. 808−845 (Chapter 21).

Molinari, A., Maldotti, A., Amadelli, R., 2013b. Heterogeneous photocatalytic systems for partial and selective oxidation of alcohols and polyols. Curr. Org. Chem. 17, 2382−2405.

Molinari, R., Marino, T., Argurio, P., 2014. Photocatalytic MRs for hydrogen production from water. Int. J. Hydrogen Energy 39, 7247−7261.

Mozia, S., 2010. Photocatalytic membrane reactors (PMRs) in water and wastewater treatment, a review. Sep. Purif. Technol. 73, 71−91.

Mozia, S., Darowna, D., Szymański, K., Grondzewska, S., Borchert, K., Wróbel, R., Morawski, A.W., 2014. Performance of two photocatalytic membrane reactors for treatment of primary and secondary effluents. Catal. Today 236, 135−145.

Palmisano, G., Augugliaro, V., Pagliaro, M., Palmisano, L., 2007. Photocatalysis: a promising route for 21st century organic chemistry. Chem. Commun. 3425–3437.
Pathak, P., Meziani, M.J., Castillo, L., Sun, Y.P., 2005. Metal-coated nanoscale TiO_2 catalysts for enhanced CO_2 photoreduction. Green Chem. 7, 667–670.
Patsios, S., Sarasidis, V., Karabelas, A., 2013. A hybrid photocatalysis–ultrafiltration continuous process for humic acids degradation. Sep. Purif. Technol. 104, 333–341.
Pidou, M., Parsons, M.A., Raymond, G., Jeffrey, P., Stephenson, T., Jefferson, B., 2009. Fouling control of a membrane coupled photocatalytic process treating grey water. Water Res. 43, 3932–3939.
Puma Li, G., Salvado-Estivill, I., Obee, T.N., Hays, S.O., 2009. Kinetics rate model of the photocatalytic oxidation of trichloroethylene in air over TiO_2 thin films. Sep. Purif. Technol. 67 (2), 226–232.
Sellaro, M., Fontananova, E., Brunetti, A., Palmisano, L., Bellardita, M., Drioli, E., Barbieri, G., 2015. Photocatalytic membranes based on TiO_2 catalysts and fluorinated polymers for CO_2 conversion. In: 12th International Conference on Catalysis in MRs (ICCMR12), Szczecin, Poland (Oral).
Tsuru, T., Kan-no, T., Yoshioka, T., Asaeda, M., 2003. Photocatalytic membrane reactor for gas-phase reaction using porous titanium oxide membranes. Catal. Today 82, 41–48.
Tsuru, T., Kan-no, T., Yoshioka, T., Asaeda, M., 2006. A photocatalytic MR for VOC decomposition using Pt-modified titanium oxide porous membranes. J. Membr. Sci. 280, 156–162.
Varghese, O.K., Paulose, M., LaTempa, T.J., Grimes, C.A.A., 2009. High-rate solar photocatalytic conversion of CO_2 and water vapor to hydrocarbon fuels. Nano Lett. 9 (2), 731–737.
Wang, J., Wen, F.-Y., Zhang, Z.-H., Zhang, X.-D., Pan, Z.-J., Zhang, P., Kang, P.-L., Tong, J., Wang, L., Xu, L., 2006. Investigation on degradation of dyestuff wastewater using visible light in the presence of a novel nano TiO_2 catalyst doped with upconversion luminescence agent. J. Photochem. Photobiol. A Chem. 180 (1–2), 189–195.
Wu, J.C.S., 2009. Photocatalytic reduction of greenhouse Gas CO_2 to fuel. Catal. Surv. Asia 13, 30–40.
Zhang, H., Quan, X., Chen, S., Zhao, H., 2006. The removal of sodium dodecylbenzene sulfonate surfactant from water using silica/titania nanorods/nanotubes composite membrane with photocatalytic capability. Appl. Surf. Sci. 24, 8598–8604.
Zhang, W., Ding, L., Luo, J., Jaffrin, M.Y., Tang, B., 2016. Membrane fouling in photocatalytic membrane reactors (PMRs) for water and wastewater treatment: a critical review. Chem. Eng. J. 302, 446–458.

Further Reading

Drab, D.M., Willauer, H.D., Olsen, M.T., Ananth, R., Mushrush, G.W., Baldwin, J.W., Hardy, D.R., Williams, F.W., 2013. Hydrocarbon synthesis from carbon dioxide and hydrogen: a two-step process. Energy Fuel 27, 6348–6354.
Fu, J., Ji, M., Wang, Z., Jin, L., An, D., 2006. A new submerged membrane photocatalysis rector (SMPR) for fulvic acid removal using a nano structured photocatalyst. J. Hazard. Mater. 131, 238–242.
Kertèsz, S., Cakl, J., Jiránková, H., 2014. Submerged hollow fiber microfiltration as a part of hybrid photocatalytic process for dye wastewater treatment. Desalination 343, 106–112.
Koci, K., Obalová, L., Lacný, Z., 2008. Photocatalytic reduction of CO_2 over TiO_2 based catalysts. Chem. Pap. 62, 1–9.
Martino, G., 2000. Catalysis for oil refining and petrochemistry, recent developments and future trends. Stud. Surf. Sci. Catal. 130, 83–103.
Qu, A., Xie, H., Xu, X., Zhang, Y., Wen, S., Cui, Y., 2016. High quantum yield graphene quantum dots decorated TiO_2 nanotubes for enhancing photocatalytic activity. Appl. Surf. Sci. 375, 230–241.
Sarasidis, V.C., Plakas, K.V., Patsios, S.I., Karabelas, A.J., 2014. Investigation of diclofenac degradation in a continuous photo-catalytic membrane reactor. Influence of operating parameters. Chem. Eng. J. 239, 299–311.
Zhang, X., Du, A.J., Lee, P., Sun, D.D., Leckie, J.O., 2008. Grafted multifunctional titanium dioxide nanotube membrane: separation and photodegradation of aquatic pollutant. Appl. Catal. B Environ. 84, 262–267.

CHAPTER 7

PMRs in Photodegradation of Organic Contaminants: Water and Wastewater Treatment

Ali Moslehyani[1,3,4], Siti K. Hubadillah[1,2], Mohd Hafiz Dzarfan Othman[1,2], Ahmad F. Ismail[1,2], Takeshi Matsuura[2,4]

[1]Advanced Membrane Technology Research Center (AMTEC), Universiti Teknologi Malaysia, Johor Bahru, Malaysia; [2]Faculty of Chemical & Energy Engineering (FCEE), Universiti Teknologi Malaysia, Johor Bahru, Malaysia; [3]University of Ottawa, Ottawa, ON, Canada; [4]University of Toronto, Toronto, ON, Canada

7.1 Introduction

"Water" is one of the natural precious gifts to mankind and perhaps one of the most important substances in our natural resources of life, next to air. Unfortunately, there is a growing concern on water shortage that is recognized widely in the world as a critical alarm (Jairath, 2010; McInerney, 2009), where the deteriorating quality and growing demand for clean water sources have created a significant challenge around the world (McInerney, 2009; Hoekstra, 2014; Ridoutt and Pfister, 2010; Enright, 2000). Because almost 750 million people of our planet are suffering to have safe drinking water, as reported by World Health Organization (WHO) (Organization, 2015; Hotez et al., 2016; Ismail et al., 2013; Mobaraki et al., 2015), the water scarcity by industrialization, growth of population, and other activities will lead to a dramatically poor condition on the Earth (Hotez et al., 2016; Mekonnen and Hoekstra, 2016; Moslehyani and Ismail, 2013; Mobaraki et al., 2016). As a result, a wide range of emerging contaminants such as inorganic matter (heavy metals, boron, etc.) and organic pollutants (pharmaceuticals, pesticides, oils, dyes, etc.) can be traced in both drinking water and wastewater (Han et al., 2017). Generally speaking, these contaminants can persist, causing severe environmental and health problems. For example, inorganic pollutants such as heavy metals are the most commonly investigated because of their serious health risk to human body, even death (Hubadillah et al., 2017). Whereas, organic pollutants such as endocrine

Current Trends and Future Developments on (Bio-) Membranes. https://doi.org/10.1016/B978-0-12-813549-5.00007-4

disrupting compounds (EDCs), including pesticides, halogenated aromatic compounds, and alkylphenols, have received most attention because that can alter endogenous hormone activity and homeostasis, thus potentially disrupting the action of sex and other natural hormones at all stages of human development (Moosa et al., 2017).

Accordingly, several potential technologies are well reported in literature on both organic and inorganic pollutant treatments such as ion exchange, coagulation/flocculation, and adsorption. In the studies of Golbaz et al. (2014), removal of phenol, chromium, and cyanide from water were conducted by coagulation and precipitation method. The coagulation method efficiently removed chromium, but poor removal of cyanide was found. In fact, it was also observed that the coagulation failed to remove organic phenol from water. Organic pollutants such as phenol are toxic and can cause several environmental and health problems. They originate from domestic sewage, sewage treatment plants, agriculture wastewater, and industrial effluents.

Taking into consideration that these organic pollutants need to be removed from water and wastewater, researchers are developing novel technologies for efficient and economic production of water by wastewater treatment. Over the last decades, a great deal of interest has been focused on the photodegradation of organic pollutants present in water and wastewater with application of titanium dioxide (TiO_2) as a photocatalyst. This superior application was first discovered by Fujishima and Honda in 1972 through the photocatalytic splitting of water on TiO_2 electrodes (Coronado, 2013). TiO_2 as a semiconductor photocatalyst has drawn a lot of attention over the past four decades especially toward water treatment because it is nontoxic, stable, readily available, and cheap.

However, the photocatalyst particles have to be separated from the treated water after the detoxification, which means that other steps are required to complete the process. A very promising method for solving problems concerning separation of the photocatalyst as well as products and by-products of photodecomposition from the reaction mixture is application of photocatalytic membrane reactors (PMRs). PMRs have the following advantages with respect to conventional photoreactors (Molinari and Palmisano, 2005):

1. Confining of the photocatalyst in the reaction environment by means of the membrane.
2. Control of a residence time of molecules in the reactor.
3. Realization of a continuous process with simultaneous photocatalyst and products separation from the reaction environment.

Moreover, application of a PMR instead of a conventional photoreactor allows avoiding some additional operations, such as coagulation, flocculation, sedimentation, which are necessary to remove photocatalyst from the treated solution. One benefit from this is energy saving and reducing the size of installation.

7.2 Photocatalytic Membrane Reactors for Photodegradation of Organic Contaminants

Nowadays, photodegradation processes are widely accepted for water and air purification because of their competence to degrade organic components without using any chemicals and without producing harmless products. As well, PMRs have also been accepted as useful tools for wastewater treatment. Experiments have been carried out to photodegrade many types of wastewater using different light sources to provide photodegradation energy. Summary of photocatalytic applications using photocatalytic membranes and PMRs is given in Table 7.1. Some of the wastewater pollutants that have been treated by photocatalytic degradation are oil, dye, phenol family, pathogenic, hospital, and heavy metal (Bahnemann, 2004; Bhatkhande et al., 2002; Qu et al., 2013).

7.2.1 Oil and Grease

Many sectors of industries, such as metallurgical, transportation etc., are contaminating clean water. The concentration of organic compounds, mainly hydrocarbons, in oily water in discharge streams is 50 ppm, which needs to be considered for purification based on most of water discharge polices including Clean Water Act (CWA) of the United States of America, European Union (EU), and Asian Sewage and Industrial Effluent Discharge Standards Regulation (Lyon and Stein, 2009; Rincón and La Motta, 2014; Loehr and Navarra, 1969; Issariyakul et al., 2007). Therefore, many technologies have been proposed to solve this problem, which include chemical adsorption, coagulation, distillation, chemical demulsification, biological degradation, membrane separation, and PMRs. The combination of photodegradation and membrane processes has attracted attention of scientists lately (Moslehyani et al., 2016).

Moslehyani et al. (2015b) applied various PMR designs for photodegradation of oil in water and separation of photocatalyst suspension. The authors used flat sheet, hollow fiber, and nanofibrous membranes. Most of the membranes had pore sizes in the UF range. The PMRs have shown superior performance in degradation of toxic hydrocarbon compounds and purification of oily wastewater (Moslehyani et al., 2015c, 2015d). Cheng et al. (2017) presented photocatalytic treatment of palm oil mill effluent (POME) over tungsten oxide (WO_3) photocatalyst under UV irradiation.

Ong et al. (2014) investigated the performance of a submerged PMR with polyvinylidene fluoride titanium dioxide (PVDF-TiO_2) hollow fiber membranes for the separation and degradation of synthetic oily wastewater under UV irradiation. The major focus of this work was to assess the performance of submerged PMR for synthetic cutting oil wastewater treatment based on several key operating parameters, i.e., TiO_2 loading (embedded in membrane matrix), module packing density, initial feed concentration, and

Table 7.1: Summary of photocatalytic membranes and slurry photocatalytic membrane reactors toward photodegradation of organic contaminants in water.

Pollutants Group	PMR Setup	Membrane	Photocatalyst	Irradiation	Pollutant Name	Efficiency	Drawbacks	References
Oil	Slurry	Polyvinylidene fluoride	Multiwalled carbon nanotube	UVC	Malaysian petroleum refinery	>90%	Formation of cake layer—membrane fouling	Moslehyani et al. (2015a)
Dye	Slurry	Polyethersulfone NF	TiO_2-P25	UV	Congo red Patent Blue	99%	Membrane fouling	Molinari et al. (2004)
	Slurry	NF/UF	ZnO	UV	Industrial wastewater from printing industries	100%	Membrane fouling Low permeation using UF	Hairom et al. (2015)
	Slurry	UF	TiO_2-P25	UV	Methylene blue	95%	Performance is disturbed due to the agglomeration of TiO_2	Sopajaree et al. (1999)
	Immobilized	UF (Ceramic)	TiO_2	UV	Direct Black 168	72%	Incomplete dye degradation	Zhang et al. (2006)
	Immobilized	UF (Ceramic)	N-doped TiO_2 Graphene oxide (GO)—modified TiO_2	UV Visible	Methylene Blue Methyl Orange	57% 29%	Dead-end filtration mode	Athanasekou et al. (2015a)
	Immobilized	UF (Ceramic)	N-doped TiO_2	UV	Direct fast Scarlet 4BS	99%	Cake layer formation	Sopajaree et al. (1999)
Pharmaceuticals	Slurry	NF	TiO_2-P25	Sunlight	Lincomycin	93.64%—97.78%	Total organic carbon (TOC) accumulation	Augugliaro et al. (2005)
	Slurry	NF	TiO_2-P25	UV	Furosemide	5%—30%	No rejection during photocatalytic test	Molinari et al. (2006)
	Immobilized	UF	TiO_2-P25 Laboratory made TiO_2	UV Visible	Diphenhydramine	73% 28%	Dead-end filtration mode	Pastrana-Martínez et al. (2015)
	Immobilized	MF	TiO_2	UV-A lamp	Ibuprofene	50%	Low flux and membrane fouling	Fischer et al. (2015)

MF, Microfiltration; *NF*; Nanofiltration; *UF*, Ultrafiltration; *UV*, Ultraviolet; *UVC*, Ultraviolet C.

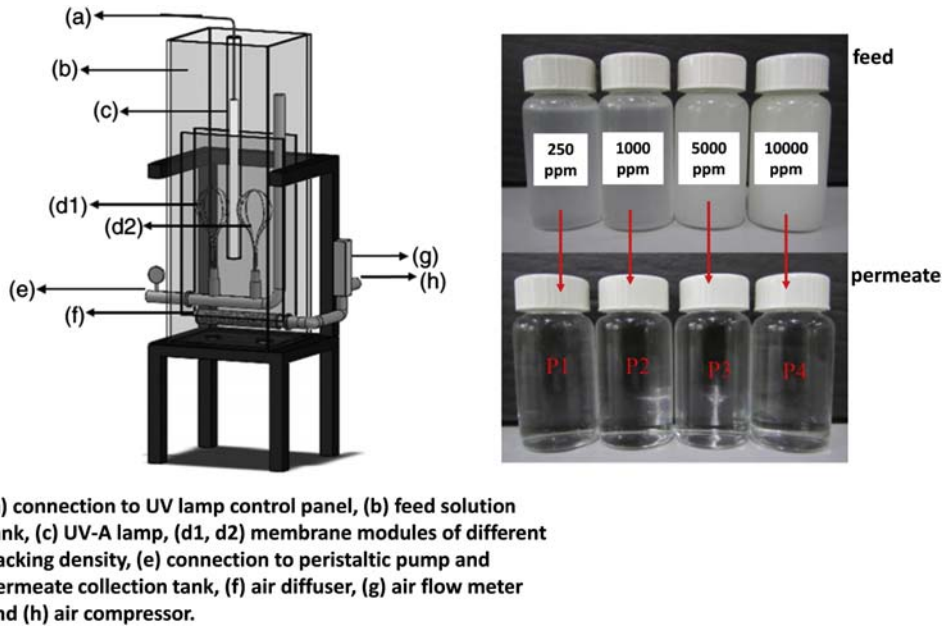

(a) connection to UV lamp control panel, (b) feed solution tank, (c) UV-A lamp, (d1, d2) membrane modules of different packing density, (e) connection to peristaltic pump and permeate collection tank, (f) air diffuser, (g) air flow meter and (h) air compressor.

Figure 7.1
Photocatalytic membrane reactor laboratory setup and oily wastewater before and after treatment. *Reproduced from Ong et al., 2014. Reprinted with the permission from Elsevier.*

air bubble flow rate (ABFR). The results showed that total organic carbon (TOC) degradation using PVDF-TiO_2 membrane was remarkably higher compared with neat PVDF membrane. In addition, it was found that both TOC degradation and membrane flux were seriously deteriorated when excessive TiO_2 loading and module packing density were used. Although thicker oil layer tended to form at high feed concentration that adversely affected photocatalytic degradation and water flux, the introduction of higher ABFR could reduce the impacts to certain extent. With respect to TOC degradation and oil rejection, the in-house-made membrane could achieve 80% TOC degradation and 90% rejection when it was operated under optimized conditions, as illustrated in Fig. 7.1.

7.2.2 Phenols

Many industrial production sectors, such as pharmaceutical, resin manufacture, plastic industry etc., are extensively using phenol family compounds causing phenolic wastewater. Bisphenol A (BPA) and nonylphenol (NP), which are toxic and prevalent EDCs, are typical examples (Dzinun et al., 2015). The wastewater contaminated with phenol groups can cause adverse effects in wildlife and humans by forming additional female organs, enlarged

accessory sex glands, morphological and functional gonadal dysfunction, and interference in the functioning of the endocrine system. The allowable phenol discharge to the water streams of inland surface is set to not more than 1 and 5 ppm to any streams in the world. Hence, treatment of this type of wastewater is very important to avoid many issues in the future because many industries are progressively using phenol compounds and producing phenolic wastewater. Full treatment of phenolic wastewater by photodegradation has been advised to be used by many researchers via PMR technology (Dzinun et al., 2015).

A study by Yang et al. (2011) on polypropylene (PP) membrane surface modification by reversible addition−fragmentation chain transfer (RAFT) grafting polymerization and TiO_2 photocatalysts immobilization for phenol decomposition in a photocatalytic membrane reactor was conducted. It was reported that the attachment of TiO_2 photocatalysts and the filtration performance were enhanced by the surface hydrophilic modification. It can be found from Fig. 7.2A and B that the efficiency of phenol decomposition in the presence of membranes with poly(acrylic acid) (PAAc) grafting degrees (GDs) of 2.9 wt.% and 12.9 wt.% on the surface was 12.4% and 32.5% after 6 h UV light irradiation, respectively. The low decomposition was due to that 3/4 of the UV light was absorbed by the poly(methyl methacrylate) (PMMA) plate of the reactor. In addition, the observed redshift of the peak in the UV-vis spectrum with irradiation time was supposed to be caused by the by-products of phenol degradation. The maximum concentration of intermediates appeared after 4 and 2 h for the membranes with grafting

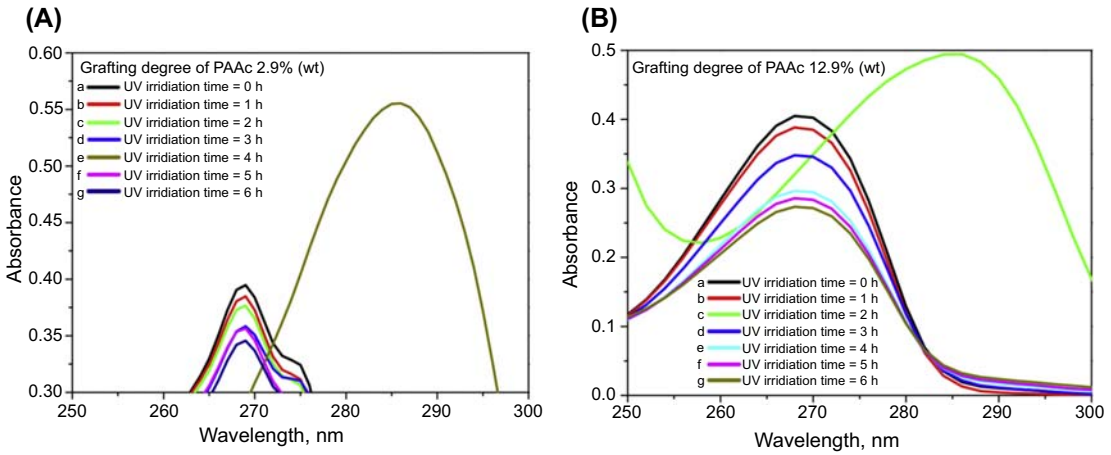

Figure 7.2

Decomposition of phenol using photocatalytic membrane reactor with TiO_2 photocatalyst immobilized on the membrane surface: (A) PAAc grafting degree of 2.9 wt.% and (B) PAAc grafting degree of 12.9 wt.%. *Yang et al., 2011. Reprinted with the permission from Elsevier.*

degrees of 2.9 wt.% and 12.9 wt.%, respectively. Dihydroxybenzene, benzoquinone (BQ), 4,4′ −dihydroxybiphenyl, and maleic anhydride were the main intermediates with absorption bands between 250 and 360 nm, higher than that of phenol (270 nm). The intermediates eventually degraded to CO_2.

Whereas, Chen et al. (2016) prepared electrospun ZnS-loaded hybrid carbon nanofiber photocatalytic membranes for phenol removal. Owing to the synergistic effect between photocatalytic activity of ZnS and excellent adsorption capacity of graphene oxide−carbon nanofibers (GO-CNFs), the resultant GO/ZnS-CNFs exhibited excellent photocatalytic activity for oxidation of 4-aminotoluene and phenol under mild conditions. The h^+, $O^{2\bullet-}$, and $^{\bullet}OH$ are the main active species for photocatalytic conversion of phenol under UV light irradiation. The direct oxidation pathway reported to be the dominant route for oxidation of 4-aminotoluene due to $^{\bullet}OH$ radicals can be scavenged by OH^- to form $O^{2\bullet-}$. Fig. 7.3 shows the time-dependent changes and the first-order reaction curve of phenol decomposition tested using a 500 W lamp. In a typical experiment, the original absorption peak of phenol was centered at 270 nm. After introducing GO/ZnS-CNFs into the phenol solution, the peak at 270 nm was decreased with increasing the irradiation time. After irradiation for about 60 min, the peak disappeared almost completely. Three major aromatic intermediates were detected: ortho-dihydroxybenzene, para-dihydroxybenzene,

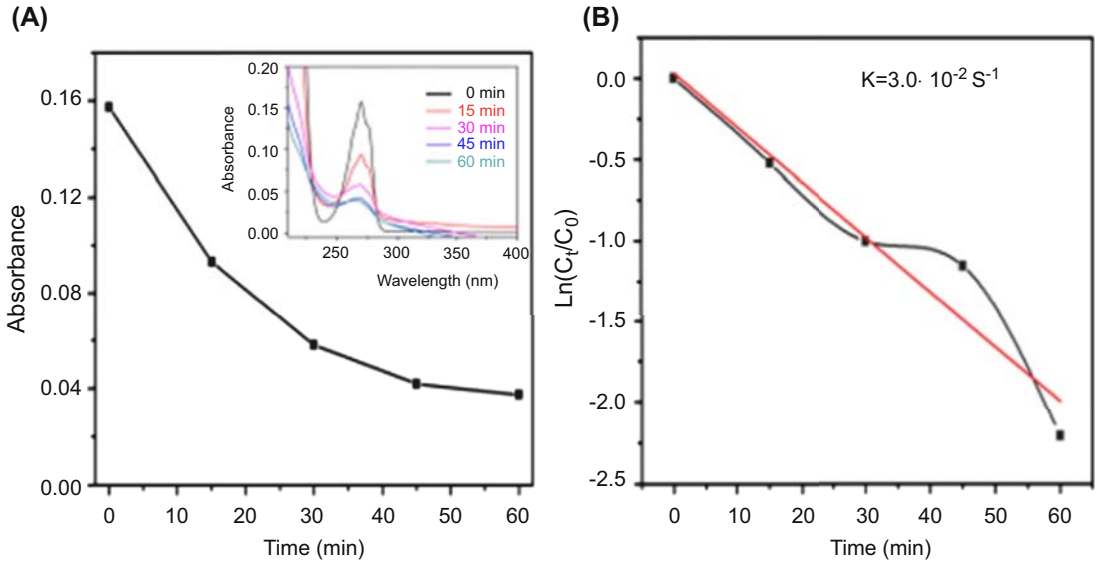

Figure 7.3

(A) Time-dependent changes of the phenol solution spectrum with GO/ZnS-CNFs and (B) the first-order reaction curve for photocatalytic conversion of phenol. *Reproduced from Chen et al., 2016. Reprinted with the permission from Elsevier.*

and 1,4-benzoquinone. The pseudo-first-order kinetic rate constant $k_{app} = 3.0 \times 10^{-2}\ s^{-1}$ was calculated from the rate equation $\ln (C_t/C_0) = -k_{app}\ t$, where C_0 is the initial concentration of phenol and C_t represents the concentration of phenol at the time t.

7.2.3 Dye

Dyes are daily used in various industries with some side effects. According to some statistics, about 20% of dye waste is entering into water streams. Hence, purification of dye-contaminated wastewater is required before any discharge to the environment. One of the promising technologies for dye wastewater treatment is PMR. PMR technology, due to the action of a photocatalyst, has a potential to break the large dye molecules into smaller ones and finally to mineralize them to water, CO_2, and inorganic salts. Mozia et al. (2005) designed a batch type PMR for dye decomposition, based on membrane distillation. Degussa TiO_2 photocatalyst (P25) was dispersed in the dye solution to the concentration of 0.3 g L^{-1}, and the experiment was carried out at 60°C for 5 h. The dyes were completely removed, and the TOC degradation was c. 80%.

Hairom et al. (2014) studied the effect of various zinc oxide nanoparticles in photocatalytic membrane reactor for Congo red (CR) dye treatment. Polypiperazine amide nanofiltration (NF) membrane was used in this study. Morphology of the membrane surface and cross sections were observed with field emission scanning electron microscopy (FESEM) as shown in Fig. 7.4. Nanoparticles synthesized with application of polyvinylpyrrolidone under vigorous stirring (denoted as ZnO-PVP-St) presented the highest photodegradation efficiency, and their contribution to the membrane flux decline was the lowest from all the ZnO samples tested. Based on the experiments with the initial dye concentration of 20 mg L^{-1} at pH 7, it was found that the optimum photocatalyst loading is 0.3 g L^{-1}, which was explained in terms of the effective surface area of ZnO-PVP-St and absorption of UV light.

Mozia et al. (2007) compared the effectiveness of methylene blue decomposition using pristine and carbon-coated TiO_2 in a photocatalytic membrane reactor combining photocatalysis with direct contact membrane distillation (DCMD). It was found that the pristine TiO_2 did not affect the permeate flux, regardless of the concentration applied, whereas during the process realized in the presence of the carbon-coated TiO_2 a deterioration of the flux was observed, being the most severe at the highest photocatalyst loading used. Moreover, in the lower range of photocatalyst concentrations (<0.5 g L^{-1}) the carbon-coated TiO_2 exhibited higher activity toward methylene blue removal than pristine TiO_2. More importantly, advantage of the presented PMR is complete separation of photocatalyst particles, as well as dye and other nonvolatile compounds. As a result, the product (distillate) has high quality.

In 2013, Zhang et al. (2013) investigated the azo dye−TiO_2 interactions on the filtration performance in a hybrid photocatalysis and ultrafiltration (UF) process. The experimental

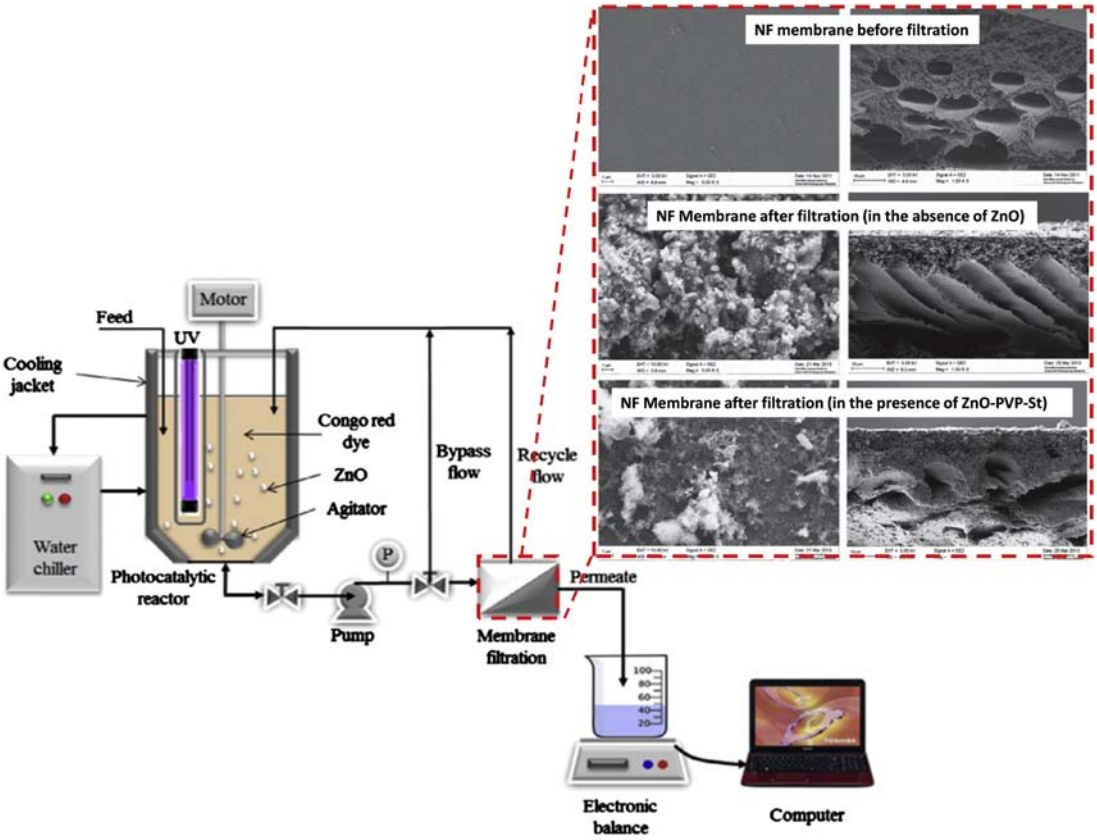

Figure 7.4

Schematic diagram for photocatalytic membrane reactor and Scanning electron microscopy image of the photocatalytic membrane. *Reproduced from Hairom et al., 2014. Reprinted with the permission from Elsevier.*

setup is shown in Fig. 7.5. The permeate flux and dye rejection behaviors of UF membrane made of polyacrylonitrile were analyzed at pH 4.0, 6.0, and 10.0. The dye−TiO_2 interaction made the size of TiO_2 aggregates to significantly increase at pH 4.0 and 6.0 and slightly decrease at pH 10.0 but led the fractal dimensions of TiO_2 aggregates to decrease in all pH conditions. These interactions hence resulted in the variation of amount and structure of deposit layer. The fractal dimension and size of TiO_2 aggregates were further applied to estimate the specific cake resistance of deposit layer by Carman−Kozeny equation. The results showed that size and fractal dimension of TiO_2 aggregates were, but not exclusive, factors dominating the permeate flux as well as the specific cake resistance. Hydrophilicity of deposit layer also played an important role in determining the performance of membrane. With the bridging effect produced by self-assemble and electronic behaviors of TiO_2 on membrane interface, the deposit layer

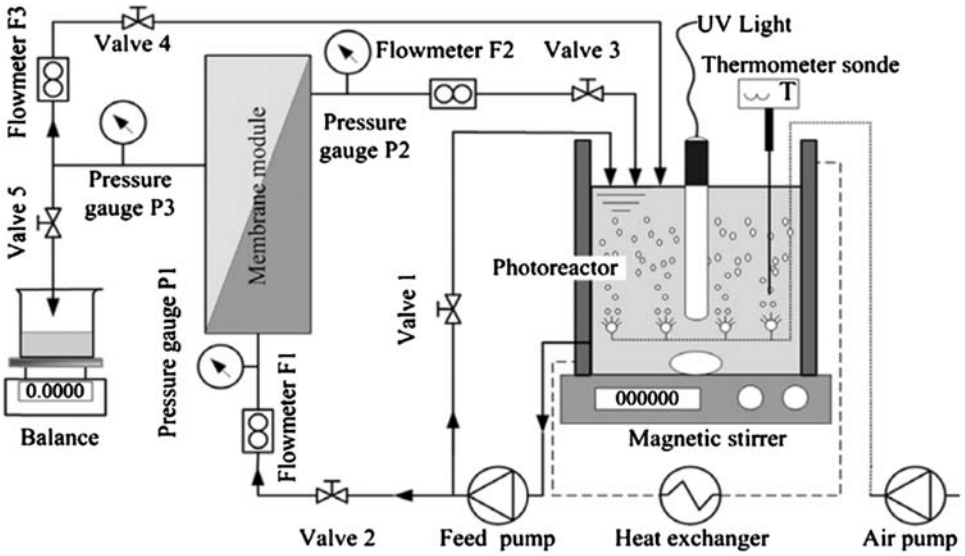

Figure 7.5
Laboratory setup for photocatalytic membrane reactor coupling photocatalysis with ultrafiltration. *Reproduced from Zhang et al., 2013. Reprinted with the permission from Elsevier.*

consisted of dye and TiO_2 significantly reduced the rejection of dyes. In the presence of TiO_2, the possible mechanism of the decrease in dye rejection was proposed in Fig. 7.6. The decrease in dye rejection can be ascribed to TiO_2 bridging between membrane interface and dyes. Self-assemble behavior was observed between TiO_2 and the interface with −COOH, −OH, − SO_2OH, −O−, and =O groups by hydrogen bond and/or coordination [34]. The bridging effect of TiO_2 not only decreased the hydrophilicity of filtration interface by binding dye but also weakened the electronic repulsion by the hydrogen bond between TiO_2 and membrane.

Damodar et al. (2010) presented a photocatalytic slurry reactor with membrane separation for dye wastewater treatment. Fig. 7.7 illustrates the laboratory setup for the coupled system. In the study, commercial polytetrafluoroethylene (PTFE) membrane with pore size and contact angle value of 0.22 μm and 120 degrees, respectively, was used. High removal performance of color (100%), TOC, and COD (∼80%) was achieved. It was reported that the photocatalyst can be effectively separated and reused using PMR, and it can be used for a long time without much loss of its activity. The TiO_2 particle size distribution showed the significant variation during continuous filtration operation. Furthermore, this study demonstrated the advantages of different aerator and stirrer settings, as well as their operating conditions for attending longer operation and reducing the frequent membrane cleaning requirement.

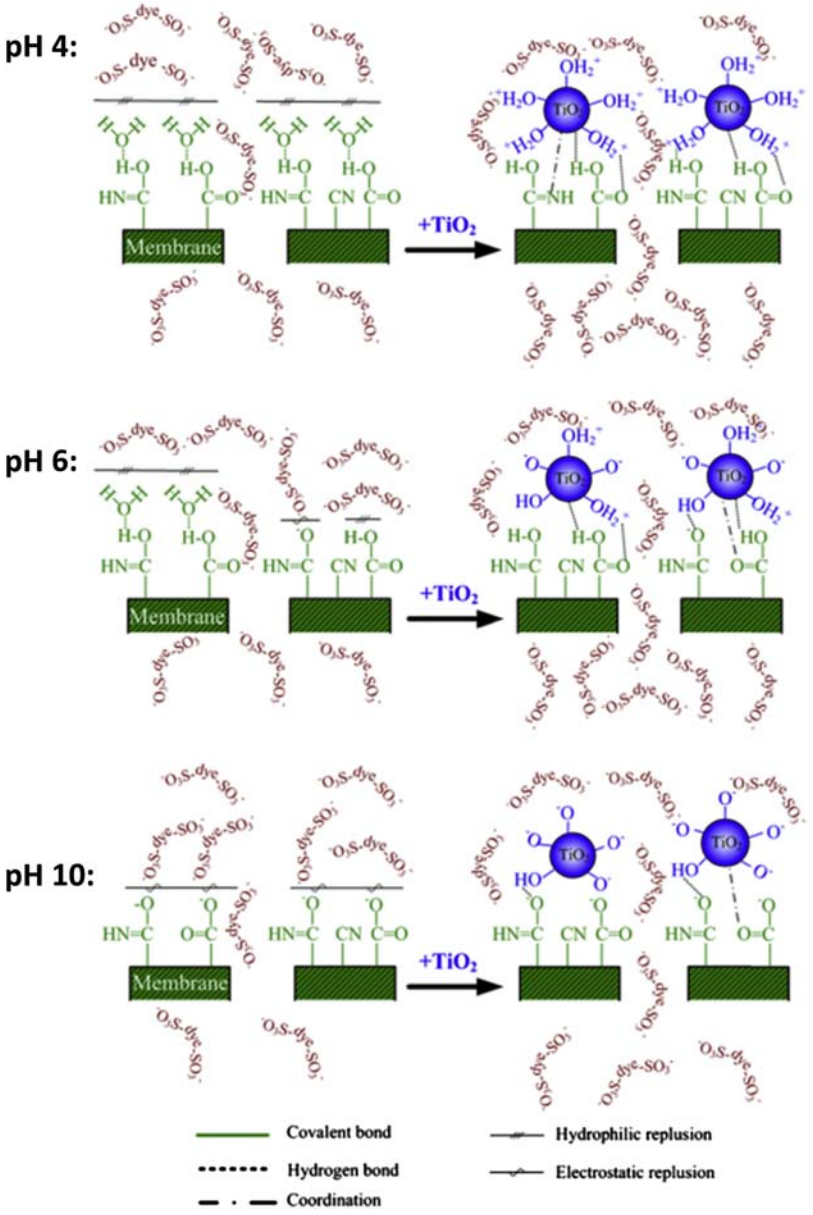

Figure 7.6

Mechanism of the decrease in dye rejection in the presence of TiO_2 at different pH. *Zhang et al., 2013. Reprinted with the permission from Elsevier.*

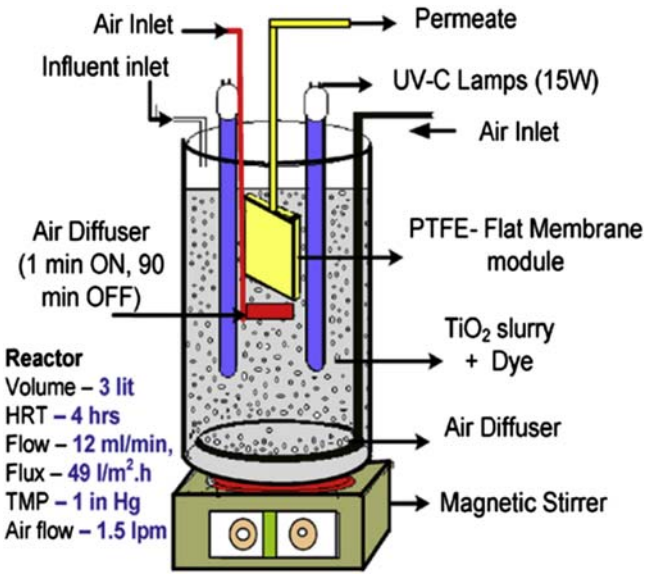

Figure 7.7
Laboratory setup for slurry photocatalytic membrane reactor coupled with polymeric membrane.
Reproduced from Damodar et al., 2010. Reprinted with the permission from Elsevier.

Athanasekou et al. (2015b) prepared ceramic photocatalytic membranes for water filtration under UV and visible light. The work demonstrates the efficiency of a hybrid photocatalysis/ultrafiltration process to eliminate or reduce the contents of synthetic dyes in water. The process involves highly active photocatalytic ceramic ultrafiltration (UF) membranes prepared with the deposition of various photocatalysts on the external and internal (pore) surfaces of UF mono-channel monoliths. A main challenge consists in swapping from the conventional slurry-type photocatalytic purification technology to a novel photocatalytic membrane filtration technology, using the most prominent recently developed TiO_2-based nanomaterials. With this objective, highly hydroxylated anatase TiO_2 was deposited on ceramic monoliths by applying sol–gel (dip-coating) techniques. Novel materials comprising modified TiO_2 nanocrystals covered with an organic shell layer as well as partially reduced graphene oxide–TiO_2 composites were synthesized and stabilized on the monoliths aiming to develop visible light–responding photocatalytic membranes. All the membranes proved to be effective against common problems faced by the conventional high flux–thin film composite polymeric nanofiltration systems, when treating waste that contains textile dyes, such as fouling tendency, increased energy consumption, and the formation of hard-to-dispose toxic-concentrated effluents of the pollutant.

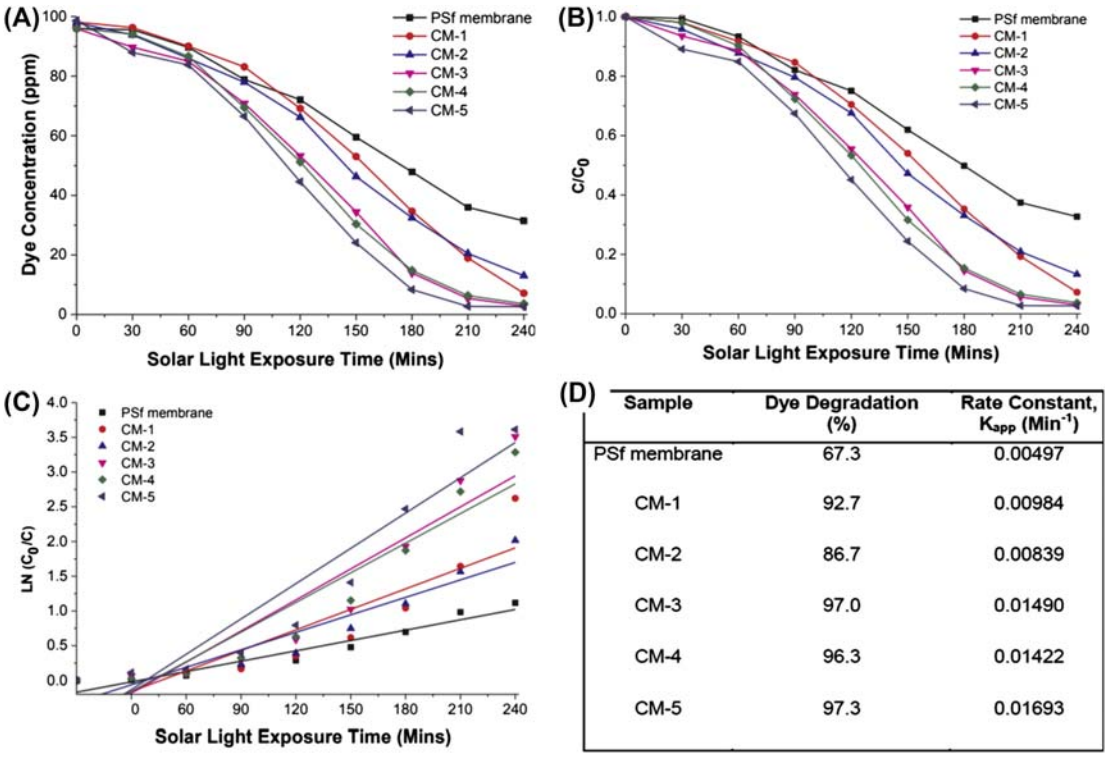

Sample	Dye Degradation (%)	Rate Constant, K_{app} (Min^{-1})
PSf membrane	67.3	0.00497
CM-1	92.7	0.00984
CM-2	86.7	0.00839
CM-3	97.0	0.01490
CM-4	96.3	0.01422
CM-5	97.3	0.01693

Figure 7.8

Photocatalytic activity of the membranes: (A) dye degradation; (B) normalized dye degradation; (C) degradation kinetics; (D) table of degradation (%) and rate constants. *Reproduced from Kuvarega et al., 2018. Reprinted with the permission from Elsevier.*

Recently the composite polysulfone membranes modified using a TiO_2 photocatalyst co-doped with nitrogen and palladium (N,Pd co-doped TiO_2) for photocatalytic dye degradation were investigated (Kuvarega et al., 2018). The entrapment of N,Pd co-doped TiO_2 into polysulfone (PSf) membranes results in enhancement of the physicochemical properties of the membranes for tailored application in photocatalysis. Improved hydrophilicity, porosity, visible light absorption, and photoactivity were achieved without compromising membrane integrity. Up to 97% of eosin yellow dye was removed after 4 h of visible light irradiation of the membrane. Fig. 7.8 shows that the rate constant of pure polysulfone (PSf) membrane was lower (0.00,497 min^{-1}) than that of the nanoparticle-loaded membranes, with CM-5 (bandgap = 3.37 eV) showing the highest degradation rate (0.01693 min^{-1}). CM-5 is the membrane with 7% of N,Pd co-doped TiO_2 (highest amount than other membrane) that dispersed in 1-methyl-2-pyrrolidone. The entrapment of N,Pd

co-doped TiO_2 therefore improved the photocatalytic performance of PSf membranes to a form almost comparable with that of N-doped TiO_2 under visible light irradiation. The very interesting part of the PMR in this study was, unlike free photocatalytic nanoparticles, the membrane can easily be taken out of the reactor and used repeatedly in photodegradation, significantly reducing the posttreatment costs.

7.2.4 Other Contaminants

Drug pollution or pharmaceutical pollution is pollution of the environment with pharmaceuticals and their metabolites, which eventually reach the aquatic environment (groundwater, rivers, lakes, and oceans) through wastewater. Drug pollution is therefore a form of water pollution. Pharmaceutical pollutants are now detected in waters throughout the world, causing aging infrastructure, sewage overflows, and agricultural runoff. Even when wastewater is treated at sewage treatment facilities, they are not equipped to remove pharmaceuticals. Moreover, these chemicals are not currently regulated by water quality laws, which make them emerging pollutants (Farré et al., 2008). Martínez et al. (2013) evaluated a coupling of membrane separation and advanced oxidation processes (AOPs) for the removal of pharmaceutical pollutants. The NF and reverse osmosis (RO) membranes were used for separation of the drugs, whereas retentate was further purified using AOPs such as heterogeneous photocatalysis or photo-Fenton process. Six pharmaceutical representatives of different families of drugs were selected as model pollutants for the assessment of separation/oxidation combined processes: sulfamethoxazole (SMX, antibiotic), diclofenac sodium (DCF, antiinflammatory), hydrochlorothiazide (HCT, diuretic, drug to treat hypertension), 4-acetamidoantipyrine (4AAA, antipyretic), nicotine (NCT, stimulant), and ranitinide hydrochloride (RNT, histamine H2-receptor antagonist that inhibits stomach acid). They have been usually found in the influents and effluents of wastewater treatment plants, being hardly affected by the conventional treatment processes. The structures of these pollutants are shown in Fig. 7.9. An efficient separation of the contaminants by the applied NF and RO membranes was achieved (<0.5 mg L^{-1} vs 10 mg L^{-1} in feed). Moreover, both photocatalysis and photo-Fenton processes were effective in decomposition of pharmaceutical compounds in retentate, reaching removal rates between 80% and 100%. However, in case of the most refractive compound, nicotine, the TiO_2 photocatalysis achieved a lower degradation efficiency.

Guo et al. (2015) developed a PMR for photocatalytic removal and inactivation of viruses. The P22 bacteriophage was used as a model virus. The performance of the proposed PMR technology was compared against that of its constituent processes—UV disinfection and microfiltration (MF). In the study, a UV lamp and a ceramic MF membrane with nominal pore size of 0.8 μm were located between two parabolic reflectors facing each other, and UV light was focused on a photocatalyst-coated outer surface of the membrane. The membrane was operated in an inside-out geometry with the permeate side irradiated by the

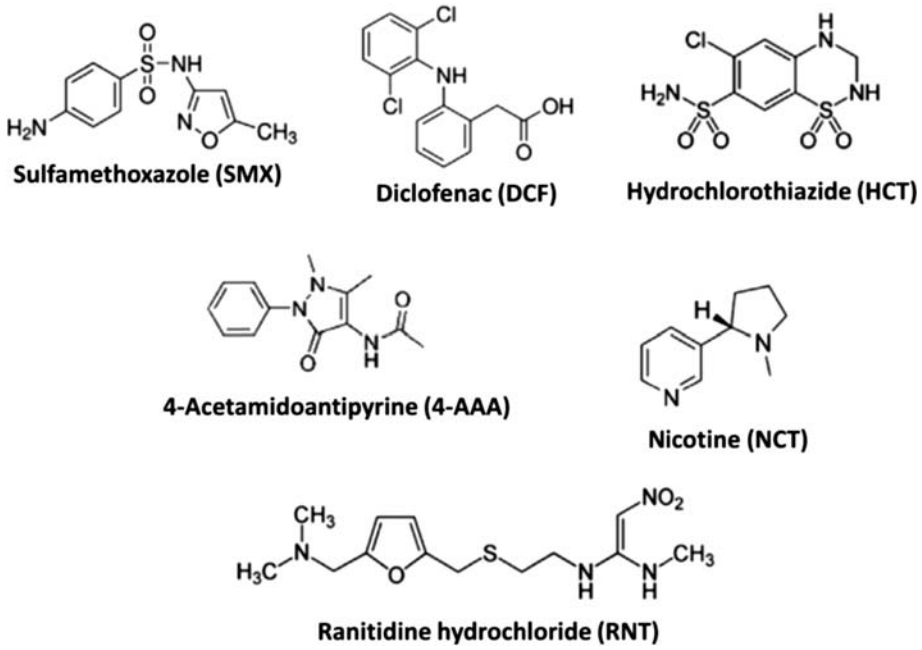

Figure 7.9

Structures of the pharmaceutical pollutants used by Martínez et al. *Reproduced from Martíńez et al., 2013. Reprinted with the permission from Elsevier.*

UV radiation (Fig. 7.10). It was postulated that the proposed hybrid process could overcome two main disadvantages of disinfection by direct UV, which are resistance of certain environmentally important pathogens to UV and low efficiency of UV disinfection in case of highly turbid waters. The performance of the system toward virus removal and inactivation can be regulated by the selection of the membrane, type of the photocatalytic coating, and by controlling UV intensity applied to the permeate stream.

7.3 Conclusions and Future Trends

Nowadays, water and wastewater pollution, especially organic type, has been a major concern, and there is an urgent need to find a solution to treat them. PMRs have been well known with their interesting results in the photodegradation of organic pollutants. Various organic pollutants such as oils, phenols, and dyes have been successfully treated through PMRs. The advantages of using PMRs in water and wastewater treatment compared with other conventional methods include the photonic activation mode of the photocatalyst, which replaces the thermal activation. In addition, PMRs offer the simple and efficient technology as compared with free photocatalytic nanoparticles, the membrane used in PMRs can easily be

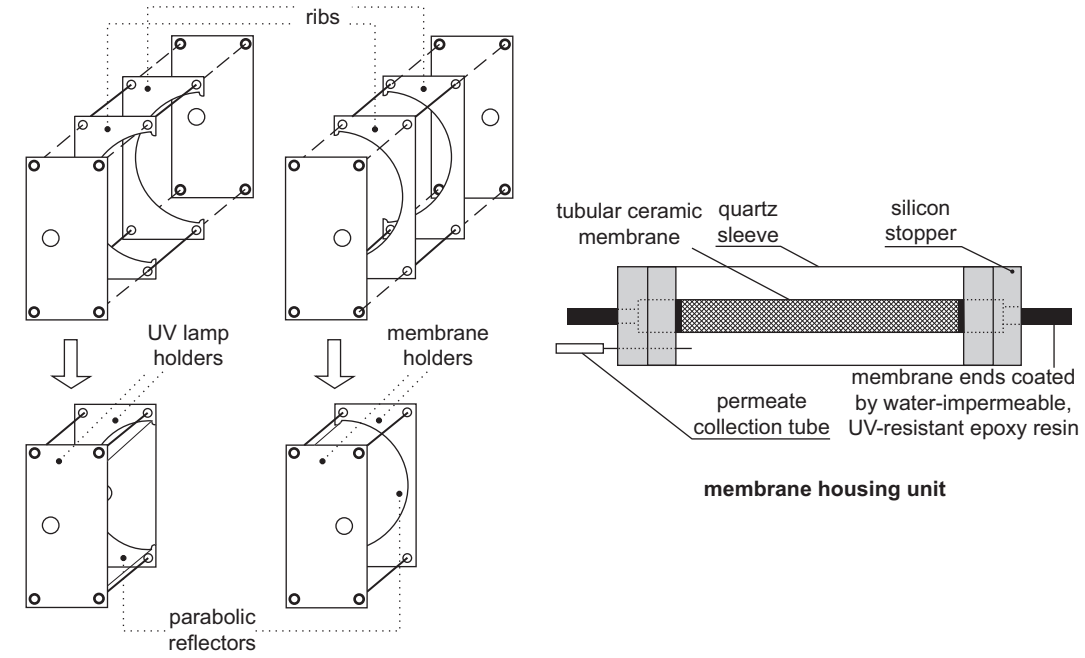

Figure 7.10
Schematic diagram of UV light holders and membrane module. *Reproduced from Guo et al., 2015. Reprinted with the permission from Elsevier.*

taken out of the reactor and used repeatedly in photodegradation, significantly reducing the posttreatment costs. However, one major drawback in PMRs is formation of dangerous intermediate products such as hydroquinone (HQ) and BQ, which were identified in traces during decomposition of phenols. Therefore, more investigations on by-products formation and toxicity during PMRs process should be undertaken. Besides, it will be more interesting if PMRs can be studied toward drinking water applications in future.

List of Abbreviations

4AAA 4-Acetamidoantipyrine
ABFR Air bubble flow rate
AOP Advanced oxidation process
BPA Bisphenol A
BQ Benzoquinone
C_o Initial concentration
COD Chemical oxygen demand
CR Congo red
C_t Final concentration at time interval

CWA Clean water act
DCF Diclofenac sodium
DCMD Direct contact membrane distillation
DL Dual layer
EDCs Endocrine disrupting compounds
EDX Energy-dispersive X-ray spectroscopy
EU European Union
GD Grafting degrees
GO Graphene oxide
GO-CNFs Graphene oxide−carbon nanofibers
HCT Hydrochlorothiazide
HF Hollow fiber
HQ Hydroquinone
HRT Hydraulic retention time
K_{app} Pseudo-first-order kinetic rate constant
MD Membrane distillation
MF Microfiltration
MMM Mixed matrix membrane
NCT Nicotine
NF Nanofiltration
NP Nonylphenol
PAAc Poly(acrylic acid)
PES Polyethersulfone
PMMA Polymethyl methacrylate
PMR Photocatalytic membrane reactor
POME Palm oil mill effluent
PP Polypropylene
PSf Polysulfone
PTFE Polytetrafluoroethylene
PV Pervaporation
PVDF Polyvinylidene fluoride
PVP Polyvinylpyrrolidone
RAFT Reversible addition−fragmentation chain transfer
RNT Ranitinide hydrochloride
RO Reverse osmosis
SEM Scanning electron microscopy
SMX Sulfamethoxazole
TMG Trimethylgallium
TOC Total organic carbon
TMP Transmembrane pressure
UF Ultrafiltration
UV Ultraviolet
UVC Ultraviolet C
WHO World Health Organization

Acknowledgments

The authors gratefully acknowledge financial support from the Ministry of Education, Malaysia, under the Higher Institution Centre of Excellence Scheme (Project Number: R.J090301.7846.4J193) and Universiti Teknologi, Malaysia, under Research University Grant Tier 1 (R.J130000.7746.4J230). The authors would also like to thank Research Management Centre, Universiti Teknologi, Malaysia, for the technical support.

References

Athanasekou, C.P., Moustakas, N.G., Morales-Torres, S., Pastrana-Martínez, L.M., Figueiredo, J.L., Faria, J.L., Silva, A.M.T., Dona-Rodriguez, J.M., Romanos, G.E., Falaras, P., 2015a. Ceramic photocatalytic membranes for water filtration under UV and visible light. Appl. Catal. B Environ. 178 (Suppl. C), 12−19.

Athanasekou, C.P., Moustakas, N.G., Morales-Torres, S., Pastrana-Martínez, L.M., Figueiredo, J.L., Faria, J.L., Silva, A.M.T., Dona-Rodriguez, J.M., Romanos, G.E., Falaras, P., 2015b. Ceramic photocatalytic membranes for water filtration under UV and visible light. Appl. Catal. B Environ. 178, 12−19.

Augugliaro, V., García-López, E., Loddo, V., Malato-Rodríguez, S., Maldonado, I., Marcì, G., Molinari, R., Palmisano, L., 2005. Degradation of lincomycin in aqueous medium: coupling of solar photocatalysis and membrane separation. Sol. Energy 79 (4), 402−408.

Bahnemann, D., 2004. Photocatalytic water treatment: solar energy applications. Sol. Energy 77 (5), 445−459.

Bhatkhande, D.S., Pangarkar, V.G., Beenackers, A.A., 2002. Photocatalytic degradation for environmental applications−a review. J. Chem. Technol. Biotechnol. 77 (1), 102−116.

Chen, H., Jiang, G., Yu, W., Liu, D., Liu, Y., Li, L., Huang, Q., Tong, Z., Chen, W., 2016. Preparation of electrospun ZnS-loaded hybrid carbon nanofiberic membranes for photocatalytic applications. Powder Technol. 298 (Suppl. C), 1−8.

Cheng, Y.W., Chang, Y.S., Ng, K.H., Wu, T.Y., Cheng, C.K., 2017. Photocatalytic restoration of liquid effluent from oil palm agroindustry in Malaysia using tungsten oxides catalyst. J. Clean. Prod. 162 (Suppl. C), 205−219.

Coronado, J.M., 2013. In: Coronado, J.M., Fresno, F., Hernández-Alonso, M.D., Portela, R. (Eds.), Design of Advanced Photocatalytic Materials for Energy and Environmental Applications. Springer London, London, pp. 1−4.

Damodar, R.A., You, S.-J., Ou, S.-H., 2010. Coupling of membrane separation with photocatalytic slurry reactor for advanced dye wastewater treatment. Separ. Purif. Technol. 76 (1), 64−71.

Dzinun, H., Othman, M.H.D., Ismail, A.F., Puteh, M.H., Rahman, M.A., Jaafar, J., 2015. Photocatalytic degradation of nonylphenol by immobilized TiO_2 in dual layer hollow fibre membranes. Chem. Eng. J. 269, 255−261.

Enright, W., 2000. The effect of terrestrial invasive alien plants on water scarcity in South Africa. Phys. Chem. Earth Part B Hydrol. Oceans Atmos. 25 (3), 237−242.

Farré, M.l., Pérez, S., Kantiani, L., Barceló, D., 2008. Fate and toxicity of emerging pollutants, their metabolites and transformation products in the aquatic environment. Trac. Trends Anal. Chem. 27 (11), 991−1007.

Fischer, K., Grimm, M., Meyers, J., Dietrich, C., Gläser, R., Schulze, A., 2015. Photoactive microfiltration membranes via directed synthesis of TiO2 nanoparticles on the polymer surface for removal of drugs from water. J. Membr. Sci. 478 (Suppl. C), 49−57.

Golbaz, S., Jafari, A.J., Rafiee, M., Kalantary, R.R., 2014. Separate and simultaneous removal of phenol, chromium, and cyanide from aqueous solution by coagulation/precipitation: mechanisms and theory. Chem. Eng. J. 253 (Suppl. C), 251−257.

Guo, B., Pasco, E.V., Xagoraraki, I., Tarabara, V.V., 2015. Virus removal and inactivation in a hybrid microfiltration−UV process with a photocatalytic membrane. Separ. Purif. Technol. 149, 245−254.

Hairom, N.H.H., Mohammad, A.W., Kadhum, A.A.H., 2014. Effect of various zinc oxide nanoparticles in membrane photocatalytic reactor for Congo red dye treatment. Separ. Purif. Technol. 137 (Suppl. C), 74−81.

Hairom, N.H.H., Mohammad, A.W., Ng, L.Y., Kadhum, A.A.H., 2015. Utilization of self-synthesized ZnO nanoparticles in MPR for industrial dye wastewater treatment using NF and UF membrane. Desalin. Water Treat. 54 (4−5), 944−955.

Han, L., Xiao, T., Tan, Y.Z., Fane, A.G., Chew, J.W., 2017. Contaminant rejection in the presence of humic acid by membrane distillation for surface water treatment. J. Membr. Sci. 541 (Suppl. C), 291−299.

Hoekstra, A.Y., 2014. Water scarcity challenges to business. Nat. Clim. Change 4 (5), 318–320.
Hotez, P.J., Pecoul, B., Rijal, S., Boehme, C., Aksoy, S., Malecela, M., Tapia-Conyer, R., Reeder, J.C., 2016. Eliminating the neglected tropical diseases: translational science and new technologies. PLoS Negl. Trop. Dis. 10 (3), e0003895.
Hubadillah, S.K., Othman, M.H.D., Harun, Z., Ismail, A.F., Rahman, M.A., Jaafar, J., 2017. A novel green ceramic hollow fiber membrane (CHFM) derived from rice husk ash as combined adsorbent-separator for efficient heavy metals removal. Ceram. Int. 43 (5), 4716–4720.
Ismail, A.F., Lau, W., Emadzadeh, D., Moslehyani, A., 2013. The Effect of SPEEK Additive on Polyethersulfonenanofiltration Membrane for Dye Removal.
Issariyakul, T., Kulkarni, M.G., Dalai, A.K., Bakhshi, N.N., 2007. Production of biodiesel from waste fryer grease using mixed methanol/ethanol system. Fuel Process. Technol. 88 (5), 429–436.
Jairath, J., 2010. Advocacy of Water Scarcity: Leakages in the Argument. The Limits to Scarcity: Contesting the Politics of Allocation, pp. 215–232.
Kuvarega, A.T., Khumalo, N., Dlamini, D., Mamba, B.B., 2018. Polysulfone/N,Pd co-doped TiO2 composite membranes for photocatalytic dye degradation. Separ. Purif. Technol. 191 (Suppl. C), 122–133.
Loehr, R.C., Navarra Jr., C.T.D., 1969. Grease removal at a municipal treatment facility. J. Water Pollut. Cont. Fed. R142–R154.
Lyon, G.S., Stein, E.D., 2009. How effective has the Clean Water Act been at reducing pollutant mass emissions to the Southern California Bight over the past 35 years? Environ. Monit. Assess. 154 (1), 413–426.
Martínez, F., López-Muñoz, M.J., Aguado, J., Melero, J.A., Arsuaga, J., Sotto, A., Molina, R., Segura, Y., Pariente, M.I., Revilla, A., Cerro, L., Carenas, G., 2013. Coupling membrane separation and photocatalytic oxidation processes for the degradation of pharmaceutical pollutants. Water Res. 47 (15), 5647–5658.
McInerney, P., 2009. Toward a critical pedagogy of engagement for alienated youth: insights from Freire and school-based research. Crit. Stud. Educ. 50 (1), 23–35.
Mekonnen, M.M., Hoekstra, A.Y., 2016. Four billion people facing severe water scarcity. Sci. Adv. 2 (2), e1500323.
Mobaraki, M., Ismail, A.F., Moslehyani, A., 2015. Taguchi Experimental Design of Oily Wastewater Treatment in Photocatalytic Membrane Reactor Hybrid Process.
Mobaraki, M., Ismail, A.F., Yusof, N., Moslehyani, A., 2016. Taguchi optimization for nanocomposite PVDF ultrafiltration membrane for oily water treatment.
Molinari, R., Palmisano, L., 2005. Water Encyclopedia. John Wiley & Sons, Inc.
Molinari, R., Pirillo, F., Falco, M., Loddo, V., Palmisano, L., 2004. Photocatalytic degradation of dyes by using a membrane reactor. Chem. Eng. Process Process Intensif. 43 (9), 1103–1114.
Molinari, R., Pirillo, F., Loddo, V., Palmisano, L., 2006. Heterogeneous photocatalytic degradation of pharmaceuticals in water by using polycrystalline TiO2 and a nanofiltration membrane reactor. Catal. Today 118 (1), 205–213.
Moosa, A., Shu, H., Sarachana, T., Hu, V.W., 2017. Are endocrine disrupting compounds environmental risk factors for autism spectrum disorder? Horm. Behav. In Press.
Moslehyani, A., Ismail, A.F., 2013. Effect of Silver ion Exchange Halloysite Nanotubes on the Performance of Polyethersulfone Mixed Matrix Membrane for Bacterial Removal.
Moslehyani, A., Ismail, A., Othman, M., Isloor, A.M., 2015d. Novel hybrid photocatalytic reactor-UF nanocomposite membrane system for bilge water degradation and separation. RSC Adv. 5 (56), 45331–45340.
Moslehyani, A., Ismail, A., Othman, M., Matsuura, T., 2015b. Design and performance study of hybrid photocatalytic reactor-PVDF/MWCNT nanocomposite membrane system for treatment of petroleum refinery wastewater. Desalination 363, 99–111.

Moslehyani, A., Ismail, A., Othman, M., Matsuura, T., 2015c. Hydrocarbon degradation and separation of bilge water via a novel TiO 2-HNTs/PVDF-based photocatalytic membrane reactor (PMR). RSC Adv. 5 (19), 14147−14155.

Moslehyani, A., Ismail, A.F., Othman, M.H.D., Matsuura, T., 2015a. Design and performance study of hybrid photocatalytic reactor-PVDF/MWCNT nanocomposite membrane system for treatment of petroleum refinery wastewater. Desalination 363 (Suppl. C), 99−111.

Moslehyani, A., Mobaraki, M., Matsuura, T., Ismail, A., Othman, M., Chowdhury, M., 2016. Novel green hybrid processes for oily water photooxidation and purification from merchant ship. Desalination 391, 98−104.

Mozia, S., Tomaszewska, M., Morawski, A.W., 2005. A new photocatalytic membrane reactor (PMR) for removal of azo-dye Acid Red 18 from water. Appl. Catal. B Environ. 59 (1), 131−137.

Mozia, S., Toyoda, M., Tsumura, T., Inagaki, M., Morawski, A.W., 2007. Comparison of effectiveness of methylene blue decomposition using pristine and carbon-coated TiO2 in a photocatalytic membrane reactor. Desalination 212 (1), 141−151.

Ong, C.S., Lau, W.J., Goh, P.S., Ng, B.C., Ismail, A.F., 2014. Investigation of submerged membrane photocatalytic reactor (sMPR) operating parameters during oily wastewater treatment process. Desalination 353 (Suppl. C), 48−56.

Organization, W.H., 2015. Investing to Overcome the Global Impact of Neglected Tropical Diseases: Third WHO Report on Neglected Tropical Diseases 2015. World Health Organization.

Pastrana-Martínez, L.M., Morales-Torres, S., Figueiredo, J.L., Faria, J.L., Silva, A.M.T., 2015. Graphene oxide based ultrafiltration membranes for photocatalytic degradation of organic pollutants in salty water. Water Res. 77 (Suppl. C), 179−190.

Qu, X., Alvarez, P.J., Li, Q., 2013. Applications of nanotechnology in water and wastewater treatment. Water Res. 47 (12), 3931−3946.

Ridoutt, B.G., Pfister, S., 2010. A revised approach to water footprinting to make transparent the impacts of consumption and production on global freshwater scarcity. Global Environ. Change 20 (1), 113−120.

Rincón, G.J., La Motta, E.J., 2014. Simultaneous removal of oil and grease, and heavy metals from artificial bilge water using electro-coagulation/flotation. J. Environ. Manag. 144, 42−50.

Sopajaree, K., Qasim, S.A., Basak, S., Rajeshwar, K., 1999. An integrated flow reactor-membrane filtration system for heterogeneous photocatalysis. Part II: experiments on the ultrafiltration unit and combined operation. J. Appl. Electrochem. 29 (9), 1111−1118.

Yang, S., Gu, J.-S., Yu, H.-Y., Zhou, J., Li, S.-F., Wu, X.-M., Wang, L., 2011. Polypropylene membrane surface modification by RAFT grafting polymerization and TiO2 photocatalysts immobilization for phenol decomposition in a photocatalytic membrane reactor. Separ. Purif. Technol. 83 (Suppl. C), 157−165.

Zhang, H., Quan, X., Chen, S., Zhao, H., Zhao, Y., 2006. Fabrication of photocatalytic membrane and evaluation its efficiency in removal of organic pollutants from water. Separ. Purif. Technol. 50 (2), 147−155.

Zhang, J., Wang, L., Zhang, G., Wang, Z., Xu, L., Fan, Z., 2013. Influence of azo dye-TiO2 interactions on the filtration performance in a hybrid photocatalysis/ultrafiltration process. J. Colloid Interface Sci. 389 (1), 273−283.

CHAPTER 8

PMRs in Photocatalytic Synthesis of Organic Compounds

Raffaele Molinari, Pietro Argurio
University of Calabria, Rende (CS), Italy

8.1 Introduction. General Overview of Photocatalytic Membrane Reactors in Photocatalytic Synthesis of Organic Compounds

Traditional industrial processes employed for making chemical products are becoming unsustainable in terms of resources and environmental impact (Molinari et al., 2010, 2013; Palmisano et al., 2007a; Li et al., 2011; Herrmann et al., 2007). In particular, although in the last decades the chemical industries have made great improvements in terms of efficiency of their processes, the need to identify renewable feedstock, reduce the use of toxic or scarce amount of catalysts, and the generation of hazardous waste effluents remain some of the unsolved problems that require the development of new sustainable approaches by the scientific community.

The application of heterogeneous photocatalysis (PC) to organic synthesis has attracted high interests to develop, in perspective, environmentally benign synthetic processes (Molinari et al., 2015a). Heterogeneous PC is an advanced oxidation process (AOP) based on the use of light and a solid semiconductor (the photocatalyst) to generate oxidizing and reducing species. The photonic activation mode of the photocatalyst, which replaces the thermal activation, represents the main difference of PC compared with conventional catalysis (Herrmann, 2005). The electronic structure of a semiconductor is characterized by a valence band (VB) and a conduction band (CB) separated by a bandgap of energy. When photons with energy ($h\nu$) equal to or higher than the bandgap energy (Eg) excite the semiconductor, electron (e^-)—hole (h^+) couples are formed by promotion from VB to CB.

Because of the highly unselective reactions involved in the photocatalytic processes, they have been widely applied in processes in which complete oxidation of organic and inorganic pollutants to innocuous substances have been carried out for remediating aqueous or gaseous effluents (Wang et al., 2016; Ozawa et al., 2016; Konstantinou and Albanis, 2004).

Current Trends and Future Developments on (Bio-) Membranes. https://doi.org/10.1016/B978-0-12-813549-5.00008-6

In the last decade, some studies have been carried out on the application of PC for synthesis. They demonstrated that high selectivity could be obtained in photooxidation and photoreduction processes in comparison with conventional methods by appropriate selection or modification of some photocatalytic parameters, such as the semiconductor surface or the excitation wavelength. In this context, the photocatalytic oxidation of organic compounds has been largely studied because the most common semiconductors have VB edges more positive than oxidation potentials of most organic functional groups (Gazi and Ananthakrishnan, 2011). Photocatalytic reductions are less frequently found because the reducing power of a CB electron is significantly lower than the oxidizing power of a VB hole (Palmisano et al., 2010; Flores et al., 2007).

Important characteristics of PC, making it in agreement with the green chemistry principles, consist of (1) use of greener and safer photocatalysts; (2) possibility to use mild oxidant/reducing agents; (3) possibility to work under mild reaction conditions; (4) requirement of very few auxiliary additives; (5) possibility to use renewable solar energy.

An important aspect to be considered in view of large-scale applications of photocatalytic processes is the recovery of the photocatalyst from the reaction environment. Photocatalytic membrane reactors (PMRs), hybrid systems obtained by coupling PC with a membrane separation, represent a very promising approach to obtain this requirement (Azrague et al., 2007; Molinari et al., 2000; Tang and Chen, 2004; Chin et al., 2007). PMRs improve the potentialities of classical photoreactors and those of membrane processes (separation at molecular level) giving a synergy for both technologies, thus minimizing environmental and economical impacts (Molinari et al., 2008, 2009). The membrane permits to operate in continuous mode in systems in which the recovery of the photocatalyst (immobilized or in suspension), the reaction and the separation of the products simultaneously occur. This approach avoids in some cases the formation of by-products, resulting competitive with other separation technologies in terms of material recovery, energy efficiency, and reduction of the environmental impact (Molinari et al., 2001). Modularity and easy scale-up are some other potential advantages of PMRs.

Despite the great potentiality of the photocatalytic process and the important advantages that can be achieved by its coupling with a membrane separation system, the research in the field of photocatalytic synthesis in PMRs still remains insufficient.

In this chapter, some results reported in the literature on the use of PMRs for partial or total photocatalytic oxidations/reductions are discussed.

One example of oxidation reaction carried out in a PMR is the one-step conversion of benzene to phenol, showing the possibility to use a photocatalytic reaction coupled to

product separation by means of a membrane contactor (MC) (Molinari et al., 2009). In this case the choice of a membrane permeable to phenol is crucial because phenol is more reactive than benzene and its permeation from the reacting solution avoids its oxidative degradation.

A similar approach has been used in the production of vanillin (VA) by the partial oxidation of ferulic acid (Camera-Roda et al., 2013). In this case the utilization of a highly selective pervaporation (PV) membrane allows the continuous recovery of VA.

One of the first examples of PMR application in reduction reaction for synthesis is represented by the production of phenylethanol, which is a compound of wide industrial interest, by the photocatalytic transfer hydrogenation of acetophenone (Molinari et al., 2015b). The results demonstrated that the efficiency of the photocatalytic reaction was improved by using a membrane reactor compared with a batch reactor. This goal was achieved, thanks to the prompt removal of the produced phenylethanol from the reacting environment, because of its extraction into the organic extracting phase.

Other interesting examples of PMR application for synthetic purposes are represented by the production of methanol by CO_2 reduction (Barton et al., 2008; Sekizawa et al., 2013) and the production of ammonia by nitrite reduction (Ranjit et al., 1995; Pandikumar et al., 2012).

Common benefits of the aforementioned integrated processes are the complete maintaining of the photocatalyst in the reacting environment, the separation at high purification degree of the product simultaneously to the reaction, thus enhancing system productivity. In these systems, the choice of the membrane module configuration is mainly determined by the type of photocatalytic reaction and the many roles membrane can assume, such as photocatalyst recovery, separation of the products, rejection of the substrate, etc. Besides, when the photocatalytic process is used as a synthetic pathway, the use of an appropriate membrane (Coronas and Santamaria, 1999; Armor, 1998) can allow the selective separation of the product minimizing its degradation.

In the following the aforementioned processes will be described and discussed with greater details.

8.2 Operating Variables Influencing Product Quality in Photocatalytic Membrane Reactors

The selection of the appropriate operative conditions is of critical importance to obtain a good performance of the PMR finalized to practical application. Thus, when developing a PMR, it is important to take into account some parameters that influence the performance of the system.

8.2.1 Photocatalyst Concentration

This parameter represents one of the main operating variables influencing PMRs performance. By working under a true heterogeneous catalytic regime, in which the photonic excitation of the photocatalyst surface represents the initial step of the process activation, the rate of the reaction is proportional to the amount of photocatalyst. However, above a certain level of mass photocatalyst, the rate of reaction reaches a plateau condition that corresponds to the maximum amount of photocatalyst in which all the surface-active sites are illuminated and occupied by the substrate. Besides, system reactivity also increases with photocatalyst amount, so that above a certain value overreaction could happen, giving an undesired conversion of the desired product. Moreover, photocatalyst aggregation and light scattering phenomena also increase with photocatalyst amount, resulting in lower system efficiency. Then, to avoid excess of photocatalyst and to ensure satisfactory reaction efficiency, the optimum amount of photocatalyst must be chosen.

8.2.2 Substrate Concentration

In general, the rate of reaction increases with substrate concentration to reach a maximum corresponding to the saturation conditions, i.e., the conditions in which all the active sites of the photocatalyst are occupied by substrate molecules. Then, it can be affirmed that the optimum amount of photocatalyst is also a function of substrate concentration. By considering the specificity of using the photocatalytic process for synthesis, maintaining high concentration of the substrate is important to favor its adsorption on the photocatalyst with respect to the other chemicals contained in the reacting environment, including the desired product. So, Molinari et al. (2009, 2015b), when studied both phenol production by partial oxidation of benzene and phenylethanol production by acetophenone hydrogenation, found that the PMR system in which the substrate concentration into the reacting environment was maintained high (close to the saturation conditions) gives the best performance. An important aspect to take into account when considering the concentration of a liquid substrate is represented by its solubility into the reacting environment. Generally, working above the solubility limit generates microdroplets of the substrate, thus decreasing the concentration of the free reacting molecules.

8.2.3 Operating pH

The operating pH largely influences two fundamental steps of the photocatalytic process: adsorption of the substrate and desorption of the desired product. Several studies

(Konstantinou and Albanis, 2004; Bekkouche et al., 2004) reported that under acidic conditions, the TiO_2 surface is positively charged, whereas in alkaline media, it is negatively charged according to the following equilibrium:

$$\text{Surface-TiOH} + H^+ \leftrightarrows \text{Surface-TiOH}_2^+$$

$$\text{Surface-TiOH} + OH^- \leftrightarrows \text{Surface-TiO}^- + H_2O$$

Depending on the substrates, an increase of pH can determine a positive or negative effect on reaction rate. Anionic species are lesser or more adsorbed at alkaline or acidic pH, respectively, owing to a different ionization state of the photocatalyst surface, as reported by Bekkouche et al. (2004) in a study of adsorption of phenol on titanium dioxide. So, in the case of benzene oxidation to phenol by using TiO_2 as the photocatalyst, alkaline pH allowed to obtain a higher phenol production caused by a lower phenol adsorption on the photocatalyst surface which reduced its degradation. Indeed, at alkaline pH, both TiO_2 and phenol (dissociated as phenolate) are negatively charged, that is the condition favoring desorption.

The operating pH also influences the permeation of substrates and products across the membrane. In particular, depending on the pH of the reacting environment, the molecules of the substrates and products could change their state from not dissociated, able to permeate, e.g., across a hydrophobic membrane, to dissociated, unable to permeate across the membrane. On this aspect, Camera-Roda et al. (2014) demonstrated that the permeation of VA across a PV membrane is affected by pH. In fact, permeation of VA is relatively high if VA is not dissociated ($pH < 6.5$), but it decreases at $pH = 7.9$ when VA is partially dissociated and becomes particularly low when VA is completely dissociated at $pH = 10.3$.

8.2.4 Wavelength and Light Intensity

The step that initiates a photocatalytic process is irradiation of the photocatalyst surface with photons with energy ($h\nu$) equal to or higher than Eg. Several authors studied the influence of wavelength (λ) and intensity of the light source and the absorption spectrum of the photocatalyst on the rate of the photocatalytic reaction (Herrmann, 2005; Emeline et al., 2000; Brosillon et al., 2008). It was found that effective activation of the photocatalyst takes place only with photons that have a λ smaller than or equal to the absorption edge of the photocatalyst and this phenomenon is predominant at low light intensity, whereas a recombination of electron–hole pairs was supposed to occur at higher light intensity.

8.2.5 Other Species

The presence of other species in the reaction environment can give positive or negative effects on the rate of the photocatalytic process depending on the reaction mechanism.

Some studies (Palmisano et al., 2007b; Zhang et al., 2006) reported the influence of dissolved metal ions on the photocatalytic reactions. In particular, metal cations, when they are used in their higher oxidation state, can act as photoelectron acceptors preventing the charge carrier recombination as schematized by the following reaction:

$$M^{n+} + e^{-} \rightarrow M^{(n-1)+}$$

Moreover, the reduced species $M^{(n-1)+}$ can react with H_2O_2 (photogenerated in the reaction ambient) to give additional $^{\bullet}OH$ by photo-Fenton reaction according to the following general expression:

$$M^{(n-1)+} + H_2O_2 \rightarrow M^{n+} + {}^{\bullet}OH + OH^{-}.$$

8.2.6 Membrane Properties

As previously reported, the main purpose in combining a membrane process with a photocatalytic reaction is the confinement of the photocatalyst into the reacting environment. Moreover, when PMRs are applied for synthesis, the specific role of the membrane is the separation of the product(s) from the reaction environment. Thus it is important to choose a membrane characterized by a high permeability with respect to the desired product, permitting its prompt and efficient selective removal and recovery. So, in the case of benzene oxidation to phenol, in their first published work on this topic, Molinari et al. (2006) demonstrated that process efficiency, quantified in terms of substrate and oxidant conversion to phenol, increases with the contact angle, i.e., the hydrophobic character of the membrane. Similarly, Augugliaro et al. (2012), studying the photocatalytic oxidation of trans-ferulic acid to VA by coupling PC with a PV step, evidenced that the choice of a nonporous PEBAX 2533 (trade name of polyether-polyamide block copolymers) membrane, characterized by a high permeability toward VA (transmembrane flux about 3.31 $g_{VA}\ h^{-1}\ m^{-2}$), permitted to remove the product from the irradiated suspension avoiding its subsequent oxidation, thus increasing process selectivity. In this system, another important parameter influencing its performance is represented by the membrane thickness. Indeed, Camera-Roda et al. (2014), concentrating its efforts on VA pervaporation with PEBAX membranes, showed that a viable method to enhance the enrichment factor of VA (VA concentration in the condensed permeate/VA concentration in the feed) is to increase membrane thickness because the resistance to VA permeation remains low while the resistance to water permeation increases.

8.3 Partial Oxidation of Organic Compounds in Photocatalytic Membrane Reactors

The aim of this section is to describe the results present in literature on the use of a membrane photoreactor for organic synthesis, developing hybrid systems in which the photocatalytic reaction and the separation of the product of interest occur in one step.

8.3.1 Benzene Hydroxylation to Phenol

Phenol is an important chemical intermediate for the synthesis of petrochemicals, agrochemicals, and plastics (Molinari et al., 2012; Liu et al., 2006). Its market demand exceeds 7 Mt/year. Today, more than 90% of the worldwide phenol production is obtained by the three-step cumene process, also called the Kellogg Brown & Root (KBR) phenol process. The high and damaging ecological impact, the production of an explosive intermediate to manage (cumene hydroperoxide), the large amount of acetone produced as by-product, and the multistep character represent some important limitations of the cumene process (Molinari et al., 2015c; Niwa et al., 2002), resulting into the need to develop alternative processes. Among the various routes, phenol production by one-step direct benzene oxidation represents an attractive alternative pathway, and many studies have been performed in the last years with the aim to develop more efficient and environmentally benign processes (Molinari et al., 2006; Liptàkova et al., 2004; Yamaguchi et al., 2005; Dong et al., 2005). In this context, the photocatalytic approach is very interesting because it is a "green process" where light and a photocatalyst are used to generate $OH^{\bullet}$ radicals to oxidize benzene (Shimizu et al., 2004; Park and Choi, 2005).

Benzene hydroxylation to phenol is a little selective because phenol is more reactive than benzene and by-products can be formed (Bellussi and Perego, 2000; Bianchi et al., 2000, 2007; Molinari and Poerio, 2010; Itoh et al., 2003; Cai et al., 2005; Wang et al., 2010a,b). The use of a membrane system, with high phenol permeability and complete rejection to the photocatalyst, seems a useful solution to avoid this limitation. On the basis of this, Molinari et al. (2009) studied the direct benzene conversion to phenol in a PMR using TiO_2 as suspended photocatalyst.

Preliminary experiments in batch (in the absence of the membrane) were performed for determining the influence of some operating parameters (pH, photocatalyst concentration, light intensity, etc.) on the efficiency of the photocatalytic reaction. The results showed that phenol production depends on the little solubilized amount of substrate, evidencing the need to use a system that provides benzene continuously to maintain a constant concentration in the aqueous ambient (the biphasic MC). The photocatalytic reaction rate increased with photocatalyst concentration, as shown in Fig. 8.1. A quick photodegradation of phenol was observed after 180 min of reaction time by operating with

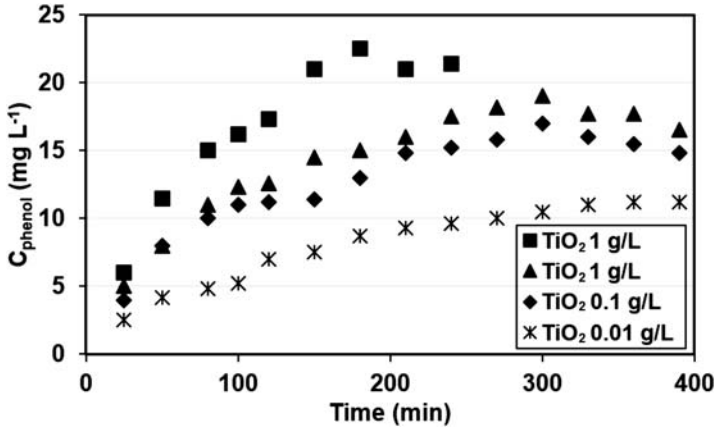

Figure 8.1
Phenol concentrations versus the time at different photocatalyst amount (pH = 5.5, intensity = 6.0 mW cm^{-2}, T = 25°C) (Elaborated from Molinari et al., 2009).

1.0 g L^{-1} TiO_2 concentration. Thus, it is preferable to use a lower photocatalyst concentration, which also limits the fouling phenomena. Regarding the influence of the operating pH on system performance, obtained results evidenced that a higher phenol concentration (20.2 vs 15.0 mg L^{-1}) was obtained by working under alkaline pH with respect to acidic one. This trend was motivated considering that at alkaline pH, both TiO_2 and phenol (dissociated as phenolate) are negatively charged, so a lower phenol adsorption on the photocatalyst surface took place thus reducing its degradation.

From these results a PMR setup was developed. In the proposed PMR, Fig. 8.2, phenol separation (box B) was performed simultaneously to the photocatalytic reaction (box A) by using benzene as both reactant and extraction solvent and a polypropylene membrane to separate the organic phase from the aqueous reacting environment. Benzene permeates through the membrane and solubilizes in the aqueous phase, where its photocatalytic conversion to phenol takes place. The produced phenol diffuses into the organic phase (benzene), where it is protected by successive oxidations to some by-products such as benzoquinone, hydroquinone, and other oxidized molecules.

Some experiments in the PMR were carried out investigating the effects of the pH of the aqueous phase on the efficiency of the overall process (PC plus membrane permeation). The results evidenced that pH reduction from 5.5 to 3.1 does not significantly influence phenol flux (1.27 mmol h^{-1} m^{-2} vs 1.06 mmol h^{-1} m^{-2} at pH 5.5). Nevertheless, the most acidic condition permitted to obtain a lower formation and extraction of oxidation by-products, allowing to control process selectivity.

To enhance the performance of the system, photocatalytic experiments with ions (Fe^{3+}, Cu^{2+}, and V^{3+}) dissolved into the organic phase were carried out. The results showed a positive effect of the presence of iron(III) ion with a phenol flux in the organic phase

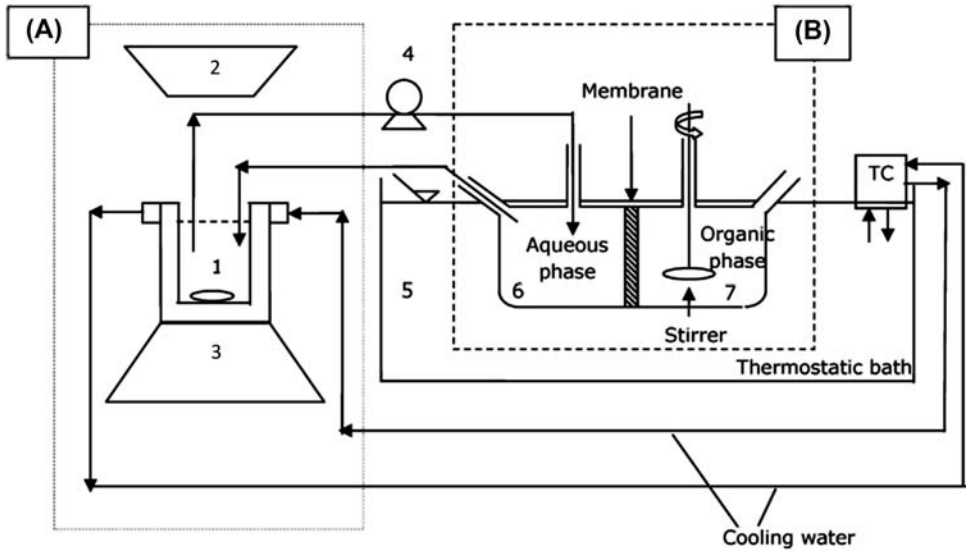

Figure 8.2
Scheme of the experimental setup: photocatalytic reactor (A) coupled with the membrane contactor (B) (1: batch reactor, 2: UV lamp, 3: magnetic stirrer, 4: peristaltic pump, 5: thermostatic bath, 6: aqueous phase, 7: organic phase, *TC*, temperature controller) (Molinari et al., 2009).

almost two times greater than those measured without salts, also as a consequence of the enhanced ionic strength (Ku et al., 2004; Dey et al., 2004).

8.3.2 Conversion of Aromatic Alcohols Into the Corresponding Aldehydes and Ferulic Acid Into Vanillin

Camera-Roda et al. (2011) photooxidized different organic alcohols, such as benzyl alcohol and 4-methoxy benzyl alcohol, into the corresponding aldehydes. The PMR system is schematically reported in Fig. 8.3. Heterogeneous PC and PV were coupled by recirculation of the retentate in a closed loop from the PV modules to the photoreactor and back to PV. The permeate coming from the PV module, obtained by condensation of the permeated vapors, represents the product stream. Both, home prepared and commercial TiO_2, were used as photocatalysts (Camera-Roda et al., 2011).

The results obtained in the integrated photocatalytic/PV system, reported in Table 8.1, compared with the ones obtained operating in batch without the membrane, evidenced that coupling the photocatalytic oxidation with the PV unit permitted to obtain enhanced yield (produced moles of benzaldehyde/reacted moles of benzyl alcohol) and conversion (reacted moles of benzyl alcohol/initial moles of benzyl alcohol). This result was ascribed to the continuous recovery of the desired product despite a little decrease of the selectivity.

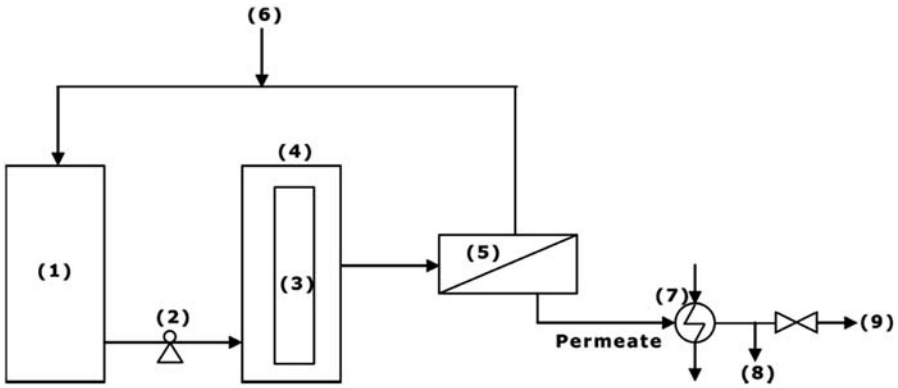

Figure 8.3

Scheme of the photocatalytic pervaporation setup: (1) thermostated tank; (2) circulation pump; (3) UV lamp; (4) annular photocatalytic reactor; (5) pervaporation unit; (6) optional feed makeup; (7) liquid nitrogen trap; (8) product stream; (9) vacuum incondensable. *Elaborated from Camera-Roda et al., 2011*.

Table 8.1: Comparison of the results obtained with and without pervaporation (PV) during the photocatalytic conversion of benzyl alcohol to benzaldehyde.

Operating Mode	Conversion (%)	Selectivity (%)	Yield (%)
Photocatalysis without PV	≈22	≈18	≈3.9
Photocatalysis with PV	≈35	≈17	≈6

Operating conditions: photocatalyst = TiO_2, photocatalyst concentration = 0.27 g L^{-1}, temperature = 60 °C, irradiation time = 8 h.

Data from Camera-Roda, G., Santarelli, F., Augugliaro, V., Loddo, V., Palmisano, G., Palmisano, L., Yurdakal, S., 2011. Photocatalytic process intensification by coupling with pervaporation. Catal. Today Off. 161, 209–213.

The higher purity of the recovered aldehyde, the complete removal of the heterogeneous photocatalyst, and the possibility to operate under mild operative conditions represent the main advantages obtained, thanks to the coupling between heterogeneous PC and PV membranes.

The same approach was employed to prepare VA by partial oxidation of ferulic acid. VA is one of the most important aromas with an annual world production of about 12,000 t (Walton et al., 2003; Korthou and Verpoorte, 2007; Rao and Ravishankar, 2000), and it is widely utilized as a flavoring or functional ingredient in food, cosmetic, pharmaceutical, and nutraceutical products (Sinha et al., 2008). Recently, some authors (Camera-Roda et al., 2011, 2013; Augugliaro et al., 2012) demonstrated that VA can be obtained by the photocatalytic reaction of some precursors, also of natural origin. However, VA is easily

degraded into other chemicals. To limit this problem, some researchers (Camera-Roda et al., 2011, 2013; Barton et al., 2008; Camera Roda and Santarelli, 2012; Böddeker et al., 1990, 1993, 1997) studied a hybrid system, in which the photocatalytic reaction was coupled with a membrane separation in a PV unit, so that the produced VA was promptly recovered during the synthesis, thus preventing its degradation.

Augugliaro et al. (Augugliaro et al., 2012) studied the photocatalytic oxidation of trans-ferulic acid, isoeugenol, eugenol, or vanillyl alcohol to produce VA in aqueous medium by using different TiO_2 samples as photocatalysts. Photocatalytic tests were carried out in two different batch systems: a cylindrical and an annular photoreactor (APR). Selectivity to VA, ranging from 1.4 to 21 mol%, was obtained by operating at room temperature. At the end of the photocatalytic runs conducted in the APR, VA was recovered by PV using a nonporous PEBAX 2533 membrane. This system allowed also the complete maintaining of the heterogeneous photocatalyst into the aqueous reacting environment. Besides, it was demonstrated that PEBAX 2533 membrane was very selective toward VA and, in the tested PC-PV system, the continuous removal of the produced VA from the irradiated suspension avoided its subsequent oxidation, thus increasing the process selectivity. Moreover, in the proposed system, the permeated VA vapors were recovered as crystals with a high degree of purity (99.8%) by freezing downstream in a liquid nitrogen trap, without the necessity to use complex extraction and recrystallization procedures.

In a recent work, Camera-Roda et al. (2014) studied the possibility to enhance the VA yield by improving the membrane performances in the PV reactor (in terms of enrichment factors and permeate flux). By studying VA pervaporation with PEBAX membrane, they found that a viable method to enhance the enrichment factor of VA is to increase the membrane thickness. Indeed, membrane resistance to water permeation increases with membrane thickness, while the resistance to VA permeation remains low. The enrichment factor can be further increased by raising the temperature, by taking advantage of the additional positive effect of the increased VA flux. Moreover, VA permeation across the PEBAX membrane was affected by the operating pH. In particular, it was found that VA permeation is relatively high at $pH < 6.5$ because VA is not dissociated, but it decreases at $pH = 7.9$ when VA is partially dissociated and becomes particularly low when VA is completely dissociated at $pH = 10.3$. However, the low volatility of the substrate (ferulic acid), and of most of the by-products, is the real reason for their very high rejection.

Summarizing, the results described in this section clearly indicate that production of some types of organics by photocatalytic partial oxidation can be highly enhanced by coupling a PV unit to the photocatalytic reactor, where the PV directly recovers the desired product from the reacting environment, thus limiting any further degradation.

8.4 Reduction Reactions in Photocatalytic Membrane Reactors

8.4.1 Photocatalytic Hydrogenation of Ketones

The feasibility to conduct reduction reactions in a PMR was studied very recently by Molinari et al. (2015b). The photocatalytic hydrogenation of acetophenone to phenylethanol was the tested reaction, conducted both under UV and visible (Vis) light. Acetophenone was chosen as a model substrate for hydrogenation of aromatic ketones (Kohtani et al., 2010) because its reduction product, phenylethanol, is used as a building block for the synthesis of bioactive compounds such as agrochemicals, pharmaceuticals, and natural products (Molinari et al., 2016).

To obtain cheaper and green process, water was tested as solvent and formic acid (FA) as hydrogen and electron donor. FA is converted into CO_2 and H_2 in the reacting environment making the reaction irreversible (Imamura et al., 2011; Wehbe et al., 2009; Molinari et al., 2017).

The equation of the tested reaction is

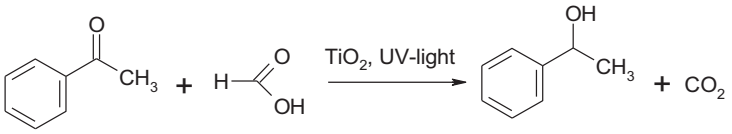

Some preliminary tests, carried out in a batch photoreactor to study the influence of some operating conditions on system performances, showed the best results in terms of phenylethanol yield (4.7%) under the following conditions: (1) 1.5 g L^{-1} of TiO_2; (2) pH = 7.5; (3) [HCOOH] = 1.97 M.

Once the optimal chemical conditions are defined, acetophenone reduction was performed in the PMR, which is schematized in Fig. 8.4. In this system, obtained by coupling an APR with an MC, the photocatalytic and the separation processes simultaneously occur. The aqueous reacting phase was withdrawn from the APR to the MC, thanks to the action of a peristaltic pump. Then the aqueous phase comes back in the APR by gravity. The APR volume was 500 mL. The MC, immersed in a thermostatic bath at the same temperature of the photoreactor, was constituted by two compartment cells (130 mL each one) separated by a flat sheet polypropylene membrane (membrane surface area 28.3 cm^2). One compartment contains the aqueous reacting phase coming from the photoreactor, while the other contains an organic extracting phase mechanically stirred by a motor. The overall volume of the aqueous reacting phase was 725 mL.

During the photocatalytic test in the PMR, the phenylethanol produced in the aqueous reacting phase was extracted into the organic extracting phase, where it was protected by successive over hydrogenation.

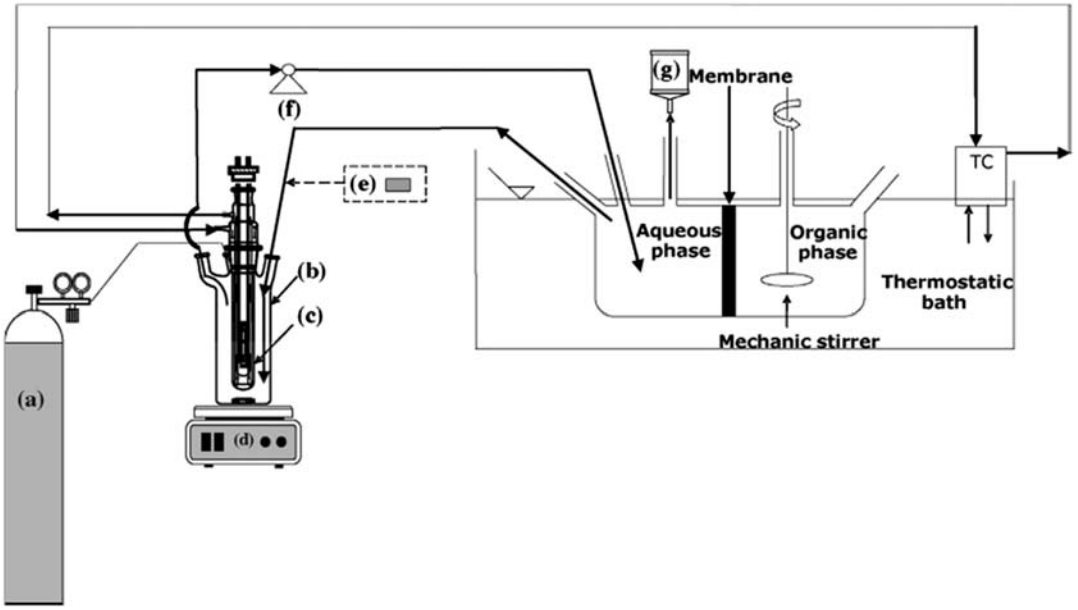

Figure 8.4
Scheme of the membrane contactor integrated with the annular photoreactor: *a*, argon cylinder; *b*, annular photoreactor; *c*, medium pressure Hg lamp with cooling jacket; *d*, magnetic stirrer; *e*, optional syringe pump for substrate feeding; *f*, peristaltic pump; *g*, degassing system; *TC*, temperature controller (Molinari et al., 2015b).

Obtained results evidenced that use of the PMR improves the efficiency of the photocatalytic reaction compared with the batch reactor (i.e., the APR without the MC) operated under the same experimental conditions. In particular, higher yield, produced amount of phenylethanol (276.20 vs 184.23 mmol), and overall phenol productivity (4.44 vs 2.96 $mg_{prod}\ g_{cat}^{-1}\ h^{-1}$) were obtained in the PMR. This behavior was obtained because of the continuous extraction of the produced phenylethanol from the aqueous reacting phase to the organic phase, which takes place simultaneously to the reaction. Thus the reaction was shifted forward to the product. Furthermore, subsequent reduction reaction of the extracted product was avoided enhancing the selectivity of the overall process.

During the experimental tests carried out in the PMR under UV light, the influence of different substrate feeding mode on system performance was investigated to improve the phenylethanol productivity and its extraction percentage into the organic extracting phase. Better results were obtained by using acetophenone as both substrate and organic phase (276.20 μmol of phenylethanol generated, 4.44 $mg_{prod}\ g_{cat}^{-1}\ h^{-1}$ phenylethanol productivity, 21.91% extraction percentage). This system permitted to obtain both the best substrate solubilization in the reacting phase and the best product extraction in the organic phase (Fig. 8.5).

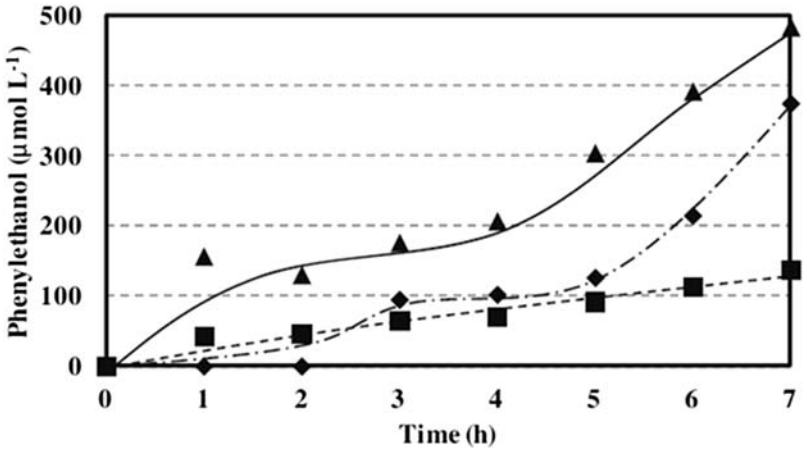

Figure 8.5

Phenylethanol concentration in the organic phase versus time by using the membrane photoreactor with different substrate feeding mode: syringe pump (◆), acetophenone dissolved in n-heptane (■), acetophenone as reactant and extractant (▲) (Molinari et al., 2015b).

Because solar light contains only 5% of UV radiation, to obtain a greener process the possibility to use Vis light as radiation source was considered. The results evidenced that bare TiO_2 was not active under Vis light irradiation. Metal doping was tested to activate TiO_2 under Vis light. In particular, TiO_2 was doped with palladium by deposition precipitation method, and the obtained Pd/TiO_2 was tested under Vis light. The Pd/TiO_2 was active under Vis light, producing a greater amount of phenylethanol (1371 μmol) and giving a productivity (22.02 $mg_{prod}\ g_{cat}^{-1}\ h^{-1}$) five times greater than that obtained by using the bare TiO_2 under UV light. Besides, the concentration of phenylethanol extracted into the organic phase increased linearly during the photocatalytic test (Fig. 8.6).

8.4.2 Photocatalytic Reduction of CO_2 to Methanol

One of the main causes of global climate change is greenhouse gas emission, mainly CO_2 (c. 36 Gt per year). Considering the necessity to reduce CO_2 emission into the environment and the need of obtaining new sustainable energy sources, in the last years, new greener technologies have been studied and developed, especially to convert CO_2 into useful chemical species and fuels (Roy et al., 2010; Dhakshinamoorthy et al., 2012).

Photocatalytic reduction of CO_2 to obtain methanol represents one of the most promising methods to be investigated. Indeed, it is a green process attractive from both economical and environmental points of view. Nevertheless, this technology presents some difficulties related to noneffective photocatalysts, low yield and poor selectivity. Photocatalyst immobilization into polymeric membrane and its use in a PMR can be an interesting and valid solution to adopt to overcome these limitations.

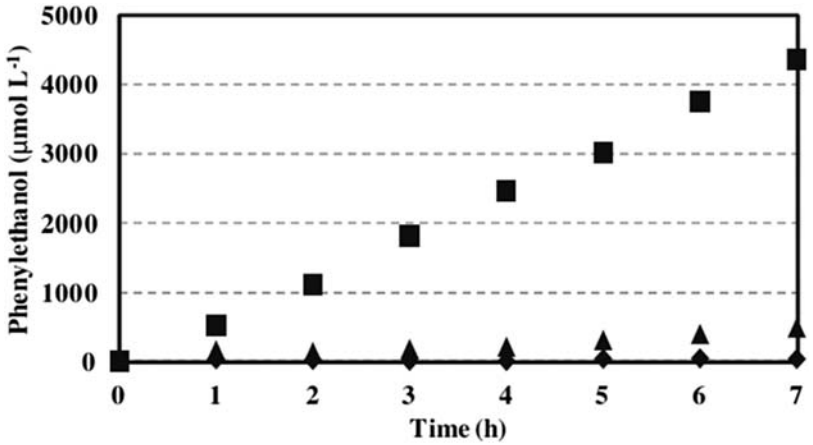

Figure 8.6

Phenylethanol extraction in the organic phase versus time by using bare TiO_2 (▲) and Pd/TiO_2 (■) under visible light and bare TiO_2 under UV light (◆) (Molinari et al., 2015b).

On the basis of this, very recently, Sellaro et al. (2016) tested the feasibility to perform the photocatalytic reduction of CO_2 in a continuous PMR operated under mild experimental conditions. Photocatalytic membranes were prepared by immobilizing bare TiO_2 into a Nafion matrix. After their characterization the photocatalytic membranes were tested for determining their photocatalytic efficiency. The photocatalytic tests were carried out under UV-Vis irradiation in liquid phase using water as the reducing agent. The photocatalytic membranes were placed into a flat sheet membrane module equipped with a quartz window for the irradiation. The module was continuously fed with a stream of CO_2 (modulated by a flow controller) and a water stream (fed by a high-performance liquid chromatography (HPLC) pump), maintaining a H_2O:CO_2 molar ratio equal to 5:1. The transmembrane pressure (TMP) was set at 2 bar. Fig. 8.7 reports a schematic diagram of the experimental apparatus.

Obtained results evidenced that the photocatalytic performances were strictly related to the photocatalyst distribution into the photocatalytic membrane rather than the photocatalyst content. Indeed, the higher methanol productivity was obtained by using the membrane with the best TiO_2 distribution. Neither CH_4 nor CO formation was observed. The main photoreduction product was methanol, with a productivity of 45 μmol $g_{TiO_2}^{-1}$ h^{-1} obtained under mild conditions. These results were obtained because of the use of the photocatalytic membrane, which allowed a continuous photoconversion of CO_2 to methanol avoiding its overreaction due to the continuous removal of the produced methanol from the reaction environment.

On the same topic, Cheng et al. (2016) proposed an optofluidic membrane microreactor, characterized by high surface area/volume ratio, enhanced photon and mass transport, and

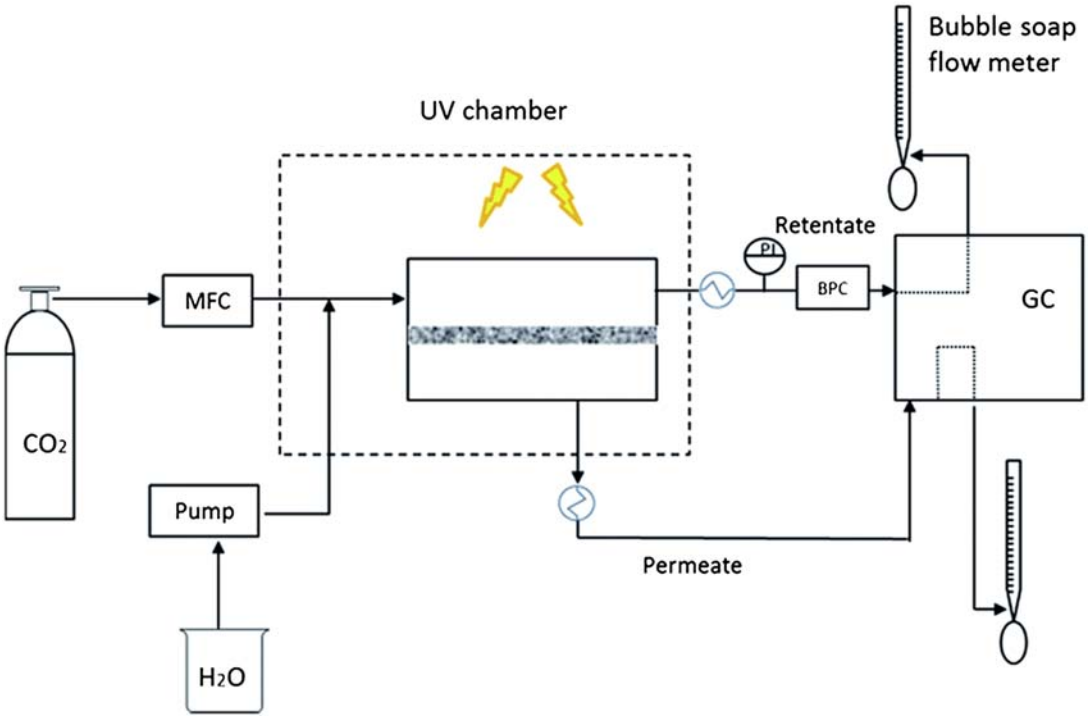

Figure 8.7
Schematic diagram of the experimental apparatus (Sellaro et al., 2016).

uniform light distribution for the photocatalytic reduction of CO_2 with liquid water. The schematization of the optofluidic membrane microreactor is shown in Fig. 8.8. In this system, two reaction microchambers (liquid and gas microchambers) are separated by a photocatalytic membrane, prepared via coating of TiO_2 onto a carbon paper followed by hydrophobic treatment by polytetrafluoroethylene (PTFE). The photocatalytic membrane obtained after the PTFE treatment was hydrophobic enough to prevent the water leakage from the liquid microchamber to the gas microchamber. During the photocatalytic tests, distilled water was fed by a pump into the liquid microchamber and CO_2 was supplied into the gas micro-chamber.. The liquid microchamber was irradiated to excite the electron–hole pairs in TiO_2. CO_2 molecules permeated across the membrane thus reaching the TiO_2 film, where they were reduced and reacted with water to generate hydrocarbon fuels.

The influence of different operating parameters such as the liquid water flow rate, the light intensity, and the photocatalyst loading on methanol yield was determined.

A maximum methanol yield of 111.0 μmol g_{cat}^{-1} h^{-1} was obtained at a flow rate of 25 mL min^{-1}, under the light intensity of 8 mW cm^{-2} and photocatalyst loading of

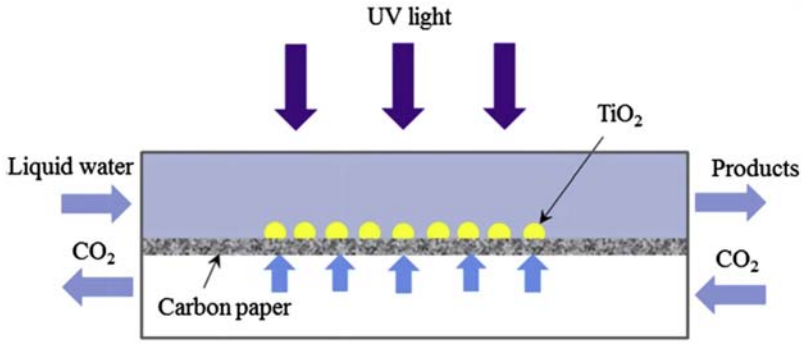

Figure 8.8
Schematic drawing of the optofluidic membrane microreactor for photocatalytic reduction of CO_2 (Cheng et al., 2016).

4.5 mg cm^{-2}. The authors compared their data with that reported in literature and concluded that the performance of the developed optofluidic membrane microreactor was among the top.

More recently, Tan et al. (2017) fabricated free-standing polyvinylidene fluoride (PVDF)−TiO_2 membranes with single, bi-, or tricrystalline titania phases, by using a combined electrospinning and hydrothermal treatment method, and tested them in CO_2 photoreduction to fuels (CH_4). Obtained results evidenced that the photomethanation activity of the prepared PVDF−TiO_2 membranes was significantly affected by both the crystal phase composition and microstructure of the photocatalyst. In particular, the sample formed by anatase (which is reported to contain a potential site for CO_2 activation) and rutile (which has an effective reduction site), in about the same ratio (55% and 45%, respectively), showed enhanced photomethanation activity. The highest photoproduction of methane from CO_2 was 19.8 μmol g_{cat}^{-1} h^{-1}.

The photocatalytic reduction of CO_2 was performed by Li et al. (2016) in a novel twin reactor producing fuels and H_2 by water splitting. This photoreactor was divided into two compartments by a modified ion exchange Nafion membrane. The H^+ ions generated by H_2O splitting permeates through the Nafion membrane and forms H_2, which reacts with CO_2 to produce mainly methanol. The highest productivity obtained was 0.98 μmol g_{cat}^{-1} h^{-1}.

8.4.3 Photocatalytic Reduction of Nitrite to Ammonia

The presence of nitrite ions $\left(NO_2^-\right)$ in drinking water (primarily from groundwater and wells) gives problems by harmful biological effects. High concentrations can cause

methemoglobinemia and represent a risk factor in developing gastric and intestinal cancers. Owing to these heath risks, a great emphasis has been placed on finding effective treatment processes to reduce nitrate concentrations to safe levels.

The photoreduction of nitrite ions represents a promising strategy in the remediation of wastewater and in nitrogen fixation into valuable compounds.

Pandikumar et al. (2012)) prepared TiO_2−Au nanoparticles (nps), composite materials ($(TiO_2-Au)_{nps}$), and embedded them in methyl functionalized silicate sol−gel (methyltrimethoxysilane [MTMOS]) and Nafion matrices. These photocatalytic membranes were employed to perform the photocatalytic reduction of nitrite to ammonia in the presence of oxalic acid as the hole scavenger. During the photocatalytic tests the photocatalytic activity increased with increasing amounts of Au_{nps} on TiO_2. The $(TiO_2-Au)_{nps}$-incorporated polymer matrices improved the photocatalytic reduction of nitrite ions to ammonia. This result was ascribed to (1) the presence of Au nanoparticles, which promotes efficient interfacial electron transfer for TiO_2 to the substrate during irradiation, avoiding electron−hole recombination; (2) the porous structure of the Nafion polymeric matrix. A lower amount of NH_3 was obtained by using the same photocatalyst in colloidal form, evidencing the advantage of using photocatalytic membrane. Besides, the immobilization of $(TiO_2-Au)_{nps}$ in the Nafion matrix is advantageous for the physical separation of the photocatalyst from the solution compared with the colloidal photocatalyst system.

8.5 Conclusions and Future Trends

The results described in the present chapter evidence that use of PMRs represents a very powerful technology of great interest at research and industrial level.

PMRs, thanks to the selective properties of the membrane, permit to achieve continuous operation in a system that allows not only the recycle and reuse of the photocatalyst but also the selective separation of the product(s).

The results obtained in the synthesis of organic compounds such as phenol, VA, phenylethanol, methanol, and ammonia demonstrated that PMRs can be considered as a useful green system for organic synthesis, although additional studies are still needed before taking advantage of their potentiality at industrial level.

Common benefits of PMR systems are the confining of the photocatalyst in the reacting environment and the separation at high purification degree of the product simultaneously to the reaction.

List of Acronyms and Symbols

AOP Advanced oxidation process
APR Annular photoreactor
Au_{nps} Au nanoparticles
CB Conduction band
Eg Bandgap energy
FA Formic acid
GC Gas chromatography
h Planck constant
HPLC High-performance liquid chromatography
KBR Kellogg Brown & Root phenol process
λ Wavelength
M Metal
MC Membrane contactor
MTMOS Methyltrimethoxysilane
Nafion Trade name of a copolymer of tetrafluoroethylene and perfluoro-3,6-dioxa-4-methyl-7-octene sulfonic acid
nps Nanoparticles
PC Photocatalysis
PEBAX Trade name of polyether-polyamide block copolymers
PMR Photocatalytic membrane reactor
PTFE Polytetrafluoroethylene
PV Pervaporation
PVDF Polyvinylidene fluoride
TMP Transmembrane pressure
UV Ultraviolet
VA Vanillin
VB Valence band
Vis Visible

References

Armor, J.N., 1998. Applications of catalytic inorganic membrane reactors to refinery products. J. Membr. Sci. 147, 217–233.

Augugliaro, V., Camera-Roda, G., Loddo, V., Palmisano, G., Palmisano, L., Parrino, F., Puma, M.A., 2012. Synthesis of vanillin in water by TiO_2 photocatalysis. Appl. Catal. B Environ. 111, 555–561.

Azrague, K., Aimar, P., Benoit-Marquie, F., Maurette, M.T., 2007. A new Combination of a membrane and a photocatalytic reactor for the Depollution of Turbid water. Appl. Catal. B Environ. 72, 197–204.

Barton, E.E., Rampulla, D.M., Bocarsly, A.B., 2008. Selective solar-Driven reduction of CO_2 to methanol using a Catalyzed p-gap based Photoelectrochemical cell. J. Am. Chem. Soc. 130, 6342–6344.

Bekkouche, S., Bouhelassa, M., Hadj Salah, N., Meghlaoui, F.Z., 2004. Study of adsorption of phenol on titanium oxide (TiO_2). Desalination 166, 355–362.

Bellussi, G., Perego, C., 2000. Industrial catalytic aspects of the synthesis of monomers for nylon production. CATTECH 4, 4–16.

Bianchi, D., Bortolo, R., Tassinari, R., Ricci, M., Vignola, R., 2000. A novel iron-based catalyst for the biphasic oxidation of benzene to phenol with hydrogen peroxide. Angew. Chem. Int. Ed. 39, 4321–4323.

Bianchi, D., Balducci, L., Bortolo, R., D'Aloisio, R., Ricci, M., Span, G., Tassinari, R., Tonini, C., Ungarelli, R., 2007. Oxidation of benzene to phenol with hydrogen peroxide catalyzed by a modified titanium silicalite (TS-1B). Adv. Synth. Catal. 349, 979–986.

Böddeker, K.W., Bengston, G., Bode, E., 1990. Pervaporation of low volatility aromatics from water. J. Membr. Sci. 53, 143–158.

Böddeker, K.W., Bengston, G., Pingel, H., Dozel, S., 1993. Pervaporation of high boilers using heated membranes. Desalination 90, 249–257.

Böddeker, K.W., Gatfield, I.L., Jähnig, J., Schorm, C., 1997. Pervaporation at the vapor pressure limit: vanillin. J. Membr. Sci. 137, 155–158.

Brosillon, S., Lhomme, L., Vallet, C., Bouzaza, A., Wolbert, D., 2008. Gas phase photocatalysis and liquid phase photocatalysis: interdependence and influence of substrate concentration and photon flow on degradation reaction kinetics. Appl. Catal. B Environ. 78, 232–241.

Cai, R., Song, S., Ji, B., Yang, W., Sun, G., Xin, Q., 2005. Phenol cogeneration with electricity by using in situ generated H_2O_2 in a H_2–O_2 PEMFC reactor. Catal. Today 104, 200–204.

Camera Roda, G., Santarelli, F., 2012. Design of a pervaporation photocatalytic reactor for process intensification. Chem. Eng. Technol. 35, 1221–1228.

Camera-Roda, G., Santarelli, F., Augugliaro, V., Loddo, V., Palmisano, G., Palmisano, L., Yurdakal, S., 2011. Photocatalytic process intensification by coupling with pervaporation. Catal. Today 161, 209–213.

Camera-Roda, G., Augugliaro, V., Cardillo, A., Loddo, V., Palmisano, G., Palmisano, L., 2013. A pervaporation photocatalytic reactor for the green synthesis of vanillin. Chem. Eng. J. 224, 136–143.

Camera-Roda, G., Cardillo, A., Loddo, V., Palmisano, L., Parrino, F., 2014. Improvement of membrane performances to enhance the yield of vanillin in a pervaporation reactor. Membranes 4, 96–112.

Cheng, X., Chen, R., Zhu, X., Liao, Q., He, X., Li, S., Li, L., 2016. Optofluidic membrane microreactor for photocatalytic reduction of CO_2. Int. J. Hydrogen Energ. 41, 2457–2465.

Chin, S.S., Lim, T.M., Chiang, K., Fane, A.G., 2007. Factors affecting the performance of a low-pressure submerged membrane photocatalytic reactor. Chem. Eng. J. 130, 53–63.

Coronas, J., Santamaria, J., 1999. Catalytic reactors based on porous ceramic membranes. Catal. Today 51, 377–389.

Dey, G.R., Belapurkar, A.D., Kishore, K., 2004. Photo-catalytic reduction of carbon dioxide to methane using TiO_2 as suspension in water. J. Photochem. Photobiol. A Chem. 163, 503–508.

Dhakshinamoorthy, A., Navalon, S., Corma, A., Garcia, H., 2012. Photocatalytic CO_2 reduction by TiO_2 and related titanium containing solids. Energy Environ. Sci. 5, 9217–9233.

Dong, T., Li, J., Huang, F., Wang, L., Tu, J., Torimoto, Y., Li, M.S.Q., 2005. One-step synthesis of phenol by O^- and OH^- emission material. Chem. Commun. 2724–2726.

Emeline, A.V., Ryabchuk, V., Serpone, N., 2000. Factors affecting the efficiency of a photocatalyzed process in aqueous metal-oxide dispersions: prospect of distinguishing between two kinetic models. J. Photochem. Photobiol. Chem. 133, 89–97.

Flores, S.O., Rios-Bernij, O., Valenzuela, M.A., Cordova, I., Gomez, R., Gutierrez, R., 2007. Photocatalytic reduction of nitrobenzene over titanium dioxide: by-product identification and possible pathways. Top. Catal. 44, 507–511.

Gazi, S., Ananthakrishnan, R., 2011. Metal-free-photocatalytic reduction of 4-nitrophenol by resin-supported dye under the visible irradiation. Appl. Catal. B Environ. 105, 317–325.

Herrmann, J.-M., 2005. Heterogeneous photocatalysis: state of the art and present applications. Top. Catal. 34, 49–65.

Herrmann, J.-M., Duchamp, C., Karkmaz, M., Thu Hoai, B., Lachheb, H., Puzenat, E., Guillard, C., 2007. Environmental green chemistry as defined by photocatalysis. J. Hazard Mater. 146, 624–629.

Imamura, K., Iwasaki, S., Maeda, T., Hashimoto, K., Ohtani, B., Kominami, H., 2011. Photocatalytic reduction of nitrobenzenes to aminobenzenes in aqueous suspensions of titanium(IV) oxide in the presence of hole scavengers under deaerated and aerated conditions. Phys. Chem. Chem. Phys. 13, 5114–5119.

Itoh, N., Niwa, S., Mizukami, F., Lnoue, T., Igarashi, A., Namba, T., 2003. Catalytic palladium membrane for reductive oxidation of benzene to phenol. Catal. Commun. 4, 243–246.

Kohtani, S., Yoshioka, E., Saito, K., Kudo, A., Miya, H., 2010. Photocatalytic hydrogenation of acetophenone derivatives and diaryl ketones on polycrystalline titanium dioxide. Catal. Commun. 11, 1049–1053.

Konstantinou, I.K., Albanis, T.A., 2004. TiO_2-Assisted photocatalytic degradation of azo dyes in aqueous solution: kinetic and mechanistic investigations: a review. Appl. Catal. B Environ. 49, 1–14.

Korthou, H., Verpoorte, R., 2007. Vanilla. In: Berger, R.G. (Ed.), Flavours and Fragrances. Springer-Verlag, Berlin, Heidelberg, pp. 203–217.

Ku, Y., Lee, W.H., Wang, W.Y., 2004. Photocatalytic reduction of carbonate in aqueous solution by UV/TiO_2 process. J. Mol. Catal. Chem. 212, 191–196.

Li, J., Yang, J., Wen, F., Li, C., 2011. A visible-light-driven transfer hydrogenation on CdS nanoparticles combined with iridium complexes. Chem. Commun. 47, 7080–7082.

Li, S., Yang, L., Ola, O., Maroto-Valer, M., Du, X., Yang, Y., 2016. Photocatalytic reduction of CO_2 by CO co-feed combined with photocatalytic water splitting in a novel twin reactor. Energ. Convers. Manage. 116, 184–193.

Liptàkova, B., Bàhidsky, M., Hronec, M., 2004. Preparation of phenol from benzene by one-step reaction. Appl. Catal. A Gen. 263, 33–38.

Liu, Y., Murata, K., Inaba, M., 2006. Direct oxidation of benzene to phenol by molecular oxygen over catalytic systems containing $Pd(OAc)_2$ and heteropolyacid immobilized on HMS or PIM. J. Mol. Catal. A Chem. 256, 247–255.

Molinari, R., Poerio, T., 2010. Remarks on studies for direct production of phenol in conventional and membrane reactors. Asia Pac. J. Chem. Eng. 5, 191–206.

Molinari, R., Mungari, M., Drioli, E., Di Paola, A., Loddo, V., Palmisano, L., Schiavello, M., 2000. Study on a photocatalytic membrane reactor for water purification. Catal. Today 55, 71–78.

Molinari, R., Grande, C., Drioli, E., Palmisano, L., Schiavello, M., 2001. Photocatalytic membrane reactors for degradation of organic pollutants in water. Catal. Today 67, 273–279.

Molinari, R., Poerio, T., Argurio, P., 2006. One-step production of phenol by selective oxidation of benzene in a biphasic system. Catal. Today 118, 52–56.

Molinari, R., Caruso, A., Argurio, P., Poerio, T., 2008. Degradation of the drugs gemfibrozil and tamoxifen in pressurized and de-pressurized membrane photoreactors using suspended polycrystalline TiO_2 as catalyst. J. Membr. Sci. 319, 54–63.

Molinari, R., Caruso, A., Poerio, T., 2009. Direct benzene conversion to phenol in a hybrid photocatalytic membrane reactor. Catal. Today 144, 81–86.

Molinari, R., Caruso, A., Palmisano, L., 2010. Photocatalytic processes in membrane reactors. In: Drioli, E., Giorno, L. (Eds.), Comprehensive Membrane Science and Engineering, vol. 3. Elsevier Science B.V, Oxford, pp. 165–193.

Molinari, R., Lavorato, C., Poerio, T., 2012. Performance of vanadium based catalyst in a membrane contactor for the benzene hydroxylation to phenol. Appl. Catal. A Gen. 417, 87–92.

Molinari, R., Argurio, P., Lavorato, C., 2013. Review on reduction and partial oxidation of organics in photocatalytic (membrane) reactors. Curr. Org. Chem. 17, 2516–2537.

Molinari, R., Argurio, P., Palmisano, L., 2015a. Photocatalytic membrane reactors for water treatment. In: Basile, A., Cassano, A., Rastogi, N.K. (Eds.), Advances in Membrane Technologies for Water Treatment-Materials, Processes and Applications, Woodhead Publishing Series in Energy: Number 75. Woodhead Publishing Limited, Cambridge, pp. 205–238.

Molinari, R., Lavorato, C., Argurio, P., 2015b. Photocatalytic reduction of acetophenone in membrane reactors under UV and visible light using TiO_2 and Pd/TiO_2 catalysts. Chem. Eng. J. 274, 307–316.

Molinari, R., Argurio, P., Poerio, T., 2015c. Vanadyl acetylacetonate filled PVDF membranes as the core of a liquid phase continuous process for pure phenol production from benzene. J. Membr. Sci. 476, 490–499.

Molinari, R., Lavorato, C., Mastropietro, T.F., Argurio, P., Drioli, E., Poerio, T., 2016. Preparation of Pd-loaded hierarchical FAU membranes and testing in acetophenone hydrogenation. Molecules 21, 394. https://doi.org/10.3390/molecules21030394.

Molinari, R., Lavorato, C., Argurio, P., 2017. Recent progress of photocatalytic membrane reactors in water treatment and in synthesis of organic compounds. A Review. Catal. Today 281, 144−164.

Niwa, S., Eswaramoorthy, M., Nair, J., Raj, A., Itoh, N., Shoji, H., Namba, T., Mizuka, F., 2002. A one-step conversion of benzene to phenol with a palladium membrane. Science 295, 105−107.

Ozawa, M., Matui, H., Suzuki, S., 2016. Preparation and photocatalytic properties of TiO_2/mica composite for acetaldehyde degradation. Jpn. J. Appl. Phys. 55. Art. No. 01AG04.

Palmisano, G., Augugliaro, V., Pagliaro, M., Palmisano, L., 2007a. Photocatalysis: a promising route for 21st century organic chemistry. Chem. Commun. 3425−3437.

Palmisano, G., Yurdakal, S., Augugliaro, V., Loddo, V., Palmisano, L., 2007b. Photocatalytic selective oxidation of 4-methoxybenzyl alcohol to aldehyde in aqueous suspension of home-prepared titanium dioxide catalyst. Adv. Synth. Catal. 349, 964−970.

Palmisano, G., Garcıa-Lopez, E., Marcì, G., Loddo, V., Yurdakal, S., Augugliaro, V., Palmisano, L., 2010. Advances in selective conversions by heterogeneous photocatalysis. Chem. Commun. 46, 7074−7089.

Pandikumar, A., Manonmani, S., Ramaraj, R., 2012. TiO_2−Au nanocomposite materials embedded in polymer matrices and their application in the photocatalytic reduction of nitrite to ammonia. Catal. Sci. Technol. 2, 345−353.

Park, H., Choi, W., 2005. Photocatalytic conversion of benzene to phenol using modified TiO_2 and polyoxometalates. Catal. Today 101, 291−297.

Ranjit, K.T., Varadarajan, T.K., Viswanathan, B., 1995. Photocatalytic reduction of nitrite and nitrate ions to ammonia on Ru/TiO_2 catalysts. J. Photoch. Photobio. A 89, 67−68.

Rao, S.R., Ravishankar, G.A., 2000. Vanilla flavour: production by conventional and biotechnological routes. J. Sci. Food Agric. 80, 289−304.

Roy, S.C., Varghese, O.K., Paulose, M., Grimes, C.A., 2010. Toward solar fuels: photocatalytic conversion of carbon dioxide to hydrocarbons. ACS Nano 4, 1259−1278.

Sekizawa, K., Maeda, K., Domen, K., Koike, K., Ishitani, O., 2013. Artificial Z-scheme constructed with a supramolecular metal complex and semiconductor for the photocatalytic reduction of CO_2. J. Am. Chem. Soc. 135, 4596−4599.

Sellaro, M., Bellardita, M., Brunetti, A., Fontananova, E., Palmisano, L., Drioli, E., Barbieri, G., 2016. CO_2 conversion in a photocatalytic continuous membrane reactor. RSC Adv. 6, 67418−67427.

Shimizu, K., Akahane, H., Kodama, T., Kitayama, Y., 2004. Selective photo-oxidation of benzene over transition metal-exchanged BEA zeolite. Appl. Catal. Gen. 269, 75−80.

Sinha, A.K., Sharma, U.K., Sharma, N., 2008. A comprehensive review on vanilla flavor: extraction, isolation and ouantification of vanillin and others constituents. Int. J. Food Sci. Nutr. 59, 299−326.

Tan, J.Z.Y., Nursam, N.M., Xia, F., Truong, Y.B., Kyratzis, I.L., Wang, X., Caruso, R.A., 2017. Electrospun PVDF−TiO_2 with tuneable TiO_2 crystal phases: synthesis and application in photocatalytic redox reactions. J. Mater. Chem. 5, 641−648.

Tang, C., Chen, V., 2004. The photocatalytic degradation of reactive black 5 using TiO_2/UV in an annular photoreactor. Water Res. 38, 2775−2781.

Walton, N.J., Mayer, M.J., Narbad, A., 2003. Vanillin. Phytochemistry 63, 505−515.

Wang, X.B., Guo, Y., Zhang, X.F., Liu, H., Wang, J., Yeung, K.L., 2010a. Catalytic properties of benzene hydroxylation by TS-1 film reactor and Pd-TS-1 composite membrane reactor. Catal. Today 156, 288−294.

Wang, X.B., Zhang, X.F., Liu, H., Yeung, K.L., Wang, J.Q., 2010b. Preparation of titanium silicalite-1 catalytic films and application as catalytic membrane reactors. Chem. Eng. J. 156, 562−570.

Wang, W.-K., Chen, J.-J., Gao, M., Huang, Y.-X., Zhang, X., Yu, H.-Q., 2016. Photocatalytic degradation of atrazine by boron-doped TiO_2 with a tunable rutile/anatase ratio. Appl. Catal. B Environ. 195, 69−76.

Wehbe, N., Jaafar, M., Guillard, C., Herrmann, J.-M., Miachon, S., Puzenat, E., Guilhaume, N., 2009. Comparative study of photocatalytic and non-photocatalytic reduction of nitrates in water. Appl. Catal. Gen. 368, 1–8.

Yamaguchi, S., Sumimoto, S., Ichihashi, Y., Nishiyama, S., Tsuruya, S., 2005. Liquid-phase oxidation of benzene to phenol over V-Substituted heteropolyacid catalysts. Ind. Eng. Chem. Res. 44, 1–7.

Zhang, T., You, L., Zhang, Y., 2006. Photocatalytic reduction of p-chloronitrobenzene on illuminated nano-titanium dioxide particles. Dyes Pigments 68, 95–100.

This page intentionally left blank

CHAPTER 9

How Far Are We From Large-Scale PMR Applications?

Anastasios J. Karabelas, Konstantinos V. Plakas, Vasileios C. Sarasidis
Centre for Research and Technology – Hellas (CERTH), Thessaloniki, Greece

9.1 Photocatalytic Membrane Reactors—Toward Technology Development

Forty five years after successfully using titanium dioxide (TiO_2) for the photoelectrochemical splitting of water (Fujishima and Honda, 1972), heterogeneous photocatalysis has received great attention by the scientific community as a promising green technology for environmental and energy applications. Numerous investigations have been carried out focusing on the removal of harmful water pollutants—organic (Kanakaraju et al., 2014; Ribeiro et al., 2015; Kaur et al., 2016) and inorganic (Cappelletti et al., 2008; Litter, 2017)—and on water disinfection (Kikuchi et al., 1997; Rincón and Pulgarin, 2004; McCullagh et al., 2007), as well as on the synthesis of industrially significant chemicals (Lu and Yao, 2014; Friedmann et al., 2016) and on hydrogen generation (Ahmad et al., 2015).

The particular interest in semiconductor photocatalytic processes for water/wastewater treatment applications apparently escalated when TiO_2 was successfully used for oxidation of cyanide ion in aqueous solutions (Frank and Bard, 1977) and later for the mineralization of halogenated hydrocarbon water pollutants, including trichloroethylene, dichloromethane, chloroform, and carbon tetrachloride (Bard, 1980; Pruden and Ollis, 1983). Since then, the effectiveness of heterogeneous photocatalysis to degrade and/or mineralize dissolved organic compounds has been very extensively investigated in laboratory studies; this work has been summarized in quite a few review papers (Blake, 1997; Gaya and Abdullah, 2008; Klavarioti et al., 2009; Malato et al., 2009; Bora and Mewada, 2017; Szczepanik, 2017), special issues (Pillai et al., 2015), and books (Pichat, 2013; Pawar and Lee, 2015; Dionysiou et al., 2016; Quintero et al., 2016). Significant research has been performed particularly on substances that are resistant to biological degradation and persistent in the environment for extended periods of time, the

Current Trends and Future Developments on (Bio-) Membranes. https://doi.org/10.1016/B978-0-12-813549-5.00009-8

so-called "recalcitrant" organics. Such organic compounds are synthetic chemicals such as pesticides, pharmaceuticals, detergents, and dyes, which have been designed for specific applications, as well as natural substances such as humic matter, lignin, natural antibiotics, or halogenated metabolites produced by marine algae and animals (Alexander, 1975).

In addition to the light source and appropriate photocatalyst, the essential component of the hybrid *photocatalytic membrane reactor* (PMR) systems considered in this chapter are the membranes required for purified water production, which also serve either as photocatalyst particle support or to separate dispersed photocatalyst particles for recycling (Mozia, 2010). There are many inherent advantages of such systems, including the mild operating conditions, the powerful oxidation occurring, which can lead to mineralization of almost all organic pollutants (with no sidestreams), and the use of relatively inexpensive and nonhazardous photocatalysts (possibly without addition of oxidizing agents). However, despite these advantages and a plethora of laboratory studies, the development of a practical PMR system for water treatment has not been achieved yet. This gap between small-scale laboratory work and large-scale applications can be attributed to several (mostly technical) types of unsettled issues, including (1) the maximization of the quantum yield, the robustness, and reusability of *photocatalyst*, (2) the efficient photocatalyst use, including the fouling-free performance of *membranes*, which ensures total rejection and recovery (for recycling) in the case of photocatalyst particle suspension, and (3) the *optimal design* of energy-efficient photocatalytic reactors catering to the needs of large-scale industrial applications. One may observe that, over the past two decades, research activity has been largely carried out along three directions to address the above types of challenges, and in particular the first one.

The preponderance of studies deal with the "heart" of the process, i.e., the photocatalytic materials, specifically, to develop photocatalysts that exhibit improved efficiencies, wide excitation wavelengths (activation in visible/solar light), low recombination rates of the photo-produced electron−hole pairs, high adsorption capacities, and minimum deactivation rates. TiO_2 is the most commonly investigated semiconductor, which can be in the form of monodispersed nanoparticles (Hernandez-Alonso et al., 2009), nanostructures (nanotubes, nanorods, nanowires, nanobelts, nanoneedles) (Nah et al., 2010; Grover et al., 2017; Hwang et al., 2017), or graphene nanocomposites (Chowdhury and Balasubramanian, 2014) or immobilized onto various substrates (Shan et al., 2010) such as glass (Daneshvar et al., 2005; Shen et al., 2017), polymeric films (Cámara et al., 2016), sand (Tokarský et al., 2013), carbonaceous nanomaterials (Leary and Westwood, 2011; Martins et al., 2017), and clay (Szczepanik, 2017). However, the development of an efficient and commercially viable photocatalyst for large-scale applications still remains a significant challenge (Leary and Westwood, 2011; Pelaez et al., 2012), even though a variety of approaches have been followed to improve the photocatalytic behavior of TiO_2 and other widely used semiconductors and their composites (ZnO, CuS, WO_3, Fe_2O_3, Fe−$ZnIn_2S_4$,

BiOBr, $BiFeO_3$, etc.), including metal particle loading, cocatalysts, dye sensitization, metallic doping, and nonmetallic doping.

Research along another direction is related to the efficient use or *recovery/reuse of the photocatalyst*. To satisfy this requirement, two approaches have been investigated. The first is the photocatalyst particle separation by means of coagulation and sedimentation (Lee and Choo, 2014) or membrane filtration (Mozia, 2010; Iglesias et al., 2016). Particular attention has been given to the photocatalyst separation by pressure-driven membrane processes such as microfiltration (MF) (Chin et al., 2007; Choo et al., 2008; Bai et al., 2013a; Khan et al., 2015), ultrafiltration (UF) (Sarasidis et al., 2011, 2014; Fernández et al., 2014a; Plakas et al., 2016a), and nanofiltration (NF) (Molinari et al., 2006; Grzechulska-Damszel et al., 2010), which permit continuous operation, among other benefits (e.g., Plakas et al., 2016a,b). The second approach involves the fabrication of membranes with embedded semiconductor materials (*photocatalytic membranes [PMs]*), which have opened promising perspectives in photocatalytic applications because they can provide photocatalytic activity and separation in a single step (Leong et al., 2014; Iglesias et al., 2016). Several reviews on hybrid photocatalysis−membrane processes have been published since 2003 (Ollis, 2003). A list of significant reviews published in the last decade is summarized in Table 9.1, which includes information regarding the designs of PMRs as well as an outline of experimental conditions and main findings in this field. A list of relevant patents, with a brief summary of inventors' claims, is also provided in Appendix (Table A1). The fairly large number of patents on PMRs contrasted to the lack of significant large-scale applications (to the best of the authors' knowledge) reflects the exciting prospects of this technology rather than the level of its maturity. In fact, it can be noted that although significant progress has been made in basic understanding of the photocatalytic mechanisms (Dionysiou et al., 2016), there are still several important technical and scale-up challenges (as subsequently discussed) that need to be successfully tackled to advance the PMR *technology readiness level (TRL)* from its present status, estimated to be at TRL 4−5 on the basis of inadequate large-scale demonstration, to maturity (TRL 8−9).

The third direction of research activities is related to the improvement of the *sustainable performance of the photocatalysis processes*. The issues of minimizing environmental burden and cost per unit of processed water, in conjunction with maximization of process reliability to satisfy societal needs, dominate in a comprehensive sustainability assessment (Pires et al., 2017; Tufa, 2015). Regarding PMR, this line of research and development (R&D) work is pursued with much less vigor (compared with the other areas) despite its significance. Nevertheless, there is noteworthy ongoing activity (Malato et al., 2009; Athanasiou et al., 2016) toward the PMR system design and optimization as well as the exploitation of solar energy for implementing the redox reactions, preferably in energy autonomous systems, in addition to efforts for the development of photocatalysts, active in

Table 9.1: A list of recent reviews on PMR systems, with brief comments on their content.

References	Scope/Content
Molinari et al. (2017)	A review is provided of experimental studies with different PMR configurations (involving pressurized or submerged membranes, photocatalytic membranes, photocatalytic reactors combined with membrane distillation, membrane dialysis, and pervaporation membrane) for water treatment aiming to degrade various organic pollutants (such as dyes, pharmaceuticals, and other pollutants) and in the synthesis of organic compounds (such as phenol, vanillin, and phenylethanol).
Iglesias et al. (2016)	Presents a critical review of photocatalytic processes that incorporate membranes, photocatalytic membrane filtration (PMF), and PMRs, and their primary applications (i.e., wastewater treatment and H_2 production). An analysis is provided highlighting advantages and drawbacks of particular configurations, including identification of corresponding intensification indices and discussion of future prospects.
Zhang et al. (2016a)	Reviews R&D progress regarding membrane fouling of PMRs and summarizes fouling evolution, fouling types, and fouling consequences in PMRs for different types of water/wastewater treatments. The relationship between photocatalytic process conditions and membrane fouling is examined, considering the dominant fouling mechanisms/types, and different control strategies are reviewed for each fouling type.
Ong et al. (2015)	Provides an update on the influences of several key operational parameters, on the efficiency of submerged membrane photocatalytic reactor (SMPR) performance in degrading organic pollutants and discusses the structure, the photocatalytic membrane properties, and membrane performance stability under UV irradiation. Approaches are recommended to overcome the persistent problems and facilitate further R&D of SMPR.
Zangeneh et al. (2015)	Compares the effectiveness of pure and modified TiO_2 for photocatalytic degradation of different organic matter and clarifies the advantages of modified TiO_2 with photoactivity under visible light. Moreover, examines the effects of important parameters on the performance of the photocatalytic reactors; describes and classifies the different types of photocatalytic reactors tested so far.
Mozia (2010)	An overview is provided of hybrid photocatalysis—membrane processes and their possible applications in water and wastewater treatment. Factors affecting the photocatalytic process are discussed, including assessment of some configurations of PMRs. Comments are included on advantages and disadvantages of coupled photocatalysis—membrane processes in terms of permeate flux, membrane fouling, and permeate quality, as well as on pressure-driven membrane processes.
Chong et al. (2010)	R&D progress is reviewed of engineered photocatalysts and photoreactor systems for water treatment, including optimization, mineralization kinetics, and modeling. The effect of operating parameters of photocatalytic reactor is assessed in terms of mineralization and disinfection. A brief discussion is also presented on LCA for retrofitting the photocatalytic system as a wastewater treatment process.
Ray (2009)	A critical assessment of studies is provided on the effect of key parameters (photocatalyst loading, circulation rate, substance initial concentration, light intensity) on the reaction rate of photocatalytic degradation of benzoic acid in TiO_2 slurry systems. Major challenges are outlined related to photocatalysis and designs/development of large-scale photocatalytic reactors for water treatment, including discussion of reactor morphologies.

LCA, life cycle assessment; *PMR*, photocatalytic membrane reactor.

visible light (Pelaez et al., 2012; Bora and Mewada, 2017), green (Ma et al., 2017), and robust (Lin et al., 2013; Zhang et al., 2016b). Such efforts should lead to the construction of technologically advanced PMR facilities, economically attractive, of minimum energy consumption and of zero- or low-waste footprint, as demanded of modern processes.

In view of the foregoing outline of "state of PMR technology," the question arises as to *how far are we from large-scale PMR applications?* It is evident that an answer to this question cannot be straightforward. Indeed, one should carefully assess the current state of promising process alternatives as well as the required and foreseen advances of the three main structural components of the PMR process, namely the photocatalytic materials (in the form of suspended particles or embedded onto membranes), the artificial or solar irradiation, and the membrane separation. Required advances should result in high-level PMR systems performance (in terms of effluent quality, operational stability, energy efficiency, and in particular, reduction in capital and operating expenses) that would render them competitive over existing and well-established techniques, such as the pollutant adsorption on traditional and novel composite materials (Wan Ngah et al., 2011; Sweetman et al., 2017; Thakur et al., 2017) and the rejection by membrane processes (NF, ultralow-pressure reverse osmosis) (Plakas and Karabelas, 2012; Mohammad et al., 2015; Le and Nunes, 2016). Regarding these established technologies, it should be stressed that, in parallel, there are efforts to improve their performance as well to address environmental and other pressures (Santhosh et al., 2016; Al Aani et al., 2017); therefore, PMR technology development for commercialization is a demanding endeavor aiming to meet ever more stringent standards and related indicators.

To address the questions on PMR raised in this chapter, consideration is given to the current TRL, the innovation gap that has prevented research outputs from reaching the market, and finally the market needs (Fig. 9.1). The essential element, for the successful

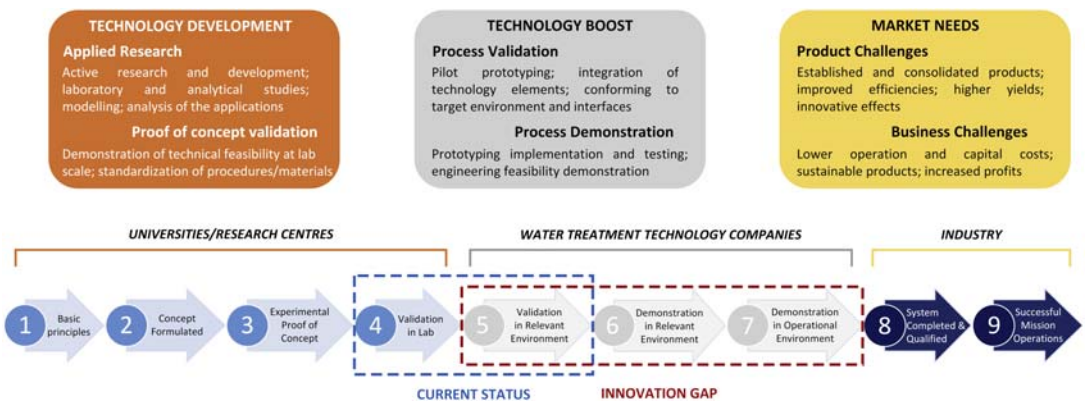

Figure 9.1
Value chain and readiness level(s) of photocatalytic membrane reactor technology.

application of PMR systems in the water-processing sector, is the capability of producing water of the desired quality, thus providing adequate public health protection while meeting the environmental and socioeconomic goals that can be practically achieved. Therefore, in the following, PMR technical issues are addressed first, followed by a critical assessment of the related economic and overall sustainability issues.

9.2 Photocatalytic Membrane Reactor Technical Issues

9.2.1 Categories of Technical Issues and Interrelations

To systematically assess PMR systems, including economic and environmental issues, precedence should be given to the treatment in fair detail of key technical issues that play a decisive role in shaping the technology and predetermine its range of applications. To proceed, it should be recognized that considerable effort is required to develop, optimize, and scale up PMR system variants (utilizing artificial and/or solar irradiation) aiming to attain a high TRL toward commercialization (Fig. 9.1). This can be achieved by overcoming various design and scale-up challenges and effectively validating the eco-innovative PMR processes for industrial applications. In this context, the research community has dealt with a multitude of significant scientific/technical issues for which, however, no standard solutions/strategies are available yet. The Venn diagram in Fig. 9.2 depicts the interrelations between the three major components of a PMR process (i.e., membranes, artificial/solar irradiation, photocatalysts); major technical issues are associated with each one of these components. These issues span scientific/technical areas from materials science to process modeling and engineering, thus rendering their solution challenging and the approach interdisciplinary.

In the ensuing critical discussion of technical issues, depicted in Fig. 9.2, emphasis will be placed on system design, photocatalysts, PMs, artificial/solar irradiation, photocatalyst separation by membrane filtration, operating issues, and relevant parameters. First, a number of *basic premises* will be set to facilitate the assessment of various PMR systems reported in the literature *for water/wastewater treatment applications*. Specifically, in the discussion of technical issues presented in this section, PMR systems will be considered that

- are of *pilot scale* (i.e., no small bench-scale experimental setups will be dealt with),
- can operate in *continuous* mode,
- can treat water/wastewater of relatively *small organic matter concentration* and low-to-moderate hardness (i.e., groundwater or surface waters for drinking water production, tertiary treatment of secondary municipal effluents for reuse, etc.),
- are mainly applicable for the efficient removal/mineralization of *recalcitrant organics* to a degree that depends on the treatment targets,
- do not require the addition of extra oxidants (e.g., H_2O_2, O_3).

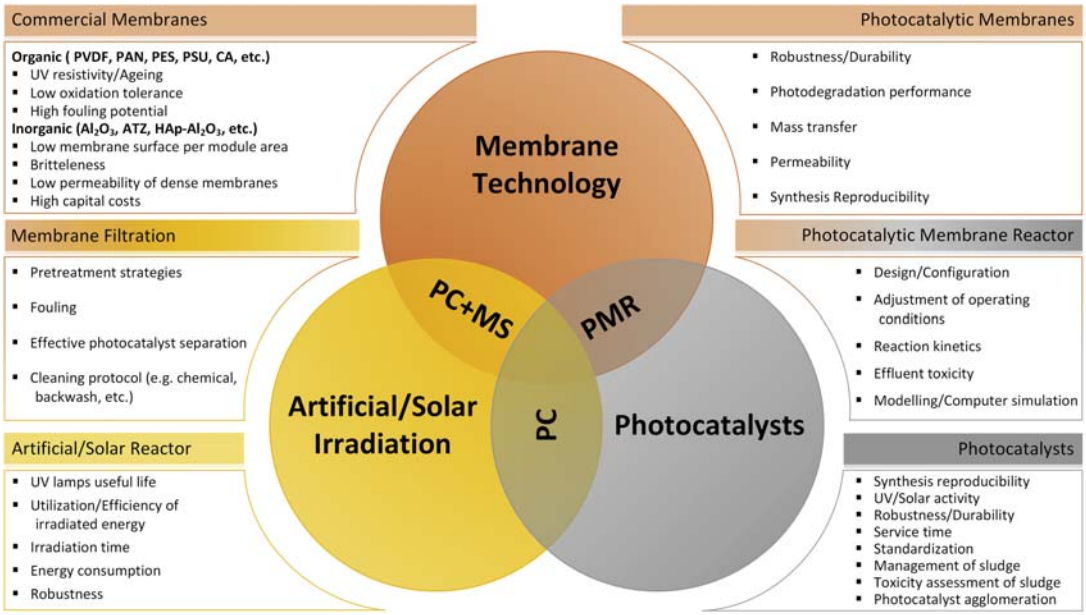

Figure 9.2

Critical technological issues and interrelation between the main components of photocatalytic membrane reactor (PMR) technology. *CA*, cellulose acetate; *MS*, membrane separation; *PAN*, polyacrylonitrile; *PC*, photocatalysis; *PES*, polyethersulfone; *PSU, polysulfone*; *PVDF*, polyvinylidene fluoride; *UV*, ultraviolet.

It should be noted that the majority of the published studies that are in line with the above considerations have been performed mostly with synthetic waters, whereas pilot PMR studies treating natural waters and real wastewaters are limited. Moreover, the best treatment performances have been reported for low pollutant concentrations because the amount of ultraviolet (UV) photons, available in both solar light and artificial illumination, presents obvious limitations regarding the pollutant concentration to be effectively treated. For this reason, in case of heavily polluted streams, photocatalysis is considered as the *next* processing step after biological treatment (Fujishima et al., 2007) or other more potent advanced oxidation processes (AOPs).

9.2.2 Assessment of Technical Issues

9.2.2.1 Photocatalytic System Morphology and Design

Meeting the main objective of PMR process design (and technology development), i.e., of minimizing specific energy consumption (SEC) and treatment cost (per unit volume of purified water) as well as overall environmental impact, for a specific purification task, critically depends on system configuration/morphology. Indeed, the latter directly affects

energy efficiency (in both artificial and solar light use), capital, and operating expenses. Therefore, selection of an optimal photocatalytic system morphology is a basic task in technology development and of high priority in the sequence of process design steps. In this chapter, the aforementioned two types of PMR systems will be considered, which depend on the condition of the photocatalyst; i.e., PMRs that use powdered photocatalysts *dispersed* in the liquid/water (*type I*) and PMRs that utilize PMs comprising photocatalysts *immobilized* on a substrate material (e.g., ceramic, polymers, stainless steel) (*type II*).

Type I PMR configurations are the most common systems treated in literature and are characterized by greater available active surface area, compared with the immobilized systems, which renders them potentially more efficient. It is noted that the inappropriate term "slurry (PMR) reactors" is usually used (and it is well entrenched in the literature) to describe this type of PMR, even though "slurries" are commonly quite concentrated solid/liquid suspensions. Usually, PMR systems use concentrations of dispersed photocatalysts of order 1 g L^{-1}. The photocatalyst particles, dispersed in the water to be purified, are circulated through a compartment or vessel to be irradiated by a light source and then are separated by membranes for recirculation/reuse, while clean permeate water is produced. Two representative pilot systems of type I PMR configurations are illustrated in Figs. 9.3 and 9.4. The unit presented in Fig. 9.3 is a patented PMR system (Photo-Cat) developed and commercialized by Purifics ES Inc. (Canada). A Photo-Cat pilot system is described and assessed for pharmaceuticals degradation (Benotti et al., 2009), hexavalent chromium removal (Stancl et al., 2015), and viruses inactivation (Gerrity et al., 2008). This system comprises UV lamps, aligned in series, whereas a cross-flow ceramic MF membrane is used for photocatalyst separation. The lamps can be individually turned on, and the total time period of fluid exposure to UV irradiation can vary depending on the number of lamps in operation, i.e., 1−30 s in the case of tests carried out by Benotti et al. (2009). The membrane can be back-pulsed to prevent photocatalyst buildup. According to the manufacturer, Photo-Cat is essentially a solid-state, automated device that operates unattended, with lamp life and service intervals exceeding 20,000 h. Fig. 9.4 presents a laboratory-scale pilot PMR that was designed and constructed in the authors' laboratory (Plakas et al., 2016a). The PMR pilot unit has total effective volume 25 L, total UVC power 52 W, and treatment capacity 1.2 m^3 d^{-1}. The main components of the pilot system are the membrane vessel and the UV treatment system. It is fully automated, including level control, periodic membrane backwashing, mechanical cleaning system of quartz sleeves of the UV lamps, and a cleaning-in-place (CIP) system. Further details on the pilot system characteristics can be found elsewhere (Plakas et al., 2016a).

Type II PMR configurations involve photocatalyst particles *embedded onto membranes*, thus overcoming technological issues associated with the postseparation/recovery of the

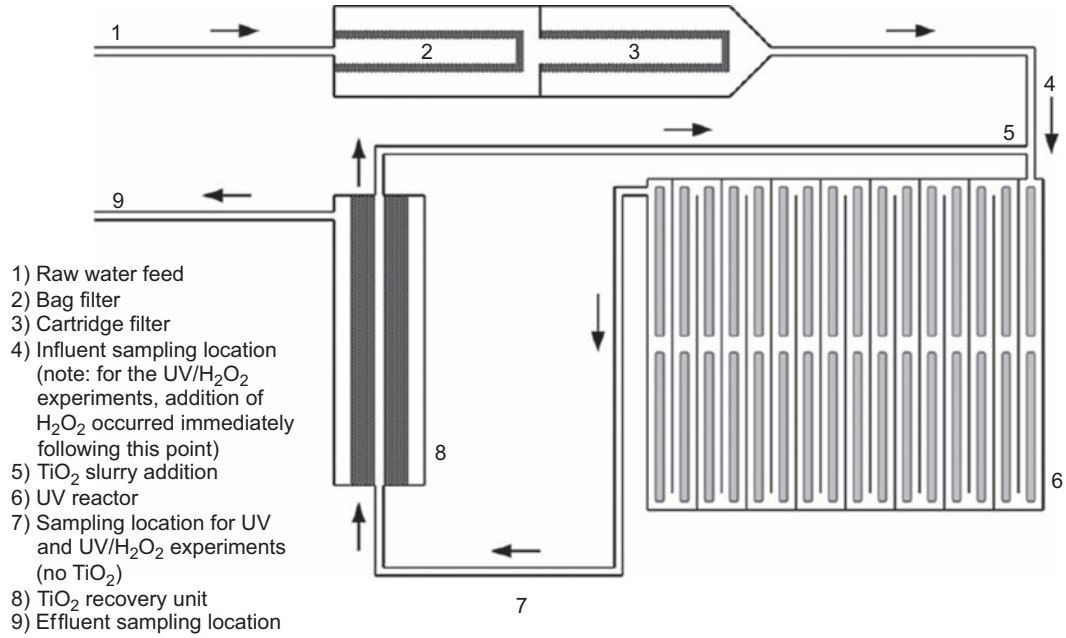

Figure 9.3
General schematic of a photocatalytic membrane reactor pilot system (Photo-Cat). *UV*, ultraviolet. *Reprinted from Benotti et al., 2009.*

photocatalyst particles from the liquid phase. In such PMRs the photocatalytic reaction readily proceeds at the membrane surface while treated water is continuously discharged with negligible loss of photocatalyst. In this kind of PMRs, there are two issues to be addressed; namely, uniform distribution of light and mass transfer of pollutants to the photocatalytic surface. In the latter case, significant research effort has been devoted to manufacture PMs with appropriate porosity and effective dispersion of the photocatalyst particles. Because of the harsh oxidation environment, inorganic membranes are preferable as support matrix over the conventional polymeric materials (Molinari et al., 2017), while special attention has been given to maximize overall system lifetime, which can be drastically decreased due to the possible photocatalyst deactivation and washout.
A promising PM system that has been recently patented by Falaras et al. (2012) is shown in Fig. 9.5. This system has been successfully tested with several PMs using mostly azo dyes as model organic compounds. The chemical vapor deposition (CVD) technique was used by this group to manufacture photocatalytic UV light active TiO_2 membranes (UF, NF) using tubular silica (Athanasekou et al., 2012), γ-alumina (Athanasekou et al., 2012; Moustakas et al., 2014), and biopolymers (Ca alginate porous hollow fibers) (Papageorgiou et al., 2012) as membrane substrates.

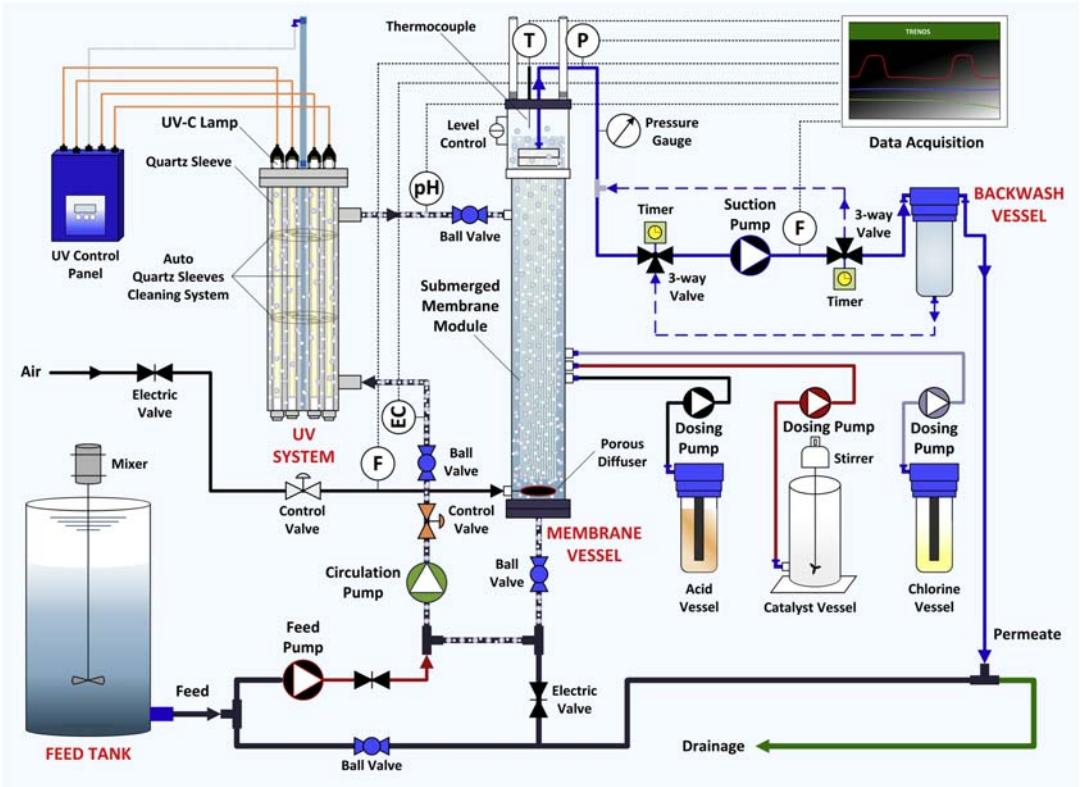

Figure 9.4
Schematic diagram of the pilot-scale continuous photocatalytic membrane reactor system. *UV*, ultraviolet. *Reprinted from Plakas et al., 2016a.*

As mentioned above, one of the major problems in semiconductor photocatalysis is the achievement of a uniform distribution of light in the photoreactor. When the semiconductor photocatalyst is used in the form of a dispersion of powder particles, or coated on an inert support material, the distribution of light throughout the reaction vessel is likely to be nonuniform, owing to absorption, reflection, and scattering by the support as well as the active photocatalyst coating. Obviously, a poor distribution of UV light in a semiconductor photocatalytic reactor will lead to a low overall efficiency of operation. Therefore, the arrangement of irradiation source in respect of the photocatalyst particles (whether in the form of dilute recirculated dispersion or embedded on fixed membranes) is a key issue in both configurations to ensure maximal and symmetrical light transmission and distribution. In the case of fixed bed reactors, as in the case of type II PMRs, two different illumination configurations are identified: light introduction from the support side

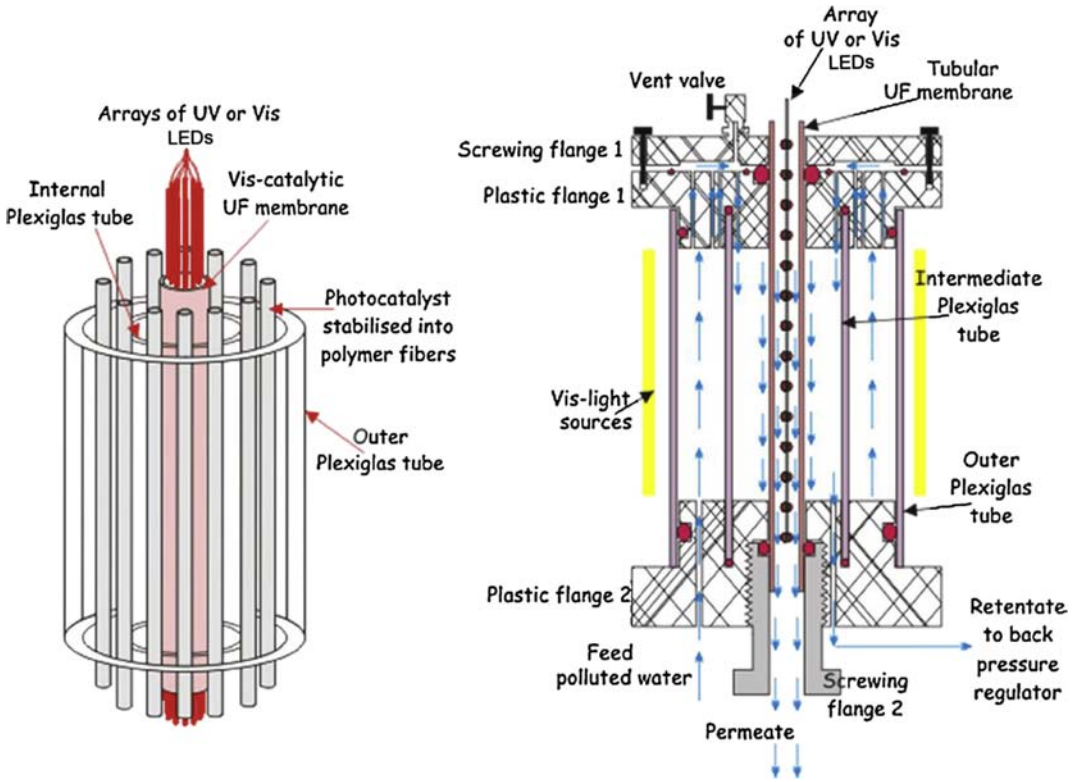

Figure 9.5

A side view of the photocatalytic membrane reactor cell (left) and schematic cross section of the reactor depicting the flow channels of the membrane cell (right). *UV*, ultraviolet. *Reprinted from Moustakas et al., 2014.*

or from the solution side. In the first case, an optimal film thickness leads to the maximum reaction rate. Increasing the film thickness beyond the optimal value would be detrimental for the reactor performance. In the second configuration, the reaction rate increases with the film thickness up to a specific value. Further increase in the film thickness does not enhance the reaction rate (Vezzoli et al., 2013).

For the usually considered case of artificial UV light source (e.g., Hg lamps encased in cylindrical sleeves) and photocatalyst in suspension, a design target is to maximize the quantum yield, within the range imposed by intrinsic physicochemical constraints (e.g., decreased photon penetration and photocatalyst agglomeration for increased photocatalyst concentration) (Manassero et al., 2017), and in turn the overall irradiation energy efficiency. Thus, the spatial arrangement of UV lamps (and the detailed

cross-sectional area between lamps available for photocatalyst suspension flow) is of significance, considering the phenomena of light absorption and photon scattering by the particles, which tend to sharply (exponentially) reduce the light intensity within several millimeters from the lamp/sleeve boundary (Ray, 2009). In such a UV light compartment configuration, it is clearly required to ensure uniform photocatalyst suspension distribution along all the lamps to take full advantage of the emitted light.

For the desirable continuous system operation, another relevant factor/constraint of practical significance in the arrangement of the UV lamps is due to the need to periodically and automatically clean the glass sleeves of lamps, to remove photocatalyst particles and other fouling materials that tend to adhere onto the glass surfaces (Lin et al., 1999a,b), reducing light transmittance, the oxidation effectiveness of the reactor, and the life of the lamp (attributed to the heat increase due to the UV light absorption by the photocatalyst). To mitigate such phenomena, automated chemical and/or mechanical cleaning can be adopted. This issue was recently brought up and successfully tackled in a novel PMR pilot (Plakas et al., 2016a), by using an automatically operated glass sleeve cleaning mechanism, without disturbing the long-term continuous plant operation. Nevertheless, the physical dimensions of the cleaning mechanism (moving along the glass sleeves) impose another constraint to be accounted for in the detailed geometric design of the photocatalytic reactor. It is noted that permanent foulants, which cannot be removed completely by typical cleaning operations, may remain on the quartz sleeves. An interesting investigation by Peng et al. (2005) revealed that after long-term regular chemical and mechanical cleaning, the wipers of cleaning systems tend to damage sleeve surfaces, creating scratches or holes with larger surface areas. Inorganic foulants such as compounds of aluminum, iron, magnesium, calcium, and phosphorus are trapped more easily and are attached tightly to the surfaces of these scratches or to each other. For the specific cases studied, chemical plus mechanical cleaning was more effective in removing deposits and in avoiding the accumulation of permanent foulants compared with the mechanical cleaning alone (Peng et al., 2005).

Another important parameter in efficient photocatalytic reactor design is related to the fluid dynamics (mixing) because the transport of reactants from the bulk of the liquid to the photocatalyst surface determines the duration of fluid−photocatalyst contacting and the overall conversion. In case of PMR units using photocatalyst suspensions, it is important to ensure that photocatalyst particles are dispersed uniformly, thus avoiding agglomeration phenomena, whereas oxygen and pollutants are dissolved effectively in the aqueous solution. A controlled aeration is usually used to satisfy both the mixing of the suspension and oxygen supply and to inhibit membrane fouling (Ryu et al., 2005; Fu et al., 2006; Chin et al., 2007; Horng et al., 2009; Sarasidis et al., 2011, 2014; Plakas et al., 2016a; Vatanpour et al., 2017). Rivero et al. (2006) used aeration not only to introduce oxygen and a perfect mixture to the reaction but also as a means to transfer the liquid from the

tank to the separation module (by airlift). In this manner, no additional pump is required for feeding the water, thus reducing the overall energy requirements. Mechanical agitation is another means to prevent agglomeration of TiO_2 particles as well as to provide shear forces that may remove TiO_2 particles from the membrane surface (Chin et al., 2007).
In continuous recirculation flow PMR units, the recirculation flow rate of the photocatalyst suspension may also drastically affect the fluid dynamics (Choo et al., 2008; Damodar et al., 2010; Sarasidis et al., 2011, 2014; Plakas et al., 2016a) and the deposition of photocatalyst particles on the walls of tanks and tubes or reaction dead zones. In the case of cross-flow membrane filtration units, the desirable turbulent regime is determined by the applied cross-flow velocities, which in turn may significantly enhance the mass transfer of the reactants to the photocatalyst and the membrane surface (Doll and Frimmel, 2005; Shon et al., 2008).

The use of solar light as an economically and ecologically attractive photon source for activating the heterogeneous photocatalytic detoxification process has been fairly extensively investigated in the past and is still an active research field (Malato et al., 2013), with a significant number of solar photocatalytic reactors reported for water decontamination and disinfection (Malato et al., 2013). Most such systems are nonconcentrating, thus utilizing direct and diffuse sunlight, although typically the UV flux is limited to c. 20–30 W m^{-2} near the Earth's surface (Bahnemann, 2004). However, the literature on solar PMR units is rather poor and is dealing mostly with solar simulators using xenon lamps (Section 9.2.2.4). Fig. 9.6 illustrates a hybrid solar membrane

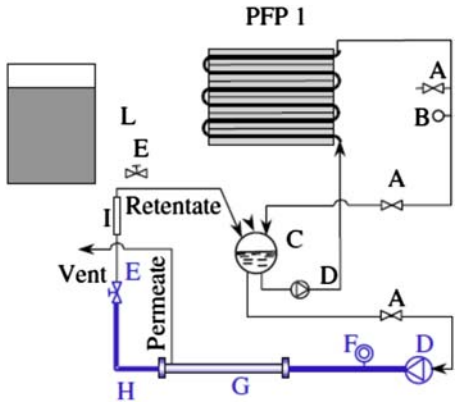

Figure 9.6

Scheme of a PFP consisted of three CPC modules in series coupled to a nanofiltration membrane module: (A) switch valve; (B) thermocouple; (C) nonreacting tank; (D) pump; (E) regulation valve; (F) manometer; (G) membrane vessel; (H) line under pressure; (I) rotameter; (L) feed tank. *CPC, compound parabolic collector*; *PFP*, plug flow photoreactor. *Reprinted from Augugliaro et al., 2005.*

photoreactor at pilot plant scale that utilizes compound parabolic collectors (CPCs) (Augugliaro et al., 2005). In this system a plug flow photoreactor (PFP) is coupled to an NF membrane module in a total recirculation loop. The aqueous suspension is continuously fed to the PFP from a nonreacting tank by means of a centrifugal pump. A high recirculation flow rate (3.34×10^{-4} m^3 s^{-1}) can lead to Reynolds number values (1.7×10^4) indicative of a turbulent regime inside the tubes. Although the morphology of the particular system is modular, its construction is not trivial because it needs a large area of weather-resistant, chemically inert, cheap, UV light—transmitting glazing. Moreover, careful control of the reaction solution is required, especially if the photocatalyst is used in suspension, rather than in the form of PMs. The critical factor in such systems seems to be the availability of the light source (effective only in sunny days) and the long residence time in the collector section, which may cause dissolved O_2 depletion. A realistic assumption of solar collector efficiency of 75% and 1% for the photocatalyst means 0.04% original solar photons are efficiently used in the process. From the standpoint of solar collecting technology, this is a rather inefficient process even when considered for a high-added-value application (Malato et al., 2009). However, the promising prospects in regard to the fabrication of new and robust photocatalysts, capable to work with bandgaps that better overlap the solar spectrum, may open the road for future industrial applications.

9.2.2.2 Photocatalysts

Since the pioneering works by Fujishima and Honda (1972) and Schrauzer and Guth (1977), photocatalysis using various semiconductors has been the focus of intense investigations by numerous researchers (Schneider et al., 2014). Various materials have been investigated and evaluated as potential photocatalysts, including metal oxides such as titanium dioxide (TiO_2), zinc oxide (ZnO), tin(IV) oxide (SnO_2), iron(III) oxide (Fe_2O_3), zirconia (ZrO_2), vanadium(V) oxide (V_2O_5), niobium pentoxide (Nb_2O_5), tungsten trioxide (WO_3), molybdenum trioxide (MoO_3), and metal chalcogenides such as zinc sulfide (ZnS), cadmium sulfide (CdS), cadmium selenide (CdSe), tungsten disulfide (WS_2), and molybdenum disulfide (MoS_2) (Hoffmann et al., 1995; Kudo and Miseki, 2009; Vinu and Madras, 2010; Schneider et al., 2014; Lee et al., 2016; Al-Hamdi et al., 2017; Lee and Wu, 2017). The *photocatalytic activity* of these materials is the result of an *interplay between a considerable number of parameters*, e.g., light absorption (linked to the bandgap), phase composition, electronic structure, particle size, exposed surface area, pollutant adsorption, degree of aggregation, mobility of charge carriers, presence of impurities, amount and kind of defects, adsorption of molecules from gas or aqueous phase, lateral interactions between adsorbed species, nature of solvent, etc. Other features of interest are the *mechanical and chemical stability*, the *corrosivity*, and the *reusability* of each photocatalytic material (Hoffmann et al., 1995; Hisatomi et al., 2014).

TiO_2, ZnO, WO_3, $SrTiO_3$, α-Fe_2O_3, and ZrO_2 exhibit favorable bandgap positions compared with other materials. Although some of the semiconductor photocatalysts, such as hematite (Fe_2O_3), are low cost and possess suitable bandgap energies for visible light absorption, they suffer from various limitations. For example, it has been reported by Fox and Dulay (1993) that Fe_2O_3 shows lower photoactivity compared with TiO_2 and ZnO because of corrosion or the formation of short-lived ligand-to-metal or metal-to-ligand charge transfer states. Metal chalcogenides semiconductors, e.g., CdS, PbS, CdSe etc., have been reported as being susceptible to photocorrosion and low stability especially in aqueous media (Mills and Le Hunte, 1997). The addition of sulfide or sulfite to the contacting solution has been described to suppress photocorrosion. These semiconductors have also been reported to show some toxicity (Beydoun et al., 1999). The formation of $Zn(OH)_2$ on the surface of the semiconductor ZnO, observed from its dissolution in water, has been reported by Bahnemann et al. (1987) to cause instability and deactivation over time. Moreover, the vacant sites on the ZnO surface also lead to photocorrosion of ZnO (Bai et al., 2013b; Chen et al., 2013). On the other hand, TiO_2 appears to be corrosion resistant and chemically stable (Carp et al., 2004).

Compared with other semiconductor photocatalysts, TiO_2 has so far been the "*photocatalyst of choice*" for destruction of organic pollutants because of its high photoactivity, low cost, nontoxic nature (environmentally benign), the ease of synthesis, and good chemical and thermal stability (Schneider et al., 2014). Generally, different TiO_2 structures have very strong oxidation power (3.0 eV for rutile and 3.2 eV for anatase), considering approximately 1.2 eV for the oxidation potential of water and approximately 3.0 eV for the hydrogen reference potential. It is generally accepted that anatase is the more active of the two TiO_2 phases, both in photocatalysis and in photoelectrochemical studies. This enhancement in photoactivity is probably due to the Fermi level of anatase, being higher than that of rutile by about 0.1 eV (Bickley et al., 1991). One commercial form of TiO_2, prepared in a similar manner to the Aerosil process, and used frequently in photocatalytic studies, is Aeroxide P25 (registered trademark of Evonik Degussa GmbH), a material that possesses a high specific surface area (approximately 50 $m^2\ g^{-1}$) and is predominantly of the anatase form with a small portion of rutile (approximately 80%−20% by weight). According to Hurum et al. (2003) "the rutile in Aeroxide P25 acts as an antenna to extend the photoactivity into visible wavelengths and the structural arrangement of the similarly sized TiO_2 crystallites creates catalytic *hot spots* at the rutile-anatase interface." Aeroxide P25 consists of aggregated primary particles of several hundred nanometers in size, having the form of fine white powder, with primary particles of approximately 21 nm mean diameter (AEROSIL, 2017). It has a hydrophilic character caused by hydroxyl groups and a high photoactivity that is attributed to the intimate contact between two phases, enhancing separation of photogenerated electrons and holes, which results in reduced recombination

(Yu et al., 2006). That is why Aeroxide P25 is recognized as the "gold standard" in photocatalysis (Mills and Lee, 2002).

Regardless of the above significant features of TiO_2 photocatalysts, their large-scale applications in water remediation appear to have been hindered by the significant quantities of electrical energy required by the UV light irradiation source. The high-energy bandgap of anatase TiO_2 can only be activated under UV light irradiation ($\lambda \leq 387$ nm), thus excluding the use of solar energy as the photoactivity source (UV represents 2%−5% of sunlight). Moreover, titania is characterized by low quantum yields (i.e., low electron transfer rate), resulting in fast recombination of the photogenerated electron−hole pairs and consequently in the termination of the photocatalytic reactions (Pelaez et al., 2012). The recombination of the charge carriers can occur with heat release via nonirradiative pathways or be accompanied by light emission via irradiative routes (Ohtani, 2013). Serpone et al. (1995) found that trapping excited electrons as Ti^{3+} species occurred on a time scale of ~30 ps and that about *90% or more of the photogenerated electrons recombine within 10 ns*. Strategies for reducing recombination and improving the photocatalytic efficiency of TiO_2 have been recently reviewed by Pelaez et al. (2012) and Fang et al. (2017), which include surface modification/complexation, such as increasing surface area and porosity, or chemical modifications, by incorporation of additional components in the TiO_2 structure, impurity doping, and heterojunction with semiconductors of similar bandgaps, sensitization, etc. Moreover, it has been possible to prepare Ti−oxide photocatalysts, enabling the absorption of light not only in the UV but also in the visible light wavelength region (which accounts for 45% of the solar spectrum) to *operate effectively under natural sunlight irradiation* (Malato et al., 2009; Pelaez et al., 2012; Schneider et al., 2014).

Photocatalytic materials have been used in a wide variety of reacting systems from suspensions to coated walls reactor and packed bed reactors, depending on the requirements of a particular reactor type. For example, the photocatalyst particles chosen for a packed bed reactor (as in the case of the PMs discussed next) need to be able to adsorb organic compounds as well as be photoactive. On the other hand, a photocatalyst appropriate for a suspension-type reactor needs to be highly photoactive, whereas the adsorption properties are of lesser concern owing to continuous mixing. In the latter case, attention should be given to minimize photocatalyst *agglomeration phenomena* (internal mass transfer resistance), which can reduce the effective photocatalyst surface area, thus resulting in reduced photocatalytic activity. Such phenomena are affected by several parameters, including the photocatalyst loading, pH, ionic strength, water composition, and recirculation rate (Yaremko et al., 2006; French et al., 2009; Ray, 2009; Li et al., 2010). For example, relatively large photocatalyst concentration (although desirable to enhance photocatalytic reaction rate) promotes particle agglomeration and renders the treated fluid turbid, thus increasing adsorption and scattering of the irradiated light, which leads to

degraded apparent quantum efficiency. Therefore, the photocatalyst load must be optimized in each system for best photocatalytic activity. Solution pH is also important, as it controls the surface charge of the photocatalyst particles. Indeed, fluid pH away from the particle point of zero charge (PZC) is required to prevent agglomeration and maintain a stable dispersion (Bora and Mewada, 2017). In the case of colloidal TiO_2 (with PZC $\sim$ 5.5−6.8) (Kosmulski, 2011), acidic pH values are preferable to obtain charged particle surfaces, leading to electrostatic repulsive forces and dispersion stability (e.g., Li et al., 2010). It is noted that the surface charge density of the TiO_2 nanoparticles may vary depending on the ionic strength and the size of the particles (Holmberg et al., 2013). Regarding the feed fluid ionic strength and composition, Song et al. (2016) reported that the presence of Cl^- can lead to agglomeration of TiO_2 particles in a suspension by suppressing the stabilizing effect of electrostatic repulsion, also reducing the effective contact surface between the photocatalyst and the pollutants. French et al. (2009) observed that divalent cations may enhance aggregation of nano-TiO_2 in soils and surface waters at significantly faster rates than NaCl suspensions with similar ionic strength and pH.

Finally, an issue that merits significant attention is the development of *standards*, for newly synthesized photocatalysts, by which their characteristics can be gauged and compared with similar materials. Standards help manufacturers develop and deliver products that have the defined characteristics desired by their customers, such as *activity*, *robustness*, and *appearance*. Thus, for the *industry*, standards ensure their *products are widely accepted and competitive*, whereas for the *consumer* they ensure *product quality* and *reliability* (Mills et al., 2012). Considering the emergence of a number of commercial products based on semiconductor photocatalysis, the International Standards Organization (ISO) has begun to address the need for quantification of their performance through the publication of a series of standards. In a recent article, Mills et al. (2012) reviewed the ISO standards related to semiconductor photocatalysis and provided recommendations for their improvement. A summary of these standards especially in the area of water purification and disinfection is given in Table 9.2. It is worth to mention the technical committee working on photocatalysis standards for the European Committee of Standardisation (CEN—Comité Européen de Normalisation), CEN/TC 386 (CEN, 2017). The latter, horizontal CEN/TC, aims at developing general standards to be applied to different elements and building constructions that will mainly concern test and analysis methods/protocols. In relation to water purification, a European Standard, with reference number prEN 17120, has been recently produced by the CEN/TC 386/WG 3 Work Programme and it is under enquiry (forecasted voting day 27/3/2018). This standard describes a test method, which is applicable to photocatalytic materials in the form of powders (suspensions in water, slurries) under UV irradiation, involving photocatalytic performance assessment through determination of phenol degradation, at specified experimental conditions, using high-performance liquid chromatography (HPLC) (CEN, 2017).

Table 9.2: Summary of published ISO standards for photocatalytic materials in the area of water purification and disinfection.

ISO	Title	Description/Comments
10676:2010	Fine ceramics (advanced ceramics, advanced technical ceramics)—Test method for water purification performance of semiconducting photocatalytic materials by measurement of forming ability of active oxygen	ISO 10676:2010 describes a test method covering photocatalytic materials formed on, or attached to, another material surface for the purpose of decomposing, and thus eliminating, the pollutants in water, using photocatalytic performance. This test method is applicable to photocatalytic materials under UV irradiation and not under visible light irradiation.
10678:2010 (DIN 52980)	Fine ceramics (advanced ceramics, advanced technical ceramics)—Determination of photocatalytic activity of surfaces in an aqueous medium by degradation of methylene blue	ISO 10678:2010 specifies a method for the determination of the photocatalytic activity of surfaces by degradation of the dye molecule methylene blue in aqueous solution using artificial UV radiation and characterizes the ability of photoactive surfaces to degrade dissolved organic molecules on UV radiation. The test method specified is also applicable to evaluation of the specific photocatalytic self-cleaning activity of surfaces covered with respective coatings. This method is not applicable to characterizing the photoactivity of surfaces on visible illumination, regarding direct soiling, degradation of gaseous molecules, and the determination of antimicrobial photoactivity of surfaces.
10677:2011	Fine ceramics (advanced ceramics, advanced technical ceramics)—Ultraviolet light source for testing semiconducting photocatalytic materials	ISO 10677:2011 describes an UV light source and specifies a method of measuring the radiation intensity, which is used in testing the performance of semiconducting photocatalytic materials in a laboratory.
27447: 2009	Fine ceramics (advanced ceramics, advanced technical ceramics)—Test method for antibacterial activity of semiconducting photocatalytic materials	ISO 27447:2009 specifies a test method for the determination of the antibacterial activity of materials that contain a photocatalyst or have photocatalytic films on the surface, by measuring the enumeration of bacteria under irradiation of ultraviolet light. It is intended for use with different kinds of semiconducting photocatalytic materials used in construction materials, flat sheet, board, plate shape, or textiles that are the basic forms of materials for various applications. It does not include powder, granular, or porous photocatalytic materials. This test method is usually applicable to photocatalytic materials produced for an antibacterial effect. Other types of performance of photocatalytic materials, i.e., decomposition of water contaminants, self-cleaning, antifogging, and air purification, are not determined by this method.

ISO, International Standards Organization; *UV*, ultraviolet.

The existing standards should extend in the future to assess the *longevity of photocatalyst materials when exposed to realistic conditions*, based on their likely area of application. For example, the water purification performance of materials should be tested over a significant period of time under nonlaboratory conditions; i.e., on real wastewater effluents. Such work should reveal the strengths and weaknesses of new photocatalytic material and help identify those with longevity, therefore promising for commercial applications (Mills et al., 2012).

9.2.2.3 Photocatalytic Membranes

PMs have emerged in the last decade, as a promising development of the supported fixed bed systems, for tackling the technological issues associated with the photocatalyst suspensions, such as the tendency of TiO_2 nanoparticles to agglomerate and scatter incident light, the need for posttreatment recovery/separation of the photocatalyst from the liquid phase, as well as photocatalyst renewal. The porosity and the large surface area of a membrane matrix tend to compensate for the significant loss of photoactivity that is often observed in simple solid supports (e.g., glass, zeolites, silica) (Shan et al., 2010), allowing the combined photocatalytic degradation and filtration of the polluted water/wastewater. PMs present several attributes, such as the potentially reduced membrane fouling and the improved permeate quality that render them significant alternatives over the conventional membrane processes (Leong et al., 2014). Specifically, the degradation of organic pollutants by oxygen-reactive radicals generated under the UV light irradiation of PMs may prevent pore blocking and the formation of a cake layer on the membrane surface. Moreover, the pollutant concentration in the retentate can be significantly reduced. However, obviously these PM attributes would manifest themselves in the case of relatively *small* organic pollutant concentrations, i.e., when the rate of coverage by organic matter of the photocatalyst-enriched membrane surface is significantly smaller than the rate of these organic pollutants' destruction. Therefore, the issue of gradual PM surface deactivation by nondegradable pollutants (including inorganic colloids) should be reckoned with.

A variety of materials including polymer (Leong et al., 2014), ceramic (Athanasekou et al., 2015) and metallic (Adán et al., 2017) have been used as immobilization substrates, whereas pure TiO_2 PMs have been also fabricated using TiO_2 nanofibers (Zhang et al., 2017), nanowires (Hu et al., 2011), or nanotubes (Liao et al., 2012). In any case, the membrane needs to be prepared with a tailored amount of photocatalyst, paying particular attention to the membrane pore size distribution and membrane photocatalytic activity toward the reaction of interest. More details on the materials, the fabrication procedures, and the designs of PMs along with their performance in reactor systems (PMRs) can be found in Chapters 3 and 6 of this book, respectively.

It is generally agreed that TiO_2 PMs exhibit enhanced filtration performance compared with conventional membranes. However, there is uncertainty regarding such PMs'

characteristics in real applications, including *photocatalytic activity*, *robustness*, *durability*, and *cost*. Despite the intensive academic/laboratory research on membrane fabrication, characterization, and testing in the field of water/wastewater purification and disinfection, PMs have not yet attracted the attention of the industry. This may not be surprising, considering the immaturity of the PMR technology in general, which does not encourage utilization by water treatment companies. Commercialization of PMs will depend on the design of effective membrane reactors as well as on the optimization of the radiant flux on the membrane surface during the short time frame that the polluted water filters through the membrane. Moreover, particular attention should be given to the key issue of membrane maintenance, especially if the rate of photocatalyst inactivation is shown (in real systems) to be significantly high, which in turn will strongly affect the frequency of PMs' regeneration and/or replacement, thus increasing the treatment cost.

As in the case of particulate photocatalysts, PMs require standards for their evaluation against other conventional or advanced materials; this is an important step forward to ensure that these materials and the respective technologies (PMR configurations) are properly tested/assessed according to established methods and criteria. Table 9.3 summarizes a number of European standards developed by CEN in regard to drinking water treatment units, which encompass treatment systems and technologies available in the marketplace today. It is noted that European Standards do not assess material safety, unlike other standards (e.g., NSF/ANSI standards). However, they effectively address structural integrity test methods and criteria, and contaminant reduction test methods and criteria. Lately, EN 12566-7:2016 was prepared by the Technical Committee CEN/TC 165 "Wastewater engineering," which applies to complete units placed in the market for the tertiary treatment of domestic wastewater by biological, physical, chemical, electrical processes including (1) units in accordance with EN 12566-3 or EN 12566-6 and (2) installations designed and constructed in accordance with CEN/TR 12566-5. This standard supports essential requirements of EU Directive(s) and can be a useful tool for marking and evaluating a PMR system as tertiary treatment unit.

9.2.2.4 Artificial/Solar Irradiation

The majority of the PMR studies focus on the utilization of artificial UV irradiation, as it possesses sufficient energy to generate electron−hole pairs (e^-−h^+) within the photocatalyst, which trigger the formation of radicals and the oxidative degradation of pollutants. Research groups commonly utilize *mercury vapor fluorescent lamps*, which emit most of the radiant energy in the germicidal wavelength at 253.7 nm also known as the UVC part of the spectrum, comprising also a line of far shorter wavelength at 185 nm (Doll and Frimmel, 2005; Meng et al., 2005; Rivero et al., 2006; Lee et al., 2006; Huang et al., 2007; Benotti et al., 2009; Zheng et al., 2015; Plakas et al., 2016a; Rajca, 2016; Vatanpour et al., 2017). Considering that TiO_2 can be activated under UV light irradiation

Table 9.3: European standards for drinking water treatment units.

Standard	Title	Scope	Requirements
EN 14652: 2005 +A1:2007	Water conditioning equipment inside buildings—Membrane separation devices	MF, UF, NF, and RO, both point of entry (POE) and point of use (POU); If pre- and postfilters are included, they must conform to the relevant standard.	*Contaminant reduction*: • Organic molecule rejection—molecular cutoff (UF, NF, RO if claimed)—90% rejection of the declared capacity of specific organics required, at specific concentrations and other test conditions as specified by the manufacturer. • Recovery rate (MF, UF, NF, RO operating in cross-flow mode)—Calculated when testing the relevant rejection rate; calculated recovery shall be at least 95% of the claimed recovery rate. • Daily production shall be at least 95% of the claimed value; measured for 1 h on day 1 and day 7, and averaged.
EN 14897: 2006 +A1:2007	Water conditioning equipment inside buildings—Devices using mercury low-pressure ultraviolet radiators	POU and POE, LP mercury lamps with 85% of total radiation intensity at 254 nm	*Test organism*: *Bacillus subtilis* *Required dosage*: 40 mJ cm^{-2} *Test conditions*: • Disinfection devices: Irradiance (measured with device sensor) across range of UV transmittance measured at three data points; sodium thiosulfate used to lower transmittance; six more data points collected across manufacturer's recommended flow rate, three are varying irradiance by adding sodium thiosulfate, three are varying irradiance by reducing lamp output; no start-up samples are collected, as system must display a signal that minimum irradiance has been reached when the system starts up.

Continued

Table 9.3: European standards for drinking water treatment units.—cont'd

Standard	Title	Scope	Requirements
EN 14898:2006 + A1:2007	Water conditioning equipment inside buildings—Active media filters	Both POU and POE, plumbed-in only, "active" media filters only	• Bactericidal treatment devices: Data at three points are while varying flow rate and UV transmittance; the data are collected at lowest, highest, and midpoint of the manufacturer's specified flow range and UV transmittance. *Organic chemical reduction*: • Maximum allowable effluent concentration based on regulated limit (EU Drinking Water Directive 98/83/EC, or, if contaminant not regulated, WHO Guidelines). • TOC concentration not specified. • 60 min cycles, 50% on/50% off, 16 h per day. • Two units tested, installed, and preconditioned in accordance with manufacturer's instructions. • Acceptance: Mean % reduction efficiency for each chemical by each filter shall be no less than the claimed efficiency or the minimum (90%) specified in the standard, and no single result shall be less than 90% of that minimum. *Taste and odor reduction*: Based on reduction of geosmin, and 2,4,6-trichlorophenol tested separately (90% reduction from 0.15 and 20 μg L^{-1} challenge, respectively). Test procedure otherwise as per organic chemical reduction above.

LP, low pressure; *MF*, microfiltration; *NF*, nanofiltration; *RO*, reverse osmosis; *UF*, ultrafiltration; *UV*, ultraviolet.

with $\lambda \leq 387$ nm, many researchers have alternatively used mercury vapor fluorescent lamps with a maximum emission wavelength of 365 nm, which falls in the UVA part of the spectrum (Ryu et al., 2005; Shon et al., 2008; Horng et al., 2009; Sarasidis et al., 2011, 2014; Fernández et al., 2014a,b; Lee et al., 2015).

The mercury vapor fluorescent lamps can be either of *low pressure (LP) or medium pressure (MP)* (i.e., gas pressure inside the lamp) with nominal power that may vary in the ranges 4−115 W and 400−17,000 W (Philips, 2017), respectively. The UV irradiation power can be as high as approximately 30% of the nominal power. It is understood that MP Hg lamps have a much higher output per lamp than LP lamps; therefore, fewer lamps can be used for a certain application, leading to reduced footprint, maintenance, and consumables overall. However, MP Hg lamps (compared with LP Hg) are less efficient and consume more energy to provide the same irradiation dose. Furthermore, because of the high output per lamp of MP systems, measures should be taken in designing process equipment to remove the generated heat and/or control the treated fluid temperature. Consequently, selecting light irradiation system depends a lot on the particular process and application. The typical life span of these lamps varies from 5000 to 17,000 h; however, their output may drastically decrease over their lifetime by 15%−40% (American Air Water® Inc., 2017).

The above issues on mercury vapor fluorescent lamps motivated researchers to explore alternative irradiation sources. Recently, light-emitting diode (LED) semiconductor devices that convert electrical energy directly into light have emerged as possible alternative light sources for photocatalysis (Wang et al., 2013; Jo and Tayade, 2014). LEDs can emit light of different wavelengths (infrared, visible, or near-UV) based on the composition and condition of the semiconducting materials, such as gallium arsenide (GaAs), gallium arsenide phosphide (GaAsP), gallium phosphide (GaP), or indium gallium nitride (InGaN). Compared with conventional mercury lamps, the advantages of using UV LEDs are as follows (Crawford et al., 2005; Eskandarian et al., 2016):

- no disposal problem (LEDs do not contain mercury);
- compact and robust design: more durable in transit and handling (no glass or filaments);
- faster start-up time;
- ability to turn on and off with higher frequency;
- lower voltages, low power requirements; and
- reduced frequency of replacement because of longer lifetime (35,000 −50,000 h).

UVA LEDs exhibit the largest available radiant flux or output power (from 1 to 4000 mW) depending on the driving current. On the contrary, the output and efficiency of UVB and UVC LEDs available on the market remain low at present; i.e., less than 2 and 1 mW, respectively (Galbraith, 2016). However, it is expected that this wavelength range will receive special attention by LED manufacturers because of the demand for an

environmentally friendly, reliable, and energy-efficient light source for applications, including sterilization and disinfection. PMR studies using visible LEDs have only recently been published in both photocatalyst suspension-type (Wang et al., 2013) and PMs-type (Athanasekou et al., 2015) membrane photoreactors, showing promising results for practical applications in the future. It is worth mentioning the patent on PMR by Falaras et al. (2012), using UVB LED arrays, where novel PM equipment is described, enabling to combine with a solar photovoltaic power unit and development of an autonomous system for the cost-effective production of drinking water (Athanasiou et al., 2016).

The least expensive source of UV radiation is *sunlight*, which accounts for about 4%–5% of radiation in the UV region of the electromagnetic spectrum. A typical UV flux near the surface of the Earth is 20–30 W m^{-2}. This corresponds to 0.2–0.3 mol photons m^{-2} h^{-1} in the 300–400 nm range provided by the sun (Mozia, 2010), which is considered sufficient to produce reactive radicals (Thompson and Yates, 2006). Applications of photocatalytic processes with sunlight have attracted considerable attention and have been reviewed elsewhere (Malato et al., 2009; Bora and Mewada, 2017). Significant research effort has been devoted to solar photocatalytic studies with both concentrating (i.e., low concentration collectors called compound parabolic concentrators), and nonconcentrating collectors; however, investigations with solar PMRs are rather limited (Augugliaro et al., 2005; Horovitz et al., 2016). Although the relevant literature is encouraging, with respect to the beneficial coupling of solar photocatalysis with membrane filtration, the shortage of applications indicates a need for substantial effort to fully exploit the suggested possibilities for process development. Future research should take into consideration the diurnal and seasonal variability of the solar light in respect of magnitude, spectral content, and distribution, including effects due to meteorological conditions and geographic latitude of application sites.

Solar simulators using xenon lamps (with ionized xenon gas at high pressure) and visible light active photocatalysts have been also utilized in several PMR studies (Liu et al., 2012; Horovitz et al., 2016; Wang et al., 2017). Xenon lamps are the closest in quality to sunlight of all artificial light. They emit a continuous spectrum with more or less equal intensities at all wavelengths throughout the visible range (roughly 400–700 nm), which approximates the neutral white color of natural daylight. Xenon lamps are available from 5 to 32,000 W, and their lifetime varies according to their design and power consumption, with one major manufacturer quoting average lifetimes ranging from 500 h (7 kW) to 1500 h (1 kW) (USHIO, 2017).

9.2.2.5 Membrane Processes

Regarding the membranes—a key component of PMR systems—it is necessary to assess here to what extent design and operating issues related to them present obstacles to the

development of this technology. Under any operating conditions, *fouling of the membranes* is the main problem, inherent in their prime/separation function, which can degrade their performance and has been studied very extensively in the past decades, with an accumulated vast relevant literature (e.g., Le-Clech et al., 2006; Tang et al., 2011; Sioutopoulos and Karabelas, 2016; Meng et al., 2017; Jiang et al., 2017); therefore, this problem requires particular attention and it is dealt with in Chapter 4 of this volume. It should be also noted that Zhang et al. (2016a) have recently presented a rather comprehensive review on membrane fouling in PMRs for water and wastewater treatment. However, referring to PMR, they concluded with an unduly strong summary assessment that "*At present, the main technical barrier to its commercialization is membrane fouling, which usually increases operating costs and decreases treatment efficiency.*" The following brief assessment, regarding membrane performance in projected large-scale PMR systems, is made considering the importance of this issue and debatable statements made in the literature (such as the foregoing assessment). Account is taken in this overview of the rich practical experience gained in recent decades with UF membrane treatment of drinking water (e.g., Allgeier et al., 2005) and of feedwaters similar to those encountered in potential PMR applications (e.g., Pearce, 2007; Henthorne and Boysen, 2015).

The function and desirable attributes of the membranes in the case of photocatalyst suspension systems is twofold, i.e., to totally separate/reject the photocatalyst particles, thus allowing their recycling, and to enhance the total rate of pollutants' removal by retaining within the PMR system undesirable colloidal and other dissolved (not mineralized) species. These requirements are not different than those of the well-established low-pressure membrane systems of large treatment capacity (commonly comprising UF and to a lesser extent MF membranes) that operate with high degree of reliability in various water treatment plants in the past 20 years, including the pretreatment of feedwater to reverse osmosis (RO) desalination plants (Voutchkov, 2009; Pearce, 2010a,b). In parallel, membranes of similar characteristics operate very successfully, even with highly polluted waters such as those treated in membrane bioreactors (MBRs) (Judd, 2014; Patsios and Karabelas, 2011) and in other similar industrial applications (Judd and Jefferson, 2003). The preponderance of such low-pressure membrane systems use *UF membranes* of nominal pore size selected on the basis of the separation task requirements, i.e., the permeate quality standards in relation to feedwater composition (Baker, 2000). It should be further noted that, in the case of significant concentration of particulate and other colloidal matter, the preferred configuration of the membrane modules is that of hollow fiber or tubular membranes *immersed* in a vessel of water to be treated, which operate under rather mild suction in the "outside−in" mode. Additionally, a periodic backwashing is implemented with predetermined frequency using the permeate, commonly using a reverse flux similar to the forward one, so that (on average) continuous nearly steady operation is achieved (Sarasidis et al., 2011, 2014; Plakas et al., 2016a).

Relatively simple CIP automatically operated systems are commonly used for membrane chemical cleaning, if the monitored pressure tends to increase above a preset level, for constant permeate recovery operation. Many studies have led to the conclusion (implemented in practice) that modest imposed permeate flux is preferable (e.g., 10–20 L m^{-2} h^{-1}) to control irreversible membrane fouling (e.g., Judd, 2014; Patsios and Karabelas, 2011); similarly, there is good understanding of the desirable protocol of backwashing, comprising commonly short (of order 1 min) backflow and an order of magnitude longer filtration (Sarasidis et al., 2011, 2014; Plakas et al., 2016a). Relatively straightforward small pilot tests are often used to specify the aforementioned operating parameters and cleaning protocol for a particular separation task.

The foreseen large-scale applications of PMR involve dispersed *primary* photocatalyst particles, such as TiO_2 and other composites in a size range of 20–40 nm (Gupta and Tripathi, 2011; AEROSIL, 2017). However, the mean photocatalyst particle size of a functioning dispersion in a PMR is usually larger, because of the unavoidable/undesirable agglomeration, as discussed in Section 9.2.2. For such a separation task, several types of UF membranes are available in the market and are used in practice with excellent record of performance (e.g., AMI® Applied Membranes Inc., 2017). The issue of optimum UF membrane pore size distribution (or mean size) is usually addressed by balancing required pressure (i.e., energy consumption) against desirable rejection; however, particularly in the case of PMR systems, pilot tests are required (with a real composition of fluid to be treated) to provide guidance for near-optimum membrane selection. Such experiments, in the context of sufficiently large-scale pilot tests, are necessary in the case of the novel PMR systems to examine the membrane performance also in respect of the pollutants' rejection and overall quality of permeate, under continuous operation. It should be added that MF membranes, of considerably larger pore size than UF and smaller operating pressure requirements, are not favored in the PMR applications discussed here, because of the tendency to suffer significant *irreversible* fouling, which is difficult to control through periodic backwashing, for sufficiently long-term continuous system operation, without very frequent (and undesirable) chemical cleaning (e.g., Katsoufidou et al., 2008).

In the case of photocatalyst particles embedded onto (mainly inorganic) membrane surfaces, the same general appraisal comments hold, in respect of the required membrane porosity, to attain a satisfactory separation of colloidal particles and possibly of other dissolved pollutants. Indeed, *UF-type* tubular membranes are considered appropriate in this case on the basis of laboratory R&D as well as practical experience (Burggraaf and Cot, 1996), even though the latter is generally smaller compared with the experience gained with *organic* hollow fiber membranes to be used is photocatalyst suspension systems. However, the issue of fouling of the membrane surface with embedded photocatalyst particles requires particular attention, as it is possible to lead to effectively inactive photocatalyst particles if the degradation rate of foulants (reaching the surface) due to

oxidation cannot cope with the rate of photocatalyst coverage by those foulants (especially the recalcitrant ones). This issue certainly requires more research (Zhang et al., 2016a) to identify optimum operating conditions for a given water purification task, although it is not expected to present insurmountable problems in the particular PMR technology development.

Based on the above overview, it can be concluded that in the case of dispersed photocatalyst systems, the low-pressure membrane technology is quite mature and the scale-up to large PMR capacities (regarding this component of the system) is expected to be straightforward, by taking advantage of already developed designs and operating rules. However, in the case of membranes with embedded photocatalyst particles, membrane design and scale-up are somewhat more complicated and deserve particular attention. Economic issues, regarding the membrane component of PMR systems, will be dealt with in the following section, using the preceding results of membrane technology assessment.

9.2.3 Assessment of Operation Issues

9.2.3.1 Mode of Operation

The desirable mode of PMR system operation of industrial interest is *continuous*, with practically constant main operating parameters (i.e., treated water volumetric throughput, pollutants' removal rate, energy requirements); however, there can be cases of practical interest (especially for relatively small treatment capacities) where semibatch or even batch operation would be used. The main issues encountered when striving to maintain continuous (practically steady) PMR operation are related to membrane performance degradation owing to fouling and material aging (e.g., pinhole development) that lead to increased operating pressure and reduced separation effectiveness, respectively; therefore, measures to *mitigate* and/or *control* such operating problems as well as reliable performance *monitoring* techniques are needed. Regarding membrane fouling control (at least for UF organic membranes to be used in type I systems), there are well-established measures in industrial practice (e.g., Judd and Jefferson, 2003; Allgeier et al., 2005) comprising automatic periodic backwashing using the permeate (at relatively small frequencies) and CIP protocols as the need arises (usually once in several days or weeks) using rather mild chemicals; these techniques have been successfully used in studies with pilot PMR (Ryu et al., 2005; Sarasidis et al., 2011; Plakas et al., 2016a,b, etc.). Similarly, techniques are available to monitor or periodically check UF hollow fiber membrane integrity (e.g., Allgeier et al., 2005; Pearce, 2010a). For the usual operating mode of *constant rate of permeate production with submerged membranes*, the monitored parameters are suction pressure and permeate quality, on the basis of which decision is taken to clean (by a CIP protocol) or replace malfunctioning membranes.

Aeration or air bubbling is another important issue in PMR system operation. Air bubbling serves two main functions, i.e., to maintain dissolved oxygen saturation in the treated water and to provide fluid agitation near the membrane surfaces (especially of the submerged type), thus inducing fluid shear stresses that tend to mitigate fouling (e.g., Judd, 2003; Allgeier et al., 2005). Excessive (nonoptimized) aeration can significantly add to SEC and to water treatment unit cost; again, useful practical experience is available for the case of submerged UF membranes in efforts to optimize aeration rate. In some studies, sparging oxygen has been used instead of air bubbling; however, the benefit of using pure oxygen in enhancing the photocatalytic reactions is doubtful (Habibi et al., 2005).

Regarding UV sources, which are commercially available in the form of mercury lamps contained within cylindrical glass sleeves for water applications, there are standard techniques available to automatically clean those sleeves from possible deposits (e.g., Schmelling et al., 2006). In a recent PMR pilot (Plakas et al., 2016a,b), such a periodically operated cleaning mechanism was proven effective for cleaning UV lamp sleeves from deposited photocatalyst particles, thus maintaining constant UV light emission. Issues related to UV power used in a PMR system are the heat release and the concomitant temperature increase of treated water, which may have overall negative effects, particularly in implementations requiring high hydraulic residence time (HRT). These significant issues have been inadequately addressed so far and should be an R&D item to include in realistic pilot studies. Finally, monitoring the photocatalyst particle performance (to identify stability degradation) is rather complicated and can be done in operating plants indirectly through a diagnosis based on temporal variation of key operating parameter values, primarily through permeate qualitative and quantitative analyses.

Regarding the type II PMR system, for which there is rather limited pilot work (Falaras et al., 2012) and experience, the continuous mode of operation is feasible. Adaptation to this system is also possible of the aforementioned techniques (currently applicable to organic hollow fiber UF membranes) to control membrane fouling and photocatalyst inactivation because of recalcitrant or nondegradable deposits. However, the issues of monitoring *both* PM photocatalytic and filtration performance, as well as restoration of those functions, are much more complicated (compared with the type I case), and there is a need to develop and demonstrate related effective techniques. For instance, there is lack of experience and uncertainty regarding the type and effectiveness of techniques to control and restore PM membrane performance stability; e.g., whether in situ or ex situ techniques would be needed, type of chemicals to avoid photocatalyst degradation.

9.2.3.2 Operating Parameters

The net rate of pollutants' oxidation/mineralization in a PMR system is strongly dependent on several operating parameters, notably photocatalyst loading, UV irradiation intensity,

HRT, aeration rate, water pH, and temperature, as discussed in Chapters 1 and 4. Another significant parameter, characteristic of membrane performance (also affecting fouling), is the permeate flux through the membrane. A large number of studies have been reported on the effect of these parameters on process efficiency (Chong et al., 2010; Mozia, 2010; Ong et al., 2015). However, these results are usually obtained with different protocols and equipment (sometimes incompletely defined) that hinder comparisons and reduce their archival value.

As outlined above, continuous steady operation is desirable for full-scale plants treating large water volumes of low organic contamination (e.g., drinking water purification, secondary municipal effluents for reuse). In the case of small volumes of wastewaters of higher organic load, semibatch or batch operation may be preferable in conjunction with low permeation fluxes (entailing increased HRT and treatment cost). However, for a given process target, all PMR systems should operate under optimum conditions, particularly regarding photocatalyst loading, UV radiant power per unit volume, and aeration rate. Table 9.4 summarizes the operating variables and the range of their values, reported in the literature for PMR systems that operate under various conditions. Therefore, these values of operating variables tend to vary significantly depending on equipment morphology and working conditions in each PMR; for example, reactors of large volume may have smaller saturated photocatalyst loadings and smaller efficiency compared with small-volume reactors. Consequently, the data in Table 9.4 should be considered as indicative, providing a general reference of the range of values reported in the literature.

Determination of a set of *optimum* operating parameters for a *sustainable* PMR system is difficult, necessitating a multiobjective optimization procedure (usually involving minimization of total treatment cost and SEC, and maximization of pollutants' degradation/mineralization), subject to several constraints. A prerequisite of such optimization is the development of a comprehensive and reliable model of the entire PMR process, as outlined in Section 9.5 and in Chapter 10 of this volume, which is not available at present. Appropriate strategies must be implemented for photocatalyst concentration, pH, and temperature control, depending on feedwater composition, to achieve efficiently the targeted photocatalytic pollutants' degradation. HRT is negatively affected by the refractory nature and the concentration of the organic pollutants to be removed; indeed, recalcitrant pollutants lead to increased HRT and PMR operating expenses.

The effects of light intensity as well as other operating variables may drastically change in the case of real water matrices compared with model systems because the photocatalytic decomposition rates of the target organic pollutants (e.g., synthetic chemicals such as pesticides, dyes, and pharmaceuticals) can be drastically hindered by other dissolved organic and inorganic compounds of the water matrix. Specifically, the less toxic natural

Table 9.4: Operation variables; main effects and range of values used in the literature for PMR systems that are of laboratory pilot scale, reported to operate in continuous mode, and treat water/wastewater of relatively small organic matter concentration (from μg L^{-1} to ng L^{-1}).

Operating Parameter	Range Values	Comments
Photocatalyst loading	0.1–2 g L^{-1} (type I) 0.5–12 %wt TiO_2 (type II)	Depends on the geometry and working conditions of the photoreactor. Its value is directly proportional to the overall photocatalytic reaction rate, up to a certain extent. The operation should take place below photocatalyst saturation level so as to avoid excess photocatalyst, agglomeration, and light scattering phenomena and ensure efficient photons absorption.
pH	4.5–8.5 (types I and II)	Affects the charge on the photocatalyst particles, size of photocatalyst aggregates, and the positions of CB and VB. Depending on the solute and the operating pH, polar attractions with opposite-charged photocatalyst particles may take place for subsequent photocatalytic reactions.
Temperature	Ambient (20–30°C) (types I and II)	Temperature affects the kinetics of the reactions and the solubility of the dissolved oxygen, which decreases with increasing reaction temperature. The optimum reaction temperature for the mineralization of organic contaminants is reported to be in the range of 20–80°C (Malato et al., 2009). Photocatalytic reaction temperatures > 80°C (e.g., in the case of solar PMRs) promote the recombination of charge carriers, thus disfavoring the adsorption of organic compounds onto the TiO_2 surface (Gaya and Abdullah, 2008).
Dissolved oxygen (aeration)	1-33 L min^{-1} (type I) No aeration (type II)	DO affects the formation of oxidants, the UVC light intensity, the stabilization of radical intermediates, the mineralization efficiency, and the suspension of the catalytic particles. Moreover, the partial pressure of oxygen may affect the mineralization rate of organics (being higher for higher partial pressures).
Hydraulic residence time (HRT)	0.5–50 h (type I)	HRT determines the effective degradation/mineralization of the organic contaminants depending on their nature and their initial concentrations. In case of real wastewaters, high HRTs are necessary owing to the slow mineralization kinetics usually achieved.
Light irradiation intensity	6-30 mW cm^{-2} (type I) 1.4–2.1 mW cm^{-2} (type II)	The photocatalytic reaction rate depends strongly on radiant flux. This dependency can be reduced from linear to zero at high intensities owing to the increased recombination of the electron–hole pair.

CB, conduction band; *DO*; *PMR*, photocatalytic membrane reactor; *VB*, valence band.

organic matter (NOM) (e.g., humic and fulvic acids, polysaccharides), which can be present in concentrations that are 10,000 times or even greater than those of the target synthetic pollutants detected in water sources (ground and surface water), would compete for the active sites on the photocatalyst surface or deactivate the photocatalyst and, subsequently, reduce the degradation rate of the target pollutants (Autin et al., 2013; Drosos et al., 2015). Moreover, NOM can foul the membrane surfaces (Katsoufidou et al., 2010; Patsios et al., 2013), thus degrading the overall system performance by reducing permeate flux. Similar to NOM, the presence of inorganic ions (e.g., Cl^-, NO_3^-, SO_4^{2-}, CO_3^{2-}, HCO_3^-) can drastically reduce the degradation efficiency because they act as holes (h^+) and hydroxyl radical scavengers (Konstantinou and Albanis, 2004). Formation of inorganic radical anions (e.g., $Cl^{\bullet}$, $NO_3^{\bullet}$) under these circumstances is possible to occur (Abdullah et al., 1990). Although the reactivity of these radicals may be considered, they are not as reactive as h^+ and $^{\bullet}OH$ (Hu et al., 2003). In the work of Autin et al. (2013), it was demonstrated that the increased alkalinity can drastically decrease the efficiency of UV/TiO_2 oxidation of metaldehyde owing to the formation of large TiO_2 aggregates. Moreover, these authors found that for a given NOM concentration, its character does not have a great influence on micropollutant removal. However, a seasonal increase of hydrophobic material will have a greater inhibitory effect than that of hydrophilic compounds (Autin et al., 2013). Additionally, investigations with real wastewater have revealed the attainment of slow mineralization kinetics (Chong et al., 2010), verifying the significant effect of the background organic and inorganic matrices. Such adverse effects would lead to increased HRT, larger reactor volumes, and energy consumption to achieve the removal of target pollutants, thus negatively impacting on treatment cost and environmental burden.

9.2.4 Performance Indicators

Appropriate performance indicators are essential for assessment of particular PMR versions as well as for comparisons with other similar water treatment processes. Energy consumption is a key issue impacting on both economic and environmental process performance. Therefore, an appropriate total energy consumption indicator is sought, related to the degree of pollutants' degradation.

PMR systems, like most AOPs that involve in situ generation of highly potent oxidants, are electric energy driven; thus minimization of energy consumption is a prime target for improved overall process efficiency. Therefore, a careful evaluation of the energy consumption of PMR technology is required, considering that the PMR process variants can achieve pollutants' removal/rejection by the membrane, in addition to their main function of pollutants' degradation either partially to simpler organic molecules or totally resulting in CO_2, H_2O (mineralization), and various inorganic ions. Regarding appropriate

indicators, Bolton et al. (2001) proposed a *figure-of-merit* for the comparison of the energy efficiency of these processes designated as *electrical energy per order* (E_{EO}), defined as the amount of electrical energy (in kWh) required to degrade the pollutant by one order of magnitude of concentration (90% degradation) in 1 m^3 of treated water, i.e.,

$$E_{EO} = \frac{P}{Flg\left(\frac{C_o}{C}\right)} \tag{9.1}$$

where P is the rated power (kW) of the PMR system, F is the water volumetric flow rate ($m^3\ h^{-1}$), and C_o and C are the initial (influent) and final (effluent) concentration of pollutants (mg L^{-1}). This definition is applicable to continuously operating systems and low concentrations of pollutants. Bolton et al. (2001) suggest that conventional methods such as NF/RO membrane separation and activated carbon adsorption are characterized by an infinite E_{EO}, considering that the pollutant is not degraded and its overall mass (both in the main stream and the sidestreams) before and after the treatment is the same.

The electrical energy consumption in a PMR system can vary widely depending on the configuration and the prevailing operating parameters, including the nature of the pollutants to be degraded, water quality parameters, and pollutants' initial concentration. Thus, it is of interest to review energy parameter values for PMR pilot studies reported in the literature, in relation to all their basic features. In Table 9.5, computed E_{EO} values are included for some literature PMR pilots that satisfy the *basic premises* set for this review in Section 9.2.1 and for which operating data are available. The schematic diagrams of PMR pilots examined and listed in Table 9.5 are illustrated in Figs. 9.3, 9.4, and 9.8.

The pilots examined in Table 9.5 use suspended/slurry photocatalyst reactors, submerged membrane modules (with two exceptions), and artificial light and reportedly implement a continuous mode of operation. It should be noted that quite a few parameter values of Table 9.5 were computed by using reported data; however, in some cases where the needed data were not available, or relevant performance data were scanty, calculations were based on reasonable assumptions. The following summary of observations, upon inspection of the contents of Table 9.5, is interesting for the purpose of this presentation.

- In almost all cases, commercial TiO_2 P-25 photocatalyst particles were used. No particular investigation of photocatalyst particle behavior (e.g., photocatalytic activity, robustness/aging issues) was reported.
- Few systems clearly reported conditions of periodic backwashing, although operation in continuous mode for a rather long time period was mentioned.
- Several PMR systems used MF (instead of UF) membranes despite well-known disadvantages of this membrane type regarding irreversible fouling, which is difficult to mitigate. Inadequate information is generally provided regarding membrane fouling issues.

Table 9.5: Design characteristics and energy consumption results for selected pilot PMR.

	Study	Units	Ryu	Meng	Lee	Rivero	Benotti	Sarasidis	Plakas	Doll	Huang
	Year		2005	2005	2006	2006	2009	2011	2016	2005	2007
Membranes	Morphology		Slurry type, submerged hollow fibers	Slurry type, submerged hollow fibers	Slurry type, submerged hollow fibers	Slurry type, external hollow fibers	Photo-Cat ceramic	Slurry type, submerged hollow fibers	Slurry type, submerged hollow fibers	Slurry type, external flat sheet	Slurry type, submerged hollow fibers
	Type		MF	UF	UF	MF	MF	UF	UF	MF	MF
	Area	(m^2)	8	1.5	0.7	0.157	NA	0.47	4.19	0.01	0.8
	Permeate Flux	($L\ m^{-2}\ h^{-1}$)	15	54	140	55	NA	14	15	100	24
	Backwashing —Pause —Pulse	(min)	3/9	Yes[a]	No	Yes[b]	0.0083/1[c]	1/9	1/9	Yes	1/10[a]
Irradiation	Type		UVA	UVC	UVC	UVC	UVC	UVA	UVC	UVC	UVC
	Number of Lamps		10	36	6	4	4/32	3	4	1	11
	Nominal Power per Lamp	(W)	30	40	40	25	191	30	39	14	29
	Total Power	(W)	300	1440	240	100	764/6112	90	156	14	319
Photocatalyst	Type		TiO_2-P25	TiO_2-P25	TiO_2-P25	TiO_2-UV100	TiO_2-P25	TiO_2-P25	TiO_2-P25	TiO_2-P25	TiO_2-P25
	Manufacturer		Degussa	IHI Co	Degussa	Hombikat	Degussa	Degussa	Degussa	Degussa	IHI Co
	Anatase-Rutile	(%)	80—20	80—20	NA	100—0	80—20	75—25	75—25	75—25	NA
Operating Parameters	Concentration	$g\ L^{-1}$	0.5 ± 0.1	0.4	1	10	0.05	0.75	0.5	1	0.4
	Water matrix		Tap	NS	Tap	RWW	NS	Tap	Tap	DE	Tap
	Pollutant		HA	4-CBA	BPA	Gray waters	DCF/ATR	SA	DCF	Clofibric acid	4-CBA
	Pollutant Concentration	($mg\ L^{-1}$)	3	70[d]	10	290[d]	2.8×10^{-4}/ 1.4×10^{-4}	2.23[e]	0.47	1.9	0.027

Continued

Table 9.5: Design characteristics and energy consumption results for selected pilot PMR.—cont'd

	Study	Units	Ryu	Meng	Lee	Rivero	Benotti	Sarasidis	Plakas	Doll	Huang
	Year		2005	2005	2006	2006	2009	2011	2016	2005	2007
	Working Volume	(L)	500	220	150	8	NA	9	25	15.9	100
	Hydraulic Residence Time	(h)	5.6	3.0	2.5	0.9	NA	1.7	0.5	15.9	4.1
	Output Volumetric Rate	($L\,h^{-1}$)	120	81	98	8.6	1440	6.6	62.9	1.0	24.4
	Mean Throughput	($L\,h^{-1}$)	90	73.3	60	8.6	1440	5.3	50.3	NA	19.2
Results	Removal (Pollutant)	(%)	90	—	95	—	99.7/ 87.5	—	90.5	98.6	50
	Removal (TOC or COD)	(%)	61.4	78.5	—	74	—	74.4	52.4	—	—
Energy Data	E_{lamps}	$kWh\,m^{-3}$	3.33	19.64	4.0	11.57	0.53/ 4.24	17.10	3.10	14.0	13.08
	E_{pumps}	$kWh\,m^{-3}$	1.88	NA	NA	NA	NA	19.38	3.15	NA	NA
	E_{air}	$kWh\,m^{-3}$	4.44	NA	NA	NA	NA	4.94	5.16	NA	NA
	E_{total}	$kWh\,m^{-3}$	9.65	NA	NA	NA	7.5/ 18.5	41.41	11.42	NA	NA
	E_{EO}	$kWh\,m^{-3}$	3.33	29.43	3.07	19.78	0.21/ 4.70	28.89	3.04	7.55	55.19

ATR, atrazine; *BPA*, bisphenol A; *COD*, chemical oxygen demand; *DCF*, diclofenac; *DE*, demineralized; *HA*, humic acids; *MF*, microfiltration; *NA*, not available; *NS*, natural surface; *PMR*, photocatalytic membrane reactor; *RWW*, real wastewater.

[a]Pause—intermittent suction.

[b]Pulse by airlift.

[c]Back pulse with air.

[d]as COD.

[e]as TOC.

- Scantly data are provided in relation to energy consumption, which are difficult to verify in several cases; therefore, assumptions were made to compute the listed E_{EO} values.
- E_{total} is the sum of other three terms; $E_{total} = E_{pumps} + E_{air} + E_{lamps}$.
- E_{EO} values listed are considered high (certainly far from a possible optimum) because of the fact that most PMR systems are overdesigned concerning the parameter *UV radiant power per unit volume* P_R (W L^{-1}).
- The system Photo-Cat (reported to be commercially available) is assessed by Benotti et al. (2009) for the removal of pharmaceuticals. In this system a MF ceramic membrane is used of unknown surface area. Owing to this and other missing data, there is uncertainty on the accuracy of listed E_{EO} value.
- Problems related to dissimilar pollutants' degradation tasks in the listed studies do not allow meaningful comparisons and assessment based on computed E_{EO}.

Summarizing, there is a wide variation of the reported energy consumption, listed in Table 9.5. Estimated electricity consumption varies between 0.2 and 55 KWh m^{-3} of treated water, depending on the size and conditions of the system considered. Small-size laboratory systems appear to have generally lower energy efficiency compared with pilots and larger-scale laboratory systems. Benotti et al. (2009) report that E_{EO} depends on the refractory nature of the molecules to be treated (in their specific case, pharmaceutically active compounds) and the level of treatment in terms of power input (i.e., number of UV lamps used). Thus, large differences are obtained between E_{EO} values for these cases. This disparity of E_{EO} values should not be surprising as, in most of the systems presented in the literature, little (if any) attention is paid to minimize energy consumption; indeed, such laboratory systems are usually overdesigned regarding the applied light source irradiation power (W) per unit working volume (L). In closing, the limited pilot studies reported in the literature (Fig. 9.7), and the uncertainties regarding estimation of a key energy consumption indicator, clearly point to the need for systematic PMR development work, as discussed in following sections.

9.3 Economic Issues

9.3.1 Equipment—Capital Expenses

A fairly detailed and reliable economic analysis of an industrial-size PMR system, relating process equipment design, construction, and operation to respective cost parameters (mainly treated water unit cost), is indispensable to PMR process developers as well as to researchers because it facilitates assessment and prioritization of those aspects and issues of the technology that need attention to achieve desirable improvements. A usual methodology applicable to typical process engineering projects can be used in the case of a novel PMR process as well. The basic task involves equipment design, specifications, and cost estimation; therefore, the type of equipment used and their availability in the market are significant in developing new processes.

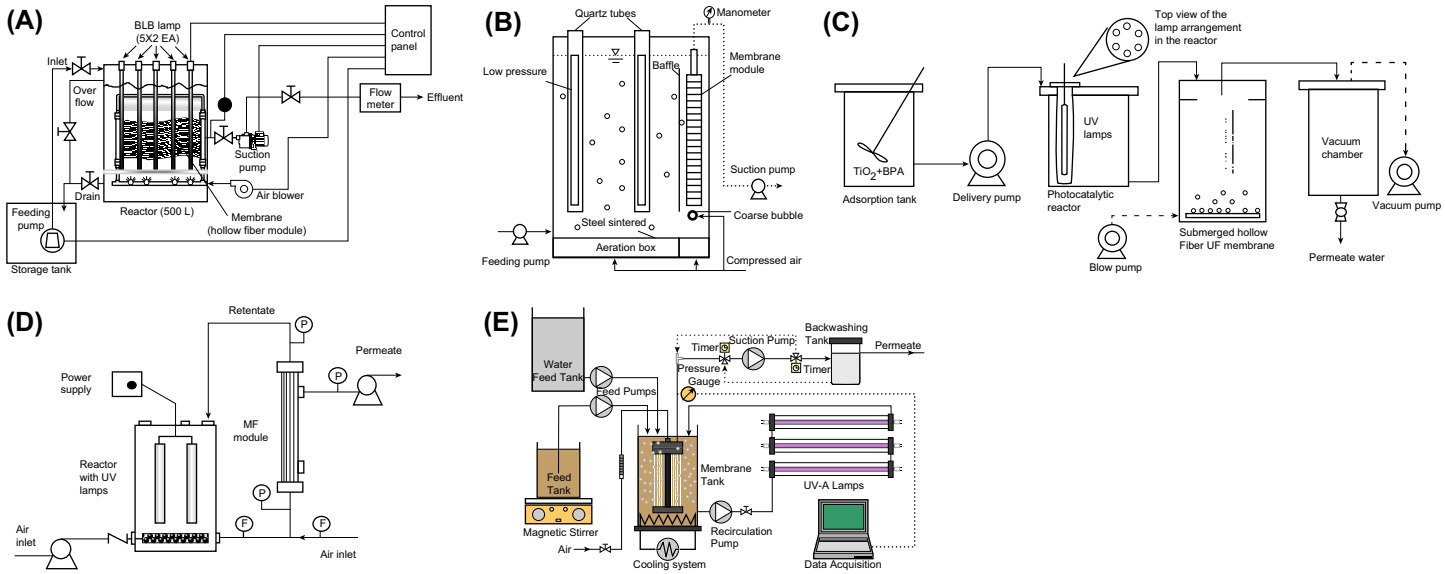

Figure 9.7

Schematic diagram of pilot-scale photocatalyst membrane hybrid reactors. *(A) Reprinted from Ryu et al., 2005. (B) Reprinted from Meng et al., 2005. (C) Reprinted from Lee et al., 2006. (D) Reprinted from Rivero et al., 2006. (E) Reprinted from Sarasidis et al., 2011.*

A typical PMR system involving UF membrane module(s) with dispersed photocatalyst comprises the following main parts:

- *Tanks*; inlet and product
- *Pumps* for feeding (water, photocatalyst suspension), recirculation, membrane backwashing
- *Membrane* module rack and vessel(s)
- *Air compressor*
- *Chemical cleaning systems*, such as CIP
- *Control and measurement instrumentation*; monitoring instruments, programmable logic controllers (PLCs)
- *UV light equipment* (bank of UV lamps or modules, LEDs) and vessels

It should be noted that all these pieces of equipment (with the possible exception of membranes and UV light equipment, for the PMR application) are standard in the industry. Even for these equipment types (i.e., membranes, UV), considerable relevant data are available and standardization has taken place, largely because of significant drinking water applications. Typical of the maturity level of these fields are the comprehensive manuals published by the US EPA on water membrane filtration (Allgeier et al., 2005) and UV disinfection (Schmelling et al., 2006). In particular, the field of membranes has evolved rather rapidly in the past two decades in terms of both equipment/module standardization and overall experience gained owing to extensive applications (e.g., Allgeier et al., 2005; Pearce, 2007). Nevertheless, some uncertainties still exist related to UF *membrane long-term* performance parameters and membrane effective lifetime for the new PMR applications, which are generally considered modest. Additionally, in the case of PMs (usually inorganic, for type II PMR), more significant design issues and related uncertainties exist, negatively impacting on cost estimation. Summarizing, it is expected that data from a novel PMR pilot operation under realistic conditions (at TRL ~ 7, Fig. 9.1) will aid to largely remove the aforementioned uncertainties (at least for type I units) and will permit fairly reliable estimates of capital and operating expenses. Additionally, the modular form of both membrane and UV equipment will facilitate up-scaling from pilot to full scale, thus rendering capital cost estimation fairly straightforward.

9.3.2 Operating Expenses

Regarding the operating expenses, translated into total *treated water unit cost* (€ m^{-3}), the particular cost items are fairly well defined; i.e., cost of capital, energy, personnel (including supervision, maintenance), chemicals, membrane, and UV lamps replacement.

Based on the experience with similar water treatment processes (e.g., Pearce, 2010b), it is foreseen that for type I systems the major cost items will be energy and capital expenses, with the greatest source of uncertainty related to energy consumption. The same assessment holds for type II PMR systems, where membrane replacement and performance restoration may be a major cost item; in these systems, the uncertainty related to membrane performance stability appears to be a major issue. In all PMR variants, the issues of optimal system geometric configuration, in connection with efficient UV light utilization, discussed in foregoing sections, are dominant and demand priority attention in the technology development tasks. A more detailed analysis of the economic aspects of PMR technology is provided in Chapter 11.

9.4 Sustainability Assessment

In recent years, it has been recognized that the selection of the appropriate water treatment technology for a specific application should be made on the basis of "triple bottom line" (TBL) approaches to sustainability, i.e., by using *environmental*, *economic*, and *social* criteria. This is critical when investing in full-scale operations because the applied technologies should satisfy well-defined and interrelated sustainability "pillars," within appropriate space and time boundaries. PMR has been characterized in literature as a green and sustainable technology, which can compete with other conventional and advanced water treatment technologies. This assessment has been mainly based on the environmental performance of the technology only at laboratory-scale experiments, without considering other relevant consequences, such as economic and social. However, evaluation of the PMR economic performance and its social impact are an integral part of the sustainability assessment that should be carried out in future studies with promising PMR systems, thus providing scientific support in the decision making for selecting the optimum among competing sustainability-enhancing technologies.

Table 9.6 presents some key sustainability issues in the form of objectives, accompanied by representative indicators and their direction (negative or positive depending on the desirable improvement). The sustainability assessment of a water treatment project should be placed in an adequately broad spatial and temporal perspective. Regarding the latter, all activities and aspects related to project should be considered, i.e., planning, design, construction, plant commissioning, operation, and even decommissioning. Spatially, an analysis should account for possible effects extending beyond the plant vicinity, as is the case of released "greenhouse gases" related with the energy consumption, and the disposal of plant effluents.

Currently used methods to assess the impacts of a water/wastewater treatment plant include the environmental impact assessment (EIA), life cycle assessment (LCA), best available technology (BAT), and the driver−pressure−state−impact−response (DPSIR)

Table 9.6: Objectives and respective indicators for the sustainability assessment of water treatment technologies; direction designates the desirable improvement.

Criteria	Objectives	Indicators	Direction
Economic	Minimization of costs	Investment costs	Negative
		Maintenance and Operation costs	Negative
Environmental	Minimization of energy use	Energy consumption	Negative
	Minimization of land use	Land area requirements	Negative
	Minimization of pollutants accumulation	Organic removal efficiency	Positive
	Minimization of odor/noise/visual impacts	Odor impact	Negative
		Noise impact	Negative
		Visual impact	Negative
	Minimization of global warming	Global warming potential	Negative
	Minimization of probability of mechanical failures	Reliability	Positive
	Minimization of chemicals utilized	Use of chemicals	Negative
	Minimization of sludge/waste production	Waste streams produced	Negative
	Optimal resource utilization/reuse	Potential for water reuse	Positive
Social	Maximization of local development	Employment	Positive
	Maximization of public acceptance	Public acceptance	Positive
	Minimization of the technological complexity	Complexity	Negative
	Level of education	Operator license	Positive
	Aesthetics	Measured level of nuisance from odor/noise	Negative

method, which are reviewed by Lior (2017). A database of 30 existing sustainability assessment methods is also reported in Zijp et al. (2017), including among others the ecological footprint, EU ecolabel, the life cycle costing (LCC), the material input per service unit (MIPS), product environmental footprint (PEF), and the sustainability assessment of technologies (SATs). A protocol to facilitate method selection is proposed in this work (Zijp et al., 2017) that covers (1) the decision context, (2) the different views of stakeholders, and (3) the selection of pertinent assessment methods. In addition, a tool for supporting utilization of the collated knowledge on method characteristics was designed in the format of a decision tree, based on the protocol steps, and implemented on a website (www.sustainabilitymethod.com).

Another approach to assess and compare process sustainability is based on the composite sustainability index (CSI), which involves numerous indicators to characterize various effects, leading to quantitative results (Lior, 2017). CSI aggregates multidimensional issues into one index, thus providing comprehensive coverage. However, it is frequently argued that CSIs are too subjective, as their results undesirably depend on the normalization method, a specific weighting scheme, and the aggregation method of subindicators.

Nevertheless, the general approach based on CSI computation is often implemented by using multicriteria analysis (MCA) techniques (Dodgson et al., 2009), which provide a theoretical framework for dealing with the complicated effects and interactions owing to the aforementioned issues. Studies using such approaches to assess sustainability have been reported in the fields of energy (Amer and Daim, 2011), manufacturing industries (Voces et al., 2012), and in the selection of technologies for secondary wastewater treatment (Molinos-Senante et al., 2014) and for tertiary treatment for water recycling (Plakas et al., 2016b).

Recently, an MCA framework was developed in authors' laboratory and used for assessing the sustainability performance of four tertiary municipal wastewater treatment technologies for effluents reuse (Plakas et al., 2016b). Three established technologies were included, i.e., powdered activated carbon adsorption coupled with UF membrane separation (PAC/UF), RO, ozone/UV light oxidation (O_3/UV), and a submerged PMR; the latter has been successfully tested in laboratory pilots (Patsios et al., 2013; Sarasidis et al., 2014; Karabelas et al., 2014) and has recently been scaled up for validation at appropriate end users' facilities (Plakas et al., 2016a). To strengthen the MCA framework, a participatory model was utilized (simple multi-attribute rating technique exploiting ranks weighting technique, SMARTER) (Edwards and Barron, 1994), which was based on a survey for capturing the judgments of decision makers in Greece (13 wastewater treatment plant operators who implement water reuse practices, serving in total more than 2 million people), thus enabling the development of a support tool for the selection of an appropriate wastewater treatment technology. The scope of the survey was the collection of critical judgments regarding the level of importance of each indicator.

Individual sustainability indicators were estimated on the basis of a comprehensive technical and scientific literature review, the real data from existing wastewater treatment plant operators using tertiary treatment (PAC/UF, RO, O_3/UV), and the long experience and expertise existing in the authors' laboratory (Plakas et al., 2016b). The numerical values of the individual sustainability indicators are summarized in Table 9.7. After the numerical weights were assigned to each sustainability indicator, a normalization of the performance matrix was performed to reformulate the entries for each indicator as single-dimensional units. Finally, the numerical value of the CSI for each wastewater treatment technology was defined (Table 9.8).

According to Table 9.8, PAC/UF is the best technology among the four, with composite index 81.04, being the most sustainable option in the economic and the environmental dimension. The RO, PMR, and O_3/UV follow with composite indices 65.16, 38.44, and 34.08, respectively. Although PMR appears to have reduced capital requirements among all the examined technologies, the operation and maintenance (O&M) costs are

Table 9.7: Quantitative and qualitative data of selected indicators for four tertiary wastewater treatment technologies assessed regarding their sustainability performance in producing recycled wastewater.

Indicators	O_3/UV	PMR	RO (With MF Pretreatment)	Activated Carbon (PAC/UF)
Investment costs (€ m^{-3} d^{-1})	224.2	10	732.5	300
O&M costs (€ m^{-3})	0.483	0.4	0.204	0.054 (PAC/sandfilter)
Energy consumption (KWh m^{-3})	3.68	3.3	0.6[a]	0.2 (PAC/UF), 0.08 (PAC/sand filter)
Land area required (m^2 m^{-3} d^{-1})[b]	0.0465	0.25	0.25	0.083
Xenobiotic efficiency removal	DCF ~93% ATR ~40%	DCF ~99.5% ATR ~87.8%	DCF > 95% ATR > 95%	DCF 79.5% ATR 74%
Odor impact	Very low to low	Very low	Moderate	(Not in the case of PAC disposal—and without regeneration)
Noise impact	Very low	Very low	Moderate	Very low
Visual impact	Very low	Very low	Moderate	Very low
Reliability	Medium	Medium	High	High
Employment (employees m^{-3} d^{-1})	0.00021	0.00046	0.00046	0.00033
Public acceptance	Moderate	Moderate	Low	Moderate
Complexity	Moderate	High	Moderate	High

ATR, atrazine; *DCF*, diclofenac; *MF*, microfiltration; *PAC*, powdered activated carbon; *PMR*, photocatalytic membrane reactor; *RO*, reverse osmosis; *UF*, ultrafiltration; *UV*, ultraviolet.

[a]Posttreatment excluded.

[b]Estimations based on existed plants of varying capacity.

Data based on analytical calculations and experimental results from relevant research activities at authors' laboratory, as well as on technical and scientific literature review. Reprinted from Plakas, K.V., Georgiadis, A.A., Karabelas A.J., 2016b. Sustainability assessment of tertiary wastewater treatment technologies: a multi-criteria analysis. Water Sci. Technol. 73 (7), 1532–1540, with permission from IWA Publishing.

Table 9.8: Dimensional scores and composite sustainability indices (CSIs) for four tertiary wastewater treatment technologies assessed regarding their sustainability performance in producing recycled wastewater.

Dimensions	O_3/UV	PMR	RO (With MF Pretreatment)	PAC/UF
Economic	9.43	16.78	11.38	25.52
Environmental	13.55	14.15	43.78	49.61
Social	11.10	7.50	10.00	5.90
Final score (composite index)	***34.08***	***38.44***	***65.16***	***81.04***

MF, microfiltration; *PAC*, powdered activated carbon; *PMR*, photocatalytic membrane reactor; *RO*, reverse osmosis; *UF*, ultrafiltration; *UV*, ultraviolet.

Reprinted from Plakas, K.V., Georgiadis, A.A., Karabelas A.J., 2016b. Sustainability assessment of tertiary wastewater treatment technologies: a multi-criteria analysis. Water Sci. Technol. 73 (7), 1532–1540, with permission from IWA Publishing.

considered high because of the energy requirements for the UV light lamps; however, the latter are based on estimates of available inadequate data. Thus, PMR stands in second place after PAC/UF. From the environmental perspective, PAC/UF is still considered as the most appropriate technology with minimum energy consumption, high reliability, and high effectiveness to tackle odor/noise/visual impacts. However, in the social sphere, the O_3/UV has received the best grades with small differences from the PMR and the RO.

A scenario analysis was also performed to make a "final check" of the robustness of the findings, including the CSI of each technology (Plakas et al., 2016b). Specifically, a multiple scenario was adopted, changing the dimensional weights of each one of the three sustainability pillars (economic, environmental, and social) from 5% to 90%. Fig. 9.8 shows the range of the CSI values for each of the four wastewater treatment technologies assessed, for the eight scenarios formed. It can be noted that PMR presents the least variability of the sustainability composite index, whereas PAC/UF and O_3/UV, the largest. The variability in the sustainability performance plays a crucial role in the selection of the final option; in fact, decision makers (or the involved stakeholders generally) occasionally exclude the most appropriate options (those derived from the analysis) even if they were the best available among alternatives because of the potential risk associated with their uncertainty (Shehabuddeen et al., 2006). Consequently, PMR technology might be considered as the most rational option, ensuring a minimum fluctuation in its sustainability performance, in an uncertain, complex, and evolving environment where the wastewater treatment technology would be operating.

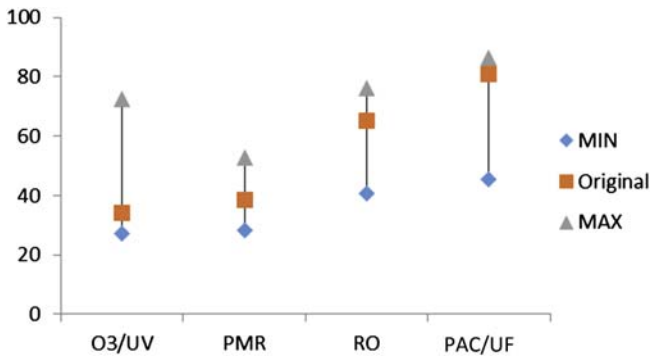

Figure 9.8

Variability of the composite sustainability index (CSI) for each of the four tertiary wastewater treatment technologies assessed regarding their sustainability performance in producing recycled wastewater. *PAC*, powdered activated carbon; *PMR*, photocatalytic membrane reactor; *RO*, reverse osmosis; *UV*, ultraviolet. *Reprinted from Plakas et al., 2016b.*

9.5 Conclusions and Future Trends

9.5.1 Overall Assessment

The PMRs are an attractive technology, *under development*, for water treatment applications, notably for purification of potable water and tertiary effluent for reuse. The technology assessment summarized in this chapter aims to identify the level of PMR maturity and the main issues hindering its development as well as to suggest R&D priorities in addressing issues toward PMR commercialization. Two types of PMR systems are considered herein, i.e., those using photocatalyst particles in suspension (type I) and other with photocatalyst particles embedded onto membranes (type II). In the implementation of both PMR types, three main process components are involved, i.e., *photocatalyst*, *light source*, and *membranes*. Technical issues, related to each one of these components and their considerable interaction, are at the heart of this technology assessment.

To quantify the assessment, in general, one can resort to the concept/index of TRL, which can be estimated on the basis of literature information; however, the TRL index (although useful) does not provide necessary details on issues hindering technology development. A comprehensive assessment considering all sustainability issues requires, among others, determination of key indicators, which are technical, environmental, economic, and social. The most important metrics to assess sustainable performance of a PMR system (for a specific treatment task) are the *SEC* and the unit *cost of processed water*, in kWh m^{-3} and € m^{-3}, respectively.

The *PMR equipment morphology* is of paramount importance, as it directly affects (among other parameters) the most critical system parameter, i.e., the total SEC. The few PMR configurations for both types reported in the literature, although promising, need significant development work, focused mainly on maximization of apparent quantum efficiency (particularly for type I PMR). In the case of artificial light sources, optimization of the detailed equipment geometry in the vicinity of those sources is needed to minimize both the energy losses, because of light absorption and scattering, and HRT that indirectly affects SEC.

Extensive laboratory work has been carried out on *photocatalysts* development, and quite a few novel UV-vis active photocatalyst types have been prepared, although for dispersion systems (type I PMR) the use of TiO_2 dominates because of its well-known attributes. However, information is lacking on the long-term photocatalyst performance characteristics, especially under realistic conditions. Specifically, the photocatalytic activity, the mechanical and chemical stability, the corrosivity, and the reusability of a new photocatalyst should be tested over a significant period of time with real water/wastewater streams. Such work should reveal the strengths and weaknesses of the new photocatalytic

materials and help identify those with longevity and therefore appropriateness for commercial applications.

Regarding *artificial light sources*, mercury vapor fluorescent lamps, i.e., of LP or MP dominate in PMR literature, as they possess sufficient energy to generate electron—hole pairs (e^-—h^+) within the heterogeneous photocatalysts (TiO_2, ZnO, etc.). The utilization of mercury vapor lamps has received considerable criticism regarding their relatively high energy consumption, short life span, and environmental impact due to lamp disposal. This criticism is certainly valid and well taken. However, the issues related to UV type should be considered in the broader context of PMR system sustainability; i.e., using mercury vapor fluorescent lamps should be assessed in a comprehensive manner as part of the overall performance of large-scale pilots that operate for long periods of time in realistic environments. Such an assessment is required to gain sufficient data and experience (including data on UV source performance) for commercial system design and comparison with other conventional or advanced treatment technologies. Recently, UV LEDs have emerged as possible alternative light sources for photocatalysis, although their available radiant flux or output power (especially of the UVB and UVC ones) is still low. Considering their significant advantages over the mercury lamps (i.e., environmentally benign, longer lifetime, robust, low power requirements) and the demand for an environment-friendly, reliable, and energy-efficient light source for applications, including sterilization and disinfection, significant research effort is concentrated by LED manufacturers to increase their power output. It is noted that this assessment covers systems designed to operate with solar irradiation as well, although the significance of the technical issues is somewhat different compared with the use of artificial light sources.

The development of *membranes* for other water treatment applications will prove helpful for advancing PMR toward commercialization. Indeed, for type I systems, the low-pressure UF membrane technology is well developed and ready for direct implementation in PMR; operating experience is extensive and well-tested techniques are available to maintain good long-term performance of such membranes. However, for type II systems, where the membranes (mostly inorganic) have the additional function of supporting the photocatalyst, more development work appears to be required.

In terms of *overall system design*, there are no particular complications, provided the aforementioned issues on the PMR components are effectively dealt with. In general, because of the modular type of PMR components (i.e., membranes and irradiation sources), no significant scale-up issues are foreseen toward commercial size units. Additionally, the type of equipment needed (particularly for the type I system) comprises mostly off-the-shelf items (membrane modules, UV light equipment, pumps, control systems), rather easy to adapt to the PMR requirements. There is uncertainty, however, regarding the type II special PM modules, which may present difficulties in large-scale fabrication.

PMR system performance depends on a number of *operating parameters* such as photocatalyst loading, solution pH, light irradiation intensity, aeration, HRT, and temperature. Their values may vary significantly depending on the geometry, the working conditions of the system, the feedwater composition (alkalinity, presence of NOM, and inorganic ions), the nature and the concentration of the target pollutants, and of course the treatment goal. It is understood that, at this early stage of PMR development, the optimum values of the operating parameters are likely to be site specific and should be determined by well-designed pilot-scale experiments (e.g., by using design of experiments [DOE] and response surface analysis [RSA] methodologies).

Dealing with *economic issues* of novel PMR is foreseen to present no complications. Indeed, estimation of capital expenses is expected to be straightforward in view of the aforementioned relative simplicity of PMR system design and the commercially available equipment for the key components, which can be adapted to the novel system requirements. Similarly, estimation of novel PMR operating expenses appears, at first look, rather straightforward in terms of cost items involved and methodology; however, significant uncertainty exists regarding the long-term photocatalyst performance in practical applications and the related expenses for photocatalyst renewal or performance restoration (in the type II case) by using costly and environmentally undesirable chemicals. Should these uncertainties be resolved, fairly accurate estimation of total treatment cost would be possible, which is essential for any type of assessment.

In respect of overall *sustainability assessment*, it is observed that to date there is no comprehensive assessment available on the sustainability of a PMR system (of type I or II) on the basis of the three pillars of sustainability (environmental, economic, and social). This is attributed mainly to the lack of full-scale PMR studies in relevant and/or operational environments and partly to unavailable methodology for comprehensive sustainability assessments. Such studies with promising PMR systems are critical, before investing in full-scale operations, because the new technologies must satisfy the quantitatively defined and interrelated sustainability criteria, within appropriate space and time boundaries. Nevertheless, preliminary efforts outlined in this chapter suggest that novel PMR systems may be superior to competing conventional technologies in terms of overall process sustainability.

The foregoing critical assessment of the promising PMR technology suggests that the respective TRL is relatively low (at $\sim$4 to 5) at present; therefore, substantial development work is required to resolve all the aforementioned issues and to render the PMR systems sustainable, attractive, and ready for commercialization (with TRL = 9). In pursuing the aforementioned PMR process development toward commercialization, significant pilot demonstration activity in real environments will be

required to optimize key design and operating parameters, such as apparent quantum efficiency, photocatalyst concentration, and HRT. After the demonstration stage, it will be possible to determine process economic and environmental indicators (i.e., total processing unit cost, CO_2/environmental footprint) with the required accuracy. It should be stressed, however, that the novel PMR hybrid process(es) would compete for a place in a market characterized by conservatism and well-established conventional processes, which operate with fair reliability for a long time. The ever more stringent environmental standards in the water sector pose an additional challenge to this novel technology. However, some distinct advantages of the PMR systems compared with conventional techniques, particularly regarding overall environmental performance (i.e., elimination or drastic minimization of sidestreams), may prove decisive in achieving commercialization. In parallel to the aforementioned development efforts, tackling the issues of PMR component and system *standardization* should be pursued. It is hoped that relevant significant steps already taken in the European Union regarding photocatalysts' standardization (in connection with some existing standards on membranes and UV light equipment) will lead to adequate system standardization, thus facilitating PMR commercialization.

9.5.2 R&D Priorities

The PMR technology, which is under development, involves three basic components (i.e., photocatalysts, photon irradiation sources, and membranes) interacting quite strongly in process equipment implementing the basic photocatalytic reaction(s). This strong interaction (indicated in Fig. 9.2) is manifested through several simultaneously occurring phenomena that impact on the basic photocatalytic process, thus rendering the prediction of the targeted outcome (i.e., the apparent degradation rate of organic pollutants) extremely difficult to predict for a process system operating under real conditions. For instance, for type I PMR, such phenomena include photocatalyst particle agglomeration as a function of treated fluid composition and related effects on species mass transfer into particles, photocatalyst particle concentration effects acting in opposite direction regarding reaction kinetics (beneficial) and light absorption and scattering (detrimental), effect of flow conditions in the vicinity of UV lamps impacting on local particle concentration distribution and on the above phenomena, organic compound adsorption on photocatalyst particles and interference with the above mechanisms, photocatalyst particle aging phenomena also affected by the above mechanisms, effects due to concentration of primary pollutants and their fragments.

The above issues that concern the basic mechanisms and phenomena (occurring at small spatial scale) have to be integrated toward development of a comprehensive model applicable to the entire equipment/system size, which is an extremely difficult task.

Despite its significance, limited work has been done in this direction, with notable contributions by Alfano et al. (2013) and Ray (2009) in the areas of photocatalytic process modeling and PMR system configuration. Most published studies have dealt with photocatalyst preparation and performance evaluation under various (not always well-defined) conditions and have provided information, which is useful in efforts to develop the PMR systems. However, as outlined in this chapter, in pursuing *PMR commercial system development*, significant challenges lie ahead, and much more data of different types (beyond process fundamentals and modeling) are required to assess the technical, economic, and environmental performance of the entire system.

To address these challenges, application of a typical chemical process engineering methodology is needed, whereby, given the process target, information on various above-mentioned particular mechanisms (largely available or to be complemented) would be synthesized through a comprehensive model, implemented in a computer-aided process simulator; such a tool would serve to carry out reliable parametric studies and performance simulations of PMR processes equipment under realistic conditions. In parallel, existing and novel equipment/system morphologies should be investigated, preferably with the aid of the aforementioned simulator. Regardless of whether a simulator is available or not, the typical engineering approach should be pursued of building and operating flexible pilot plants of significant size, *capable of operating continuously* and providing detailed data on all the aforementioned key system parameters; successful efforts in this direction have already been reported (e.g., Plakas et al., 2016a,b). Data from these pilot studies should provide correlations of the main PMR design and operating parameters as a function of system characteristics. Therefore, these *pilot studies are considered a top priority* in R&D toward PMR technology development, as they can provide valuable data to clarify the effect of key parameters (particularly SEC) as well as assess the *long-term performance* of PMR system components outlined below.

In the following, the present "state of PMR technology" is summarized and R&D priorities are suggested, regarding technical/scientific issues involved in the main PMR types.

Type I PMR (photocatalyst dispersion type system) comprises three distinct components:

1. *Photocatalysts*. Extensive information is available on the well-tested commercial and inexpensive TiO_2 as well as on other novel and promising photocatalysts; however, although there is scope in further pursuing photocatalyst development studies, *top R&D priority is placed on testing the long-term performance (*i.e., *photocatalytic activity, aging/degradation, mechanical properties) of promising photocatalysts, preferably in pilot units under realistic conditions*, as outlined above.
2. *UF membrane separation modules*. There is ample practical experience, gained in similar water treatment processes, using *organic hollow fiber* membranes, preferably of

the submerged type. PMR pilot tests with such membranes show that the available experience with UF membranes can be readily transferred to the hybrid photocatalytic systems, enabling them to achieve smooth continuous operation. However, *the long-term performance stability* of these membranes needs to be examined in realistic pilot experiments; this R&D item is of modest priority.

3. *UV light source*. Commercial mercury-type lamps are preferable at present, considering the rich operating experience and existing standardization. LED sources appear to need significant development work. The issues of UV type and optimization of irradiation power, for certain classes of PMR applications, should be treated (in conjunction with UV module and overall system configuration) as *a top priority R&D topic*, to be tackled at the level of modeling/simulation and realistic pilot testing. Regarding solar light utilization, the dominant issue of high priority is optimization of equipment configuration to cope with the temporal variability of solar irradiation.

Type II PMR (photocatalyst embedded onto membranes) comprises the aforementioned components that exhibit a greater degree of complexity.

1. A variety of embedded photocatalysts have been tested in the laboratory; however, additional research is needed, primarily in the context of *photocatalyst performance stability* (including measures to maintain it) over a long time period in continuous process applications. This is a *top R&D priority* item to be pursued preferably under realistic pilot-scale conditions.
2. *Inorganic membranes* with embedded photocatalysts are a clear choice over organic ones as the latter are subject to degradation due to UV irradiation and the oxidative environment. The issue of *recalcitrant foulants deposition* on the membranes, affecting both their photocatalytic and separation functions (in connection with item 1), is of *high priority* to address through realistic pilot testing.
3. Regarding UV light source, the same general issues hold, as outlined above, although the need to *directly* irradiate the PMs introduces additional complications to large-scale equipment design. R&D work on these design issues is definitely warranted.

A significant issue to be encountered in any PMR system application is the degree of pollutants' mineralization as well as the type and toxicity of fragments because of their incomplete degradation. High priority should be placed on relevant R&D work at both basic and pilot plant level. Finally, as outlined in preceding sections, development of appropriate ISO standards should be pursued to enable assessment of photocatalysts' performance as well as of entire novel PMR systems. Once the above scientific/technical issues have been adequately addressed and the related uncertainties removed, it is foreseen that equipment scale-up and determination of technical, economic, and environmental PMR performance indicators will be straightforward.

List of Acronyms

AOPs	Advanced oxidation processes
ATR	Atrazine
ATZ	Aluminium/titanium/zirconium (mixture of oxides)
BAT	Best available technology
BPA	Bisphenol A
CA	Cellulose acetate
CB	Conduction band
CEN	Comité Européen de Normalisation (European Committee of Standardisation)
CIP	Cleaning in place
COD	Chemical oxygen demand
CPC	Compound parabolic collector
CSI	Composite sustainability index
CVD	Chemical vapor deposition
DCF	Diclofenac
DOE	Design of experiments
DPSIR	Driver-pressure-state-impact-response
EIA	Environmental impact assessment
HA	Humic acids
HPLC	High-performance liquid chromatography
HRT	Hydraulic residence time
ISO	International Standards Organization
LCA	Life cycle assessment
LCC	Life cycle costing
LED	Light-emitting diode
LP	Low pressure
MBR	Membrane bioreactor
MCA	Multicriteria analysis
MF	Microfiltration
MIPS	Material input per service unit
MP	Medium pressure
NF	Nanofiltration
NOM	Natural organic matter
O&M	Operation and maintenance
PAC	Powdered activated carbon
PAN	Polyacrylonitrile
PEF	Product environmental footprint
PES	Polyethersulfone
PFP	Plug flow photoreactor
PLC	Programmable logic controller
PM	Photocatalytic membrane
PMF	Photocatalytic membrane filtration
PMR	Photocatalytic membrane reactor
POE	Point of entry
POU	Point of use
PVDF	Polyvinylidene fluoride
PZC	Point of zero charge
R&D	Research and development
RO	Reverse osmosis

RSA	Response surface analysis
SA	Sodium alginate
SAT	Sustainability assessment of technologies
SEC	Specific energy consumption
SMARTER	Simple Multi-Attribute Rating Technique Exploiting Ranks
SMPR	Submerged membrane photocatalytic reactor
TBL	Triple bottom line
TOC	Total organic carbon
TRL	Technology readiness level
UF	Ultrafiltration
UV	Ultraviolet
VB	Valence band
WHO	World Health Organization

List of Symbols

C	Final (effluent) concentration of pollutants (mg L^{-1})
C_o	Initial (influent) concentration of pollutants (mg L^{-1})
F	Water volumetric flow rate (m^3 h^{-1})
P	Rated power of the PMR system (kW)

References

Abdullah, M., Low, G.K.C., Matthews, R.W., 1990. Effects of common inorganic ions on rates of photocatalytic oxidation of organic-carbon over illuminated titanium dioxide. J. Phys. Chem. 94, 6820–6825.

Adán, C., Marugán, J., Mesones, S., Casado, C., van Grieken, R., 2017. Bacterial inactivation and degradation of organic molecules by titanium dioxide supported on porous stainless steel photocatalytic membranes. Chem. Eng. J. 318, 29–38.

AEROSIL, 2017. http://www.aerosil.com/lpa-productfinder/page/productsbytext/detail.html?pid=1822&lang=en.

Ahmad, H., Kamarudin, S.K., Minggu, L.J., Kassim, M., 2015. Hydrogen from photocatalytic water splitting process: a review. Renew. Sustain. Energy Rev. 43, 599–610.

Al Aani, S., Wright, C.J., Atieh, M.A., Hilal, N., 2017. Engineering nanocomposite membranes: addressing current challenges and future opportunities. Desalination 401, 1–15.

Al-Hamdi, A.M., Rinner, U., Sillanpää, M., 2017. Tin dioxide as a photocatalyst for water treatment: a review. Process Saf. Environ. Prot. 107, 190–205.

Alexander, M., 1975. Environmental and microbiological problems arising from recalcitrant molecules. Microb. Ecol. 2 (1), 17–27.

Alfano, O.M., Cassano, A.E., Brandi, R.J., Satuf, M.L., 2013. A methodology for modeling slurry photocatalytic reactors for degradation of an organic pollutant in water. In: Pichat, P. (Ed.), Photocatalysis and Water Purification: From Fundamentals to Recent Applications. Wiley-VCH Verlag GmbH & Co, Weinheim, Germany.

Allgeier, S., Alspach, B., Vickers, J., 2005. Membrane Filtration Guidance Manual, USEPA, Office of Water. Report No EPA 815-R-06–009.

Amer, M., Daim, T.U., 2011. Selection of renewable energy technologies for a developing county: a case of Pakistan. Energy Sustain. Dev. 15, 420–435.

American Air & Water®, Inc., 2017. http://www.americanairandwater.com/lamps.htm.

AMI® Applied Membranes Inc., 2017. Ultrafiltration Membranes. http://www.appliedmembranes.com/ultrafiltration-membranes-uf-membranes.html.

Athanasekou, C.P., Romanos, G.E., Katsaros, F.K., Kordatos, K., Likodimos, V., Falaras, P., 2012. Very efficient composite titania membranes in hybrid ultrafiltration/photocatalysis water treatment processes. J. Membr. Sci. 392–393, 192–203.

Athanasekou, C.P., Moustakas, N.G., Morales-Torres, S., Pastrana-Martínez, L.M., Figueiredo, J.L., Faria, J.L., Silva, A.M.T., Dona-Rodriguez, J.M., Romanos, G.E., Falaras, P., 2015. Ceramic photocatalytic membranes for water filtration under UV and visible light. Appl. Catal. B Environ. 178, 12–19.

Athanasiou, D.A., Romanos, G.E., Falaras, P., 2016. Design and optimization of a photocatalytic reactor for water purification combining optical fiber and membrane technologies. Chem. Eng. J. 305, 92–103.

Augugliaro, V., García-López, E., Loddo, V., Malato-Rodríguez, S., Maldonado, I., Marcì, G., Molinari, R., Palmisano, L., 2005. Degradation of lincomycin in aqueous medium: coupling of solar photocatalysis and membrane separation. Sol. Energy 79, 402–408.

Autin, O., Hart, J., Jarvis, P., MacAdam, J., Parsons, S.A., Jefferson, B., 2013. The impact of background organic matter and alkalinity on the degradation of the pesticide metaldehyde by two advanced oxidation processes: UV/H_2O_2 and UV/TiO_2. Water Res. 47, 2041–2049.

Bahnemann, D., 2004. Photocatalytic water treatment: solar energy applications. Sol. Energy 77, 445–459.

Bahnemann, D.W., Kormann, C., Hofmann, M.R., 1987. Preparation and characterization of quantum size zinc oxide: a detailed spectroscopic study. J. Phys. Chem. 91, 3789–3798.

Bai, H., Liu, L., Liu, Z., Sun, D.D., 2013a. Hierarchical 3D dendritic TiO_2 nanospheres building with ultralong 1D nanoribbon/wires for high performance concurrent photocatalytic membrane water purification. Water Res. 47, 4126–4138.

Bai, X., Wang, L., Zong, R., Lv, Y., Sun, Y., Zhu, Y., 2013b. Performance enhancement of ZnO photocatalyst via synergic effect of surface oxygen defect and graphene hybridization. Langmuir 29 (9), 3097–3105.

Baker, R.W., 2000. Membrane Technology and Applications. McGraw Hill.

Bard, A.J., 1980. Photoelectrochemistry. Science 207, 139–144.

Benotti, M.J., Stanford, B.D., Wert, E.C., Snyder, S.A., 2009. Evaluation of a photocatalytic reactor membrane pilot system for the removal of pharmaceuticals and endocrine disrupting compounds from water. Water Res. 43, 1513–1522.

Beydoun, D., Amal, R., Low, G., McEvoy, S., 1999. Role of nanoparticles in photocatalysis. J. Nanopart. Res. 1, 439–458.

Bickley, R.I., Gonzalez-Carreno, T., Lee, J.S., Palmisano, L., Tilley, R.J.D., 1991. A structural investigation of titanium dioxide photocatalysts. J. Solid State Chem. 92, 178–190.

Blake, D.M., 1997. Bibliography of Work on Photocatalytic Removal of Hazardous Compounds from Water and Air. NREL/TP-430–22197. National Renewable Energy Laboratory, Golden.

Bolton, J.R., Bircger, K.G., Tumas, W., Tolman, C.A., 2001. Figure-of merit for the technical development and application of advanced oxidation technologies for both electric and solar-derived systems. Pure Appl. Chem. 73, 627–637.

Bora, L.V., Mewada, R.K., 2017. Visible/solar light active photocatalysts for organic effluent treatment: fundamentals, mechanisms and parametric review. Renew. Sustain. Energy Rev. 76, 1393–1421.

Burggraaf, A.J., Cot, L. (Eds.), 1996. Fundamentals of Inorganic Membrane Science and Technology, Membrane Science and Technology Series 4. Elsevier.

Cámara, R.M., Portela, R., Gutiérrez-Martín, F., Sánchez, B., 2016. Photocatalytic activity of TiO_2 films prepared by surfactant-mediated sol–gel methods over commercial polymer substrates. Chem. Eng. J. 283, 535–543.

Cappelletti, G., Bianchi, C.L., Ardizzone, S., 2008. Nano-titania assisted photoreduction of Cr(VI): the role of the different TiO_2 polymorphs. Appl. Catal. B Environ. 78 (3–4), 193–201.

Carp, O., Huisman, C.L., Reller, A., 2004. Photoinduced reactivity of titanium dioxide. Prog. Solid State Chem. 32 (1–2), 33–177.

CEN/TC 386 - Photocatalysis, 2017. https://standards.cen.eu/dyn/www/f?p=204:7:0::::FSP_ORG_ID:653744&cs=1F934586869740A2BF8530F361AE25EBA.

Chen, T.-T., Chang, I.-C., Yang, M.-H., Chiu, H.-T., Lee, C.-Y., 2013. The exceptional photo-catalytic activity of ZnO/RGO composite via metal and oxygen vacancies. Appl. Catal. B Environ. 142–143, 442–449.

Chin, S.S., Lim, T.M., Chiang, K., Fane, A.G., 2007. Hybrid low-pressure submerged membrane photoreactor for the removal of bisphenol A. Desalination 202, 253–261.

Chong, M.N., Jin, B., Chow, C.W.K., Saint, C., 2010. Recent developments in photocatalytic water treatment technology: a review. Water Res. 44, 2997–3027.

Choo, K.H., Tao, R., Kim, M.J., 2008. Use of a photocatalytic membrane reactor for the removal of natural organic matter in water: effect of photoinduced desorption and ferrihydrite adsorption. J. Membr. Sci. 322, 368–374.

Chowdhury, S., Balasubramanian, R., 2014. Graphene/semiconductor nanocomposites (GSNs) for heterogeneous photocatalytic decolorization of wastewaters contaminated with synthetic dyes: a review. Appl. Catal. B Environ. 160–161, 307–324.

Crawford, M.H., Banas, M.A., Ross, M.P., Ruby, D.S., Nelson, J.S., Boucher, R., Allerman, A.A., 2005. Final LDRD Report: Ultraviolet Water Purification Systems for Rural Environments and Mobile Applications. Sandria National Laboratories, Albuquerque, New Mexico.

Damodar, R.A., You, S.J., Ou, S.H., 2010. Coupling of membrane separation with photocatalytic slurry reactor for advanced dye wastewater treatment. Sep. Purif. Technol. 76, 64–71.

Daneshvar, N., Salari, D., Niaei, A., Rasoulifard, M.H., Khataee, A.R., 2005. Immobilization of TiO_2 nanopowder on glass beads for the photocatalytic decolorization of an azo dye C.I. direct red 23. J. Environ. Sci. Health Part A 40, 1605–1617.

Dionysiou, D.D., Li Puma, G., Ye, J., Schneider, J., Bahnemann, D., 2016. Photocatalysis Applications. The Royal Society of Chemistry, Cambridge, UK.

Dodgson, J.S., Spackman, M., Pearman, A., Phillips, L.D., 2009. Multi-Criteria Analysis: A Manual. Communities and Local Government Publications, Wetherby, UK, West Yorkshire.

Doll, T.E., Frimmel, F.H., 2005. Cross-flow microfiltration with periodical back-washing for photocatalytic degradation of pharmaceutical and diagnostic residues—evaluation of the long-term stability of the photocatalytic activity of TiO_2. Water Res. 39, 847–854.

Drosos, M., Ren, M., Frimmel, F.H., 2015. The effect of NOM to TiO_2: interactions and photocatalytic behavior. Appl. Catal. B Environ. 165, 328–334.

Edwards, W., Barron, H.F., 1994. SMARTS and SMARTER: improved simple methods for multi-attribute utility measurement. Organ. Behav. Hum. Decis. Process. 60, 306–325.

Eskandarian, M.R., Choi, H., Fazli, M., Rasoulifard, M.H., 2016. Effect of UV-LED wavelengths on direct photolytic and TiO_2 photocatalytic degradation of emerging contaminants in water. Chem. Eng. J. 300, 414–422.

Falaras, P., Romanos, G., Aloupogiannis, P., 2012. Photocatalytic Purification Device. European Patent, EP 2409954 (A1)–2012-01-25. National Center for Scientific Research Demokritos, Innovative Research & Technology Ltd.

Fang, W., Xing, M., Zhang, J., 2017. Modifications on reduced titanium dioxide photocatalysts: a review. J. Photochem. Photobiol. C Photochem. Rev. 32, 21–39.

Fernández, R.L., McDonald, J.A., Khan, S.J., Le-Clech, P., 2014a. Removal of pharmaceuticals and endocrine disrupting chemicals by a submerged membrane photocatalysis reactor (MPR). Sep. Purif. Technol. 127, 131–139.

Fernández, R.L., Coleman, H.M., Le-Clech, P., 2014b. Impact of operating conditions on the removal of endocrine disrupting chemicals by membrane photocatalytic reactor. Environ. Technol. 35 (16), 2068–2074.

Fox, M.A., Dulay, M.T., 1993. Heterogeneous photocatalysis. Chem. Rev. 93 (1), 341–357.

Frank, S.N., Bard, A.J., 1977. Heterogeneous photocatalytic oxidation of cyanide ion in aqueous solutions at titanium dioxide powder. J. Am. Chem. Soc. 99 (1), 303–304.

French, R.A., Jacobson, A.R., Kim, B., Isley, S.L., Lee Penn, R., Baveye, P.C., 2009. Influence of ionic strength, pH, and cation valence on aggregation kinetics of titanium dioxide nanoparticles. Environ. Sci. Technol. 43, 1354–1359.

Friedmann, D., Hakki, A., Kim, H., Choi, W., Bahnemann, D., 2016. Heterogeneous photocatalytic organic synthesis: state-of-the-art and future perspectives. Green Chem. 18, 5391−5411.

Fu, J., Ji, M., Wang, Z., Jin, L., An, D., 2006. A new submerged membrane photocatalysis reactor (SMPR) for fulvic acid removal using a nano-structured photocatalyst. J. Hazard. Mater. B131, 238−242.

Fujishima, A., Honda, K., 1972. Electrochemical photolysis of water at a semiconductor electrode. Nature 238, 37−38.

Fujishima, A., Zhang, X., Tryk, D.A., 2007. Heterogeneous photocatalysis: from water photolysis to applications in environmental cleanup. Int. J. Hydrogen Energy 32, 2664−2672.

Galbraith, J., 2016. Current State of UV LED Technology. http://www.koppglass.com/blog/current-state-of-uv-led-technology/.

Gaya, U.I., Abdullah, A.H., 2008. Heterogeneous photocatalytic degradation of organic contaminants over titanium dioxide: a review of fundamentals, progress and problems. J. Photochem. Photobiol. C Photochem. Rev. 9, 1−12.

Gerrity, D., Ryu, H., Crittenden, J., Abbaszadegan, M., 2008. Photocatalytic inactivation of viruses using titanium dioxide nanoparticles and low-pressure UV light. J. Environ. Sci. Health Part A 43, 1261−1270.

Grzechulska-Damszel, J., Mozia, S., Morawski, A.W., 2010. Integration of photocatalysis with membrane processes for purification of water contaminated with organic dyes. Catal. Today 156, 295−300.

Grover, I.S., Prajapat, R.C., Singh, S., Pal, B., 2017. Highly photoactive Au-TiO_2 nanowires for improved photo-degradation of propiconazole fungicide under UV/sunlight irradiation. Sol. Energy 144, 612−618.

Gupta, S.M., Tripathi, M., 2011. A review of TiO_2 nanoparticles. Chin. Sci. Bull. 56 (16), 1639−1657.

Habibi, M.H., Hassanzadeh, A., Mahdavi, S., 2005. The effect of operational parameters on the photocatalytic degradation of three textile azo dyes in aqueous TiO_2 suspensions. J. Photochem. Photobiol. A Chem. 172, 89−96.

Henthorne, L., Boysen, B., 2015. State-of-the-art of reverse osmosis desalination pretreatment. Desalination 356, 129−139.

Hernandez-Alonso, M.D., Fresno, F., Suarez, S., Coronado, J.M., 2009. Development of alternative photocatalysts to TiO_2: challenges and opportunities. Energy Environ. Sci. 2, 1231−1257.

Hisatomi, T., Kubota, J., Domen, K., 2014. Recent advances in semiconductors for photocatalytic and photoelectrochemical water splitting. Chem. Soc. Rev. 43, 7520−7535.

Hoffmann, M.R., Martin, S.T., Choi, W., Bahneman, D.W., 1995. Environmental applications of semiconductor photocatalysis. Chem. Rev. 95, 69−96.

Holmberg, J.P., Ahlberg, E., Bergenholtz, J., Hassellöv, M., Abbas, Z., 2013. Surface charge and interfacial potential of titanium dioxide nanoparticles: experimental and theoretical investigations. J. Colloid Interface Sci. 407, 168−176.

Horng, R.-Y., Huang, C., Chang, M.-C., Shao, H., Shiau, B.-L., Hu, Y.-J., 2009. Application of TiO_2 photocatalytic oxidation and non-woven membrane filtration hybrid system for degradation of 4-chlorophenol. Desalination 245, 169−182.

Horovitz, I., Avisar, D., Baker, M.A., Grilli, R., Lozzi, L., 2016. Carbamazepine degradation using a N-doped TiO_2 coated photocatalytic membrane reactor: influence of physical parameters. J. Hazard. Mater. 310, 98−107.

Hu, C., Yu, J.C., Hao, Z., Wong, P.K., 2003. Effects of acidity and inorganic ions on the photocatalytic degradation of different azo dyes. Appl. Catal. B Environ. 46 (1), 35−47.

Hu, A., Zhang, X., Oakes, K.D., Peng, P., Servos, M.R., 2011. Hydrothermal growth of free standing TiO_2 nanowire membranes for photocatalytic degradation of pharmaceuticals. J. Hazard. Mater. 189 (1−2), 278−285.

Huang, X., Meng, Y., Liang, P., Qian, Y., 2007. Operational conditions of a membrane filtration reactor coupled with photocatalytic oxidation. Sep. Purif. Technol. 55, 165−172.

Hurum, D.C., Agrios, A.G., Gray, K.A., Rajh, T., Thurnauer, M.C., 2003. Explaining the enhanced photocatalytic activity of Degussa P25 mixed-phase TiO_2 using EPR. J. Phys. Chem. B 107, 4545−4549.

Hwang, H.J., Yang, S., Lee, H., 2017. Surface analysis of N-doped TiO_2 nanorods and their enhanced photocatalytic oxidation activity. Appl. Catal. B Environ. 204, 209–215.
Iglesias, O., Rivero, M.J., Urtiaga, A.M., Ortiz, I., 2016. Membrane-based photocatalytic systems for process intensification. Chem. Eng. J. 305, 136–148.
Jiang, S., Li, Y., Ladewig, B.P., 2017. A review of reverse osmosis membrane fouling and control strategies. Sci. Total Environ. 595, 567–583.
Jo, W.-K., Tayade, R.J., 2014. New generation energy-efficient light source for photocatalysis: LEDs for environmental applications. Ind. Eng. Chem. Res. 53, 2073–2084.
Judd, S., Jefferson, B., 2003. Membranes for Industrial Wastewater Recovery and Reuse. Elsevier.
Judd, S., 2014. Industrial MBRs. Judd and Judd Ltd., Cranfield, UK.
Kanakaraju, D., Glass, B.D., Oelgemöller, M., 2014. Titanium dioxide photocatalysis for pharmaceutical wastewater treatment. Environ. Chem. Lett. 12 (1), 27–47.
Karabelas, A.J., Plakas, K.V., Sarasidis, V.C., Patsios, S.I., 2014. The effect of humic acids on the removal of atrazine from water in a continuous photocatalytic membrane reactor. Global NEST J. 16, 516–524.
Katsoufidou, K., Yiantsios, S.G., Karabelas, A.J., 2008. An experimental study of UF membrane fouling by humic acid and sodium alginate solutions: the effect of backwashing on flux recovery. Desalination 220 (1–3), 214–227.
Katsoufidou, K.S., Sioutopoulos, D.C., Yiantsios, S.G., Karabelas, A.J., 2010. UF membrane fouling by mixtures of humic acids and sodium alginate: fouling mechanisms and reversibility. Desalination 264 (3), 220–227.
Kaur, A., Umar, A., Kansal, S.K., 2016. Heterogeneous photocatalytic studies of analgesic and non-steroidal anti-inflammatory drugs. Appl. Catal. A General 510, 134–155.
Khan, S., Kim, J., Sotto, A., Van der Bruggen, B., 2015. Humic acid fouling in a submerged photocatalytic membrane reactor with binary TiO_2–ZrO_2 particles. J. Ind. Eng. Chem. 21, 779–786.
Kikuchi, Y., Sunada, K., Iyoda, T., Hashimoto, K., Fujishima, A., 1997. Photocatalytic bactericidal effect of TiO_2 thin films: dynamic view of the active oxygen species responsible for the effect. J. Photochem. Photobiol. A Chem. 106, 51–56.
Klavarioti, M., Mantzavinos, D., Kassinos, D., 2009. Removal of residual pharmaceuticals from aqueous systems by advanced oxidation processes. Environ. Int. 35, 402–417.
Konstantinou, I.K., Albanis, T.A., 2004. TiO_2-assisted photocatalytic degradation of azo dyes in aqueous solution: kinetic and mechanistic investigations: a review. Appl. Catal. B Environ. 49 (1), 1–14.
Kosmulski, M., 2011. The pH-dependent surface charging and points of zero charge V. Update. J. Colloid Interface Sci. 353, 1–15.
Kudo, A., Miseki, Y., 2009. Heterogeneous photocatalyst materials for water splitting. Chem. Soc. Rev. 38, 253–278.
Le, N.L., Nunes, S.P., 2016. Materials and membrane technologies for water and energy sustainability. Sustain. Mater. Technol. 7, 1–28.
Leary, R., Westwood, A., 2011. Carbonaceous nanomaterials for the enhancement of TiO_2 photocatalysis. Carbon 49 (3), 741–772.
Le-Clech, P., Chen, V., Fane, T.A.G., 2006. Fouling in membrane bioreactors used in wastewater treatment. J. Membr. Sci. 284 (1–2), 17–53.
Lee, J.-W., Kwon, T.-O., Thiruvenkatachari, R., Moon, I.-S., 2006. Adsorption and photocatalytic degradation of bisphenol A using TiO_2 and its separation by submerged hollow-fiber ultrafiltration membrane. J. Environ. Sci. 18 (1), 193–200.
Lee, K.C., Choo, K.H., 2014. Optimization of flocculation conditions for the separation of TiO_2 particles in coagulation–photocatalysis hybrid water treatment. Chem. Eng. Process. Process Intensif. 78, 11–16.
Lee, K.C., Beak, H.-J., Choo, K.-H., 2015. Membrane photoreactor treatment of 1,4-dioxane-containing textile wastewater effluent: performance, modeling, and fouling control. Water Res. 86, 58–65.

Lee, K.M., Lai, C.W., Ngai, K.S., Juan, J.C., 2016. Recent developments of zinc oxide based photocatalyst in water treatment technology: a review. Water Res. 88, 428−448.

Lee, G.-J., Wu, J.J., 2017. Recent developments in ZnS photocatalysts from synthesis to photocatalytic applications — a review. Powder Technol. 318, 8−22.

Leong, S., Razmjou, A., Wang, K., Hapgood, K., Zhang, X., Wang, H., 2014. TiO_2 based photocatalytic membranes: a review. J. Membr. Sci. 472, 167−184.

Li, G., Lv, L., Fan, H., Ma, J., Li, Y., Wan, Y., Zhao, X.S., 2010. Effect of the agglomeration of TiO_2 nanoparticles on their photocatalytic performance in the aqueous phase. J. Colloid Interface Sci. 348, 342−347.

Liao, J., Lin, S., Pan, N., Li, S., Cao, X., Cao, Y., 2012. Fabrication and photocatalytic properties of free-standing TiO_2 nanotube membranes with through-hole morphology. Mater. Charact. 66, 24−29.

Lin, L.-S., Johnston, C.T., Blatchley, E.R., 1999a. Inorganic foulant at quartz: water interfaces in ultraviolet photoreactors − I. Chemical characterization. Water Res. 33 (15), 3321−3329.

Lin, L.-S., Johnston, C.T., Blatchley, E.R., 1999b. Inorganic fouling at quartz: water interfaces in ultraviolet photoreactors − II. Temporal and spatial distributions. Water Res. 33 (15), 3330−3338.

Lin, L., Chai, Y., Yang, Y., Wang, X., He, D., Tang, Q., Ghoshroy, S., 2013. Hierarchical Gd-La codoped TiO_2 microspheres as robust photocatalysts. Int. J. Hydrogen Energy 38, 2634−2640.

Lior, N., 2017. Sustainability as the quantitative norm for water desalination impacts. Desalination 401, 99−111.

Litter, M., 2017. Last advances on TiO_2-photocatalytic removal of chromium, uranium and arsenic. Curr. Opin. Green Sustain. Chem. 6, 150−158.

Liu, L., Liu, Z., Bai, H., Sun, D.D., 2012. Concurrent filtration and solar photocatalytic disinfection/degradation using high-performance Ag/TiO_2 nanofiber membrane. Water Res. 46, 1101−1112.

Lu, H., Yao, J., 2014. Recent advances in liquid-phase heterogeneous photocatalysis for organic synthesis by selective oxidation. Curr. Organ. Chem. 18 (10), 1365−1372.

Ma, R., Wang, L., Wang, S., Wang, C., Xiao, F.-S., 2017. Eco-friendly photocatalysts achieved by zeolite fixing. Appl. Catal. B Environ. 212, 193−200.

Malato, S., Fernández-Ibáñez, P., Maldonado, M.I., Blanco, J., Gernjak, W., 2009. Decontamination and disinfection of water by solar photocatalysis: recent overview and trends. Catal. Today 147, 1−59.

Malato, S., Fernández-Ibáñez, P., Maldonado, M.I., Oller, I., 2013. Solar photocatalytic processes: water decontamination and disinfection. In: Suib, S.L. (Ed.), New and Future Developments in Catalysis, Solar Photocatalysis. Elsevier B.V., Oxford, pp. 371−393.

Manassero, A., Satuf, M.L., Alfano, O.M., 2017. Photocatalytic reactors with suspended and immobilized TiO_2: comparative efficiency evaluation. Chem. Eng. J. 326, 29−36.

Martins, A.C., Cazetta, A.L., Pezoti, O., Souza, J.R.B., Zhang, T., Pilau, E.J., Asefa, T., Almeida, V.C., 2017. Sol-gel synthesis of new TiO_2/activated carbon photocatalyst and its application for degradation of tetracycline. Ceram. Int. 43, 4411−4418.

McCullagh, C., Robertson, J.M.C., Bahnemann, D.W., Robertson, P.K.J., 2007. The application of TiO_2 photocatalysis for disinfection of water contaminated with pathogenic micro-organisms: a review. Res. Chem. Intermed. 33, 359−375.

Meng, Y., Huang, X., Yang, Q., Qian, Y., Kubota, N., Fukunaga, S., 2005. Treatment of polluted river water with a photocatalytic slurry reactor using low-pressure mercury lamps coupled with a membrane. Desalination 181, 121−133.

Meng, F., Zhang, S., Oh, Y., Zhou, Z., Shin, H.-S., Chae, S.-R., 2017. Fouling in membrane bioreactors: an updated review. Water Res. 114, 151−180.

Mills, A., Le Hunte, S., 1997. An overview of semiconductor photocatalysis. J. Photochem. Photobiol. A 108 (1), 1−35.

Mills, A., Lee, S.-K., 2002. A web-based overview of semiconductor photochemistry-based current commercial applications. J. Photochem. Photobiol. A Chem. 152, 233−247.

Mills, A., Hill, C., Robertson, P.K.J., 2012. Overview of the current ISO tests for photocatalytic materials. J. Photochem. Photobiol. A Chem. 237, 7–23.
Mohammad, A.W., Teow, Y.H., Ang, W.L., Chung, Y.T., Oatley-Radcliffe, D.L., Hilal, N., 2015. Nanofiltration membranes review: recent advances and future prospects. Desalination 356, 226–254.
Molinari, R., Pirillo, F., Loddo, V., Palmisano, L., 2006. Heterogeneous photocatalytic degradation of pharmaceuticals in water by using polycrystalline TiO_2 and a nanofiltration membrane reactor. Catal. Today 118, 205–213.
Molinari, R., Lavorato, C., Argurio, P., 2017. Recent progress of photocatalytic membrane reactors in water treatment and in synthesis of organic compounds. Catal. Today 281, 144–164.
Molinos-Senante, M., Gómez, T., Garrido-Baserba, M., Caballero, R., Sala-Garrido, R., 2014. Assessing the sustainability of small wastewater treatment systems: a composite indicator approach. Sci. Total Environ. 497–498, 607–617.
Moustakas, N.G., Katsaros, F.K., Kontos, A.G., Romanos, G.E., Dionysiou, D.D., Falaras, P., 2014. Visible light active TiO_2 photocatalytic filtration membranes with improved permeability and low energy consumption. Catal. Today 224, 56–69.
Mozia, S., 2010. Photocatalytic membrane reactors (PMRs) in water and wastewater treatment. A review. Sep. Purif. Technol. 73, 71–91.
Nah, Y.-C., Paramasivam, I., Schmuki, P., 2010. Doped TiO_2 and TiO_2 nanotubes: synthesis and applications. ChemPhysChem 11, 2698–2713.
Ohtani, B., 2013. Titania photocatalysis beyond recombination: a critical review. Catalysts 3 (4), 942–953.
Ollis, D.F., 2003. Integrating photocatalysis and membrane technologies for water treatment. Ann. N.Y. Acad. Sci. 984, 65–84.
Ong, C., Goh, P.S., Lau, W.J., Ismail, A., Ng, B.C., Choo, C.M., 2015. The impacts of various operating conditions on submerged membrane photocatalytic reactor (SMPR) for organic pollutant separation and degradation: a review. RSC Adv. 5, 97335–97348.
Papageorgiou, S.K., Katsaros, F.K., Favvas, E.P., Romanos, G.E., Athanasekou, C.P., Beltsios, K.G., Tzialla, O.I., Falaras, P., 2012. Alginate fibers as photocatalyst immobilizing agents applied in hybrid photocatalytic/ultrafiltration water treatment processes. Water Res. 46, 1858–1872.
Patsios, S.I., Karabelas, A.J., 2011. An investigation of the long-term filtration performance of a membrane bioreactor (MBR): the role of specific organic fractions. J. Membr. Sci. 372, 102–115.
Patsios, S.I., Sarasidis, V.C., Karabelas, A.J., 2013. A hybrid photocatalysis–ultrafiltration continuous process for humic acids degradation. Sep. Purif. Technol. 103, 333–341.
Pawar, R., Lee, C.S., 2015. Heterogeneous Nanocomposite-photocatalysis for Water Purification. Elsevier Inc.
Pearce, G., 2007. The case for UF/MF pretreatment to RO in seawater applications. Desalination 203, 286–295.
Pearce, G.K., January/February 2010a. SWRO pre-treatment: integrity and disinfection. Filtr. Sep. 32–35.
Pearce, G.K., January/February 2010b. SWRO pre-treatment: cost and sustainability. Filtr. Sep. 36–38.
Pelaez, M., Nolan, N.T., Pillai, S.C., Seery, M.K., Falaras, P., Kontos, A.G., Dunlop, P.S.M., Hamilton, J.W.J., Byrne, J., O'Shea, K., Entezari, M.H., Dionysiou, D.D., 2012. A review on the visible light active titanium dioxide photocatalysts for environmental applications. Appl. Catal. B Environ. 125, 331–349.
Peng, J., Qiu, Y., Gehr, R., 2005. Characterization of permanent fouling on the surfaces of UV lamps used for wastewater disinfection. Water Environ. Res. 77 (4), 309–322.
Philips, 2017. http://www.lighting.philips.com/main/prof.
Pichat, P., 2013. Photocatalysis and Water Purification: From Fundamentals to Recent Applications. Wiley-VCH Verlag GmbH & Co. KGaA, Weinheim Germany.
Pillai, S.C., Štangar, U.L., Byrne, J.A., Perez-Larios, A., Dionysiou, D.D., 2015. Photocatalysis for disinfection and removal of contaminants of emerging concern. Chem. Eng. J. 261, 1–2.

Pires, A., Morato, J., Peixoto, H., Botero, V., Zuluaga, L., Figueroa, A., 2017. Sustainability assessment of indicators for integrated water resources management. Sci. Total Environ. 578, 139−147.

Plakas, K.V., Karabelas, A.J., 2012. Removal of pesticides from water by NF and RO membranes − a review. Desalination 287, 255−265.

Plakas, K.V., Sarasidis, V.C., Patsios, S.I., Lambropoulou, D.A., Karabelas, A.J., 2016a. Novel pilot scale continuous photocatalytic membrane reactor for removal of organic micropollutants from water. Chem. Eng. J. 304, 335−343.

Plakas, K.V., Georgiadis, A.A., Karabelas, A.J., 2016b. Sustainability assessment of tertiary wastewater treatment technologies: a multi-criteria analysis. Water Sci. Technol. 73 (7), 1532−1540.

Pruden, A.L., Ollis, D.F., 1983. Degradation of chloroform by photoassisted heterogeneous catalysis in dilute aqueous suspensions of titanium dioxide. Environ. Sci. Technol. 17, 628−631.

Quintero, C., Carlos, J., Xu, Y.-J., 2016. Heterogeneous Photocatalysis: From Fundamentals to Green Applications. Springer-Verlag Berlin Heidelberg.

Rajca, M., 2016. The effectiveness of removal of nom from natural water using photocatalytic membrane reactors in PMR-UF and PMR-MF modes. Chem. Eng. J. 305, 169−175.

Ray, A.K., 2009. Photocatalytic reactor configurations for water purification: experimentation and modeling. In: de Lasa, H.I., Rosales, B.S. (Eds.), Advances in Chemical Engineering, vol. 36. Elsevier Inc., pp. 145−184

Ribeiro, A.R., Nunes, A.C., Pereira, M.F.R., Silva, A.M.T., 2015. An overview on the advanced oxidation processes applied for the treatment of water pollutants defined in the recently launched Directive 2013/39/EU. Environ. Int. 75, 33−51.

Rincón, A.-G., Pulgarin, C., 2004. Effect of pH, inorganic ions, organic matter and H_2O_2 on *E. coli* K12 photocatalytic inactivation by TiO_2: implications in solar water disinfection. Appl. Catal. B Environ. 51, 283−302.

Rivero, M.J., Parsons, S.A., Jeffrey, P., Pidou, M., Jefferson, B., 2006. Membrane chemical reactor (MCR) combining photocatalysis and microfiltration for grey water treatment. Water Sci. Technol. 53 (3), 173−180.

Ryu, J., Choi, W., Choo, K.-H., 2005. A pilot-scale photocatalyst-membrane hybrid reactor: performance and characterization. Water Sci. Technol. 51 (6), 491−497.

Santhosh, C., Velmurugan, V., Jacob, G., Jeong, S.K., Grace, A.N., Bhatnagar, A., 2016. Role of nanomaterials in water treatment applications: a review. Chem. Eng. J. 306, 1116−1137.

Sarasidis, V.C., Patsios, S.I., Karabelas, A.J., 2011. A hybrid photocatalysis ultrafiltration continuous process: the case of polysaccharide degradation. Sep. Purif. Technol. 80, 73−80.

Sarasidis, V.C., Plakas, K.V., Patsios, S.I., Karabelas, A.J., 2014. Investigation of diclofenac degradation in a continuous photo-catalytic membrane reactor. Influence of operating parameters. Chem. Eng. J. 239, 299−311.

Schmelling, D., et al., 2006. Ultraviolet Disinfection Guidance Manual for the Long Term 2 Enhanced Surface Water Treatment Rule, USEPA, Office of Water (4601). Report No EPA 815-R-06−007.

Schneider, J., Matsuoka, M., Takeuchi, M., Zhang, J., Horiuchi, Y., Anpo, M., Bahnemann, D.W., 2014. Understanding TiO_2 photocatalysis: mechanisms and materials. Chem. Rev. 114, 9919−9986.

Schrauzer, G.N., Guth, T.D., 1977. Photocatalytic reactions. 1. Photolysis of water and photoreduction of nitrogen on titanium dioxide. J. Am. Chem. Soc. 99, 7189−7193.

Serpone, N., Lawless, D., Khairutdinov, R., Pelizetti, E., 1995. Size effects on the photophysical properties of colloidal anatase TiO_2 particles: size quantization versus direct transitions in this indirect semiconductor? J. Phys. Chem. 99 (45), 16646−16654.

Shan, A.Y., Mohd Ghazi, T.I., Rashid, S.A., 2010. Immobilisation of titanium dioxide onto supporting materials in heterogeneous photocatalysis: a review. Appl. Catal. A General 389, 1−8.

Shehabuddeen, N., Probert, D., Phaal, R., 2006. From theory to practice: challenges in operationalising a technology selection framework. Technovation 26, 324–335.
Shen, C., Pang, K., Du, L., Luo, G., 2017. Green synthesis and enhanced photocatalytic activity of Ce-doped TiO_2 nanoparticles supported on porous glass. Particuology 34, 103–109.
Shon, H.K., Phuntsho, S., Vigneswaran, S., 2008. Effect of photocatalysis on the membrane hybrid system for wastewater treatment. Desalination 225, 235–248.
Sioutopoulos, D.C., Karabelas, A.J., 2016. Evolution of organic gel fouling resistance in constant pressure and constant flux dead-end ultrafiltration: differences and similarities. J. Membr. Sci. 511, 265–277.
Song, L., Zhu, B., Gray, S., Duke, M., Muthukumaran, S., 2016. Hybrid processes combining photocatalysis and ceramic membrane filtration for degradation of humic acids in saline water. Membranes 6 (1), 18.
Stancl, H.O., Hristovski, K., Westerhoff, P., 2015. Hexavalent chromium removal using UV-TiO_2/ceramic membrane reactor. Environ. Eng. Sci. 32 (8), 676–683.
Sweetman, M.J., May, S., Mebberson, N., Pendleton, P., Vasilev, K., Plush, S.E., Haybal, J.D., 2017. Activated carbon, carbon nanotubes and graphene: materials and composites for advanced water purification. J. Carbon Res. C 3 (2), 18.
Szczepanik, B., 2017. Photocatalytic degradation of organic contaminants over clay-TiO_2 nanocomposites: a review. Appl. Clay Sci. 141, 227–239.
Tang, C.Y., Chong, T.H., Fane, A.G., 2011. Colloidal interactions and fouling of NF and RO membranes: a review. Adv. Colloid Interface Sci. 164 (1–2), 126–143.
Thakur, S., Govender, P.P., Mamo, M.A., Tamulevicius, S., Thakur, V.K., 2017. Recent progress in gelatin hydrogel nanocomposites for water purification and beyond. Vacuum. https://doi.org/10.1016/j.vacuum.2017.05.032.
Thompson, T.L., Yates, J.T., 2006. Surface science studies of the photoactivation of TiO_2 new photochemical processes. Chem. Rev. 106, 4428–4453.
Tokarský, J., Matějka, V., Neuwirthová, L., Vontorová, J., Kutláková, K.M., Kukutschová, J., Čapková, P., 2013. A low-cost photoactive composite quartz sand/TiO_2. Chem. Eng. J. 222, 488–497.
Tufa, R.A., 2015. Perspectives on environmental ethics in sustainability of membrane based technologies for water and energy production. Environ. Technol. Innov. 4, 182–193.
USHIO, 2017. https://www.ushio.com/product/uxl-xenon-short-arc/.
Vatanpour, V., Karami, A., Sheydaei, M., 2017. Central composite design optimization of rhodamine B degradation using TiO_2 nanoparticles/UV/PVDF process in continuous submerged membrane photoreactor. Chem. Eng. Process. 116, 68–75.
Vezzoli, M., Farrell, T., Baker, A., Psaltis, S., Martens, W.N., Bell, J.M., 2013. Optimal catalyst thickness in titanium dioxide fixed film reactors: mathematical modeling and experimental validation. Chem. Eng. J. 234, 57–65.
Vinu, R., Madras, G., 2010. Environmental remediation by photocatalysis. J. Indian Inst. Sci. 90, 189–229.
Voces, R., Diaz-Balteiro, L., Romero, C., 2012. Characterization and explanation of the sustainability of the European wood manufacturing industries: a quantitative approach. Expert Syst. Appl. 39 (7), 6618–6627.
Voutchkov, N., February 2009. SWRO pre-treatment system: choosing between conventional and membrane filtration. Filtr. Sep. 46.
Wan Ngah, W.S., Teong, L.C., Hanafiah, M.A.K.M., 2011. Adsorption of dyes and heavy metal ions by chitosan composites: a review. Carbohydr. Polym. 83, 1446–1456.
Wang, P., Fane, A.G., Lim, T.T., 2013. Evaluation of a submerged membrane vis-LED photoreactor (sMPR) for carbamazepine degradation and TiO_2 separation. Chem. Eng. J. 215–216, 240–251.
Wang, Q., Yang, C., Zhang, G., Hu, L., Wang, P., 2017. Photocatalytic Fe-doped TiO_2/PSF composite UF membranes: characterization and performance on BPA removal under visible-light irradiation. Chem. Eng. J. 319, 39–47.
Yaremko, Z.M., Tkachenko, N.H., Bellmann, C., Pich, A., 2006. Redispergation of TiO_2 particles in aqueous solutions. J. Colloid Interface Sci. 296, 565–571.
Yu, J., Yu, H., Cheng, B., Zhou, M., Zhao, X., 2006. Enhanced photocatalytic activity of TiO_2 powder (P25) by hydrothermal treatment. J. Mol. Catal. A 253, 112–118.

Zangeneh, H., Zinatizadeh, A.A.L., Habibi, M., Akia, M., Hasnain Isa, M., 2015. Photocatalytic oxidation of organic dyes and pollutants in wastewater using different modified titanium dioxides: a comparative review. J. Ind. Eng. Chem. 26, 1–36.

Zhang, W., Ding, L., Luo, J., Jaffrin, M.Y., Tang, B., 2016a. Membrane fouling in photocatalytic membrane reactors (PMRs) for water and wastewater treatment: a critical review. Chem. Eng. J. 302, 446–458.

Zhang, A.-Y., Wang, W.-K., Pei, D.-N., Yu, H.-Q., 2016b. Degradation of refractory pollutants under solar light irradiation by a robust and self-protected ZnO/CdS/TiO_2 hybrid photocatalyst. Water Res. 92, 78–86.

Zhang, L., Zhang, Q., Xie, H., Guo, J., Lyu, H., Li, Y., Sun, Z., Wang, H., Guo, Z., 2017. Electrospun titania nanofibers segregated by graphene oxide for improved visible light photocatalysis. Appl. Catal. B Environ. 201, 470–478.

Zheng, X., Wang, Q., Chen, L., Wang, J., Cheng, R., 2015. Photocatalytic membrane reactor (PMR) for virus removal in water: performance and mechanisms. Chem. Eng. J. 277, 124–129.

Zijp, M.C., Waaijers-van der Loop, S.L., Heijungs, R., Broeren, M.L.M., Peeters, R., Van Nieuwenhuijzen, A., Shen, L., Heugens, E.H.W., Posthuma, L., 2017. Method selection for sustainability assessments: the case of recovery of resources from waste water. J. Environ. Manag. 197, 221–230.

Appendix

Table A1: List of patents on PMR technology for water/wastewater treatment applications.

Title/Patent No	Inventors/Date	Field of the Invention
Photo-catalytic membrane reactor, US 20110150734 A1	Izumi Kumakiri, Rune Bredesen, Henrik Reader, Christian Simon 23/6/11	This invention relates to a process and a reactor for liquid or gas treatment. The process is based on the same principles as catalytic wet air oxidation, but it is implemented by the combined use of a porous membrane contactor, photocatalysts, and a light source. The photocatalytic membrane contactor may be used in liquid–gas, liquid–liquid, or gas–gas photocatalytic applications. One typical application is to treat water containing hardly degradable organics.
Photocatalytic reactor and process for treating wastewater US 20080179178 A1	Pablo Arturo Venegas Cabello, Maria Christina Yeber Ortiz, Anna Lorena Narvaez Dinamarca et al. 31/7/08	This invention is related to a photocatalytic reactor with a modular configuration, based on UV light sources, a supported photocatalyst (TiO_2), and gas ozone for producing hydroxyl radicals, using AOPs, wherein the photocatalyst is supported over glass sheets as fixed strips within the reactor, at an established distance from the UV light source, and wherein the wastewater is treated as "batches" being recirculated and returned to the circuit. It is reported as useful for purifying and disinfecting wastewater from confined aquaculture.

Continued

Table A1: List of patents on PMR technology for water/wastewater treatment applications.—cont'd

Title/Patent No	Inventors/Date	Field of the Invention
Photocatalytic reaction systems for water purification US 20090148359 A1	Hsin Shao, Min-Chao Chang, Ren-Yang Horng 11/6/09	Multiple photocatalyst carriers are used in the photocatalytic reaction tank, surrounding the light source. Each photocatalyst carrier carries a plurality of photocatalyst particles. A photocatalysts separation tank is connected to the photocatalytic reaction tank, with at least one light source. A nonwoven fabric membrane filtration module is arranged in the photocatalysts separation tank, filtering off the photocatalyst.
Photocatalytic method for treatment of contaminated water EP 0819649 A1	Makhmutov Fanilji Akhatovich, Tsareva Elena Ivanovna, Mishkin Roman Nikolaevich 21/1/98	This invention includes irradiation with UV and a photocatalytically active porous membrane of dynamic or ceramic type made of a semiconducting material. This invention applies to the field of natural and wastewater purification and water treatment, in particular to water purification from toxic and hardly degradable aromatic and chlorinated compounds.
Water purification system by means of a photocatalytic process EP 1870379 A1	Claudio Dr. Terruzzi 26/12/07	The invention consists of a photocatalytic process comprising a tank containing polluted water, a water-purifying device, and a channeling system to transport the polluted water from the tank to the purification device; the purification device also comprises a container containing said water and a plurality of photocatalytic elements, realized by a matrix containing basic substances and including photocatalyst particles and a plurality of UV lamps suitable to illuminate the photocatalytic elements.
Method for photocatalytic decontamination EP 0697012 B1	Brian Edward Butters, Anthony Leonard Powell 2/6/99	This invention relates generally to a method and system for the continuous and efficient photocatalytic decontamination of contaminated fluid. The system provides for the irradiation of a slurry between defined surface(s) such that substantially all of the contaminants are removed from the slurry, and a turbulent flow of the slurry is achieved. Furthermore, it provides separation of decontaminated effluent

Continued

Table A1: List of patents on PMR technology for water/wastewater treatment applications.—cont'd

Title/Patent No	Inventors/Date	Field of the Invention
		from the slurry by using ceramic membrane filters. Air is applied to the ceramic membrane filters at relatively high pressures to remove any photoreactive photocatalyst particles that have collected in the ceramic filter.
Photocatalytic purification device EP 2409954 A1	Polycarpos Falaras, Georgios Romanos, Panagiotis Aloupogiannis 25/1/12	This invention relates to a photocatalytic reactor for removing organic contaminants from fluids such as water. The reactor comprises a first flow channel for receiving fluid from an inlet means, a second flow channel for delivering fluid to an outlet means, a selectively permeable filtration membrane intermediate to the first and second flow channels, having a first surface that receives fluid from the first flow channel and an opposite second surface defining, at least in part, the second fluid flow channel, and at least one photocatalyst support disposed in the first flow channel. The fluid therefore undergoes three photocatalytic treatment stages and a filtration stage during its passage through the reactor.
Oxidation reaction device combining nanofiltration membrane with photocatalysis CN 202430036 U	Wentao HE, ZhiJun Hou 12/9/12	The invention relates to sewage treatment plants and more particularly to photocatalysis and nanofiltration membrane by UV filter—combined sewage treatment plant. The reaction device comprises a reaction chamber, an aeration device, an ultraviolet lamp, a pressure pump, a nanofiltration membrane component, and a return flow system. The reaction device has the advantages of mildness in reaction, high treatment efficiency, thoroughness in degradation, clean and green process, and energy conservation.
Photocatalysis-membrane separation coupling process unit and operation method thereof CN 103253728 A	Song Hongchen, Wang Jianming 21/8/13	This invention provides a photocatalysis—membrane separation coupling process unit comprising a photocatalysis unit, an upper die, and a membrane separation assembly. Through coupling of photocatalysis and membrane separation,

Continued

Table A1: List of patents on PMR technology for water/wastewater treatment applications.—cont'd

Title/Patent No	Inventors/Date	Field of the Invention
		the unit can both rapidly and highly efficiently separate and purify a water body and control pollution of the membrane during separation and purification of the water body.
Photocatalytic oxidation-membrane separation circulating fluid bed reaction device CN 101875001 B	Liping Xie, Yan Liu 25/12/12	This invention relates to an integrated optical oxidation—membrane separation reaction. The device comprises a photocatalytic reactor and a membrane separation circulating reactor, wherein the photocatalytic reactor comprises a photocatalytic reactor shell; the membrane separation circulating reactor comprises a membrane separation circulating reactor shell arranged on the upper part of the side of the photocatalytic reactor shell; the photocatalytic reactor shell is internally provided with an ultraviolet light source; the membrane separation circulating reactor shell is internally provided with an immersed membrane assembly; the immersed membrane assembly is connected with a water outlet; The invention claims higher mass transfer efficiency and light energy utilization ratio by adopting the photocatalytic oxidation—membrane separation circulating fluid bed reaction device, which greatly enhances the efficiency of photocatalytic oxidation reaction.
Novel photocatalysis filter tank device and water treatment system CN 102701317 A	Hong Zhong Zhang, Ming Hua Wang, Yanqin Yang, Hualin Zhang, Meina Guo, Xuejing Kang, Xilong Hao, Shaoming Fang, Jihong Zhao 3/10/12	The invention discloses a photocatalyst filter device loaded with titania-coated beads. The novel photocatalysis filter tank device organically combines the conventional biomembrane filtering tank with the advanced photocatalysis treatment process; it is compact in layout, allows a light source to be uniformly distributed in the filter material, has a good hydraulic power condition, can fully utilize light energy, does not need aeration, does not generate sludge and secondary pollution, is convenient to operate and simple to maintain, has high water quality

Continued

Table A1: List of patents on PMR technology for water/wastewater treatment applications.—cont'd

Title/Patent No	Inventors/Date	Field of the Invention
Membrane separation concentrated water treatment method and integral coupling device CN 101786689 B	Jun Chuan Wang 9/5/12	purification efficiency and sterilization capability, and is mainly applied to the fields of reclaimed water reuse and wastewater treatment. The invention discloses a membrane separation method and the integrated concentration of water coupling device. The membrane separation concentrated water treatment method comprises the following steps: membrane separation concentrated water is pretreated and then enters a suspension-type photocatalytic reactor, subjected to photocatalytic reaction under the UV radiation and, simultaneously, improves the degradation rate and the degradation effect of pollutant through the combination of photocatalytic and ultrasonic effects; the wastewater after photocatalytic oxidation and ultrasonic degradation enters a submerged filtration system to be filtered and then is divided into filtered water and the concentrated water.

This page intentionally left blank

CHAPTER 10

Modeling Photocatalytic Membrane Reactors

Kwang-Ho Choo
Kyungpook National University, Daegu, Republic of Korea

10.1 Introduction

Modeling the performance of photocatalytic membrane reactors and their corresponding reaction kinetics plays a crucial role in their process design and operation in many chemical and environmental engineering processes (Lee et al., 2015; Shahrezaei et al., 2012; Sopajaree et al., 1999). Several factors affect the development of photocatalytic membrane processes, including the properties and concentration of the target compounds (i.e., reactants), the reactor configuration and operational mode, and background species, to name a few. Because photocatalysis is a heterogeneous reaction involving solid (i.e., photocatalyst) and liquid phases, mass transfer of a reactant from the liquid to the solid phase is an important parameter, which is related to the agitation (i.e., convection) of the bulk solution and attachment of the reactants to the photocatalyst surface (Dijkstra et al., 2003). Furthermore, light illumination on the catalysts is critical to activate and initiate the photocatalytic reactions. Finally, the interactions of photogenerated reactive oxygen species (e.g., •OH and O_2^{-}·) with the target materials cause the latter species to degrade over time (Chong et al., 2010). Taken together, these issues must be carefully considered to accurately model photocatalytic membrane reactors and the reactions therein.

Mathematical modeling of a photocatalytic membrane reactor can be performed in two steps: (1) evaluation of the reaction kinetics and (2) development of mass balances for a target material. Kinetic tests are performed in batch reactors, and so the variation of a reactant is monitored over time. Subsequently, model parameters (e.g., the reaction order and rate constant) are estimated and determined using the batch reactor data. The mass balance of a target material in a continuous flow system is developed as follows:

$$\text{Accumulation} = \text{Input} - \text{Output} - \text{Consumption} \tag{10.1}$$

Current Trends and Future Developments on (Bio-) Membranes. https://doi.org/10.1016/B978-0-12-813549-5.00010-4

Usually, an ordinary differential equation with respect to time (i.e., only one independent variable) can be formulated. A partial differential equation with respect to time and direction (i.e., x, y, or z) can be obtained if the mass transfer or specific directional movement of a reactant is considered in the photocatalytic membrane reactor system.

Regarding modeling photocatalytic membrane reactors, this chapter primarily focuses on the process configuration to understand different types of reactor operation schemes and flow regimes. Additionally, the kinetic model equations used to evaluate the reaction rate in photocatalytic membrane systems under various operating conditions are evaluated. Using first- and zeroth-order kinetics, continuous flow reactor models are developed and evaluated using Eq. (10.1) for nonsteady- and steady-state conditions.

10.2 Reactor Configurations

10.2.1 Photocatalytic Reactors With Catalytic Membranes

Fig. 10.1 shows several different types of photocatalytic membrane reactors that have been developed for water and wastewater treatment (Lee et al., 2001; Molinari et al., 2002; Mozia, 2010; Mozia et al., 2007). As shown in Fig. 10.1A, the formation of a photocatalyst layer on top of a flat ultrafiltration membrane followed by irradiation with UV light on a catalyst-coated membrane was devised and tested to investigate the degradation of toxic organic contaminants (e.g., 4-nitrophenol) in feed water (Molinari et al., 2000). This approach was easily implemented using a stirred ultrafiltration cell with photocatalyst deposition on the membrane. However, the cake layer of the photocatalysts on the membrane was not mechanically stable and it readily detached. Additionally, only the top portion of the photocatalyst layer was effective for photocatalytic reactions, indicating that optimal usage of the deposited photocatalysts was not achieved. Moreover, increasing the deposition of photocatalysts on the membrane may not improve contaminant degradation. For instance, the degradation of 4-nitrophenol with different amounts of TiO_2 photocatalysts (0.76–4.08 mg cm^{-2}) afforded almost identical removal efficiencies ($\sim$50%), which was lower than that obtained using suspended catalysts ($\sim$80%).

A concern of photocatalytic reactors with catalytic membranes is aging or damage of the membrane by UV light or reactive oxygen species produced during photocatalysis. Indeed, some polymeric membranes made of cellulose acetate, polyacrylonitrile, and polysulfone were damaged with direct UV radiation (365 nm) on the membrane at an intensity of 6.2 mW cm^{-2} in distilled water (Molinari et al., 2000). However, no perceptible damage was observed with polyvinylidene difluoride or polytetrafluoroethylene membranes (Chin et al., 2006; Molinari et al., 2000). In general, the thickness of the photocatalyst cake played an important role in membrane deterioration, with thicker cakes resulting in less membrane damage. In other words, the bottom layer of the photocatalysts was not

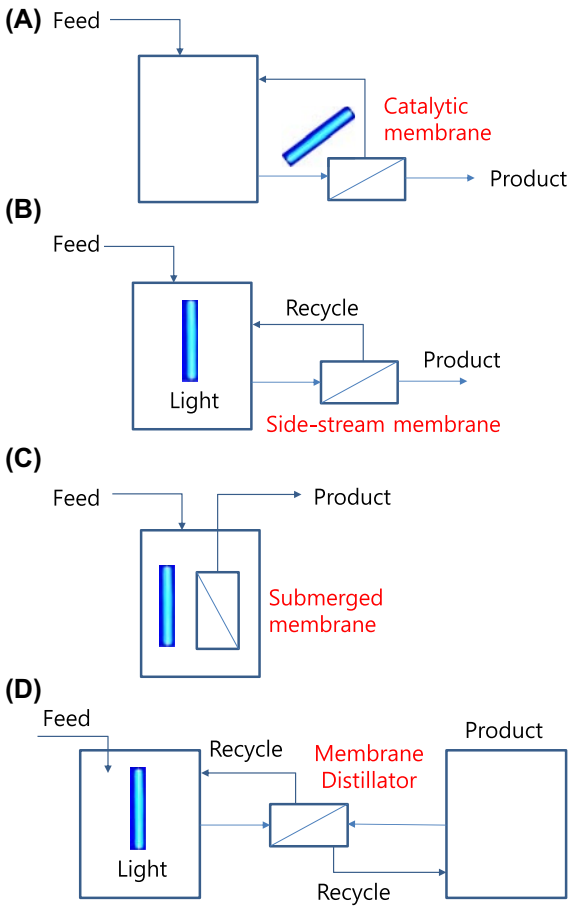

Figure 10.1
Types of photocatalytic reactors with (A) catalytic membrane, (B) sidestream membrane, (C) submerged membrane, and (D) membrane distillator.

illuminated by UV light, therefore protecting the membrane base. Fabrication of inorganic composite membranes with a photocatalytically active top (skin) layer and TiO_2 nanotubes was successful, which prevented membrane damage from light radiation (Albu et al., 2007; Romanos et al., 2012; Wang et al., 2008; Zhang et al., 2006, 2014). However, efficient light radiation on the catalytic membrane surface remains a major challenge to be resolved with these types of photocatalytic membranes and processes.

10.2.2 Photocatalytic Reactors With Sidestream Membranes

Coupling a photocatalytic reactor with a sidestream membrane involves suspension of the photocatalysts in the reactor followed by their separation (rejection) by the membrane (Fig. 10.1B) (Jiang et al., 2010; Lee et al., 2001; Molinari et al., 2001). The retentate

containing the photocatalysts returns to the photocatalytic reactor, while a constant catalyst concentration is maintained. To illustrate, the majority of TiO_2 photocatalyst (P25) grains suspended in water was found to be > 0.4 μm; consequently, they were rejected almost completely by a 0.1 μm microfiltration membrane (Choo et al., 2008a). With this configuration, efficient light radiation on the suspended catalysts can be achieved, giving rise to maximal catalytic activity. In particular, suspended photocatalysts can initially sorb organic matter rapidly and then degrade it over time (Choo et al., 2008b; Yao et al., 2009). The sorption of organics onto the photocatalysts plays an important role in retaining pollutants inside the reactor because unsorbed organics may otherwise pass through the membrane pores before photocatalytic degradation.

10.2.3 Photocatalytic Reactors With Submerged Membranes

More compact process designs composed of suspended photocatalysts and submerged membranes have also been developed (Fig. 10.1C), which have a similar configuration to submerged membrane bioreactors (Choo et al., 2008a; Fu et al., 2006; Ryu et al., 2005). In this approach, both photocatalysis and catalyst separation occur in a single tank. The catalysts can be suspended and well mixed by stirring and/or aeration devices, which can also interfere with catalyst deposition on the membranes (Choo et al., 2008b; Jiang and Choo, 2016; Ryu et al., 2005). Periodic backwashing either using a permeate or gas (N_2 or air) is able to dislodge the photocatalysts from the membrane, making the membrane functional at a relatively high permeation flux (Jiang and Choo, 2016).

However, membrane deterioration by light radiation remains a concern for this process configuration. Unlike the configuration with catalytic membranes (Fig. 10.1A), suspended photocatalysts are present between the light source and the membrane. In addition to this gap, some photocatalysts may accumulate and form a cake layer on the membrane during filtration. Thus, the liquid buffer zone and cake layer may prevent the membrane from being exposed to light. Nevertheless, no membrane damage has yet been reported with this configuration.

10.2.4 Hybrid Photocatalysis–Membrane Distillation

Another reactor configuration (liquid/vapor phase separation) that combines photocatalysis and membrane distillation was introduced in place of pressure-driven liquid/liquid phase separation, such as microfiltration, ultrafiltration, and nanofiltration (Mozia et al., 2005, 2007). A modified configuration, which has a submerged membrane distillation module in a photocatalytic reactor with a microwave heating device, was developed to remove dyes and mitigate fouling (Qu et al., 2014). Incorporation of membrane distillation and

photocatalysis in this configuration fouls the membrane less because vaporized water molecules move through the hydrophobic membrane pores without any convective movement of particulate matter (including photocatalysts) toward the membrane surface. Additionally, a temperature gradient across the membrane plays a major role in water extraction. Notably, high-quality treated water can be obtained with a photocatalytic membrane distillator; however, passage of volatile organics through the membrane is possible (Mozia et al., 2007). Other issues to overcome concerning the stability of this process are membrane wetting and the energy demand for heating the feed solution, which is undesirable unless the production of highly purified water is essential.

10.3 Reaction Kinetic Models

10.3.1 First- and Zeroth-Order Reaction Kinetics

The reaction behaviors in photocatalytic membrane reactors are expected to follow a two-phase heterogeneous photocatalytic reaction mechanism. One of the most popular kinetic models that can explain the rate (r) of photocatalytic degradation of contaminants over illuminated photocatalysts is described by the Langmuir–Hinshelwood equation (see Fig. 10.2), which adopts the following form (Konstantinou and Albanis, 2004; Sopajaree et al., 1999; Turchi and Ollis, 1990):

$$r = \frac{dC}{dt} = -\frac{k_0 KC}{1 + KC} \tag{10.2}$$

where C is the reactant concentration (e.g., organic contaminants), t is the reaction time, k_0 is the reaction rate constant, and K is the adsorption coefficient of the reactant on the catalysts. This original model is useful for the analysis of photocatalytic kinetics of organic materials in photocatalytic membrane reactors (Sopajaree et al., 1999; Tahiri Alaoui et al., 2009). The model parameters k_0 and K can be estimated by means of linearization of Eq. (10.2), that is, the reciprocal of Eq. (10.2) as shown in Fig. 10.2B. In addition, the nonlinear integrated form of Eq. (10.2) is derived as follows:

$$\ln C_t + KC_t = \ln C_0 + KC_0 - k_0 Kt \tag{10.3}$$

The model parameters k_0 and K can also be obtained by means of a trial-and-error approach during determination of the best linear regression coefficient of Eq. (10.3).

Additionally, Eq. (10.2) is often modified based on the reaction conditions. If the term KC is much smaller than 1, Eq. (10.2) can be simplified to the following pseudo–first-order reaction equation:

$$r = \frac{dC}{dt} = -k_0 KC = -k_1 C \tag{10.4}$$

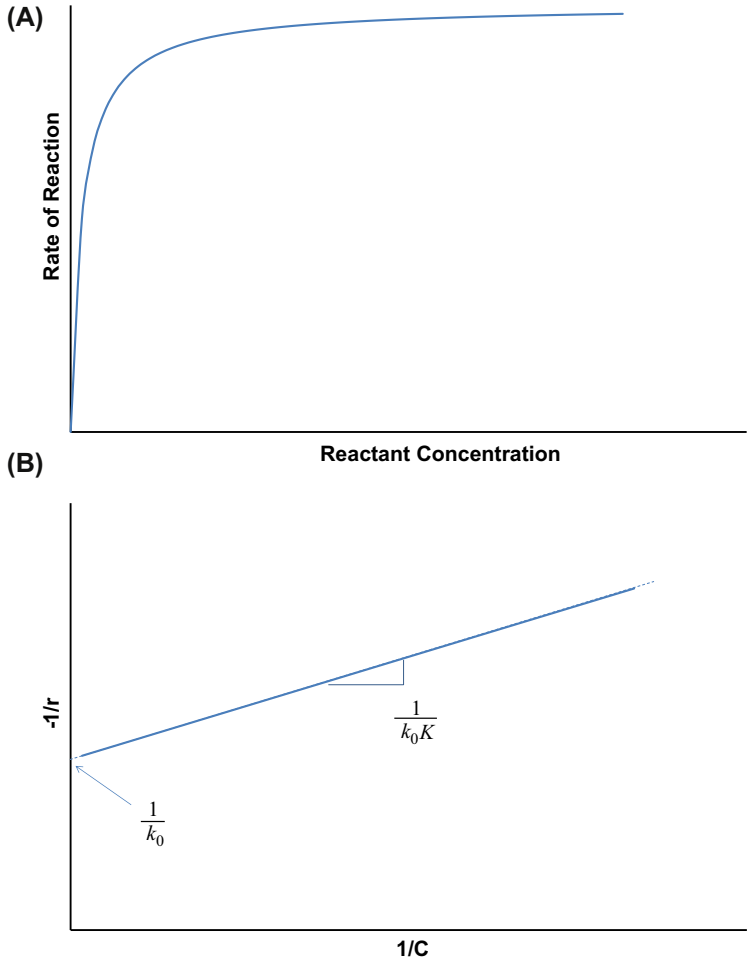

Figure 10.2
(A) The Langmuir–Hinshelwood model profile and (B) an estimation of the model parameters.

Eq. (10.4) is useful to estimate the reaction kinetics when the adsorption coefficient, reactant concentration, or both are fairly small. The integrated form of Eq. (10.4) is:

$$\ln \frac{C_t}{C_0} = -k_1 t \tag{10.5}$$

where C_t and C_0 are the reactant concentrations at time t and 0, respectively. Fig. 10.3A shows a linear plot of ln C_t versus t. As seen, the pseudo–first-order reaction model fits the degradation rate of organic contaminants using TiO_2-mediated photocatalytic membrane reactors for water and wastewater treatment well (Fu et al., 2006; Huang et al., 2008; Lee et al., 2015; Molinari et al., 2006).

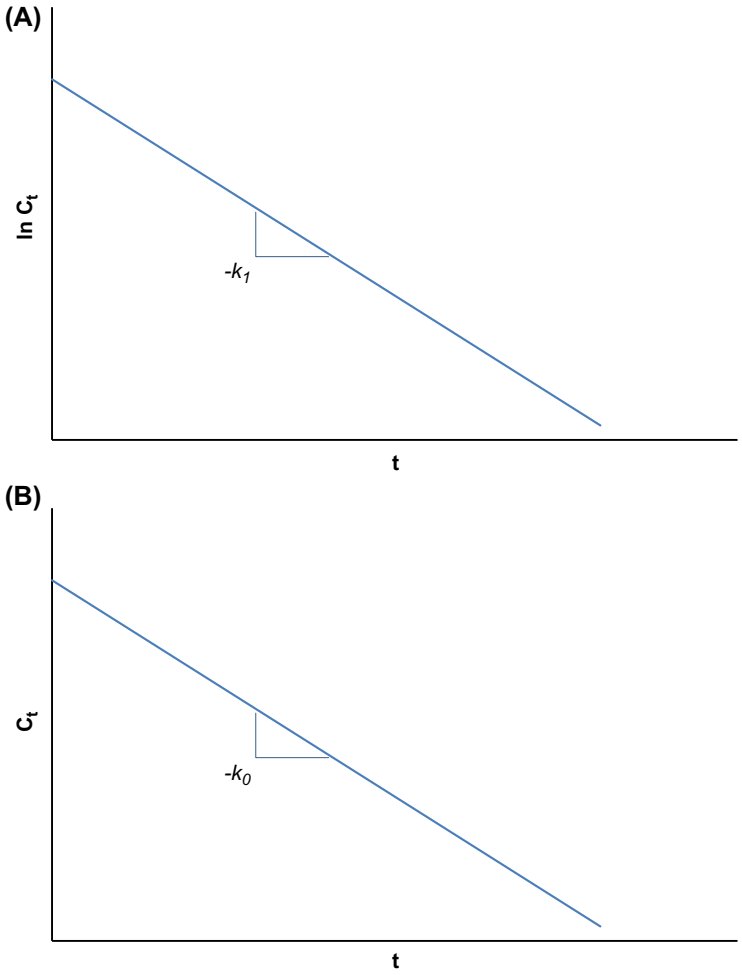

Figure 10.3
Linear plots of the integrated forms of (A) first- and (B) zeroth-order kinetic model equations.

If the term KC is greater than 1, Eq. (10.2) is converted to the following pseudo−zeroth-order reaction equation:

$$r = \frac{dC}{dt} = -k_0 \tag{10.6}$$

The integrated form of Eq. (10.6) is:

$$C_t = C_0 - k_0 t \tag{10.7}$$

In this case, the concentration of a reactant is expected to decrease linearly over time (Fig. 10.3B). This pseudo−zeroth-order kinetics can be applied to estimate the degradation

rate of organic pollutants with relatively high concentrations, for example, 2,4-dihydroxybenzoic acid (0.24–2.59 mM) (Azrague et al., 2007), 4-acetamidoantipyrine (10 mg L^{-1}) (Martínez et al., 2013), nicotine (10 mg L^{-1}) (Martínez et al., 2013), and formic acid (50–370 mg L^{-1}) (Dijkstra et al., 2001). Fig. 10.3 shows the linearized plots of the concentration profile as a function of time for zeroth- and first-order kinetics. Note that analyzing reaction kinetics based on the zeroth-order model is relatively rare compared with the first-order model and the original Langmuir–Hinshelwood model because photocatalytic membrane processes have been primarily developed and applied for the degradation of refractory, toxic micropollutants at very low concentrations.

10.3.2 Noninteger Reaction Kinetics

In addition to the above kinetic models based on the Langmuir–Hinshelwood mechanism, the general form of *n*th-order reaction kinetics, which normally describes homogeneous reactions of a reactant, can be applied to photocatalytic membrane reactors using the following form:

$$r = \frac{dC}{dt} = -k_n C^n \tag{10.8}$$

The integrated form of Eq. (10.8) can be expressed as:

$$C_t^{1-n} = C_0^{1-n} - (1-n)k_n t \tag{10.9}$$

The order (n value) of the reaction and rate constant (k_n) are determined based on nonlinear fitting of the experimental data (see Fig. 10.4). Fractional (noninteger) order reaction kinetics was adopted to describe the reduction ($n = 0.5$) of chromium(VI) to chromium(III) (Sabate et al., 1992) and the degradation ($n = 0.3$) of a dye (i.e., Acid Red 4) (Wang et al., 2008). It was found that among the three kinetic models tested (i.e., zeroth-, half-, and first-order reactions) for the photocatalytic reduction of chromium, half-order ($n = 0.5$) reaction kinetics best fitted the observed data.

The rate coefficient for the degradation of Acid Red 4 achieved by the photocatalytic membrane was found to be dependent on the light intensity (L in mW cm^{-2}) and catalyst mass loading (W in g) (Wang et al., 2008). The value of n for the initial dye concentrations and light intensities ranging from 0.013 to 0.052 mM and from 1 to 6 mW cm^{-2}, respectively, was estimated to be 0.3 by a trial-and-error approach. The rate constant $k_{0.3}$ ($mM^{0.7}/s$) was also expressed as a function of the catalyst dosage and light intensity:

$$k_{0.3} = \frac{0.0024WL^{0.5}}{1 + 18.1W} \tag{10.10}$$

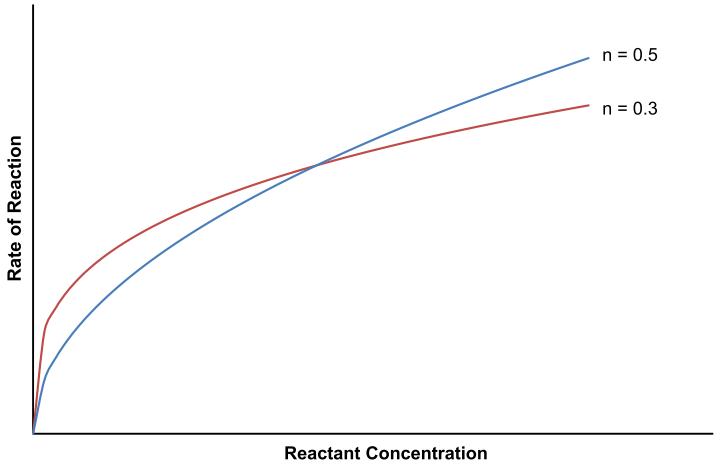

Figure 10.4
Rate of reaction as a function of reactant concentration for noninteger (fractional) reaction kinetics.

The effects of catalyst dosage and light intensity on the photocatalytic rate have been reported in the treatment of several organic pollutants, such as trichloroethylene (Choo et al., 2008a), 1,4-dioxane (Lee et al., 2015; Lee and Choo, 2013), formic acid (Dijkstra et al., 2001), bisphenol A (Chin et al., 2007), and secondary effluent organic matter (Jiang and Choo, 2016). The rate constant continues to increase with greater light radiation, as indicated in Eq. (10.10), although a maximal catalyst dosage does occur with respect to organic degradation. Excessive catalyst dosing should be avoided because the catalysts can coat the membrane surface, leading to a decline in the flux by either the catalysts alone or in combination with other constituents present in the feed solution (Lee et al., 2001). Table 10.1 summarizes the reaction rate kinetics of various target compounds reported in the literature.

10.3.3 Two-Step Reaction Kinetics

A concave-down concentration profile (i.e., two-step reaction kinetics) for the membrane photocatalysis of large molecules (e.g., humic acid) was observed (Fig. 10.5); the profile behavior became more pronounced as the light intensity diminished (Choo et al., 2008b). Such a two-step kinetic mechanism occurs if the initial substrate is converted to an intermediate and then mineralized to carbon dioxide (Chong et al., 2010; Rota et al., 1996). Ideally, the intermediate has a relatively small sorption capacity on the photocatalysts so that it can desorb easily following photocatalysis, giving rise to a concave-down concentration profile of bulk phase organic matter. Hence, the two-step

Table 10.1: A summary of the reaction kinetics for target compounds investigated using photocatalytic membrane reactors.

Kinetic Model	Catalyst	Target	Initial Target Level	Reference
Langmuir–Hinshelwood	Degussa P25 TiO_2	Methylene blue	11–42 mg L^{-1}	Sopajaree et al. (1999)
Langmuir–Hinshelwood	Anatase (98%) P25 TiO_2	Indigo carmine, brilliant green	20 mg L^{-1}	Tahiri Alaoui et al. (2009)
First order	Nanostructured TiO_2/silica gel	Fulvic acid	11.95 mg L^{-1} as C	Fu et al. (2006)
First order	Degussa P25 TiO_2	Suwannee River natural organic matter	10 mg L^{-1} as C	Huang et al. (2008)
First order	Degussa P25 TiO_2	1,4-Dioxane	850 μg L^{-1}	Lee et al. (2015)
First order	Degussa P25 TiO_2	Furosemide, clofibric acid, naproxen, carbamazepine, ranitidine, ofloxacine, phenazone	5–10 mg L^{-1}	Molinari et al. (2006)
First order	Degussa P25 TiO_2	Sulfamethoxazole, diclofenac, hydrochlorothiazide, ranitidine hydrochloride	10 mg L^{-1}	Martínez et al. (2013)
Zeroth order	Degussa P25 TiO_2	2,4-Dihydroxybenzoic acid	37–400 mg L^{-1}	Azrague et al. (2007)
Zeroth order	Degussa P25 TiO_2	4-Acetamidoantipyrine, nicotine	10 mg L^{-1}	Martínez et al. (2013)
Zeroth order	Degussa P25 TiO_2	Formic acid	50–370 mg L^{-1}	Dijkstra et al. (2001)
Fractional order ($n = 0.5$)	Degussa P25 TiO_2	Cr(VI)	17.5–33.4 mg L^{-1}	Sabate et al. (1992)
Fractional order ($n = 0.3$)	Degussa P25 TiO_2	Acid Red 4	4.94–19.8 mg L^{-1}	Wang et al. (2008)
Two-step reaction	Degussa P25 TiO_2	Aldrich humic acid	2–10 mg L^{-1}	Choo et al. (2008b)
Two-step reaction	Degussa P25 TiO_2	Natural organic matter	1.3–5.9 mg L^{-1}	Yao et al. (2009)
Two-step reaction	PHOTOPERM CPP/313	Phenol, 2,6-dimethyl phenol, 1,2,3-benzenetriol, 4-chlorophenol, 2,4-dichlorophenol	0.056–9.9 mM	Rota et al. (1996)

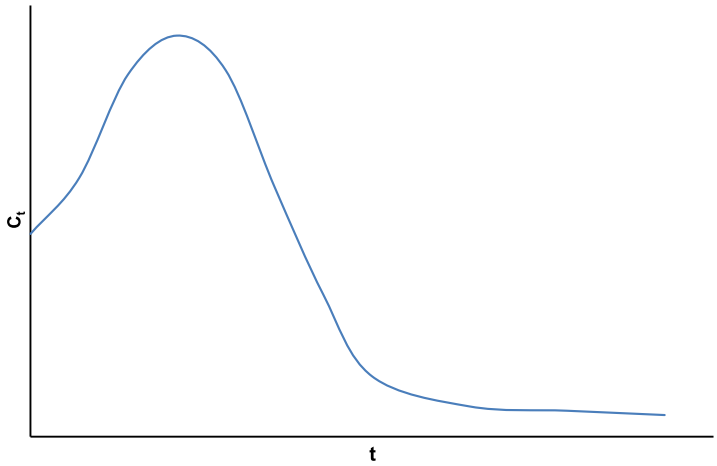

Figure 10.5
A concave-down concentration profile as a function of time for a two-step reaction.

TiO_2-mediated photocatalytic reactions (including stepwise sorption onto the catalyst) can be written as follows:

$$TiO_2 + R \overset{K'}{\leftrightarrow} TiO_2 - R \tag{10.11}$$

$$TiO_2 - R \overset{k'}{\rightarrow} TiO_2 + I \tag{10.12}$$

$$TiO_2 + I \overset{K''}{\leftrightarrow} TiO_2 - I \tag{10.13}$$

$$TiO_2 - I \overset{k''}{\rightarrow} TiO_2 + CO_2 \tag{10.14}$$

where R is the reactant (initial substrate), I is the intermediate, K' is the first-step adsorption coefficient, k' is the first-step rate constant, K'' is the second-step adsorption coefficient, and k'' is the second-step rate constant. Eq. (10.12) can be considered a photoinduced desorption because of the conversion of the initial substrate to an intermediate, which can deteriorate the quality of the treated effluent (membrane permeate). Thus, coating the membrane using other adsorbents (e.g., iron oxide particles) with high sorption capacities was performed and found to help minimize the release (desorption) of intermediates to the aqueous phase (Yao et al., 2009).

10.3.4 Effects of Background Species

Some background species such as bicarbonate and chloride ions act as scavengers for hydroxyl radicals that are produced during the photocatalytic membrane processes

(Choo et al., 2008a; Sabate et al., 1991). Scavenging •OH radicals generates carbonate radicals and chlorine atoms, which have less oxidizing capabilities. Subsequently, these species can scavenge electrons generated from the catalyst to yield carbonate and chloride ions, respectively. The scavenging chain reactions can be expressed as follows:

$$HCO_3^- + \bullet OH \rightarrow CO_3^{\bullet -} + H_2O \quad (10.15)$$

$$CO_3^{2-} + \bullet OH \rightarrow CO_3^{\bullet -} + OH^- \quad (10.16)$$

$$CO_3^{\bullet -} + e^- \rightarrow CO_3^{2-} \quad (10.17)$$

$$Cl^- + \bullet OH \rightarrow Cl^{\bullet} + OH^- \quad (10.18)$$

$$Cl^{\bullet} + e^- \rightarrow Cl^- \quad (10.19)$$

As a result, these scavenging reactions can reduce the oxidation efficiency of organic matter in aqueous media. Indeed, it was found that a large amount of bicarbonate ions present in textile wastewater substantially reduced the reaction rate constant (Lee et al., 2015). However, the rate constant increased fourfold when the bicarbonate ion concentration (as $CaCO_3$) decreased from 300 to <50 mg L^{-1}. The scavenging effect of chloride ions was also found to be significant during treatment of seawater organic matter using a photocatalytic membrane reactor because of the abundance of chloride ions in seawater (Kim et al., 2010). Although the organics became oxidized, their mineralization (i.e., conversion to carbon dioxide) was marginal, which was probably due to the relatively weak oxidation efficiency of the chloride ions and their scavenging chain reactions. The impact of other anions, such as nitrate and sulfate, to photocatalysis was found to be relatively marginal.

Other factors that affect the reaction kinetics in photocatalytic membrane reactors are the dissolved oxygen content, because it can act as an electron acceptor and form superoxide radicals ($O_2^{\bullet -}$), and electron–hole recombination, which must be minimized for optimal performance. A maximum first-order rate constant was obtained during a photocatalytic membrane treatment of fulvic acid when the specific airflow rate (per reaction volume) increased from 3.125 to 28.125 $m^3\ m^{-3} h^{-1}$ (Fu et al., 2006). The increase in rate constant can be attributed to enhanced mass transfer caused by aeration as well as the role of oxygen to capture photogenerated electrons. At very high airflow, however, air bubbles are not beneficial for photocatalysis. Indeed, a negative airflow effect was observed in reactor treatments using a submerged photocatalytic membrane for bisphenol A (Chin et al., 2007) and secondary effluent organic matter (Jiang and Choo, 2016). This is possibly because air bubbles can scatter light that would otherwise irradiate the photocatalysts; moreover, they may interfere with the sorption of organics onto the photocatalysts. Another important factor that can affect membrane

photocatalysis is a turbid material in the feed solution because it can accumulate inside the reactor and block light radiation. Notably, colloidal particles (within a few NTU levels) left over in secondary effluent did not significantly impact the photocatalytic rate (Jiang and Choo, 2016).

10.4 Continuous Flow Reactor Models

10.4.1 Continuously Stirred Tank Reactor Model with First-Order Kinetics

The reactor configurations illustrated in Fig. 10.1 can be regarded as continuously stirred tank reactors. Here, bulk solution is recycled or remained for a specific residence time in the reactor. Thus, a mathematical model for these reactors can be developed based on mass balance. An ordinary differential equation for the photocatalytic membrane reactor with a given volume (V) can be written as:

$$V\frac{dC}{dt} = QC_0 - QC - rV \tag{10.20}$$

If the pseudo−first-order reaction rate is suitable for a specific reaction, Eq. (10.20) can be rewritten incorporating Eq. (10.3) as follows:

$$V\frac{dC}{dt} = QC_0 - QC - k_1CV \tag{10.21}$$

Eq. (10.21) can be rearranged as a function of the hydraulic resistance time (θ) as:

$$\frac{dC}{dt} = \frac{C_0 - C}{\theta} - k_1C \tag{10.22}$$

and the integrated form of Eq. (10.22) can be expressed as:

$$C_t = \frac{C_0}{1 + k_1\theta}\left\{1 + k_1\theta e^{-\left(\frac{1}{\theta}+k_1\right)t}\right\} \tag{10.23}$$

Fig. 10.6A shows the concentration profile as a function of time at different hydraulic residence times using Eq. (10.23). This nonsteady-state model equation can be converted to a steady-state form assuming that the time goes to infinity. The steady-state concentration (C_∞) of a reactant remaining in the reactor is:

$$C_\infty = \frac{C_0}{1 + k_1\theta} \tag{10.24}$$

Additionally, it can be hypothesized that no rejection of the reactant occurs by the membrane other than photocatalytic degradation; the reactant concentration in the final membrane permeate is considered to be the same as C_∞. The fraction

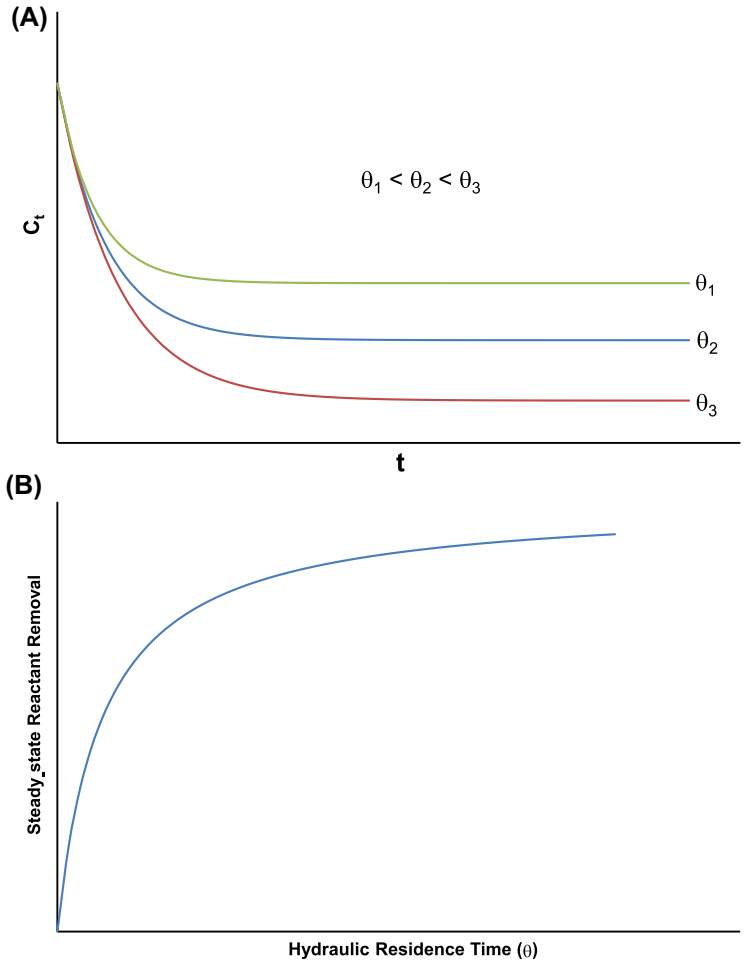

Figure 10.6
Continuously stirred tank reactor modeled with first-order reaction kinetics: (A) nonsteady-state concentration profiles of a reactant with time and (B) steady-state removal of a reactant as a function of hydraulic residence time (θ).

of a reactant removed in the steady state by the photocatalytic membrane reactor can thus be expressed as:

$$1 - \frac{C_\infty}{C_0} = \frac{k_1\theta}{1 + k_1\theta} \tag{10.25}$$

However, if some of the reactant is rejected by the membrane, its level in the final permeate can be estimated by multiplying the rejection ratio by its concentration remaining in the reactor. Fig. 10.6b shows the steady-state reactant removal as a function of hydraulic residence time using Eq. (10.25). Here, no rejection by the membrane was

considered. It was found that Eqs. (10.23) and (10.25) fit the 1,4-dioxane concentration profile well during textile wastewater treatment by a photocatalytic membrane reactor and satisfactorily predicted the removal efficiency at steady state, respectively (Lee et al., 2015). However, the total organic carbon removal did not well agree with model predictions. This is presumably because of multistep reactions involving large organic molecules present in the textile wastewater, as discussed above (Choo et al., 2008b).

10.4.2 Continuously Stirred Tank Reactor Model With Zeroth-Order Kinetics

Another applicable mathematical model for continuously stirred tank reactors with zeroth-order reaction kinetics can be derived based on mass balance. Combining Eqs. (10.6) and (10.20) gives rise to an ordinary differential equation for the photocatalytic membrane reactor as follows:

$$V\frac{dC}{dt} = QC_0 - QC - k_0V \tag{10.26}$$

Eq. (10.26) is rearranged as a function of the hydraulic resistance time (θ) as:

$$\frac{dC}{dt} = \frac{C_0 - C}{\theta} - k_0 \tag{10.27}$$

and the integrated form of Eq. (10.27) is:

$$C_t = C_0 - k_0\theta\left(1 - e^{-\frac{1}{\theta}t}\right) \tag{10.28}$$

Fig. 10.7A shows the concentration profile as a function of time at different hydraulic residence times using Eq. (10.28). The steady-state concentration (C_∞) of a reactant remaining in the reactor and the fraction of the reactant removed at a steady state are expressed, respectively, as:

$$C_\infty = C_0 - k_0\theta \tag{10.29}$$

$$1 - \frac{C_\infty}{C_0} = \frac{k_0\theta}{C_0} \tag{10.30}$$

Fig. 10.7B shows the steady-state removal as a function of hydraulic residence time using Eq. (10.30). Table 10.2 summarizes the mathematical solutions for nonsteady-state and steady-state reactant concentrations for photocatalytic membrane reactors based on continuously stirred tank reactors with zeroth- and first-order reaction kinetics.

10.4.3 Numerical Methods for Complex Continuous Flow Reactors

The continuous flow reactor model varies depending on the type and operation of the reactors and photocatalytic reaction kinetics. In this regard, numerical analyses are useful

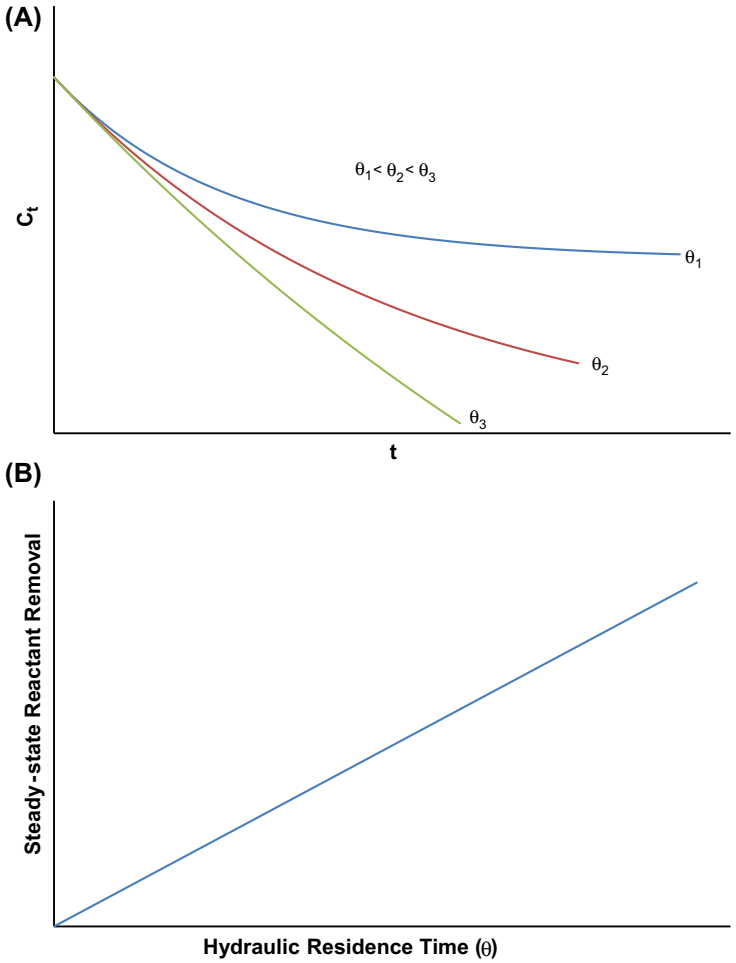

Figure 10.7
Continuously stirred tank reactor modeled with zeroth-order reaction kinetics: (A) nonsteady-state concentration profiles of a reactant with time and (B) steady-state removal of a reactant as a function of hydraulic residence time (θ).

to solve such complicated model equations (Brandi et al., 2000; Cassano and Alfano, 2000). A variety of numerical techniques are available and applicable to virtually any differential equation (Chapra and Canale, 2010; Jenson and Jeffreys, 1977). The ordinary differential equation associated with Eq. (10.20) falls into an initial value problem (Come, 1979), which can be expressed generally as:

$$\frac{dC}{dt} = f(C,t) \tag{10.31}$$

$$C(0) = C_0 \tag{10.32}$$

Table 10.2: Mathematical solutions for ordinary differential equations developed for photocatalytic membrane reactors using a continuously stirred tank reactor flow system.

Flow Systems	Kinetic Model	Nonsteady-State Concentration (C_t)	Steady-State Concentration (C_∞)
Continuously stirred tank reactor	First order	$\frac{C_0}{1+k_1\theta}\left\{1+k_1\theta e^{-\left(\frac{1}{\theta}+k_1\right)t}\right\}$	$\frac{C_0}{1+k_1\theta}$
Continuously stirred tank reactor	Zeroth order	$C_0 - k_0\theta\left(1-e^{-\frac{1}{\theta}t}\right)$	$C_0 - k_0\theta$

A simple approach to obtain the numerical solution of Eq. (10.32) is to use a forward difference method with time interval Δt, called the Euler method, which yields:

$$\frac{C_{i+1}-C_i}{\Delta t} = f(C_i, t_i) \tag{10.33}$$

$$C_{i+1} = C_i + (\Delta t) f(C_i, t_i) \tag{10.34}$$

Although this method is not very accurate and is rarely used, it nevertheless illustrates how to solve ordinary differential equations using a numerical technique. One of the most widely used methods is the fourth-order formula of the Runge–Kutta method (Hornbeck, 1975):

$$C_{i+1} = C_i + \frac{(\Delta t)}{6}\{g_1 + 2g_2 + 2g_3 + g_4\} \tag{10.35}$$

where

$$g_1 = f(C_i, t_i) \tag{10.36}$$

$$g_2 = f\left(C_i + \frac{\Delta t}{2} g_1, t_{i+1/2}\right) \tag{10.37}$$

$$g_3 = f\left(C_i + \frac{\Delta t}{2} g_2, t_{i+1/2}\right) \tag{10.38}$$

$$g_4 = f(C_i + \Delta t\, g_3, t_{i+1}) \tag{10.39}$$

$$t_{i+1/2} = t_i + \frac{\Delta t}{2} \tag{10.40}$$

However, it is beyond the scope of this chapter to derive and discuss the theoretical background of this method. Interested readers are referred to other relevant sources for details (Iserles and NøRsett, 1990; Munthe-Kaas, 1999). In addition to the Runge–Kutta methods, many other methods, such as the Adams multistep formulas and predictor–corrector methods, can be used to estimate the solutions of ordinary differential equations. Indeed, several computer software programs already include such numerical methods that can be straightforwardly applied to such problems.

Acknowledgment

This work was supported by the Mid-career Researcher Program (No. 2016R1A2B2013776) from the National Research Foundation of Korea.

References

Albu, S.P., Ghicov, A., Macak, J.M., Hahn, R., Schmuki, P., 2007. Self-organized, free-standing TiO_2 nanotube membrane for flow-through photocatalytic applications. Nano Lett. 7 (5), 1286−1289.

Azrague, K., Aimar, P., Benoit-Marquié, F., Maurette, M.T., 2007. A new combination of a membrane and a photocatalytic reactor for the depollution of turbid water. Appl. Catal. B Environ. 72 (3−4), 197−204.

Brandi, R.J., Alfano, O.M., Cassano, A.E., 2000. Evaluation of radiation absorption in slurry photocatalytic reactors. 1. Assessment of methods in use and new proposal. Environ. Sci. Technol. 34 (12), 2623−2630.

Cassano, A.E., Alfano, O.M., 2000. Reaction engineering of suspended solid heterogeneous photocatalytic reactors. Catal. Today 58 (2−3), 167−197.

Chapra, S.C., Canale, R.P., 2010. Numerical Methods for Engineers. McGraw-Hill, New York.

Chin, S.S., Chiang, K., Fane, A.G., 2006. The stability of polymeric membranes in a TiO_2 photocatalysis process. J. Membr. Sci. 275 (1−2), 202−211.

Chin, S.S., Lim, T.M., Chiang, K., Fane, A.G., 2007. Factors affecting the performance of a low-pressure submerged membrane photocatalytic reactor. Chem. Eng. J. 130 (1), 53−63.

Chong, M.N., Jin, B., Chow, C.W.K., Saint, C., 2010. Recent developments in photocatalytic water treatment technology: a review. Water Res. 44 (10), 2997−3027.

Choo, K.-H., Chang, D.-I., Park, K.-W., Kim, M.-H., 2008a. Use of an integrated photocatalysis/hollow fiber microfiltration system for the removal of trichloroethylene in water. J. Hazard Mater. 152 (1), 183−190.

Choo, K.-H., Tao, R., Kim, M.-J., 2008b. Use of a photocatalytic membrane reactor for the removal of natural organic matter in water: effect of photoinduced desorption and ferrihydrite adsorption. J. Membr. Sci. 322 (2), 368−374.

Come, G.M., 1979. Mechanistic modelling of homogeneous reactors: a numerical method. Comput. Chem. Eng. 3 (1), 603−609.

Dijkstra, M.F.J., Buwalda, H., de Jong, A.W.F., Michorius, A., Winkelman, J.G.M., Beenackers, A.A.C.M., 2001. Experimental comparison of three reactor designs for photocatalytic water purification. Chem. Eng. Sci. 56 (2), 547−555.

Dijkstra, M.F.J., Koerts, E.C.B., Beenackers, A.A.C.M., Wesselingh, J.A., 2003. Performance of immobilized photocatalytic reactors in continuous mode. AlChE J. 49 (3), 734−744.

Fu, J., Ji, M., Wang, Z., Jin, L., An, D., 2006. A new submerged membrane photocatalysis reactor (SMPR) for fulvic acid removal using a nano-structured photocatalyst. J. Hazard Mater. 131 (1−3), 238−242.

Hornbeck, R.W., 1975. Numerial Methods. Quantum Publishers, Inc., New York.

Huang, X., Leal, M., Li, Q., 2008. Degradation of natural organic matter by TiO_2 photocatalytic oxidation and its effect on fouling of low-pressure membranes. Water Res. 42 (4−5), 1142−1150.

Iserles, A., NøRsett, S.P., 1990. On the theory of Parallel Runge—Kutta methods. IMA J. Numer. Anal. 10 (4), 463−488.

Jenson, V.G., Jeffreys, G.V., 1977. Mathematical Methods in Chemical Engineering. Elsevier.

Jiang, H., Zhang, G., Huang, T., Chen, J., Wang, Q., Meng, Q., 2010. Photocatalytic membrane reactor for degradation of acid red B wastewater. Chem. Eng. J. 156 (3), 571−577.

Jiang, L., Choo, K.-H., 2016. Photocatalytic mineralization of secondary effluent organic matter with mitigating fouling propensity in a submerged membrane photoreactor. Chem. Eng. J. 288, 798−805.

Kim, M.-J., Choo, K.-H., Park, H.-S., 2010. Photocatalytic degradation of seawater organic matter using a submerged membrane reactor. J. Photochem. Photobiol. A-Chem. 216 (2−3), 215−220.

Konstantinou, I.K., Albanis, T.A., 2004. TiO2-assisted photocatalytic degradation of azo dyes in aqueous solution: kinetic and mechanistic investigations: a review. Appl. Catal. B Environ. 49 (1), 1−14.

Lee, K.-C., Beak, H.-J., Choo, K.-H., 2015. Membrane photoreactor treatment of 1,4-dioxane-containing textile wastewater effluent: performance, modeling, and fouling control. Water Res. 86, 58−65.

Lee, K.-C., Choo, K.-H., 2013. Hybridization of TiO2 photocatalysis with coagulation and flocculation for 1,4-dioxane removal in drinking water treatment. Chem. Eng. J. 231, 227−235.

Lee, S.-A., Choo, K.-H., Lee, C.-H., Lee, H.-I., Hyeon, T., Choi, W., Kwon, H.-H., 2001. Use of ultrafiltration membranes for the separation of TiO2 photocatalysts in drinking water treatment. Ind. Eng. Chem. Res. 40 (7), 1712−1719.

Martínez, F., López-Muñoz, M.J., Aguado, J., Melero, J.A., Arsuaga, J., Sotto, A., Molina, R., Segura, Y., Pariente, M.I., Revilla, A., Cerro, L., Carenas, G., 2013. Coupling membrane separation and photocatalytic oxidation processes for the degradation of pharmaceutical pollutants. Water Res. 47 (15), 5647−5658.

Molinari, R., Grande, C., Drioli, E., Palmisano, L., Schiavello, M., 2001. Photocatalytic membrane reactors for degradation of organic pollutants in water. Catal. Today 67 (1−3), 273−279.

Molinari, R., Mungari, M., Drioli, E., Di Paola, A., Loddo, V., Palmisano, L., Schiavello, M., 2000. Study on a photocatalytic membrane reactor for water purification. Catal. Today 55 (1−2), 71−78.

Molinari, R., Palmisano, L., Drioli, E., Schiavello, M., 2002. Studies on various reactor configurations for coupling photocatalysis and membrane processes in water purification. J. Membr. Sci. 206 (1−2), 399−415.

Molinari, R., Pirillo, F., Loddo, V., Palmisano, L., 2006. Heterogeneous photocatalytic degradation of pharmaceuticals in water by using polycrystalline TiO_2 and a nanofiltration membrane reactor. Catal. Today 118 (1−2), 205−213.

Mozia, S., 2010. Photocatalytic membrane reactors (PMRs) in water and wastewater treatment. A review. Sep. Purif. Technol. 73 (2), 71−91.

Mozia, S., Tomaszewska, M., Morawski, A.W., 2005. A new photocatalytic membrane reactor (PMR) for removal of azo-dye Acid Red 18 from water. Appl. Catal. B Environ. 59 (1−2), 131−137.

Mozia, S., Tomaszewska, M., Morawski, A.W., 2007. Photocatalytic membrane reactor (PMR) coupling photocatalysis and membrane distillation—Effectiveness of removal of three azo dyes from water. Catal. Today 129 (1−2), 3−8.

Munthe-Kaas, H., 1999. High order Runge-Kutta methods on manifolds. Appl. Numer. Math. 29 (1), 115−127.

Qu, D., Qiang, Z., Xiao, S., Liu, Q., Lei, Y., Zhou, T., 2014. Degradation of Reactive Black 5 in a submerged photocatalytic membrane distillation reactor with microwave electrodeless lamps as light source. Sep. Purif. Technol. 122, 54−59.

Romanos, G.E., Athanasekou, C.P., Katsaros, F.K., Kanellopoulos, N.K., Dionysiou, D.D., Likodimos, V., Falaras, P., 2012. Double-side active TiO_2-modified nanofiltration membranes in continuous flow photocatalytic reactors for effective water purification. J. Hazard Mater. 211−212, 304−316.

Rota, F., Cavassi, M., Niego, D., Gorlani, R., Vianelli, L., Tatti, L., Bruzzi, P., Moroni, A., Bellobono, I.R., Bianchi, M., Muntau, H., 1996. Mathematical modelling of photomineralization of phenols in aqueous solution, by photocatalytic membranes immobilizing titanium dioxide. Chemosphere 33 (11), 2159−2173.

Ryu, J., Choi, W., Choo, K., 2005. A pilot-scale photocatalyst-membrane hybrid reactor: performance and characterization. Water Sci. Technol. 51 (6−7), 491−497.

Sabate, J., Anderson, M.A., Aguado, M.A., Giménez, J., Cervera-March, S., Hill, C.G., 1992. Comparison of TiO2 powder suspensions and TiO2 ceramic membranes supported on glass as photocatalytic systems in the reduction of chromium(VI). J. Mol. Catal. 71 (1), 57−68.

Sabate, J., Anderson, M.A., Kikkawa, H., Edwards, M., Hill, C.G., 1991. A kinetic study of the photocatalytic degradation of 3-chlorosalicylic acid over TiO2 membranes supported on glass. J. Catal. 127 (1), 167−177.

Shahrezaei, F., Mansouri, Y., Zinatizadeh, A.A.L., Akhbari, A., 2012. Process modeling and kinetic evaluation of petroleum refinery wastewater treatment in a photocatalytic reactor using TiO_2 nanoparticles. Powder Technol. 221, 203–212.

Sopajaree, K., Qasim, S.A., Basak, S., Rajeshwar, K., 1999. An integrated flow reactor-membrane filtration system for heterogeneous photocatalysis. Part I: Experiments and modelling of a batch-recirculated photoreactor. J. Appl. Electrochem. 29 (5), 533–539.

Tahiri Alaoui, O., Nguyen, Q.T., Mbareck, C., Rhlalou, T., 2009. Elaboration and study of poly(vinylidene fluoride)–anatase TiO_2 composite membranes in photocatalytic degradation of dyes. Appl. Catal. Gen. 358 (1), 13–20.

Turchi, C.S., Ollis, D.F., 1990. Photocatalytic degradation of organic water contaminants: mechanisms involving hydroxyl radical attack. J. Catal. 122 (1), 178–192.

Wang, W.-Y., Irawan, A., Ku, Y., 2008. Photocatalytic degradation of Acid Red 4 using a titanium dioxide membrane supported on a porous ceramic tube. Water Res. 42 (19), 4725–4732.

Yao, P., Choo, K.-H., Kim, M.-H., 2009. A hybridized photocatalysis–microfiltration system with iron oxide-coated membranes for the removal of natural organic matter in water treatment: effects of iron oxide layers and colloids. Water Res. 43 (17), 4238–4248.

Zhang, H., Quan, X., Chen, S., Zhao, H., Zhao, Y., 2006. Fabrication of photocatalytic membrane and evaluation its efficiency in removal of organic pollutants from water. Sep. Purif. Technol. 50 (2), 147–155.

Zhang, X., Wang, D.K., Lopez, D.R.S., Diniz da Costa, J.C., 2014. Fabrication of nanostructured TiO_2 hollow fiber photocatalytic membrane and application for wastewater treatment. Chem. Eng. J. 236, 314–322.

CHAPTER 11

Economical Aspects in Photocatalytic Membrane Reactors

Wolfgang M. Samhaber[1], **Minh Tan Nguyen**[2]
[1]*Johannes Kepler University Linz, Linz, Austria;* [2]*Hanoi University of Science and Technology, Hanoi, Vietnam*

11.1 Introduction

Different ways of operating a photocatalytic membrane reactor (PMR) in laboratory scale have been reviewed recently in a comprehensive form by Molinari et al. (2017), and photocatalytic applications have been reported in different publications extensively, e.g., by Molinari et al. (2010), Brunetti et al. (2017), and Mozia (2010).

The main fields of applications of this technology can be divided in two groups. The first is dealing with purification processes and the second is focused on synthesis steps; however, combined reactions are often investigated to get an increased efficiency of the system. In Figs. 11.1 and 11.2, those different ways of operating PMRs and combinations of photocatalytic and membrane separation systems are illustrated schematically.

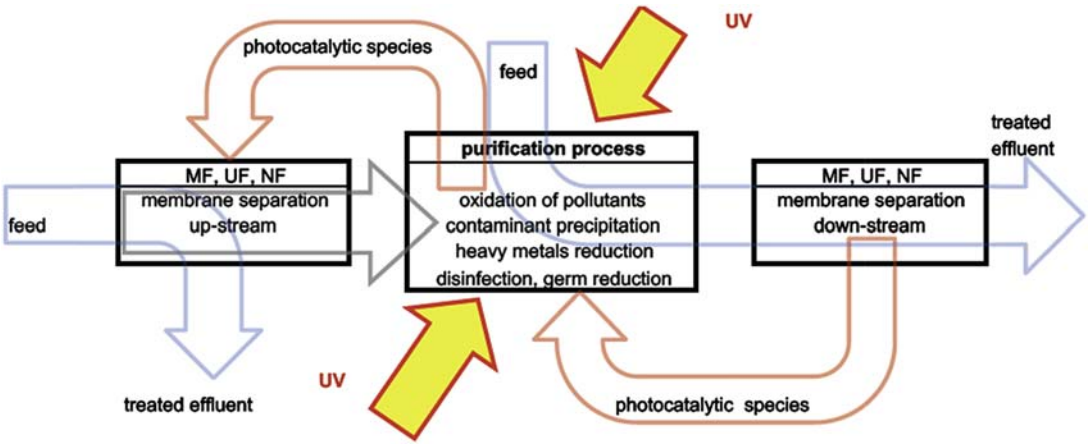

Figure 11.1
Hybrid photocatalysis–membrane process concepts for purification purposes.

Current Trends and Future Developments on (Bio-) Membranes. https://doi.org/10.1016/B978-0-12-813549-5.00011-6

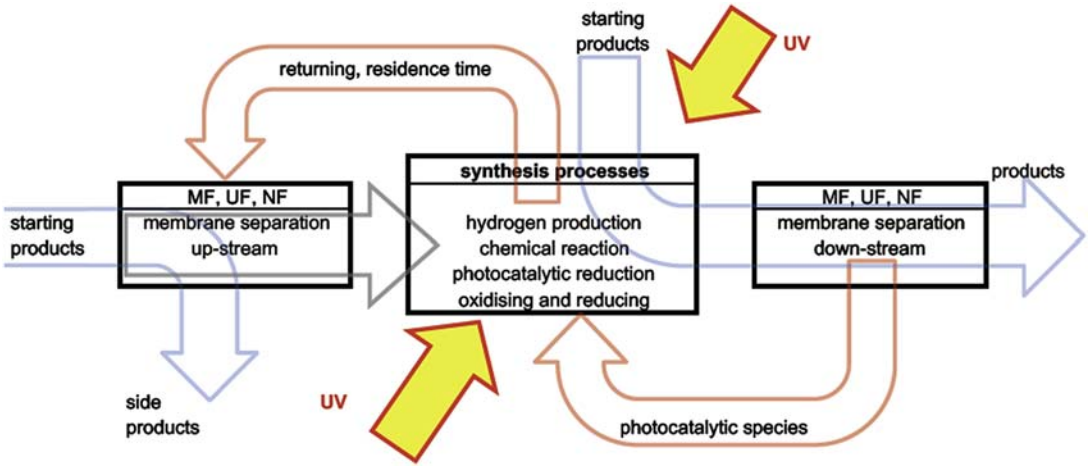

Figure 11.2
Schematic diagram of hybrid photocatalysis–membrane system combinations for synthesis processes.

Considering the combination of photocatalytic systems with membrane separation, however, different possibilities exist, which are defined by certain process or reaction-related requirements. On this view, the membrane unit can be put on the entrance or upstream side of the reaction system, e.g., for a selective pretreatment of the feed, or on the downstream side to keep the photocatalyst in the process and/or to bring back not yet treated dissolved components to the photocatalytic reactor.

In the same way, it will be shown in Fig. 11.2 for synthesis processes, where the upstream or downstream steps are separating, e.g., inhibitors, maintaining residence time, recycling feed products, reducing side products, or just keep the photocatalyst particles within the system.

Many pathways for purifying waste stream and cleaning up water with different concepts and membranes in combination with photocatalytic reactions have been discussed so far. Basics of photocatalysis can be taken from Chapter 1 of this book.

Combining membranes with photocatalytic reactors, two different concepts of PMR systems can be distinguished: the system with suspended photocatalyst and the system with the photocatalytic particles fixed on or in the membrane. Suspended photocatalytic particles can be retained in the reaction system by a cross-flow or a submerged membrane system. The system can be operated partly or entirely in batch or continuous mode, and the membrane unit can control or assist the process.

The membranes of interest for being used in PMRs are generally microfiltration (MF) (Damodar et al., 2010), ultrafiltration (UF) (Grzechulska-Damszel et al., 2010;

Damodar et al., 2010; Mozia et al., 2006), nanofiltration (NF) (Grzechulska-Damszel et al., 2010; Zheng et al., 2013; Berberidou et al., 2009; Grzechulska-Damszel and Morawski, 2009; Molinari et al., 2004), and, in few cases, reverse osmosis (RO) membranes (Berberidou et al., 2009), which are applied in pressure-driven mode, where the feed, retentate, and permeate phases are liquid. Only a few applications are dealing with gaseous or vapor phases such as pervaporation or membrane distillation (MD). Newly, the combination with membrane distillation (Grzechulska-Damszel et al., 2010; Mozia et al., 2006) has also been proposed for the treatment of dyehouse effluents.

Regarding the separation properties, the membrane itself must proof its mechanical and chemical stability in such photocatalytic processes (Mozia et al., 2015).

Thinking of economics and cost aspects of the PMR and focusing on the part of the membrane unit and a possible technical realization, the upscaling requirements have to be rigorously considered.

Small scales in laboratory applications have a large surface in proportion to the operated volume. In scaling up, the surface is expanding with a quadratic function of the length and the volume is linked with the third power. The figure that is given by the treated volume in a certain time with a certain membrane area has to be kept more or less constant during upscaling.

Cross-flow as well as submerged membrane systems can be more easily scaled up, because the needed membrane surfaces can be realized outside of the reaction system. The pressure-driven cross-flow systems are operated by applying a positive pressure on the retentate side, whereas the submerged membrane systems are operated by a suction pressure applied at the permeate side.

The difference between these separating systems is that the transmembrane pressure controls permeate flux of the cross-flow systems, whereas the permeate flux of submerged units are adjusted by the limit of the applicable suction pressure. The applied pressures influence the operational costs. Lower pressures of the submerged systems have corresponding cost advantages during operation in comparison with the pressurized cross-flow systems.

Some selected examples that are described in the literature will be discussed later on in terms of size, construction, or design in order to illustrate diverse ideas and possibilities of the membrane reactor combinations.

The combination of photocatalysis and membranes is based on the fact that photocatalysis exhibits an oxidation potential, and the membrane separation especially with NF membranes owns a selective separation potential for retaining and removing pollutants. Different concepts have been described in literature. The use of particulate photocatalysts

requires a recirculation of the photocatalyst, and it is additional necessary to uncouple the hydraulic residence time from the residence time of the organic compounds in the photocatalytic reactor system, which can be achieved by selective membrane separation (Chong et al., 2010; Grzechulska-Damszel et al., 2010; Chooa et al., 2008; Augugliaro et al., 2005; Martınez et al., 2013).

11.1.1 Membrane Concepts With Photocatalyst

To integrate a membrane separation unit into a photocatalytic process system, it is necessary to select the most suitable type of membrane (RO, NF, UF or MF), the right membrane materials (ceramic, polymeric), and the proper process configuration (tubular, flat-sheet, spiral, capillary, or hollow fibers); all of these possible selections have an influence of course on performance and on price.

To reject or to separate dissolved components in clear influent solution, NF- or UF-type membranes are to be chosen. In Fig. 11.3 the photocatalytic process is shown with the photocatalytic system as the master of the purification process. A UF or an NF step is set downstream of the photocatalytic reactor for recycling of not yet completely treated organics back to the reaction chamber. Besides retaining and back transport, photocatalytic particles can also be recovered and returned back into the reactor. For separation of organics, mostly polymeric membrane can be used, but in case of suspended

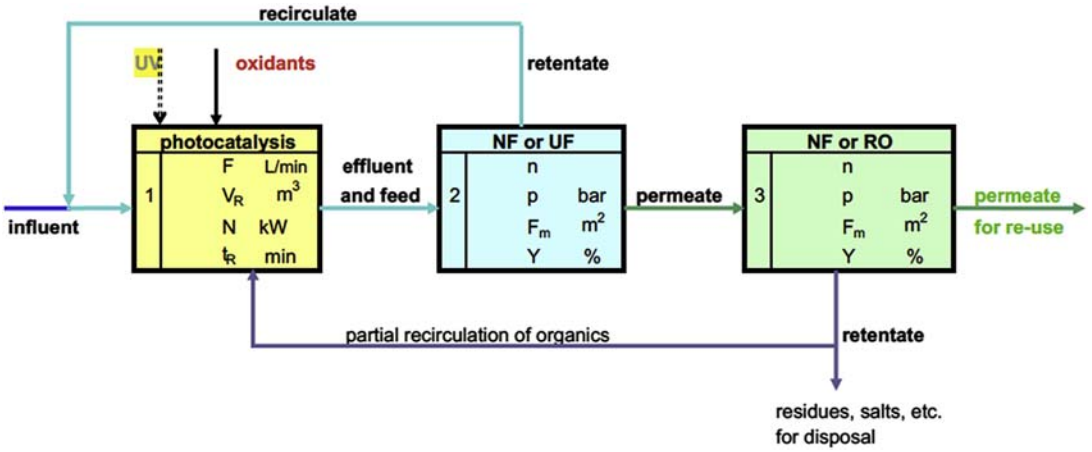

Figure 11.3

Photocatalysis as the master process responsible for the reduction of organics and fouling matter with a UF or NF membrane to control residence time and recycling organics by NF and partially by RO and polishing the water for reuse (n: concentration factor; p, bar: operational pressure; F_m, m^2: membrane area; F, L min^{-1}: flow rate; Y, %: retention; V_R, m^3: reactor volume; N, kW: energy demand; t_R, min: the reaction time).

photocatalytic particles the selection of abrasion-resistant membrane types and configuration are highly necessary. A further possibility would be to split the particle recovery from the dissolved organics separation with two different membranes. In combining recovering and polishing membrane steps of MF, UF, NF, and RO with photocatalysis, the efficiency of the reaction system must proof the higher cost of those process extensions. UF or NF permeate can be fed to separation steps with a dense NF or RO membrane with almost no fouling risk to separate additional unwanted salts and possibly residual organics to produce high-quality water for reuse.

Certain key figures are shown in Fig. 11.3, which are necessary to specify the size of the equipment and represent the requirement for the estimation of capital operation costs. For the reaction system, we need to define the reaction volume (V_R), the flow rate or the reaction time, and the energy demand. Again, for the membrane separation unit, we need to specify the membrane area, which is a result of the permeate volume to be produced per time over the specific permeate flux, which can be achieved by applying a certain pressure with the real process stream.

Permeate fluxes result primarily from factors such as membrane type, operation pressure, concentration, osmotic pressure, viscosity, and temperature. Based on practical experiences, we can assume for a rough cost preliminary fluxes, which have to be proofed before the system will be designed for a realization.

In this sense, we can take an estimated membrane flux for RO and NF between 15 and 30 L ($m^{-2}\,h^{-1}$), for UF some more between 25 and 50 L ($m^{-2}\,h^{-1}$), and for MF between 50 and 100 L ($m^{-2}\,h^{-1}$).

Fluxes are much affected by the turbidity of the influents, undissolved fine dispersed organic solids, which are also influencing the photocatalytic reaction because of the reduced transparency for the UV radiation.

Clear influent streams with less complex dissolved compounds and a high optical transmission will be the effluent stream of choice, which could be treated favorably. Suspended fine or colloidal solids in the feed water have in anyway to be pretreated to prevent fouling. Finally, it must be kept in mind that additional improvements of the reaction process through NF and RO step like in Fig. 11.3 will have to be justified through cost advantages in the operation.

Generally, in all membrane applications, the appearance of an unwanted fouling is a costly issue. Fouling of membranes is often considered as a weakness of membrane processes. In any way, it has to be taken care of the fouling stuff before entering a reaction system, which is connected with a membrane separation unit. Fouling should certainly not be accepted as a disadvantage in membrane application. It has to be avoided almost in all surface-defined processes such as in membrane separation as well as in heterogeneous

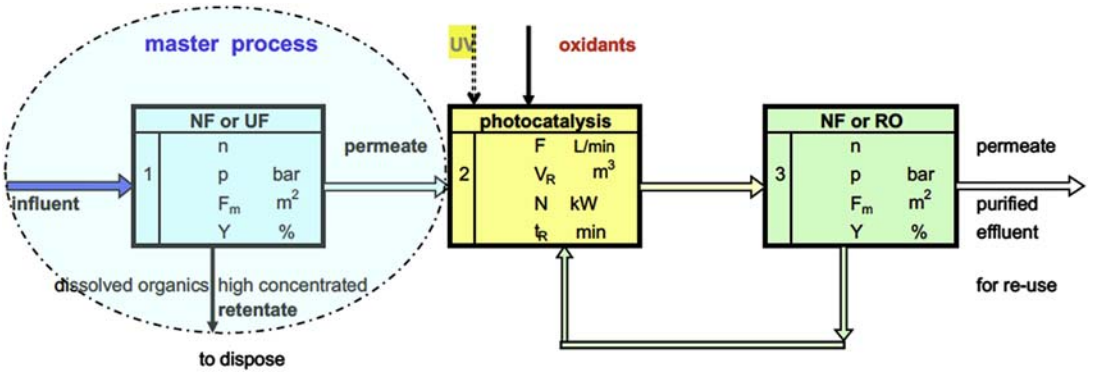

Figure 11.4

Membrane process as the master process removing the major organic load of the influent whereby photocatalysis acts as a polishing step (n: concentration factor; p, bar: operational pressure; F_m, m^2: membrane area; F, L min^{-1}: flow rate; Y, %: retention; V_R, m^3: reactor volume; N, kW: energy demand; $t_{R,}$ min: the reaction time).

photocatalytic processes. The development of a proper pretreatment recipe is therefore a challenging task but is paying off later in a multiple way.

Another way of combining membranes and photocatalysis is shown in Fig. 11.4. In this schematic basic diagram, an organic rejecting membrane type such as an NF or UF membrane is used in the first step to separate the influent in a high concentrated retentate stream and a low loaded permeate stream. The permeate stream, which will be obtained in the first membrane step, has received already a high grade of purification but is further subjected to a following cleaning step by a photocatalytic reactor.

The reactor is placed downstream to the NF or RO membrane step and therefore has a serving function, and the NF or RO membrane step represents the master process. The photocatalysis has the polishing function to reduce still residual compounds, which cannot completely be rejected by nonporous hydrophilic solution/diffusion membranes. Conventionally activated carbon adsorption is used for that task, and a photocatalytic system is an alternative process in this function and has to be competitive in this way.

This concept is comparable with a general NF treatment concept at the source, and the feed therefore has to be pretreated if necessary in order again to avoid membrane fouling as already mentioned before.

The retained dissolved organic solutes are separated in the first step in a concentrated retentate stream, which would have to be thermally oxidized or disposed in accordance with relevant regulations. The permeate stream, which is already poor in organic contents and transparent, is posttreated in the photocatalysis, which can again be classified as a polishing step.

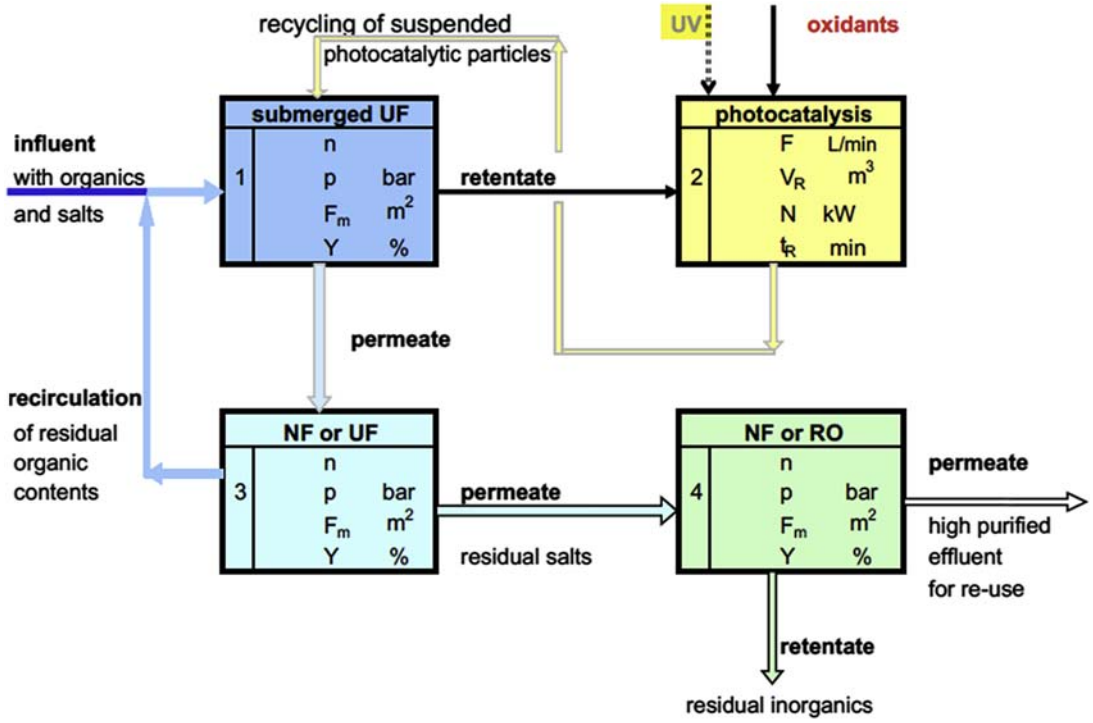

Figure 11.5

Processing of streams containing organic and inorganic contents through a photocatalytic reactor with suspended photocatalytic particles combined with a submerged UF membrane unit (n: concentration factor; p, bar: operational pressure; F_m, m^2: membrane area; F, L min^{-1}: flow rate; Y, %: retention; V_R, m^3: reactor volume; N, kW: energy demand; t_R, min: the reaction time).

Fig. 11.5 shows the processing of process streams containing organic and inorganic contents through a photocatalytic reactor with suspended photocatalytic particles combined with a submerged UF membrane unit. The backflow of the photocatalytic system contains substances, which have not yet been reacted or oxidized, and suspended photocatalytic particles, which will be separated from the treated water to the UF permeate. With the recirculation rate of the UF retentate, on the one hand, the residence time within the reactor can be defined and, on the other hand, the photocatalytic particle will be brought back into the reaction system. The UF permeate will be introduced as the feed to the downstream NF separation step, where organic compounds are retained and returned to the influent feed. The NF step should be arranged in such a way that the residence time of persistent organic compounds could be increased within the system. The NF permeate again can be treated downstream optionally to separate residual inorganic contents by RO step to achieve high-quality water source.

The influent stream needs respective pretreatment, whereby the effluent stream of choice has to be transparent to enable a proper photocatalytic degradation of the organic content. A favorable and optimal feed would be again a clear effluent stream with less complex constituents together with a high optical transparency.

11.2 Cost Estimation for Photocatalytic Membrane Reactor System

Because of the different nature of the photocatalytic part and membrane part of PMR system, cost estimation for PMR system will be discussed on the basis of separate cost consideration for the photocatalytic part and the membrane part.

11.2.1 Cost Estimation for Photocatalytic Part

Cost estimation for photocatalytic part can be realized by following the advanced oxidation processes (AOPs) process cost estimation procedure proposed by Kommineni et al. (2000) and Mahamuni and Adewuyi (2010). Table 11.1 shows details on the cost breakdown as have been taken by these authors (Mahamuni and Adewuyi, 2010; Kommineni et al., 2000).

11.2.1.1 Calculation of Capital Expenditure of Photocatalytic Part Following Mahamuni and Adewuyi (2010)

The overall kinetics of the photocatalytic degradation of pollutant has been identified by most researchers to be either a first-order or a zeroth-order reaction (Melin, 1999; Bolton et al., 2001). Aiming at the development of a standard figure-of-merit for comparing AOP processes, Bolton et al. (2001) used a simple mechanism model for AOP processes:

$$B \rightarrow Z\bullet \qquad r_1 = c.P_{elec}/V \tag{11.1}$$

$$Z\bullet + C \rightarrow \text{products} \qquad r_2 = k_C[Z\bullet][C] \tag{11.2}$$

$$Z\bullet + S_1 \rightarrow \text{products} \qquad r_{3a} = k_{S1}[Z\bullet][S_1] \tag{11.3a}$$

$$Z\bullet + S_2 \rightarrow \text{products} \qquad r_{3b} = k_{S2}[Z\bullet][S_2] \tag{11.3b}$$

$$Z\bullet + S_i \rightarrow \text{products} \qquad r_{3i} = k_{Si}[Z\bullet][S_i] \tag{11.3c}$$

where c, constant; P_{elec} (kW), electrical power input to the system; V (L), treated volume; B, initial compound, which can be water or some added substance (e.g., H_2O_2 or O_3); Z•, highly reactive intermediate (e.g., •OH, H•, hydrated electron, etc.); C, a particular organic contaminant; S_1, S_2,…, S_i, scavengers for the Z• radical; r_1 (Ms^{-1}), rate of formation of Z• radical; G ($Einstein^{-1}$), total absolute photon flow emitted from the lamp in all directions in a useful wavelength range; χ, fraction of photons that are absorbed in solution; $\phi_{Z\bullet}$,

Table 11.1: Cost breakdown of a photocatalytic unit.[a]

Cost Breakdown	Cost (US$)
Capital expenditure (CAPEX)	**1.2 S**
(*The investment costs contain the full treatment system and its setting up*)	
Reactor cost	*P (provided by vendors)*
Piping, valves, electrical (30%)	0.3 P
Site work (10%)	0.1 P
Subtotal 1	*1.4 P = Q*
Contractor O&P (15%)	0.15 Q
Subtotal 2	*1.15 Q = R*
Engineering (15%)	0.15 R
Subtotal 3	*1.15 R = S*
Contingency (20%)	0.2 S
Operating expenditure (OPEX)	
Replacement parts	*Based on vendor's estimation*
Laboratory costs:	*Based on hours of service life*
• Water sampling cost	
• General O&M costs:	
• General system oversight	
• Maintenance: pressure gauges, control panels, leakages, etc.	
• System-specific O&M costs:	
• Inspection	
• Replacement	
• Repair	
Analytical costs for sampling conducted weekly	
Chemical costs:	*Based on dose and price estimated by vendor*
• Consumables	
• Chemicals involved with the AOP (TiO_2, etc.)	
Power cost	*Based on consumption estimates provided by vendor*
Amortization of the annual capital cost	Assumptions: 30-year period, at a discount rate of 7%

P: reactor cost; Q: subtotal 1; R: subtotal 2; S: subtotal 3.

[a]The % values are taken from vendor data in the MTBE report from NWRI (National Water Research Institute, USA) (Melin, 1999).

quantum yield for the generation of Z•; r (Ms^{-1}), overall rate of the process; k_C, second-order rate constant; r_2 (Ms^{-1}), rate of reaction of Z• with C with second-order rate constant k_C; r_{3a}, r_{3b},…, r_{3i}, rate of reaction of Z• with scavengers S_1, S_2,…, S_i; and k_{S1}, k_{S2}, …, k_{Si}, second-order rate constant k_{S1}, k_{S2}, …, k_{Si}.

For the case of a photochemical process:

$$c = \frac{G\chi\phi_{Z\bullet}}{P_{elec}}$$

Therefore, overall rate of the process can be obtained as follows:

$$r = \frac{\frac{c \cdot P_{elec} \cdot k_{C.} \cdot [C]}{V}}{k_C \cdot [C] + \sum_i k_{S_i} \cdot [S_i]} \tag{11.4}$$

In case [C] is high, so that $k_C[C] \gg \sum_i k_{S_i}[S_i]$ or, in other words, reaction 2 with contaminant dominates over the scavenging of Z• in reaction 3, then the reaction rate will be zero order in C $\left(r = \frac{c \cdot P_{elec}}{V}\right)$.

In case [C] is low, so that $k_C[C] \ll \sum_i k_{S_i}[S_i]$, then the reaction rate will be first order in C with:

$$k_1' = \frac{\frac{60 \cdot c \cdot P_{elec} \cdot k_C}{V}}{\sum_i k_{S_i} \cdot [S_i]} \tag{11.5}$$

Hyman et al. (2001) stated that the differentiation between "low" and "high" concentration range here depends substantially on the characteristics of AOP processes. According to Herrmann (1999), for photocatalysis processes, low and high concentration ranges are defined as $C < 10^{-3}$ M and $C > 5.10^{-3}$ M, respectively.

In case of low concentration, the first-order degradation can be written as follows:

$$\ln \frac{C_0}{C} = k_i' \tau \tag{11.6}$$

Time for 90% degradation can be calculated by:

$$\tau_{90} = \frac{2.3025851}{k_i'} \tag{11.7}$$

For high concentration or zeroth-order degradation:

$$C = C_0 - k_C \tau \tag{11.8}$$

Time for 90% degradation can be calculated by:

$$\tau_{90} = \frac{0.9 C_0}{k_C} \tag{11.9}$$

Capacity of the reactor is then:

$$V_{90} = U \tau_{90} \tag{11.10}$$

where k_1' (min^{-1}), pseudo−first-order rate constant; τ_{90} (min), time required for 90% degradation of the contaminant; U ($L\ min^{-1}$), design flow rate of the photocatalytic reactor; V_{90} (L), treated volume at 90% degradation; ε (WL^{-1}), energy density; E (W), energy supplied by single reactor; and N, number of reactor.

Energy density, ε, can be derived from referred publications or calculated from the data in the publications. Total energy requirement in the reactor is $V_{90}\varepsilon$.

The energy supplied by single reactor, E (W), can be taken from vendor quotations.

The required number of reactor $N = U\tau_{90}\varepsilon$.

With the unit costs of a photocatalytic reactor C (US$), the capital costs of the equipment are:

$$P = NC = C\frac{U\tau_{90}\varepsilon}{\mathrm{E}}\ (\mathrm{US\$}) \tag{11.11}$$

Consequently, for the case of low concentration of the organic contaminant, we have:

$$P = A\frac{U\dfrac{2.3025851}{k_i'}\varepsilon}{\mathrm{E}} \tag{11.12}$$

and for the case of high concentration:

$$P = A\frac{U\dfrac{0.9C_0}{k_C}\varepsilon}{\mathrm{E}} \tag{11.13}$$

Eqs. (11.12) and (11.13) reveal clearly that capital cost of AOP processes, in general, and of photocatalysis, in particular, is influenced mainly by the removal efficiency and flow rate but not by the concentration of the influent. This displays a good correlation with the experimental results from diverse studies (Mahamuni and Adewuyi, 2010; Kommineni et al., 2000; Johne and Nguyen, 2016).

11.2.1.2 Calculation of Amortization of the Annual Capital Cost

Amortization of the capital cost P can be calculated according to the formula (Adewuyi, 2001):

$$A = \frac{Pr}{1 - \left(\dfrac{1}{1+r}\right)^n} \tag{11.14}$$

where A, periodic amortization payment; r, periodic interest rate divided by 100 (nominal annual interest rate also divided by 12 in case of monthly installments); and n, total number of payments (for a 30-year loan with monthly payments $n = 30 \times 12 = 360$).

11.2.1.3 Calculation of Operating Expenditure

As exhibited in Table 11.1, OPEX consists of part replacement costs, labor costs, analytical costs, chemical costs, and electrical and energy costs.

Part replacement costs can be assumed to be 45% of the annual electrical power consumption costs as for UV system (Yuan and Tol, 2004; Hyman and Dupont, 2001).

Labor costs consist of water sampling cost and general and system-specific O&M costs. General O&M labor was assumed to be 312 h $year^{-1}$ for all the systems. According to Melin (1999), the labor rate was assumed to be \$80 h^{-1} for all AOP systems. Nevertheless, Mahamuni and Adewuyi (2010) did not consider labor costs for photocatalyst systems.

Analytical costs are based on the sampling frequency, the labor required to carry out the analysis of the samples, and the cost of analytical chemicals. Melin (1999) proposed a rate of \$200h^{-1} for these costs.

Chemical costs include the costs of consumables such as hydrogen peroxide and chemicals involved in the AOP such as TiO_2 photocatalyst. Prices for H_2O_2 and TiO_2 are obtained from standard industrial suppliers such as ICIS Pricing and Inframat Advanced Materials (icis):

H_2O_2 (50%): \$4 per gallon
TiO_2: \$300 per kg

Electrical costs are based on the power consumption by the photocatalysis. Electricity rate is assumed to be \$0.08 kWh^{-1}. Power consumption can be calculated by multiplying the annually consumed electrical energy by the electricity rate.

Kommineni et al. (2000) have made evaluation for several AOP processes based on the cost estimation provided from different manufacturers/vendors.

Basis of the cost estimation for methyl-tert-butyl ether (MTBE) degradation proposed by the authors was as follows (Kommineni et al., 2000):

- Flow rate: 600 gpm (2271 L min^{-1})
- Influent MTBE: 200 μg L^{-1}
- Effluent MTBE: 5 μg L^{-1}

Table 11.2: Cost estimation overview (Kommineni et al., 2000).

Manufacturers/ Vendors	**Calgon Carbon Corporation**	**Applied Process Technology, Inc.**	**Oxidation Systems, Inc.**	**Hydroxyl Systems, Inc.**
AOP Process	H_2O_2/Medium Pressure UV	H_2O_2/O_3	Hydrodynamic Cavitation with H_2O_2	**TiO_2 photocatalysis under UV**
TOC Concentration 0.8 mg L^{-1}				
Capital cost	$488,800	$1,777,400	$461,200	**$1,730,800**
Annual operation and maintenance costs	$264,000	$136,800	$185,500	**$391,000**
Total amortized operating cost (per 1000 gallons treated)	$0.96	$0.89	$0.71	**$1.68**
TOC Concentration 2 mg L^{-1}				
Capital cost	$488,800	$1,777,400	$461,200	**$1,730,800**
Annual operation and maintenance costs	$264,000	$139,900	$204,400	**$542,200**
Total amortized operating cost (per 1000 gallons treated)	$0.96	$0.90	$0.77	**$2.16**
TOC Concentration 8 mg L^{-1}				
Capital cost	$488,800	$1,777,400	$461,200	**$1,730,800**
Annual operation and maintenance costs	$316,900	$149,300	$229,600	**$831,300**
Total amortized operating cost (per 1000 gallons treated)	$1.13	$0.93	$0.85	**$3.08**

As it can be seen from Table 11.2, the change in total organic carbon (TOC) concentration did not have an effect on the size of the reactor (capital cost) in all AOP systems. The amortized operating cost (per 1000 gallons treated, equivalent to 378 m^3) in most cases depends also not much on the change of TOC concentration. Nevertheless, increasing TOC concentration tends to have great influence on the performance of TiO_2/UV system and makes this technology more cost-intensive. Because the treatment of higher TOC concentration effluent will surely lead to shorter photocatalyst lifetime, oftener reactor and lamp cleaning.

Kommineni et al. (2000) stated that H_2O_2/O_3 and H_2O_2/medium-pressure UV are most promising processes because of their high technical as well as economic feasibility in terms of MTBE oxidation. TiO_2 photocatalysis under UV irradiation was considered to be an emerging technology characterized by many advantages with respect to the treating of water with low contaminant concentrations. Nevertheless, the process still needs to be thoroughly studied before being used in large-scale remediation or drinking water treatment applications.

Mahamuni and Adewuyi (2010) evaluated the economic feasibility of the use of ultrasonic energy for wastewater treatment on industrial scale by conducting a comprehensive cost estimation of various AOP processes following the algorithm described above.

Basis of the cost estimation:

- Flow rate: 1000 L min^{-1} (264 gpm)
- Contaminants: phenol, trichloroethylene (TCE), and reactive azo dyes
- 90% degradation

The treatment cost (US$/1000 gallons) was derived from capital costs, operating costs, and operation parameters of the treatment with the assumption that the treatment plant is running throughout the year (52 weeks) continuously. Kinetic data taken from published literature and calculated from data given in the literature were used for the determination of 90% degradation time. Reactor capacity is then calculated by multiplying the residence time (or 90% degradation time) with the desired flow rate (1000 L min^{-1}).

Table 11.3 shows the results of the cost estimation for two established AOP processes and photocatalysis extracted from the work of Mahamuni and Adewuyi (2010). Obviously, it can be seen here that the treatment costs of photocatalysis are much higher than those of O_3 and H_2O_2/UV processes for the degradation of different organic pollutants such as phenol, TCE, and reactive azo dyes.

The treatment costs using the O_3 system are the lowest in all three cases. The cost for phenol degradation ranges from 0.32 US$ m^{-3} using O_3 to 2285 US$ m^{-3} using TiO_2/UV system. Those costs for reactive azo dye degradation increase from 1.08 US$ m^{-3} using O_3 to 195.5 US$ m^{-3} using TiO_2/UV systems. In case of TCE degradation, the TiO_2/UV process becomes more competitive and the gap between the treatment costs of these technologies essentially narrowed. It drops from 3.99 US$ m^{-3} of TiO_2/UV to 0.62 US$ m^{-3} of O_3 systems.

Mahamuni and Adewuyi (2010) have also calculated electrical energy per mass (EE/M) or electrical energy per order of magnitude per m^3 (EE/O) to evaluate the electrical efficiency of AOP processes. These are two figures-of-merit proposed by Bolton et al. (2001) based on electrical energy consumption of two different phenomenological kinetic data.

Table 11.3: Extracted calculation results from Mahamuni and Adewuyi (2010).

AOP Process	k	P_{elec} kW	τ_{90} min	V L	C_0 μg L^{-1}	C μg L^{-1}	ε (W mL^{-1})	EE/O or EE/M	Cost \$ m^{-3}
Phenol Degradation									
O_3 (2 mg L^{-1})	0.0279 min^{-1}	0.036	82.53	0.1	235.53	23.528	0.36	495.18	0.32
UV/H_2O_2	0.0524 min^{-1}	0.15	90	0.75	1100	5.53	0.15	130.51	81.50
Photocatalysis	**0.433 ppm min^{-1}**	**0.45**	**180**	**0.1**	**100**	**2.36**	**0.45**	**138,263**	**2285.02**
Reactive Azo Dye Degradation									
O_3 (12.4 mg L^{-1})	0.01108 min^{-1}	0.036	207.814	1.2	20	2	0.03	103.91	1.08
UV/H_2O_2	0.0124 min^{-1}	0.186	60	4.5	100	84.35	0.0147	559.2	19.71
Photocatalysis	**0.0207 ppm min^{-1}**	**0.5**	**111.24**	**0.7**	**402.6**	**40.26**	**0.7143**	**3654.68**	**195.47**
TCE Degradation									
O_3 (6 mg L^{-1})	0.0209 min^{-1}	0.036	25	0.1	2.2	1.3	0.36	656.51	0.62
UV/H_2O_2	0.4418 min^{-1}	0.02	14.84	5	2.194	0.003	0.004	0.35	0.88
Photocatalysis	Apparent rate constant = 49.57 μg Ls^{-1}; Adsorption equilibrium constant = 0.000466 L μg	**0.45**	**30**	**7.2**	**15**	**0.21**	**0.0625**	**2,112,914**	**3.99**

11.2.1.4 Electrical Energy per Mass

- Definition: Electrical energy per mass (EE/M) is the electrical energy in kilowatt hours (kWh) required to bring about the degradation of a unit mass (1 kilogram, kg) of a contaminant C in polluted water or air.
- EE/M can be best used when [C] is high (i.e., phenomenologically zero order in C).
- EE/M (kWh kg) can be calculated by formula (11.15):

$$\mathrm{EE/M} = \frac{P\tau 1000}{VM60(C_i - C_f)} \tag{11.15}$$

For photochemical process of the zeroth-order rate:

$$\frac{60G\chi\phi_{z\bullet}}{V} = \frac{(C_i - C_f)}{\tau}\ (\mathrm{M\ min^{-1}})$$

Eq. (11.15) can be written in another way as:

$$\mathrm{EE/M} = \frac{P1000}{M60G\chi\phi_{Z\bullet}} \tag{11.16}$$

EE/M is inversely proportional to the fundament efficiency factors such as G, χ, and $\phi_{Z\bullet}$.

11.2.1.5 Electrical Energy per Order

- Definition: Electrical energy per order (EE/O) is the electrical energy in kilowatt hours (kWh) required to bring about the degradation of a contaminant C by one order of magnitude in 1 m^3 (1000L) of contaminated water or air.
- EE/M can be used when [C] is low (i.e., cases that are overall first order in C).
- EE/O values (in kWh per order per m^3) can be calculated using formula (11.17):
  - For batch operation:

$$\mathrm{EE/O} = \frac{P_{elec}\cdot\tau\cdot 1000}{V\cdot 60\cdot\log\left(\frac{C_i}{C_f}\right)} \tag{11.17a}$$

  - For flow-through operation:

$$\mathrm{EE/}O = \frac{P_{elec}\cdot\tau\cdot 1000}{F\cdot 60\cdot\log\left(\frac{C_i}{C_f}\right)} \tag{11.17b}$$

In case of first-order kinetics, we have $\log\left(\frac{C_i}{C_f}\right) = 0.4343k_1'\tau$ and $F = \frac{V_r\cdot P_{elec}}{\tau}$.

Thus, Eq. (11.17a) can be rewritten as:

$$\mathrm{EE/O} = \frac{38.4 \cdot P}{V_r k_1'} \tag{11.18a}$$

Together with Eq. (11.5), Eq. (11.18a) can be converted into Eq. (11.18b):

$$\mathrm{EE/O} = \frac{0.640 \cdot P \cdot \sum_i k_{S_i} [S_i]}{G \cdot \chi \cdot \phi_Z \cdot k_C} \tag{11.18b}$$

Like EE/M, EE/O is also inversely proportional to fundamental efficiency factors such as G, χ, and ϕ_Z.

EE/M and EE/O demonstrate a direct link to the electrical efficiency. Lower value of these figures-of-merit corresponds to more energy-efficient system.

Table 11.3 contains a part of calculation results of Mahamuni and Adewuyi (2010). Electrical energy per mass (EE/M) or electrical energy per order of magnitude per m^3 (EE/O) of photocatalysis is extremely higher than that of O_3 and UV/H_2O_2 processes. In the present case, this would mean that photocatalysis can still hardly be realized in industrial scale for 90% degradation of phenol, TCE, and reactive azo dyes at the flow rate of 1000 L min^{-1} (264 gpm) owing to its gigantic energy cost.

The huge differences between EE/M or EE/O values of photocatalysis and those of UV/H_2O_2 can be partly explained with the reciprocal proportionality to the fraction of light absorbed (χ). Within the slurry reactor, high turbidity of photocatalyst suspension leads to extreme drop in UV transmittance and therefore causes the low fraction of light absorbed (χ), which leads to high EE/M or EE/O values. Apart from this, phenomena such as absorbance and scattering in nanocolloidal suspensions result in a loss of energy of the incident beam (Le et al., 2015). Moreover, high energy density is also required to avoid the great aggregation tendency of the photocatalyst suspension. Le et al. (2015) studied the effect of aggregate size on the photocatalytic activity of Aeroxide P25 (Evonik) with a laboratory-scale plug flow reactor and stated that the required energy would increase 170 times to halve the Aeroxide P25 size and that a reduction in particle size from 380 to 250 nm leads to an enhancement of the reaction rate constant of 1 g L^{-1} P25 suspension by 23%.

The H_2O_2/UV process has been widely commercialized in the last few years. The UV-EL GmbH & Co. KG in Germany is one of the companies supplying various H_2O_2/UV systems for different purposes (Johne and Nguyen, 2016).

Figs. 11.6–11.8 show different installed H_2O_2/UV systems of UV-EL GmbH & Co. KG in the last few years.

Figure 11.6
Processing of UXPM OX Series. AOP (advanced oxidation process) for wastewater from Microelectronics, Project UV-EL & V3 Corporation Ltd., Russian Federation, 2017; UV equipment: medium-pressure lamp; power: 2 × 11.5 kW. (Use admission from UV-EL GmbH & Co. KG.)

Figure 11.7
UXPM OX Series. AOP (advanced oxidation process) for UV wet oxidation for treatment of groundwater (elimination of cyanide), Germany, 2013; UV equipment: medium-pressure lamp; power: 2 × 7 kW. (Use admission from UV-EL GmbH & Co. KG.)

Figure 11.8

UXPM OX Series. AOP (advanced oxidation process) for UV wet oxidation for treatment of wastewater in electroplating industry (hypophosphite/phosphite oxidation) from Project UV-EL & bibra Abwassertechnik GmbH, Germany, 2015; UV equipment: medium-pressure lamp; power: 7 kW. (Use admission from UV-EL GmbH & Co. KG.)

Based on data collected while implementing projects of the company, Johne from UV-EL GmbH & Co. KG (Johne and Nguyen, 2016) summarized typical energy consumption of H_2O_2/UV system for diverse applications with different wastewater characterizations. Table 11.4 shows that H_2O_2/UV is quite energy-intensive. It is because approximately 80% of operational costs of H_2O_2/UV processes come from energy consumption.

Table 11.4: Typical energy consumption of H_2O_2/UV system (Johne and Nguyen, 2016).

Applications	P [kWh m^{-3}]
Treatment dye effluent	1–3
Treatment of groundwater	0.5–3
Treatment of wastewater (phenol, PCE/PCB, xylol, chloroform, cyanide, phosphite, etc.)	1–10
Specific application in the chemical and pharmaceutical industry	3–20

Furthermore, research of UV-EL GmbH & Co. KG on feasibility of the combination between H_2O_2/UV and photocatalysis revealed that the use of the UV reactor, which is equipped with a nano-TiO_2-coated inner wall, can reduce the energy costs in the treatment of textile wastewater (Johne and Nguyen, 2016). This can be a new possibility for commercial application of photocatalysis. This application is currently in a longtime testing phase in pilot scale.

Energy costs take a dominant part of operational costs of photocatalysis. Therefore, economic feasibility of the process can be considerably improved by using the immobilized photocatalyst instead of slurry reactor. In this case, the energy costs for dispersing can be eliminated and the energy loss due to low UV transmittance can also be minimized remarkably.

Besides, more reliable cost estimations of the photocatalytic part can only be attained through an extension of empirical work and investigations in larger-scale processes.

11.2.2 Cost Estimation for Membrane Part

Applying a membrane separation unit in combination with a photocatalysis, the synergistic benefits of these additional process steps must pay for it.

MF, UF, or NF can be used as pretreatment steps to increase the efficiency of the photocatalysis or be applied as a posttreatment after the photocatalysis for further purification and returning of residual organic matter to the reaction system.

In both process concepts, the membrane separation steps will not only contribute significantly in the recycling, removing, retaining, or returning of organic solutes to increase the reaction efficiency but also require a major contribution in the treatment costs. Samhaber and Nguyen (2014) supplied detailed cost calculations of NF step within the combination of membrane and photocatalysis for the treatment of dyehouse effluents.

For the estimation of costs, which will come along with an additional membrane separation step, it is important to know in what range of system capacity the costs have to be taken into account and what influences the costs of the applied membrane processes. For a rough and a quick estimation, a simple approach will be described and demonstrated in the following.

The estimation procedure for the membrane units is based on experiences in the realization of industrial membrane plants for the production of different products and water and wastewater treatment. Based on those experiences, cost figures were developed to allocate costs for rough cost estimation (range of $\pm 30\%$) in relation to the value of membrane replacement costs (MRCs), which is directly connected with the required

membrane area. The membrane area again is a result of designed membrane unit throughput together with the achievable membrane fluxes.

In the application of membrane separation units, it is the challenge to keep the specific membrane cost figure low by achieving a less frequent membrane replacement in a viewed application. MRCs in industrial application are generally in the range of 10%–20% of the total investment costs of a plant.

In wastewater treatment, it is as a rule of thumb to afford MRCs, which are less than 10% of the equipment costs depending on the size of the plant, which is also connected with the specific estimation cost for realizing the plant given in Fig. 11.1.

The annual operating costs, as computed in Table 11.5, are 6.80 times higher than MRCs and amount from 204 to 408 US$ according to the specific MRCs, which we have assumed herewith to be in the range of 30–60 US$ m^{-2} of spiral wound membrane used in the focused treatment plant.

The estimated figures of fixed and variable cost are empirical cost data collected from membrane plant with membrane areas from 100 to 500 m^2 with a cost accuracy of ±30% depending on the design pressure, quality of technical construction, and level of system automation.

Table 11.5: Compilation of costs in multiples of membrane replacement costs (Samhaber and Nguyen, 2014).

spec. Membrane Replacement Costs (sMRC) for Spiral Membrane Elements		30	to	60	US$ m^{-2}
	Volumetric Permeate Capacity	10	to	30	L m^{-2} h^{-1}
Assumption 1	*Membrane lifetime (MLT)*	1	a		
Fixed costs	Amortization	2,55	x	MRC	
	Maintenance 20% of amortization	0,50	x	MRC	
		3,05		MRC	
Variable costs	Membrane costs	1,00	x	MRC	
	Energy costs	0,50	x	MRC	
	CIP-costs	0,25	x	MRC	
	Labor costs	2,00	x	MRC	
	Running costs	3,75	x	MRC	
	Total operating costs	**6,80**	**x**	**MRC**	

Based on those figures in Table 11.5, we can roughly estimate the operating cost of a membrane unit application, which has to achieve a given throughput of permeate based on a specified feed or output capacity. The estimated achievable permeate fluxes as already mentioned earlier can be usually figured out for different membrane type applications as follows.

For an RO and NF, it can be approached between 10 and 30 L ($m^{-2}h^{-1}$), for UF, some more between 25 and 50 L ($m^{-2}h^{-1}$), and for MF, between 50 and 100 L ($m^{-2}h^{-1}$).

To illustrate this cost estimation procedure, a short example for an NF unit should be carried out. The first steps of this approach are shown in Table 11.6. We assume an application like in Fig. 11.4 where in the first step a treatment of a 20 m^3 d^{-1} organic containing water stream should be carried out. The treatment system should be operated during 200 days per year. For cleaning-in-place (CIP) it is foreseen 4 h per day, where the net operating time per day then makes 20 h. With the assumed 200 operating days per year, we get the specific permeate capacity between 200 and 600 L ($m^{-2}d^{-1}$) or with the calculation for 1 year of 40–120 m^3 ($m^{-2}a^{-1}$).

Depreciation and maintenance costs thereby incurred independently if the plant is in operation or possibly not in use, e.g., if there is no demand to treat dye effluents. In the

Table 11.6: Cost estimation example for a treatment capacity of 20 m^3 dye effluent per day (Samhaber and Nguyen, 2014).

EXAMPLE	20	$m^3 d^{-1}$	Dyehouse effluent treatment	
Assumption 2	*10*	L $m^{-2} h^{-1}$	*Specific permeate capacity*	
Assumption 3	*4*	*h CIP/d*	*24 h/d operation*	
	200	L $m^{-2} h^{-1}$	Specif permeate capacity per day	
Resulting size of NF plant	100	m^2	membrane area size (MAS)	
Basis: sMRC range from	30	to	60	US$ m^{-2}
Mean value of	sMRC	45,00	US$ m^{-2}	
With assumption 1		1	a	Membrane lifetime MLT
The total membrane replacement costs can be estimated with MAS between				
Total MRC from	3.000	to	6.000	US$ a^{-1}
Days per year	365	Days/year		
Days of operation	200	Days/year		
With the specific cost estimation of table 1				
of	6,80	x MRC		
The total operating costs can be estimated between				
Total operating costs	**15.314**	**to**	**30.629**	**US$ a^{-1}**

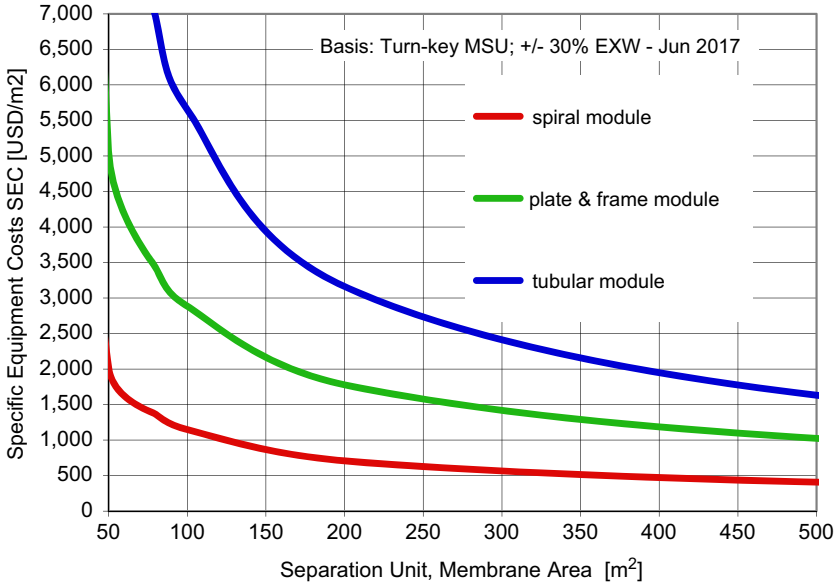

Figure 11.9
Specific equipment cost (SEC) per m^2 of membrane area (Samhaber and Nguyen, 2014).

maintenance cost, the periodical CIP is included, which is needed even if the membrane plant is not in operation.

As for the amortization period, we have taken generously a 10-year period, which might not be generally applicable depending on local situations or financial regulations.

Fig. 11.9 is a compilation of empirical data of realized membrane plant with different module configurations such as tubular, plate and frame, or spiral wound. The given specific equipment costs are turnkey costs of frame-mounted separation plant including the CIP system, without the costs for local installation of buffer tanks and all out-side the battery limits of the separation plant, which are considered to be ex-works prices.

We can take from Fig. 11.9 the specific equipment costs, which then give us the estimated purchase price for the equipment by multiplying it with the necessary plant size.

The needed plant size in our application example, which is pointed out in Table 11.6, is defined with 100 m^2 membrane area. As we are using a spiral wound configuration, the specific equipment costs can be taken from Fig. 11.9 with about 1150 US$ m^{-2}, which again results in an equipment purchase price of 1150 times 100 m^2 membrane area which is needed, which results in an equipment purchase price of 115,000 US$ (±30%

depending on quality of materials, instrumentation, control devices, process automation standards, etc.) as for the capital investments.

As calculated in Table 11.6, the total operating costs will be 15,314 US$ (with MRCs of assumed 3000 US$) or 30,629 US$ (for 6000 US$ MRCs), respectively.

With those figures, we can calculate the treatment cost of 1 m^3 of effluents to be treated, which results depending again on the respective MRCs in the range between 3.83 and 7.66 US$ m^{-3}.

11.2.2.1 Membrane Unit Treatment Costs and Sensitivities

The daily required effluent treatment capacity and the time for membrane cleaning together with the mean specific achievable permeate flux can be taken for the preliminary design of the membrane plant size. Possible influences in flux performances are not taken in consideration herein. With the amortization costs, the invested capital of a plant, which can be estimated on the basis of the plant size, will be paid off over a certain period time. The number of years for paying off the capital expenditures is one cost-sensitive factor. Another major cost factor for the total operating costs is given with the annual operating hours. These influences are affecting to a great extent the total specific treatment costs caused by the membrane step.

The total mean treatment costs of our example can be calculated with 5.74 US$ of an NF membrane plant with a capacity of 20 m^3 of effluents per day. With the assumption of a membrane flux of 10 $Lm^{-2}h$ and 200 operating days per year which means that 4000 m^3 of effluents would be treated within 1 year, those treatment costs could be reduced to an amount of 4.20 US$ if the plant would be operated the whole year round, which results in a yearly treatment capacity of 7300 m^3.

The number of the treatment days per year, which represents a significant influence in the treatment costs too, is pointed out in Fig. 11.10.

A good performing plant can be assessed by the achieved quality of treated effluent. For a profitable or useful application, a stable flux and proper cleaning conditions have to be established.

In Fig. 11.11 the total specific effluent treatment costs in US$ per treated m^3 of effluents are shown versus the mean plant permeate flux, which can be achieved in the considered treatment process. With that dependency and an assumed 10-year amortization period, the total specific treatment costs are calculated for an assumed

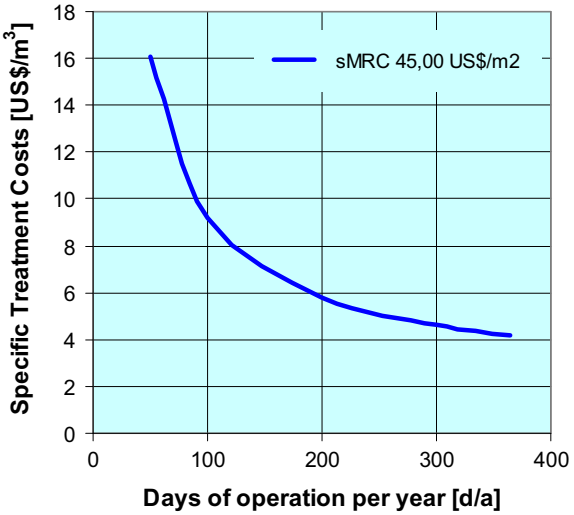

Figure 11.10

Total specific dyehouse effluent treatment costs versus the operating time in d/a with mean MRC value of 45 US$ (Samhaber and Nguyen, 2014).

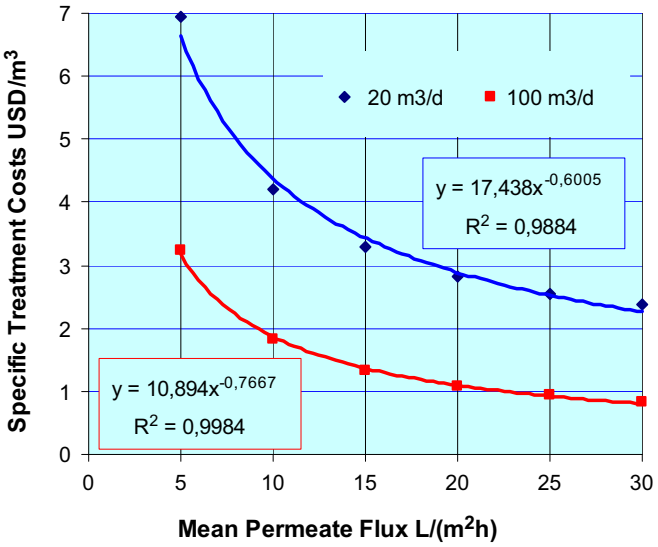

Figure 11.11

Specific total operating costs, treatment capacities of 20 and 100 $m^3\ d^{-1}$, 365 days per year treatment operation (Samhaber and Nguyen, 2014).

365 days per year operation and for plant capacities of 20 and 100 $m^3\ d^{-1}$. In Fig. 11.11 the resulted treatment costs in US$ m^{-3} of effluents are outlined versus the achievable mean permeate flux of the NF process.

11.3 Conclusions and Future Trends

The combination of membranes with photocatalysis is capable to increase the efficiency of reaction processes whereby the existing synergies between the reaction and separation will be used in an optimal way. Membranes such as UF and NF exhibit the ability to reject or selectively separate organic compounds. Membrane pretreatment steps would improve, on the one hand, the transparency of the feed solution and, on the other hand, can separate components before the reaction step, which do not need or not have to be treated in the reactor and would make it just more difficult to degrade.

Viewing the application of a membrane step for selectively removing or separating dissolved matter before the photocatalytic reaction to purify wastewater could be necessary to set an MF or UF step before the NF step during upscaling the system.

Promising results in laboratory tests are not always easily transferable into industrial scale, and it has to be kept in mind that highly selective membrane processes might have an additional treatment step to achieve a well-performing longtime operation of an RO, NF, UF, or MF. Investment costs for industrial plant including the necessary pretreatment equipment can be high. Focusing industrial applications, it is a rule of thumb that costs are associated almost directly with the numbers of process steps involved.

Considering the purification of certain waste effluent streams, there is one possibility to set the treatment plant at the source to avoid the disadvantage of dilution of contaminants to be treated. Formerly, wastewater treatment was located at the end of pipe, and as a consequence, the treatment of high-volume flows was necessary. If different sources of organic matter in various effluents are given, the process flows at the source have to be primarily treated.

The treatment of diluted systems after the biological degradation step is also described as a polishing step of effluents, which can be performed conventionally through natural UV radiation in large surface ponds or unconventionally with reduced surface demands in photocatalytic systems, which are known as the so-called advanced oxidation processes. The photocatalytic systems exhibiting higher efficiencies and shorter residence times and membrane separation again can bring back those organic compounds, which are not readily degraded within the hydraulic residence time of the reaction system. Membranes on the down-stream side of photocatalytic reactors are used to recycle suspended

photocatalytic particles and additionally it can retain compounds for further treatment as already mentioned before.

Membrane steps for reaction systems with their highly selective properties can be justified simply because of missing a conventional and proper separation technique. Nevertheless, membrane separation units will be parallel to the photocatalytic reaction system, a major cost factor, but will ascertain high qualities of treated process streams and will demonstrate that the combination with a photocatalytic reactor has synergies in practical applications.

List of Abbreviations

AOP Advanced oxidation processes
CIP Cleaning-in-place
EE/M Electrical energy per mass
EE/O Electrical energy per order
MF Microfiltration
MRC Membrane replacement costs
MTBE Methyl-tert-butyl ether
NF Nanofiltration
PMRs Photocatalytic membrane reactors
RO Reverse osmosis
SEC Specific equipment cost
TCE Trichloroethylene
TOC Total organic carbon
UF Ultrafiltration
UV Ultraviolet

Notation

k_1' Pseudo−first-order rate constant (min^{-1})
V_r Reactor volume (L)
ϕ Quantum yield for the generation of $Z^{\bullet}$
B Initial compound, which can be water or some added substance (e.g., H_2O_2 or O_3)
C A particular organic contaminant
c Constant in Eq. (11.1)
C_i, C_f Initial and final contaminant concentrations (mol L^{-1})
E Energy supplied by single reactor
F Flow rate (L/min)
F, Flow rate in the flow-through system ($m^3\ h^{-1}$)
F_m Membrane area (m^2)
G Total absolute photon flow emitted from the lamp in all directions ($Einstein^{-1}$) in a useful wavelength range
k_C Second-order rate constant
k_{S1}, k_{S2}, …, k_{Si} Second-order rate constant k_{S1}, k_{S2}, …, k_{Si}
M Molecular weight of the contaminant (g mol^{-1})
n Concentration factor of membrane unit
N Energy demand (kW)

N Number of reactor
P Reactor cost
p Operational pressure (bar)
$\mathbf{P_{elec}}$ Electrical power input to the system (kW)
Q Subtotal 1
r Overall rate of the process (Ms^{-1})
R Subtotal 2
$\mathbf{r_1}$ Rate of formation of Z• radical (Ms^{-1})
$\mathbf{r_2}$ Rate of reaction of Z• with C with second-order rate constant
$\mathbf{k_C}$ Second-order rate constant
$\mathbf{r_{3a}}$, $\mathbf{r_{3b}}$,…, $\mathbf{r_{3i}}$ Rate of reaction of Z• with scavengers S_1, S_2,…, S_i
S Subtotal 3
$\mathbf{S_1}$, $\mathbf{S_2}$,…, $\mathbf{S_i}$ Scavengers for the Z• radical
$\mathbf{t_R}$ The reaction time (min)
U Design flow rate of the photocatalytic reactor (L min^{-1})
V Treated volume (L)
$\mathbf{V_{90}}$ Treated volume at 90% degradation (L)
$\mathbf{V_R}$ Reactor volume (m^3)
Y Retention (%)
Z• Highly reactive intermediate (e.g. •OH, H•, hydrated electron, etc.)
τ Retention time in the reactor (min)
χ Fraction of photons that are absorbed in solution
$\boldsymbol{\varepsilon}$ Energy density (WL^{-1})
$\boldsymbol{\tau}$ Treating time (min)
$\boldsymbol{\tau_{90}}$ Time required for 90% degradation of the contaminant (min)

References

Adewuyi, Y.G., 2001. Sonochemistry: environmental science and engineering applications. Ind. Eng. Chem. Res. 40, 4681–4715.

Augugliaro, V., GarcıÅa-LoÅLpez, E., Vittorio Loddo, V., Malato-RodrıÅLguez, S., Maldonado, I., Marcı‘, G., Molinari, R., Palmisano, L., 2005. Degradation of lincomycin in aqueous medium: coupling of solar photocatalysis and membrane separation. Sol. Energy 79, 402–408.

Berberidou, C., Avlonitis, S., Poulios, I., 2009. Dyestuff effluent treatment by integrated sequential photocatalytic oxidation and membrane filtration. Desalination 249, 1099–1106.

Bolton, J.R., Bircher, K.G., Tumas, W., Tolman, C.A., 2001. Figures-of-merit for the technical development and application of advanced oxidation processes. Pure Appl. Chem. 73 (4), 627–637.

Brunetti, A., Zito, P.F., Giorno, L., Drioli, E., Barbieri, G., 2017. Membrane reactors for low temperature applications: an overview. Chem. Eng. Process. Process Intensif. (in press).

Chong, M.N., Jin, B., Chow, C.W.K., Saint, C., 2010. Recent developments in photocatalytic water treatment technology: a review. Water Res. 44, 2997–3027.

Chooa, K.H., Changa, D., Park, K.W., Kim, M.H., 2008. Use of an integrated photocatalysis/hollow fiber microfiltration system for the removal of trichloroethylene in water. J. Hazard Mater. 152, 183–190.

Damodar, R.A., You, S.J., Ou, S.-H., 2010. Coupling of membrane separation with photocatalytic slurry reactor for advanced dye wastewater treatment. Separ. Purif. Technol. 76, 64–71.

Grzechulska-Damszel, J., Morawski, A.W., 2009. Removal of organic dyes in the hybrid photocatalysis/nanofiltration system. Asia Pac. J. Chem. Eng. 4, 239–245.

Grzechulska-Damszel, J., Mozia, S., Morawski, W.A., 2010. Integration of photocatalysis with membrane processes for purification of water contaminated with organic dyes. Catal. Today 156, 295–300.

Herrmann, J., 1999. Heterogeneous photocatalysis: fundamentals and applications to the removal of various types of aqueous pollutants. Catal. Today 53 (1), 115−129.

Hyman, M., Dupont, R.R., 2001. Groundwater and Soil Remediation: Process Design and Cost Estimating of Proven Technologies. American Society of Civil Engineers, ASCE Press, ISBN 0784404275.

http://www.icispricing.com and http://www.advancedmaterials.us/.

Johne, S., Nguyen, M.T., 2016. NaViTex from research to applications implementation of scientific results for textile Industry. In: Closing Workshop - "Concept Development for Textile Wastewater Treatment in Vietnam Using Photocatalytic Oxidation with Titanium Dioxide Nanoparticles (NaViTex)" 18.03.2016, Danang, Vietnam.

Kommineni, S., Zoeckler, J., Stocking, A., Liang, P.S., Flores, A., Rodriguez, R., Browne, T., Roberts PE, R., Brown, A., 2000. 3.0 Advanced Oxidation Processes. Center for Groundwater Restoration and Protection National Water Research Institute.

Le, H.N., Babick, F., Kühn, K., Nguyen, M.T., Stintz, M., Cuniberti, G., 2015. Impact of ultrasonic dispersion on the photocatalytic activity of titania aggregates. Beilstein J. Nanotechnol. 6, 2423−2430. https://doi.org/10.3762/bjnano.6.250.

Mahamuni, N.N., Adewuyi, Y.G., 2010. Advanced oxidation processes (AOPs) involving ultrasound for waste water treatment: a review with emphasis on cost estimation. Ultrason. Sonochem. 17, 990−1003.

Martınez, F., et al., 2013. Coupling membrane separation and photocatalytic oxidation processes for the degradation of pharmaceutical pollutants. Water Res. 47 (15), 5647−5658.

Melin, G. (Ed.), 1999. Treatment Technologies for Removal of Methyl Tertiary Butyl Ether (MTBE) from Drinking Water: Air Stripping, Advanced Oxidation Processes, Granular Activated Carbon and Synthetic Resin Sorbents. Center for Groundwater Restoration and Protection, National Water Research Institute, CA.

Molinari, R., Pirillo, F., Falco, M., Loddob, V., Palmisano, L., 2004. Photocatalytic degradation of dyes by using a membrane reactor. Chem. Eng. Process 43, 1103−1114.

Molinari, R., Caruso, A., Palmisano, L., 2010. Photocatalytic processes in membrane reactors. Compr. Membr. Sci. Eng. 3, 165−193.

Molinari, R., Lavorato, C., Argurio, P., 2017. Recent progress of photocatalytic membrane reactors in water treatment and synthesis of organic compounds. A review. Catal. Today 281, 144−164.

Mozia, S., 2010. Photocatalytic MRs in water and wastewater treatment. A review. Sep. Purif. Technol 73, 71−91.

Mozia, S., Tomaszewska, M., Morawski, A.W., 2006. Removal of azo-dye Acid Red 18 in two hybrid membrane systems employing a photodegradation process. Desalination 198, 183−190.

Mozia, S., Szymański, K., Michalkiewicz, B., Tryba, B., Toyoda, M., Morawski, A.W., 2015. Effect of process parameters on fouling and stability of MF/UF TiO_2 membranes in a photocatalytic membrane reactor. Separ. Purif. Technol. 142, 137−148.

Samhaber, W.M., Nguyen, M.T., 2014. Applicability and costs of nanofiltration in combination with photocatalysis for the treatment of dye house effluents. Beilstein J. Nanotechnol. 5, 476−484.

Yuan, Z., Tol, R.S.J., 2004. Evaluating the costs of desalination and water transport. Water Resour. Res. 41 (3), 1−16.

Zheng, Y., Yu, S., Shuai, S., Zhou, Q., Cheng, Q., 2013. Color removal and COD reduction of biologically treated textile effluent through submerged filtration using hollow fiber nanofiltration membrane. Desalination 314, 89−95.

This page intentionally left blank

Index

'*Note:* Page numbers followed by "f" indicate figures and "t" indicate tables.'

C

D

E

F

G

H

I

K

L

M

N

O

P

Q

R

S

T

U

V

W

X

Z

CURRENT TRENDS AND FUTURE DEVELOPMENTS ON (BIO-) MEMBRANES

PHOTOCATALYTIC MEMBRANES AND PHOTOCATALYTIC MEMBRANE REACTORS

EDITED BY
ANGELO BASILE, SYLWIA MOZIA, AND RAFFAELE MOLINARI

The book will give a comprehensive review on the present state of the art in the area of photocatalytic membranes and photocatalytic membrane reactors.

- Reviews new hybrid separation techniques based on photocatalysis and membranes
- Offers a detailed description of the various photocatalytic membrane reactors and their function
- Includes solutions for removal of emerging contaminants from water such as pharmaceutical and personal care products
- Numerous reactor configurations are discussed and various membrane materials for photocatalytic membranes are presented
- Includes modeling and economical aspects of the various processes

In recent years, there is an increased interest in photocatalytic membrane reactors (PMRs), hybrid systems coupling photocatalysis and membrane separation. There are two main configurations of PMRs: (1) reactors with photocatalyst suspended in feed solution and (2) reactors with photocatalyst supported in/on the membrane, i.e., reactors with photocatalytic membranes (PMs). The main application of PMRs is in water and wastewater treatment; however, the possibilities of using these systems in chemical synthesis are also considered. ***Photocatalytic Membranes and Photocatalytic Membrane Reactors*** offers a comprehensive review on the present state of the art in the area of PMs and PMRs. The book gives an overview of the basis of photocatalysis and membrane separation, basic aspects of PMs and PMRs as well as applications, modeling and economical aspects of PMs and PMRs. Although PMRs exhibit numerous advantages over the conventional photoreactors in case of water and wastewater treatment as well as organic synthesis, further investigations are still needed to improve the performance of these hybrid processes. The book addresses the main issues associated with PMR design and tries to answer the question *"how far is from the laboratory scale to the application of PMRs in industry."*

Angelo Basile is a senior researcher at the ITM-CNR where he is responsible for research related to ultrapure hydrogen production and CO_2 capture using Pd-based membrane reactors. As of 2014, he also holds the post of full professor of chemical engineering processes.

Sylwia Mozia is a full professor at the Institute of Inorganic Chemical Technology and Environmental Engineering, West Pomeranian University of Technology, Szczecin (Poland). Her research interests focus mainly on water/wastewater treatment with the application of (hybrid) membrane processes and advanced oxidation techniques.

Raffaele Molinari is a full professor of fundaments of chemical technologies at the Department of Environmental and Chemical Engineering, University of Calabria. His research interests are membrane processes; catalytic and photocatalytic membrane reactors; complexation reactions coupled with membranes; and saving, recovery, and recycle of matter and energy by membrane processes.

Chemical Engineering

ISBN 978-0-12-813549-5

9 780128 135495

ELSEVIER

elsevier.com/books-and-journals